TITANIUM AND TITANIUM ALLOYS

Scientific and Technological Aspects

Volume 3

J. C. Williams · A. F. Belov

Springer

TITANIUM AND TITANIUM ALLOYS

Scientific and Technological Aspects

Volume 3

The Metallurgical Society of AIME Proceedings
published by Plenum Press

Refractory Metal Alloys: Metallurgy and Technology
Edited by I. Machlin, R. T. Begley, and E. D. Weisert

Research in Dental and Medical Materials
Edited by Edward Korostoff

Developments in the Structural Chemistry of Alloy Phases
Edited by B. C. Giessen

Corrosion by Liquid Metals
Edited by J. E. Draley and J. R. Weeks

Metal Forming: Interaction Between Theory and Practice
Edited by A. L. Hoffmanner

Titanium Science and Technology (4 Volumes)
Edited by R. I. Jaffee and H. M. Burte

Metallurgical Effects at High Strain Rates
Edited by R. W. Rohde, B. M. Butcher,
J. R. Holland, and C. H. Karnes

Physics of Solid Solution Strengthening
Edited by E. W. Collings and H. L. Gegel

Shape Memory Effects in Alloys
Edited by Jeff Perkins

Titanium and Titanium Alloys: Scientific and
Technological Aspects (3 Volumes)
Edited by J. C. Williams and A. F. Belov

TITANIUM AND TITANIUM ALLOYS

Scientific and Technological Aspects

Volume 3

Library of Congress Cataloging in Publication Data

International Conference on Titanium, 3d, Moscow State University, 1976.
Titanium and titanium alloys.

Organized by the Academy of Sciences of the USSR, in association with the Metallurgical Society of AIME and others, and held at Moscow State University, May 18–21, 1976.
Includes index.
1. Titanium—Congresses. 2. Titanium alloys—Congresses. I. Williams, James Case, 1938- II. Belov, Aleksandr Fedorovich. III. Akademiia nauk SSSR. IV. Title.
TN693.T5I57 1976 669'.732 79-9156
ISBN 978-1-4757-1760-0 ISBN 978-1-4757-1758-7 (eBook)
DOI 10.1007/978-1-4757-1758-7

Proceedings of the Third International Conference on Titanium, organized by the Academy of Sciences of the USSR, in association with The Metallurgical Society of AIME, American Society for Metals, the Metals Society (London), and the Japan Institute of Metals, in Moscow, on May 18–21, 1976.

© 1982 Springer Science+Business Media New York
Originally published by Plenum Press, New York in 1982
Softcover reprint of the hardcover 1st edition 1982

All rights reserved

No part of this book may be reproduced, stored in a retrieval system, or transmitted, in any form or by any means, electronic, mechanical, photocopying, microfilming, recording, or otherwise, without written permission from the Publisher

DECOMPOSITION OF THE MARTENSITE IN TWO-PHASE TITANIUM ALLOYS

T. L. Trenogina and R. M. Lerinman

Institute of Metal Physics, the Urals Scientific Centre, USSR Academy of Sciences

U.S.S.R.

The present work is devoted to an electron microscope study of the decomposition of hexagonal martensite in $\alpha+\beta$ titanium alloys. As previous investigations have shown, martensite decomposition in titanium alloys is heterogeneous in character.[1,2] In this connection it is of interest to study the martensite substructure and its effect on the decomposition kinetics, dispersity and distribution density of precipitating phases.

For this investigation, the alloyVT9 (Ti-6.5Al-3.5Mo2Zr-0.2Si) quenched from the β-field was used. Upon quenching from 1050°C, hexagonal martensite forms and a very small quantity of β-phase is retained. Observations show the internal structure of martensite plates to be varied. One can note the following kinds of internal structure of martensite:

1. Rows of parallel dislocations (Fig. 1);
2. Blocks of dislocation origin with a slight disalignment (Fig. 2);
3. Complicated dislocation pile-ups and networks (Fig. 3);
4. Twins with a twinning plane $\{1011\}_{\alpha'}$ (Fig. 4).

According to the existing phenomenological theory of crystallography of the martensitic transformation, martensite forms by an invariant plane deformation which generally consists of a homogeneous lattice-invariant shear.[3]

Principal distortions for the transformation of b.c.c. to h.c.p. lattice are:

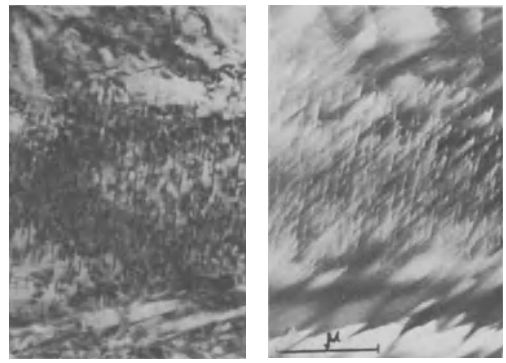

(a) (b)

Fig. 1: a) Rows of dislocations in martensite. Quenched from 1100°C (1hr) + tempered at 550°C for 1hr. Z.N. $[1\bar{3}\bar{2}2]_{\alpha}$; b) Precipitates of β-phase on the rows. D.F. micrograph from $(020)_{\beta}$ reflection. x29000

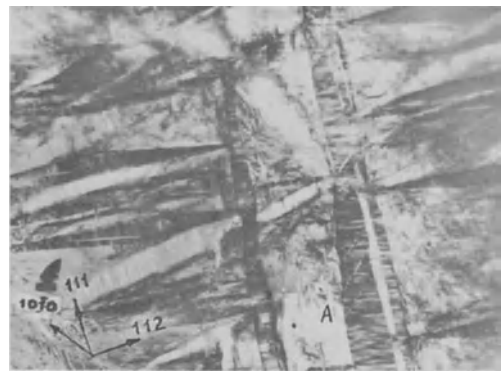

Fig. 2: Block structure of martensite. Quenching from 1050°C 15 min. Z.N. $[110]_{\beta} \parallel [0001]_{\alpha}$. A-twins.

$$\varepsilon_i = \eta_i - 1,$$

where

$$\eta_1 = \frac{a_\alpha}{a_\beta}\sqrt{3/2}\,, \quad \eta_2 = \frac{a_\alpha}{a_\beta}\,, \quad \eta_3 = \frac{c_\alpha}{a_\beta}\sqrt{2}$$

and where a_α and c_α = lattice parameters of α-phase (h.c.p.),

a_β = lattice parameter of β-phase (b.c.c.).

For the investigated alloy $a_\beta = 3.299$, $a_\alpha = 2.949$ and $c_\alpha = 4.677$Å and $c/a = 1.586$*; $\varepsilon_1 = 9.5$; $\varepsilon_2 = 10.5$ and $\varepsilon_3 = 0.3\%$.

Since $\varepsilon_3 = 0$ is small, it can be taken as 0. At $\varepsilon_3 = 0$ no additional lattice-invariant shear is required as the lattice deformation itself proves to be an invariant plane strain. In this case it can be accomplished by a simple shear with an invariant (habit) plane.

Using the computation of habit plane indices employed in (3) for the case when $\varepsilon_3 = 0$ it was found that for the investigated alloy they should be $\{575\}_\beta$. Loci of habit plane normals were determinated by trace analysis. They are plotted on the Figure 5 assuming the Burgers orientation relationship is fulfilled. Experimental results are in satisfactory agreement with the computations. Therefore, one can actually assume that during β→α'-transformation the only deformation in the investigated alloy is the lattice deformation. It appears to be close to the deformation for the lattice change proposed by Burgers for β→α-transformation in Zr. It is a shear in $\langle 11\bar{1}\rangle$ direction on a {112} plane.

Proceeding from the fact that the deformation of β→α-transformation is identical to the shear for the β→α lattice change according to Burgers, one can suppose that accommodation of stresses between α'-crystals and the β-matrix occurs by formation of translation blocks with the output of dislocations on their boundaries. A similar mechanism of translation block formation is offered for the case of α-phase growth.[4] Rows of parallel dislocations observed in martensite plates of the investigated alloy (Fig. 1) appear to be connected with the formation of such blocks in the β→α'-transformation. The following testifies in favor of this suggestion:

1. Trace analysis showed the dislocations to be located on planes $\{10\bar{1}0\}_\alpha \parallel \{112\}_\beta$ along $\langle 1\bar{2}10\rangle_\alpha \parallel \langle 11\bar{1}\rangle_\beta$ so that they are likely to be screw dislocations with $\vec{\beta} = 1/3\ \langle 1\bar{2}10\rangle$;

*Parameter values were determined by X-ray method.

Fig. 3: Dislocation pileups and twins in martensite. Quenched from 1050°C (1hr) + tempered 600°C, 2hr. A - Dislocation pileups, B - twins. x17000

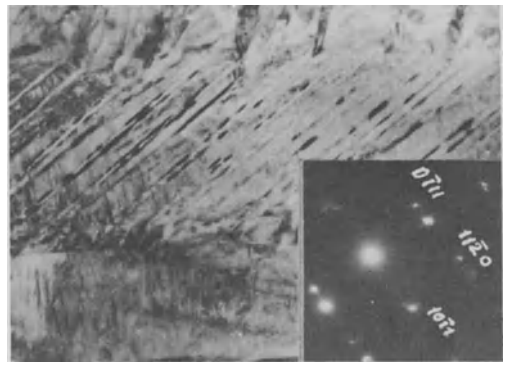

Fig. 4: β-phase precipitates on twin boundaries in martensite. Quenched from 1050°C (1hr) + tempered at 600°C for 2hr. Z.N. $[001]_\beta \| [1101]_\alpha$, Z.N. of twins $[1101]_\alpha$. x37000

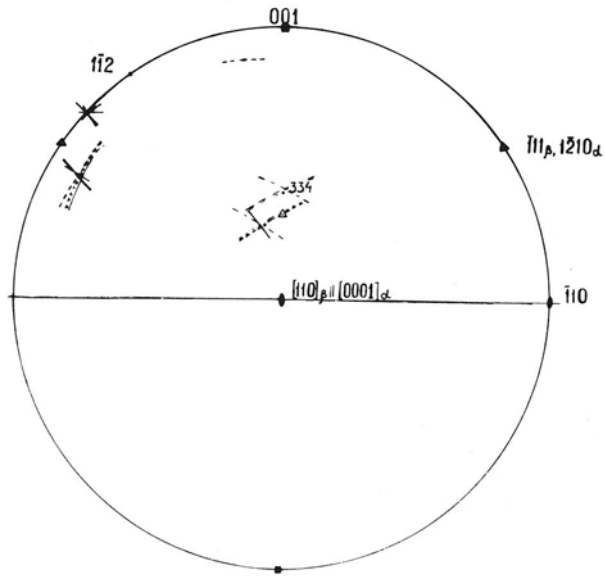

Fig. 5: Trace analysis of habit planes of martensite plates. --- and === quenching after β-deformation.

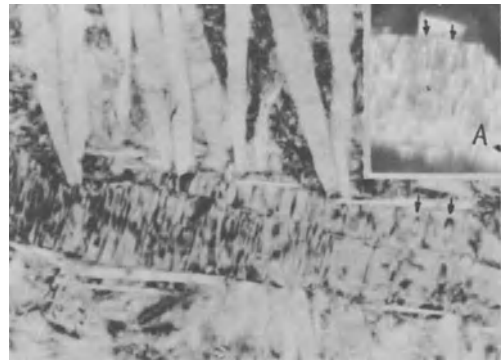

Fig. 6: Dislocation loops in the alloy after quenching from 1050°C for 1hr + tempering at 550°C for 100hr. A - D.f. micrograph from $(10\bar{1}0)_\alpha$ reflection. x50000

2. The amount of shear necessary for $\beta \rightarrow \alpha'$-transformation computed according to Wechsler-Otte[5] is about 0.026 of the shear for slip on $\{10\bar{1}0\}$ along $<1\bar{2}10>$. This amount of shear corresponds to the formation of a single dislocation every 80 planes. Spacing between the dislocations then must be roughly 200Å, which agrees with that observed (Fig. 1).

The formation of translation blocks can occur in spite of the fact that it does not completely remove the stresses at the martensite plate-matrix boundary plane. For the complete relaxation of stresses to occur, a little shear along this plane and tension in the direction normal to it are also necessary. As these deformations are small (below 3%), they can be accommodated at the expense of elastic deformation of the plate and the matrix.

In general, during martensitic transformation a complicated stressed state of the material is formed due to the collision of martensite plates during their formation, anistropy of linear expansion of α-phase and the development of stresses at the martensite-matrix boundary surface. Therefore one can understand the observed breakdown of martensite crystals into disoriented blocks (Fig. 2) or the formation of dislocation pile-ups (Fig. 3,A) and twins in them (Fig. 3,B). All of this leads to relaxation of stresses. The process of breakdown into disoriented blocks is similar to the formation of disoriented microbands in the presence of an inhomogeneous stressed state in deformation of mono- and polycrystals.[6]

On the basis of the Bowles-Mackenzie[7] theory, the lattice-invariant shear for transformation from b.c.c. to an orthorhombic (or h.c.p.) lattice must occur by twinning on $\{110\}_{b.c.c.}$ in an irrational direction (class of solutions A). The shear value on the plane $(110)_\beta \parallel (1\bar{1}01)_{\alpha'}$ estimated according to Wechsler-Otte[5] amounts to ~ 0.03 of a twinning shear. Therefore, in this alloy, twins must not occur. However, a good many internal twinned martensite plates are observed fairly often. Sometimes both twins and blocks of dislocation origin are observed in large plates simultaneously (Figs. 2 and 4). Presumably in this case twinning is a consequence of deformation due to the shock of martensite crystals formed later. That twins in martensite of the investigated alloy do not result from the transformation, but from the deformation is confirmed by the following:

1. Contrast of blocks continues behind the twins and is sometimes visible in the twins proper (Figs. 2,A and 4).

2. Deformation of α-titanium at room temperature does not occur by twinning on $\{10\bar{1}1\}$, but at elevated temperatures, as shown in (8), this very type of twinning deformation is possible. M_s of

Fig. 7: β-particles: A-on dislocation networds, B - on martensite plate boundaries. Quenched from 1050°C (1hr) + tempered at 600°C for 2hr.

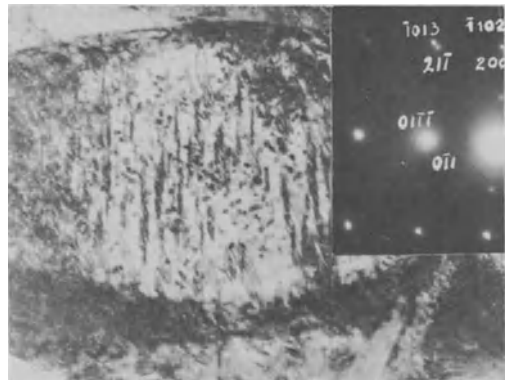

Fig. 8: Ordering in α-plates. Quenched from 1050°C (1hr) + tempered 500°C, 100hr. Z.N. $[\bar{1}0\bar{1}]_{\beta} \| \| [\bar{5}14\bar{3}]_{\alpha, \alpha_2}$. x30000

the investigated alloy is much higher than the ambient temperature.

Heating the quenched alloy initiates the decomposition of martensite. At low temperatures and short durations of tempering, microstructural changes were not observed. After tempering at 550°C for 5 hr, X-ray and electron microscope study revealed the beginning of β-phase precipitation from α'-martensite. β-phase particles seem to be more distinct and are seen earlier at twin boundaries (Fig. 4). The twinning plane $\{10\bar{1}1\}$, that is the habit plane of the twins, is parallel to $\{110\}_\beta$, where the α- and β-phase lattices are in good matching. It is a favorable site for the germination of β-phase. β-precipitates appear also at the boundaries of smaller martensite plates and on rows of dislocatins with $\vec{\beta} = 1/3 \langle 1\bar{2}10\rangle$ on $\{10\bar{1}0\}_\alpha \parallel \{112\}_\beta$ planes in larger plates (Fig. 1). After tempering at 550°C for 100 hr the formation of dislocation loops occurs in some α-plates in which disoriented blocks were observed after quenching (Fig. 6). Elevation of temperature and increased duration of tempering results in the formation of β-phase in the loops. β-phase is also precipitated at dislocation pile-ups in large α-plates and at martensite plate boundaries (Fig. 7).

Fig. 9: Recrystallized α-phase. Quenched from 1050°C (30min) + tempered 600°C, 100hr. Z.N. $[\bar{1}0\bar{1}]_\beta \parallel [5\bar{1}\bar{4}\bar{3}]$. x30000

At 550°C for 100 hr, conditions for the development of an ordering process are created as a result of martensite depletion in Mo and the enrichment in Al during the precipitation of β-phase. Faint superstructural reflections are seen on the electron diffraction patterns taken from large plates (Fig. 8). Ordering is of Ti_3Al type. Superstructural reflections remain on the electron diffraction patterns after 50 hr at 600°C and 5 hr at 650°C.

Mechanical tests of the alloy showed that the strength and the relative elongation are lowered at that stage of tempering (600°C, 5 hr) when β-phase precipitates are seen in all martensite plates on dislocations, twin boundaries and blocks; β-phase also precipitates on plate boundaries and an ordered α_2-phase is formed in the plates. With a further increased duration of tempering and the elevation of temperature β-phase particles begin to coagulate, forming β-islands at the boundaries of blocks and plates proper. Simultaneous recovery and recrystallization processes take place in the martensite plates. The plate body becomes free from dislocations, becoming a monolith. At the tempering temperature 650°C, recrystallization begins already after 30 min. The process of recrystallization in the former martensite plates occurs mainly by means of coalescence. Therefore, inside the recrystallized α-plates, β-phase islands are left. The most obvious is the gradual disappearance of boundaries between parallel α-plates with the same orientation (Fig. 9) which merge together in a single body with β-phase veins. The recrystallization results in a further decrease of strength and elevation of tensile ductility.

Basic elements of martensite substructure of the investigated alloy are blocks and twins. The β-phase precipitation as a continuous film on twin boundaries and on the martensite plate boundaries being about deterioration in mechanical properties. The precipitation at the dislocation pile-ups and networks remains highly dispersed for a long time. By changing the martensite substructure one can probably prevent a sharp decrease of tensile ductility of the alloy in the state strengthened by heat treatment. In reference 9 it is shown that the deformation of martensite improves the mechanical properties of alloy Ti-6Al-4V after tempering, especially at 600°C. Evidently the introduction of additional dislocations as well as the formation of dislocation networks and pile-ups in the martensite results in optimum tensile ductility of the alloy in the state strengthened by heat treatment.

Deformation in the β-field favors the formation of complicated dislocation networks and pile-ups in the martensite and also makes it fine as a result of the inheritance of parent β-phase dislocations.[10] Hence β-deformation will lead to better tensile ductility of the alloy in the state strengthened by heat treatment in comparison with the properties of the undeformed alloy. A necessary condition for the favorable influence of β-deformation is considerable deformation without recrystallization.

REFERENCES

1. Poljak, E. V. and Sokolova, A. Yu., Structural transformations in two-phase titanium alloys, Sb. "Novij konstrukcionnij material titan," "Nauka," M., 1972, p. 66.

2. Williams, J. C. Critical Review. Kinetics and phase transformations, "Titanium Science and Technology," Plenum, New York, 1973, 3, 1433.

3. Kelly, A. and Groves, G. W., Crystallography and crystal defects. Longman, London, 1970.

4. Murzayeva, G. V. and Lerinman, R. M., Electron microscopic investigation of metastable β-phase decomposition in titanium alloy TS6. "Fiz. metal. metalloved.," 1970, 28, 813.

5. Wechsler, M. S. and Otte, H. M., The generalized theory of the martensitic cubic to orthorombic phase transformation. "Acta Met.," 1961, 9, 117.

6. Urusovskaja, A. A., Formation of regions with disoriented lattice at deformation of mono- and polycrystals. "Sb. Nekotorie voprosi fiziki plastichnosti kristallov," Izd. AN SSSR, 1960, 75.

7. Mackenzie, J. K. and Bowles, J. S., The crystallography of martensite transformations-IV. Body centered cubic to orthorhombic transformations. "Acta Met.," 1957, 5, 137.

8. Nath, B. and Lorimer, G. W., The effect of thermomechanical history of the structure and properties of a Ti-6Al-4V alloy. Proceedings of the Third International Conference on the Strength of Metals and Alloys., Cambridge, England, 1973, 1, 123.

10. Trenoghina, T. L., Yelkina, O. A., Lerinman, R. M., Zvereva, Z. V., Beloborodova, A. T. and Makhnev, E. S., Electron microscope study of effect of thermomechanical conditions of deformation on the structure two-phase α+β-titanium alloys. "Fiz. metal. metalloved.," 1975, 40, 1227.

THE INVESTIGATION OF THE TITANIUM STRUCTURE AFTER SHOCK WAVE LOADING

A. R. Kutsar and V. N. German

I. P. Bardin Central Research Institute of Ferrous Metallurgy

U.S.S.R.

INTRODUCTION

The analysis of the previous data on phase transformations under shock wave loading[1] shows that the same polymorphic transitions occur in short duration conditions of dynamic compression as in static high-pressure experiments. Until quite recently the α - ω transformation in titanium was not detected during shock loading.

Under static pressures titanium undergoes α - ω transformation between 40 and 90kbar.[2,3] But no phase transition was noticed in that range at shock measurements. The kink on the D - U diagram occurred at 175kbar[4] and was correlated with the α - β transition. This was verified by observing β-phase in the titanium samples after unloading. Retention of β-phase also detected by Pashkov and Polyakova, as described in reference 5. The structure and property changes in Ti after explosive shock loading were also correlated with the α - β transformation.[6] The occurrence of the Ti α - ω transition during dynamic compression was established for the first time in[7]. It was also shown that considerable quantity of ω-phase may be retained after unloading.

Because of the presence of ω-phase at atmospheric pressure it became possible to study the structure and phase composition of titanium as a function of loading conditions. The aim of the present work is to gain additional knowledge of the mechanism and characteristics of the α - ω transformation at shock wave loading.

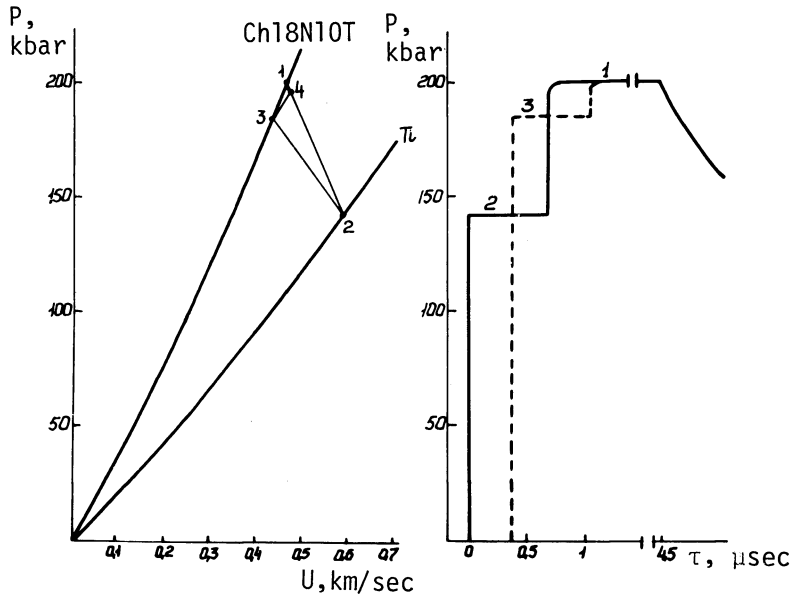

Fig. 1: Shock loading scheme for the titanium sample in the container of stainless steel Ch18N10T. a) Pressures (P) and particle velocities (U) in the container and the sample, 2,4,1- P-U states on the entrance interface (steel-titanium); 3,1 - P-U states on the back interface (titanium-steel).
b) Pressure (P) vs time (T) for the entrance (——) and back (----) sample surfaces; pressures in state 4 and 1 are practically the same.

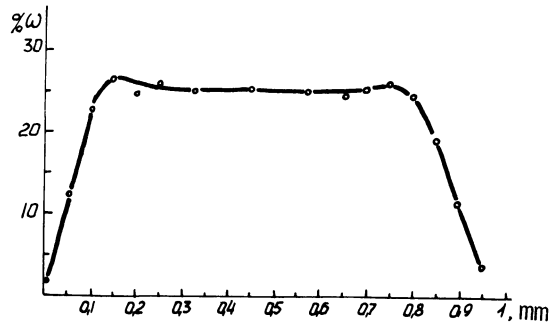

Fig. 2: -phase distribution along cross section of titanium sample after loading to 200 kbar at the initial temperature 120°K (steel container).

EXPERIMENTAL PROCEDURE

Titanium VT-1-0 in the form of a cylinder (16mm diameter by 2mm thick) and iodide grade titanium (16mm diameter by 1mm thick) were used for this investigation. The samples were enclosed in a cylindrical container of stainless steel CH18N10T. Plane shock waves of 120, 200, 350 and 500kbar were produced by the method of contact explosure. The waves were produced by the impact of the metal driver plate accelerated by an explosive charge with the container top surface. This procedure was used earlier[7] and described in detail.[8]

Since the sample and container materials are of different dynamic impedance, loading to the nominal pressure of 120, 200, 350 and 500kbar was done by stages. P-U and P-T loading diagrams (200kbar) for titanium are given as examples in Fig. 1. It is seen from Fig. 1 that the pressure close to maximum initial pressure in the container (state 1) is achieved in the sample in $\sim$1μsec while the whole compression impulse duration is $\sim$4,5μsec. Similar behavior is observed at the other pressures. In several experiments a titanium container was used to get singlewave loading. In that case only state 2 (Fig. 1) with $\sim$4,5μsec duration is realized and pressures of 90, 140, 265 and 390kbar passing through the sample are attained in the first shock wave.

X-ray methods were used to investigate ω-phase content by measuring $(011)_\alpha$ and $(110)_\omega$ line intensities. Surface layers of 0.1-0.15mm thick were removed by etching in hydroflouric acid. For transmission electron microscopy, discs of 4mm diameter were cut from the samples, mechanically thinned to 0, 1-0, 2mm and then chemically polished in the 1:4 mixture of hydroflouric and nitric acids until suitable thin foils were obtained.

EXPERIMENTAL RESULTS

No ω-phase was detected in titanium samples after shock wave loading of 120-500kbar (steel container) at the initial temperature of 290°K. At the lower initial temperature of 120°K ω-phase was 6, 25, 39 and 54% at 120, 200, 300 and 500kbar, respectively.

After singlewave loading of 90kbar (titanium container, initial temperature 120°K) traces of ω-phase were detected; 140kbar loading resulted in 25% ω-phase. In the experiments with singlewave loading to 265 and 386kbar three titanium samples (eash 2mm thick) were enclosed in container, 0,1mm titanium foil being put between them. No ω-phase was detected in these samples. During these experiments containers were subjected to considerable heating, which is evidenced by a blue discoloration on the surface.

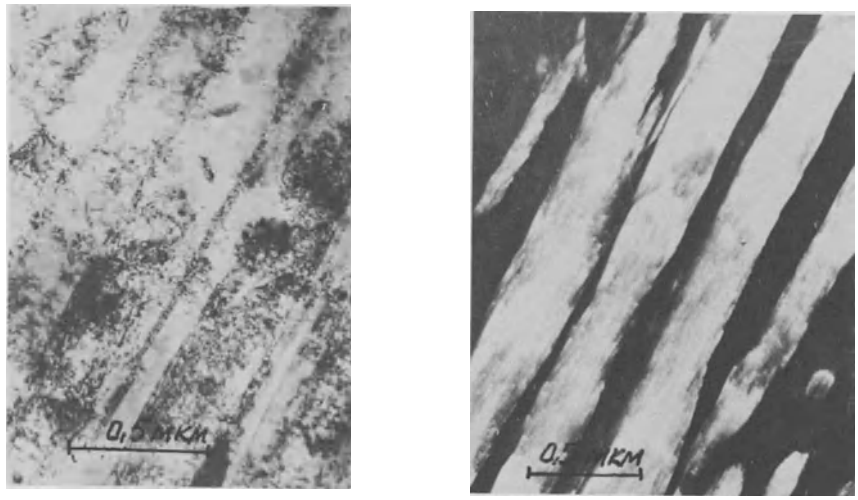

Fig. 3: Structure of shock-loaded titanium (140 kbar, 120°K, titanium-container)
a)α- and ω-crystals.
b)Dark-field image in ω-phase pattern spot.

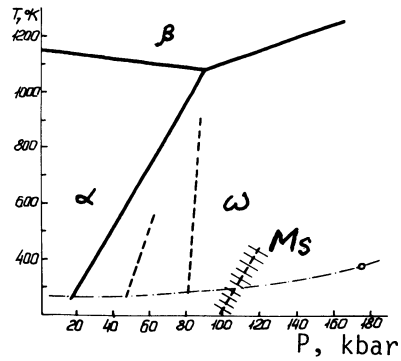

Fig. 4: T-P diagram of Ti.
——— phase equilibrium lines (Ref. 12);
-.-.- Hugoniot for Ti, o-phase transition point (Ref. 4);
--- isothermal α→ω transformation lines (Ref. 2,3);
////// line of the athermal martensite α→ω transformation (M_s).

Four experiments at 350kbar and 120°K were done to determine phase composition stability. ω-phase content was 34, 20, 21 and 24%. The second loading 350kbar, 120°K of the samples with 21 and 24% ω-phase resulted in ω-phase increase to 34 and 35%, respectively.

ω-phase content along the cross-section of the titanium sample was examined by means of X-ray studies. Several layers of 0,05mm were consecutively removed and the ω-phase distribution after 200kbar loading at 120°K is shown in Fig. 2. Similar behavior was observed in other samples containing ω-phase.

Electron microscopy was done after singlewave loading to 140kbar and multiwave loading to 200kbar at the initial temperature of 120°K. In both cases ω-phase was in the form of platelets 0,1-03μm thick (Fig. 3), which were fragmented and had higher defect concentration than α-phase. Analysis of diffraction patterns from the α and ω-crystals showed that both the $(001)_\alpha$ and $(011)_\omega$ planes, and the $[100]_\alpha$ and $[\bar{2}\bar{1}1]_\omega$ directions were parallel,which correlates with the orientation relationship between α and ω-phases in static-pressure treated titanium.[9] The same results were obtained in the study of iodide titanium.

DISCUSSION

It is well known that the high velocity (close to that of sound) of the athermal martensite transformation is caused by cooperative lattice reconstruction.[10] ω-phase formation during several microseconds at temperatures of 200-300°K allows one to assume the athermal martensite mechanism of α→ω transformation.[7] Analysis of the lattice deformation for an α to ω-phase transition[9] shows, in fact, that such reconstruction requires atomic displacements for the distances less than those of interatomic.

The present data about orientation relationships between the α and ω-phases in conjunction with the characteristic thin platelet form of ω-phase crystals, together with kinetic conditions of its formation, allows one to make the unambiguous conclusion that Ti α→ω transformation under shock loading proceeds by athermal martensite mechanism.

At the same time the investigation of α→ω transformation in titanium at static pressures shows rather slow isothermal isobaric kinetics.[2,3]

In connection with essential differences between static and shock kinetics it is possible to plot another line (region) of athermal martensite α→ω transition, together with the well known

isothermal line (region). The existence of two different kinetic lines (regions) is expected from the general kinetic scheme of phase transformations at high pressures.[11]

The T-P diagram of titanium proposed in[12] is given in Fig. 4. The region of α - ω transformation corresponds to 40-90kbar at static pressures, thus the sample after 100kbar loading consists mainly of ω-phase.[9]

Small quantities of ω-phase were detected after shock loading at 90 and 120kbar (initial temperature of 120°K; ∿200°K at shock wave compression). Thus these pressures should be close to the start line of the athermal martensite $\alpha \rightarrow \omega$ transformation (M_s).[10] For a first approximation the M_s line may be plotted to[11] parallel to the line of α - ω equilibrium through the point with coordinates: ∿100kbar, 200°K (Fig. 4).

From the proposed diagram it follows that the phase transition detected in[4] should be correlated with α - ω transition, but not with α - β one. The fact that ω-phase is retained after shock loading at pressures (200kbar) close to the transformation pressure (175kbar)[4] confirms that the volume change at 175kbar during shock transition (1,1%)[4] corresponds to the one of α- ω transformation (1,5%).[12]

Phase composition changes in Ti indicate that the $\alpha \rightarrow \omega$ transition in shock wave loading can be extended to considerable pressure ranges. This correlates with the features of athermal martensite transformation, that every value of overcooling corresponds to definite quantity of martensite phase.[10] Further evidence for this explanation is that at the second loading the quantity of ω-phase increased, but didn't exceed the maximum value after the first loading (35%).

As to β-phase,[8,9] its formation on the surface is associated with peculiarities of shock loading at the surface. These peculiarities were reported earlier[7] and temperatures were discussed in detail recently.[13] Since Hugoniot of the surface layers is in fact that of the porous substance,[13] it is characterized by the essentially higher temperatures and may intersect the ω - β transition line on the T-P diagram. At the same time Hugoniot of the massive titanium may be in the region of ω-phase stability (pressure inside the sample and on the surface being equal). This fact and the elevated residual surface temperatures result in differences between phase composition on the surface and in the bulk of the sample (Fig. 2).

According to the Ti T-P phase diagram, it is possible to explain mechanical property changes after shock wave loading at

P∿200kbar and the absence of considerable effects after loading at 70kbar.[6,14] It follows from Fig. 4 that for strengthening of Ti by α - ω transformation Hugoniot should intersect not only the α→ω line for martensite transformation (M_s). In addition large quantities of ω-phase are expected at pressures considerably exceeding M_s pressures.

The α - ω transformation at dynamic compression causes strengthening of Ti.[6,14] ω-phase retention gives additional possibilities to regulate structure and properties of titanium and its alloys by shock loading.

CONCLUSIONS

The present work shows that phase composition, structure and properties of Ti after shock wave loading may be satisfactorily explained by α - ω transformation with the athermal martensite mechanism, which is expected to be the main mechanism of phase transformations in solids at shock compression.

Since in static pressure conditions thermally activated (diffusion) transformations may occur, transition pressures at dynamic and static loading may differ considerably. This must be taken into account in studying phase transformations at dynamic compression.

ACKNOWLEDGMENTS

The authors would like to thank Professor L. M. Utevskii for his interest and encouragement and Dr. M. P. Usikov for the help in electron microscopic study.

REFERENCES

1. Altshuler, L. V., The usage of shock waves in high pressure physics. - "Uspehi Fizicheskih Nauk", 1965, 85, pp 233-246.

2. Bundy, F. P., G. E. Research Lab., Rept. N 63-R1-3481C, 1963.

3. Zilberstein, V. A., Nosova, G. I. and Estrin, E. I. α-ω transformation in Ti and Zr. - "Fizika Metallov i Metallovedenie", 1973, 35, pp. 584-589.

4. McQueen, R. G. The equation of state of solids from shock wave studies. - In: High Velocity Impact Phenomena, N.Y., 1970, pp. 341-343, 536.

5. Pashkov, P. O. and Polyakova, U. U. About surface phenomena at high velocity impact of metals. - "Diklady AN SSSR", 1972, pp. 332-337.

6. Koul, M. K. and Breedis, J. F., Strengthening of titanium alloys by shock deformation. In: The Science, Technology and Application of Titanium. Oxford, 1970, pp. 817-828.

7. Kutsar, A. R., German, V. N. and Nosova, G. I., α-ω transformation in titanium and zirconium in shock waves. "Doklady AN SSR", 1973, 213, pp. 81-84.

8. Dulin, J. N. et al. Phase transformation of boron nitride at dynamic compression. "Fizika Tverdogo Tela", 1960, 11, pp. 1252-1257.

9. Usikov, M. P. and Zilberstein, V. A., The orientation relationship between the α and ω-phases of titanium and zirconium. "Phys. Stst. Solid.", 1973, 19, pp. 53-58.

10. Kurdumov, G. V., Phenomena of quenching and tempering in steel. Moscow, "Metallurgia", 1960, pp. 20-45.

11. Estrin, E. I., Kinetics of phase transformations under pressure and synthesis of high pressure phases. In: Problemy metallovedeniya i fiziki metallov. Moscow, "Metallurgia", 1973, N12, pp. 6-13.

12. Kutsar, A. R., T-P diagram of hafnium and phase transitions in shock waves. "Fizika Metallov i Metallovedenie", 1975, 40, pp. 787-793.

13. Urtiew, P. A. and Grover, R., Temperature deposition caused by shock interactions with material interfaces. "J. Appl. Phys.", 1974, 45, pp. 140-145.

14. Deribas, A. A., Physics of strengthening and welding by explosion. Novosibirsk, "Nauka", 1972, pp. 106-110.

EMBRITTLEMENT AND "SPONTANEOUS" CRACKING OF A HARDENED ($\alpha+\beta$) TITANIUM ALLOY DURING AGING

I. V. Gorynin, A. M. Parshin, S. S. Ushkov and
I. I. Yarmolovich

Central Research Institute of Shipbuilding Technology

U.S.S.R.

In aging of small half-finished products of the titanium alloy (Ti-6Al-2.5Mo-2Fe-1Cr-1Mn) hardened in the upper limit of ($\alpha+\beta$) region, we have discovered a hitherto unknown phenomenon of "spontaneous" cracking of titanium alloys under no external load. The fracture occurs in the form of fine cracks, single or numerous, directed from the periphery to the center of the blank (Fig. 1).

General Characteristics of "Spontaneous" Cracking

Based on the results of visual examination of the blanks after aging, a region has been plotted for heat treatments producing the fracture or absolutely brittle condition of the blanks. The region is outlined by a C-shaped curve (Fig. 2). The intensity of cracking depends on a number of processing parameters, the most important of which is a hardening temperature. After water hardening at a temperature of 800° or below, fracture of the blanks has not been observed during subsequent aging times up to 5000 hrs. Hardening in the upper limit of ($\alpha+\beta$) region leads to cracking within the aging temperature range of 250-500°. Hardening in β-region at a temperature of 950° accelerates cracking: the region of cracking shifts to shorter durations and widens in the direction of low and high aging temperatures (Fig. 2b). The rate of heating the blanks before hardening has no effect on the cracking of this kind, while a higher rate of cooling does. Section size effect is of considerable importance. With the surface conditions being equal, the smaller size of the blank results in the longer time to crack initiation. on 65mm diameter blanks at temperatures 350-400° cracks have been observed in 60 hours, on 18mm diameter rods in 200 hours and

Fig. 1: Appearance of cracks arising on stampings aging

a) 870° c 1h, water

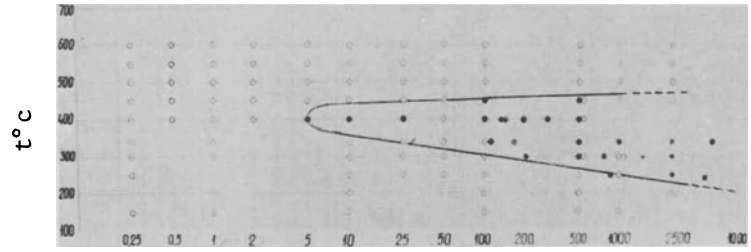

b) 950° c, 1h, water

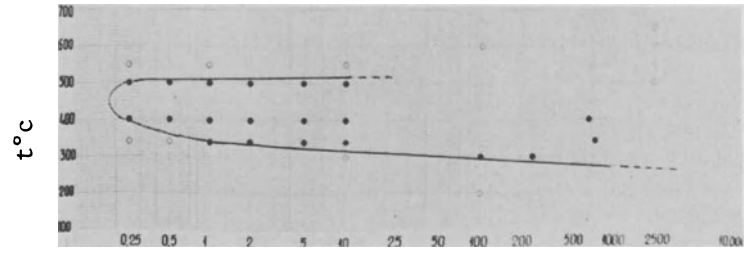

t,h

Fig. 2: Temperature-time region of macrocrack initiation in the titanium alloy during aging
a) after water hardening at 870° for 1 hour
b) after water hardening at 950° for 1 hour
o - no cracks
● - cracks present

on plates 6mm thick in 230-300 hours. The cracks have rarely been observed on cross-sections. The machined specimens tend to crack much later than the unmachined ones. The presence of a brittle gas-saturated layer on the surface reduces the time to cracking. It should be noted that the blanks with a large length to cross-section ratio undergo considerable distortion. The crack initiation in aging is preceded by a sharp decrease in the strain capacity of the material. Yet at the early stages of low temperature aging the alloy hardened in the upper limit of $(\alpha+\beta)$-region exhibits an increase in its strength and a decrease in its ductility. Aging for 25-30 hours results in zero ductility long before cracking of the specimens in tensile tests. The fracture of the specimens occurs at the elastic tensile strain before the yield strength and ultimate strength are achieved. At temperatures of 400-600° the alloy becomes completely embrittled after aging from 15 minutes to 1 hour. Increasing the duration of aging shifts the region of brittle fracture in the direction of low temperatures and at the same time an increase in ductility has been observed after aging at high temperatures.

Embrittlement of the material which precedes cracking has been observed in the tests both at room and elevated temperatures (Table I).

The probability of cracking of the blanks during aging has been verified on other titanium alloys: the dilute $(\alpha+\beta)$ alloy Ti-5.5Al-2Mo-2Cr-1Fe-0.2S; the alloy of critical composition Ti-2.5Al-7.5Mo-1Cr-1Fe and the β-alloy Ti-3Al-8Mo-11Cr. The tests have shown that the dilute $(\alpha+\beta)$ alloy and the β-alloy are not susceptible to cracking. "Spontaneous" cracking during aging is characteristic of $(\alpha+\beta)$ high alloys.

The Reasons of Embrittlement and Cracking

Undoubtedly, the embrittlement and subsequent cracking are a common process occurring in the hardened $(\alpha+\beta)$ high alloys during aging.

The results of X-ray diffraction analysis indicate that the alloy hardened at 870° is composed of 66% of β-phase with the lattice parameter 3.251A°, the rest being α-phase. When the hardened material is heated, decomposition of the metastable β-solid solution takes place and a β-phase rich in alloying elements is produced. The decomposition rate increases with increased aging temperature and results in a decrease of the lattice parameter of β-solid solution. The early stages of decomposition tend to exhibit asymmetrical traces of β-phase which are the result of the formation of microvolumes depleted or rich in alloying elements. Like in other precipitation-hardening materials,[1] decomposition, in our opinion, proceeds by way of a long continuous diffusion process

Table I

Effect of aging duration at 400° on the mechanical properties of the alloy hardened at 870°

Heat treatment	Test temperature 400°				Test temperature 20°			
	σ_B kg/mm	$\sigma_{0,2}$ kg/mm	δ %	ψ %	σ_B kg/mm	$\sigma_{0,2}$ kg/mm	δ %	ψ %
Water hardening	-	-	-	-	103.1	97.3	16.9	38.7
Aging for 30 min	125.8	115.3	7.0	20.0	128.0	120.0	brittle fracture	
Aging for 1 hour	128.0	121.0	5.6	12.0	143.0	brittle fracture		
Aging for 2 hours	134.0	123.5	5.6	12.8	150.0	brittle fracture		
Aging for 5 hours	135.0	130.0	brittle fracture		brittle fracture			

which involves the formation of concentration fluctuations, segregations, origination of nuclei in the dilute microvolumes with subsequent intermediate coherent and non-coherent states and the equilibrium α-phase having an interface with β-matrix. The decomposition involves dilatometric effects, like in other precipitation-hardening materials, such as aluminum alloys[2,3], Fe-Ni alloys[4] and other titanium alloys.[5] For blanks hardened at 870°C, subsequent aging in the temperature range of 270-400° results in a change from thermal expansion to contraction. Increasing the temperature above 400° leads to intensive expansion. The machined specimens do not show similar effects.

A change of linear dimensions of the specimens also takes place during isothermic soaking. The reduction of the specimen length begins at a temperature of 150-170°. The value of the reduction increases as isothermic soaking temperature is increased. A maximum length reduction occurs at a temperature of 400°. At higher temperatures contraction decreases and above 500° only expansion takes place. The relationship between the value of contraction and the exposure duration has an attenuating effect. However, at a temperature of 400° contraction is accomplished in a 15 minute exposure,whereas at low temperatures its completion takes tens of hours.

The contraction of the specimens results in a phenomenon known as the "negative creep."

A value of contraction depends mainly on the phase composition of the hardened material. The martensite α'-phase hardened alloys have no dilatometric effect during continuous heating and appears only during isothermic exposure. Considerable volumetric effects are characteristic of β-phase hardened alloys and the higher its volumetric content and the less their alloyage, the greater a degree of contraction. The reason for the contraction of the specimens might be due to a decrease of the lattice parameter of β-solid solution. Such is attributed to a redistribution of the alloying elements between individual microvolumes at the early stages of decomposition, and the ratio of specific volumes of the matrix and the precipitating phase.[4,6] The macroscopic contraction is the result of the two simultaneous processes: (1) a decrease of the lattice parameter due to the enrichment of the lattice with β-stabilizing elements which leads to the contraction of the specimen, and (2) the formation of α-phase which has a greater specific volume than β-phase which causes the expansion of the specimen. At a certain stage of aging, the formation of isolated particles of α-phase compensates for the contraction. This is due to the decrease of the lattice parameter of β-solid solution and at temperatures above 500° results in the expansion of the specimens.

Thus, the decrease of volume is caused by the structural changes in β-solid solution which occur at these stages of decomposition.

However, the presence of non-uniform volumetric changes in the blanks may give rise to internal stresses.

The value of the first order stresses in the hardened blanks measured by strain gauges is small and does not exceed 2kgf/mm. In the blanks aged at 400° this value is 11-16kgf/mm. Thus, during aging the value of the first order stresses increases but are not of sufficient magnitude to cause cracking. Probably the main role in cracking is played by the second order stresses. The structural stresses at the early stages of decomposition are due to multidirectional volumetric changes at the boundaries of the incipient α-phase - β-matrix and the initial α-phase surrounding the β-matrix, i.e. these stresses are the result of the heterogeniety in the phase composition of the alloy and non-uniformity of the microvolumetric changes.

A value of microstrain in the lattice was measured using the even moments method and the harmonic analysis of the X-ray trace 211 of β-phase after photographing the sections in the diffractometer "ΔPOH-15" in nickel filtrated characteristic radiation of copper. The measurements have indicated that in the low temperature range of aging the value of microstrains increases with increased temperature and time. An average value of unrelaxed microstresses along the boundaries of extension and contractions is σ_1 = 100 - 130kgf/mm, σ_2 = 40 - 65kgf/mm. Stress relaxation cannot be achieved by plastic displacements in the β-matrix which is embrittled by decomposition and high internal stresses concentrated in the narrow regions along the boundaries of α-phase - β-matrix. These stresses can be relieved by the emergence of microcracks.

Even though decomposition proceeds by way of successive changes in the lattice, crack formation in the aging β-alloy does not occur. The structural stresses arise at the early stages of decomposition and cause embrittlement of the material. Apparently, additional conditions are needed for crack initiation and propagation. One of these conditions is the heterogeneity of the initial structure in terms of the presence of α-phase areas in the β-matrix. Significant in this respect is an experiment on the cracking of blanks of (α+β) high alloys containing various amounts of aluminum (0-6%) and, consequently, various amounts and qualities of the initial α-phase. It has been found that a decreased amount of aluminum results in a longer time to crack initiation. In blanks of the alloys containing no aluminum cracking has not been observed at all. The role of α-phase particles in the general picture of cracking is attributed to the fact that they have a greater specific volume than the β-phase and a high modulus of elasticity. The presence of the particles make for additional distortion of the β-matrix which itself is subject to volumetric changes in decomposition. Another factor which affects the crack formation is the non-

uniformity of a post-hardening phase composition in the mid-section of large blanks both in terms of the α- and β-phase ratio and their alloyage, and through incomplete in-depth hardening. As a result, structural changes in large blanks proceed non-uniformity, both in velocity and magnitude, with respect to volumetric changes. For example, the specimens cut from the surface layer of the 950° hardened blank 65mm in diameter elongated to 0.07% in dilatometer tests, while the internal layers, including the axial region, undergo contraction. This results in the initiation of the first order regional stresses which facilitate individual microcracks to merge into one main crack and help in its propagation.

In light of the above, cracking is not expected to occur in β-alloys which have no structural heterogeneity in the form of initial α-phase particles whose decomposition rate is extremely slow or where the amount of metastable β-phase is small after hardening. Nevertheless, the second order structural stresses do arise and lead to embrittlement and low toughness even in those cases where the ductility is still high.

Cracking in aging is not a specific feature of (α+β) high alloys only. The processes investigated in the titanium alloys develop in a similar manner in other precipitation-hardening materials. The crack formation in aging has been observed in pipes made from a nickel alloy, in aging aluminum alloys,[7] in beryllium bronzes, and copper-gold alloys.[8]

Consequently, this phenomenon in (α+β) high titanium alloys is a particular case of the general phenomenon of cracking during aging of many precipitation-hardening materials due to structural stresses.

Conclusions

The embrittlement and further cracking of (α+β) high titanium alloys during aging are caused by structural stresses at the early stages of decomposition due to the heterogeneity of the phase alloy and non-uniform microvolumetric changes. The likelihood of "spontaneous" cracking may be reduced by changing alloyage, decreasing the aluminum content in the alloy or decreasing a phase composition after hardening, and aging at a temperature of 500° or above.

References

1. Kelly, A. and Nicholson, R., "Precipitation hardening." Uspehi phiziki metallov, vol 10 "Metallurgy," 1966.

2. Guinler, A., "Non-uniform metallic solid solutions." Foreign literature publishing house, Moscow, 1962.

3. Jagodic, P., "Studie des Zerfallprozesses der Ferten Losung in einer Niedriglegierten Aluminum-Zink-Legie-rung." Aluminum, 1971, N5, s.319.

4. Gitgarts, M. I., Ivashin, V. V. and Tolstoy, A. V., "The volume change in nimonik aging." Fizika metallov i metallovedeniye, 1972, v.33, issue 4, p.820.

5. Lashko, N. F., Khatsinskaya, I. M. and Ermolova, M. I., "The volume change at the decomposition of metastalbe phases of titanium alloys." Fizika metallov i metallovedeniye, 1972, vol.33, issue 2, p. 275.

6. Hickman, B. S., "Precipitation of the omega phase in titanium-vanadium alloys." J. Inst. Metals, 1968, vol 96, No. 11, p. 330.

7. Elistratov, A. M., "The X-ray investigation of initial stages of δ-decomposition of Ag-Al system." Akademiya Nauk SSSR, 1955, 101, 3, p. 437.

8. Syutkin, P. N., Syutkina, V. I. and Yakovleva, A. S., "The spontaneous cracking of ordered Cu-Au alloy." Fizika metallov i metallovedeniye, 1969, 27, 5, p. 904.

TRANSFORMATION IN UNSTABLE BETA-TITANIUM ALLOYS

M. A. Nikhanorov and V. V. Latsh

Scientific and Technical Society of Engineering Industry

U.S.S.R.

Numerous investigations are devoted to phase transformations occurring in aging of unstable beta-phase titanium alloys.[1-7] In this work results of the influence of step aging conditions on the decomposition of the beta-phase in thermally unstable beta-titanium alloys are presented.

The titanium alloy TC6 with two oxygen levels and the low oxygen alloy BT15 are examined. The compositions of these alloys are given in Table I.

After forging all the stocks were turned and annealed in vacuum at 750 for 4 hours. The effect of heat treatment was estimated based on the results of hardness, microhardness, and tensile tests. Microstructures were examined by means of optical and electron microscopy. Some specimens were analyzed by x-ray diffraction.

X-ray analysis was performed in a chamber RCU-114 and on a diffractometer URS-501, using filtered Cu-radiation. The position of the samples being examined by x-ray diffractometry in the chamber RCU-114 was varied by an average angle of rotation at about ± 5°. Diffraction patterns were taken on rotating specimens. Before x-ray investigation a layer 0.4-0.5mm thick was removed from the sample surface by electroetching to a mirror finish.

The phase composition of the alloy TC6 in different aged conditions was examined by transmission electron and electron diffractometry.

Table I

Alloy Compositions

Alloy grade	Content, % Al	Mo	V	Cr	Fe	Si	C	N_2	O_2
TC6	4.05	6.97	10.25	3.2	0.10	0.07	0.02	0.017	0.065
TC6	3.4	6.84	10.16	3.02	traces	0.03	0.05	0.006	0.15
BT15	7.65	-	10.76	3.24	0.08	0.03	0.02	0.007	0.045

Note: alloys are melted into 100 kg ingots.

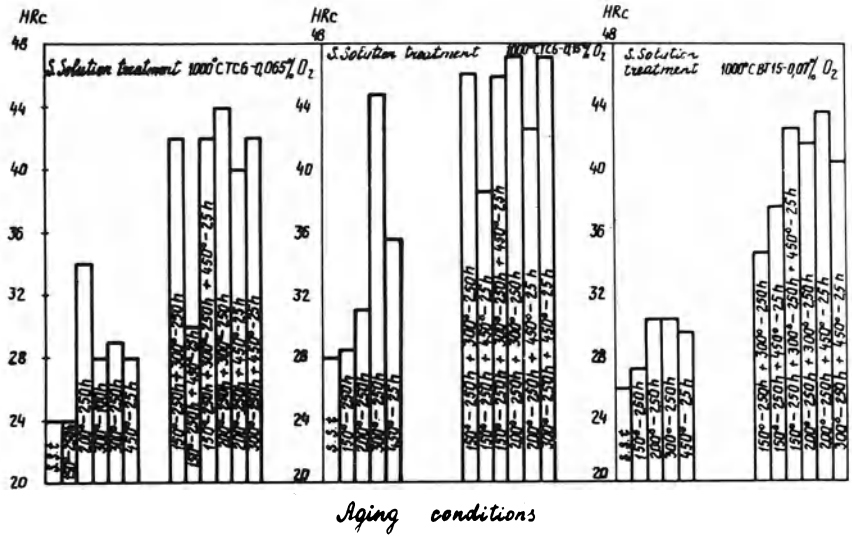

Fig. 1: The effect of step aging conditions on the hardness of the alloys TC6 and BT15, solution treated at 1000° before aging.

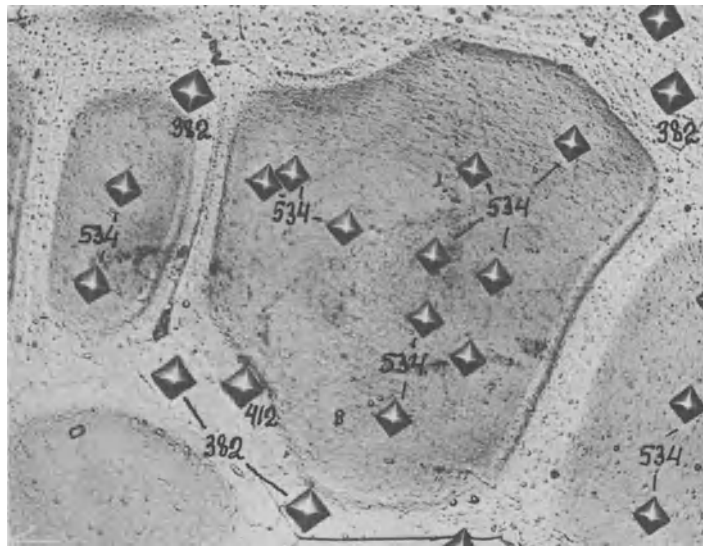

Fig. 2: A microstructure of the alloy TC6 (0.065 O_2) after a solution treatment at 1000° and aging at 200°C-250 h x400

Table II

Phase Compositions of Alloys TC6 and BT15 After Step Aging (X-ray Method)

Heat treatment conditions					Phase composition
Solid. solut. t,°C	Aging t,°C	Aging time, h	Aging t, °C	Aging time, h	
			Alloy TC6		
900	200	200			$\beta_i+\beta_{enr}+\omega$
900	200	250	300	250	$\beta_{i(vdl)}+\alpha_{(dl)}$
950	200	250			β_i
950	200	250	300	250	$\beta_{i(vdl)}+\alpha_{(dl)}$
950	200	250	450	25	β_i
950	300	250	450	25	$\beta_{i(vdl)}+\alpha_{(dl)}$
1000					β_i
1000	150	250			β_i
1000	200	250			$\beta_i+\beta_{(enr)}+\omega$
1000	150	250	300	250	$\beta_{i(dl)}$
1000	200	250	300	250	$\beta_{i(vdl)}+\alpha_{(dl)}$
1000	200	150	450	25	$\beta_{i(vdl)}+\alpha_{(dl)}$
1000	300	250			$\beta_{i(vdl)}+\alpha_{(dl)}$
			Alloy BT15		
900					β_i
900	300	250			β_i
900	200	250	300	250	β_i
1000	300	250	-	-	β_i
1000	200	250	300	250	$\beta_{i(vdl)}+\alpha_{(vdl)}$

Symbols: β_i - initial beta-phase, β_{enr} - enriched beta-phase, dl - diffuse lines, vdl - very diffuse lines.

Influence of Step Aging Conditions on Beta-Phase Decomposition in TC6 and BT15 Alloys

As previously indicated,[6] the formation of the omega-phase during the aging of the solid solution treated alloy TC6, containing 0.065% O_2, results in a considerable hardness increase. The process of the omega-phase formation slows down as the oxygen content increases. X-ray diffraction indicates that there is no omega precipitation after aging at 300°C and that the beta-phase transformation is followed by the dispersed alpha-phase precipitation.

A series of experiments was conducted to investigate more intensively the processes observed at low aging temperatures.

Step aging conditions of the alloy TC6 with two oxygen levels (0.065 and 0.15%) and the 0.075% oxygen alloy BT15 are given below.

After solid solution treatment from 800, 900, 950, 1000°C:

a) aging at 150, 200, 300, 450°C,
b) double aging at 150+300, 150+450, 200+300, 200+450, 300+450°C,
c) three-step aging at 150+300+450°C.

Aging time at 150, 200, 300°C is about 250 hours and at 450°C-25 hours.

After solution treatment at 800°C the first step aging time was varied in the range of 250-1000 hours.

The first and the second step aging times were chosen based on preliminary investigations. Figure 1 shows hardness changes in the TC6 and BT15 alloys solution treated at the temperature 1000°C and aged under the above mentioned conditions.

The preliminary low temperature aging at the temperatures 150 and 200°C followed by the additional aging at the temperature 300 or 300+450°C results in a great hardness increase in the low oxygen alloys TC6 and BT15. The hardness value of the 0.065 oxygen alloy TC6 specimens step-aged at 150-200°C, 250 h+300°C, 250h, reached 40-43 HRC while after aging at 300°C for 250 and 500 hours it was 28 and 32 HRC, respectively. At these low temperature aging conditions the hardness of the alloy TC6 increased more intensively than that of the alloy BT15.

The effect of the low temperature aging is reduced directly as the oxygen content in the alloy increases.

A metallographic analysis makes it possible to observe structural transformations in the alloys as a result of low temperature

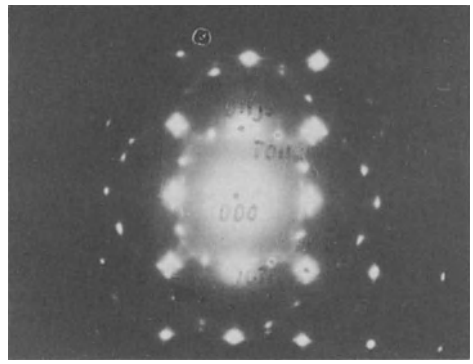

Fig. 3: A diffraction pattern of the alloy TC6, solution treated at 1000°C and aged at 200°C - 250h + 300°C - 250h. x 75000

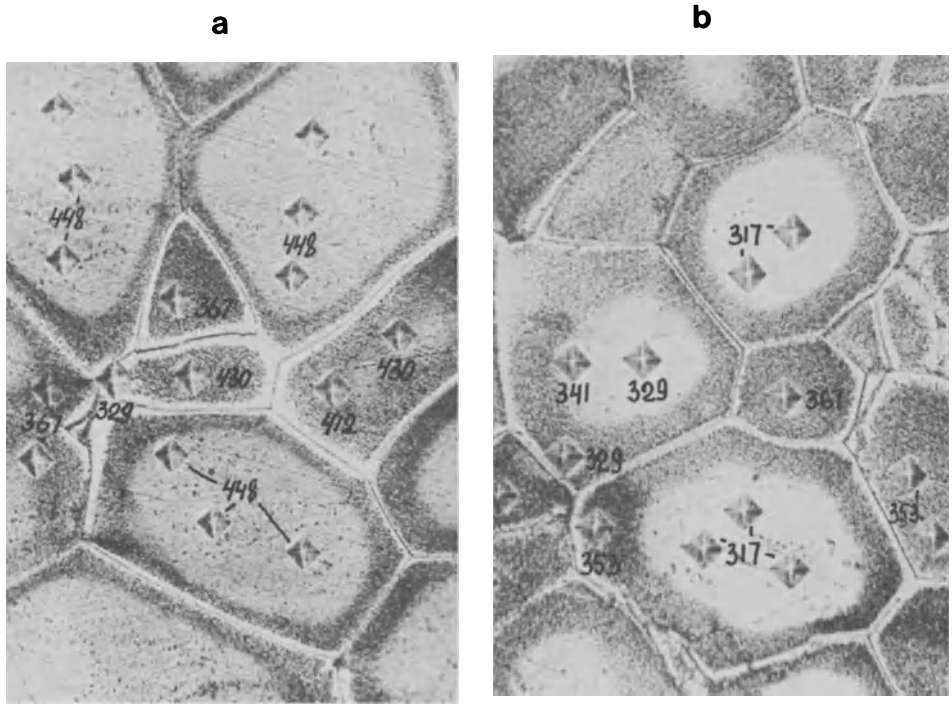

Fig. 4: A microstructure of the alloy TC6 (0.065 O_2) solution treated at 800°C and aged at 200°C - 1000h + 300°C - 100h +450°C - 25h a) and reversed under above conditions plus 570°C for 5 min (b). x 400

aging. Just after aging at 150 and 200°C, regardless of the solid solution treatment temperature (800-1000°C), the structure of the alloy investigated consists of uniform beta-phase grains. A further aging at 300°C after a preliminary aging at temperatures of 150-200°C considerably changes the structure of the low oxygen alloys TC6 and BT15. In this case new areas with sharply outlined boundaries were observed inside beta-grains. (Fig. 2).

The electron microscopy of alloys indicated besides the beta-phase the presence of a large amount of a new phase, dispersed precipitations, which were alpha-solution particles according to x-ray diffraction analysis. The diffuseness of the lines from these phases means a highly stressed alloy (Table II).

The data obtained by means of transmission electron microscopy allowed the control of the size, shape, distribution, and the type of phases precipitated either just after aging at the temperature 300°C or after step aging at 200°C (250 h) + 300°C (250 h). After both aging conditions, besides the matrix beta-phase, there was observed alpha-phase precipitations in the structure where the size and shape differed considerably from one another depending on heat treatment conditions. After ordinary aging at the temperature 300°C for 250 hours some platelets reach the size of 1000 Å. The alpha-phase particles formed after a step aging are considerably more dispersed. The dimensions of these particles are in the range 200-300 Å and similar to those of the omega-phase particles formed after exposure at 200°C. In Figure 3 an electron diffraction pattern after the step aging is given.

The microstructure produced after a prolonged step exposure (150-200°C)+300°C is also retained after a long tempering to 450°C in the case of the alloys aged at (150-200°)+300°C+450°C. As a result of the latter treatment some badly etched areas are also observed in the grain but its periphery qualitively changes and effectively etches. Studying the near boundary areas of the grain at a high magnification showed that they have a two-phase structure. The microhardness of these near boundary areas is 360-370 H_{50} and that of the areas inside the grains as a result of aging under following conditions 200+300°C and 200+300+450°C is 530-450 H_{50}, respectively. (Fig. 4a).

To define the formed structure some step aged specimens were thermally recovered.

In this work the recovery treatment was performed at the temperature 570°C for 5 min depending on a specimen size and subsequent water cooling.

The investigations of the microstructure, hardness and micro-

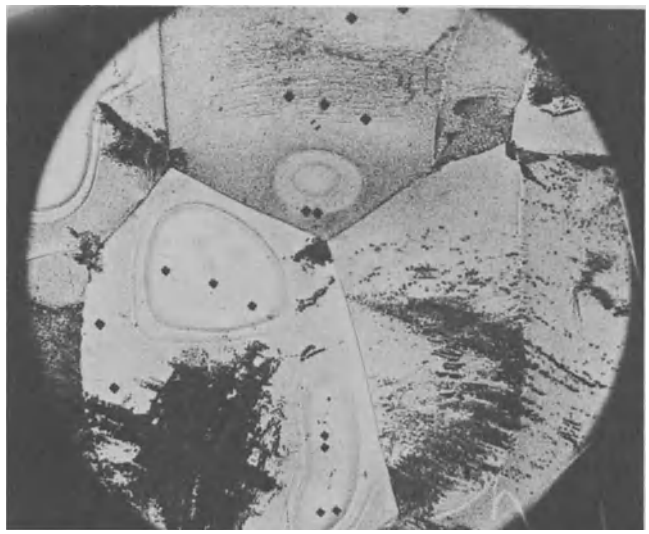

Fig. 5: A microstructure of the alloy TC6, aged at 200°C - 250h + 300°C - 250h after tensile test. x 100

hardness after "recovery" showed that the specimens step aged at 200+300°C, after being solution treated at the temperature 800-1000°C, were practically fully reversed. The areas with sharply defined boundaries observed in primary beta-grains, before the recovery treatment, completely disappeared and in addition, the hardness reduced to the value typical for the beta-phase. X-ray diffraction analysis showed only the presence of the beta-phase in the structure. The structure of the specimens heat treated under the following conditions (200+300+450) was partially transformed and showed microhardness changes in weakly etched areas inside primary beta-grains. If the hardness in these areas after step aging was 460 H_{50}, "the recovery" treatment reduced it to the value of that of the initial beta-phase (307 H_{50}). The "recovery" did not influence the periphery of the grain and its hardness remained unchanged (350 H_{50}) (Fig. 4b).

The research of the step aging influence on the structure behavior and its hardness displayed the possibility of a new phase formation during the subsequent higher temperature aging stage (300°C) only after a sufficient exposure time during the first stage aging at the temperature 150-200°C, allowed the necessary stability of the omega-phase. This is justified by the preliminary investigation results obtained while defining the aging period at the first low temperature stage. They showed that the first stage exposure

time for about 100 hours did not result in structural and hardness alterations after the secondary aging.

Comparing all the obtained data concerning hardness, microhardness, structure behavior investigated by optical and electron microscopy, and also by x-ray diffraction analysis before and after recovery treatment showed a new phase being an alpha-phase coherent with beta-solid solution.

In the above step-aging conditions the omega-phase is not redissolved in the beta-phase during the second stage aging owing to the enhanced stability reached at the first aging. It is further transformed thermodynamically into a more stable alpha-phase at this temperature. The omega-phase transforms in-situ into alpha-coherent phase without diffusion. This is proved by the similarity of the omega-phase particle sizes (150-250 Å) formed after an exposure to the temperature 200°C and those of the alpha-coherent phase particles (200-300 Å) after aging at 300°C.

The omega-phase substitutional transformation into alpha-coherent phase is confirmed based on the reversed transformation of the alpha-coherent phase into beta-solid solution, depending on the external tensile stresses and the "recovery treatment."

The new alpha-coherent phase can be retained in the equilibrium-phase temperature range for a long time. During our experiments the presence of the alpha-coherent phase is defined after a long exposure at 200 300 450. After this treatment two forms of the alpha-phase can coexist in one grain simultaneously: near the grain boundary - a stable (equilibrium) alpha-phase, and in the grain interior - an unstable phase formed directly due to the omega-phase. This is proved by metallographic analysis and hardness data defined during "the recovery."

After "the recovery treatment" the alpha-coherent phase is not rearranged into the stable alpha-phase but reversed into the beta-phase indicating a different mechanism of formation of these phases.

Based on this existing conception the equilibrium alpha-phase is formed due to its nucleation and growth in the beta-matrix. The formation of the isolated alpha-phase is induced by lattice defects - firstly, by dislocations caused by a proceeding plastic deformation, and also by interstitial elements (oxygen, nitrogen) leading to a beta-phase lattice distortion.

The alpha-coherent phase is formed in a high alloy titanium with an unstable beta-phase during step aging only as a result of a rearrangement of a stabilized omega-phase at the second step. The omega-phase is stabilized due to a long isothermal tempering of

these alloys during the first step-aging which result in stress relaxation in the omega-phase lattice. At the second higher temperature step-aging (300°C for this type of alloy), which corresponds to the nucleation of the alpha-phase, the omega-phase is not redissolved into the beta-matrix due to its elevated stability, and further rearrangments by slip into this structure, parameters of which are similar to those of the alpha-phase.

The lattice defects (dislocations) induced into an alloy by prior deformation or by substitutional elements present in a structure favor an equilibrium alpha-phase formation, and make an omega-phase and alpha-coherent phase formation difficult.

The alpha-coherent phase formed during the step aging due to the influence of external tensile stresses at room temperature can be reversed into the beta-phase (Fig. 5). The reversing is observed by means of metallographic and x-ray analysis and by monitoring hardness values.

Conclusions

A new intermediate alpha-coherent phase is discovered and a mechanism and conditions for its formation during a heat treatment of high strength alloys are studied. It is found that the alpha-coherent phase can be reversed into the beta-phase under the influence of external tensile stresses at the room temperature.

References

1. Bagarjatskiy, Yu. A., Tagunova, T. V. and Nosova, G. I., Problemy metallovedenija i fiziki metallov. Moskow, Metallurgizdat, 1958, s. 210.

2. Harman, E. L. and Troiano, A. R., Trans. ASME, 1961, 43, 43.

3. Ageev, N. V. and Petrova, L. A., Titan i ego splavy, N.7, Moskow, Izd vo Akad. Nauk USSR, 1962, s. 131.

4. Novikov, I. I., Pol'kin, I. S. and Kasparova, O. V., Izd vo Akad. Nauk USSR, Metally, 1966, N. 2, s. 131.

5. Hickman, B. S., J. of Materials Science, 1969, v. 4, s. 554.

6. Nikhanorov, M. A. and Latsh, V. V., Fizika metallov i metallovedenie, 1971, v. 31, s. 342.

7. Nikhanorov, M. A., Fizika metallov i metalloved, 1971, v. 32, s. 1057.

INTERNAL FRICTION STUDIES IN STABLE AND METASTABLE BETA TITANIUM ALLOYS

S. Mishra and M. K. Asundi - Metallurgy Division

Bhabha Atomic Research Centre

Trombay, Bombay-400 085 India

INTRODUCTION

The structures obtained on rapid cooling to room temperature from the phase of the titanium base alloys containing Mo, V and/or Nb are either martensitic (α') or $\beta + \omega$ (athermal) or β, depending upon the concentration of the alloying elements. The temperature, T_ω, at which the athermal ω transformation is initiated, decreases with increasing concentration of solute additions[1,2] (oxygen included)[3]. The athermal ω is observed to be reversible in Ti-Mo and Ti-V alloys.[2] Whereas the thermal ω occurs in a broader composition range and changes its lattice parameter with time at aging temperatures.

Internal friction techniques have been used in studying the defect structures in these metastable phases and their possible formation modes. The interpretations of the internal friction peaks (P_1, the low temperature peak for example) have been at variance[1,4,5,6,7] and the present investigation attempts to explain the cause for the peak. It also reports many new relaxation maximas observed in Ti-Mo, Ti-V and also in the commercial variety βIII alloy.

Experimental Procedure

The internal friction experiments are carried out in (a) Kê type normal torsional pendulum (maximum 2Hz) and (b) Koiwa type inverted torsional pendulum operating in the frequency range 0.5 to 16Hz.[9] The Kê type was utilized for the elevated temperature studies while the inverted pendulum operated in the low temperature range. Higher than 2Hz oscillations could be recorded automatically. The alloys studies are, (a) titanium-17±2%Mo and (b) Ti-43%Mo; (c) Ti-56%V and (d) the commercial βIII alloy having 11.5%Mo, 6%Zr, 4.5%Sn and 0.13% oxygen. The binary alloys are prepared from crystal bar titanium and high purity Mo and V metals. The alloys are melted in an electron beam furnace in the form of 'fingers' which were subsequently cold rolled and drawn into 1mm. dia. wires. Interstitial additions to the alloys are made by soaking the wires in the high temperature beta range for sufficient time to allow the diffusion of the interstitial elements. The sample length used is 150mm. The creep effects in these samples have been ignored as they have been found to be negligible.

RESULTS AND DISCUSSION

In all, six peaks have been observed. They are P_1,P_2,P_3,P_4, P_5 and P*. The first five peaks occur at increasing temperatures. The lowest being peak P_1 at about -180°C (0.8Hz) and the highest peak P_5 at about 410°C (1.0Hz).

Peak P_1

Peak P_1 is observed clearly in Ti-17Mo, βIII alloy, Ref.Fig.1 and Figs.2(a) and 2(b). The origin of this peak was first ascribed by Nelson et al.[7] as due to stress induced, thermally activated exchange of unit cell of athermal ω with β phase at the diffuse interface of the two phases. However, Doherty and Gibbons[1] contended that it was due to a relaxation process entirely in the beta phase and associated with a reorientation of a complex of atoms entrapped by extrinsic vacancies. Sommer et al.[6] based on the work of De Fontaine et al.[2], suggested that the atom reshuffling during the formation of the athermal ω phase (reversible) in unstable β matrix as the cause for the peak. This model was further supported by Vigier et al.[4] based on their work on βIII alloys. The present investigations shows the the peak P_1 is due to an interaction of dislocations (in the annealed condition) with vacancies and oxygen atoms in the metastable β phase. Since oxygen and vacancies are intimately associated, the observed effects are due to a combination of these two. The reasons for the above conclusion are: (a) the peak height increases with oxygen concentration and the peak temperature is not affected by oxygen. This rules out β+ω (athermal) transformation since T_ω is affected by oxygen[3];

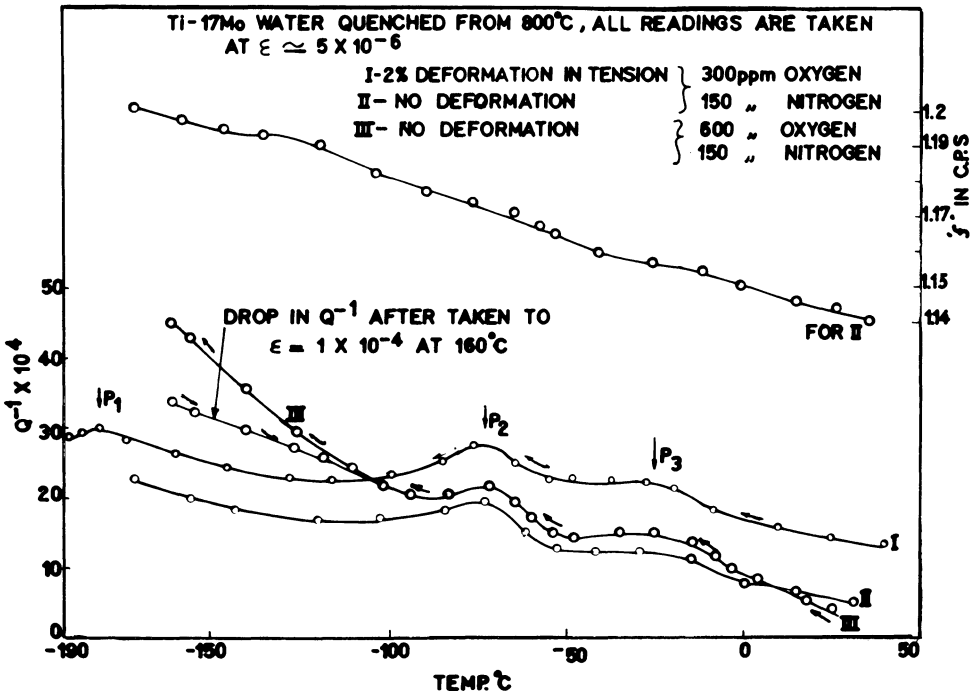

Fig. 1 - Effect of oxygen content and low temperature deformation on the Q^{-1} vs temperature plot. Frequency changes shown.

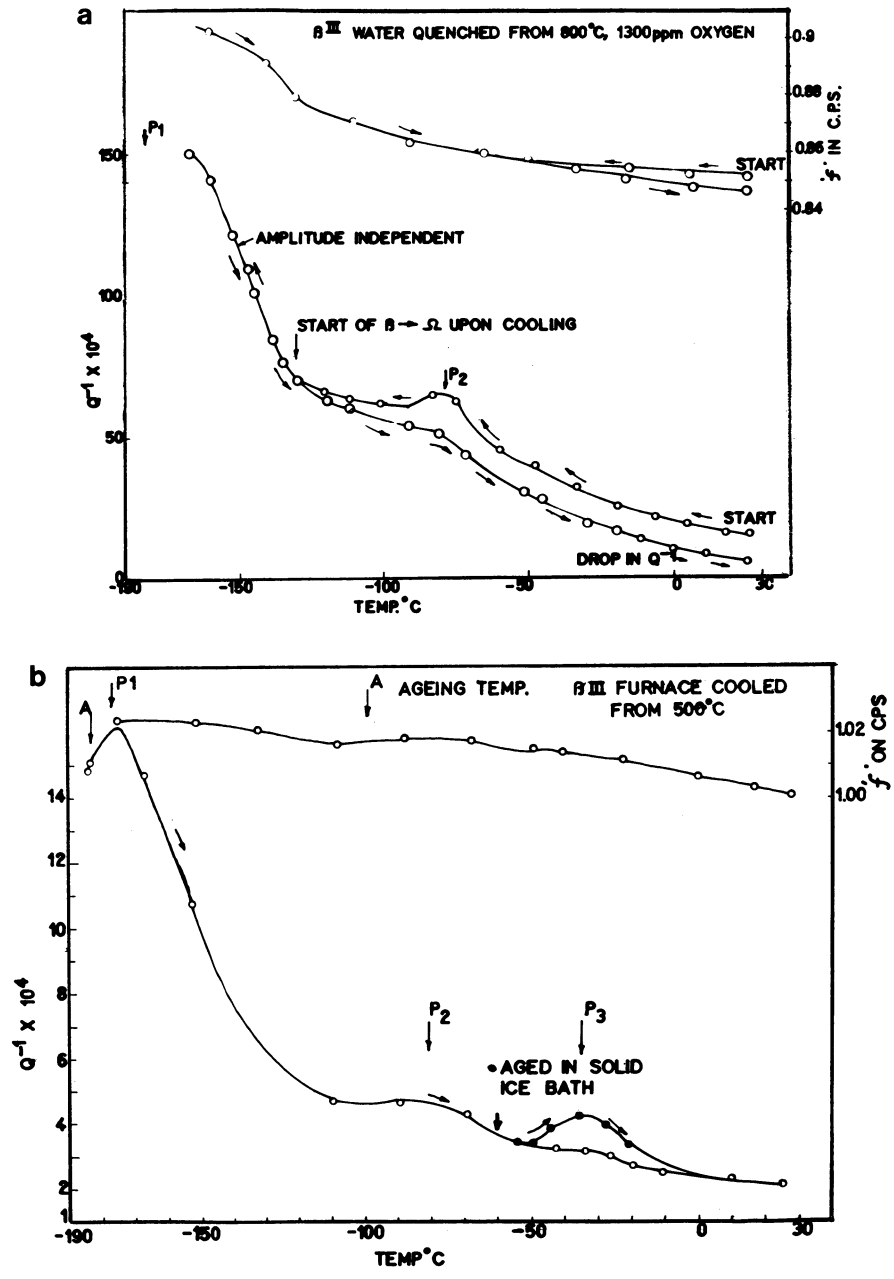

Fig. 2 - (a) Q^{-1} vs. temperature plot. Frequency changes indicated. (b) Q^{-1} vs. temperature plot, effect of dry ice bath soaking on peak P_3, Frequency changes indicated.

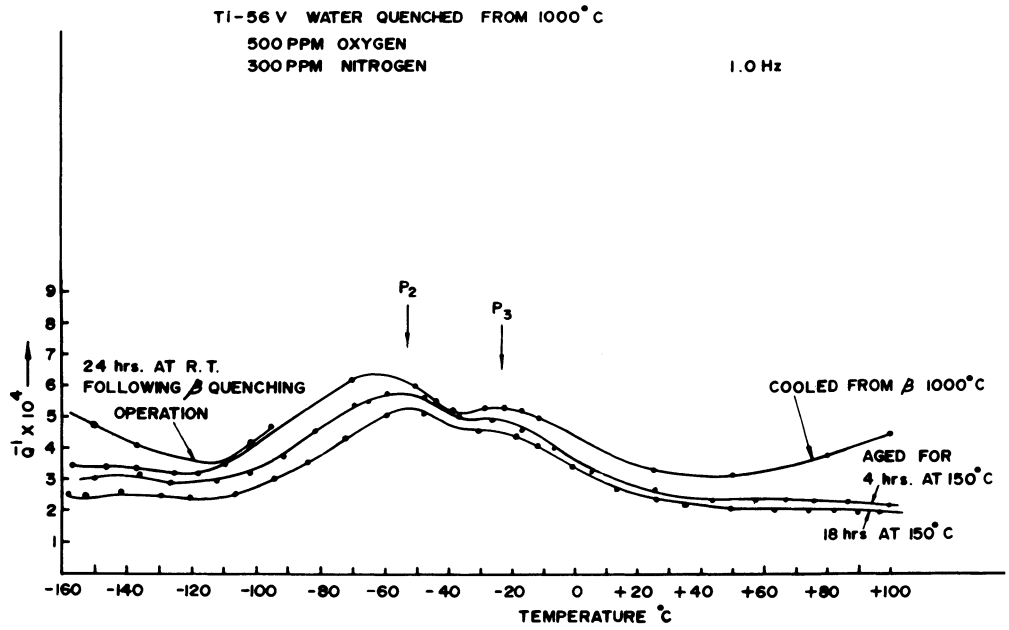

Fig. 3 - Q^{-1} vs. temperature plot. Effect of aging at R-T as well as at 150°C.

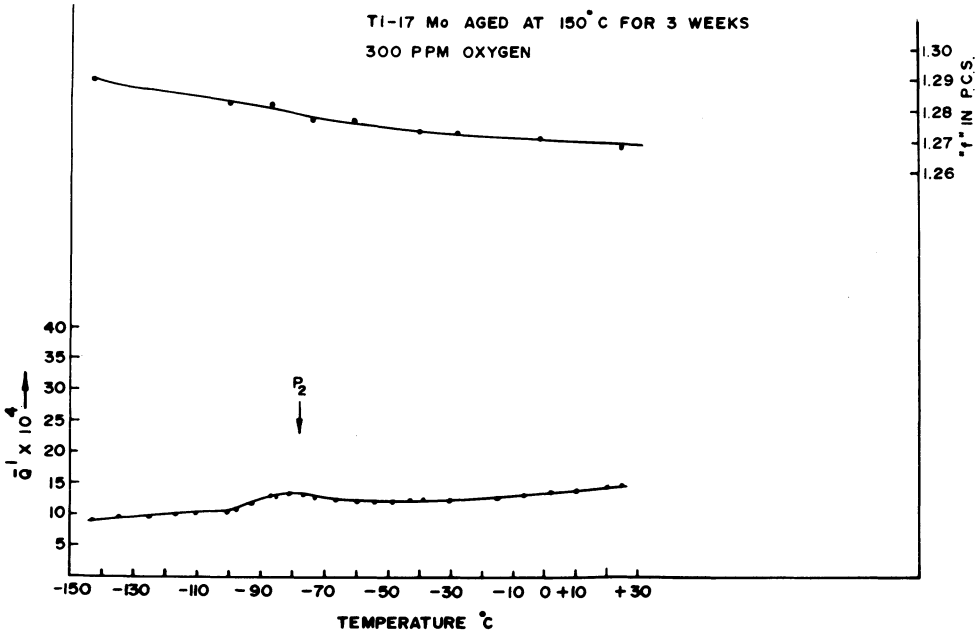

Fig. 4 - Q^{-1} vs. temperature plot. Frequency changes are indicated.

TABLE I

SUMMARY OF THE RESULTS

Sr. No.	Alloy Systems	Relaxation peak	Peak Temperature in °C	Frequency of observations in Hz.	ΔH Activation energy in Kcals/gm. mol.	τ_o in sec.
1	Ti-17Mo β^{III} alloy Ti-43 Mo; Ti-56V	P_1 -	-93 -180	120 (KHZ) 0.8	5 "	2.2×10^{-14} (1) $1 \times 10^{-9 \pm 2}$ (4)
2	β^{III} alloys Ti-17Mo Ti-43Mo Ti-56V	P_2	-90 to -70 (depending upon the alloy concentrations)	1.0	13 ± 2	1×10^{-14}
3	Same as above.	P_3	-55 to -45	1.0	15 ± 2	"
4	Ti-17 Mo β^{III} Ti-43Mo Ti-56V	P_4 P_4	+230(for oxygen) 260(for carbon) 310(" oxygen) 360(" nitrogen)	1.0 "	38 ± 3 C-35± 3 O-43± 3 N-43± 3	10^{-15} 5×10^{-16}
5	Ti-17Mo β^{III} alloy Ti-43Mo	P_5	410	1.0	43	-
6	Ti-17Mo	P*	300 to 360°C	1.0	40 ± 5	-

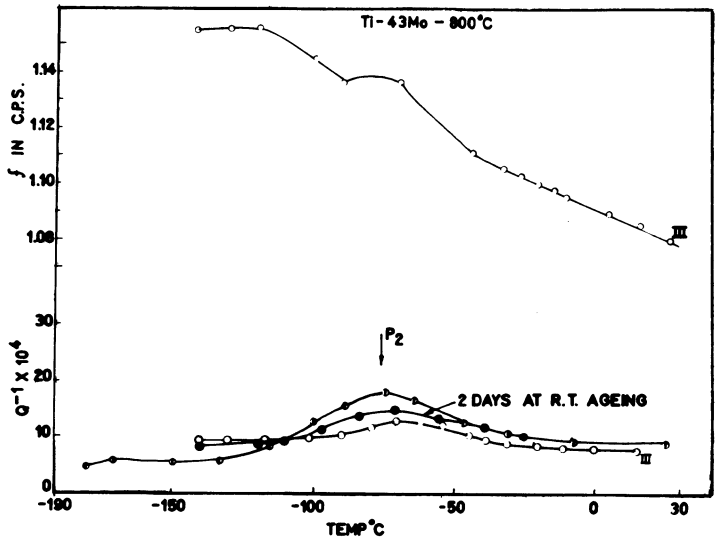

Fig. 5 - Q^{-1} vs. temperature plot. The specimen contained 500 ppm oxygen.

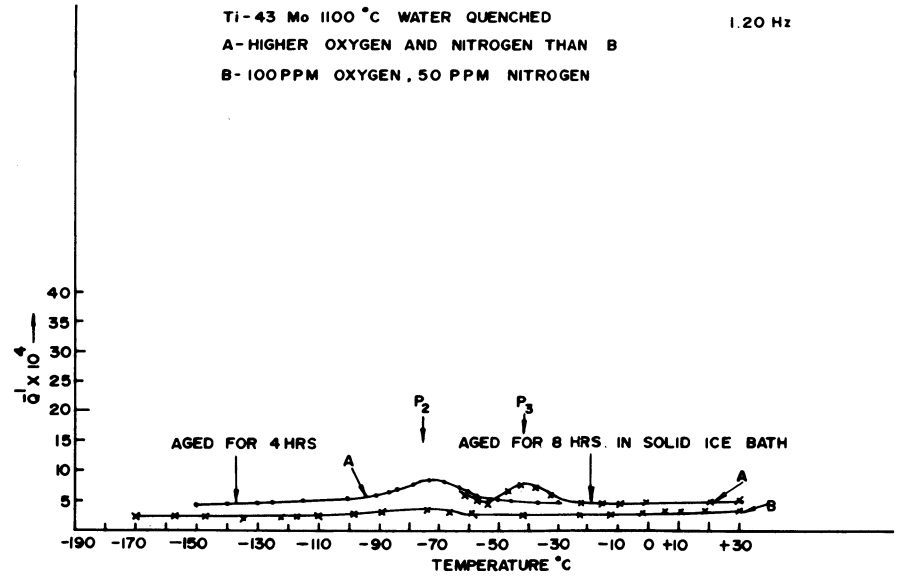

Fig. 6 - Q^{-1} vs. temperature plot. Effect of oxygen and nitrogen contents and dry ice soaking on peaks P_2 and P_3.

(b) Figs.2a and 2b indicate that this peak originates from the metastable β phase; the peak height is proportional to the quantity of β; (c) the β→ω (athermal) transformation is indicated (from Fig.2c) at -140°C and it appears that a part of ω is not reversible; (d) atom shuffle process should have been more difficult with oxygen presence in the lattice but as observed oxygen actually aids the proposed mechanism; (e) the value of $\tau_0 = 1 \times 10^{-9\pm2}$ sec[4] which again supports the dislocation interactions; (f) It is expected that the oxygen solubility would be maximum for an optimum alloying addition to give maximum β metastability which in turn is responsible for peak P_1. For richer alloys the oxygen solubility proportionately decreases and for dilute alloys the metastable beta phase is less; (g) Belko et al.[8] measured internal friction during diffusionless phase transformations in Cu-Ni alloys. The relaxation peaks associated with this type of atom shuffle process are quite different than Peak P_1 in the sense that there is observed a temperature lag in the peak temperatures while heating and cooling operations.

Peaks P_2 and P_3

Peaks P_2 and P_3 are observed at -75°C and -40°C respectively at 1Hz as shown in Fig.3, Fig.4, Fig.5 and Fig.6. These peaks are due to interstitial-vacancy pair mechanism in the metastable β matrix. P_2 is associated with oxygen and vacancy pair whereas P_3 is due to nitrogen-vacancy pairs. The appearance of the P_3 in molybdenum alloys occurs only on aging at -60°C for sufficiently long time to allow the vacancies to migrate to the nitrogen atoms. Aging at R-T or above tends to decrease the peak height of P_2 and P_3 (See Fig.3 & 5) due to possible decrease in the amount of the metastable beta phase. The effect of quenching temperature on the metastable beta phase. The effect of quenching temperature on the peak height for Ti-43Mo for the peak P_2 is shown in Fig.7. The maxima occurs at about 800°C quenching temperature as this is the temperature at which the optimum number of oxygen-vacancy pairs would be existing.

Peak P_4

Peak P_4 occurs at about 230°C at 1.0Hz for all the Ti-Mo alloys as well as for the βIII alloys, Ref.Fig.8, Figs.9(a & b) and Fig.10. These are ascribed as due to the Snoek relaxation in the bcc structure involving oxygen atoms. These are observed either in the metastable beta Ref. Fig.10 or in the stable beta field Ref. Figs.9 (a & b). The explanation offered by Vigier at al.[4] for P_4 in their observation in βIII does not seem to be adequate. It is noted that both P_1 and P_4 are dependent upon the oxygen content, hence they are linearly related to each other in conformity with the earlier observations.[4] The P_4 in the Ti-V alloy occurs at about 315°C for 1.0Hz for oxygen. In addition, two more Snoek peaks are observed

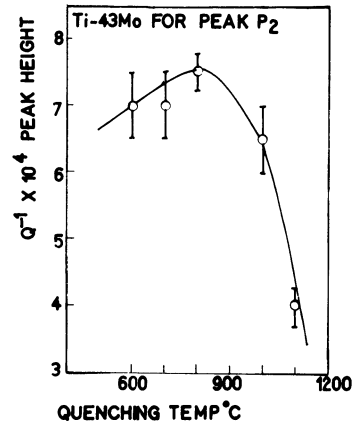

Fig. 7 - The effect of quenching temperatures on the peak heights, the alloy sample contained 500 ppm oxygen.

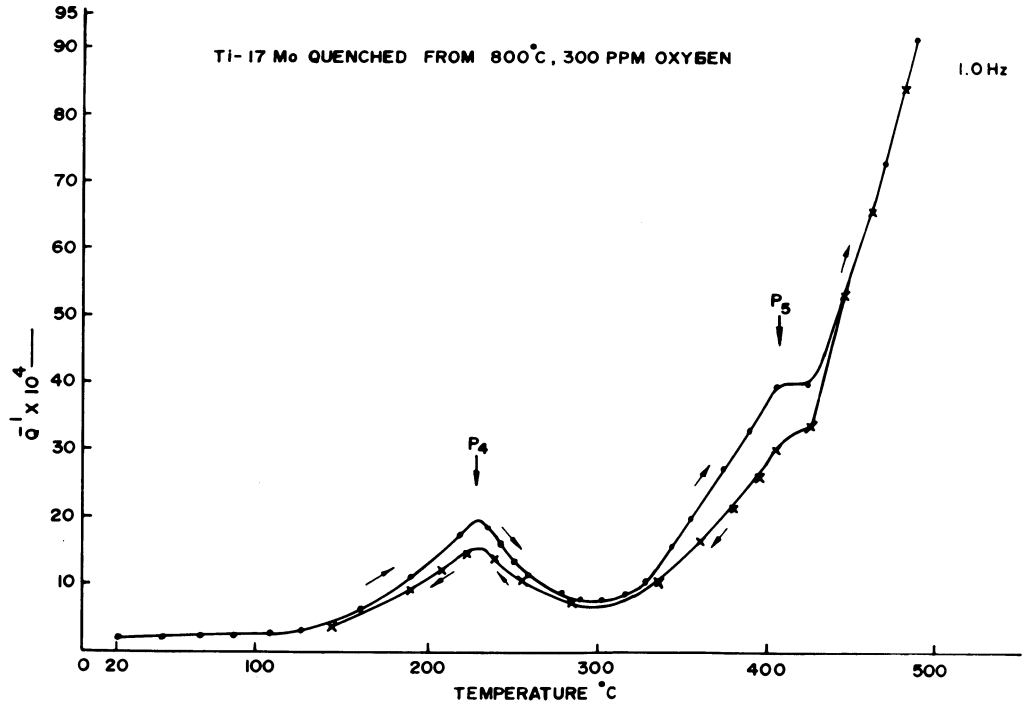

Fig. 8 - Q^{-1} vs. temperature plot at high temperatures.

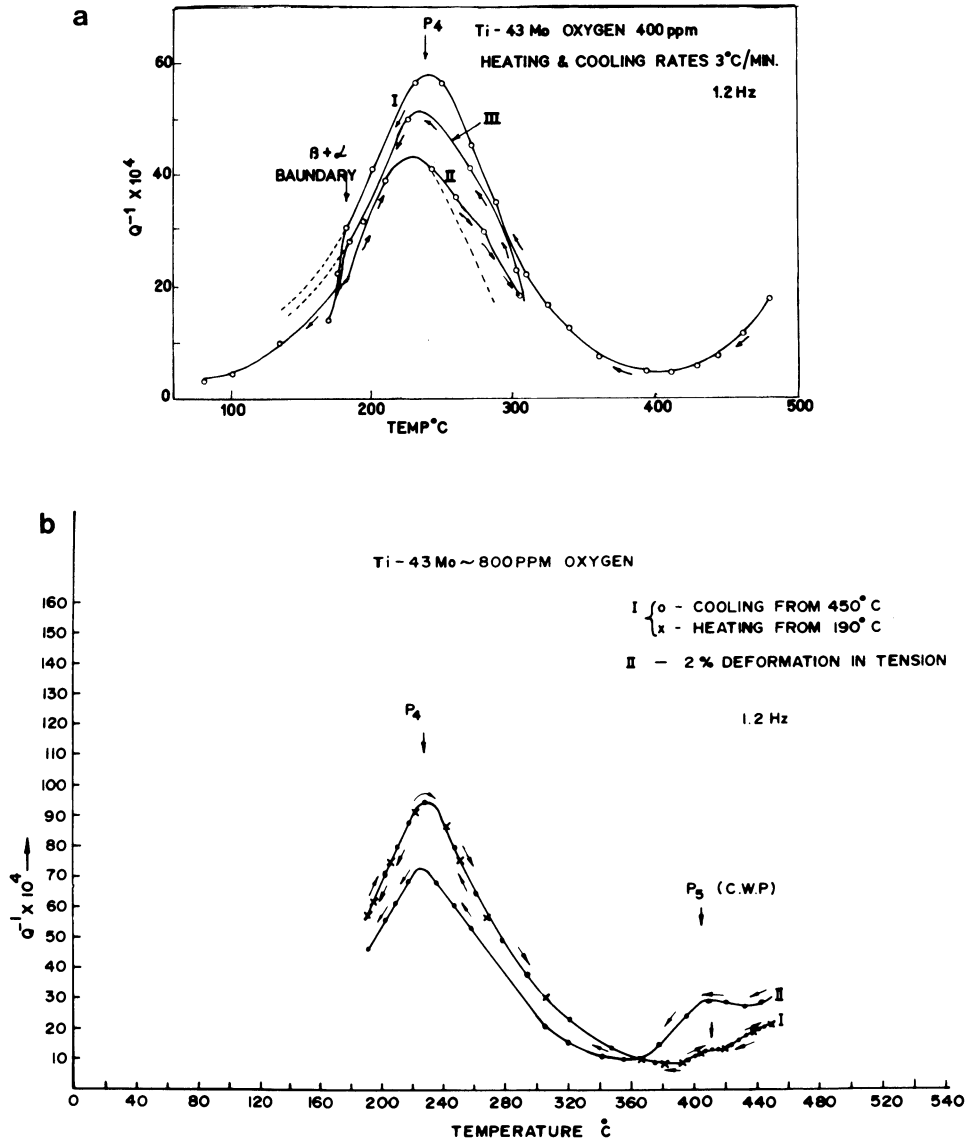

Fig. 9 - (a) Q^{-1} vs. temperature plot at high temperatures. (b) Q^{-1} vs. temperature plot at high temperatures. Effect of oxygen content and deformation, shown.

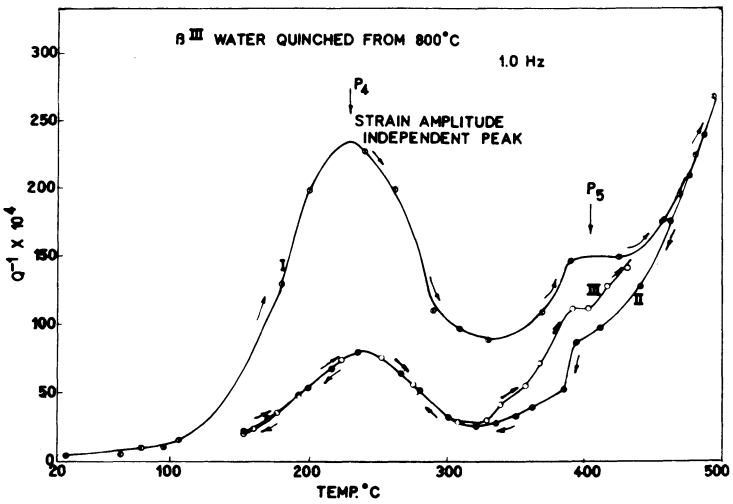

Fig. 10 - The high temperature Q^{-1} vs. temperature plot.

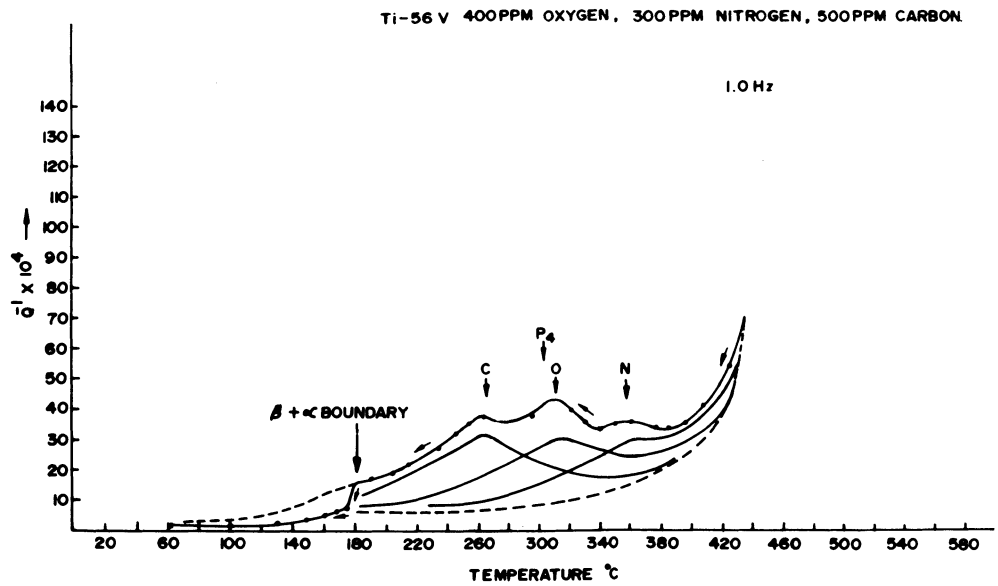

Fig. 11 - The Snoek peaks for various interstitials like oxygen, nitrogen and carbon.

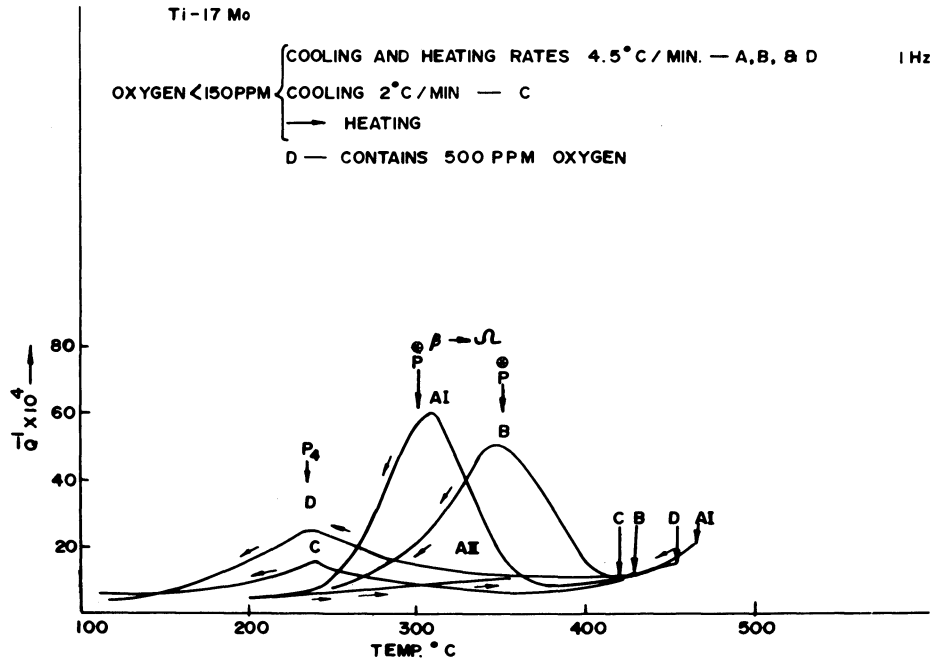

Fig. 12 - β to ω (athermal) transformation peak. Effect of oxygen content, cooling rates and the Mo content of the metastable, shown.

for carbon and nitrogen at about 260°C and 360°C respectively. Fig.9(b) and Fig.11 also show the $\beta+\alpha$ boundary by a sudden loss in Snoek relaxation magnitude during cooling. The Snoek peaks reported earlier have now been analyzed to be due to substitutional interstitial interaction peaks occurring at higher temperatures for the same frequency.

Peak P_5

P_5 is a cold worked peak (C.W.P.) seen in Figs.8, 9(a) and 10. Introduction of cold work increases P_5 and reduced P_4 during cooling from 450°C due to the fact that some of the oxygen causing P_4 are transferred to the dislocation and build up P_5. The necessity for cold work is not there if dislocations are produced by thermal ω precipitation which is expected to generate dislocations Fig.8 and 10.

Peak P*

Peak* is connected with the diffusionless ω transformation occurring during fast cooling and the activation energy for the peak is found to be 40 ± 5 kcal/gm.mole, Ref.Fig.12. The peak P* is only observable in alloys containing less oxygen such that T_ω is $\sim$ 400°C[2] for this composition. With increasing oxygen content as well as with slower rate of cooling the peak P* gets suppressed. The occurrence of the peak temperature is a function of the Mo content of beta phase. The cause of the peak is due to $\beta \rightarrow \omega$ (athermal) transformation. It is expected that the formation and dissolution of the diffusionless omega embryos takes place during cyclic stressing. All the pertinent data are summarized in Table I.

ACKNOWLEDGMENTS

The authors are grateful to Shri C. V. Sundaram, Head, Metallurgy Division, Bhabha Atomic Research Centre, for his interest and encouragement.

REFERENCES

1. Doherty, J. E. and Gissons, D. F., Internal Friction Studies in Some Titanium and Zirconium based Alloys, Acta Met. 1971, Vol. 19, pp.275-282.

2. De Fontaine, D., Paton, N. E. and Williams, J.C., The Omega Phase Transformation in Titanium Alloys as an example of displacement controlled reactions, Acta Met., 1971, Vol. 19, pp. 1153-1162.

3. Paton, N. E. and Williams, J. C., The Influence of Oxygen Content on the Athermal Transformation, Scripta Met., 1973, Vol. 7, No. 6, pp.647-650.

4. Vigier, G., Merlin, J. and Gobin, P. F., Etude De L'alliage De Titane βIII Variations De Module, Scripta Met., 1974, Vol. 8, No. 7, pp. 843-850.

5. Goasdoue C., Ho, P. S. and Sass, S. L., Ultrasonic Study of the beta-omega phase transformation in Zr-Nb Alloys, Acta Met., 1972, Vol. 20, pp. 725-733.

6. Sommer, A. W., Motokura, S., Ono, K. and Buck, O., Relaxation Processes in Metastable Beta Titanium Alloys Acta Met., 1973, Vol. 21, pp. 489-497.

7. Nelson, C. W., Gibbons, D. G. and Hehemann, R. F., Acoustic Relaxation in Zirconium-Niobium Alloys, J. Appl. Phys. 37, 1966, pp. 4677.

8. Belko, V. N., Darinskiy, B. M., Postnikov, V. S. and Sharshakov, I. M., Internal Friction during Diffusionless Phase Transformation in Cu-Ni Alloys. Fiz. Metal Metalloved 27, 1969, No. 1, pp. 141-147.

9. Mishra, S. and Asundi, M. K., Internal Friction Studies in Titanium base alpha and alpha plus beta alloys, Titanium Science and Technology, Jaffee, R. I. and Burte, H. M. (ed.) Plenum Press, New York, London, 1973, p. 669.

AGING CHARACTERISTICS OF BETA TITANIUM ALLOYS

T. Nishimura, M. Nishigaki and H. Kusamichi

Kobe Steel, Limited
Kobe, Japan

Introduction

Titanium alloys have been used in aerospace areas for their high strength-density ratios. Most of them have been alpha or alpha-beta titanium alloys, which have a difficult point of the lower cold deformability. On the contrary, beta titanium alloys which consist of a metastable beta structure stabilized to the room temperature in addition of the beta stabilizing element such as Mo, V and Cr, have a good cold deformability as well as the excellent aging properties and recently have been investigated actively for the various compositions.[1]-[3] It was found in the previous investigations[4]-[9] that Ti-Mo base beta alloys, Ti-15Mo-5Zr and Ti-15Mo-5Zr-3Al have a good combination of corrosion resistance, cold deformability, weldability and mechanical properties.

In the work reported here, in order to make clear the aging phenomena in these two beta titanium alloys, tensile tests, hardness measurement, light and electron microscopy, X-ray diffraction observation have been carried out. In this manner the strengthening mechanisms in the beta titanium alloys have been studied. On the basis of these observations, the best combinations of tensile

properties for the alloys by the optimum heat treatment are determined.

Experimental procedure

The experimental work was carried out with the two beta titanium alloys, Ti-15Mo-5Zr and Ti-15Mo-5Zr-3Al double-melted in a consumable-electrode arc furnace. The as-melted ingots were forged into billets 60 mm x 60 mm at 1100°C and hot rolled to bars of 9.5 mm diameter. The chemical compositions of the materials are shown in Table 1.

Table 1. Chemical compositions of alloys (wt%)

Alloy	Mo	Zr	Al	Fe	C	O	N
Ti-15Mo-5Zr	14.74	4.76	-	0.046	0.008	0.183	0.0058
Ti-15Mo-5Zr-3Al	14.97	5.04	2.93	0.043	0.006	0.165	0.0129

In order to investigate the effects of the solution temperatures, the specimens were heated in the range of 50°C below the beta transus temperature (Tβ) to 150°C above Tβ, followed by a water quench of a cooling rate 3400°C/min. The beta transus temperatures of Ti-15Mo-5Zr and Ti-15Mo-5Zr-3Al are 730°C and 785°C, respectively. The solution-treated specimens were aged at 500°C up to 5000 min. The specimens solution-treated at Tβ were aged in the temperature range 300°C to 550°C up to 5000 min. The solution-treated specimens, and solution-treated and aged specimens were used for tensile tests, hardness measurement, light and electron microscopy and X-ray diffraction. The relative intensities of the X-ray diffraction were used for estimating the relative amounts of the phases which form during aging. The relative intensity of the alpha phase, $I\alpha$, and that of the omega phase, $I\omega$, were determined using the diffraction intensity of the beta phase as follows :

$$I\alpha = I\,(10\bar{1}0)_\alpha / I\,(200)_\beta$$

$$I\omega = I\,(11\bar{2}2)_\omega / I\,(200)_\beta$$

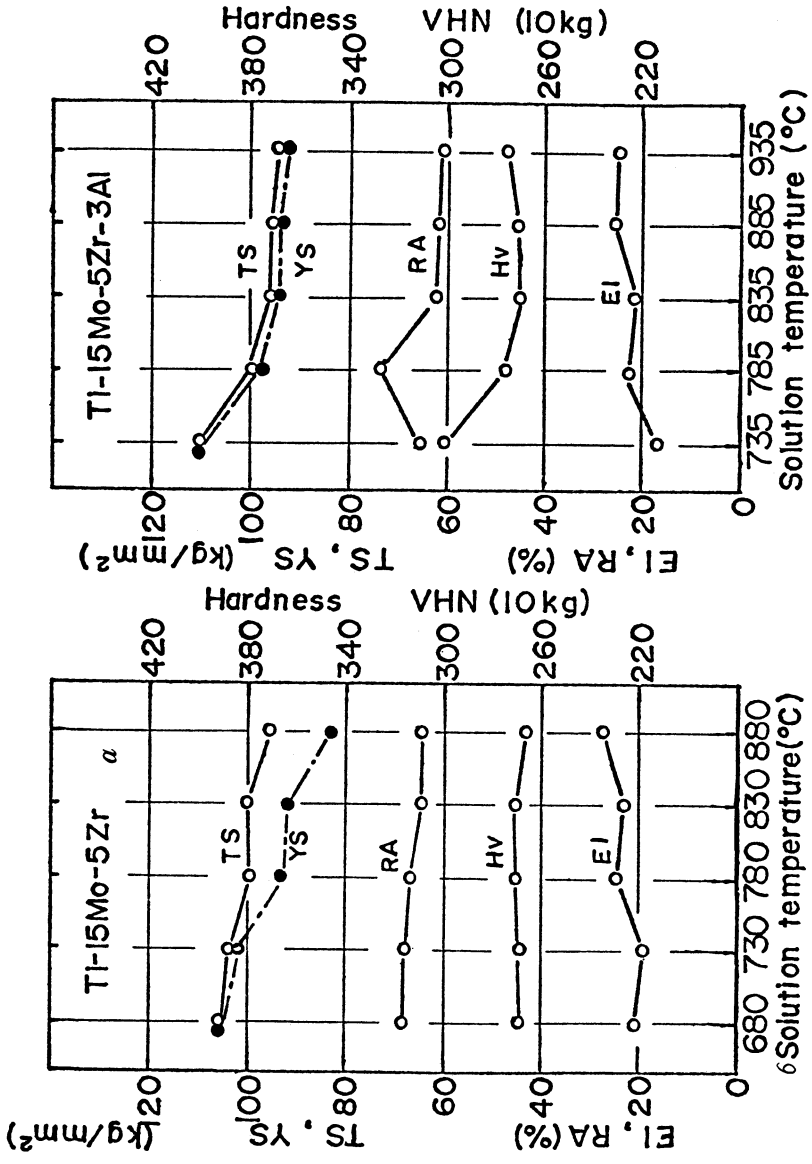

Fig. 1 - Effect of solution temperatures on the tensile properties of solution treated beta titanium alloys.

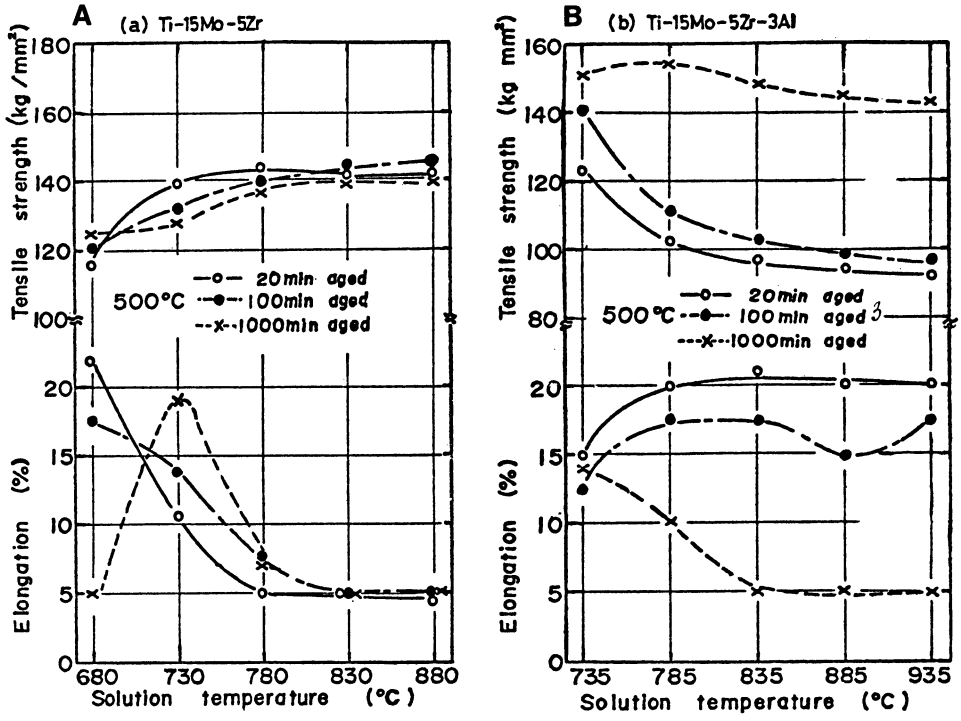

Fig. 2 - Effect of solution temperatures on the tensile properties of aged beta titanium alloys
(a) Ti-15Mo-5Zr
(b) Ti-15Mo-5Zr-3Al

$I\ (10\bar{1}0)_\alpha$, $I\ (11\bar{2}2)_\omega$ and $I\ (200)_\beta$ are the diffraction intensities of the crystal planes, $(10\bar{1}0)_\alpha$, $(11\bar{2}2)_\omega$ and $(200)_\beta$, respectively.

Results and discussion

1. Effect of solution temperature

The tensile properties of the as-quenched solution-treated specimens are shown in Fig. 1. In the both alloys Ti-15Mo-5Zr and Ti-15Mo-5Zr-3Al, the tensile strength is higher in the specimens solution-treated 50°C below T_β due to the existence of the alpha phase, while it decreases with increasing solution temperatures because of the enlargement of the beta grains. The correlations between the yield strength and the beta grain diameter d (mm) are shown as follows :

Ti-15Mo-5Zr $\quad YS\ (kg/mm^2) = 67.2 + 4.8 \times d^{-1/2}$

Ti-15Mo-5Zr-3Al $\quad YS\ (kg/mm^2) = 89.2 + 1.1 \times d^{-1/2}$

The larger dependence of the yield strength on the beta grain size in Ti-15Mo-5Zr is related to its easiness of the stress induced transformation, while that of Ti-15Mo-5Zr-3Al is not large since aluminum in the beta phase stabilizes the beta phase and suppresses the stress induced transformation.[7]

The tensile properties of the solution-treated and aged specimens are shown in Fig. 2. In the alloy Ti-15Mo-5Zr, a little increase in tensile strength occurred after aging in the specimens solution-treated below T_β , while the pronounced hardening was observed for specimens solution-treated at and above T_β. The beta phase of the specimen solution-treated below T_β is more stable for the existence of the alpha phase in as-solution-treated condition, which leads to the suppression of the omega phase and the less hardening during aging. In the solution-treatment above T_β, the tensile strength increased over 140 kg/mm^2 due to the precipitation of the omega phase and showed a slight tendency of decreasing, which is related to the reversion of the omega phase and the

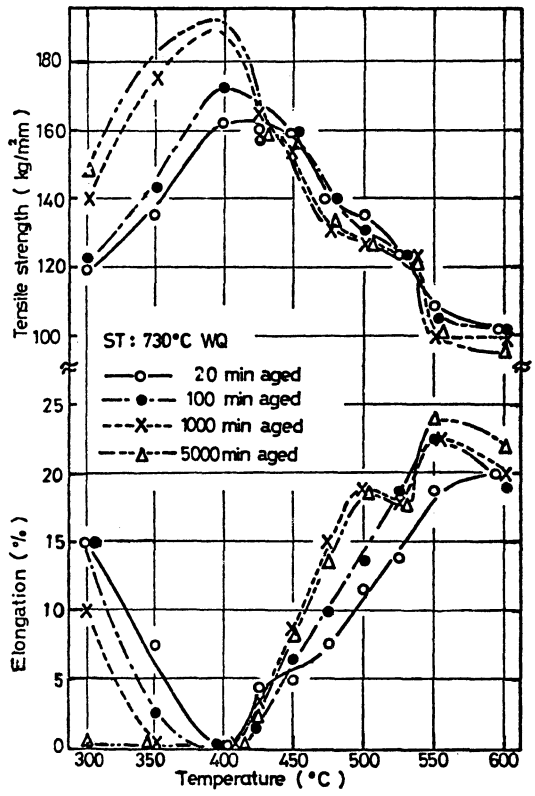

Fig. 3 - Isochronal curve of tensile properties of various aging temperatures for Ti-15Mo-5Zr.

precipitation of the alpha phase. The better ductility was obtained for the materials with the finer beta grain structure produced by the solution-treatment at the lower temperatures.

In the alloy Ti-15Mo-5Zr-3Al, the age hardening became larger with increasing aging time in the solution-treatments both below and above T_β. The better ductility was obtained with the lower solution temperatures. In this alloy the omega formation did not occur during aging at 500°C. Consequently the age hardening is attributed to the alpha precipitation. The beta phase of the specimen solution-treated below T_β is more stable also in this alloy, but has an ability to form the alpha phase during aging and shows the age hardening since the formation of the alpha phase is a strengthening mechanism in this alloy.

It was found from these observations that the optimum solution temperatures to produce the good combination of the tensile properties were T_β for Ti-15Mo-5Zr and below T_β for Ti-15Mo-5Zr-3Al.

2. Aging properties

The isochronal curves of tensile properties during aging for Ti-15Mo-5Zr are shown in Fig. 3. In the range 300° to 400°C, the pronounced age hardening with loss in ductility occurred with increasing aging time. The embrittlement such as zero elongation was observed. In the range 425° to 450°C, the tensile strength increased to 160 kg/mm^2 in the early stages and then decreased gradually with recovery of ductility, which is related to the alpha precipitation from X-ray observation. In the aging at 475° to 500°C, the tensile strength increased to 140 kg/mm^2, followed with a slight softening and the improvement in ductility. The tensile strength increased to 120 kg/mm^2 in the aging at 525°C, and showed a slight or no increasing in the aging at the higher temperatures. The changes of strength during aging showed the quite opposite tendency as compared with ductility, as shown in Fig. 3.

The relative intensities of the omega and alpha phases by the X-ray diffraction are shown in Fig. 4. As shown in Fig. 3 and

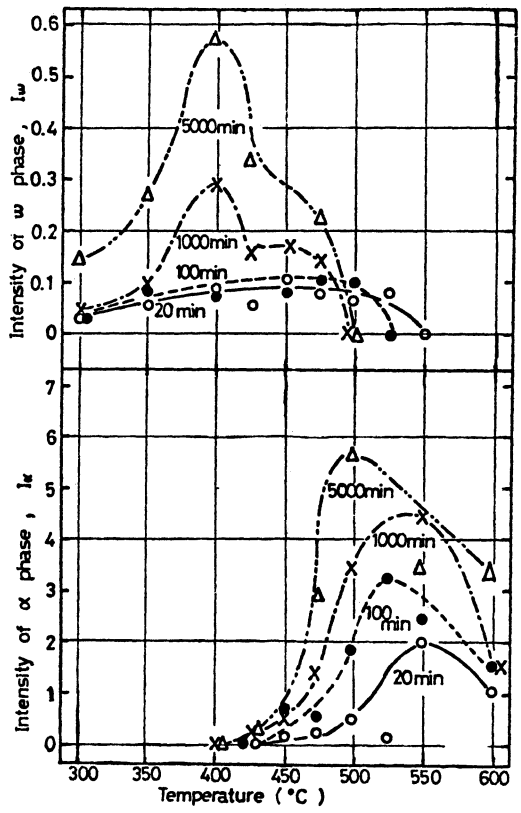

Fig. 4 - Amount of omega and alpha phases during aging for Ti-15Mo-5Zr.

Fig. 4, it is found that the formation of the omega phase is a strengthening mechanism and that of the alpha phase is a softening mechanism in Ti-15Mo-5Zr. In order to obtain a good combination of mechanical properties in this alloy, the adequate coexistence of the omega and alpha phases is necessary by the heat treatment.

The different aging phenomena were observed in Ti-15Mo-5Zr-3Al since aluminum suppresses the omega precipitation and strengthens greatly the alpha phase. The isochronal curves of tensile properties during aging for Ti-15Mo-5Zr-3Al are shown in Fig. 5. The maximum age hardening was obtained in the range 425° to 450°C, but the embrittlement such as zero elongation was not observed in this alloy. The results of X-ray diffraction for Ti-15Mo-5Zr-3Al are shown in Fig. 6. As shown in Fig. 6, the omega precipitation in the aging below 425°C and the alpha formation above 425°C were observed. The coexistence of the omega and alpha phases was not observed in this alloy. In the higher temperatures above 425°C, the maximum in the tensile strength and the minimum in elongation varied to the lower aging temperatures with increasing aging time, which were related to the maximum amount of the alpha phase, as shown in Fig. 6. Consequently, the precipitation of the alpha phase is a strengthening mechanism during aging at the higher temperatures in Ti-15Mo-5Zr-3Al.

On the basis of these observations, the good combination of strength and ductility is obtained by the aging treatment at 475°C after the solution treatment at T_β in Ti-15Mo-5Zr, which produced the structure of the adequate coexistence of the omega and alpha phases. The optimum heat treatment for Ti-15Mo-5Zr-3Al is the aging at 500°C after the solution treatment 50°C below T_β, which results in the alpha precipitation. The mechanical properties of the alloys are shown in Table 2.

3. Duplex aging

The aging transformation diagrams from the X-ray diffraction observation are shown in Fig. 7, which are consistent with the

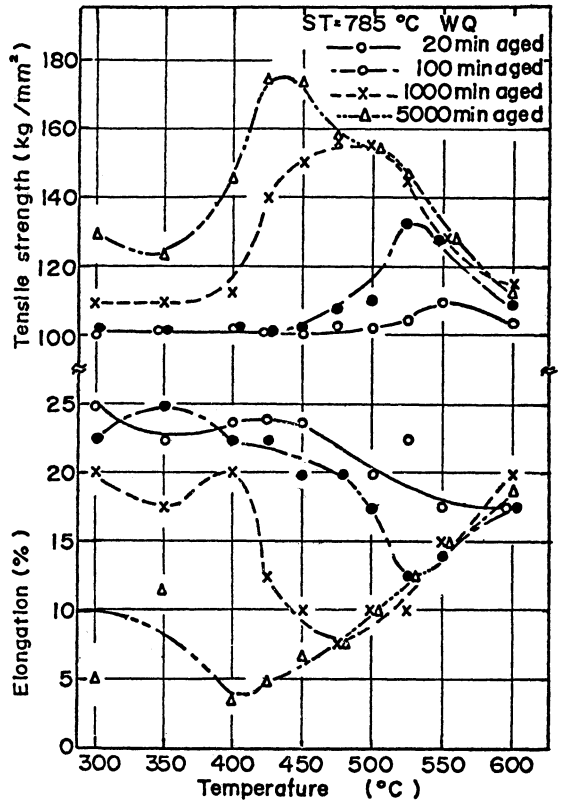

Fig. 5 - Isochronal curve of tensile properties at various aging temperatures for Ti-15Mo-5Zr-3Al.

Table 2. Mechanical properties of beta titanium alloys aged at the optimum conditions

Alloy	Heat treatment	TS (kg/mm^2)	El (%)	RA (%)	Hardness HV (10kg)	NTS/TS ratio	Charpy value (kg.m/cm^2)	Fatigue strength (kg/mm^2)
Ti-15Mo-5Zr	730°C WQ +475°C x100min	140.5	10.0	53.8	394	0.94	2.43	56.9
Ti-15 Mo-5Zr-3Al	735°C WQ +500°C x1000 min	150.5	13.8	58.7	412	1.06	3.06	70.0

previous report studied by the dilatometric method.[5] As shown in Fig. 7, the addition of 3% aluminum lowers the formation temperature range of the omega phase and spreads that of the alpha phase. The duplex aging conditions were determined from these aging transformation diagrams. The first aging temperature was selected the lower aging temperature, 300°C, at which the fine distribution of the omega precipitates was supposed for Ti-15Mo-5Zr. The higher aging temperatures were selected for the second aging temperature to produce the adequate coexistence of the omega and alpha phases in Ti-15Mo-5Zr. In Ti-15Mo-5Zr-3Al, the first aging treatment was carried out at 425°C, which is the lower temperature of the alpha formation, followed by the second aging treatments at 475°C and 500°C. The mechanical properties obtained by the duplex treatments are shown in Table 3. The tensile strengths of 167.8 kg/mm^2 for Ti-15Mo-5Zr and of 161.9 kg/mm^2 for Ti-15Mo-5Zr-3Al were obtained without large loss in ductility.

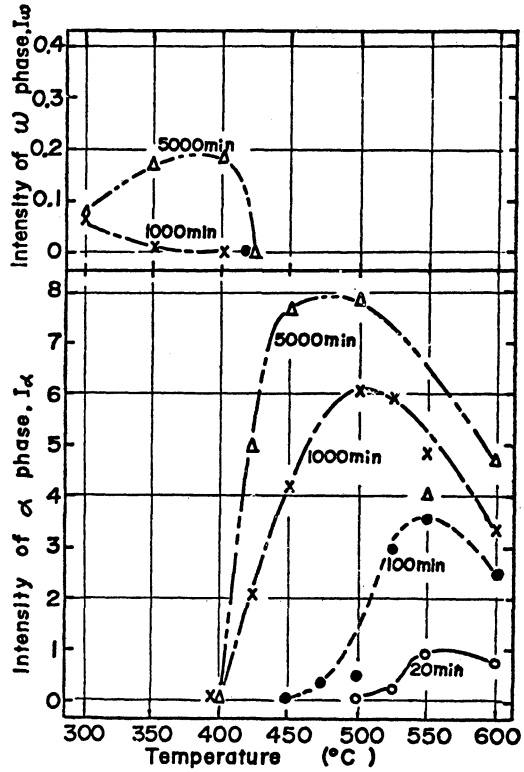

Fig. 6 - Amount of omega and alpha phases during aging for Ti-15Mo-5Zr-3Al.

Table 3. Mechanical properties of duplex aged beta titanium alloys

Alloy	Aging treatment	TS (kg/mm^2)	El (%)	RV (%)	HV (10 kg)
Ti-15Mo-5Zr	300°C x 500 min + 425°C x 200 min	151.0	1.2	5.7	456
	300°C x 500 min + 475°C x 100 min	167.8	7.5	44.0	417
Ti-15Mo-5Zr -3Al	425°C x 1000 min + 475°C x 1000 min	161.9	10.0	52.0	413
	425°C x 1000 min + 500°C x 1000 min	159.0	10.0	58.1	417

Solution treatment Ti-15Mo-5Zr : 730°C x 60 min WQ
Ti-15Mo-5Zr-3Al : 735°C x 60 min WQ

Conclusion

(1) In Ti-15Mo-5Zr, the age hardening with embrittlement such as zero elongation was observed in the aging treatment below 400°C, which was related to the omega precipitation. In the higher aging temperatures, the decrease of age hardening and recovery of ductility were observed, attributed to the reversion of the omega phase and the formation of the alpha phase. For the good combination of strength and ductility, the adequate coexistence of the omega and alpha phases was needed by the aging treatment. The tensile strength of 140.5 kg/mm^2 and elongation of 10% were obtained by the aging treatment at 475°C.

(2) In an aluminum containing alloy, Ti-15Mo-5Zr-3Al, the precipitation amount of the omega phase was suppressed and the temperature range of the omega formation was lowered below 425°C. In the higher aging temperatures, only the alpha formation was observed. The alpha formation is a main strengthening mechanism in this alloy and

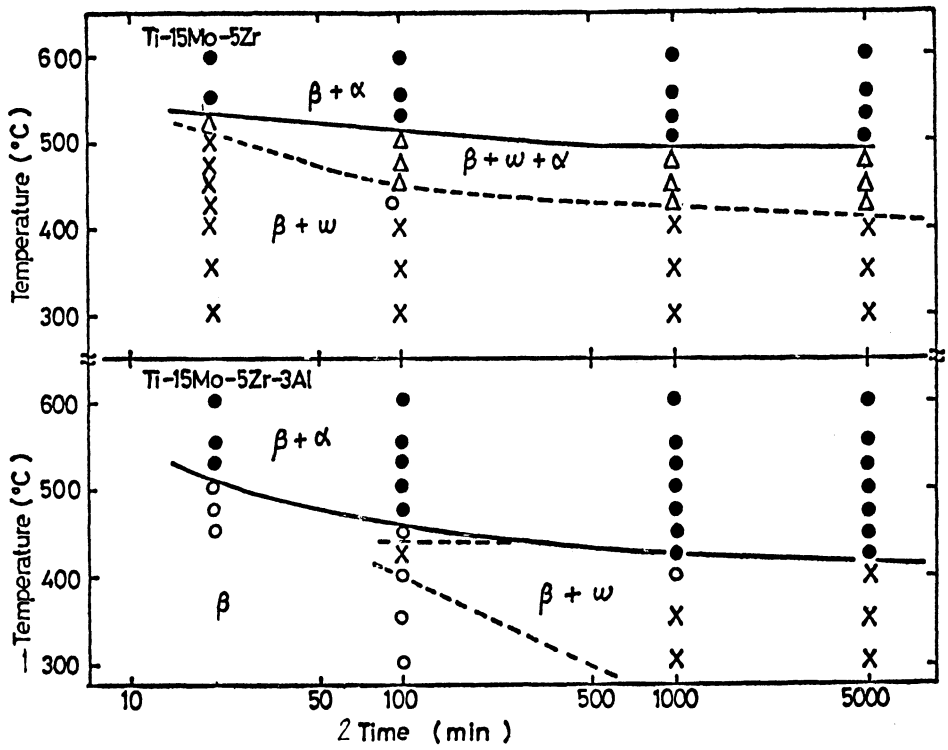

Fig. 7 - Aging transformation diagrams for Ti-15Mo-5Zr and Ti-15Mo-5Zr-3Al.

the embrittlement such as zero elongation did not occur. The tensile strength of 150.5 kg/mm^2 and elongation of 13% were obtained by the aging treatment at 500°C.

(3) There is difference of the strengthening mechanisms between Ti-15Mo-5Zr and Ti-15Mo-5Zr-3Al. In the aluminum-free alloy, Ti-15Mo-5Zr, the omega formation is a only strengthening mechanism, while the omega and alpha formations increase the strength of the aged Ti-15Mo-5Zr-3Al. Aluminum content of the alpha phase is higher than that of the matrix in Ti-15Mo-5Zr-3Al, and therefore the alpha precipitates are very hard since aluminum strengthens the alpha phase strongly. As the omega formation was suppressed by the addition of aluminum, the alpha formation is a main strengthening mechanism in Ti-15Mo-5Zr-3Al.

(4) The finer beta grain structure after solution treatment is needed for the good mechanical properties. The optimum solution temperatures are T_β for Ti-15Mo-5Zr and 50°C below T_β for Ti-15Mo-5Zr-3Al.

(5) The tensile strength was improved by the duplex aging treatment to 167.8 kg/mm^2 for Ti-15Mo-5Zr and 161.9 kg/mm^2 for Ti-15Mo-5Zr-3Al without large loss in ductility.

DECOMPOSITION OF THE SOLID SOLUTION THE THE ALL-BETA βIII

G. Vigier, J. Merlin, and P.F. Gobin

Groupe d'Etude de Métallurgie Physique et de Physique des matériaux., I.N.S.A. de Lyon
69621 Villeurbanne, France

The decomposition of the solid solution in the βIII alloy (Ti-11,5 Mo-6Zr-4,5 Sn) is of interest because various transformations occur inside : from diffusional transformations (α and isothermal ω phases) to displacive transformations (athermal ω phase). The decomposition has been studied by two main techniques :

- elastic modulus measurements by the resonant frequency method in the range 0,5 khz to 10 khz
- internal friction measurements in the cycle and kilocycle range from 10°K to 600°K

These techniques are interesting because the formation of the various phases leads to very important increases of modulus and to two anelastic phenomena (1) (2) (3) (4) a P_1 peak and a P_2 peak at about -170°C and 250°C at one cycle (5) (fig 1) : the P_2 peak is associated with the instability of solid solution before the diffusional transformation β→w isothermal and the P_1 peak is associated with the instability of solid solution before the displacive transformation β→w athermal.

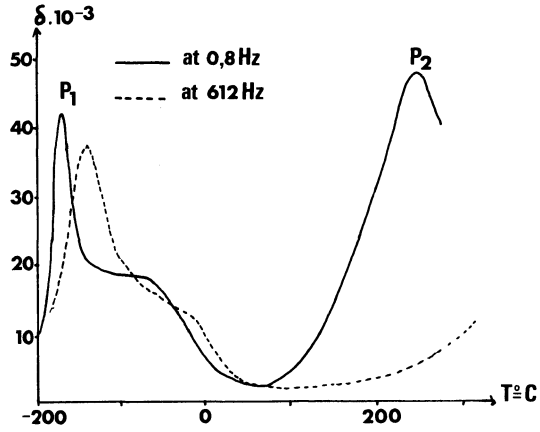

Fig. 1 - Internal friction spectra from -200°C to 300°C.

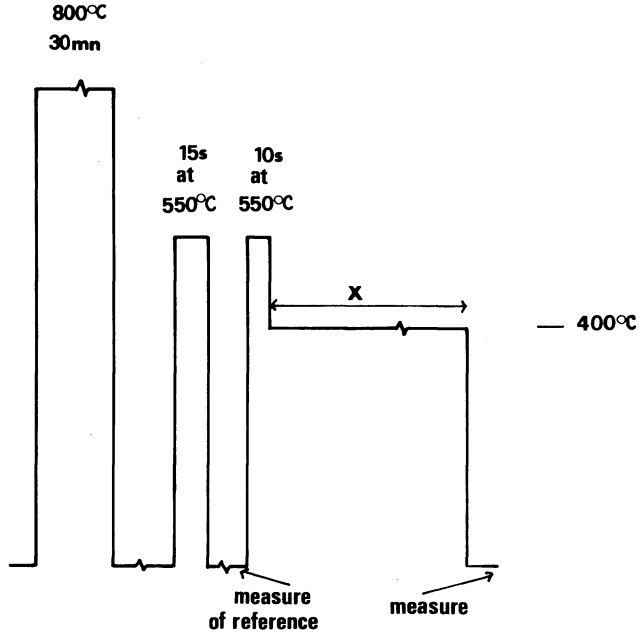

Fig. 2 - Thermal treatment effected for drawing the isothermal curves.

I FORMATION TEMPERATURE RANGES AND KINETICS OF GROWTH OF THE VARIOUS PHASES

We have defined a treatment (described by the fig. 2) that gives the best solid solution. Isothermal curves between 20°C and 630°C have been drawn by Young modulus (E) and Coulomb modulus (G) measurements (fig 3).

Two kinds of curves have been distinguished (this distinction has been corroborated by transmission electron microscopy observations) (6) :

- from 20°C to 375°C, the curves are associated with the ω precipitation : $\Delta G/G \rightarrow 0,87$ and $\Delta E/E \rightarrow 0,63$
- from 400°C to 630°C, the curves are associated with the α precipitation : $\frac{\Delta G}{G} \rightarrow 0,50$ and $\frac{\Delta E}{E} \rightarrow 0,34$.

These curves have been normalized and we have drawn the T.T.T. diagram (fig 4) (with the supposition that the modulus variation is proportional to the volume transformed (7).

The shape of modulus variation curves and the micrographic observations lead us to separate the α formation range in two parts :

- below 590°C : the α precipitation is semi-coherent, and the α phase nucleates on dislocations and grain boundaries.
- above 590°C : the α precipitation is incoherent and the α phase nucleates only on grain boundaries.

The upper temperature of ω phase formation from a solid solution is approwimatively 410°C.

Whithin the ω formation range, an anomaly is caracterised by two facts (9).

- an abnormaly rapid increase of modulus below 200°C
- this anomaly, observed between 200°C and 20°C, disappears when 10% of the ω phase has precipitated.

Therefore this anomaly could be attributed to the process of nucleation, because the growth is normal in all the ω precipitation range. At very low temperature the instability of the b.c.c lattice leads

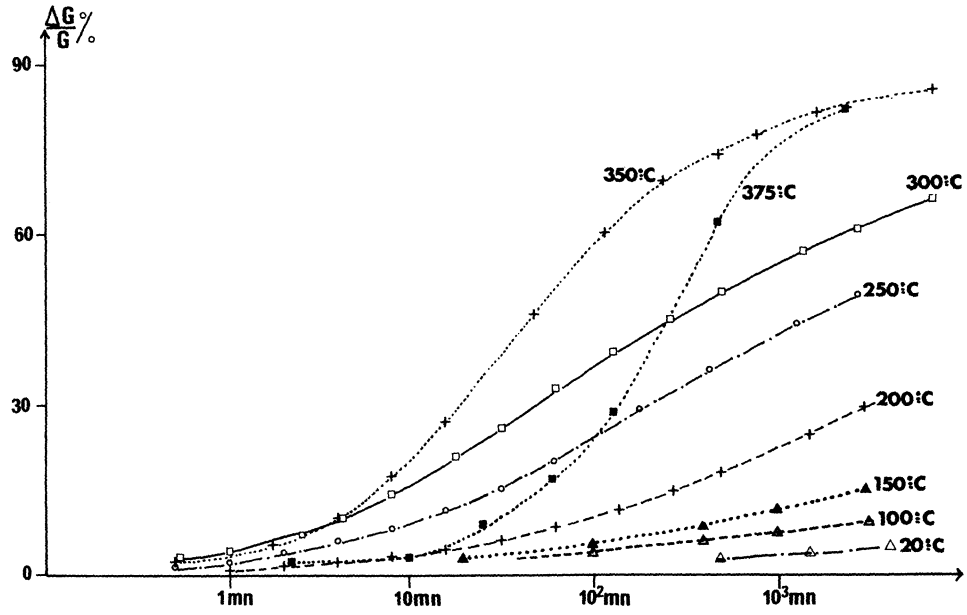

Fig. 3A - Evolution of the Coulomb modulus during the ω precipitation.

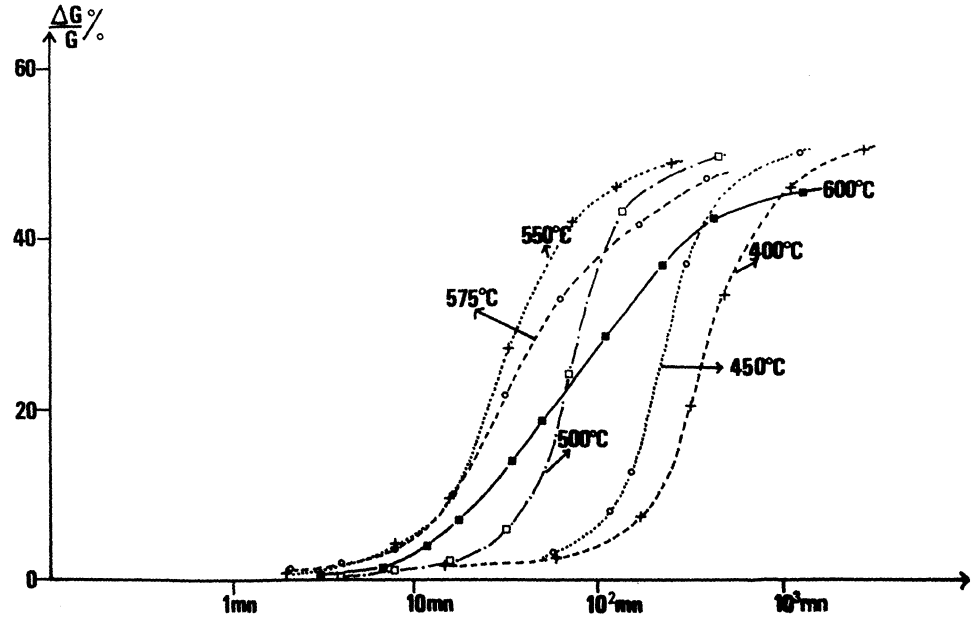

Fig. 3B - Evolution of the Coulomb modulus during the α precipitation.

to the athermal ω phase ; pretransformation phenomena have been observed : internal friction peaks (3) (4), diffuse diffraction effects (8). It is possible that the causes of these pretransformation phenomena may be responsible for the isothermal ω formation in the range where this anomaly of nucleation is observed. If that is so, the diffusion having little or no influence at all on the process of germination, the vacancy concentration must not affect strongly this process. Effectively we have observed on an aging at 85°C that the modulus increase is nearly the same on a water quenched specimen and on a reverted specimen. Therefore it would be possible to associate the ω isothermal phase below 200°C with an intermediar tranformation in which displacive process and short range diffusional process would occur.

Moreover it could be shown that the ω phase, formed below 410°C may be up to about 500°C, but a treatment of reversion (15s to 60s at 550°C) is able to dissolve this phase completely without generating the α phase.

The study of the P_1 peak allowed us to determine the ωs temperature (the start temperature for athermal ω formation). The linear displacement defects (10) which lead to the transformation would be responsible for this peak : an external stress would modify the population of these defects in preferred direction thereby giving rise to energy dissipation. The peak height must be maximum just above ωs since such a temperature corresponds to the greatest population of linear displacement defects. While, for a reverted specimen, at 0,8 hz the peak is observed at about 100°K and its magnitude is δ (logarithmic decrement) = 42.10^{-3}, whereas at 612 hz the peak is observed at about 120°k and its magnitude is $\delta = 38.10^{-3}$. The evolution of the peak magnitude when the temperature goes from 100°K to 120°K allows us to suppose that the ωs temperature is not yet reached. The drastic decrease of internal friction between 90°K and 60°K (fig 5), whatever the structural state of the alloy, at 0,8hz as well as 612hz, would show that ωs is in this temperature range.

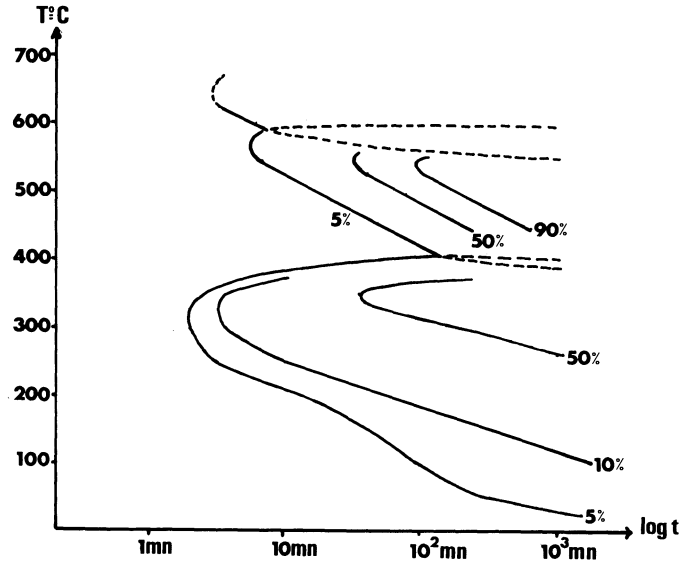

Fig. 4 - T.T.T. diagram.

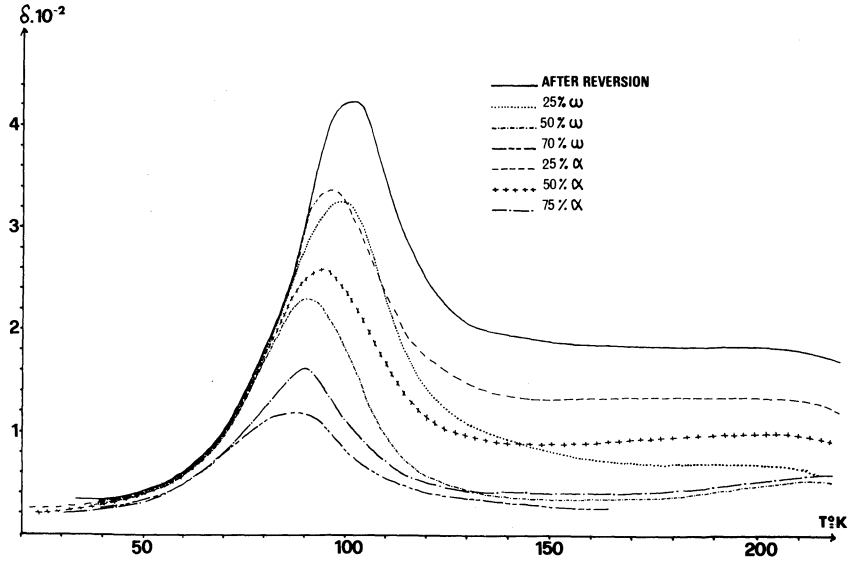

Fig. 5 - Evolution of the P_1 peak during the ω and α precipitation.

II PRECIPITATION DESCRIPTION OF DIFFERENTS PHASES

The α or ω phases have been formed in various quantities, then we have shown the influence of these phases on the P_2 peak. The ω quantity formed during raising of temperature at the time of internal friction test (from 20°C to 300°C, at a rate of 120°C/hour) has been estimated from elastic modulus variations. This quantity is representative of the alloy stability in various structural states or more exactly of the stability of the non-transformed β phase.

From Fig 6 it can be seen

i) the α phase formed before the internal friction test has little action on the quantity and the rate of formation of the ω phase during raising of temperature. Therefore the α phase (when its precipitable percentage does not exceed 50%) does not stabilize the β phase. During the α precipitation the titanium concentration in the matrix does not change continuously but on the contrary an important fraction of the matrix stays with the initial composition βo. It is only on the vicinity of the α precipitates that the matrix is stable.

$$\beta o \rightarrow k\ (\alpha + \beta E) + (1-k)\ \beta o$$

in which βE is the matrix composition at equilibrium and k tends to 1 when the aging time increases.

ii) The ω phase formed before the internal friction test reduces the quantity and the formation rate of the ω phase very much during raising of temperature. That is probably due to an homogencous re-partition of the ω particles which inhibits the formation of new particles and to a continuous decrease of the titanium concentration in the all matrix : the β phase is more stable.

$$\beta o \rightarrow \omega + \beta'$$

in which β' is the Mo-Ti solid solution going continuously from βo to βE.

On the fig 7 and 8 we can see the effect of the α and ω precipitation on the P_2 peak two facts appear :

i) The temperature of the peak can be associated with the stability of the solid solution

ii) The height of the peak is proportional to the square of the

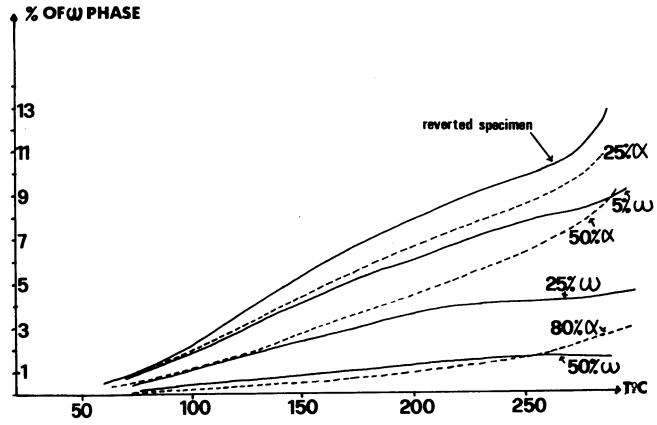

Fig. 6 - Percentage of precipitable ω phase formed during the internal friction test.

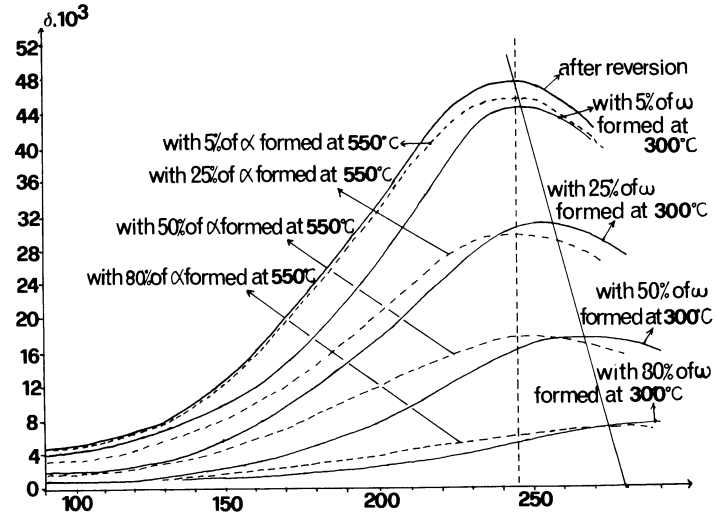

Fig. 7 - Evolution of the P_2 peak during the α and ω precipitation.

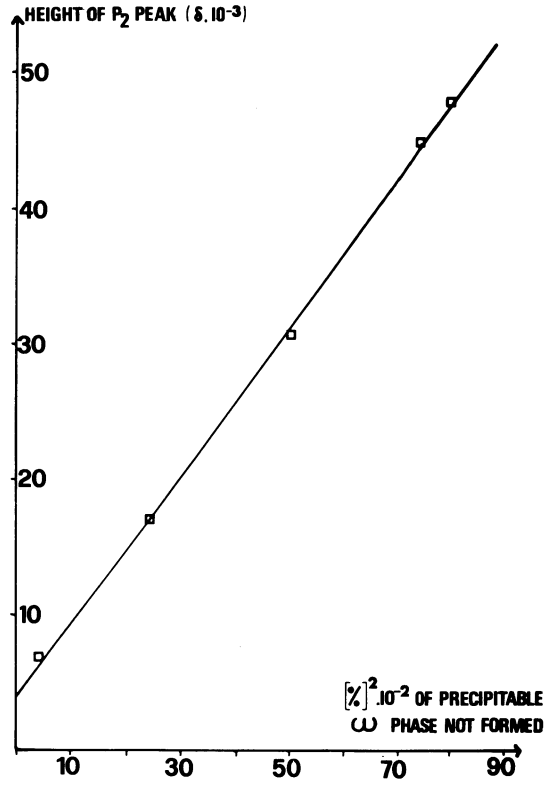

Fig. 8 - Variation of the height of the P_2 peak with the square of the fraction of ω phase which is to be formed.

titanium quantity in supersaturation in matrix, and that independently of the titanium repartition. Indeed we can see that the height of the peak is proportional to the square of the fraction of α or ω phases which are to be formed when the peak has a maximum height (fig 8) and this fraction can easily be related with the number of the titanium atoms which stays in supersaturation in the alloy.

III CONCLUSION

The solid solution decomposition in the alloy βIII can be summarized by the following table :

Temperature	PHASE	FORMATION	TRANSFORMATION TYPE
750°C			
	α incoherent phase	by diffusion from grain boundaries	localized and discontinuous precipitation
590°C			
	α semi-coherent phase	by diffusion from dislocation and grain boundaries	localized and discontinuous precipitation
410°C			
	ω coherent phase	by diffusion within the matrix	generalized and continuous precipitation
200°C			
	ω coherent phase + displacement defects	by displacement and by diffusion within the matrix	Intermediar transformation
0°C			
	displacement defects	by displacement	displacive transformation
-180°C			
-210°C			
	displacement defects + athermal ω	by displacement	displacive transformation

Acknowledgements

We wish to express our gratitude to the Ugine-Acier laboratory for their support in this investigation.

BIBLIOGRAPHY

(1) F. GANESAN R.J. Dc ANGELIS G.A. SARGENT Journal of less common Metals 1974 - Vol 34 p.209.

(2) A.W BOWEN Scripta Metallurgica 1971 vol 5 p. 709

(3) J.E DOHERTY D.F GIBBONS Acta Metallurgica 1971 vol 19 p.275

(4) A.W SOMMER S. MOTOKURA K.ONO O. BUCK Acta Metallurgica 1973 vol 21 p. 489

(5) G. VIGIER J. MERLIN P.F GOBIN Scripta Metallurgica 1974 vol 8 p.843

(6) G. VIGIER J. MERLIN P.F GOBIN Mémoires Scientifiques de la revue de Métallurgie 1975 n°9 p.677

(7) G. VIGIER Thèse Docteur-Ingénieur LYON FRANCE 1975

(8) D. DE FONTAINE Acta Metallurgica 1969 vol 18 p.275

(9) G. VIGIER J. MERLIN P.F GOBIN Journal of Less Common Metals to be published

(10) D. DE FONTAINE O. BUCK Philosophical Magazine 1973 vol 27 p.967

MARTENSITE FORMATION AND DECOMPOSITION IN ALLOYS OF TITANIUM CONTAINING β-STABILIZING ELEMENTS

H.M. Flower, R. Davis and D.R.F. West

Dept. of Metallurgy and Materials Science
Imperial College of Science and Technology, London, U.K.

Synopsis

An investigation is reported of martensite formation in certain Ti-Mo, Ti-V and Ti-Nb alloys and of the decomposition of martensite on ageing. A transition from hexagonal to orthorhombic martensite occurred with increase in solute content. On ageing the orthorhombic martensite structures, spinodal decomposition took place, accompanied by substantial strengthening. Reversion of α'' to β can also occur in some alloys.

1. Introduction

β-stabilising elements such as molybdenum and vanadium have been widely used in commercial titanium alloys and a complex range of transformations can occur when both binary and multi-component alloys are quenched from the β phase field and aged. In the present work a series of binary Ti-Mo, Ti-V and Ti-Nb alloys have been studied over the composition range for which M_f lies above room temperature.

2. Experimental Procedure

The basis materials were sponge titanium and high purity molybdenum, vanadium and niobium. 30g alloys ingots were prepared by arc melting, with nominal compositions (wt%) as follows: Ti-2,4,6 and 8%Mo; Ti-2,4.2,7.4 and 10.6%V; Ti-0.5,1,8,14 and 20%Nb. Oxygen analysis was not carried out for all the alloys, but the molybdenum-containing alloys are known to have relatively high oxygen contents (∿2000-3000 ppm); the other alloys are anticipated to contain ∿1500 ppm oxygen. The ingots were hot-rolled to strip (∿1 mm thick); samples were then solution treated in argon-filled capsules for 1/2 hr. at 1100°C, followed by water-quenching. Ageing was carried out in the range 375-600°C for times up to 10,000 minutes.

3. Results

3.1. Martensite formation

The martensitic structure in the Ti-2%Mo alloy consisted of the acicular morphology with a small proportion of massive morphology, while the alloys with 4-8%Mo were entirely acicular. The Ti-2%V alloy contained predominantly acicular martensite after water quenching. In the Ti-0.5%Nb alloys the massive form dominated while the Ti-1%Nb was predominantly acicular. Layers of retained β were observed in the 2 and 4%Mo alloys, in the Ti-2%V alloy and in the Ti-0.5 and 1%Nb alloys. These β layers were similar to those previously reported for dilute Ti-Mo alloys[1].

The martensite structures in some of the alloys were studied by X-ray examination of the as-quenched material and/or selected area diffraction examination of appropriately aged material (see Discussion). Previous X-ray work[2] has shown that a transition from hexagonal (α') to orthorhombic (α'') martensite occurs in the binary systems at ∿4%Mo, 10%V and 11%Nb respectively. The present results are consistent with this previous work, orthorhombic α'' being found in the following alloys: Ti 4-8%Mo; Ti 10.6%V; Ti 14 and 20%Nb.

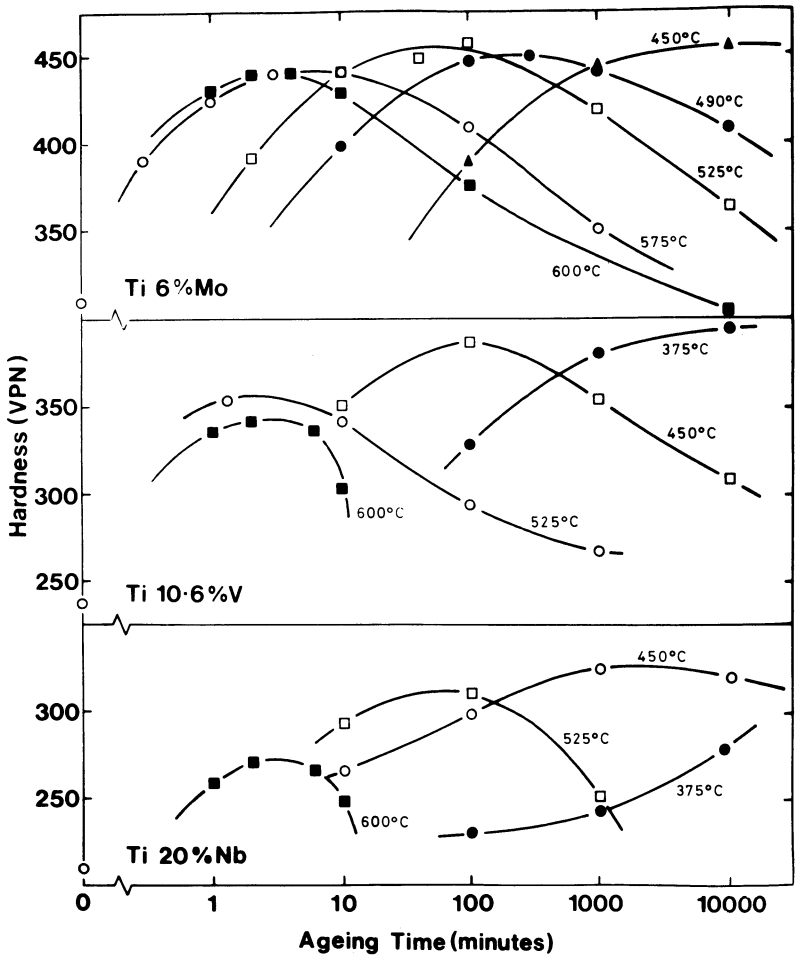

Fig. 1 - Hardness vs aging time curves for α'' alloys. The age hardening is due to spinodal decomposition in the Ti-6%Mo and Ti-6%V alloys, while in Ti-20%Nb hardening is due to competing precipitation and β reversion reactions. The behavior of Ti-4 and 8%Mo was similar to that of Ti-6%Mo but the hardness increments were smaller for the 4%Mo alloy. Ti-14%Nb showed much less hardening than Ti-20%Nb.

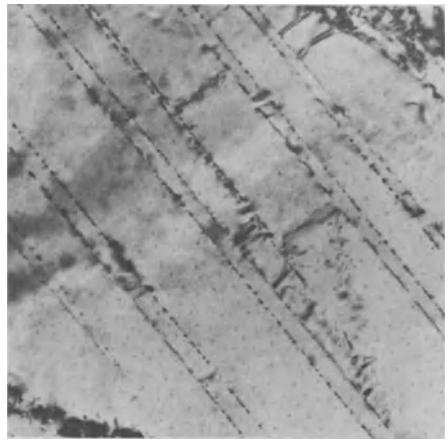

0.1μm

Fig. 2 - Ti-7.4%V. Aged 10^4mins. 375°C, showing heterogeneous nucleation of β at twin boundaries and on dislocations; homogeneous nucleation in the α' matrix. X124,000

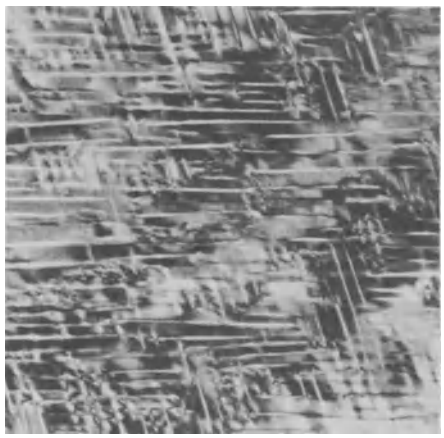

Fig. 3a 0.1μm

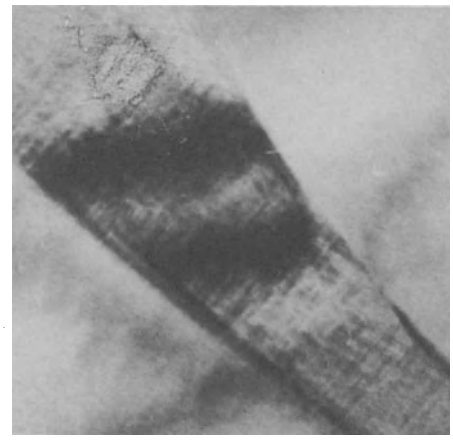

Fig. 3b 200A

Fig. 3 - Ti-10.6%V. (a) Aged 10^4mins. 375°C. $(001)_{\alpha''}$ foil showing periodic "precipitate" structure, X 124,000. (b) Aged 10 min. 375°C. Periodic spinodal structure prior to coarsening. X588,000

The substructure of both the massive and acicular hexagonal α' consisted predominantly of dislocations (although some twins were present in the acicular crystals); the orthorhombic α'' was characterised by the presence of faults and twins.

3.2. Ageing characteristics

Hardness changes. Ageing of the hexagonal martensitic structures containing Ti-2%Mo, Ti-4.2 and 7.4%V and Ti-8%Nb produced no significant hardening effect in the range 375-600°C for times ranging up to ∿10,000 minutes. However, substantial hardening effects were found in the same temperature range on ageing the orthorhombic martensites (e.g. Fig. 1). The level of hardness was highest in the Ti-Mo alloys, probably because of the higher oxygen contents.

Structural changes. In the hexagonal α' martensites the only precipitate detected was the equilibrium β phase which nucleated entirely heterogeneously, with the exception of Ti-7.4%V in which ageing at 375°C produced homogeneous nucleation (Fig. 2). Six variants of the β precipitates formed. Single surface trace analysis showed that the habit plane was irrational and contained the [0001] direction. Examination of martensite plates tilted into the basal orientation permitted accurate determination of the habit plane which was found to deviate 2° from $\{1\bar{4}30\}$ in the direction of the adjacent $\{1\bar{3}20\}$ for Ti 2%Mo while in Ti 7.4%V the deviation was 4°. In all cases the orientation relationship between the α and β phases was found to be close to the ideal Burgers relationship:

$$(0001)_\alpha \,||\, (011)_\beta . \quad [11\bar{2}0]_\alpha \sim || \, [11\bar{1}]_\beta$$

These results are similar to those reported earlier for Ti 1%Mo[1] where there is the crystallographic similarity between α formed by shear in β and β formed by diffusion in α (as in the present case).

The structural changes that occurred on ageing the orthorhombic martensites differed completely from those occurring in the hexagonal martensites. In the Ti-Mo system the Ti 6%Mo alloy was chosen for detailed study. This alloy aged at 450°C, and the orthorhombic Ti-V

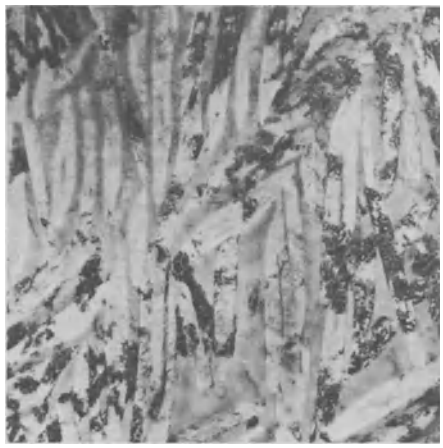

Fig. 4a

500A

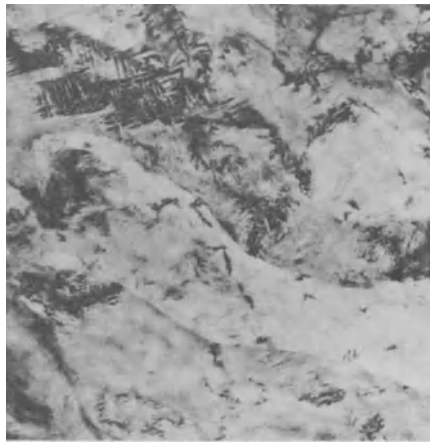

Fig. 4b

Fig. 4 - Ti-6%Mo. (a) Aged 40 mins. 525°C. The periodic structure is continuous up to grain boundaries. X288,000 (b) Aged 575°C 1 min $[001]_{\alpha''}$ SADP showing satellite reflections.

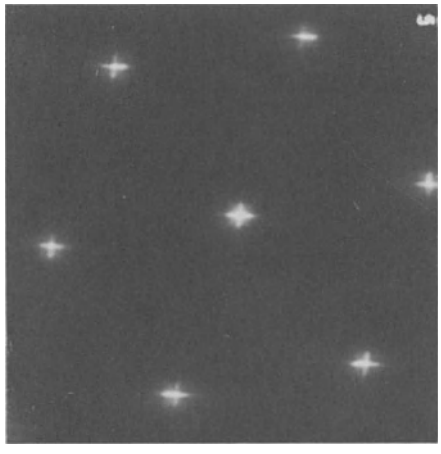

Fig. 5a

0.5μm

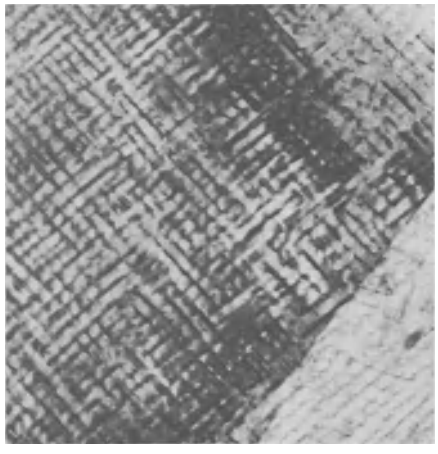

Fig. 5b

0.5μm

Fig. 5 - Ti-20%Nb. (a) Aged 10 mins. 450°C. Complex structure producing ring diffraction patterns. X45,000 (b) Aged 1000 min. 525°C, α plates in β matrix. X45,000

and Ti-Nb alloys aged at 375°C showed the same type of feature consisting of a regular "periodic" or modulated structure which coarsens to a periodic precipitate array, e.g. Fig. 3a shows an (001) α" region in the Ti-10.6%V alloy aged for 10,000 minutes at 375°C. The periodic structure showed only two crystallographic "variants", whose "habit planes" were ~$\{430\}_{\alpha''}$, in contrast to the six variants of β precipitates observed on ageing the hexagonal martensites. The periodic structures were observed from the earliest ageing times studied (e.g. Fig. 3b) and in the case of the Ti 6 and 8%Mo alloys and the Ti-Nb alloys they were even detected in the as-quenched state. The "spacing" of the periodicity increased with ageing time, e.g. in the Ti-6%Mo alloy it was ∿25Å in the as-quenched state and ∿75Å after 10,000 mins at 450°C. The periodic structure was continuous up to grain boundaries, e.g. Fig. 4a. Other defects such as twin boundaries, stacking faults and dislocations played no part in nucleating the structure, and the modulations were continuous across dislocations and up to twin boundaries. The precise periodicity of the modulated structure gave rise to "satellite" reflections in selected area diffraction patterns (Fig. 4b). These observations are consistent with the decomposition of α" by a spinodal mechanism.

Comparison of Figs. 3 and 2 shows how much further advanced was the ageing reaction in the Ti-10.6%V α" alloy than in the Ti-7.4%V α' alloy, given the same ageing treatment. This implies that the lack of precipitation in the latter alloy was not due to slow diffusion at 375°C, but rather to the relatively high activation energy for precipitation as compared with the absence of a nucleation barrier in a spinodal transformation.

With increasing ageing temperatures various structural changes were observed as the systems changed towards equilibrium: (i) as the spinodal products coarsen the solute-rich regions can transform to β and the solute depleted regions to α; (ii) heterogeneous nucleation of β can take place and consume the spinodal products, the matrix

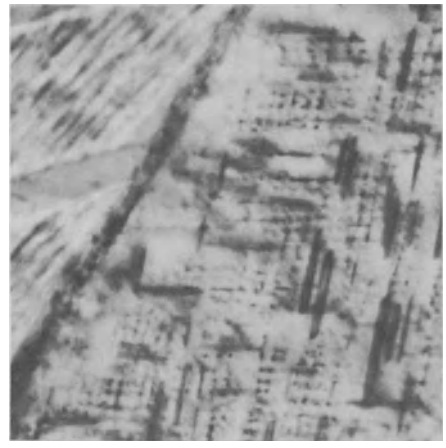

Fig. 6 - Ti-14%Nb. Aged 100 min. 525°C. The [001] grain on the right shows the spinodal structure being consumed by 2 heterogeneously nucleated β variants. A P.F.Z. is developing along the grain boundary as a result of β precipitation. X188,000

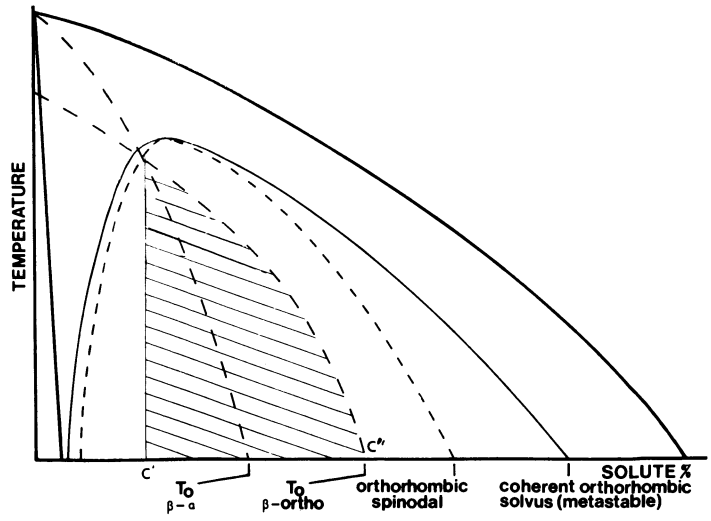

Fig. 7 - Schematic representation of phase relationships in the Ti-Mo, Ti-V and Ti-Nb systems.

being converted to the equilibrium α phase; (iii) α and β can be nucleated and grow cooperatively as a cellular product which consumes the spinodal product; (iv) the reversion of α'' to β can occur.

In the Ti-Mo and Ti-V alloys on ageing at temperatures up to 600°C the main change was coarsening of the spinodal products. However, in the Ti-Mo alloys a cellular reaction occurred competitively with this, and in the Ti-10.6%V alloy some reversion of α'' to β was observed at ≥525°C.

The behaviour of the Ti-Nb alloys is complex and is not clearly understood. On ageing the Ti-20%Nb alloy ≥450°C, microstructures were produced in which the original martensite structure could not be detected, e.g. in Fig. 5a showing the alloy aged for 10 minutes at 450°C, no α'' plates were visible and the structure was highly strained, producing ring diffraction patterns. Some precipitation can be seen, and increase in ageing time or temperature resulted in the production of α + β structures characteristic of α precipitated in β, e.g. Fig. 5b. These observations suggest that α'' reverts to β >∿400°C. Complex structures can be produced when reversion and precipitation occur on ageing and partial retransformation to martensite takes place on cooling. Only when β has precipitated sufficient α to lower the M_s below room temperature will the structure present at the ageing temperature be directly observable.

In the Ti-14%Nb alloy evidence of reversion was obtained at 600°C. At lower temperatures in addition to spinodal coarsening, β phase particles (2 variants only) were observed to nucleate heterogeneously and to consume the spinodal product (Fig. 6). The matrix lattice parameters changed progressively from those of the original α'' structure towards equilibrium α. The matrix was however, still orthorhombic at the stage when β nucleation occurred.

4. Discussion

4.1. As-quenched structures

The formation of retained β in the dilute alloys indicates that in titanium alloys with high M_s temperatures (>∿700°C) water quenching is insufficiently rapid to inhibit completely diffusional reactions. Martensitic and diffusional transformations both occur and β layers form enriched in β stabilising elements. As the solute content is increased and M_s decreases, the diffusional contribution decreases, and fully martensitic structures are produced, until retained β forms when M_f lies below room temperature.

The transition from α' to α" martensite may be represented schematically by T_o curves for α'/β and α"/β, T_o being the temperature at which the two phases have the same free energy at the same composition. These curves represent upper limits for M_s and lower limits for β reversion and the α'/β and α"/β T_o curves must cross in order for the α'/α" transition to occur (Fig. 7). The "cross-over" composition represents the upper limit (c') for this transition.

Concerning the martensite morphology, the microstructural change from dislocated to twinned martensite cannot be uniquely associated with the crystallographic transition from hexagonal to orthorhombic, since twinning is observed at compositions where the martensite is still hexagonal.

4.2. Aged Structures

A change in precipitation characteristics is expected at the α'/α" transition because of the lower symmetry of the orthorhombic as compared with the hexagonal form. This is demonstrated by the fact that six β precipitate variants can form in α' in which the [0001] direction is a hexad axis, while in α" [001] is only a diad axis and only two β variants can form (e.g. as in the overaged Ti-14%Nb alloy). In fact this observation on aged alloys can be used to

demonstrate clearly whether the original as-quenched structures were orthorhombic or hexagonal.

The most significant change in passing from the α' to the α'' range is that from nucleation and growth of β to the formation of the periodic decomposition product on ageing the martensite. The microstructural data provide evidence that spinodal decomposition is occurring. The presence of a spinodal necessarily implies the existence of a metastable orthorhombic miscibility gap in each of the three alloy systems studied. The equilibrium and metastable coherent phase diagrams for such a situation are shown schematically in Fig. 7. Since the miscibility gap refers to the orthorhombic structure the consequences of its presence can only be observed if the product of water quenching from the β phase field is itself orthorhombic, i.e. the alloy must produce an orthorhombic martensite. In the diagram the composition at which α'' forms is already well within the spinodal so the transition between nucleation and growth in α' martensite (for which there is no coherent miscibility gap) and spinodal decomposition should be abrupt and must occur in association with the transition from α' to α''. Correspondingly if an alloy has a composition above c''% solute it does not form martensite at room temperature and again spinodal decomposition will not be possible (unless there is a miscibility gap for the bcc phase). Thus whether or not spinodal decomposition can be achieved depends on the values of c' and c'' and these will vary from system to system. The experimental evidence shows that spinodal decomposition occurs in the range Ti-4-8%Mo; Ti-10%V and Ti-14-20%Nb. The diagram also indicates the possibility that an alloy which forms α'' on quenching can, if heated above T_o, revert, at least partially, to β. (This can happen for temperatures that lie within the miscibility gap.) The reversion of Ti-20%Nb at or above 450°C and Ti-10.6 %V at or above 525°C both illustrate this situation. Other observations on α'' → β reversion have been previously reported[6,7], including Ti-Nb alloys[6]. The overall temperature composition limits over which spinodal

decomposition can be observed are illustrated by the 'ruled' area indicated in the diagram.

It is believed that these alloys constitute the first examples of noncubic metallic systems reported to undergo spinodal decomposition; (several low symmetry mineral systems undergo such reactions). However, examination of micrographs of the decomposition products observed in other orthorhombic titanium alloys[7-9] Ti-W, Ti-Mo-Si, and Ti-Al-Sn-Zr-Mo, suggests that spinodal decomposition may occur in these systems also. If, by further alloying, the critical cooling rate for α'' formation can be reduced without loss of spinodal decomposition it is possible that this age-hardening behaviour could be used practically to produce high strength titanium alloys.

5. Conclusions

In water-quenched dilute Ti-Mo, Ti-V and Ti-Nb alloys some β retention occurs in the α' structures as a result of diffusion. On ageing the hexagonal α' structures in the range 375-600°C heterogeneous precipitation of β phase occurs, with no significant hardening. Ageing of the orthorhombic α'' structures involves a spinodal mode of decomposition, giving rise to substantial hardening. The spinodal decomposition products coarsen with increase in temperature and time and undergo transformation to α and β; various competing reactions can occur including cellular decomposition, and reversion of α'' to β.

6. Acknowledgements

Acknowledgements are made to Professor J.G. Ball for the provision of research facilities, to Imperial Metal Industries (Kynoch) Ltd. for supply of materials and for carrying out oxygen analysis, and to Messrs. H.V. Cheetham, A.G. Furniss, D.H. Lancefield and A. Treasure for carrying out some of the experimental work on the Ti-V and Ti-Nb alloys. One of the authors (R.D.) acknowledges the award of a research studentship from the Science Research Council.

Bibliography

1. Flower, H.M., Henry, S.D. and West, D.R.F., J. Mat. Sci. 1974 9, p.57.
2. Bagariatskii, Nosova, G.I. and Tagunova, T.V., Sov. Physics, Doklady, 3, 1959, p.1014.
3. Hirsch, P.B., Howie, A., Nicholson, R.B., Pashley, D.W., and Whelan, M.J., Electron Microscopy of Thin Crystals 1967, Butterworths.
4. Bywater, K.A. and Christian, J.W., Phil. Mag. 1972, 25, p.1275.
5. Gomez, M.H. Unpublished work.
6. Jepson, K.S., Brown, A.R.G., and Gray, J.A. The Science, Technology and Application of Titanium, Pergamon Press, 1970, p.677.
7. Williams, J.C., Titanium Science and Technology, Plenum Press, 1972, p.1433.
8. Williams, J.C. and Hickman, B.S. Met. Trans, 1, 1970, p.2648.
9. Young, M. Levine, E. and Margolin, H., Met. Trans. 5, 1974, p.189.

AN EVALUATION OF DIRECT AGING TO ACHIEVE OPTIMUM MECHANICAL PROPERTIES FOR THE METASTABLE BETA Ti-8Mo-8V-2Fe-3Al ALLOY

R. Chait and T.S. DeSisto

Army Materials and Mechanics Research Center
Watertown, Massachussetts 02172, U.S.A.

Metastable beta titanium alloys are usually given a conventional solution treating and aging heat treatment to achieve high strength. This has been the case for the alloy Ti-8Mo-8V-2Fe-3Al. The present paper examines an alternate heat treatment for Ti-8823, that of direct aging after fabrication. Material for this study was fabricated by extrusion processes that provide reduction of a) 30%; and b) 83-84% during hot working for which two different heat treatments are considered: a conventional solution treatment and age, and a direct age. The extrusion temperature was also varied for the material that had undergone the larger amount of reduction. Static tension, torsion, and fracture toughness properties are determined for various through-the-thickness locations. Also reported are crack growth data and uniaxial S-N fatigue curves obtained from tests run at an R ratio of 0.1. The information from these tests enables a comparison between the solution treated and aged, and the direct aged conditions for the larger amount of reduction. Except for the crack growth behavior these data are compared to that obtained from material that has received 30% reduction during hot working.

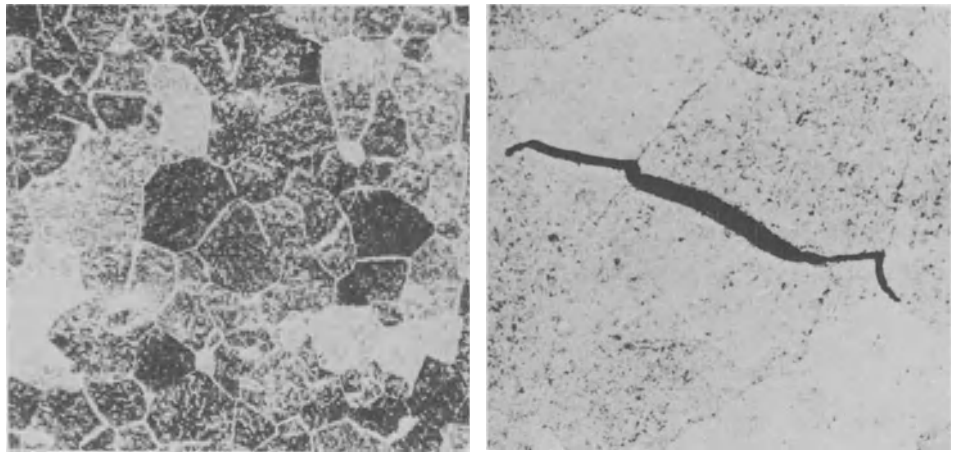

(a) 84% Reduction (Mag. 100X) (b) 30% Reduction (Mag. 125X)

Fig. 1 - Effect of reduction during hot working on beta grain size. Micrograph shown in (b) was taken from the cross section of broken tension specimen and shows the appearance of crack formation in the grain boundaries.

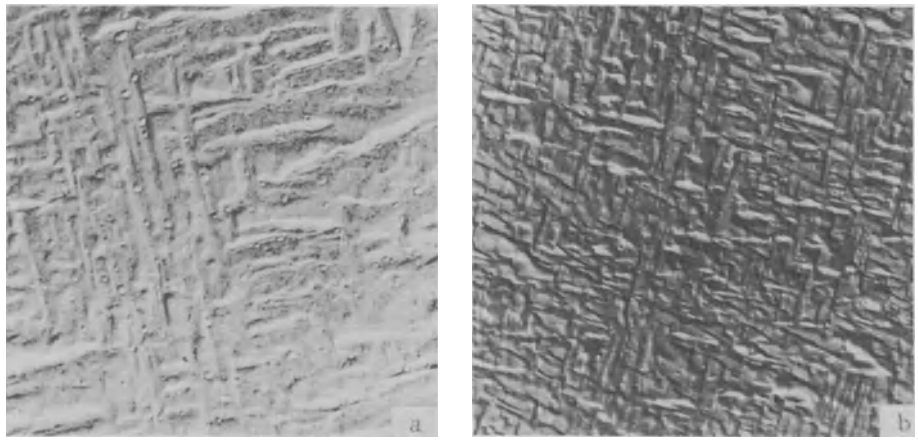

Fig. 2 - Electron micrograph of microstructure at (a) OD and (b) MW of material given 83% reduction during hot working followed by STA heat treatment. X10,000

Introduction

The metastable beta Ti-8Mo-8V-2Fe-3Al alloy, henceforth referred to as Ti-8823, is a candidate alloy for structural forgings and extrusions because of its excellent hardenability. Conventional heat treating practice of Ti-8823 consists of a solutionizing and aging heat treatment (STA) generally in the range 1450°F-1475°F and 900°F-1000°F, respectively (1). Recent efforts (2,3) have characterized the static strength and fracture toughness of heavy section forgings and extrusions given the STA heat treatment. The present paper considers an alternate heat treatment for heavy sections: direct aging (DA) after hot working. For heavy sections that have been reduced 83-84% during extrusion, baseline tension, torsion, and fracture toughness values are determined for the DA heat treatment and compared to that resulting from the STA heat treatment. The paper also emphasizes a comparison based on important fatigue properties for which little data are available in the literature. In addition to the effect of heat treatment, the influence of the amount of hot working as well as the hot working temperature is considered.

Materials, Processing History, and Test Procedure

The two heats of Ti-8823 alloys that were involved in this investigation were melted by Titanium Metals Corporation of America and have the composition shown in Table I. Heat I provided material for the extrusion (84% continuous reduction) of cylindrical hollows having the approximate dimension 11-3/8 in. OD x 3-1/8 in. wall, while from Heat II an 8-3/4 in. OD x 3 in. wall cylindrical hollow (30% continuous reduction) and a 3 in. diameter solid cylindrical round (83% continuous reduction) were obtained. Other important details pertaining to the fabrication as well as the heat treatment are shown in Table II.

Cylindrical tension (0.252 in. diameter) and full-sized Charpy specimens were taken in the longitudinal and transverse directions at various through-the-thickness locations, i.e., OD, MW or ID

TABLE I CHEMICAL COMPOSITION

Heat Identification	Element (Weight Percent)							
	Al	V	Mo	Fe	C	O	H	N
I	3.12	7.99	8.17	1.77	0.022	0.16	0.007	0.018
II	3.08	8.08	7.80	2.07	0.035	0.133	0.006	0.010

TABLE II EXTRUSION AND HEAT TREATMENT DETAILS

Heat Identification	Extrusion Temp. and Amount of Hot Work	Final Product Form	Solutionizing Temp. and Time Prior to WQ	Aging Temp. and Time Prior to AC	Notation
I	1700°F - 30% Reduction	Cylindrical Hollow	1475°F - 1-1/2 Hr	1000°F - 8 Hr	STA
	1650°F, 1850°F, and 2000°F - 83% Reduction*	Solid Round	1475°F - 1-1/2 Hr -	1000°F - 8 Hr 1000°F - 8 Hr	STA DA
II	1700°F - 84% Reduction†	Cylindrical Hollow	1475°F - 1-1/2 Hr -	1000°F - 8 Hr 950°F - 8 Hr	STA DA

*Direct extrusion performed by Canton Extrusion Corporation, Canton, Ohio.
†Modified direct extrusion performed by Cameron Iron Works, Houston, Texas.
All reductions were the result of single-step extrusion operations.

locations. According to recent ASTM definitions the longitudinal and transverse directions correspond to the LR and CR orientations.

The tension tests were performed on a 120,000-lb capacity universal hydraulic testing machine at a platen displacement of 0.005 in./min. The torsion tests representing selected through-the-thickness locations were conducted on a 2000 in.-lb capacity Instron testing machine. The Charpy specimens were precracked in a ManLabs Model FCM 300B machine and tested to failure in three-point bending to determine an approximate plane strain fracture toughness designated K_Q. Transverse compact tension specimens (CR orientation) were machined for plane strain K_{IC} toughness determination. The initial portion of the crack was located at the MW and propagated toward the ID location. Precracking of the compact tension specimen was performed on a 20,000-lb capacity MTS closed loop hydraulic test system

TABLE III ROOM TEMPERATURE MECHANICAL PROPERTIES

Final Extrusion Form		Condition		Tension: 0.2% Yield Strength ksi OD	MW	ID	Ultimate Tensile Strength ksi OD	MW	ID	Elongation % OD	MW	ID	Reduction of Area % OD	MW	ID	Fracture Toughness K_{IC} or K_Q ksi$\sqrt{in.}$ OD	MW	ID
Cylindrical Hollow (30% Reduction)		STA	L	177.5	181.3	174.2	178.9	182.1	181.4	1.1	1.3	2.0	2.4	2.1	5.4	-	-	-
			T	177.3	180.0	175.6	180.0	182.5	180.6	1.4	1.9	2.4	2.4	2.6	3.4	-	51.5*	-
Solid Round (83% Reduction)	Extrus. Temp.	STA	L	145.9	154.0	-	162.7	165.0	-	10.0	5.0	-	11.0	5.5	-	-	-	-
			T	-	155.2	-	-	168.4	-	-	4.2	-	-	4.8	-	-	34.9*	-
	1650°F	DA	L	164.0	164.5	-	176.8	177.6	-	10.5	6.0	-	16.2	6.4	-	-	40.6	-
			T	-	-	-	-	-	-	-	-	-	-	-	-	-	-	-
	1850°F	STA	L	155.7	158.0	-	168.0	170.0	-	10.0	10.0	-	17.3	15.2	-	-	-	-
			T	-	-	-	-	-	-	-	-	-	-	-	-	-	41.2*	-
		DA	L	164.0	159.5	-	178.6	174.0	-	11.0	11.0	-	21.5	17.0	-	-	-	-
			T	-	-	-	-	-	-	-	-	-	-	-	-	-	48.6*	-
	2000°F	STA	L	147.9	144.9	-	158.7	161.5	-	14.0	14.0	-	27.6	22.4	-	-	-	-
			T	-	-	-	-	-	-	-	-	-	-	-	-	-	48.0*	-
		DA	L	165.8	167.5	-	180.0	182.0	-	12.0	11.0	-	23.1	11.8	-	-	-	-
			T	-	-	-	-	-	-	-	-	-	-	-	-	-	53.1*	-
Cylindrical Hollow (84% Reduction)		DA	L	173.8	177.2	176.7	190.5	194.2	190.8	9.8	6.0	8.0	14.2	7.6	10.0	43.4	44.6	45.6
			T	184.2	184.8	183.9	196.4	196.2	196.2	5.0	6.3	6.0	6.9	10.3	8.4	43.4	49.9*	48.6
		STA	L	160.0	175.1	179.5	175.8	184.5	185.6	9.3	3.7	3.0	14.0	5.5	4.0	42.1	37.3	41.5
			T	168.9	184.2	178.1	181.6	190.2	186.1	4.0	3.0	4.0	5.1	4.9	6.5	43.2	39.3	44.1

*Compact tension specimens tested in accordance with ASTM Standard E-399.

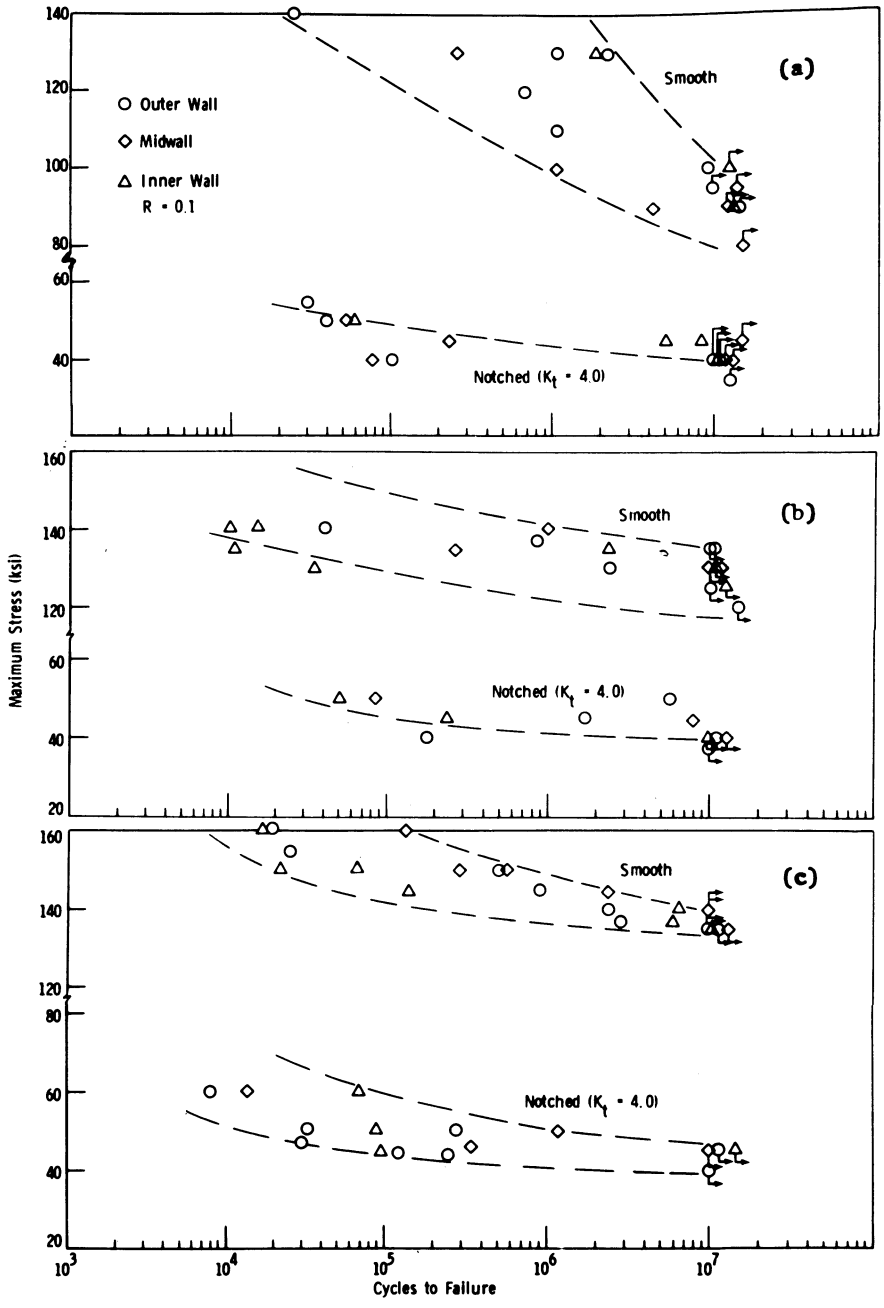

Fig. 3 - S-N curves for (a) STA material reduced 30%, (b) STA material reduced 84%, and (c) DA material reduced 84%.

and tested to failure in a 10,000-lb Instron tension machine. All precracking and testing procedures with the exception of the crack-front profile conformed to the current ASTM Standard (4). Although it is felt that these data are valid and should be reported as K_{IC} plane strain fracture toughness values, the difference between any two crack length measurements exceeds the allowable limit given in the ASTM Standard.

Stress-controlled uniaxial S-N fatigue data obtained from smooth (0.200-0.250 in. diameter) and notched (K_T=4) specimens were generated at room temperature on an SF-10U Satec fatigue machine at a frequency of 15 Hz and an R ratio ($\sigma_{min}/\sigma_{max}$) of 0.1. Here, only the longitudinal direction is considered for both levels of hot working. For the material reduced 84% (STA and DA heat treatments) crack propagation rates were determined on uniaxially loaded 1/4-in.-thick compact tension specimens tested in air and in water on the closed-loop hydraulic apparatus at a frequency of 15 Hz.

Results and Discussion

The strength, ductility, and toughness results for all extrusions are shown in Table III. Uniform high strength and excellent fracture toughness is seen for the material with the lowest amount of hot working with the STA heat treatment. Ductility is lowest with this material because of the large grain size (Fig. 1). As suggested by Bohanek (5) continuous hot working (e.g., extrusion) at sufficient reductions will reduce the grain size of large section products to a level where improved ductility is realized. The smaller grain size for the material receiving the larger amount of hot working is also shown in Fig. 1. Under tensile loading crack initiation is located in the grain boundaries as shown in Fig. 1. Larger cracks were observed in the larger grain size material (6) accounting for the grain size dependency noted above. For a given amount of reduction, increasing the extrusion temperature will reduce the beta grain size and result in the generally higher ductility values shown in Table III.

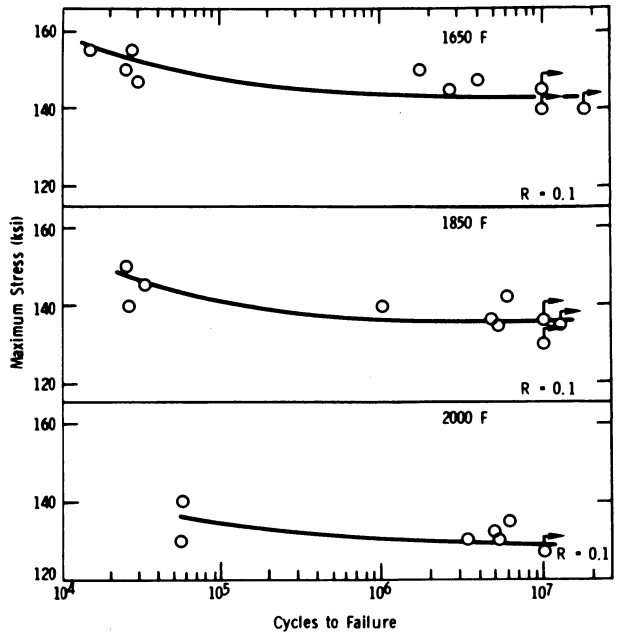

Fig. 4 - S-N curves for DA material extruded at temperatures shown.

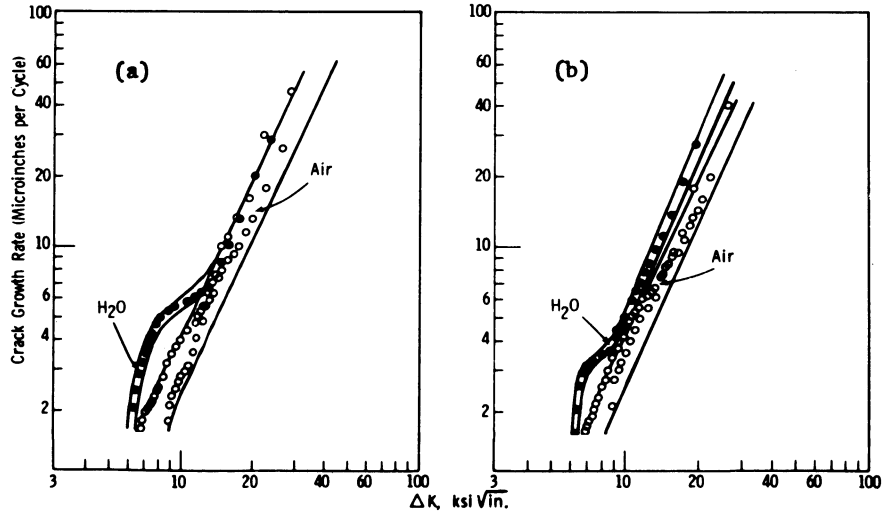

Fig. 5 - Crack propagation behavior of material given (a) direct aged and (b) STA heat treatment after 84% reduction. Shown are the rates for both air and H_2O.

It is important to note that for the material given the larger amount of hot working, the STA heat treatment results in nonuniform strength properties through-the-section. Most notable is the lower strength at the OD. Bohanek (5) also observed lower strength levels at the OD and suggested that it may be due to recrystallization that occurred as a result of lower working temperatures at the OD. For the cylindrical hollow extrusions, thermocouples attached to the billet just prior to extrusion showed the temperature to be approximately 1540°F on the skin of the billet after transfer from the 1700°F furnace. Unrecrystallized regions of metastable beta at the OD were observed, indicating that the temperature near the OD was very close to the recrystallization temperature. Subsequent solutionizing at 1475°F probably results in some additional recrystallization. Upon recrystallization there is probably a loss of dislocation structure which reduces the ability to produce a fine network of precipitated alpha during aging (7). Note the larger alpha precipitates near the OD as compared to that near the MW location (Fig. 2).

For the material reduced 83-84%, replacing the STA heat treatment with the DA heat treatment after extrusion improves the uniformity of the strength properties through-the-section. It is a generally fine alpha precipitate that accounts for the uniform properties. It is interesting to note that 1) increasing the extrusion temperature does not have a significant effect on the strength level and 2) the torsional yield (σ_{tys}) and ultimate strength (σ_{tus}) are higher for the DA heat treatment than for the STA heat treatment. For example, σ_{tys} (DA) = 185 ksi while σ_{tus} (STA) = 180 ksi and σ_{tus} (DA) = 229 ksi while σ_{tus} (STA) = 185 ksi.

Direct aging also offers more uniform and higher fracture toughness values. This appears to be dependent on the smaller amount of intergranular fracture of the DA material. This may be related to a coarse alpha precipitate morphology near the grain boundary. Note that increasing the extrusion temperature increases the fracture toughness of both DA and STA materials.

It is also interesting to note that ductility values of the material given the larger reduction were not adversely affected by the generally higher strength values offered by the DA heat treatment. For example, for the material reduced 84% the ductility level at the OD was about the same for both STA and DA materials despite a difference of about 15 ksi in strength. Metallographic examination of the cross section of broken halves of tension specimens indicated that the grain boundary cracks such as shown in Fig. 1 were smaller and less numerous for the DA material (6).

Results of high cycle uniaxial fatigue tests for the longitudinal orientation are shown in Figs. 3 and 4 where the maximum stress is plotted as a function of the number of cycles to failure (S-N curves). Because the OD, MW, and ID locations are represented, there is some scatter and as a result a band has been drawn through the data in Fig. 3. For purposes of discussion the stress level at 10^7 cycles will be referred to as the fatigue strength (σ_{fs}), and the ratio of σ_{fs} to the ultimate tensile strength is termed σ_{fs}/σ_{uts}.

S-N curves for the material that has received 30% reduction during hot working followed by STA heat treatment is shown in Fig. 3a. For smooth specimens $\sigma_{fs} \approx 95$ to 100 ksi ($\sigma_{fs}/\sigma_{uts} \approx 0.53 - 0.55$), while for notched specimens σ_{fs} is reduced to approximately 45 to 50 ksi. For the same STA condition, increasing the amount of hot working to 84% resulted in a marked increase in fatigue strength as shown in Fig. 3b. For example, the OD location shows fatigue strengths in the range of 120 to 135 ksi, considerably above previously reported results for STA material (5). At the OD this corresponds to $\sigma_{fs}/\sigma_{uts} \approx 0.68$ to 0.77, while at the MW and ID, $\sigma_{fs}/\sigma_{uts} \approx 0.70$.

For material direct aged after 84% reduction (Fig. 3c), σ_{fs}/σ_{uts} is also about 0.70. Despite the generally higher strength levels, the σ_{fs}/σ_{uts} is about the same as for the STA material with an equal amount of reduction. For example, at the OD location σ_{fs} is about the same for both STA and DA heat treatments despite an increase in

σ_{uts} of about 15 ksi, for the DA material. It thus appears that there are other factors beside strength level that influence the fatigue behavior of metastable beta titanium alloys. It is suggested that the increase in fatigue strength of the material reduced 84% could very well be influenced by the smaller beta grain size (cf. Fig. 1) in much the same way that the fatigue strength of Ti-6Al-4V is dependent on the alpha grain size (8). In light of the slight decrease in σ_{fs} with increasing extrusion temperature (smaller grain size) as shown in Fig. 4, additional work is required before a more definitive statement can be made. However, from a cursory fractographic examination of the broken specimens it did appear that the crack initiation site was well removed from the surface of the specimen indicating some microstructural influence. Lastly, it should be noted that $\sigma_{fs}/\sigma_{uts} \simeq 0.82$ for the material reduced 83% at 1650°F and given the DA heat treatment. This was the highest ratio reported for any heat-treated condition.

Turning to notched fatigue behavior it is seen that $\sigma_{fs} \simeq 45$ to 50 ksi for material reduced 30% and given an STA heat treatment. Increasing the amount of hot work in combination with a DA or STA heat treatment does little to improve notched fatigue behavior. A clue to this behavior may be found in results of recent acoustic emission studies on the notched and unnotched Ti-8823 fatigue specimens (9). These studies indicate that it is possible to separate the crack initiation from the crack propagation phase of the failure process of both types of specimens tested at R = 0.1. At the lower load the time spent to initiate the critical crack size in the notched specimen is about 15 times greater than for the unnotched specimen. Because the critical crack size is controlled by the fracture toughness value, it is not surprising to find that the materials with the highest fracture toughness lead to the best notched fatigue properties.

Crack propagation rates were determined for the material reduced 84% and given the STA and DA heat treatment. Fig. 5 shows results of tests conducted in air and water on a da/dn - ΔK plot where da/dn

is the crack growth rate and ΔK is the difference between the stress intensity factor at maximum and minimum loads for a particular crack length. In terms of the Paris power law relationship $da/dn = C\Delta K^m$, it is seen (Fig. 5) that in air there is little difference between the slope of the scatter band representing the data from the STA and DA heat treatments ($m_{STA} \approx 0.23$ and $m_{DA} \approx 0.22$). However, the crack propagation rates for both heat treatments were affected by the presence of water. For the STA heat treatment, a higher crack propagation ratio was observed in water than in air throughout the entire ΔK range, while for the DA heat treatment such an increase was most noticeable in the lower ΔK range.

Summary and Conclusions

This study has focused on the evaluation of direct aging as means for heat treating heavy sections fabricated from Ti-8823 metastable beta alloy. For sections given large amounts of continuous reduction (extrusion), direct aging affords more uniform and generally higher strength, ductility, and toughness levels than does solution treating and aging. For a given heat-treated condition, increasing the amount of hot working or increasing the extrusion temperature reduces the beta grain size. Such a reduction in grain size favorably influences ductility. High cycle fatigue resistance for the materials (both STA and DA heat treatments) which have undergone a large amount of reduction is excellent (fatigue strength/ultimate tensile strength ratios in the approximate range 0.70 to 0.80). Crack propagation behavior in air appears to be independent of heat treatment while that in an aggressive environment is affected by heat treatment.

Acknowledgment

The authors very much appreciate the dedication of Mrs. A. V. Gallagher and her staff in the preparation of this manuscript.

References

1. Wood, R. A., MCIC Report 72-11, Battelle-Columbus Laboratories, Columbus, OH, September 1972.

2. Broadwell, R. G., Coyne, J. E., "The Fracture Toughness-Tensile Property Relationships of Deep Hardenable Titanium Alloys," AIME Spring Meeting, Las Vegas, NV, May 1970.

3. Chait, R., DeSisto, T. S., "The Fracture Toughness of Three Heavy Section Titanium Alloys," AMMRC PTR 72-5, Army Materials and Mechanics Research Center, Watertown, MA, October 1972.

4. ASTM Standard E-399, ASTM Philadelphia, PA 1975, Part 10, 561.

5. Bohanek, E., "Evaluation of Several Commercial Heats of Ti-8Mo-8V-2Fe-3Al," Technical Report No. 45, Titanium Corporation of America, Toronto, OH, August 1970.

6. Chait, R., Metallurgical Transactions, 1975, Vol. 6A, 2301.

7. Adair, A. M., Roberson, J. A., Proc. Second Int. Conf. on Strength of Metals and Alloys, American Society for Metals, Metals Park, OH, 1970, Vol. 3, 932.

8. Lucas, J. J., Konieczny, P. P., Metallurgical Transactions, 1971, Vol. 2, 911.

9. Acquaviva, S. J., Chait, R., "Monitoring Fatigue Failure of a High Strength Titanium Alloy by Acoustic Emission Techniques," AMMRC PTR 75-2, Army Materials and Mechanics Research Center, Watertown, MA, June 1975.

INTENSIFICATION OF CHEMICAL-THERMAL TREATMENT OF TITANIUM AND ITS ALLOYS

L. N. Larikov, V. B. Brick, V. F. Mazanko and
V. M. Falchenko
Institute of Metal Physica, UkrSSR Academy of Sciences
U.S.S.R.

In order to increase the depth of the protective surface layer and the productivity of the technical process, the high temperature treatment of metals is usually used. The increase of the temperature, however, leads to the undesirable growth of the grains and substantially decrease of the mechanical properties of the metal (alloy) as a whole. In this connection new approaches for intensification of the thermal-chemical treatment are of great interest.

To intensify the diffusion process in titanium thermal cycling, associated with $\alpha \rightleftarrows \beta$ transformation in titanium, and rapid plastic deformation $\dot{\varepsilon} = 20\ sec^{-1}$ were used. The investigations of the diffusion processes by radioactive-tracer method for temperatures ranging from 755°C to 1030°C were made for titanium of different purity (iodide titanium and VT-1 mark titanium) the isotypes Ti-44 and Co-60 were used. Taking into consideration that the diffusion anomalies in titanium are associated with the presence of dislocation type defects in metal,[1] a special pretreatment of samples was used to minimize these defects. This pretreatment consists of the titanium deformation by about 20% and the recrystallization annealing of 10x10x10mm samples under 850°C during 20 hours, pressure in chamber being equal to 10^{-5} torr. After this procedure the average size of grains was 0.2mm.

Influence of $\alpha \rightleftarrows \beta$ Transformation on the Parameters of the Titanium Self-and Interdiffusion

The influence of $\alpha \rightleftarrows \beta$ transformation on the titanium self-and

interdiffusion was investigated on the instrument[2] using both the isothermal regime of the annealing and cyclic heating (cooling) near the $\alpha \rightleftarrows \beta$ transition temperature 883.5°C. When the selfdiffusion in β-modification was investigated, the annealings were made with the rate of 100 and 1 degrees/min with the exposition during 5 min after every heating at the β-modification temperature (the minimum temperature being equal to 600°C and 840°C accordingly). In α-modification case the cyclic annealings were made with the rate of 25 and 1 degrees/min with the exposition during 10 min at the α-modification temperature (the maximum temperature being equal to 990°C and 930°C). The interdiffusion investigations of $Co^{60} \rightarrow Ti$ under the cyclic annealing conditions were made only for the β-modification of the titanium. The rate of the heating (cooling) was about 100 degrees/min.

The diffusion coefficient were determined by means of the precise sectioning technique method.[3] For the calculation of the effective diffusion coefficient the formula[1] taking into account the temperature change was used.[4] In the case of the rapid plastic deformation calculation of the D_{ef} was made taking into account of the diffusion equation solution for the plastically deformed medium.[5]

$$TGS = - \frac{0.1086}{\sum_{i=i}^{n} D_i t_i + D_{ef} t} \qquad (1)$$

Here D_{ef} - is diffusion coefficient which can be calculated; t-is the total annealing time for all cycles at given temperature; $\sum_{i=i}^{n} D_i t_i$ - is the sum of the products of the diffusion coefficients for different temperatures and the corresponding time intervals.

Figure 1 shows the temperature dependence of the effective self- and interdiffusion coefficients for isothermic and cyclic annealing regimes. In Figure 1 it can be seen that the experimental points lie in a straight line, therefore the self- and interdiffusion coefficient change in the investigated interval can be described by an Arrhenius relation. It should be noted that the results of the self-diffusion in β-titanium under isothermal conditions of the annealing are in a good agreement with the datum of the works.[1,6] The selfdiffusion in the region of titanium α-modification was not reliably investigated previously. However, the observable value of the selfdiffusion coefficient change at $\alpha \rightarrow \beta$ transition in titanium is of the same order as in zirconium[7] metal which is the analogue of titanium.

From comparison of the self- and interdiffusion coefficients

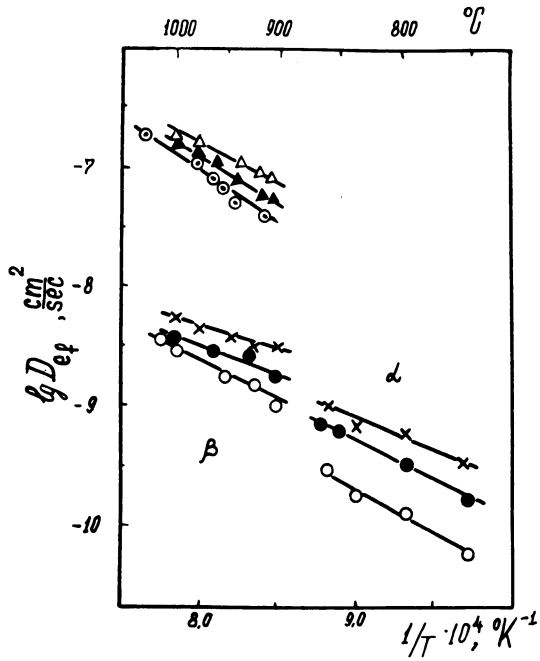

Fig. 1: Temperature dependence of effective coefficients of self- and interdiffusion, Co-60→Ti, in α- and β-modifications of titanium: ○, ⊘ - for isothermal and ●, X, Δ, ▲ - for cyclic annealings; ●, X, Δ-100 cycles and ▲ -50 cycles; ● -V = 1 degrees/min, Δ, ▲ - 100 degrees/min; X - 100 degrees/min (for β-modification) and 25 degrees/min (for α-modification).
○, ●, X - for self-diffusion, Ti-44→Ti.
⊘, Δ, ▲ - for interdiffusion, Co-60→Ti.

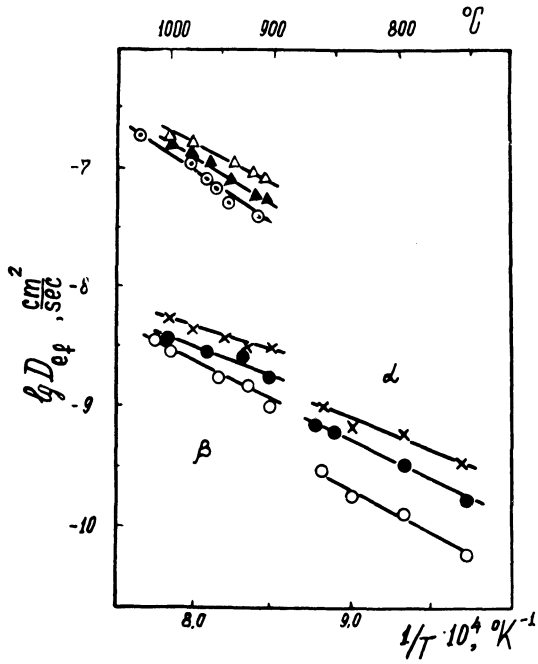

Fig. 2: Temperature dependence of effective coefficients of Co-60 in titanium: i - impulse loading ($\dot{\varepsilon}$ = 20 sec^{-1}); 2 - molten state; 3 - steady isothermal annealing.

obtained under different annealing conditions following the $\alpha \rightleftarrows \beta$ transformation which takes place at cyclic heating (cooling), there is an essential diffusion mobility increase of atoms in the α- and β-titanium modification. The effect of the selfdiffusion rate increase is observed also at the comparatively low heating (cooling) rates. For high-temperature modification the largest effect is observed at temperatures near the phase equilibrium point T_o=883.5°C.For the low-temperature modification this effect increases as the difference between sample temperature and T_o increases.

The increase of the number of $\alpha \rightleftarrows \beta$ transition traverses as evaluated from $Co^{60} \rightarrow Ti$ interdiffusion data leads to the rise of diffusion rate with respect to the data D_{ef}, obtained in isothermal annealing conditions, Fig. 1. Considering the influence of $\alpha \rightleftarrows \beta$ transformation on the diffusion parameters in α- and β-modification it is useful to pay attention to the regularities of the transformation process itself. The investigation of $\alpha \rightleftarrows \beta$ transformation in titanium was made by means of the isochronal annealing in range $1 \cdot 10^{-2}$ - $1 \cdot 10^{2}$ degrees/min on an X-ray diffractometer equipped with the high-temperature device GPWT-1500, that the $\alpha \rightleftarrows \beta$ transformation in titanium take place in interval 20-40 degrees only by progressive heating (cooling); where the isothermal exposure was made the process transformation is stopped.

The cooling from β-modification region lead to formation α-modification with typical martensitic relief. The repeated $\alpha \rightleftarrows \beta$ transformations lead to development sub-and grain structure of α-modification associated with passing dynamic recrystallization. The similar kinetic regularities of $\alpha \rightleftarrows \beta$ transition and the morphology of α-modification crystals testify about martensitic mechanism transformation of titanium. This was in agreement with the data communicated in another works, for example[8]. Therefore, the increase of the diffusion rate processes in titanium takes place by martensitic mechanism transformation.

It should be noted that the increase of the rate of self-diffusion by the martensitic mechanism transformation took place also for cobalt and thallium.[9,10] But the effect of raising of atom diffusion mobility in these metals when transformation was going according to normal mechanism was practically absent.

The use of cyclic annealings (with the crossing of phase of transformation temperature) was approached for the chemical-thermal treating of the manufactures of VT-1 titanium with the 0.01mm thick Co-60 coating made by galvanic method.

It was proved that condition of multiple $\alpha \rightleftarrows \beta$ transformation the Co protective layer thickened, scale-resistance of items im-

proved, and total technological time of chemical thermal treating was two times less. As it was mentioned the stated condition of chemical-thermal treating was accompanied also by the formation of fine-grain structure matrix beneficial for mechanical qualities of items.[11]

The Influence of Rapid Plastic Deformation on Diffusion in Ti

Investigation of rapid plastic deformation influence on atom diffusion mobility were carried out on VT-1 titanium samples. Rapid deformation of Ti was carried out on special apparatus characteristics of which gave us the possibility to vary plastic deformation speed and temperature in wide range.[12] In this case the speed of deformation was constant and was equal to 20 sec^{-1} while deformation rate of samples did not exceed 10-15%, the time of deformation was near 0.005 sec.

Diffusion mobility of Co-60 in Ti was studied within temperature interval of from 650°C to 1100°C including both α- and β-modification. Diffusion rates were calculated by method described in the work.[13] The effective diffusion coefficients of Co in Ti received by this method (deformation speed = 20 sec^{-1}) are presented in Figure 2. On the same figure the well known temperature plots corresponding to effective coefficients diffusion which were obtained under conditions of rapid plastic deformation can be laid on straight line. This circumstance gives us the possibility to make a conclusion that the change in values of the effective diffusion coefficient of Co in Ti in rapid deformation within investigated temperature intervals as well as in case of steads isothermal annealing can be described by an Arrhenius dependence.

The analysis and comparison of data given in Figure 2 show that values of D_{ef} for rapid ($\dot{\varepsilon}$=20 sec^{-1}) plastic deformation are anomalously high and few orders exceeds not only the rates of Co diffusion in Ti determined in steady isothermal annealing but which is most interesting, rates of diffusion in molten metal. It is seen from Figure 2 that increase of the effective diffusion coefficient values during rapid deformation rises when the temperature reduces and considerably differ in α- and β-modifications of Ti. The comparison given on Figure 2 shows that the increase D_{ef} values for Co in β-Ti with close-packed (hcp) lattices in rapid deformation is noticeably higher than with friable (bcc) lattice of β-Ti and makes with the extrapolation of $\alpha \rightleftarrows \beta$ phase transformation temperatures two orders. In the result if diffusion coefficient Co in Ti in steady conditions during $\alpha \rightarrow \beta$ transformation jumps approximately one order up in conditions of rapid deformation we observe the opposite effect that is that diffusion coefficient during $\alpha \rightarrow \beta$ transformation

decreases also approximately on one order (Fig. 2).

Hence, plastic deformation with the speed of 20 sec^{-1}, cycle heating (cooling) with the crossing of $\alpha \rightleftarrows \beta$ transformation point lead to substantial rise of atom diffusion mobility in Ti, value of increase of D_{ef} in case of rapid deformation depending on the metal lattice type and being considerably higher indensity packed α-modification.

Mechanism of Influence of Polymorphous Transformation and Rapid Plastic Deformation on Atom Diffusion Mobility

As stated before during phase transformation martensitic mechanism of $\alpha \rightleftarrows \beta$ transformation is responsible for observed increase of atom diffusion mobility in α- and β-Ti.

This conclusion corresponds with the image of influence of interphase boundary on defect generation during its movement. It is known that for martensitic mechanism of transformation the presence of semicoherent sliding boundary containing screw dislocations is characteristic for growing crystals. During motion in real crystal jumps (bends) are formed on the latter. Their nonconservative motion with sufficiently high speeds is accompanied by generation of point defects of vacancy type.[16,17] As a result the atom diffusion mobility in crystal matrix rises. In condition of normal mechanism of transformation large corner boundary are powerful sink of different defects themselves. This mechanism of growth as known[18] leads to formation of comparatively nondefectless crystals, which do not possess an abnormally high atom diffusion mobility. In other words, the observed acceleration diffusion mobility during polymorphous transformation, going by martensite mechanism in investigated range of speeds of heating (cooling) can be explained within the frame of usual vacancy diffusion mechanism.

But in case of rapid plastic deformation (20 sec^{-1}), where rate of diffusion in solid phase is several orders higher than that in molten metal, observed effect cannot be described within the frame of above mentioned mechanism. To explain the observed abnormally high rate of diffusion in solid phase, it will probably be necessary to enlist new, non-traditional view on possible mechanism of diffusion. Most probably that the described effect can be linked to the fact that considerable tensions and deformations appearing in Ti during rapid plastic deformation lead to essential rise of motion speed of screw dislocations with jumps (bends). As a result their nonconservative motion in crystal is accompanied by generation of not only vacancies but of the considerable quantity of interstitial

atoms[17,19] by the high mobility of which the anomalous acceleration of diffusion can be explained.

Therefore, rapid plastic deformation leading to anomalous acceleration of diffusion mobility of atoms can be widely used for intensification of processes of chemical-thermal processing of Ti and its alloys. It will give the possibility to raise the efficiency of process owing to the sharp reducing of processing time and to improve the exploitation qualities of products at the expense of deepening the penetration of saturation element into metal.

References

1. Le Claire, A. D., Diffusion in body-centered cubic metals, American Society for Metals, 1964.

2. Falchenko, V. M., sb. Siffuzionye processy v metalakh, Izd. "Naukova Dumka," Kiev, 1968, 71.

3. Gruzin, P. L., Dokl. Akad. Nauk SSSR, 1952, 86, 2, 289.

4. Gertzriken S. D. and Dekhtyar, I. Ya., Solid state diffusion in metals and alloys, State Publishing House for Physical-Mathematical Literature, M., 1960.

5. Lybov, B. Ya and Fastov, N. S., Fizika metalov i metallovedeniya, 1960, 10, 310.

6. Murdock, I. F., Diffusion in body-centered cubic metals, American Society for Metals, 1964.

7. Lyashenko, V. A., Bykov, V. N. and Pavlinov, L. V., Fizika metalov i metallovedeniya, 1959, 8, 3, 362.

8. McQuillan, A. D. and McQuillan, M. K., Titanium in Industry, London, 1952.

9. Brick. V. B., Larikov, L. N. and Falchenko, V. M., Ukrainsky Fizichesky Jurnal, 1975, 20, 3, 397.

10. Brick, V. B., Larikov, L. N. and Falchenko, V. M., Metalofizika, Izdaniye Akad. Nauk USSR, Kiev, 1976, No. 63.

11. Larikov, L. N., Falchenko, V. M., Mazanko, V. F., Stetzenko, I.V., and Yurchenko, I. F., Buleten izobreteniy, N 19, 1975, N471398.

12. Larikov, L. N., Falchenko, V. M., Mazanko, V. F., Gurevich, S.M., Kharchenko, G. K. and Ignatenko, A. I., Avto-maticheskaiya svarka, 1974, No. 5, 19.

13. Larikov, L. N., Falchenko, V. M., Mazanko, V. F., Gurevich, S. M., Kharchenko, G. K. and Ignatenko, A. I., Dokl. Akad. Nauk SSSR, 1975, 221, 5, 1073.

14. Morgan, D. W. and Kitchener, I. A., Trans. Farad. Soc., 1954, 50, 51.

15. Sparke, B., James, D. W. and Leak, G. M., J. Iron Steel Inst., 1965, 203, 152.

16. Frank, F. C., Acta Met., 1953, 1, 15.

17. Friedel, J., Dislocations, Pergamon Press, Paris, 1964.

18. Larikov, L. N. and Zasimchuk, E. A., Izuchenie defektov Kristallicheskogo stroeniya metallov i splavov, "Naukova Dumka," Kiev, 1966, 70.

19. Hirth, J. and Lother, J., Theory of dislocations, New York, 1972.

EFFECT OF BORONISING ON ADHESIVE WEAR CHARACTERISTICS OF TITANIUM

H. S. Alsalim and T. S. Eyre

Brunel University, Uxbridge, Middlesex UBB 3PH

England

A pin-on-disc technique has been used to investigate the adhesive wear (galling) characteristics of C.P. Ti and I.M.I.318 under dry sliding conditions. Both materials exhibit running-in before equilibrium wear is established and also show mild/severe transitional behaviour. The wear characteristics of I.M.I.318 are considerably superior to C.P. Ti. Boronising, which is a surface diffusion process, produces titanium borides which inhibit adhesive wear and prevent metal transfer from the pin to the disc surface. The load-bearing capacity of both materials is considerably increased by boronising.

INTRODUCTION

Titanium and its alloys have now become major materials of construction in the general engineering, chemical and aircraft industries. Its good combination of strength, low weight and corrosion resistance, however, have to be balanced against its poor tribological properties. The poor galling and fretting characteristics of these alloys have necessitated the development of a wide range of surface treatments which include diffusion, electroplating and sprayed and plasma coatings. The galling characteristics of titanium have been attributed to its electron structure[1] and its low capacity for strain hardening which is associated with the c/a ratio of its hexagonal structure. One of the methods, therefore, of improving its frictional and wear properties is to alloy with a metal which increases the c/a ratio and in this respect aluminum is particularly beneficial[2]. All conventional boundary lubricants have been shown to be entirely ineffective on titanium, although those containing iodine appear to be satisfactory[3].

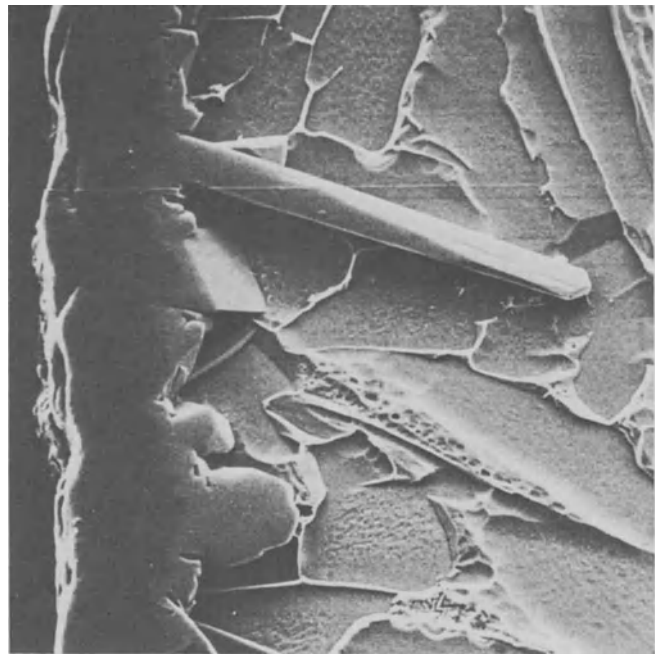

Fig. 1: Microstructure of boronized I.M.I.318 (x1.1K)

High friction leading to stick-slip behaviour and poor adhesive wear behaviour against both itself and steel have been major industrial problems both during processing and application of these alloys. A particular feature of this problem is the metal transfer which occurs to produce smeared layers on the counterface materials. The surface treatments commercially used vary considerably in their ability to prevent adhesion. One of the major problems in their development has been the lack of a suitable experimental technique to discriminate between the various features of wear behaviour. The use of the pin-on-disc technique used in this investigation has helped considerably in the understanding of adhesive wear and the role of boronising.

This paper describes the effect of boronising of commercial purity titanium (C.P. Ti) and I.M.I.318 (6%Al, 4%V) on friction and wear sliding against steel. Boronising is a surface diffusion treatment carried out in a pack medium during which boron diffuses into the surface to form metallic borides. The outermost layer is likely to be TiB_2 but other chemically different borides are also present as indicated by the phase diagram. The boronised structure of I.M.I.318 is shown in Figure 1, which shows at least two distinct layers and a saw tooth interface with the matrix. Some boride spikes are also present and these penetrate to a depth of 0.08 mm and it is this microstructure which contributes to the good adhesion of the coating to the substrate. The thickness of the boronised layer is between 0.025 to 0.045 mm and its surface hardens is approximately 200 H_V in comparison with 500-525 H_V for the α/β substrate.

Wear Evaluation

Titanium wear pins (6.25 mm diameter, 3 cm long) with a flat and were rubbed against a low alloy steel disc (0.4% C, 1.1% Cr. 1.5% Ni) which had been heat treated to a hardenss of 350 H_V. The rubbing speed was kept constant at 300 cm per second. The load applied to the wear pin was varied over a wide range (2 kg to 32 kg). This wear technique, usually referred to as the pin-on-disc, has ben widely used by other investigators and one of the present authors has been an identical technique to investigate the properties of boronised steel[4]. Friction force and wear of the pin were measured continuously using linear displacement transducers. The duration of test varied from 90 to 300 minutes depending upon the response of the materials. A particular feature of this technique is the continuous graphical record of friction and wear. Examination of the graphical record enables different stages of wear to be recognised and separated. For each material tested a new pin and new disc were used for each test and these were chemically cleaned immediately prior to the commencement of the test. All experiments were carried out dry in normal labaoratory atmosphere at 60-70% relative humidity and a temperature between 15-22°C. For each

(a)

Fig. 2: Appearance of C.P. Ti debris from different wear regions.
a) first metallic region
b) oxidative region
c) second metallic region

(b)

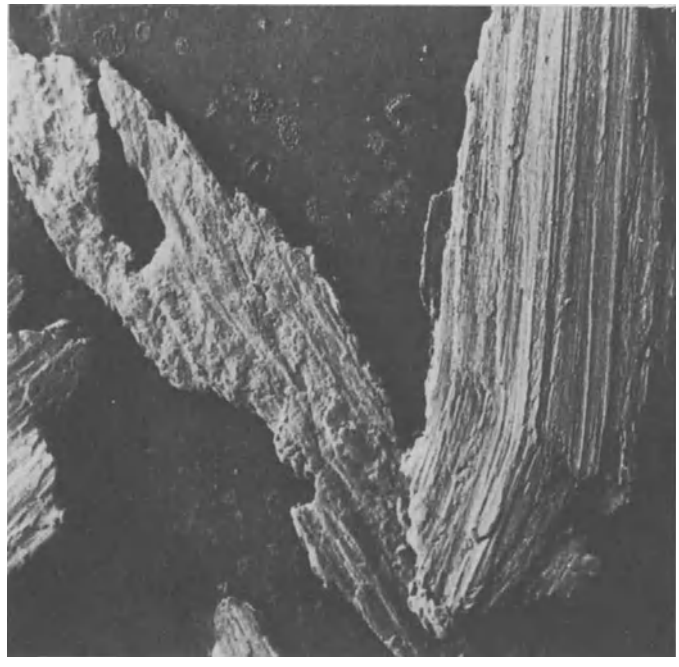

(c)

material tested at least ten separate experiments were carried out. Sufficient tests were carried out for each material and condition to obtain a transitional wear diagram.

Results

Wear rate (gm per cm of sliding) depends on load. For all materials there is a transition from a low wear rate (mild wear) to a high wear rate (severe wear) at some critical load. The transitions are sharp with the exception of that for commercial titanium. For both materials the effect of boronizing is to reduce mild wear rate and increase the transition load.

Commercial titanium exhibited metallic wear at the lowest load with titanium particles transferred to the steel disc surface and the production of a metallic debris. From 3.0 to 7.5 kg an oxide layer formed on the disc surface, but spalled away to form a fine oxide debris. The wear rate increased considerably as the load increased. Metallic wear commenced at 7.5 kg with the production of debris which was larger than that produced at loads below 3.0 kg. The size and appearance of the various debris fractions are shown in Figure 2, which would suggest that the two regions of adhesive wear appear similar but different in scale. At higher loads wear takes place by gross plastic flow accentuated by the effect of frictional heating. The effect of boronising was to inhibit metallic wear at leads below 3.0 kg and considerably reduce mild wear at all loads up to the transition at 7.5 kg. This intermediate region of oxidative wear is promoted by work hardening and sufficient friction heating to cause oxidation.

The wear characteristics of I.M.I.318 are a considerable improvement on C.P. Ti. The effect of boronising is even more remarkable, the mild wear rate being reduced by over an order of magnitude and increasing only slightly as the load increases. The mild/severe transition load is increased from 10.5 kg to 30 kg.

The mild/severe transition diagram does not do justice to all the wear characteristics of these materials because in the case of the non-boronised metals the equilibrium wear rates were preceded by some running-in wear of a metallic nature. This behavior was seen in I.M.I.318 at 6.4 kg where the running-in wear was completely inhibited by boronizing and a considerable time elapsed before the coating was worn off the wear pin, which then resulted in a higher wear rate. The wear rate during running-in was considerably higher (4.23×10^{-7} gm/cm) than the equilibrium wear rate (3.2×10^{-8} gm/cm) and

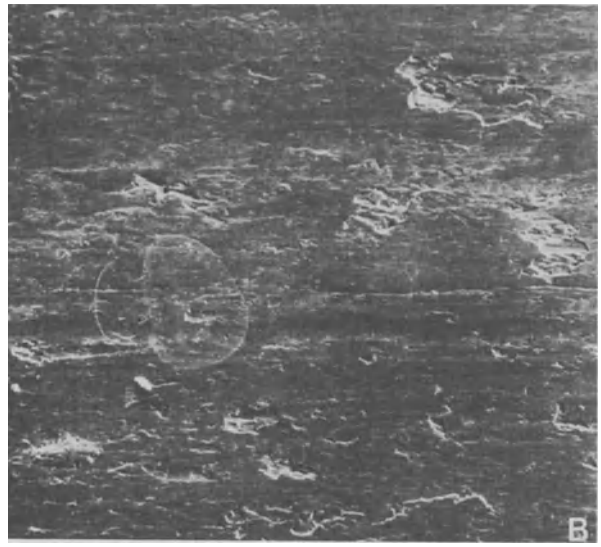

Fig. 3: Wear tracks on steel disc counterface (x 200) 6.4 Kg 300 cm per sec)
a) Non-boronized showing adhesive wear and metal transfer
b) Boronized showing no adhesive or metal transfer

(a)

Fig. 4: Adhesive wear of I.M.I. 318 on steel c counterface.
a) Direct view of steel surface and adhered titanium metal x 200
b) Taper section through (a) x 1K
c) Electron image for titanium x 1K

(b)

(c)

the actual weight loss (0.27gm) accounted for approximately 70 percent of the total wear. This would probably have been enough for engineering components to have been sufficiently damaged to prevent further use. Running-in weight loss increases with load for both metals. The actual improvement brought about by boronizing, therefore, is greatest at higher applied loads. Even when the boronized layer has been worn off the subsequent wear rate is considerably lower than that for non-boronized surfaces at the same applied load. This indicates, therefore, that the counterface surfaces have become conditioned by virtue of the production of a smoother topography and a harder surface structure.

Adhesive wear (galling) of I.M.I.318 is shown in Figure 3 which is characteristic also of C.P. Ti and this feature is produced both during running-in and above the mild/severe transition load. Titanium is transferred from the wear pin by shear and metal transfer and adheres to the disc surface, producing a rough smeared appearance. Use of the taper microsection scanning-electron microscopy technique described elsewhere[5] shows the intimate nature of the Ti/steel interface (Figure 4). This technique allows simultaneous examination of the wear surface and the substrate. It is possible to see the plastic flow which is similar in appearance to structures produced by explosive forming. Boronising completely suppresses this type of behaviour until severe wear occurs at very much higher loads with much higher surface temperatures being observed.

Discussion

Both C.O. Ti and I.M.I.318 exhibit mild/severe wear characteristics and in this respect are similar to many other metals and alloys[6.7]. Both alloys exhibit classic adhesive (galling) wear with metal transfer from the pin to the disc surface. Wear of I.M.I. 318 is considerably less than that of C.P. Ti and it may be used at much higher loads before severe wear occurs. The effect of boronising is to produce a very hard, strongly adherent coating containing titanium borides. This coating retains its hardness up to a temperature of approxiamtely 1000°C and this could be an advantage in hot wear applications. Its thermal stability also resists the softening effect of friction heating.

Boronising inhibits adhesive wear and consequently prevents running-in wear and also reduces the equilibrium mild wear rate. Prevention of adhesive wear is more likely to be due to chemical inertness of the boride surface rather than its high hardness. The life of the coating is inversely related to the applied load and even after the coating has been worn away, wear rates are still considerably reduced, probably because a harder and smoother surface has been produced. This effect is similar to that detected on other chemical diffusion surfaces on steel [4]. The mild/severe transition

load is increased and when severe wear commences it occurs with the generation of considerable heat (> 750°C). From other investigations into abrasive wear resistance of titanium alloys[8] it was concluded that hardness is the controlling factor. It would appear, therefore, that the high hardness of the boronised layer could also bring about increased abrasive wear resistance.

CONCLUSIONS

1. Hard thermally stable titanium boride coastings can be produced by a simple pack process.

2. Boronising prevents adhesive (galling) wear and consequently considerable reductions are obtained in wear rates and the mild/severe transition load is increased.

3. The boronised layer is eventually worn away, but even after its removal the wear rates are still lower than would be expected on non-boronised titanium.

ACKNOWLEDGMENTS

One of the authors (H. Alsalim) is grateful to the Science Research Council for their support in the form of a Research Fellowship. Both authors than Borax Consolidated Ltd. for their continued encouragement and the provision of financial support. We are grateful to Imperial Metal Industries for the supply of titanium.

REFERENCES

1. Nosovskỳ, I. G., Zaporozhets, A. A., Investigation of Friction and Wear of Certain Metals in Liquid Nitrogen. Sov.Mat.Sci. 4 (1968) 416.

2. Buckley, D. H., Johnson, R. L., Friction, Wear and Adhesion Characteristics of Titanium-Aluminim Alloys in Vacuum. NASA, TN D-3235, Jan. 1966.

3. Owens, R. S., Roberts, R. W., Barnes, W. J., Iodine as an Extreme Pressure Lubricant Additive. Wear, 9 (1966), 79.

4. Eyre, T. S., Effect of Boronising on Friction and Wear of Ferrous Metals. Wear, 34, (1965), 383-397.

5. Eyre, T. S., Dutta, K., Some Applications of the Scanning Electron Microscope in Wear Studies. ASLE, 31 (10), October 1975, 521-529.

6. Eyre, T. S., Wilson, F., Wear of Grey Cast Iron Under Unlubricated Sliding Conditions. ASLE, 29, February 1973, 65-72.

7. Welsh, N. C., The Dry Wear of Steels. Phil.Trans.Roy.Soc. (london), A257 (1965), 31-70.

8. Bayer, R. G., Baker, D., Ku T.C., Abrasive Wear by Paper. Wear, 12, 1968, 277.

ANTISEIZING PROPERTIES OF TITANIUM ALLOYS UNDER DIFFERENT CHEMICAL AND HEAT TREATMENT

Ju. M. Vinogradov, V. D. Dovzhenko and E. M. Polikarpova

Research Institute of Chemical Engineering

U.S.S.R.

Chemical and heat treatment (CHT) of titanium alloys for preventing their failure upon friction is based on general principles designed for ferroalloys but has its own characteristic properties related to the different chemical nature of these metals. The development of antiseizing CHT of ferroalloys was made based on the conception that a decrease in friction between metal surfaces and prevention of seizure upon friction was achieved by modifying friction surfaces with chemical compounds. As a result friction surfaces have lower resistance to shear, microcontact rupture upon friction is localized and is not followed by the tearing out of depth metal.[1,2] From this conception it is stemmed that to obtain a high antiseizing effect chemical interaction between active compounds entering into the composition of salt baths used for CHT (or into the composition of material lubrication) and friction metal surfaces[3] is necessary. In accordance with this conception the choice of chemical compounds for chemical and heat treated titanium alloys is made with the use of the method of thermography applied advantageously upon the development of sulphurization methods for ferroalloys.[3] Chemical interaction was determined by the appearance of characteristic current on the heating curve of a differential thermocouple.

In order to evaluate the change in antifriction and antiseizing properties of titanium alloys different types of friction machine were used, namely: a four-roll friction machine that shows the load at which the seizing of rubbing specimens begins; a friction machine with backward-rotary motion of specimens based on the disk-spherical slider arrangement. At multiple passes of this machine the friction coefficient was measured at specific pressure in the range from 10 to 30 kgf/mm^2 and an average rate of sliding equal to 0.04m/min.

Table I

Alloy grade	Without being CH treated	CH treated
BT1-0	10	120
BT-5	35	55
BT3-1	30	75
BT-16	22	105
OT4-1	18	120
AT-3	20	120
AT-6	45	80

The following grades of titanium used in the machine building industry of the USSR were studied: BT1-0, OT4-1, OT4-Y, BT3-1, BT-6, AT-3, AT-6, etc.*

The recording of thermograms on the Kurnakov pyrometer allowed the following regularities of modifying titanium alloys to be revealed. Unlike ferroalloys for which the greatest effect is obtained when the surface is enriched with chemical compounds including the VI group elements (sulphur, selenium, tellurium) for titanium alloys these compounds give a less significant effect. The more active effect is obtained upon treatment of titanium alloys in salt baths containing the VII group compounds, in particular iodine compounds.

Figure 1 shows a thermogram of interaction between AT-3 titanium alloy and cadmium iodine. Two thermoeffects are seen: the melting of cadmium iodine at 390°C and interaction between cadmium iodine and AT-3 titanium alloy cutting. The close temperature range was obtained for other titanium alloys.

BT1-0 chemically pure titanium showed the highest activity upon chemical interaction. The higher the alloying of titanium the weaker is the modifying effect. In this respect there is an analogy with the processes of ferroalloy sulphurization.

*Editor's Note: Chemistry should be given.

Tests performed on the friction machines have confirmed a high efficiency of chemical and heat treated titanium alloys in a cadmium iodine salt bath. It is seen from Table I that CHT increases a seizing load measured on the four-roll friction machine by several times. The highest effect is obtained with BT1-0, OT4-1, AT-3 titanium alloys.

Seizing loads of titanium alloys in kgf obtained on the four-roll friction machine are given in Table I.

Owing to CHT it is possible to use titanium alloys in friction couples without lubrication. And conversely, without CHT these alloys are highly sensitive to catching. When measuring the friction coefficient under the severe conditions (a spherical slider 8mm in diameter was running with friction against a disk without librication a non-treated couple was exposed to seizing immediately. When the disk was subjected to CHT sliding occurred without seizure. In Table II the friction coefficients are given that were obtained at the beginning and the end of the test.

BT1-0 and BT-14 titanium alloys served as a construction material for the disk give the best results with the friction coefficient is practically constant. The use of BT3-1 alloy shows an increase in the friction coefficient by a factor of 1.5-2.0.

The friction coefficient characterizing seizure of titanium alloys corresponds to the value of 0.5-0.7.

The positive results obtained gave the basis for testing the developed method of CHT for threaded joints made from titanium alloys.

Before using this method in the working conditions laboratory tests on threaded friction couples were performed. The nuts were made from OT4-1 alloy and subjected to chemical and heat pretreatment while the screws were made from BT3-1 and BT-6 alloys without any pretreatment.

As part of the tests simulation of the running of a real bolt joint subjected to frequent assembly and disassembly was carried out. Screw thread pressure varied from zero to a maximum by the sinusoidal law. The rate of relative displacement of contact screw threads varied from a maximum to zero according to the variation in specific pressure of 200kgf/cm^2 at the end of joint tightening.

For a non-treated joint seizure occurred after 2-3 turns of the nut. With the treated nut its running ability extended to more than 1000 tightenings. Figure 2 shows wear following 500 tightenings which was 2-4mg for the screws and 15-20mg for the nuts. The threaded couple with BT-6 screw shows its advantage in lower wear.

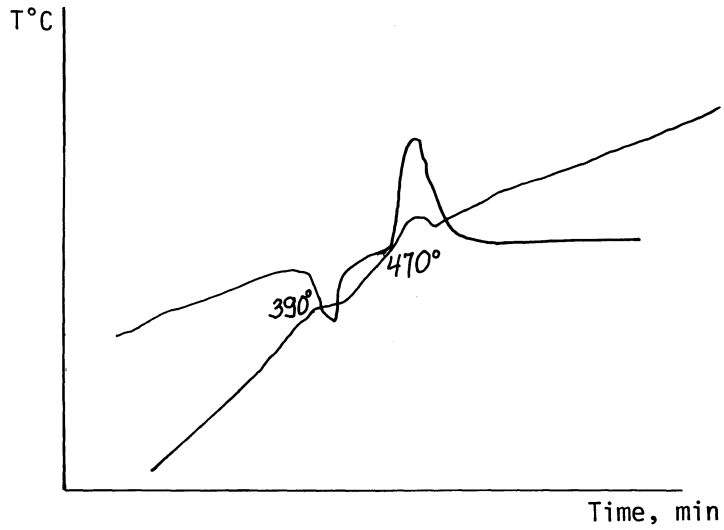

Fig. 1: Thermogram of interaction between cadium iodine and AT-3 titanium alloy.

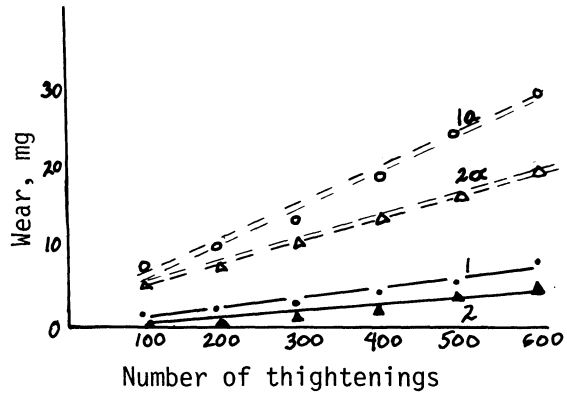

Fig. 2: Wear variation upon repeated loading:
1 - BT3-I screws; 2 - BT-6 screws
Ia and 2a - OT4-I conjugated nuts

Table II

The Friction Coefficients for Different Titanium Alloys

Construction material for spherical slider	Construction material for flat specimen	Friction coefficient	
		per cycle	at the end of tests
BT1-0	BT1-0	0.14	0.15
BT1-0	BT3-1	0.20	0.40
BT1-0	BT-14	0.17	0.22
BT3-1	BT1-0	0.19	0.14
BT3-1	BT3-1	0.14	0.27
BT3-1	BT-14	0.14	0.18
BT-14	BT1-0	0.16	0.16
BT-14	BT3-1	0.20	0.32
BT-14	BT-14	0.19	0.19
BT-16	BT1-0	0.17	0.17
BT-16	BT3-1	0.20	0.40
BT-16	BT-14	0.16	0.18
Steel 30X1CA	BT1-0	0.17	0.27
Steel 30X1CA	BT3-1	0.24	0.40
Steel 30X1CA	BT-14	0.20	0.26
Alloy AA-19	BT1-0	0.40	0.50
Alloy AA-19	BT3-1	0.48	0.60
Alloy AA-19	BT-14	0.38	0.45

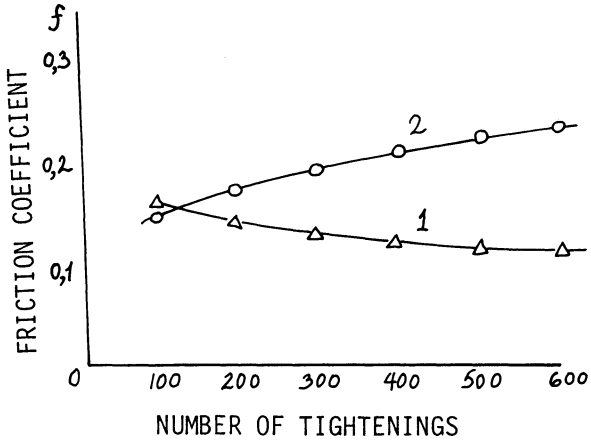

Fig. 3: The variance of friction coefficients upon repeated tightenings of BT3-I (I) and BT=6 (2) screws and OT4-I nuts

The friction coefficients remained low; following the first 200 tightenings they became practically stable in the range from 0.18 to 0.20 for the BT-6 screw and from 0.12 to 0.14 for the Bt3-1 screw (Fig. 3).

With the results obtained CHT was used for fabricating separators of COC-501T-2 type from AT-6 and AT-3 alloys chosen based on the set of mechanical properties.

AT-3 nuts were treated in the cadmium iodine bath. As rig trials showed the threaded couples had been running trouble free for a preset service life (4000 repeated tightenings) with low and stable friction coefficients of 0.1-0.12 without any seizure in conjugated screw threads.

CHT in the cadmium iodine bath for titanium alloys has been introduced at a machine building plant. It takes from 40 min. to one hour. As a result of CHT the titanium alloy surface is modified in the order of 5-10 in depth and turns into dark grey or blue color. The process is simple, inexpensive and very economical.

A new method of chemical and heat treatment belongs to the treatment methods based on chemical interaction between metal sur-

faces and active chemical compounds followed by the appearance of a modified surface layer. It is established that iodine compounds may be used for titanium alloys. For titanium alloys CHT in the cadmium iodine salt bath leads to a significant reduction in the friction coefficient and provides seizureless friction without lubrication. Comparison to the well-known surface treatment methods with the aim of improving their antiseizing properties and wear resistance has shown that a new method of chemical and heat treatment for titanium alloys is the most effective and economical.

References

1. Frink, M. , Transactions of the American Society, Steel Treatment, 1930, 17, VIII.

2. Vinogradov, Ju. M., Influence of lubrication on seizing upon Cutting Metals, Machine Part Surface Quality. Sb. 1, AN SSSR, M. 1951.

3. Vinogradov, Ju. M., Friction and wear of modified metals, "Nauka," Moscow, 1972.

Discussion

Section IX. Phase Transformations in Titanium Alloys. Thermal and Thermomechanical Treatment Techniques

L. I. Zakharova

Is there an α_2-phase in zirconium alloys and, if there is, does it have any similarity with the α_2-phase in titanium alloys?

J. C. Williams

The comparable ordered phase in Zr base alloys is ZR_3Al which has a face-centered cubic Ll_2 structure. I think that these two phases are completely different and the DO_{19} α_2-phase, as such, simply does not exist in zirconium systems. Zirconium-aluminum and titanium-aluminum alloys are of great interest. It is yet not clear what elements are to be added for the α_2-phase ordering prevention in titanium-aluminum alloys.

V. S. Tompsinsky

Do you use high-temperature X-ray diffraction and what promise does this method hold for the future?

J. C. Williams

We make use of the high-temperature X-ray diffraction and consider it to have a very strong potential. The difficulty I foresee is that the information available to us relates only to a thin surface layer. And since we can contaminate this surface when the temperature is raised, interpretation of the final result becomes difficult.

R. I. Jaffee

1. Why are the coherent precipitation sequences in titanium alloys, for example $\beta+\omega$ and $\alpha+\alpha_2$, not as useful as it is in nickel-base alloys? The precipitation of the γ'-phase in nickel-base alloys is known to have a special importance for high-temperature strength.

2. Why are precipitations of intermetallics from the α and β-phases also not useful? As has been indicated by Professor Williams, the chief precipitate that we make practical use of is the α-phase. Meanwhile, studies have been recently reported which investigated Ti_2Cu precipitation from the α-phase, which can be considered as useful. There is also evidence of other intermetallics precipitation during β-phase decomposition.

3. Why is it that we have no HSLA titanium alloys? HSLA is a term used for steels and implying high-strength low alloy. For the most part, titanium alloys are high alloys. The characteristics of the HSLA alloyed steels are that precipitation occurs during controlled rolling. What would be an equivalent situation in titanium alloys?

I don't think we have paid enough attention to such factors as rolling temperatures and the possibilities of controlling grain size by controlling rolling process. One should, perhaps, study β-enriched alloys having an element capable of precipitating during deformation, for example, in the form of carbide, but more stable than titanium carbide.

4. Have we made full use of the possibilities of transformation to martensite? Most of the works on transformation from β to martensite of various types deal with the reverse transformation. If martensite is made up of very sluggish alloy elements one could get a reversion with an increase in dislocation density similar to the reversions possible in iron-nickel alloys.

5. What uses have been made of transformation from liquid titanium to solid titanium? Is it possible to produce very useful microcrystalline or even amorphous titanium alloys by rapid cooling from the melt? What elements would be useful? One looks for deep eutectic forming elements. These aren't many in titanium, perhaps silicon is the only one, but I suggest that perhaps eutectoid forming elements like iron, copper, nickel might be useful in amorphous titanium alloys. That is something we can talk about for years ahead.

J. C. Williams

1. One of the causes for the inadequate appeal of $\alpha+\alpha_2$-phase mixture is, in my opinion, the fact that α_2-phase (Ti_3Al) does not have the positive temperature dependence of the yield strength that Ni_3Al exhibits. As to the $\beta+\omega$ mixture, our work at Rockwell and that elsewhere has shown that $\beta \rightarrow \omega$ precipitation is extremely sensitive to composition and heat treatment and probably cannot be controlled adequately in practice.

2. I agree with you. The precipitation of compounds did not find acceptance due to the fact that they always precipitate according to an eutectoid reaction which occurs in eutectic systems having a tendency to severe freezing segregation.

If titanium powder metallurgy gains wide acceptance and ingot inhomogeneity is eliminated, this question can be reopened. At least it will be possible to carry out research in this area to explore the potential of the eutectoid alloys. Not only technological, but also economic questions must also be examined in the case of powder metallurgy.

3. High-strength low alloy (HSLA) alloys

To obtain the required properties in β alloys, these must be processed by the same method used for high-strength steels. I don't think that β alloys obtained in this way can be used for the manufacture of large-size semi-fabricated products. They will primarily be used in production of forgings as well as sheets and plates. This will require a very careful control of the manufacturing process. Because of the solute concentration needed to retain the β-phase, these would not be truly "low alloy" but this is only semantics.

4. As to martensite, many studies are known to discuss the problem of stress-induced martensite. According to my observations, stressed martensite is always orthorhombic, rather than hexagonal. One of the problems associated with the use of orthorhombic martensite is the problem of ductility, especially after tempering.

5. As regards liquid-solid titanium transformation, it should be noted that our chemists have some new amorphous materials containing significant percentage of titanium.

Unfortunately, I do not remember the relevant compositions.

All these problems are of great interest and deserve to be studied. But,in many cases,the study of these problems is restrained by economic factors, rather than technological ones.

U. Zwicker

1. Do you think that type Iα precedes type IIα?

2. If type IIα is precipitated from solid solution, does α dissolve in the matrix, what happens with it?

J. C. Williams

1. We do not have the confirmation of the fact that type Iα is different from type IIα in its composition. Last December I read a lecture in the USSR where, judging by the questions, S. G. Fedotov is also involved in this activity. He asked about oxygen content. It is possible that oxygen takes part in varying these structures. It is difficult, however, to determine the cause of this process. We suspect that there is a difference in composition, but have not proved it experimentally up until now.

In type IIα, there are localized zones of modified structure and composition. Subsequently, it will be necessary to use analytical electron microscopy techniques to study this. I think that this investigation method will bring more detailed results.

2. We think that type IIα is formed by nucleation at the boundary type Iα followed by growth. Our data indicate that on completion of type IIα formation the type Iα has disappeared.

F. L. Lokshin

We have listened here to very interesting presentations by J. C. Williams and I. S. Polkin. I would like to dwell on some aspects important for the theory and practice of titanium alloy heat treatment.

It is noticed that, in some alloy compositions having a martensite transformation starting temperature above 600°C, quenching results in partial β-solid solution decomposition. Regions were observed in metastable diagrams having two martensitic phases, which is inexplainable to terms of thermodynamics alone.

We investigated the effect of cooling rate on the phase composition of a number of commercial and binary alloys. During cooling from β-region at rates above 150-200°C/sec, these alloys develop a single phase structure of α' or α" martensite, depending on the chemical composition. At lower cooling rates, two-phase or three-phase structures of the type of α'+β, α"+β, α'+ω+β, or α"+ω+β are obtained. By changing lattice parameters, it was possible to establish that, at cooling rates below 150-200°C/sec, the phase transformation processes should be considered as intermediary of the type of bainitic process in steel. Such phase modification occurs by diffusional redistribution of alloying elements and formation of enriched and depleted regions with subsequent decomposition of the depleted zone by the diffusionless martensite transformation. As titanium alloys have low thermal conductivity, a cooling rate of above 200°C/sec can be obtained at a specimen thickness of not greater than 2-4 mm. This is the

reason why during quenching of actual products the pure martensitic transformation is practically never realized.

At the present moment, the processes of metastable phase decomposition, particularly at their initial stages, are lacking adequate understanding. To achieve this, we used accelerated heating. The initial stage of the decomposition of all metastable phases is found to occur with diffusion redistribution of alloying elements and formation of enriched and depleted regions. As holding time at a given temperature increases, the difference in $C_{enrich}-C_{depl}$ continuously enhances. When β-solid solution decomposition takes place in a depleted region, $\omega \rightarrow \alpha'' \rightarrow \alpha' \rightarrow \alpha$ is consecutively obtained. When martensite decomposition occurs in an enriched region, $\alpha'' \rightarrow \omega \rightarrow \beta$ is consecutively obtained.

E. S. Makhnev

A wide diversity of phase transformations is typical for titanium alloys, i.e. diffusional, non-diffusional types; direct and reverse martensite transformation have been discovered. While in steel these transformations can be readily studied by magnetic method, the absence of ferromagnetic properties in titanium alloys prohibits the use of this method and other methods capable of direct monitoring of transformation process do not produce kinetic curves and formation times for various phases. We feel it extremely desirable to direct researchers' efforts towards developing novel instrumentation for volumetric investigations.

J. C. Williams referred to the limitations of high-temperature X-ray techniques. Magnetic electromagnetic-susceptibility method largely appears to be acceptable. Such data are of late being reported in literature. My wish is for all of us, at the next International Conference, which will take place in four years, to become eyewitnesses of the development of methods for direct monitoring of phase transformations. When such data becomes available, it will be possible to create newer, well-grounded titanium alloy processing methods.

Critical Review

INFLUENCE OF TECHNOLOGICAL FACTORS ON STRUCTURE AND PROPERTIES OF TITANIUM ALLOYS

J. D. Alexander

Rolls-Royce (1971) Limited

It is now widely, although unfortunately not universally, accepted by the users, that materials contain defects. The nature and size of the defects are critical factors in the use of the material and the methods of controlling defects should be major factors governing the future development policies of the material supply industry.

It is obvious that any material supply must show its capability to control the grosser defects. In the aerospace industry there have been a number of incidents where oxygen and nitrogen rich areas have been present in components which have caused failure of highly stressed components in service. These failures in the late 1960's caused the industry to consider very carefully the source of the defects. In the USA, the major effort was on the cleanness of the initial sponge and the methods of dispersing the contaminated material. The controls of AMS 2380 achieved after considerable discussion and effort by the combined forces of users and suppliers was a significant step forward. The triple melting of titanium for highly stressed critical parts has resulted in an improved confidence situation with the user. There are some excellent disciplines required in this document and each user has interpreted and enlarged upon them in his own way.

It is not, however, the details of the requirements that are important, but the total philosophy of control that it instills. The user expects that the supplier is continually reviewing his melting and processing techniques to avoid macrosegregation and inclusions. It is the total awareness of the potential problems that is required. Having achieved the awareness and the understanding

of the source of the problems then each individual supplier must be treated in a different way. This is now the cause of the revisions of AMS 2380. Each supplier has a different sponge source and practice, a different method of making additions etc. To the user it is logical that different methods of manufacture and different controls are required for each supplier. We do not consider it illogical to demand triple melting from one supplier and double melting for the same standard of product from another.

It is apparent that the supplier industry is giving much more attention to cleanness and controls than ever before. The need for regular furnace cleaning has been established after it was shown that oxygen and nitrogen rich areas in the final product could be due to oxidized spatter from the furnace walls and ledges falling into the final melt.

The correct control of tools used in the machining of ingots between melts has been investigated. Problems on the selection, inspection and mixing procedures of masteralloys have been with titanium since its inception and even today these can create problems.

Hot topping is also an important parameter which has given problems due to alloy segregation. The user requires the industry to provide evidence that this is under control and the supplier understands the mechanism of his melting procedure. Given this understanding, we believe computerized step down procedure for the finishing of the final melt is essential. Given this understanding demonstrated by an individual supplier, there is no reason why Non-Consumable Electrode Melting cannot be considered.

All these good practices are, however, aimed at the gross defects which must be removed so that the titanium industry can be totally credible. That point has been reached and the user is now looking for the more subtle problem which can be equally damaging. The material behavior approach is now considering in more detail than before the effects of structure and substructures of the alloys, and in particular the various parts of the structure. Most alloys contain alpha phase. At what size and under what conditions does alpha cease to be a strengthening element and become a harmful defect? It is now known that the transformed β phase contains α which can be aligned and when the alpha is so aligned it can behave as one block of α in terms of its propensity to cleavage. Thus the form of transformed β in any alloy becomes a major factor in material behavior and the aligned α block size is important. In an α β processed alloy, the primary α shape has been of concern for many years and test evidence is now showing the behavior of the primary α. It is, however, not only the blocky and stringy α that is of concern but the form distribution and chemical compos-

ition that requires to be controlled by inspection and process control.

The nature of close packed hexagonal structure alpha titanium makes slip and hence conforming strain difficult in a multi-element structure. Failures of high stressed parts have shown the need for uniform structure and that local variations in composition and structure must be avoided. Variations in the composition of the alpha units with respect to aluminum and oxygen can decrease the ability of the alpha to absorb strain. This is particularly important in the high aluminum alloys where the propensity to unit cracking is high, particularly in adverse environments. The role of hydrogen in the limited slip behavior of alpha is still under investigation although its manifestations in terms of bulk properties are known.

The influence of texture in alpha can be postulated by consideration of the limited slip and the redistribution of microstresses in the material. In other words, texturing of the alpha gives the worst properties of the material in one direction since it is exposed to the microstresses where as in randomly oriented alpha material the microstress on any one alpha colony is reduced by the surrounding grains.

Can α, therefore, ever be considered as anything other than a hazard? The work to which the total industry needs to address itself more positively is in the understanding of the behavior of α, the influence of size, effect of surrounding material and its composition. The latter point is significant not only in the absolute composition of the α in terms of alloying elements but is composition in terms of hydrogen and other interstitial elements and the effect of these on the behavior of the α.

To this end, research work should not only be aimed at the relationship of grain size to static and dynamic material properties but much more to the point of crack initiation, the crack path and the reasons for the crack growth behavior. The work on texture and crack behavior in the UK is of particular note in its attempts to relate properties to detailed structure.

There is still a lot of information to be gained in the effect of these points on the understanding of material behavior. Even more is the work required to relate this understanding to the total material manufacturing route.

The method of manufacture of primary concern to the structure is the hot working from ingot to billet for α/β processed alloys since it is this route which sets the α form. For this reason we are most concerned that for our forgings we have a well defined

billet structural standard consistent with a clearly defined final product standard. If the material supplier produces the correct structure by careful control of his process which has been shown to be feasible forging scrap is reduced, a more consistent product achieved and a better part utilization acquired.

For α/β and β processed alloys, the hot working operations affect not only the shape and texture of the alloy but the composition. This field requires recognition and control.

In short, when titanium does not contain defects it is its own worst enemy in terms of its structure. Phase I of titanium development is near its end. Phase II is beginning.

STRUCTURE OF SEMIFINISHED ALPHA + BETA TITANIUM ALLOY PRODUCTS

I.N. Kaganovich, M.V. Efimova, Z.F.Zvereva, Yu.I. Potapenko and V.K. Kataya
All-Union Institute of Light Alloys

U.S.S.R.

Development of semi-finished products manufactured from alpha +beta titanium alloys has necessitated a thorough study of the interrelation between the structure and phase composition of these alloys, and their mechanical properties. For the necessary combination of mechanical properties to be assured, semi-finished products manufactured from titanium alloys must have a homogeneous macrostructure and a fine-grained microstructure. The structure of semiproducts from alpha+beta alloys is determined by their thermomechanical deformation behaviour.

A number of investigators [1,2] have established the impossibility of correcting the coarse-grained structure of titanium alloys by thermal treatment alone. This is explained by the small extent of intracrystalline mechanical hardening of the metal in the process of polymorphic transformation and the characteristic property of titanium associated with the intensive grain growth in the transition to the beta state. The principal way to obtain a fine-grained metal for titanium alloys is, therefore, to combine deformation with heating. Thermal treatment will, mainly, change the phase composition, shape and size of structural components.

To obtain the structure of necessary quality, a process flow diagram has been developed for the manufacturing of every semiproduct. Anomalous structures are, nevertheless, encountered in actual practice. Among the most frequent types of structural defects, resulting from the deformation conditions, in semi-finished products manufactured from titanium alloys are:

1. Heterogeneous and coarse-grained macrostructure.
2. Striations.
3. Local manifestations of the coarse alpha phase.

1. HETEROGENEOUS AND COARSE-GRAINED MACROSTRUCTURE

Heterogeneous and coarse-grained macrostructures are most frequently encountered in die-forged semiproducts.

Coarse-grained macrostructure (Fig.1) results from the insufficient transformation in the cast metal with the hightemperature deformation, due to:

a) the cooling-down of metal, in the process of deformation, to below the temperature of polymorphic transformation;
b) a small extent of deformation in the whole volume of the metal or some of its areas in the zones of inhibited deformation.

Heterogeneous macrostructure (Fig.2) is,in our opinion, being formed as a result of the cooling of the metal, during its high-temperature forging, down to or somewhat below the region of critical temperatures. With the deformation proceeding further at the alpha+beta region temperatures, and during subsequent annealing, the bulk of the metal has time to recrystallize, but some of the material does not recrystallize.

Both the possible warming-up of the metal during deformation and its chemical heterogeneity can contribute to the formation of such structures.

The heterogeneous structure is eliminated with the help of such a thermomechanical process of deformation that, fully proceeding in the beta region, guarantees the size reduction of cast crystallites in the ingot. In case there is no certainty that the process of cast structure diminution terminates in the beta region, it is expedient to apply additional annealing in the beta region at 30-70°C above the polymorphic transformation temperature. In all cases, the manufacturing process terminates in the deformation at the alpha+beta region temperatures.

2. STRIATIONS

Striations manifest themselves as part of the structure having the form of striae, extending in a certain direction, against the background of a homogeneous structure.

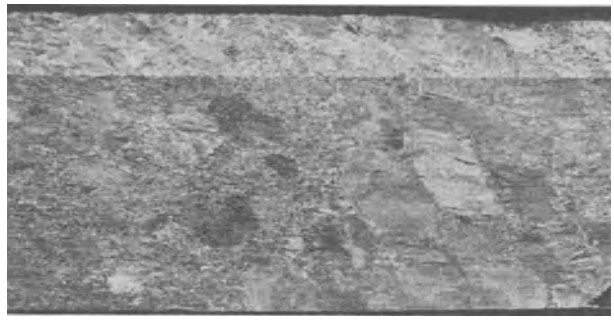

Fig. 1: Coarse-grained macrostructure of an article manufactured from BT9 alloy.

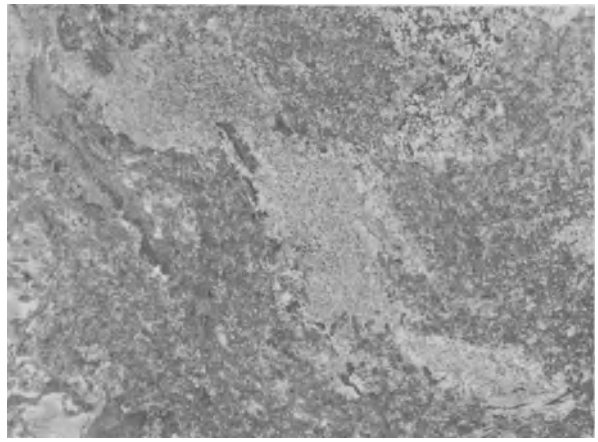

Fig. 2: Nonuniform macrostructure of an article manufactured from BT9 alloy.

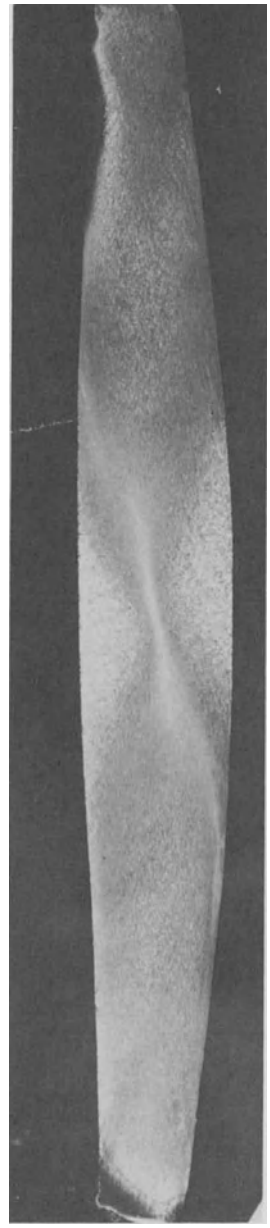

Fig. 3: Striation in a vane forging manufactured from BT3-1 alloy.

Striations are most frequently encountered when the material is, predominantly deformed in one direction; e.g., thick sheets and plates, moldings, vane forging etc.

The nature of striation can be:

a) deformation dependent;

b) caused by chemical heterogeneity.

Striations of solely deformational origin can have several causes:

a) non-uniform or heterogeneous deformation during the manufacturing process;
b) surface layers of the metal being cooler than its central zone.

In vane forgings, e.g., structural heterogeneity of the striation type (Fig.3) is caused by the localized deformation due to the forging temperature decreasing 60-80°C below that of polymorphic transformation.

To prevent the formation of pronounced localized deformation zones, the temperature of deformational heating, when forging the vanes, must be strictly regulated and correspond to 30-50°C below T_{cr}.

Raising the forging temperature above the indicated will result in the coarsening of the structure and even in overheating due to the high recrystallization rate. Forging the semi-products at temperatures below those recommended will again result in the appearance of striated zones. Striation in the vanes renders their mechanical properties unstable and, in the zones of localized deformation, may even lead to cracking.

Thick sheets and plates were, as a rule, manufactured by hot rolling from the beta region with one heating cycle. The final stage of the rolling process was carried out at the temperatures of alpha+beta region, which lead to the development of striation (Fig.4), as it is impossible for the recrystallization processes to take place at these temperatures. The mechanical properties of hot-rolled sheets were extremely unstable.

Application of heavy-duty rolling-mill equipment makes it possible to reduce the heating temperature of hot-rolled metal to the temperatures of alpha-beta region, so as to decrease the surface gas saturation, but, at the same time, it increases the possibility of getting a coarse striated structure.

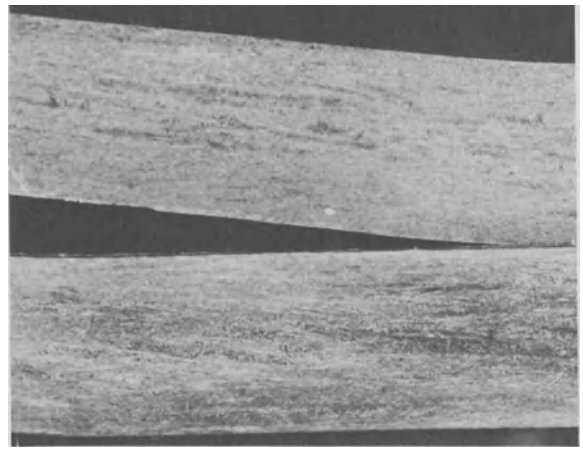

Fig. 4: Striation in a rolled sheet 20 mm thick.

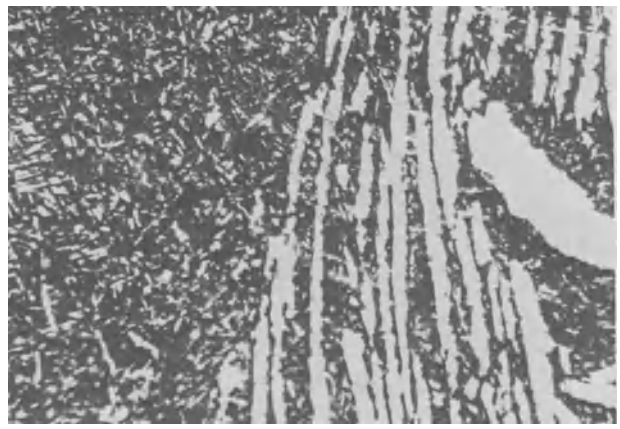

Fig. 5: Inclusions of alpha phase in an article manufactured from BT3-1 alloy.

When elaborating the technological process for the manufacturing of high-thickness sheets b rolling,with subsequent warm or cold deformation either absent or very limited, it becomes necessary to search for conditions eliminating the formation of striated structure during hot rolling. One of the ways to improve the micro-

structure is to combine the hot and the warm rolling within one heating cycle by cooling down and subsequently deforming the metal in the conditions of the warm rolling process.

Rolling with cooling has, however, some serious disadvantages: there is no possibility to control the cooling temperature in a reliable way; a thermal gradient over the strip thickness appears, due to low heat conduction, which aggravates the structural heterogeneity.

The most effective and economical way of improving the structure, raising the level and stability of the mechanical properties of titanium sheets and plates is hot rolling with two heating cycles in the following sequence: hot rolling of a slab with the deformation primarily in the upper interval of the alpha+beta region, cooling the strip down to room temperature, heating at the temperature of alpha+beta region (50-60°C below T_{cr}), rolling the strip to size with area reduction of at least 40%.[3]

The microstructure of thick sheets and plates obtained in this way is characterized by the absence of striation and clearly defined boundaries of beta grains, and by the presence of a uniform despersed mixture of alpha+beta phases, with a sharply raised level and stability of mechanical properties, especially these of the plastic parameters.

3. LOCAL PRECIPITATION OF THE COARSE ALPHA PHASE

One of the varieties of anomalous structures in articles manufactured from titanium alloys is the microstructural heterogeneity in the form of coarse precipitations of the alpha phase (Fig.5). This type of heterogeneity is formed as a result of the slabs staying for a long time in the upper interval of alpha+beta region temperatures when being heated before deformation, due to the process of alpha-phase coagulation. As a rule, anomalous microstructure of the coagulated alpha+beta type is found in large-size vane forgings manufactured from slabs obtained by smith forging with its inherent non-uniform deformation. The coarse alpha phase is first of all, found in the zones of inhibited deformation. For every alloy there is a corresponding temperature at which the growth of the alpha phase is maximum. Alpha-phase inclusion, practically, does not affect the mechnical properties in static rupture but reduces the fatigue strength.

By substituting the rolled slab, which, as a rule, has a homogeneous fine-grained microstructure, for the forged blank and by limiting the duration of slag heating in the alpha+beta region before the forging we can eliminate the coarse alpha-phase.

PHASE COMPOSITION EFFECT IN THE MANUFACTURING OF VANE FORGINGS BY THE HIGH-HEAT MECHANICAL TREATMENT

The process of manufacturing forgings from BT9 alloy using HHMT can serve as an example of how the changes in phase composition affect the mechanical properties.

As it is known, strengthening with HHMT is based on the fixation in the material of a structural state, created with plastic deformations in the region of high temperatures, due to rapid cooling (hardening) after the deformation.

The duration of the pause between the end of the deformation and the hardening has been found to produce a remarkable effect on the set of mechanical properties, as, depending on this, different quantitative rations of phases can be obtained. In the case of hardening taking place directly after the deformation BT9 alloy is hardened to martensite, the alloy, in this case, combining high ultimate strength with low plasticity. With the duration of the pause increasing the quantity of the beta phase also increases. The optimum combination of strength and plastic characteristics of BT9 alloy after HHMT is reached by hardening to the beta phase.

CONCLUSION

The article reviews the causes for the appearance of anomalous structures in semi-finished products manufactured from alpha+beta titanium alloys and outlines the ways which make it possible to manufacture articles with a homogeneous fine-grained structure.

REFERENCES

1. Bochvar G.A. Structure and properties of cast titanium alloys and their interrelation with the conditions of phase recrystallization. Synopsis of Candidate's Thesis. Moscow, 1966.

2. Sadovsky V.D. et al. Journ. "Fizika metallov i metallovedeniye", vol. 10, No.3, 1960.

3. Shul'kin S.M. et al. Characteristic features of the technology for the manufacturing of 48-OT3 titanium alloy hot-rolled sheets. Journ. "Metallurgiya", No.2, 1959.

INFLUENCE OF THE PARAMETERS OF A LAMINATED STRUCTURE ON THE MECHANICAL PROPERTIES OF TITANIUM ALLOYS

M. Ya. Brun, N. Z. Pertsovsky, G. V. Shakhanova, and V. L. Rodionov

All-Union Institute of Light Alloys

U.S.S.R.

I. Introduction

Titanium alloys display a great variety of laminated structures. The mechanical properties of semi-finished products with such structures, ductility in particular, vary over a wide range.[1-3] Thus, for the two-phase alloys with a laminated structure. BT3-1, BT9, and others in an annealed state the reduction in area varies from very low values (5-10%) up to relatively high values (30-40%) approaching the ductility level of these alloys with globular structure. The difference in fatigue strength, fracture toughness, and other properties may also be significant (up to 25-30%) for various types of laminated structures.

It was found in our earlier investigations[3,4] that the microstructural pattern of deformation and fracture of titanium alloys with a laminated structure subjected to tensile bending tests depends on the size of the initial β-grains (D), on the size of the intergranular α-clusters (d), and on the thickness of α-laminae (b). The main goal of this investigation was, therefore, to study the effect of the structural parameters D,d, and b upon the mechanical properties of various titanium alloys.

II. Experimental Procedure

The study was carried out using rolled rods and forgings of different size made of the α-alloy BT5-1 (Ti - 5Al - 2.5Sn), the pseudo α-alloy OT4 (Ti - 3Al - 1,5Mn), and the medium (α+β) alloys VT3-1 (Ti - 6Al - 2Cr - 2.5Mo - 0.2Si) and BT9 (Ti - 6.5Al -

2Zr - 3Mo - 0.2Si). Each alloy was studied in several ingots. The various laminated structures were obtained by changing the conditions of deformation and by preliminary B-heat treatment. The final heat treatment (annealing) was performed at temperatures below that of the $(\alpha+\beta) \rightarrow \beta$-transition.

The rods and forgings were used for determining the ultimate tensile strength (σ_b), the ultimate elongation (δ), the total reduction of area (ψ), the impact strength (a_H), the work of fracture under impact bending of specimens with a fatigue crack (a_{cf}), the fracture toughness (K_{IC}), and the fatigue strength (σ_{-1}).

The mechanical properties, except for K_{IC}, were determined on standard specimens by standard procedures. The single-notched specimens 12x24x90 mm in size with a fatigue crack were employed for the fracture toughness tests.

The microstructure of all the specimens was studied after the tests. The dimensions of structural constituents were estimated by the secant method.[5] Several specimens were subjected to the X-ray diffraction study to determine the lattice parameter of the β-phase (a_β) from the line $(321)_{\beta\text{-Ti}}$, and the total disorientation angle of the α-laminae ($\Delta\alpha$) from the boradening of the line $(001)_{\alpha\text{-Ti}}$ in some β-grains.

III. Results and Discussion

The dependence of the mechanical properties of the BT3-1 and BT5-1 alloys on the laminated-structure parameters D,d, and b is shown in Figure 1. One of the causes of a considerable scatter in the experimental data is the fact that each diagram is constructed without taking account of the other structural parameters. Nevertheless, these diagrams show a certain relationship between the dimensions of the structural constituents and the mechanical properties,ductility in particular. For instance, as the size of β-grains increases, the ductility decreases in all the alloys, whereas the dependence of the mechanical properties of the $(\alpha+\beta)$-alloys on the size of α-clusters and the thickness of α-laminae is pronounced.

When α-clusters grow up to 25-30 μm and α-laminae become as thick as 2.5-3.5μm the BT3-1 and BT9 alloys display a sharp increase in ductility and decrease in strength. With further

[x]The authors are grateful to A. I. Gnevko, G. A. Deryagin, and Yu.K. Shtovba for their assistance in performing the experiments.

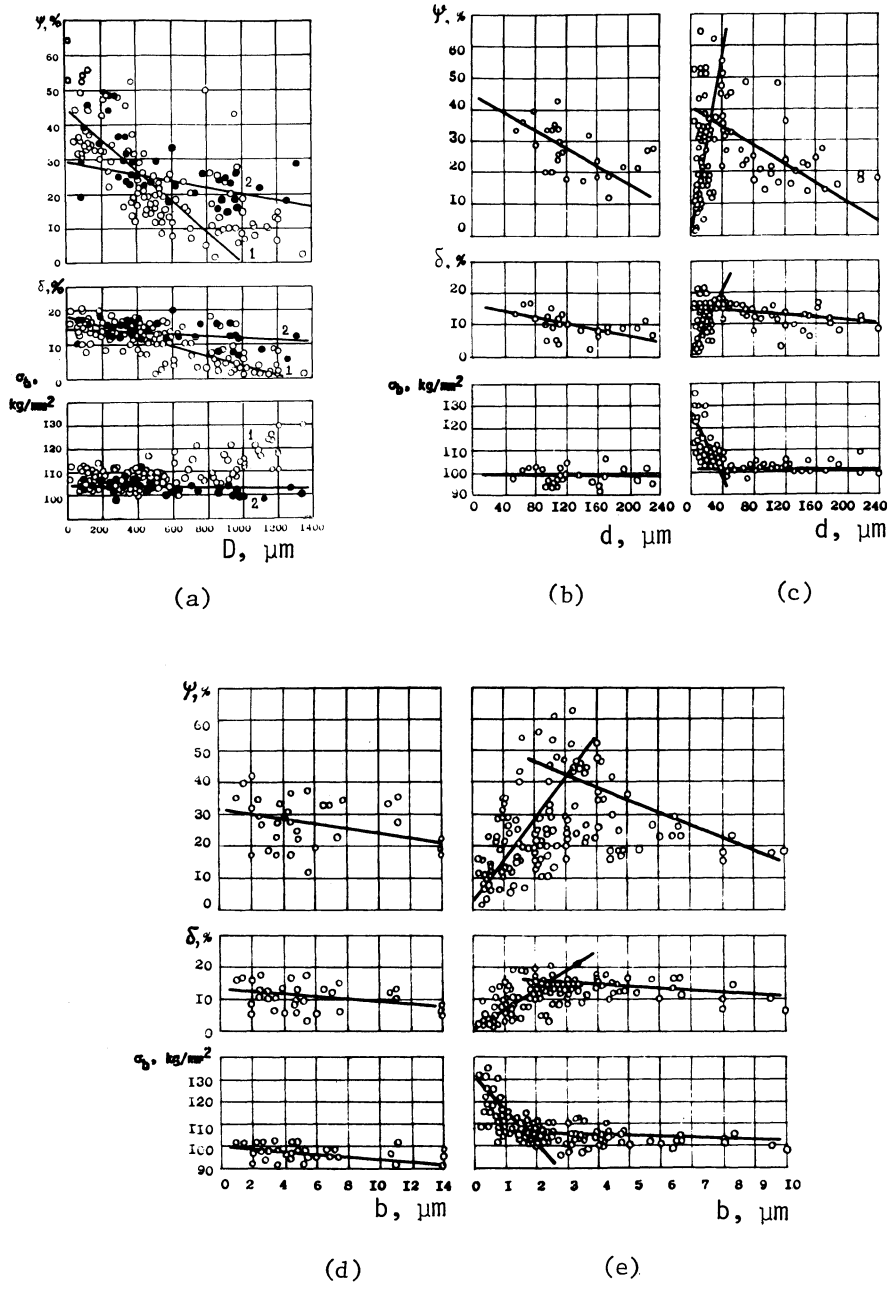

Fig. 1: The effect of the laminated-structure parameters upon the mechanical properties of the BT3-1 (a,c,e) and BT5-1 (b,d) titanium alloys.
to Fig. 1a: (1) d < 30Mμ; (2) d> 30μm .

coarsening of the intergranular structure a smooth decrease in ductility is observed at an almost constant strength level.

The sharp increase in ductility and reduction in strength with increasing thickness of α-laminae at b<3 μm seems to be due to the improvement of the internal structure of the phases present as they approach the equilibrium state. This is evidenced by changes in the lattice paramter of the β-phase and in the disorientation angle of α-laminae in β-grains, depending on the thickness of α-plates in the BT3-1 alloy (Figure 2). As the laminae become thicker, the paramter a_β decreases and at b≈3μm takes on a constant value. The disorientation angle Δα varies in a similar way.

It is known from (6) that as the (α+β)-alloys approach the equilibrium state, the parameter a_β decreases, which is due to changes in the composition and in the volume fractions of the α-andβ-phases. It can be expected that the equilibrium state of VT3-1 alloy is established at a given thickness of α-laminae which corresponds to a predetermined thickness of interlayers of the β-phase.

At b>3μm the phase composition does not seem to change and the observed smooth decrease in ductility is in agreement with the widely adoped ideas about the influence of the structural constituent dimensions on the mechanical properties.

In the same way it is possible to explain the pronounced dependence of the mechanical properties of (α+β)-alloys on the size of α-clusters, since the parameters d and b have been found to be interrelated within certain limits. In α-clusters less than 25-30μm in size, α-laminae 3.0-3.5μm thick are usually present, the growing clusters being, as a rule, accompanied by an increase in laminae thickness.

As shown earlier,[4] the non-monotonic variation of the mechanical properties of titanium alloys with the size of α-clusters is determined by the specific features of the deformation process. At d > 25-30μm the deformation is the result of coarse glide inside the α-clusters, whereas at d < 25μm the deformation is localized along their boundaries and spreads usually througout the β-grain.

The effect of the structural parameters upon the mechanical properties is similar for all the alloys under consideration. However, their different chemical composition accounts for their different phase composition and, consequently, for the specific structure in each particular case. It has been found that the minimum thickness of α-laminae in the structures of the investi-

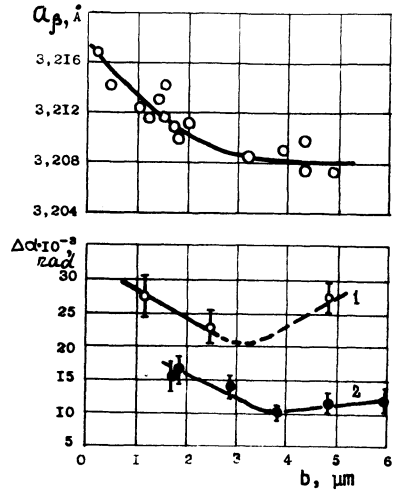

Fig. 2: The variations in the lattice parameter of β-phase (α_β) and in the total disorientation angle of α-laminae in β-grains ($\Delta\alpha$) as a function of the thickness of α-laminae (b) in the VT3-1 alloy.

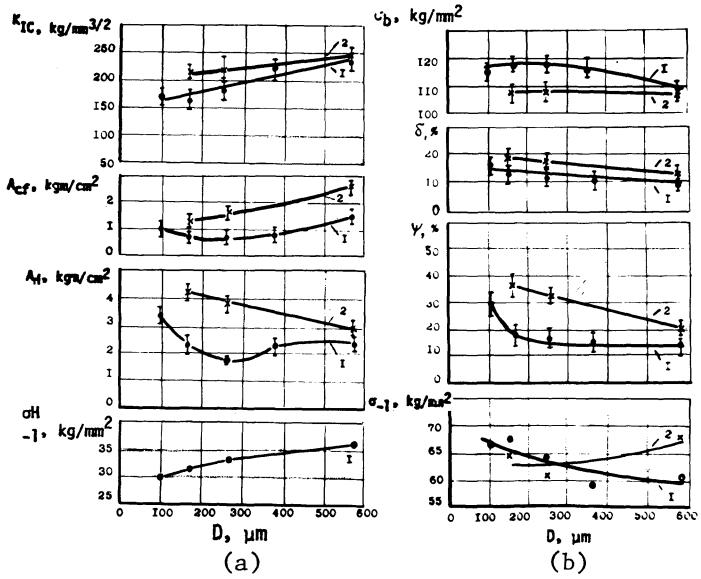

Fig. 3: The effect of the size of β-grains (D) on the mechanical properties of 20 mm - diameter rolled rods made of the BT3-1 alloy; (1) b = 0.9-1.1 mm; d = 15-25μm; (2) b = 2.5-3.5μm; d = 30-35μm):
a = test specimens with a notch;
b = unnotched test specimens.

gated semifabricated products is smaller, the greater the content of β-stabilizers: b_{min} = 3.5μm in the BT5-1 alloy; 1.5μm in the CT4 alloy; and 0.1-0.2μm in the BT3-1 and BT9 alloys. It means that in the BT5-1 alloys the equilibrium phase composition is usually achieved, which explains the weak sensitivity of the mechanical properties of this alloy to the structure, whereas in the BT3-1 and BT9 alloys the structural sensitivity is very strong.

This accounts for the absence of ascending branches in the ductility dependence on the parameters d and b for the BT5-1 alloy (see Figure 1). The OT4 alloy differs from the BT3-1 and BT9 alloys in that such branches in the corresponding graphs are less pronounced.

In order to obtain a quantitative evaluation of the relationship between the mechanical properties of titanium alloys and the parameters of the laminated structure the probabistic-statistical methods of correlation and regression analyses were employed.[7] The values σ_b, δ and ψ were assumed to be random (y), and the structural parameters D,d and b served as argument (x). On the basis of the data of Figure 1, the existence of a linear relationship of the type

$$y = a + cx \tag{1}$$

were suggested, and the area of each graph was divided into two sections corresponding to the fine intergranular structure ($d < 30\mu m, b < 3\mu m$) and to the coarser one ($d > 30\mu m$).

Calculation of the correlation coefficient has provided support for Equation (1) chosen as the required equation of linear dependence. Equations of linear regression describing the dependence of the mechanical properties of the alloys on each structural parameter have also been obtained. The corresponding regression lines are depicted in Figure 1.

Based on the regression equations we have derived generalized formulas of the type

$$y = a_0 + a_1 D + a_2 d + a_3 b \tag{2}$$

describing the general form of the dependence of the mechanical properties on the three structural parameters studied above.

Thus, for the BT3-1 alloy Equation (2) has the following form (σ_b in kg/mm^2; δ and ψ in %; D,d, and b in μ):

a) at $d < 30\mu m$ and $b < 3\mu m$

$$\sigma_b = 156 - 0.005\,D - 1.0\,d - 15.0\,b$$
$$\delta = 6 - 0.013\,D + 0.5\,d + 6.0\,b$$
$$\psi = 3 - 0.045\,D + 1.2\,d + 12.5\,b$$

b) at $d > 30\mu m$ $\sigma = 104 - 0.002\ D - 0.005\ d - 0.3\ b$
$\delta = 18 - 0.005\ D - 0.014\ d - 0.6\ b$
$\psi = 55 - 0.016\ D - 0.10\ d - 3.5\ b$

The values of mechanical characteristics calculated by these formulas are in good agreement with the results of standard mechanical tests.

These formulas show that the effect of the size of the β-grain upon the characteristics δ and ψ is approximately 100 times less, and that of the size of α-clusters is 10 times less than the effect of the α-laminae thickness. But since the actual sizes of β-grains are hundreds of microns and of α-cluster tens of microns, and the thickness of α-laminae is microns and fractions of a micron, the degree of influence of each of these parameters upon ductility in formulas of the type (2) is expressed in one-order values.

Thus, at $b > 3\mu m$ the reduction of area in all the alloys studied decreases by about three per cent with a 100 μm increase in β-grain size, a 10 μm increase in α-cluster size, or a 1μm increase in the thickness of α-laminae. At $\delta < 3\mu m$ even minute changes in the size of the structural elements produce a significant effect on the properties. In this case the effect of the structural parameters for the BT3-1 and BT9 alloys is 3-5 times as strong as at $b > 3\mu m$.

It follows from the data obtained that in order to ensure a high level of ductility, whatever the chemical composition and the technology of semi-product manufacturing, the optimal parameters of laminated structures of titanium alloys are: the smallest possible β-grain, α-clusters 30-50μm in size, and α-laminae 3.0-3.5μm thick, which corresponds to the equilibrium state of α and β-phases in the alloys under investigation. The refinement of an intergranular structure or its coarsening with respect to the above parameters leads to a lower ductility. At the same time, if we do not proceed from the maximum ductility, the satisfactory level of δ and ψ can be achieved by various combinations of the parameters D,d and b, even for large β-grains (up to 700-1000μm), since cluster sizes and α-phase laminae thicknesses close to optimal values can be obtained by heat treatment.

Figure 3a shows the experimental results for the effect of the laminated-structure parameters on some mechanical properties of rolled rods made of the BT-3-1 alloy for specimens with different types of notches. For comparison, Figure 3b presents the results of tensile and fatigue tests for unnotched speimens made of the same material.

These results show that the impact toughness a_H, determined on the specimens of the Menage type with a notch radius of 1 mm,

the fatigue strength of the unnotched specimens, and the ductility characteristics δ and ψ decrease with coarsening β-grains. At the same time, the fracture toughness K_{IC}, the fracture work a_{cf}, and the fatigue strength of specimens with a sharp notch at τ = 0.1 mm increase with D. It can be seen from Figure 3 that except for the short-time strength σ_b and the fatigue strength σ_{-1}, the coarsening of the intergranular structure up to the optimal (in terms of ductility) values of the parameters d and b leads to the improvement of all the properties studied.

The study of the microstructural features of deformation and fracture of specimens with different structures subjected to fracture-toughness and impact-bending tests has shown that the increase in K_{IC} and a_{cf} with coarsening laminated structure results from the sidening of the zone in which these processes occur, and consequently, from the increase in required energy. As has been found in our previous studies, at the initial stage of the test the specimens with a notch or a crack, unlike un-notched specimens, display a drastic localization of deformation in the zone, whose size depends both on the concentrator's depth and radius and on the dimensions of the structural constituents determining the length of coarse slip bands in α-clusters or deformation bands spreading throughout the β-grain.

Consequently, the sharper the notch and the larger the α-clusters and β-grains, the greater the localizated deformation zone relative to the enhanced stress concentration zone and the greater the amount of metal involved in the deformation and fracture. In particular, this is evidenced by the more frequent and abrupt changes in the direction of the crack motion, which lead to an increase in its length with coarsening β-grain (Figure 4).

Therefore, in testing specimens with cracks, the material with a coarser structure is preferable, whereas in testing specimens with a notch at a lower deformation locatization the reverse may be true.

Unlike the dimensions of β-grains and α-clusters whose influence upon the characteristics under consideration depends on the concentration coefficient, the thickening of α-lamellae leads to an increase in a_H, as well as in K_{IC} and a_{cf}, probably as a result of the enhanced frictional effect of the developing crack. In this case a change in σ_{-1} is less pronounced, because in specimens with such a structure the work of crack formation decreases with increasing work of crack propagation owing to a lower strength level.

IV. Conclusion

As a result of the studies carried out by means of the

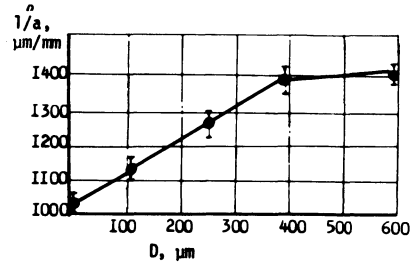

Fig. 4: The effect of the size of β-grains (D) on the relative length of the crack (l/a) in the Sharpy type specimens made of the BT3-1 alloy;
(l is the crack length, a is the specimen width).

quantitative metallography and statistical methods, quantitative relationships between the mechanical properties of various titanium alloys subjected to static tensile tests and the parameters of a laminated structure have been established. The formulas calculated can be used for evaluating mechanical properties.

The structural parameters providing the optimal level of mechanical properties have been determined. The most distinct effect of the structure upon the properties is manifest for non-equilibrium phase composition; this effect is stronger, the higher the content of β-stabilizers in the alloy. As has been shown, among the titanium alloys investigated the (α + β)-alloys BT3-1 and B19 possess the highest structural sensitivity.

The influence of the laminated-structure parameters on the mechanical properties of specimens with various types of notches under different loading conditions has been studied using the BT3-1 alloy. The coarsening of the structure has been shown to cause an increase in the materials's structural strength, which is due to an extension of the zone of localized deformation.

References

1. Glazunov, S. G., Moiseev, V.N., "Constructive Titanium Alloys," Moscow, "Metallurgiya" Publishing House, 1974.

2. Greenfield, W. V., Pierce, C. M., Hall, J. A., Titanium Sci. and Tech., N.Y.-London, 1973, 3, 1731-1743.

3. Pertsovski, N. A., Brun, M. Ya., Shakhanova, G. V., Fizika metallov i metallovedenie, 1970, 30, No. 5, 1047-1054.

4. Pertsovski N. Z., Shakhanova, G. V., Brun M. Ya., Fizika metallov i metallovedenie, 1973, 36, No. I, 154-161.

5. Saltykov, S. A., "Stereometric metallography," Moscow, "Metallurgiya" Publishing House, 1970.

6. Nosova, G. I., "Phase Transitions inj Titanium Alloys," Moscow, "Metallurgiya" Publishing House, 1968.

7. Aivazyan, S. A., "Statistical Studies of Dependences," Moscow, "Metallurgiya" Publishing House, 1968.

METHODS OF REFINING COARSE-GRAINED STRUCTURES OF TITANIUM ALLOYS

L.A. Elagina, A.I. Gordienko, O.P. Evmenov, and V.V. Ivashko

All-Union Institute of Light Alloys, and Physical Technical Institute, BSSR Academy of Sciences U.S.S.R.

INTRODUCTION

The specific features of titanium alloys are their tendency towards grain growth at temperatures $\geqslant T_{trans.}$ and the resulting drastic deterioration of their mechanical properties and ductility in particular (beta embrittlement). Since the coarse-grained structure of titanium alloys cannot be improved by phase transformation hardening(1), the main method of grain refinement is at present a rather laborious process including sufficient beta deformation and considerable ($\geqslant$ 50%) alpha+beta deformation. The latter makes it possible to obtain a fine-grained structure of globular or fibrous type and, accordingly, high strength and ductility, but it fails to provide an optimum level of high-temperature strength and fracture toughness which can be attained (with adequate ductility) only in the case of a limited beta-transformed (plate-like alpha) structure (D_{grain} = 150 to 200 μm depending upon the alloy and temper.).

In our previous work it was shown that it is possible, in principle, to improve coarse-stripped structures by 10- to 40% alpha+beta deformation and subsequent beta annealing.

The objective of the present investigation was to look into the possibility of refining coarse-grained structures by this method.

MATERIAL AND EXPERIMENTAL TECHNIQUES

The quantitative methods of refining the beta grain were

studied using cast and deformed material. The cast billets (dia. 40x40 mm; 80x65x12-45 mm) were longitudinally cut from vacuum-arc-melting ingots (dia. 350-420 mm, alloys BT3-1 and BT18) and scull-melting ingots (dia. 650x65 mm, alloy BT9); the deformed billets (60x10x5 mm) were cut from rolled bars, 55 mm in dia., of the same alloys with a special coarse grained (D_{mean} = 500 m) beta-transformed structure.

The cast billets were deformed by upsetting in a press at $V_{str.}$ = 0.1 mm/s under isothermal conditions. The reduction was 3-60% and the upsetting temperature was 900°, 950°, 980° and 1050°C.

The deformed billets with a coarse-grained structure were rolled at $V_{def.}$ = 0.5 mm/s at temperatures of 750°, 950°, and 1050°C and ε=10, 20, 30, and 60% in one pass. The upset and rolled billets were cut into specimens and annealed. The upset specimens were annealed in a furnace at temperatures of 800°-1150°C during 0, 0.2, 0.5, 1.5,5, 10, 30, 90, and 180 min with subsequent air cooling ($V_{cool.}$ = 8-10 deg/s). Rapid continuous resistance heating (V_h = 10 and 25 deg/s) of the deformed specimens to 950°-1200°C was employed to estimate the possibility of additional grain refinement and to study the initial stages of recrystallization. As soon as the predetermined temperature had been reached, heating stopped automatically and the specimens were quenched in water.

The grain size was determined on diametral (in upsetting) and longitudinal (in rolling) macrosections and microsections of billets under an optical microscope with the method of random secants. A special technique of sample preparation and etching was used to determine the grain boundaries. The fine structure was investigated using foils, under an electron microscope, MNB-100K X9000. The mechanical properties at room temperature were estimated using standard specimens (dia. 5 mm, gauge length-25 mm) after conventional heat reatment.

RESULTS

To obtain systematic information on the process of recrystallization of the beta phase in titanium alloys and to select reasonable coarse-grained structure refinement parameters, we have studied the dependence of the beta-grain size on temperature and the degree of the preliminary alpha+beta deformation on temperature, aging time, and heating rate during subsequent beta annealing.

Annealing of cast billets deformed in the alpha+beta region at temperatures below the transformation temperature causes no marked change in their macrostructure, and the refinement is ob-

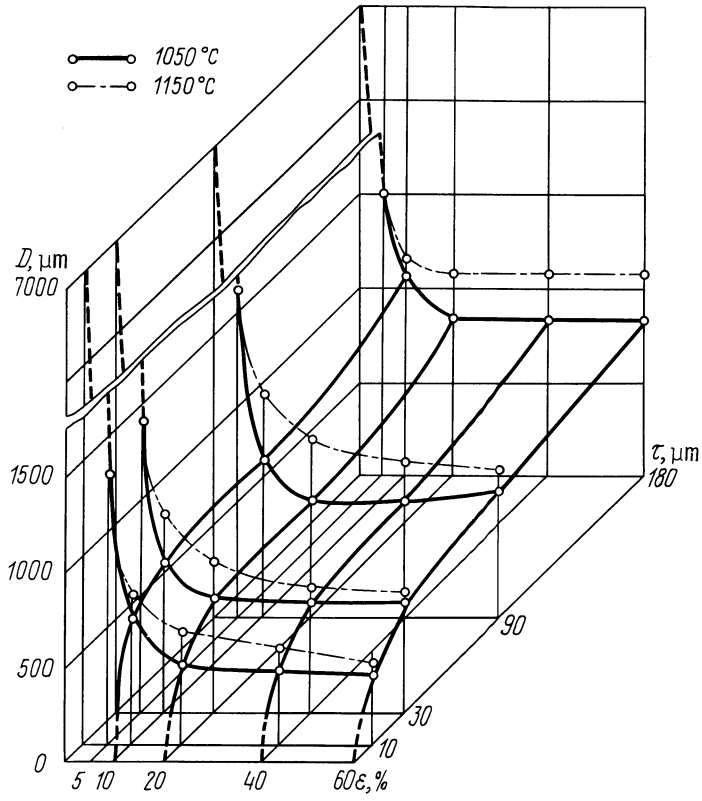

Fig. 1: The recrystallization diagram of alloy BT3-1 (cast billet, $t_{def.}$ = 950°C, furnace heating).

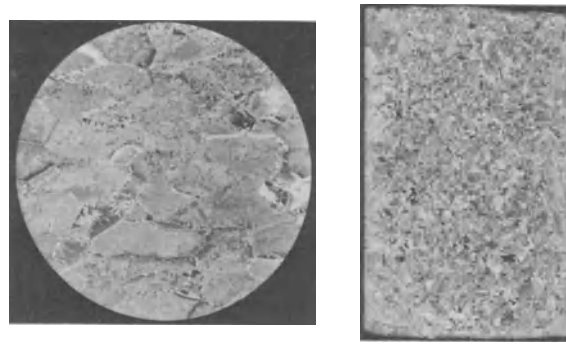

(a) (b)

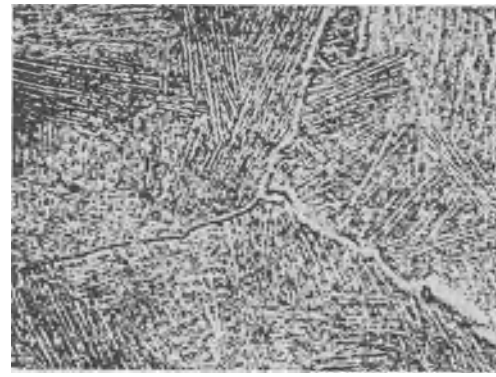

(c)

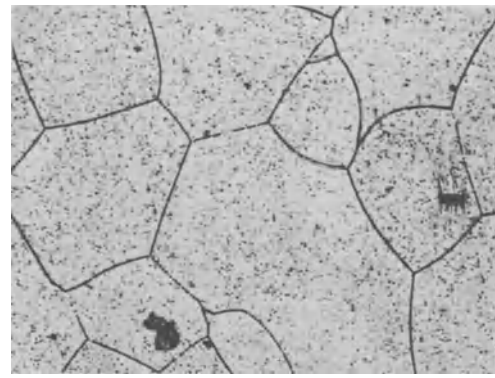

(d)

Fig. 2: Macrostructure - a, b, (1:1) and microstructure- c, d (x250) of alloy BT3-1.
a, b: initial as-cast state;
c, d: ε = 20% at 950°C - 1050°C, 30 min.

served only on heating to the temperatures of the beta region.

As seen from the diagram, annealing at temperatures above the transformation temperature after alpha+beta deformation is accompanied by considerable refinement of the cast structure. Certain refinement after beta annealing can be observed starting from ε=3-7%, depending on the deformation temperature; but reliable efficient grain refinement (with allowance for deformation nonuniformity) by a factor of 8 to 10 throughout the volume in all alloys examined occurs after upsetting with the degree of deformation of 10 to 20 per cent (Fig.1-3). With a further increase in deformation - up to 40 per cent and more - the refinement effect is stabilized. The fact that considerable refinement is achieved at relatively low deformation of low-ductility cast and coarse-grained materials premits this phenomenon to be used in practice. As follows from Fig.3, the most effective improvement of the mechanical properties of cast billets of scull-melted alloy BT9 after annealing at 1050°C takes place in the case of preliminary deformation at 950°C with the degree ε=20 per cent. The ductile characteristics (δ and ψ) increase from 4.5 to 10 and from 8 to 21 per cent, respectively, with a slight increase in strength (σ_c increases approximately by 3 kg/mm^2.)

A rise in alpha+beta deformation temperature causes the refinement effect to decrease, especially at low reductions. For example, as a result of the increase in the upsetting temperature for alloy BT9 from 900° to 980°C (ε=20%), the grain size after subsequent annealing at 1050°C increases approximately three times. In the case of similar deformation in the beta region (1050°C) the effect of grain refinement after beta annealing is altogether absent.

The dependence of the grain size of beta-annealed cast billets of alloy BT3-1 ($D_{mean} \sim 7000\mu$) on preliminary deformation at 950°C, according to the data of metallographic analysis, is presented in Fig.1. Similar partial recrystallization diagrams have been plotted for alloys BT9 and BT18 with the initial melted grain value D_{mean} = = 2000μ and D_{mean} = 8000μ, respectively.

With increasing temperature and annealing time, the size of newly formed grains increases, too, the most efficient growth (as is evident from Fig. 1,4) being observed for the first 30 or 60 seconds.

The use of rapid resistance heating (without isothermal aging) instead of furnace heating in annealing makes it possible to obtain a still finer grain. As follows from the recrystallization diagrams plotted for the scull-melted alloy BT9 with the initial size of cast grain D_{mean} = 2.0 mm, the size of new grains after deformation with =10, 20, and 40 per cent in the case of furnace beta annealing

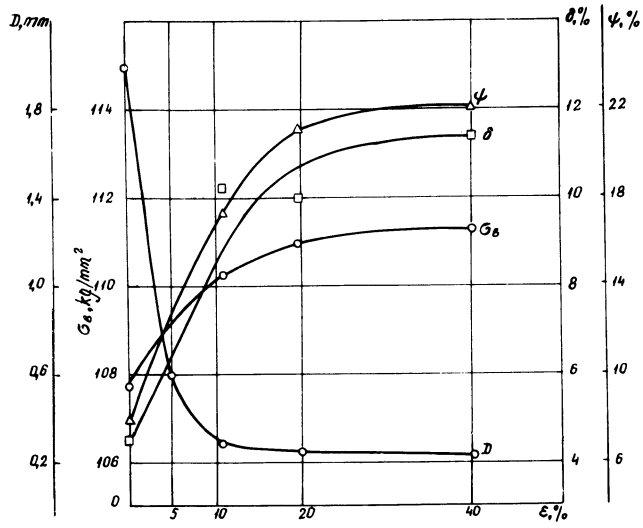

Fig. 3: Influence of the degree of deformation at 950°C on the grain size and the mechanical properties and of alloy BT9 after beta annealing (1050°C, 30 min).

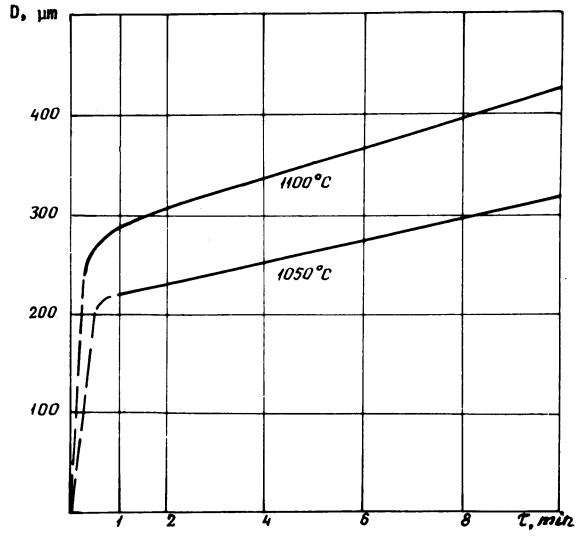

Fig. 4: Influence of the annealing temperature and time on the grain size of alloy BT3-1 (t_{def} = 950°C, ε =20%)
- - partial recrystallization.

during 30 min at 1050°C is 300, 250, and 200 μm (Fig.2), and after resistance heating to 1200°, 1150° and 1100°C for the same degrees of upsetting it is 200, 100, and 70 μm, respectively, which is attributed to an appreciable reduction in the time of specimens stay at β-temperatures owing to the use of rapid heating.

Fig. 5 presents a diagram of variation in the grain size of coarse-grained specimens (D_{mean} = 500 μm) of alloy BT9 (produced from a rolled billet) as a function of deformation in rolling (t^o = 950°C) and of the temperature of subsequent resistance β-heating (V_h = 25 deg/s). The specimens were cooled in air water.

From Fig.5 one can see that the general pattern of the formation of a more fine-grained structure in deformed initial billet, as with a cast one, obeys the behaviour characteristic of the recrystallization process: with increasing degree of preliminary alpha+beta deformation, a finer grain is formed; the temperature of the start and completion of the refinement process decreases (in alloy BT9 deformed by 10 and 40 percent at 950°C the process is completed at 1060°C and 1020°C, respectively, in both cases at temperatures well in excess of the complete phase transformation temperature of 980°C); the higher the temperature and the longer the time of beta annealing, the larger the grain.

The 10-20% deformation (D_{mean} = 500 μm) at 950°C with subsequent resistance heating to 1050°-1100°C enables one to obtain a grain size of about 50-75μ. Yet, in the β-deformed specimens with ε=20 percent, traces of partial recrystallization are detectable only on heating to 1200°C, but even at ε=35% under these conditions the degree of recrystallization does not exceed 10 per cent.

DISCUSSION

A metallographic analysis (x500) of the structure of specimens of the alloys under study immediately after (α+β) deformation reveals no noticeable signs of recrystallization.

After alpha+beta annealing in a furnace the specimens subjected to minor preliminary alpha+beta deformation (10-20%) display fine recrystallized grains of the alpha phase predominantly along the boundaries of old beta grains (at 750°C in alloy BT18 and at 800°C in alloys BT3-1 and BT9). This process, however, does not develop throughout the grain volume on account of the inhibiting action of the beta phase interlayers, nor does it have any marked effect on the macrostructure of billets.

According to the data of electron microscopy[x)] (x900) of alloy BT18, in the as-cast state inside the alpha plates separated by thin

interlayers of the beta phase one can observe individual dislocations (Fig.6a) whose number markedly increases after 5% deformation (at 970°C); in the specimens deformed by 20 per cent the alpha plates have a polygonal structure (misorientation angle is 3°), which is rather stable in subsequent annealing (990°C) up to temperatures of the $\alpha+\beta\rightarrow\beta$ transformation ($t_{trans.}$ = 1010°C). The occurrence of separate recrystallized grains inside the alpha plates was detected only after deformation with ε=40% (Fig.6).

The formation growth of new beta grains and, accordingly, the refinement of coarse-grained plate-like structures at a sufficient ("critical") degree of alpha+beta deformation occur only on heating to beta-region temperatures when the phase transformation has been completed and the barrier action of particles of the residual alpha phase has been obviated.

At the initial stages of the process, at low alpha+beta deformation, one can observe "distortion" of the boundaries, and the nucleation of new beta grains occurs predominantly at deformation localization points, i.e., along the boundaries of old grains and at the slip lines (Fig.6) e.d.. In contrast to steels, in titanium alloys no critical growth of grains is observed at low reduction. As seen from Fig. 6e, on rapid heating at the first stages of formation of new grains the initial grain boundaries are retained; they disappear only during the primary and agglomeration growth of new grains (Fig.6f). The final size of new grains, dependent on the initial grain size, is determined, as demonstrated above, by the temperature and degree of alpha+beta deformation, which account for the quantity of nuclei and their distribution in the matrix, and and by the temperature-time conditions of beta annealing, which govern the rate of growth of these nuclei.

The pattern of the formation and growth of new grains in the alloys under study in beta annealing after alpha+beta deformation and the possibility of the formation of a new, finer structure only after sufficient preliminary deformation testify to the fact that the observed refinement effect results from the recrystallization process.

The beta phase transformation on cooling does not make it possible to follow the mechanism of nucleation of new beta grains. It may, however, be assumed, on the basis of electron microscopy data that in titanium alloys with a small quantity of beta phase, such as alloy BT18, the beta phase under transformation inherits a rather stable subgrain structure of the alpha phase, and the recrystallization process occurs either through coalescence of subgrains or through migration of their boundaries. As regards alpha+beta alloys,such as BT9 and BT3-1, with a larger quantity of beta

x) Electron microscopy of foils was carried out in collaboration with Semenova N.M.

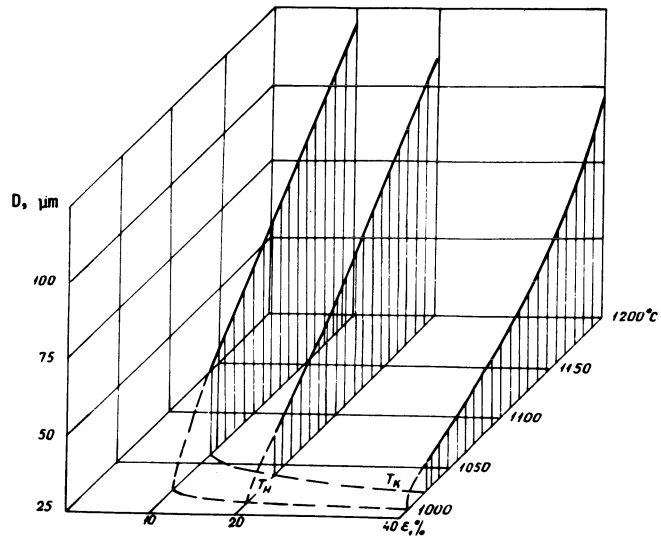

Fig. 5: The recrystallization diagram of alloy BT9 (rolled billet, D_{mean} = 500μm, t_{def} =950°C, resistance heating, V_h = 25 deg/s.
$T_H T_k$ - temperature of the start and completion of the recrystallization process.

phase, it is conceivable that deformed particles of the beta phase itself may also be the centers of new grains therein.

CONCLUSION

(i) Recrystallization diagrams of alloys BT3-1, BT9, and BT18 have been plotted and the possibility of effective refinement of coarse-grained structures, including cast ones, by means of minor alpha+beta deformation (ε = 10-20%) and of subsequent recrystallization beta annealing have been demonstrated.

(ii) It has been found that the use of rapid heating, in place of furnace heating, in beta annealing ensures a better refinement of the beta grain.

(iii) Some suggestions have been made regarding the possible mechanisms of refinement of coarse-grain structures.

REFERENCE

1. Sadovsky, V. D. and Bogachev, Fizika metallov i meyallovedeniye, 1960, v. 10, 132.

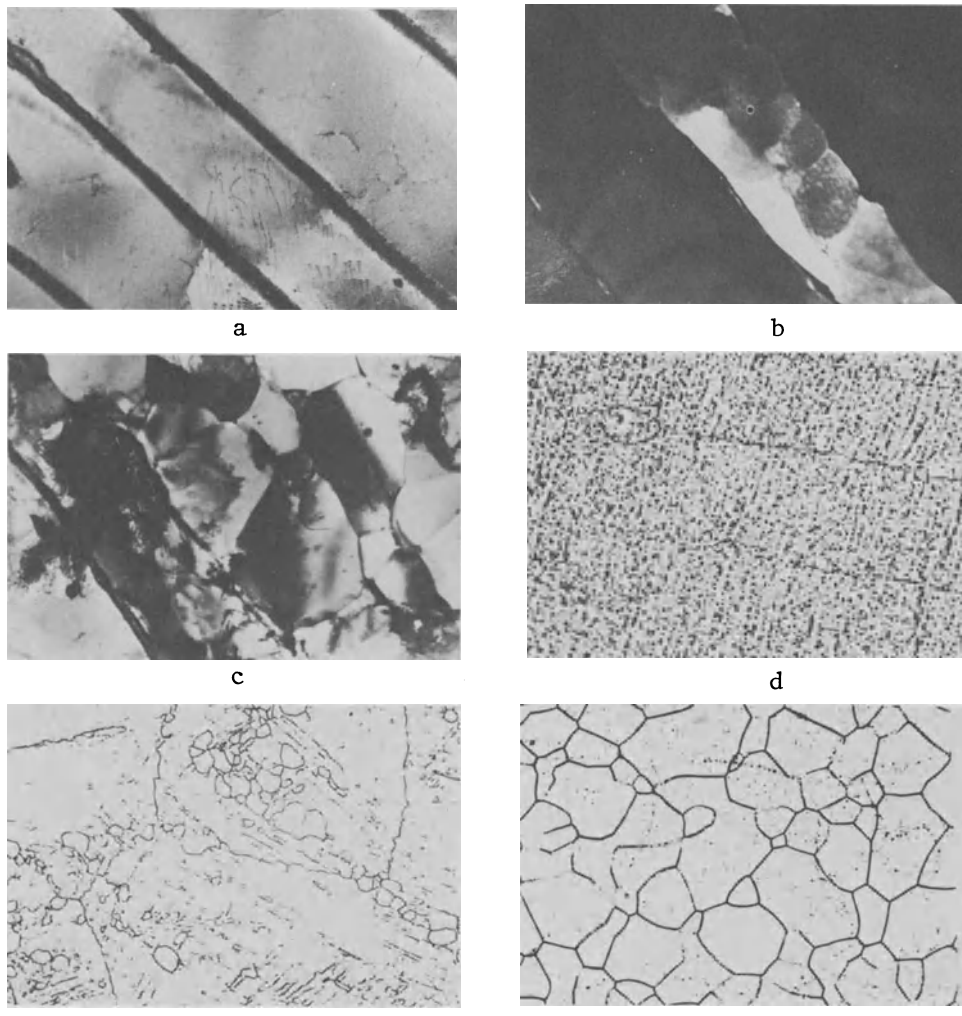

Fig. 6: Structure of alloys BT9 (e,f) and BT18 (a,b,c,d,)

e): ε= 15%, t_{def} = 950°C, resistance heating, t_h = 1040C, V_h = 25 deg/s, x 100;

f): ε = 15%, t_{def} = 950°C, resistance heating, t_h = 1150 C, V_h = 25 deg/s, x100;

d): ε = 10%, t_{def} = 970°C, resistance heating, t_h = 1020 C, V_h = deg/s, x 250;

a): as=cast state, x 9000;

b): ε = 20%, t_{def} = 950°C, x9000;

c): ε = 40%, t_{def} = 950°C, x9000.

THE INFLUENCE OF POLYGONIZED STRUCTURE ON THE PROPERTIES OF HEAT-TREATED BETA TITANIUM ALLOYS

I. S. Polkin, N. M. Semenova and A. B. Notkin

All-Union Institute of Light Alloys

U.S.S.R.

It has been shown in some papers that a polygonized structure in titanium beta alloys is formed after hot deformation. For example, a polygonized structure was obtained by upsetting the BT15 alloy at 860°C with 50% reduction[1] and by extruding the Beta-III alloy at 760°C.[2] The authors indicate a favorable effect of subgrains on the mechanical properties of aged beta-alloys. However, up till now no systematic investigations of the effect of various deformation conditions (temperature, reduction in area) on the character of polygonized structure and its influence on mechanical properties of heat-treated alloys has been carried out.

The aim of this work was to study the structure of the beta-solid solution of BT15 and Beta III alloys under different conditions of hot deformation and to establish the optimum type of structure for obtaining satisfactory ductility in combination with a high strength in the aged state.

Forged rods, 80mm in diameter, of BT15 (Ti-3Al-7Mo-11Cr) and Beta III (Ti-6Zr-11Mo-5Sn) alloys were used for this investigation. Hot deformation was effected by upset forging at 900° and 1150°C with 10, 20, 50, and 75% reduction with the single deformation not exceeding 10%. The final thickness of upset discs was 15mm. After each mode of hot deformation, three variants of water quenching were used, namely, without any interval and with intervals of 30 and 60 seconds. The samples for the investigation were cut out from the central part of the discs.

The basic method used for studying the structure was the transmission electron microscopy. Optical metallography was also used. The preparation of foils was carried out by usual methods.[3]

RESULTS

Hot deformation has yielded three types of structures: polygonized, combined (polygonized + recrystallized), and recrystallized.

The polygonized structure of the Beta III alloy was obtained as a result of upsetting of samples at 900°C with reduction from 10 to 75% and at 1150°C with reductions of 10 and 20%. The polygonized structure in the alloy BT15 was observed after deformation at 900°C with upsetting up to 20%. At higher reductions a combined structure was formed. After deformation at 1150°C with 50-75% reductions recrystallized structure prevailed in both alloys.

It has been determined by transmission electron microscopy that the nature of the polygonzied structure changes with increasing reductions.

Deformation by 10% at 900°C leads to the formation of narrow elongated subgrains with relatively rectilinear boundaries (type-I substructure) (Fig. 1a). It is possible to detect such subgrains only on extinction contours by tilting the sample, which is attributed to the very small angles of disorientation (not more than 1°). Trace analysis has shown that the most probable plane,where the rectilinear boundaries of subgrains are located, is the {112} plane. With an increase in the degree of deformation the rectilinearity of boundaries disappears. The subgrains become more nearly equiaxial, and although some remnants of the elongated structure remain (Fig. 1b), the angle of disorientation increases. The selected area diffraction patterns, obtained for some subgrains, show a splitting of reflections in azimuth up to 5°. We refer to this type of polygonized structure as type-II structure.

It follows from a comparison of structures observed under optical and electron microscopes that the type-I substructure is formed in equiaxial grains after the deformation. The type-II substructure is observed in deformed, elongated grains.

An interval increase between deformation and quenching up to 60 seconds resulted in an enlargement of subgrains.

The formation of three types of structures (polygonized, combined, and recrystallized) in the beta solid solution has a significant influence on the mechanical properties of the aged alloys (see Table I).

As can be seen from the presented data, the best combination of strength and ductility in the aged state is achieved with the formation of the type-II substructure in the Beta III alloy. A

Table I

Change of Mechanical Properties of Aged Beta III and BT15 Alloys Depending on the Type of the Type of the Initial Structure

Alloy	Type of primary structure	Hot deformation conditions		Mechanical properties		
		deform. temperature C	reduction %	σb_2 kg/mm	δ %	ψ %
Beta III hot deformation, aged at 480°, 8 hrs	polygonized, type-I	900	10-20	142	5	11
	polygonized, type-II	900	75	143	7	18
	combined	1050	20	140	5	12
	recrystallized	1050	50-75	142	3	5
BT15 hot deformation, aged at 450°, 25 hrs	polygonized, type-I**	900	10	150	5	10
	combined	900	20-75	120	8	20
	recrystallized	1050	50-75	100	15	39

*The data were obtained on water-quenched samples after deformation without an interval.

**Because recrystallization takes place in alloy BT15 during deformation at 900°C, we failed to obtain a structure with the prevalent type-II substructure.

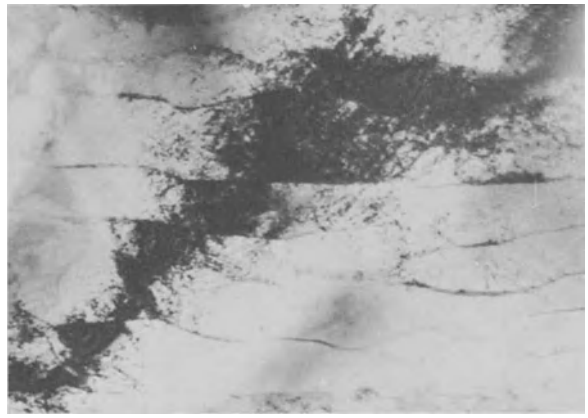

(a)

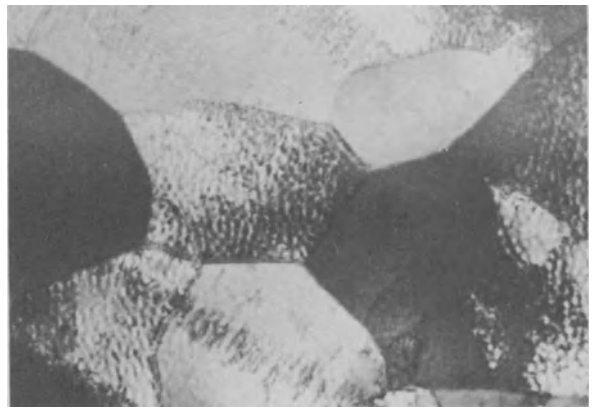

(b)

Fig. 1: Electron photomicrograph of the structure of beta III alloy after hot deformation at 900°C (water quenching without interval):
(a) 10% reduction. Type I substructure;
(b) 75% reduction. Type II substructure.

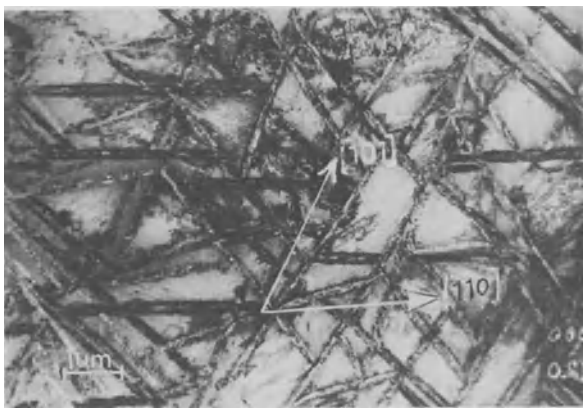

(a)

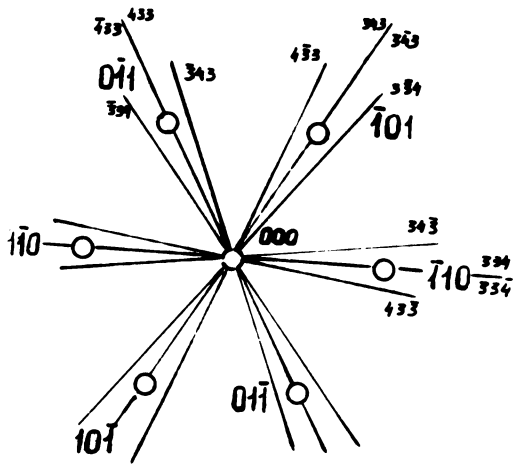

(b)

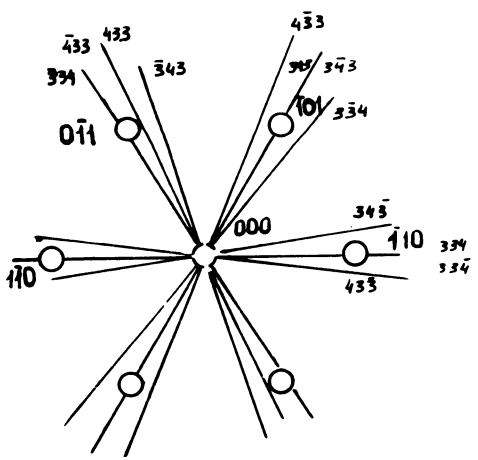

(c)

Fig. 2: Electron photomicrograph of the structure of beta III alloy after aging (480°, 8 hrs) of preliminarily recrystallized material (a) and diagram of selected area diffraction patterns for the axis of zone (III)$_{bcc}$ with plotting of all theoretically possible traces of the habit plane (b) and experimentally observed traces (c).

step-by-step aging (480°C, 8 hours + 560°, 15 minutes) increased the elongation to 7-8% and the reduction in area to 24-26% with the tensile strength preserved at the level of 150kg/mm^2.

The influence of the interval was manifested by the degradation of the plastic characteristics of the samples cooled with an interval of 60 seconds. After an interval of 30 seconds the level of properties did not differ from the data presented in Table I.

The formation of combined and recrystallized structures resulted in a difference in the properties of the investigated alloys. Because the beta phase in recrystallized grains of the BT15 alloy had not undergone decomposition, the formation of combined and recrystallized structures resulted in a lower strength and higher ductility. An intensive decomposition took place in the recrystallized grains of the Beta III alloy.

The polygonized structure obtained in the beta solid solution has a considerable influence on the nature of precipitation of the alpha phase, which is reflected by a substantial size reduction of the alpha-phase particles and the uniform distribution of this phase over the entire volume.

Another feature is the decreasing number of orientations of alpha plates in the polygonzied beta solid solution in comparison with the number of orientations allowed by the Bürgers orientation relationship (OR) generally observed in the aged recrystallized material.

The number of orientations was evaluated by comparing the traces of the habit planes of the alpha plates for the aged polygonized and recrystallized material with the orientations allowed by the Bürgers orientation relationship. For this purpose, the habit of the alpha plates[4] was determined, which is the {334} plane for the Beta-III alloy.

Knowledge of the indices of the habit plane made it possible to plot diagrams, in which all the possible traces of the alpha plates were plotted on definite sections of the beta-phase reciprocal lattice. The analysis of structures in the aged state consisted in determining the beta-phase zone axis in the region under investigation, performing a trace analysis, and comparing the experimentally observed traces with the theoretical diagrams.

All of the OR-allowed variants of the alpha-phase (Fig. 2a, b, c) are present in the structure of recrystallized samples after aging.

A lesser number of orientations of the alpha-phase is formed during the aging of the polygonized structure with a small angle of disorientation between subgrains (type -I structure) than after the

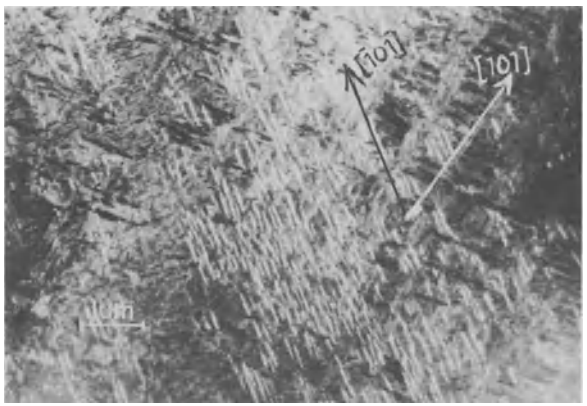

(a)

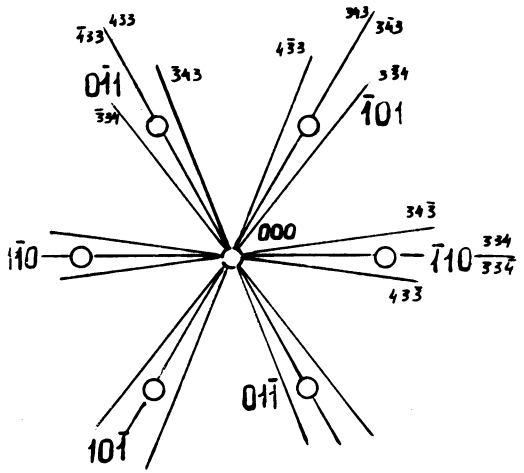

(b)

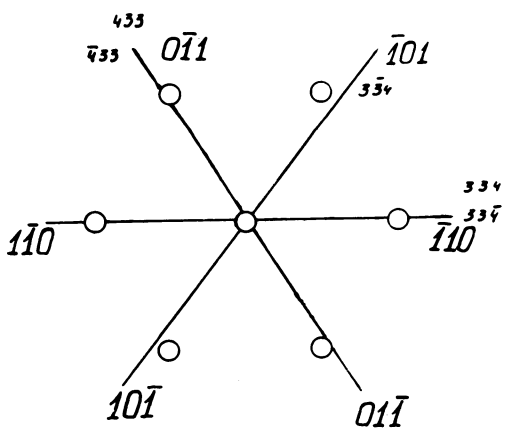

(c)

Fig. 3: Electron photomicrograph of the structure of beta III alloy after hot deformation at 900°C, 10% reduction (type I substructure) and subsequent ageing at 480°, 8 hrs (a) and diagrams of selected area diffraction patterns for the axis of zone $(III)_{bcc}$ with plotting of all theoretically possible traces of the habit plane (b) and experimentally observed traces (c).

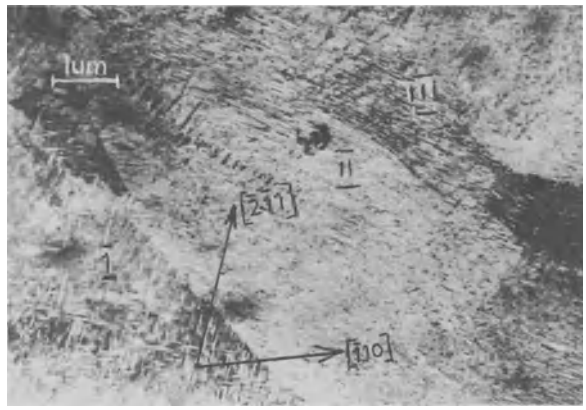

(a)

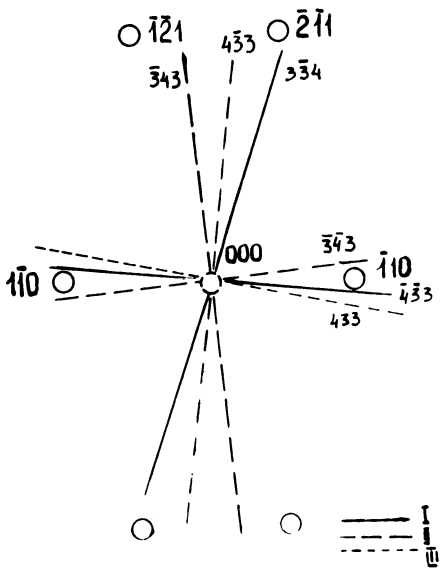

(b)

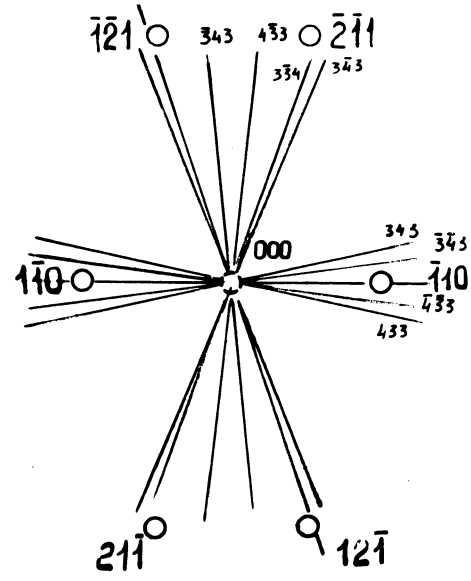

(c)

Fig. 4: Electron photomicrograph of the structure of beta III alloy after hot deformation at 900°C, 75% reduction (type II substructure) and subsequent ageing at 480°C, 8 hrs (a) and diagrams of selected area diffraction patterns for the axis of zone $(113)_{bcc}$ with plotting of all theoretically possible traces of the habit plane (b) and experimentally observed traces (c).

aging of the recrystallized material (Fig. 3). Besides, in the type-I substructure the direction of the alpha plates does not vary from subgrain to subgrain.

In subgrains with a disorientation of 3-5° (type-II substructure), likewise, a limited number of alpha plate orientations prevails; however, the neighboring subgrains differ in the orientation and direction of the alpha plates.

Figure 4 shows the structure of the Beta-III alloy after hot deformation at 900°C with 75% reduction (type-II substructure) and subsequent aging at 480° for 8 hours.

A comparison of the diagrams (Fig. 4, b and c) indicates that each of the three subgrains A, B, and C has a limited number of orientations, and the direction of traces of the alpha plates in each of the subgrains differs from that in the neighboring subgrains.

The decrease in the number of orientations of the alphs plates in comparison with the structure of the recrystallized material, where all possible orientations of the alpha-phase are realized with respect to the orientation relationship, is due to the fact that the alpha-phase nucleate on dislocations that form the boundaries of subgrains. A similar phenomenon was observed during the investigation of martensite transformation[5] in pre-deformed austenite.

CONCLUSION

The results of this investigation show that the properties of the aged Beta III and BT15 alloys are determined by the structure of the primary beta solid solution formed during hot deformation.

It has been established that the optimum type of structure is the polygonized one with relatively equiaxial subgrains disoriented by no less than 5°.

The main advantages of the polygonized structure are, firstly, the possibility of more homogeneously distributed products of decomposition of the beta solid solution, which eliminates the heterogeniety of mechanical properties, and secondly, the possibility of improving the plastic characteristics in the aged state.

The positive effect in the aging of the polygonized structure seems to be due to the fact that subgrains with a disorientation of not less than 3-5° behave like grains, because each subgrain, much like a grain, has a set of orientations different from those of the neighboring subgrains.

It has been found that in the polygonized structure, after aging, the number of alpha-phase orientations is reduced in comparison with the number of OR-allowed orientations formed in the recrystallized material.

REFERENCES

1. Trenogina, T. L., Murzaeva, G. V., Lerinman, R. M., Potanenko, Y. I. and Kaganovich, I. M., Electron Diffraction Microscopic Analysis of Structural Changes Occurring in Heat-Treatment and Machining of Titanium Alloys. Physics of Metals and Science of Metals, 1973, v. 36, No. 6, 1242-1252 (in Russian).

2. Adair, A. M. and Roberson, J. A., The Influence of Thermomechanical Processing on the Structure and Properties of Extruded Beta III Titanium. Proc. Second S. Conf. on the Strength of Metals and Alloys, 1970, v. III, 932.

3. Blackburn, M. J. and Williams, J. C., The Preparation of Thin Foils of Titanium Alloys. Trans. AIME, 1967, v. 239, No. 2, 287.

4. Utevsky, L. M., Electron Diffraction Microscopy in the Science of Metals. Metallurgy Publishing House, 1973 (in Russian).

5. Bokros, J. C. and Parker, E. R., The Mechanism of the Martensite Burst Transformation in Fe-Ni Single Crystals. Acta Met., 1963, v. 11, No. 12, 1291-1301.

TRANSMISSION ELECTRON MICROSCOPY STUDY OF STRUCTURAL CHANGES HOT DEFORMATION OF TITANIUM ALLOYS

R. M. Lerinman, T. L. Trenogina and O. A. Yolkina

Institute of Metal Physics, the Urals Scientific Centre
USSR Academy of Sciences
U.S.S.R.

The investigation of microstructural changes during hot deformation of titanium alloys is of great practical interest especially for the establishment of optimal regimes of high-temperature mechanical treatment and for the study of possibility of application of hot deformation of $\alpha+\beta$ alloys in β field. Deformation in the β field offers well-known technological advantages as well as improvements in plane strain fracture toughness and creep strength resistance.(1) At the same time, β deformation, as numerous investigations reveal, decreases tensile ductility of the alloys in comparison with deformation in $\alpha+\beta$ field. However in (1) it was demonstrated that the proper choice of deformation conditions in beta field of Ti-6Al-4V results in the same tensile ductility as after $\alpha+\beta$ deformation. The main prerequisite being extensive deformation with no recrystallization.

Unfortunately, no investigation of the fine structure of this alloy was carried out, even though it appears to be desirable for understanding the reasons of this effect.

The present work is devoted to an electron and light microscopy study of hot deformation effects on dislocation structure and transformation product structure obtained during quenching after deformation of $\alpha+\beta$ alloy VT9 and β alloy VT15. The microstructure of alloy VT15 is not only of interest in itself but also because it models the dislocation structure of the β phase after hot deformation in $\alpha+\beta$ alloys. Due to the high stability of β phase in this alloy, the process of phase transformations is avoided during quenching. In alloy VT9, martensite is formed in the process of water quenching or the mixture $\alpha+\beta$ phases formed during air cooling makes it

almost impossible to observe this dislocation structure.

MATERIALS AND PROCEDURE

The chemical composition of the alloys VT15 and VT9, of which the specimens were prepared, is given in Table I.

The specimens were deformed by upsetting on a 35-ton universal tensile tester (static loading) using a special fusible lubricant. Deformation regimes used were: deformation temperature of alloy VT15-900°C and 1100°C, alloy VT9-950°C, 1000°C and 1100°C. The alloy VT15 was held at these temperatures for 15 min, alloy VT9 for 1 hr, while reductions ranged from 0 to 60%. Subsequently, the specimens were cooled in water or air.

Thin foils for electron microscopic analysis were prepared by electropolishing in the mixture of perchloric acid and acetic anhydride at +15°C, then in the mixture of perchloric acid, methyl alcohol and n-butyl alcohol at -50°C.

RESULTS AND DISCUSSION

Alloy VT15 After Deformation in the β Field (at 900°C)*

With increased reduction, dislocation structure of the original β grain is changed. In water quenched samples, at 10%-deformation, there appear single dislocations and dislocation networks in the grains while at 30%-deformation initial grains are broken into subgrains as a result of dynamic polygonization of the alloy (Fig. 1).

The subgrain sizes vary from 0.5 to 2-3μm (original grain sizes range from 20μm to 160μm). The subgrain boundaries consist of dislocation arrays and dislocation networks. Inside such polygons there are single dislocations and their pile-ups. Previously [2] it was found that in the process of air cooling after deformation, recovery and polygonization were more complete and subgrains were almost clear of dislocations.

Grain boundaries, which were smooth prior to deformation, became serrated as a result of localization of shear at boundaries already after 10%-deformation, while grains themselves still remain equiaxial. With further increase of reduction the alloy grains become appreciably elongated, their boundaries becoming progressively serrated.

*Temperature $\alpha+\beta \rightarrow \beta \simeq 700°C$.

Table I

Alloy	Al	Mo	Cr	Zr	Si	Fe	N	C
VT15	2,60	7,87	11,0		0,13	0,17		
VT9	6,20	3,20		1,90	0,24	0,18	0,02	0,04

Editor's Note: I believe VT9 contains tin also.

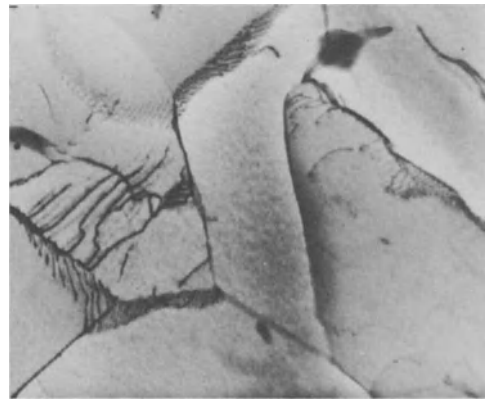

Fig. 1: Polygonized structure of alloy VT15 after 30% deformation at 900°C and water quenching, x25000

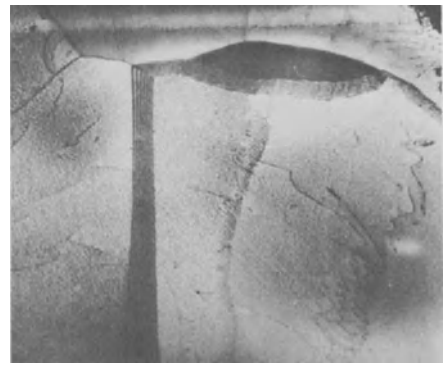

Fig. 2: Recrystallization nucleus in alloy BT15 after 60% deformation at 900°C and water quenching, x 14000

Fig. 3: Polygonized structure and stacking faults of alloy VT15 after 60%-deformation and water quenching, x 25000

After 60%-deformation recrystallization nuclei at original grain boundaries are observed (Fig. 2). Grains themselves are broken into polygons, inside which one can see single dislocations and their pile-ups.

Alloy VT15 After Deformation in β Field (at 1100°C)

Heating of the alloy at 1100°C leads to considerable coarsening of grains. After water quenching, single dislocations are observed in the grains with pile-ups and stacking faults, in agreement with(3). Dislocation density is greater than in the case of lower quenching temperatures, which is accounted for by greater quenching stresses at higher quenching temperatures and a higher diffusion mobility of impurity atoms which provides a possibility of creating stable concentration atmospheres of these atoms in the vicinity of dislocations during subsequent cooling. The stable concentration atmospheres decrease dislocation mobility.(4)

Starting at 10%-deformation the alloy grains are elongated and their boundaries serrated. Electron microscope study of thin foils showed that at reductions of 10, 30 and 60% the grains develop polygonal dislocation substructure (Fig. 3) which, as expected, is coarser than that observed after deformation at 900°C.

Alloy VT15 which was deformed at 1100°C and water quenched is characterized by the appearance of greater stacking faults than after mere quenching from 1100°C. An especially large number of stacking faults are observed at 60%-deformation mainly in subgrain boundaries(Fig. 3).

Alloy VT9 After Deformation in α+β Field (at 950°C)*

Temperature 950°C approximately corresponds to the recrystallization point of cold-deformed alloy VT9. As was shown by microscopic investigation, hot deformation of this alloy up to 60% does not yet result in recrystallization. However, microscopic study makes it possible to observe certain boundaries inside original β grains (Fig. 4a). It is hard to determine directly the type of the boundaries (high or low angle boundaries) because dislocation structure formed by hot deformation is disguised by the martensite. On the basis of study of the hot-deformed β alloy VT15 one can suppose that coarse initial β grains in alloy VT9 are broken into subgrains in the process of dynamic polygonization. The examination of electron microdiffraction patterns revealed that one deals with subgrains, whose misalignment does not exceed a few degrees. Subgrain sizes 0.5-10μm, as a rule, determine the length of plates of ortorhombic α''martensite, as the plates are retarded or stopped at the subgrain boundaries (Fig. 4b). However, there are cases

*Temperature $\alpha+\beta \rightarrow \beta \simeq 1020°C$.

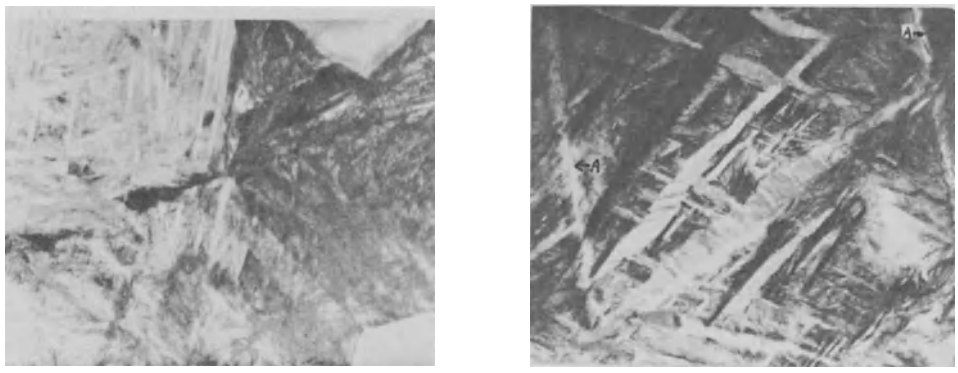

Fig. 4. Polygonized structure of alloy BT9 after deformation at 950°C and water quenching. Reductions are as follows: a)30% and b)60%. A-subboundary. x17000

Fig. 5: Polygonized structure of α grains of alloy VT9 after 60%-deformation at 950°C and water quenching. x 12500

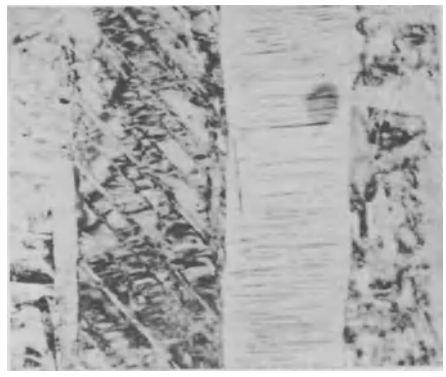

Fig. 6. Microstructure of alloy BT9 after quenching from 1100°C and tempering at 500°C for 15 min. x3000

when martensite passes through sub-boundaries. Inheritance of austenite sub-boundaries by martensite crystals was also observed in alloyed steels.[5,6] The polygons are also formed in residual α phase during the process of hot deformation. The polygon boundaries represent dislocation networks or walls (Fig. 5).

With increased deformation, the plates of residual α phase inside β grains are noticeably reduced in size while β phase grains are elongated. Thus after 60%-deformation initial β grains appear as long fibres with serrated boundaries. As for α plates their length becomes approximately 5 times smaller than in the alloy deformed by 30%. In residual α phase after 60%-deformation at 950°C along with the boundaries of subgrains, there are also high angle boundaries. Partial recrystallization of α phase appears to occur already at 60%-deformation.

During air cooling of alloy VT9 no martensite transformation takes place. Alpha phase plates with complicated dislocation networks are precipitated in original beta grains.[2] Evidently alpha phase also inherits dislocation structure produced in the process of hot deformation.

Alloy VT9 After Deformation in β Field (at 1100°C)

Deformation at 1100°C also gives rise to elongation of initial β grains and serration of their boundaries. In a deformed alloy hexagonal martensite produced by quenching from this temperature is finer, than in an undeformed alloy (conf. Fig. 6 and 7). Substructure of martensite plates- blocks of dislocation type and twinned type with twinning plane $\{1\bar{1}01\}_{\alpha'}$ is well resolved by electron microscopy method in an undeformed alloy. It loses its clarity in electron microscope images of alloy quenched after deformation which is presumably associated either with peculiarities of structure or with difficulties of preparing thin foils in this stressed state. Taking into consideration that no essential changes in the size of martensite crystals, their boundaries and substructure take place, the investigation of low-tempered specimens, rather than quenched ones, was conducted.

The examination of electron microscopic images showed that the refinement of martensite crystals occurs due to creation of polygonal substructure in initial β grains as is the case at α+β deformation. The polygon boundaries are serrated which is presumably a consequence of both interaction of glissile dislocations between sub-boundaries and retarding of martensite plates (Fig. 7). The latter explains also the observed curving of martensite plate boundaries. In the martensite of a deformed alloy complicated dislocation networks are noticed more frequently than in an undeformed alloy (Fig. 7). All this is a result of inheritance of a disloca-

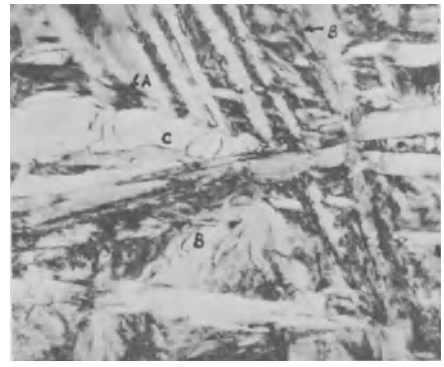

(a)

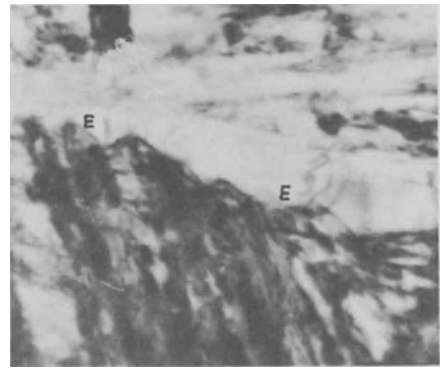

(b)

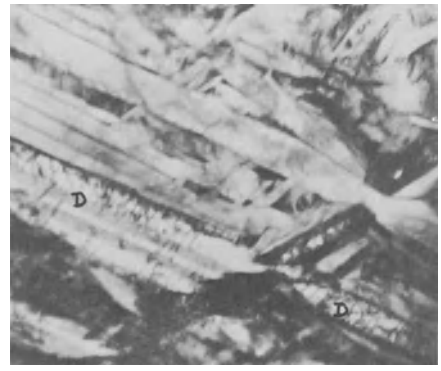

(c)

Fig. 7: Microstructure of alloy BT9 after 30%-deformation at 1100°C, water quenching and tempering at 500°C for 15 min. A,B-subboundaries, C-curved boundaries of martensite crystals, D-dislocation networks in martensite, x 30000, E-subboundary A after tilt, x 5000

Fig. 8: Recrystallization nuclei in alloy BT9 after 60%-deformation at 1100°C and water quenching, x 150

tion structure formed during hot deformation. Similar effects are also noticed in steel.[6,7] Martensite crystal refinement in the alloys studied decreases the quantity of twins inside the crystals. It is a well-known fact that twinning is made difficult in small volumes.

With the increased amount of hot deformation the original β grains are more and more elongated. After 60%-deformation they acquire the shape of fibres. Polygonization in these grains begins to be replaced by recrystlalization. At this reduction, nucleation of recrystallized grains is most often observed at initial grain boundaries (Fig. 8). Martensite substructure in the recrystallized grains becomes clearly distinguished.

Partial recrystallization leads to heterogeneity of structure and development of recrystallized grains in a variety of grain sizes which can bring about a deterioration of mechanical properties. The investigation of the effect of temperature and the amount of deformation on mechanical properties of alloy VT8 which is similar to VT9 has shown that tensile ductility actually decreases beginning from 60%-reduction at 1080°C and from 80% at 1040°C.

It should be noted that serration of grain boundaries and sub-boundaries will hinder the process of sliding along them which results in rising creep strength of the alloy. The relative fraction and role of serrated sub-boundaries and grain boundaries at β deformation is greater than at α+β deformation. It is presumably one of the basic reasons for a higher level of creep strength of the alloy after β deformation. More even interphase boundaries are prominent after α+β deformation.

Thus it was shown that there is an optimal interval of amount of reduction at high-temperature deformation in both β field and α+β field where homogeneous polygonized structure is formed. Polygonal structure with dislocation sub-boundaries and dislocations inside polygons are observed both in initial α and β grains. The formation of homogeneous polygonized structure results in finer dispersion of transformation products of parent β phase. Substructure of phases created during the process of cooling changes is due to the inheritance of enhanced density of crystal lattice defects in deformed parent β phase and due to the refinement of these phases.

It was shown that not only grain boundaries, but also sub-boundaries in hot-deformed titanium alloys have a serrated appearance. These are expected to result in the elevation of high-temperature strength of the alloy.

Partial recrystallization occurring at the reduction that is greater than optimal, bring about the deterioration in mechanical properties of the alloy.

Optimal amount of reduction in β field for the alloy VT9 fall within the limits of $30 < \varepsilon < 60\%$.

REFERENCES

1. Coyne, J. E., The beta forging of titanium alloys, Science, technology and application of titanium, Pergamon Press, 1970, 97

2. Trenogina, T. L., Murzayeva, G. V., Lerinman, R. M., Potapenko, Yu.I. and Kaganovich, I. N., Electron microscopic investigation of structural changes during high-temperature mechanical treatment of titanium alloys, Fiz. metal. metalloved., 1973, 36, 1242.

3. Semenova, N. M. and Utevskij, L. M., Peculiarities of structure of beta titanium alloys after high-temperature heating, Fiz. metal. metalloved., 1970, 30, 1297.

4. Bochvar, G. A., Semenova, N. M. and Utevskij, L. M., Stacking faults and annealing twins in titanium alloys with thermically unstable β phase, Fiz. metal. metalloved., 1969, 28, 1041.

5. Vinnikov, L. Ja., Pankova, M. N. and Utevskij, L. M., Inheritance of dislocation structure of hot-deformed austenite by martensite, Sb. Problemi metllovedenija i fiziki metallov, Moskow, Metallurgizdat, 1972, No. 1, 157.

6. Kozlova, A. G. and Utevskij, L. M., Investigation of martensite structure forming in deformed austenite, Sb. Metallofizika, 54, Kiev, Izd. "Naukova dumka," 1974, 48.

7. Bernstein, M. L., Zaiymovskiy, V. A., Kaputkina, L. M., Laptjev, D. V., Matevosjan, A. P., Smoljakova, L. A., Spasskij, M. N. and Stremel, M. A., Influence of thermomechanical strengthening on structure and properties of martensite, Sb. Metallofizika, 55, Kiev, Ize. :"Naukova dumka," 1974, 49.

INFLUENCE OF FORGING SKIN ON FATIGUE STRENGTH OF DIE FORGINGS IN Ti-6Al-4V MATERIAL

J. Broichhausen
Rhein.-Westf. Techn. Hochschule, Aachen

H. van Kann
Otto Fuchs Metallwerke, Meirnerzhagen, West Germany

In view of their relatively high material and machining costs it appears desirable to produce titanium die forgings approaching the final contours as closely as possible. This does not only permit the most economical use of forging stock, but also helps to reduce the actual machining effort. As with other materials, one endeavours to supply titanium die forgings which have to be machined in the attachment areas only.

Despite the peculiarities associated with the forming of titanium [1], modern die-forging technology has now advanced to the point where certain parts can be produced with enough precision to eliminate the need for machining, at least partially.

The object of the investigations described below is to establish the influence of hot-forming conditions on the fatigue behaviour of titanium die forgings. Actual fatigue life [2] is dependent on a number of factors, such as:

- Orientation of the main direction of forming in relation to the direction of stressing
- Forming temperature, in particular whether the transformation temperature is exceeded
- Material structure, especially the forging skin/base material interface which may be gas-enriched
- Surface finish of the actual die forging.

In order to separate the influence of these factors on fatigue behaviour, test specimens as detailed in Table 1 were produced.

The first test series (Series A) served to quantify the following criteria:

- Main direction of flow (grain flow)
- Forming temperature (forging in the alpha-beta or beta range)
- Surface finish
- Heat treatment.

Further tests (Series B) were performed to obtain information on the influence of protective coating, time of heating, mechanical and chemical post treatment.

The gauge length of Series A specimens is so designed that the broad sides are machined, while the unmachined narrow sides are still covered with the forging skin.

In order to establish notch effect factor β_k* actual fatigue strength was determined on a test series of completely machined specimens.

The Series B specimens were finish-forged in the die, so that no machining at all was required over their gauge length. Only the specimens of one test series were machined all over for determining the β_k* value. In contract to Series A specimens, the entire gauge length of these specimens is covered with the forging skin. The forging stock (30 mm dia. bar material) was preheated to 930 +/- 10°C. At 45 minutes the pre-heating time was deliberately chosen rather long for material of this diameter to obtain a pronounced oxygen-enriched surface layer and to clearly determine its potential influence on fatigue life. For heating prior to actual forging, the test series was divided into batches of 10 specimens to ensure uniform time at temperature.

The die-forging operation was performed with untreated stock and also with a protective coating for temperature insulation between the material and die as well as reduced sliding resistance in the die and lower gas absorption. After final heat treatment (2 h - 700°C/air) the test specimens were trimmed, shot blasted and finally pickled with a mixture of nitric acid, hydrofluoric acid and water to remove not only any scale, but also the diffused layer.

Table 1.

Series	Grain Flow	Surface Coating	Forging Temp. °C	Final Heat Treatment	Test Cross Section	Fatigue Strength σ_{zdW} N/mm²				Notch Effect Factor βk^*
A	Long.	no	900 ($\alpha+\beta$)	2 h/700°C/AC	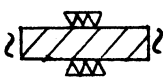	270 (470) [1]				1,74
	Transv.					[400] [2] (460) [1]				1,15
	Long.			1 h/950°C/WQ + 4 h/540°C/AC		210 (540) [1]				2,52
	Transv.					290 (540) [1]				1,86
	Long.		1090 (β)	2 h/700°C/AC		250 (410) [1]				1,64
	Transv.					230 (360) [1]				1,56
	Long.			1 h/950°C/WQ + 4 h/540°C/AC		240 (530) [1]				2,21
	Transv.					220 (530) [1]				2,41
B [3]	Transv.	no	930 ($\alpha+\beta$)	2 h/700°C/AC	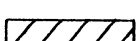	250	270	260	250	1,70 - 1,96
		yes				240	260	200	220	1,77 - 2,35
		no			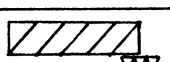	490	460	470	470	-

1. σ_{zdW} found on completly machined round specimens

2. See text

3. The results of series B are splitted in 4 subseries, which were forged in one lot

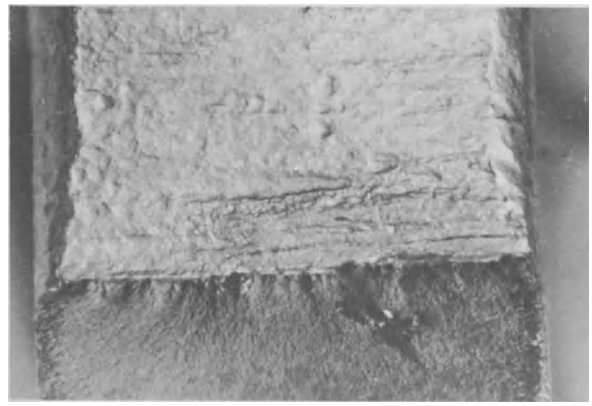

Fig. 1: Sharp Grooves
$\sigma_a = \pm 270\ N/mm^2$
cycles $N = 0{,}016 \cdot 10^6$

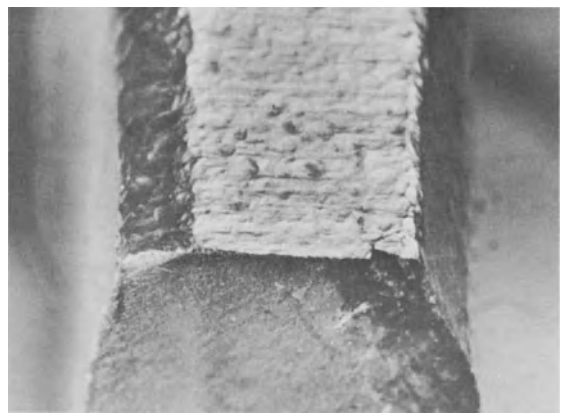

Fig. 2: Round Grooves
$\sigma_a = \pm 300\ N/mm^2$
cycles $N = 22 \cdot 10^6$

Fig. 3: Pronounced depressions
$\sigma_a = \pm 260\ N/mm^2$
$N = 0{,}091 \cdot 10^6$

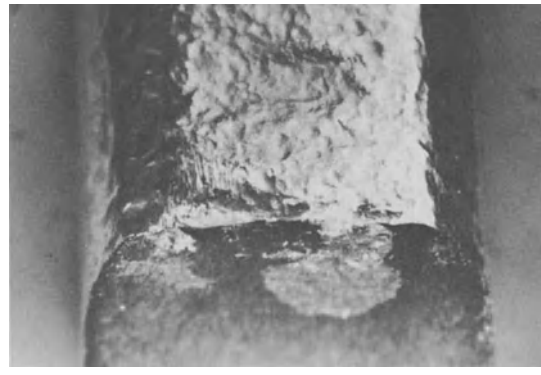

Fig. 4: Local notches
$\sigma_a = \pm 270\ N/mm^2$
cycles $N = 17{,}5 \cdot 10^6$

Macroscopic surface examinations have shown that the various test specimens exhibit the typical characteristics of forging skins and unmachined flash lines, as follows:

- Sharp grooves transverse to the longitudinal axis (Fig. 1)
- Rounded grooves transverse to the direction of stressing (Fig. 2)
- Pronounced depressions (Fig. 3)
- Local notches (Fig. 4)
- Sharp notches (Fig. 5).

After light polishing, the surface of test specimens with fatigue strengths well below the expected values also shows crater formations (Fig. 6).

The conclusions drawn on the basis of the macroscopic examinations are as follows:

- Surface defects such as sharp grooves, depressions and crater formations tend to reduce fatigue life considerably
- Rounded grooves and local notches have a less detrimental effect on strength.

The results of light-microscopic examinations are summarised below:

- As evidence by Fig. 7, the actual shape of surface notches has a dignificant influence on fatigue life
- Even these examinations do not permit to correlate certain types of structure safely, although it appears that in general the strength of acicular material is lower than that of irregularly fine globulitic material (Fig. 8)
- At the forging-skin/base-material interface the structure is uniform irrespective of the actual manufacturing process (with or without protective coating) as well as the mechanical descaling and pickling which are normally applied.

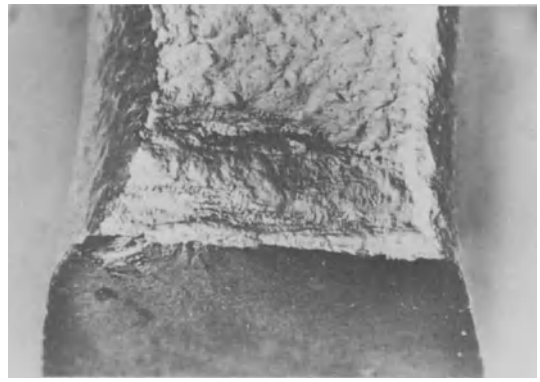

Fig. 5: Sharp notches
$\sigma_a = \pm$ 270 N/mm^2
cycles N = 0,074 • 10^6

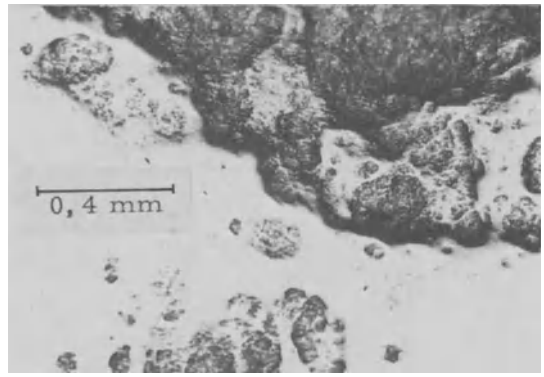

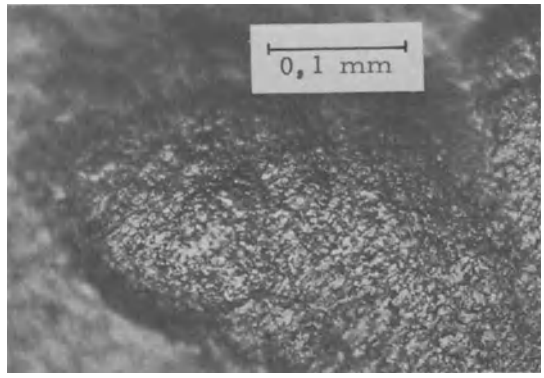

Fig. 6: Crater Formations
$\sigma_a = \pm$ 270 N/mm^2
cycles N = 0,074 • 10^6

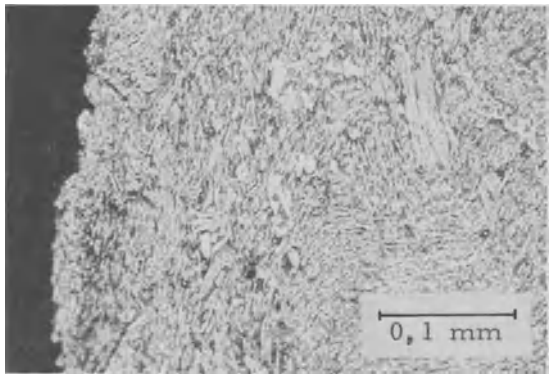

$\sigma_a = \pm 280\ N/mm^2$
$N = 21 \cdot 10^6$

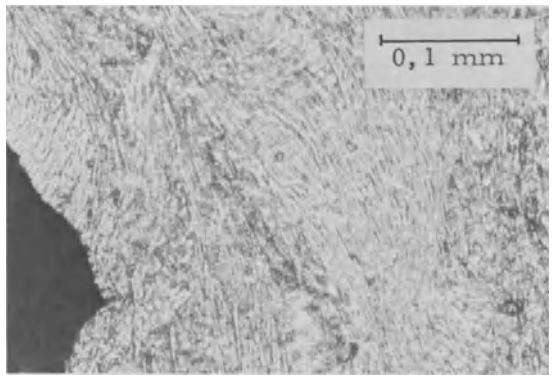

$\sigma_a = \pm 270\ N/mm^2$
$N = 0,35 \cdot 10^6$

Fig. 7:
Shape of surface notches

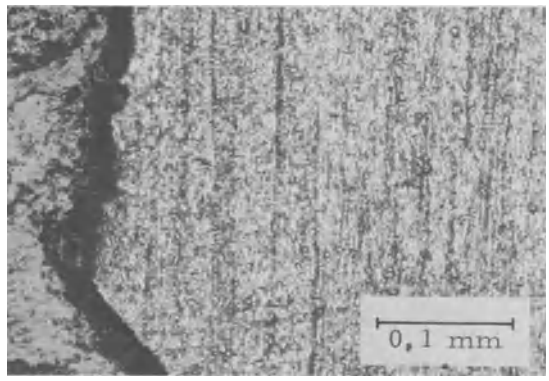

$\sigma_a = \pm 270\ N/mm^2$
$N = 0,35 \cdot 10^6$

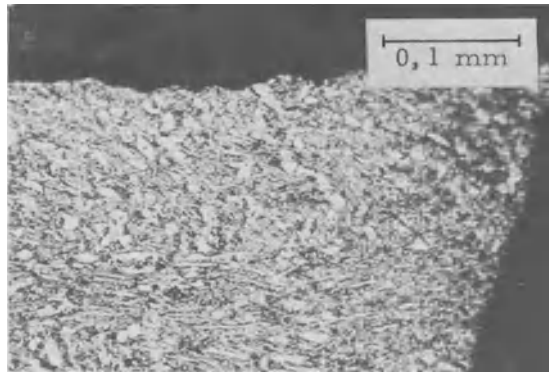

$\sigma_a = \pm 440\ N/mm^2$
$N = 25 \cdot 10^6$

Fig. 8:
Micro-structure of specimens with different fatigue behaviour

The above investigations indicate that the fatigue life of titanium die forgings is essentially dependent on the actual surface finish. In comparison with completely machined forging surfaces, the normal unmachined forging skin tends to reduce fatigue strength to an estimated 50%. Further investigations will therefore be carried out to establish the influence of common industrial surface treatments on the fatigue strength of die-forged test specimens. Initial results show that chemical milling, for instance, helps to offset to a large extent the heavy reduction of fatigue strength associated with unmachined specimens. A paper on this test programme will be published at a later date.

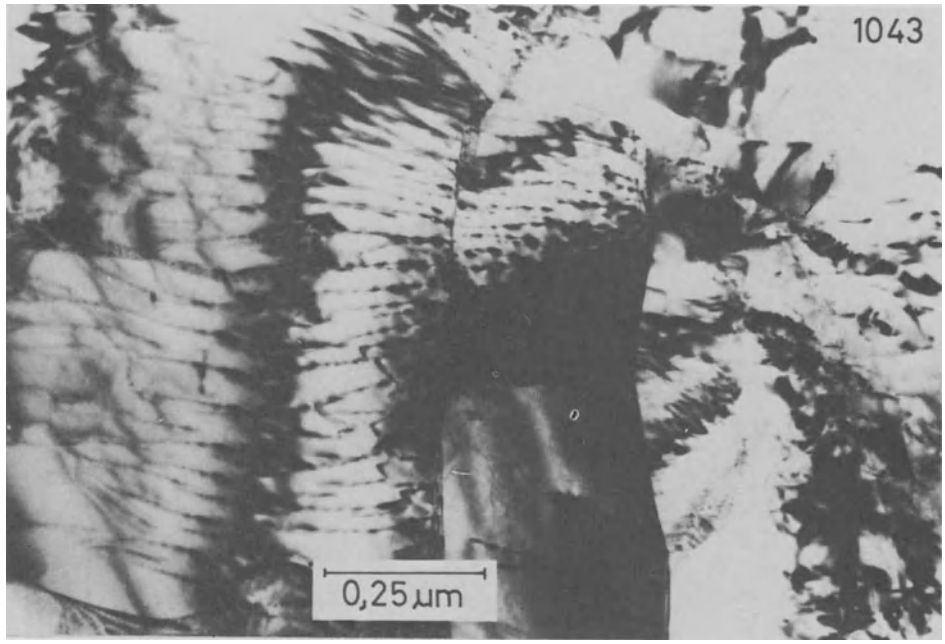

Fig. 9: Micro-structure with high dislocation density

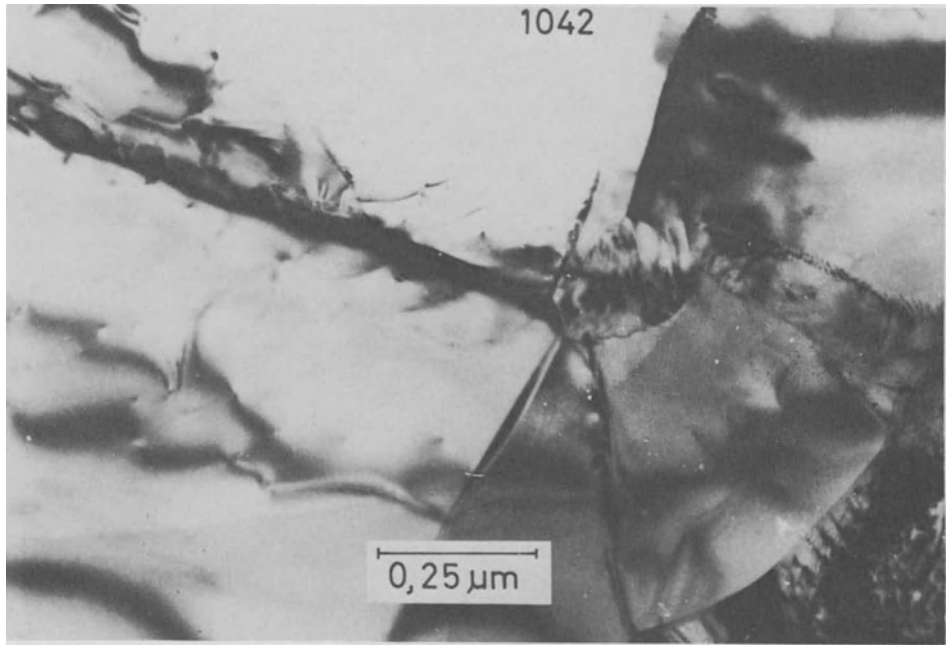

Fig. 10: Micro-structure with low dislocation density

The fatigue strength (tensional-compressional fatigue strength σ_{zdW}) was determined in single-stage tests, and the results were evaluated in the form of a streee-cycle diagram based on the lower limit values.

The test results are summarised in Table 1. In respect of Series A, the following conclusions can be drawn:

- The orientation of the main direction of forming in relation to the direction of stressing does not have any definite influence on tensional-compressional fatigue strength; the test results were found to be inside the expected scatter range.

- The forging temperature does not clearly influence the fatigue strength either.

- Actual heat treatment does not have any conclusive influence on fatigue strength.

- Compared with completely machined test specimens, the fatigue strength is reduced by the forging skin to approx. 40-60%.

- The notch effect factor β_k* of solution treated and aged (STA) titanium is significantly higher than that of annealed material.

As regards Series B specimens, the following has been established:

- The effect of any protective coating on fatigue strength is negligible.

- In agreement with the results obtained on Series A specimens, the fatigue strength is reduced by the forging skin to approx. 42-59% of the values for completely machined specimens.

- The notch factor ranges from 1.70 to 2.35.

The value [2] shown in Table 1 was not included on the above comparison because the reason for its high level is still unknown. As a matter of fact, the relevant tests have not yet been completed. In view of the above and the fact that some scatter ranges are very large [3], further investigations will be carried out.

On test specimens that had not been completely machined all incipient fatigue cracks were found to be located in areas of unfavourable surface finish. One should remember, however, that actual fatigue life also appears to be considerably influenced by the micro structure. The results of current investigations[4] indicate the following:

- The dislocation density and the degree of recovery of deformed areas have a significant influence on fatigue strength. For instance, according to Fig. 9 the material with lower tensional-compressional fatigue strength (σ_{zdW} = 220 N/mm^2) has a much greater dislocation density than the material with high fatigue strength (σ_{zdW} = 380 N/mm^2) Fig. 10. The degree of recovery was found to have the same effect, i.e. the fatigue strength increases as the material recovers.

REFERENCES

1. Kann, H. van:
Der Einflub der Verformungsbedingungen beim Gesenkschieden auf die mechanischen Eigenschaften von Gesenkschmiedestücken aus Titan-Legierungen. TZ für prakt. Metallbearbeitung 6 1 (1967), pp. 325/30.

2. Broichhausen, J. and H. van Kann:
Influence of Forging Conditions on the Fatigue Behaviour of Ti-6Al-4V Material. Titanium Science and Technology. Plenum Press. New York-London 1973, Vol. 3, P. 1785.

3. Broichhausen, J. and H. van Kann:
Einflubfaktoren auf die Dauerschwingfestigkeit von Ti-6Al-4V. 6. Int. Leichtmetall-Tagung Leoben/Wien 1975, S. 258/60. Aluminum-Verlag, Düsseldorf 1975.

4. Broichhausen, J.:
Wechselbeziehung zwischen Mikrostruktur und Schwingungsfestigkeit der Titan-Legierung Ti-6Al-4V. Z. Metallkunde (1976). To be published soon.

THE INFLUENCE OF HYDROGEN ON HOT DEFORMABILITY OF TITANIUM ALLOYS WITH DIFFERENT PHASE COMPOSITIONS

B. A. Kolachov, L. A. Livanov and V. K. Nosov

Moscow Aviation Technology Institute

U.S.S.R.

In a number of papers [1-4] it was established that an addition of hydrogen to titanium alloys increased their plasticity and reduced resistance to deformation in hot forming processes. The favorable effect of hydrogen on deformability of titanium alloys depends upon their phase composition. This paper deals with the results of high temperature tensile tests and resistance to cracking in compression tests of VT1-0 titanium and its VT3-1, Ti9Al and ST5 alloys with hydrogen content from 0.004 wt% (vacuum annealed) up to 0.6 wt%. VT1-0 titanium and VT3-1 alloy in the form of forged rods 20 by 20mm and Ti9Al and ST5 alloys in the as-cast state were used for the study.

EXPERIMENTAL RESULTS

Tensile properties of VT1-0 titanium with different hydrogen contents in the temperature range of 600-800°C at the strain rate of 2.5mm/min are given in Table I. The favorable effect of hydrogen on deformability of VT1-0 titanium is shown from the essential reduction of yield point. The greater reduction in area is characteristic of the hydrogenated samples. The reduction of the total elongation of the hydrogenated samples is due to the sharp local plastic deformation within the neck and the decrease, as a result, of the uniform elongation. The latter may be due to the decrease in strain hardening intensity in the hydrogenated material. A large number of defects such as pores whose amount and sizes increase with decreasing test temperature are found on the longitudinal sections of the samples containing 0.005 wt% hydrogen (Fig. 1a). Internal defects were not observed in samples containing 0.2 and

0.3 wt% hydrogen (Fig. 1b), which gives evidences of greater deformability of hydrogenated titanium at high deformation temperatures.

The decrease in the yield strength of $\alpha+\beta$ VT3-1 alloy with hydrogen addition occurs at 600-800°C. As shown in Table II, the yield strength of the alloy at these temperatures monotonically decreases with increasing hydrogen content. at 900°C the yield strength values are nearly the same for hydrogen concentrations of 0.o; 0.2 and 0.3 wt% remaining, however, below the yield strength of the alloy with 0.005 wt% hydrogen. At the β-phase field temperatures the yield strength values are approximately the same for all hydrogen contents investigated being 2-3kg/mm^2. The favorable effect of hydrogen on the reduction in area of VT3-1 alloy distinctly takes place only at 600°C. In the temperature range of 700 - 900°C the values of reduction in area for VT3-1 alloy with all hydrogen contents investigated are high.

If the addition of hydrogen to VT1-0 titanium caused the decrease in elongation, the increase in elongation with rising hydrogen contents is characteristic of VT3-1 alloy in the whole temperature interval investigated (Table II). It should be noted that the highest elongation values were due to the formation of two or more necks.

The favorable effect of hydrogen is the most pronounced in compression tests of high aluminum alloys: binary Ti9Al alloy and ST5 alloy based on titanium aluminide Ti_3Al.[5] These tests were run using the experimental procedure described in paper.[2]

The results of compression tests of cylindrical samples of Ti9Al alloy prior to the initiation of the first crack under the static loading are summed up in the form of the volume diagram of plasticity in Figure 2. The experimental data obtained show high sensitivity of plasticity and resistance to deformation of the alloy to the phase composition. During compression in the β-phase field (1150-1200°C),samples of Ti9Al alloy with 0.006 wt% hydrogen deform to high reductions without internal defects; however, the lateral surface is covered with sharp folds. The highest plasticity of the alloy is near the transition temperature $\alpha \underset{\leftarrow}{\overset{\rightarrow}{\beta}} \beta$ (1100°C). At this temperature the samples do not fail when testing on the 125 ton press at the maximum reduction (80-85%), specific compression pressure at the reduction ε = 70% being 5kg/mm^2. At α-phase field temperatures the threshold reduction of the alloy is characterized by the severe dependence upon the temperature. In the $\alpha+\alpha_2$-phase field temperature range (750-850°C) even small reductions (10-15%) resulted in the formation of cracks on the lateral surface of the samples.

Table I

Tensile Properties of VT1-0 Titanium with Different Hydrogen Contents in the Temperature Range of 600 - 800°C

Temperature °C	Tensile properties	Hydrogen Contents, wt% 0.005	0.1	0.2	0.3
600	σ_{02}, kg/mm^2	10.5	8.5	7.4	5.8
	δ , %	19.0	33.7	20.1	16.4
	ψ , %	70.7	85.9	86.8	94.6
700	σ_{02}, kg/mm^2	6.9	5.7	5.0	2.2
	δ , %	61.0	51.1	46.0	43.5
	ψ , %	92.0	93.5	97.8	97.7
800	σ_{02}, kg/mm^2	3.7	2.1	1.5	1.3
	δ , %	78.0	55.9	43.5	55.0
	ψ , %	93.8	93.7	98.5	99.3

Table II

Tensile Properties of VT3-1 Alloy with Different Hydrogen Contents in the Temperature Range of 600 - 900°C

Temperature °C	Tensile properties	Hydrogen Contents, wt% 0.005	0.1	0.2	0.3
600	σ_{02}, kg/mm^2	55.6	53.8	49.7	36.4
	δ ,%	22.0	25.5	26.8	36.0
	ψ ,%	68.1	87.2	83.2	98.5
700	σ_{02}, kg/mm^2	38.7	29.4	26.5	24.5
	δ ,%	35.6	58.1	59.3	109.5*
	ψ ,%	94.5	97.3	98.7	98.5
800	σ_{02}, kg/mm^2	17.9	13.5	11.1	7.8
	δ ,%	49.2	62.7	89.5*	151.0*
	ψ ,%	100	100	100	98.0
900	σ_{02}, kg/mm^2	6.1	3.9	4.1	4.0
	δ ,%	79.5	103.8*	126.0*	129.1*
	ψ ,%	97.3	100	100	100

*There are some necks on the samples.

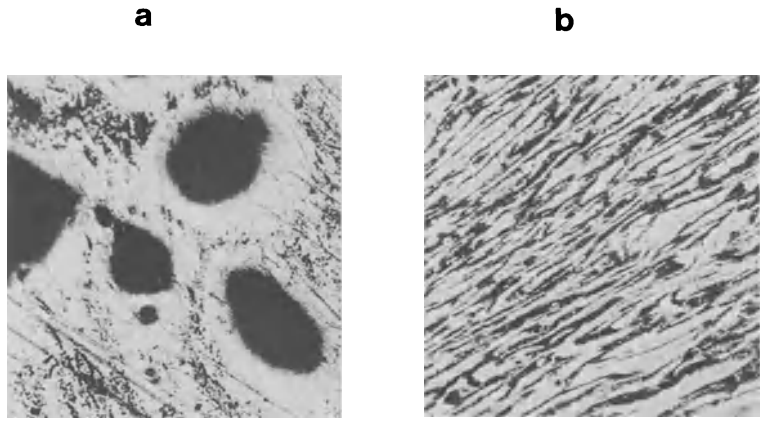

Fig. 1: The microstructure of VTI-0 titanium samples within the neck after the tests at 600°C, x 200
a) 0.005 wt% hydrogen, b) 0.3 wt% hydrogen

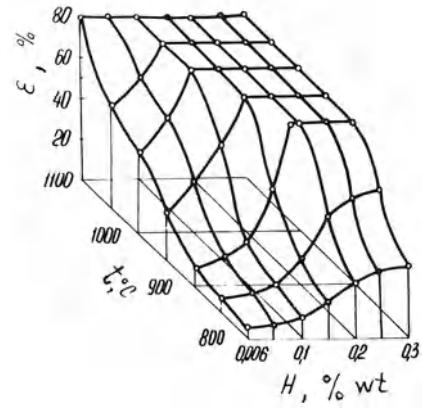

Fig. 2: The effect of hydrogen on the threshold-reduction of Ti9Al alloy in compression tests.

The favorable effect of hydrogen on the plasticity of the alloy takes place already with the addition of 0.1 wt% hydrogen. This hydrogen concentration reduces the maximum plasticity temperature of the alloy from 1100°C to 1000°C (Fig. 2). By further increasing hydrogen contents up to 0.15-0.3 wt% the plasticity increases still greater. The effect of the favorable influence of hydrogen on the compression Ti9Al alloy plasticity was proved by the pneumatic hammer dynamic compression tests. For instance, at 1000°C the samples with 0.006 wt% hydrogen fractured by cleavage after a deformation of 50%, while the samples with 0.1 wt% hydrogen deformed to 80-90% without fracturing.

Hydrogen not only increases the threshold reduction but essentially reduces deforming stresses. Figure 3 shows the specific compression pressure values of Ti9Al alloy with hydrogen concentrations investigated at 1000°C and 900°C. Similar calculations of specific compression pressure values are carried on for all the test temperatures. They showed that with increasing compression temperature the favorable effect of hydrogen on the reduction of specific compression pressure was enhanced.

The samples containing 0.004; 0.15; 0.25 and 0.6 wt% hydrogen were tested in compression to estimate the effect of hydrogen on the processes plasticity of ST5 alloy. As seen in Figure 4, the addition of comparatively small amount of hydrogen (0.15 wt%) significantly increases the threshold compression reduction of the alloy. At the compression temperature of 900°C the first cracks in the alloy containing 0.15 wt% hydrogen were detected at the reduction of 70% whereas the samples with 0.004 wt% hydrogen do not allow 35% compression. The process plasticity of the alloy is especially enhanced by the addition of 0.6 wt% hydrogen, which enables the sample of the alloy based on titanium aluminide Ti_3Al to be compressed above 50% at 800°C. Even at 700°C the samples of ST5 alloy with 0.6 wt% hydrogen are compressed 20-25% without fracture and 75-80% at 900°C.

The increase in plasticity of hydrogenated samples of ST5 alloy is accompanied by the significant decrease in specific pressure as with Ti9Al alloy. Figure 5 illustrates the dependence of specific compression pressure of the alloy with different hydrogen contents upon the reduction at 1000°C. The decreasing specific pressure also takes place at lower temperatures, e.g. at 900°C the compression yield strength decreases from 63 kg/mm^2 in the alloy with 0.004 wt% hydrogen to 38kg/mm^2 in the alloy with 0.25 wt% hydrogen and to 28kg/mm^2 in that containing 0.6 wt% hydrogen.

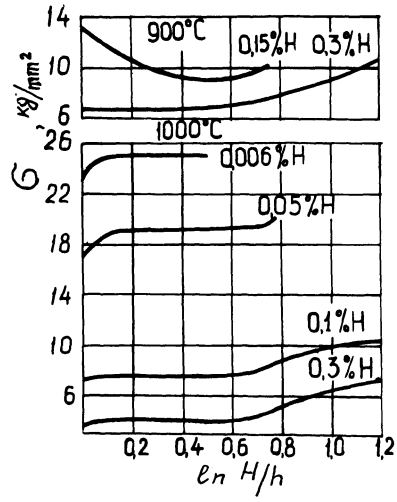

Fig. 3: The dependence of specific compression pressure of Ti9Al alloy with different hydrogen contents upon the reduction at 900°C and 1,000°C.

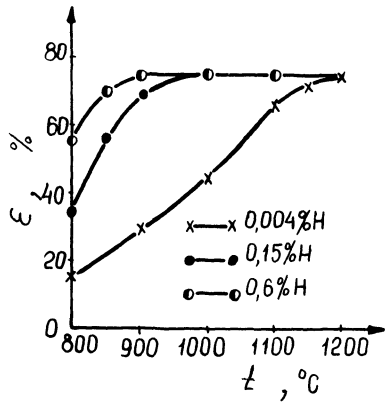

Fig. 4: The effect of hydrogen on the threshold reduction of ST5 alloy in compression tests.

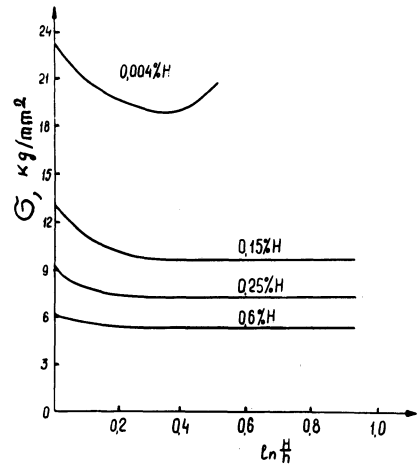

Fig. 5: The dependence of specific compression pressure of ST5 alloy with different hydrogen contents upon the reduction at 1,000°C.

The Mechanism of Hydrogen Plasticization of Titanium Alloys

To explain the favorable effect of hydrogen on the deformability of titanium alloys the following preliminary hypotheses may be suggested:

- alloying titanium alloys by hydrogen contributes to the β-phase stabilization at lower temperatures;
- in high aluminum alloys hydrogen hampers or completely suppresses the embrittling α_2-phase precipitates;
- hydrogen increases the diffusion component of plasticity and involves new slip systems in the hydrogenated material.

The favorable effect of hydrogen on the deformability of VT1-0 titanium takes place at the α+β phase field temperatures. The increase in the amount of the β-phase in VT3-1 alloy with increasing hydrogen contents is confirmed by the data of the microstructural and x-ray phase analysis on the URS-50IM diffractometer. The thermal analysis of Ti9Al alloy (the differential record of the curves of heating on thermogravimetric plant ATVU-10A) showed that when heated the alloy with the initial hydrogen content undergoes α→α+β→β transitions at 1065°C and 1090°C. The α→α+β transition temperature of the alloy with 0.1 wt% hydrogen decreases to 910°C and the

$\alpha+\beta\rightarrow\beta$ transition temperature lowers to 980°C. In the alloy containing 0.4 wt% hydrogen the $\alpha+\beta$ phase field exists from the temperature of the beginning of the heating records (550°C) to 915°C. The addition of hydrogen to Ti9Al alloy at first (0.1 wt%H) results in decreasing the amount of α_2-phase in the course of hydrogenating annealing and then with 0.4 wt%H to its full dissolution. The amount of the β-phase in ST5 alloy increases whereas the α_2-phase amount decreases at the same time. The comparison of the data obtained shows that the favorable effect of hydrogen on the deformability of titanium alloys takes place in the greater degree the more there is aluminum in this alloy. This proves that the suppression of the α_2-phase participates as the result of hydrogenation is one of the decisive factors determining the effect of hydrogen plasticization.

The results obtained give evidences that the addition of hydrogen too hard to deform titanium alloys will allow production of deformed semi-products from the alloys, hot plastic deformation of which is very difficult or practically unreal. However, to eliminate hydrogen embrittlement during service, semi-products from titanium alloys made using the effect of hydrogen plasticization should be vacuum-annealed to safe hydrogen concentrations.

SUMMARY

1. The addition of hydrogen to titanium alloys increases their plasticity and decreases their resistance to deformation in the hot forging temperature interval.

2. The favorable effect of hydrogen on the deformability of titanium alloys is associated, first of all, with the change of their phase composition. Hydrogen increases the amount of the β-phase and contributes to the dissolution of embrittling α_2-phase in high aluminum alloys.

REFERENCES

1. Zwicker, U. and Walter, G., The USA patent, No. 2892742, cl. 148-11, 5.

2. Kolachev, B. A., Nosov, V. K., Livanov, V. A. et al, On the effect of hydrogen on the process plasticity of the Ti9Al alloy. "Izvest. Vuz'ov." Non-ferrous Metallurgy, 1972, No. 4, 137-142.

3. Kolachev, B. A., Livanov, V. A., Nosov, V. K. et al, About the favorable hydrogen effect on the deformability of ST4-titanium alloy. "Kuznechnoshtampov. Proiz. (in Russian), 1975, No. 1, 29-32.

4. Kolachev, B. A., Nosov, V. K., Shchipunov, G. I. and Fainbron, S. M., On high temperature tooth of creep in titanium alloys with intermetallic strengthening, "Fizika metallov i metalloved," 1975, v. 39, p. 611-616.

5. Nartova, T. T., Some problems of physical and chemical theory of high-temperature strengthening and new refractory titanium alloys ST-1; ST-3; St-4 and ST-5, in Titanium Alloys in New Technique, Moskva, Nauka, 1968, p. 176-186.

THE EFFECT OF SOME TECHNOLOGICAL FACTORS ON THE STRUCTURE AND PROPERTIES OF THE EQUIATOMIC TITANIUM-NICKEL ALLOY*

L.P. Fatkullina, V.A. Smalshenko

All-Union Institute of Light Alloys

U.S.S.R.

The equiatomic titanium-nickel alloy (45 wt.% titanium, 55% nickel) exhibits a number of of unique properties: high plasticity, resistance to corrosion, and deformation memory.[1,2].

The object of the paper is to demonstrate the effect of temperature, deformation, and conditions of the subsequent annealing on the structure and properties of the TiNi alloy. The samples were subjected to deformation on the press at a temperature of 20°C with 5, 10, 15, and 20% reductions, and at temperatures of 400-900°C with 5, 20, 30, 50, and 70% reductions. Annealing was done in electric resistance furnaces, and the hardness, electric resistance, grain size, and mechanical properties were determined with the use of standard techniques.

Moreover, the structure and properties of the hot-extruded and hot-rolled semifabricated products with the various reductions in the initial state, the worked state, and after annealing at temperatures of 100 - 900°C were studied. The effect of the "shape memory" was determined by the following methods: (1) the samples, annealed at various temperatures, were bent to an angle of 90° with a radius of 5 mm or they were subjected to (2) tensile deformation at a speed of 0.8 mm/min for 8 - 10% elongation and then they were heated to a temperature of 300°C. The degree of the shape restoration was found by the formula:

$$\text{for the bend tests, } \Phi\% = \frac{90-\Theta}{90} \cdot 100$$

*Dudenkov V.M., Alimkhanova E.S., Rudeva G.M. contributed to the present work.

where Θ is the non-restored angle;

for the tensile tests, $\overset{\rightarrow}{\leftarrow} \Phi\% = \frac{L_1 - L_2}{L_o} \cdot 100\%$

L_o is the initial length of the sample at 20°C;

L_1 is the length of the stretched sample at 20°C after removal of the stress;

L_2 is the length of the stretched sample after heating to 300°C and cooling in the air down to 20°C.

Experimental results presented in Fig.1 show the effect of the cold deformation on the grain size, electrical conductivity and hardness. It can be seen that increasing the reduction up to 15% leads to an increase in the hardness and decrease in electric conductivity and grain size. As a result of a 20% cold deformation the hardness slightly decreases, electric conductivity increases and the bandwidth on the radiographs gets narrow, which is perhaps due to the initial stages of recrystallization.(3)

The annealing of the cold-deformed samples at 100-300°C results in the increases hardness, electric resistance (Fig.2) and bandwidth on the radiographs. On making tensile tests at the same temperature an increase in the yield point is evident.

Increasing the annealing temperature results in the decreased hardness and electric resistance. The minimum values of hardness and electric resistance were noted after annealing at a temperature of 700°C. This suggests that at 700°C there occurs recrystallization. The radiographic methods failed to establish the temperature of the recrystallization initiation since the phase strain hardening appearing at the formation of martensite distorts a true bandwidth on the radiographs.

Figs.3 and 4 show the results obtained on measuring the hardness and grain size of the TiNi alloy following the deformation by 5 - 70% at 400 - 900°C.

The deformation at temperatures of 400 - 550°C causes the structural disintegration* and hardening of the material. Increasing the amount of αreduction by more than 50% leads to some softening, which is probably connected with the alloy recrystallization, whose initiation temperature drops as the %reduction increases.

*Ed.Note - The authors may be referring to a strain induced martensitic transformation

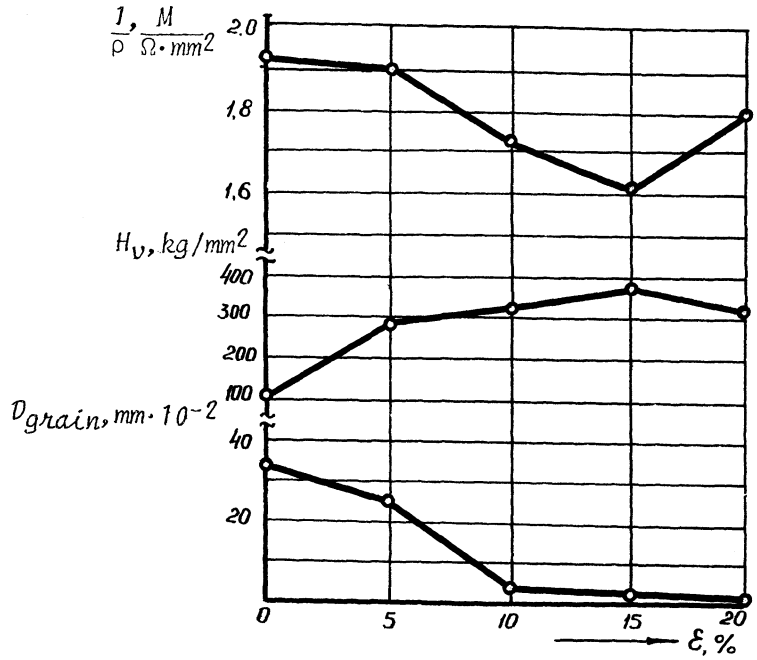

Fig. 1: Effect of the reduction at 20°C on the grain size, hardness and electric conductivity of the TiNi alloy.

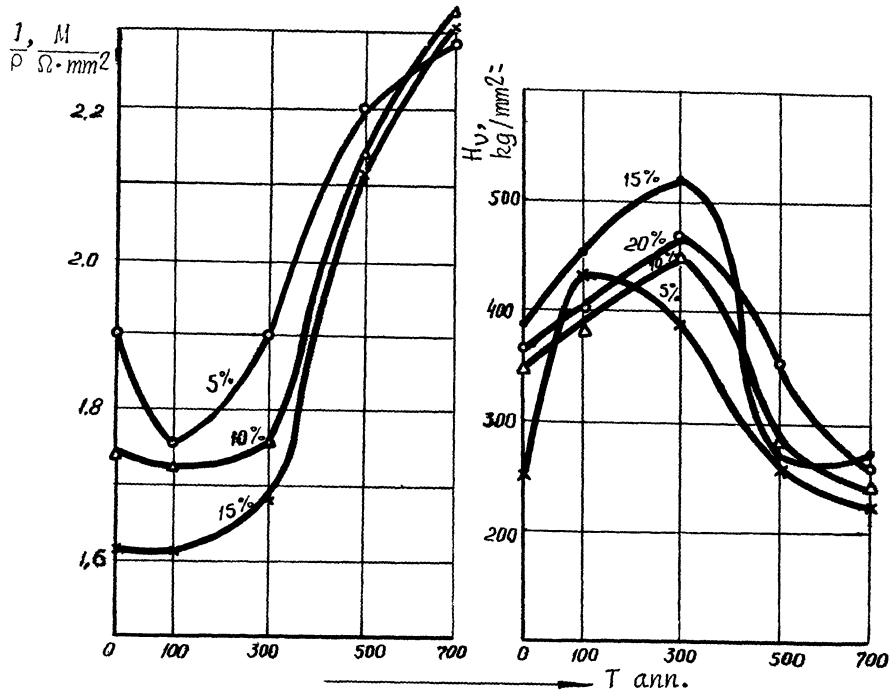

Fig. 2: Effect of the annealing on the hardness and electric conductivity of the TiNi alloy subjected to deformation at 20°C.

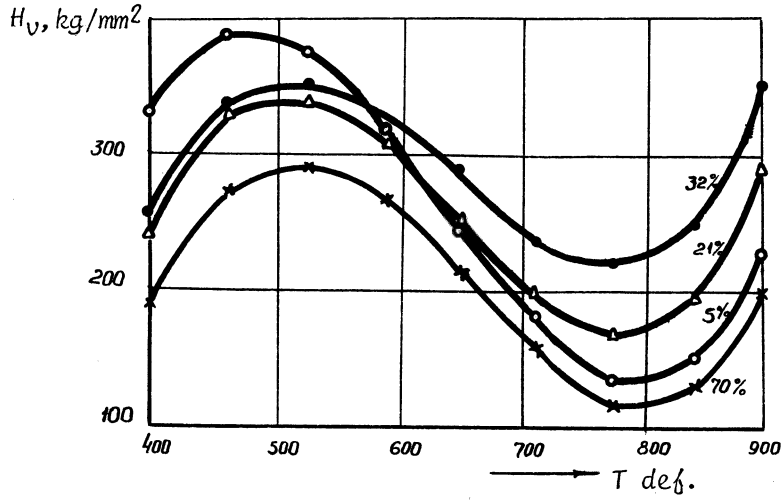

Fig. 3: Effect of the temperature and reduction on the hardness of the TiNi alloy.

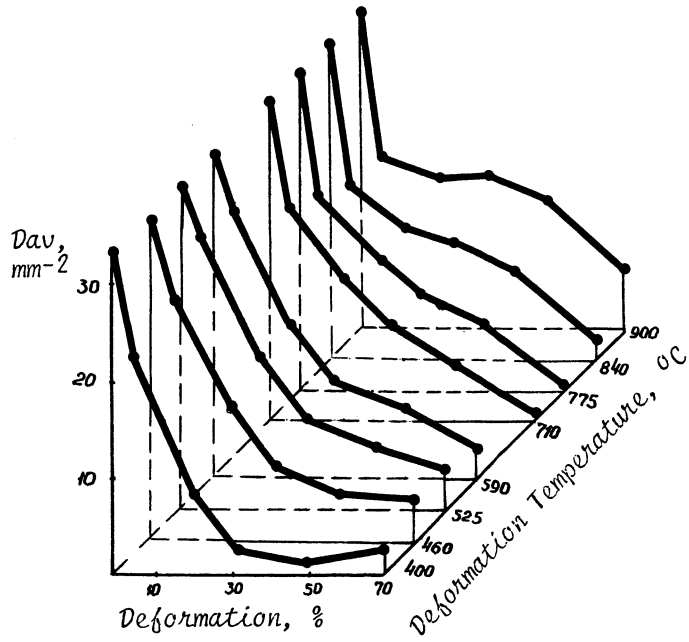

Fig. 4: Effect of the temperature and reduction on the grain size of the TiNi alloy (diagram of the 2nd type recrystallization)

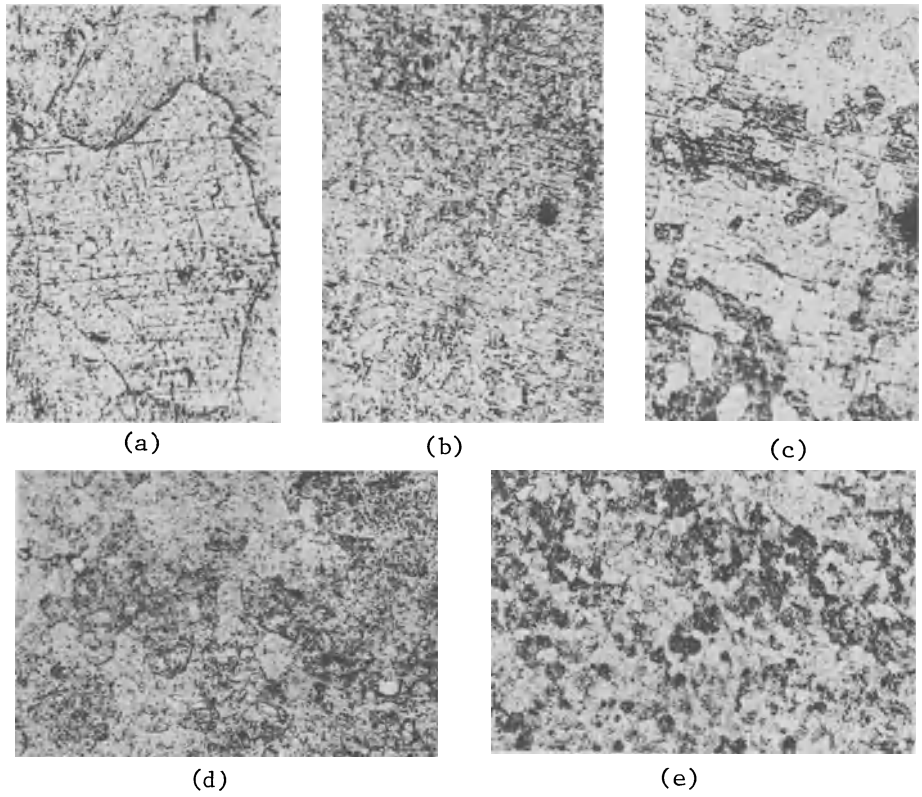

Fig. 5: Microstructure of the TiNi alloy

- in the initial state; (a)
- 15% deformation at 20°C; (b)
- same as (b) + annealing at 700°C for 1 hour; (c)
- 15% deformation at 400°C; (d)
- 50% deformation at 400°C; (e).

magnification at250.

When deformation takes place in the temperature interval 600 - 900°C, the material shows no hardening but the grain size is reduced.

The microstructural analysis reveals that both at the cold and hot deformations a higher degree of deformation causes a reduction in the grain size, which at the same time remains equiaxial (Fig.5).

The metallographic methods failed to reveal the texture of deformation.

In the event of the hot deformation, even at 900°C, grain growth is not observed, i.e. the processes of the secondary recrystallization are restrained.

Thus, the results obtained suggest that it is wise to perform the hot deformation at temperature over 700°C where the material undergoes no hardening and remains fine-grained.

Some products from the TiNi alloys, i.e. hot-extruded rods 240 mm and 20 mm in diameter, hot-rolled bars 18 mm and 8 mm in diameter, were examined in the initial state and following annealing at temperatures of 100 - 900°C. TABLE I lists the corresponding mechanical properties and percentage of the shape restoration, and Fig.6 shows the structure of these semi-products after some annealing conditions. Analytical results demonstrate that as the diameter of the semi-product decreases, i.e. with an increase in the material reduction, the grain size decreases, the ultimate strength and plasticity become higher. Annealing exerts practically no effect on the grain size and mechanical properties of hot-deformed stet-products but affects considerably the shape memory effect. The maximum memory effect is found following annealing at 500°C. As a result of annealing at higher temperatures the degree of the shape restoration is markedly less, which is probably due to the development of the process of recrystallization.

The present investigations enable one to make the following conclusions:

(1) The deformation of the TiNi alloy in the temperature interval 20 - 550°C causes a considerable hardening of the material and structure disintegration.

(2) The deformation at temperatures of 600 - 900°C is not associated with any hardening of the material but encourages a substantial grain size reduction.

(3) A secondary recrystallization was not found to take place in the TiNi alloy.

TABLE I

Mechanical properties of the TiNi alloy semifabricated products

Type of product	Annealing temperature	Mechanical properties at 20°C				
		ultimate strength kg/mm^2	yield strength kg/mm^2	%elong	%R.A.	%of the shape restoration
Rod 240 mm dia	No annealing	46.6	22.2	7.9	15.1	17
	400	41.0	19.7	11.0	17.6	17
	500	50.6	19.6	9.0	17.0	66
	600	43.2	19.3	9.0	15.4	57
	700	39.4	20.1	9.8	17.1	36
	800	46.8	18.2	11.2	19.4	19
Rod 16 mm dia	No annealing	84.0	15.0	24.0	16.0	
	400	87.0	17.0	19.0	13.0	
	500	85.0	18.5	16.0	14.0	
	600	86.5	19.5	21.0	15.8	
	700	81.0	18.0	16.5	15.5	
	800	79.0	16.0	16.0	13.0	
Rod 8 mm dia	No annealinging	92.9	17.7	31.7	39.3	
	400	92.7	16.5	27.1	29.7	45
	500	94.9	17.0	38.0	46.9	70
	600	88.3	16.9	28.4	37.5	55
	700	99.5	17.4	34.4	45.7	40
	800	87.9	16.5	38.9	47.0	35

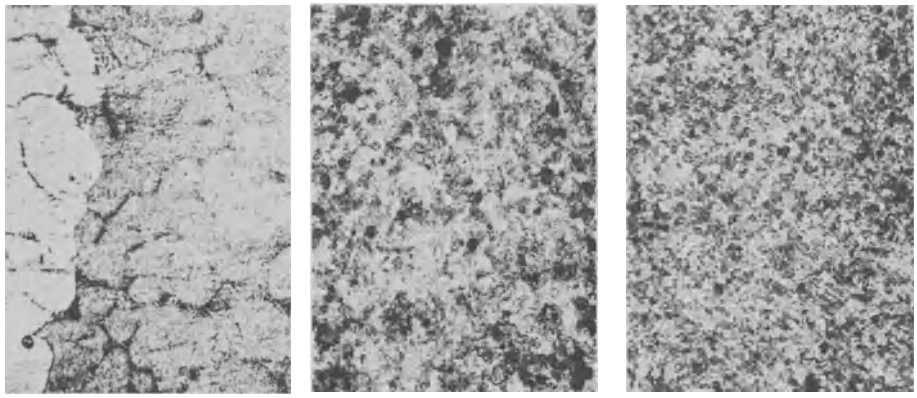

a b c

Fig. 6: Microstructure of hot-extruded rods with diameters of 240 mm (a) and 20 mm (b); hot-rolled rods with diameters of 18 mm (c) and 8 mm (d).
magnification x70

(4) Annealing of the semi-products at temperatures of 400 - 900°C does not change the grain size and their mechanical properties.

(5) The maximum effect of the deformation memory in semi-fabricated products is found to take place after annealing at 500°C.

REFERENCES

1. Kornilov I.I., Belousov O.K., Kachur E.V. Physics of metals and General metallurgy, 1971, vol. 32, issue 2, 32-35.

2. Solovyov L.A., Khachin V.N. Physics of metals and General metallurgy, 1974, vol. 38, issue 2, 433-435.

3. Gorelik S.S. Recrystallization of metals and alloys. "Metallurgiya" Publ. House, Moscow, 1967.

THERMOMECHANICAL PROPERTIES AND STRESS CORROSION OF RMI Ti-3Al-8V-6Cr-4Mo-4Zr

R. J. Stokes, R. J. De Angelis,

and G. A. Sargent

U.S. Army Missle Command, Redstone Arsenal, Alabama
*Metallurgical Engineering and Materials Science Department. University of Kentucky, Lexington, KY

1. ABSTRACT

RMI 38-6-44 is a newly developed beta titanium alloy of nominal composition, 3 percent aluminum, 8 percent vanadium, 6 percent chromium, 4 percent molybdenum, and 4 percent zirconium. This alloy can be easily worked at room temperature and combinations of mechanical working and thermal treatments produce a variety of complex microstructures. A broad range of engineering properties can be obtained as a result of these processes. This paper presents the procedures and results of a systematic investigation of the effects of various thermomechanical processes on the mechanical properties, corrosion resistance, susceptibility to stress corrosion and structure of this alloy. Investigations were conducted on material receiving 0 percent, 40 percent, and 80 percent cold work with no heat treating and material receiving zero percent, 40 percent, and 80 percent cold work and various heat treatments. Aging temperatures used were between 370-565°C for times varying from 15 minutes to 96 hours. Maximum yield strengths of 155 Kg/mm^{2} were obtained. A discussion of properties is presented and correlation between these properties and existing microstructures are discussed.

2. INTRODUCTION

The alloy Ti-11.5Mo-6Zr-4.5Sn, called Beta III, was specifically designed as a compound-free alloy to eliminate the

embrittlement problems experienced with other titanium alloys. Work on Beta III has included studies on formability, weldability, engineering properties, and structure (1). It was found that the metastable transition omega phase was present in the alloy. Investigations to define the structural characteristics of the omega phase in this alloy and other titanium alloys have been conducted (2, 3, 4).

The continued search for a compound-free deep hardening, low density, short-time aging response alloy led to the development of the Ti-3Al-8V-6Cr-4Mo-4Zr alloy (5). This is a new deep-hardening beta composition alloy. The large amount of beta stabilizing elements in this composition results in sluggish transformation characteristics which give deep hardening. The metallurgy of this alloy is similar to other beta alloys such that solution annealing retains the more ductile body-center-cubic beta phase at room temperature The Ti-3Al-8V-6Cr-4Mo-4Zr alloy formulation was based on consideration of mechanical properties, density, raw material cost, meltability, hot workability, cold workability, formability, and a practical method of heat treatment. The alloying concept was based on achieving a high beta stability but less than Ti-13V-11Cr-3Al (6). This allows for response to heat treatment in relatively large sections in a reasonable aging cycle. The high beta stability of Ti-13V-11Cr-3Al has necessitated aging cycles as long as 72 hours, while the Ti-3Al-8V-6Cr-4Mo-4Zr normally requires only 6 to 24 hours (6).

3. EXPERIMENTAL PROCEDURES

The chemical composition of the RMI alloy is shown in Table 1.

Table 1
CHEMICAL COMPOSITION OF RMI 38-6-44 Ti ALLOY

Aluminum	3.39%
Vanadium	8.16%
Chromium	6.45%
Molybdenum	4.86%
Zirconium	3.9%

A sheet of material measuring 20 x 60 x 0.5 cm. was cut into three equal strips. Approximately 3.175 mm of material was removed from the outside edges of the sheet to prevent edge cracking. Figure 1 shows a block diagram of the processing sequence used to produce finished sheet material of 0.10 cm. thick. Sheet tensile specimens (2.5 cm. gauge) and stress corrosion specimens (7.6 cm. by 0.64 cm) were prepared from

the processed material by grinding. Specimens were aged in dry argon for times ranging from 15 minutes to 96 hours, and at temperatures from 370°C to 565°C. The mechanical properties of the heat treated specimens were measured on an Instron machine equipped with an extensometer. Elongation was measured on the specimen after failure, and Young's modulus of elasticity was calculated from the slope of the experimental curve. Corrosion and stress-corrosion testing were performed in a salt spray cabinet using a 3.5-percent neutral salt solution at 35°C and 95 to 98 percent relative humidity. After exposure for 2200 hours, the specimens were removed and their mechanical properties were evaluated. Stress-corrosion specimens were loaded to 75 percent of their yield strength using the snap-in bent beam fixture and loading and exposed to the salt fog environment for 4000 hrs. Metallographic specimens were prepared by standard procedures. These were swab etched using a 2% HF, 4% HNO_3, 94% H_2O solution. Typical microstructures are shown in Fig. 2.

4. RESULTS AND DISCUSSION

The tensile properties of the solution treated and cold rolled RMI alloy are compared with those of other commercial titanium alloys in Fig. 3. Although the cold rolled properties of the RMI alloy are similar to the other alloys very high yield strength with good ductility can be obtained by thermomechanical processing. It was found the aging unworked material at 370°C gives moderate strength with good ductility. Cold working prior to aging increases strength, but sharply reduced ductility. Ultimate tensile strength was increased on solution-treated material from 88.1 to 105.01 Kg/mm^2 after aging 96 hours at 370°C. The highest ultimate tensile strength obtained on material aged at 370°C was 129.4 Kg/mm^2 on material that had been cold worked 40 percent and aged for 8 hours.

High strength levels are obtained with low ductility with material aged at 480°C. The highest ultimate tensile strength recorded for any of the samples tested during this investigation was 161.9 Kg/mm^2. This material had received 80 percent cold working and 4 hours aging at 480°C. Even at this extremely high strength level the material still had 3 percent elongation.

Aging at 538°C gives high strengths with good ductility. After only 2 hours aging at 538°C, an ultimate tensile strength of 153.8 Kg/mm^2 with 4 percent elongation was obtained. Ultimate tensile strengths of near 140.6 Kg/mm^2 and good elongations were demonstrated by specimens aged at 565°C, while low to moderate ductility with high ultimate strengths near 140.6

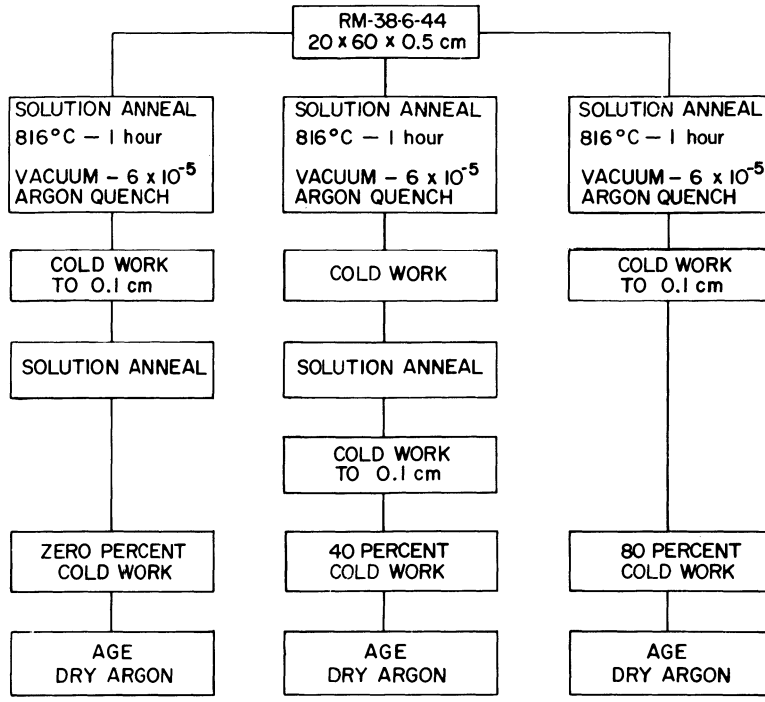

Fig. 1. Block diagram showing material processing sequences.

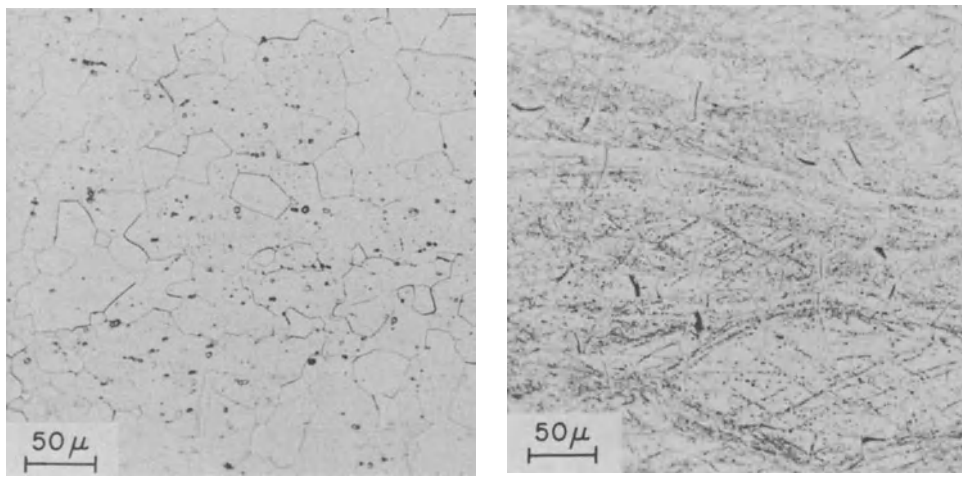

(a) (b)

Fig. 2. (a) Microstructure in solution treated condition.
(b) Microstructure after solution treatment and aged 2 hours at 538°C.

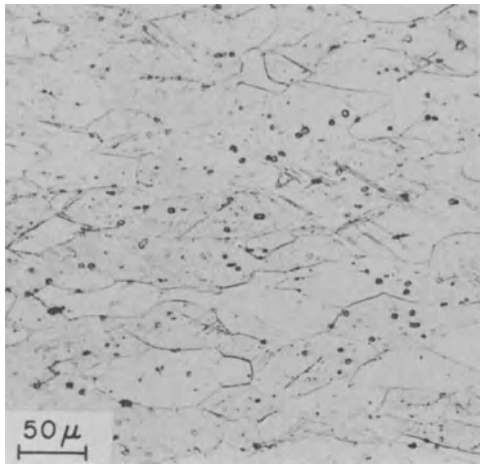

(c)

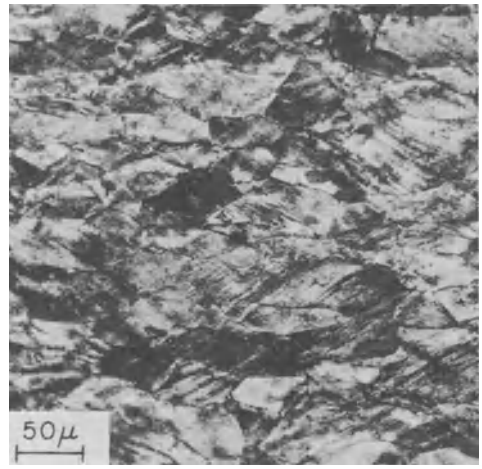

(d)

Fig. 2. (cont.) (c) Microstructure of Material solution treated, cold worked 40 percent, no aging.
(d) Microstructure of material solution treated, cold worked 40 percent, aged 2 hours at 538°C.

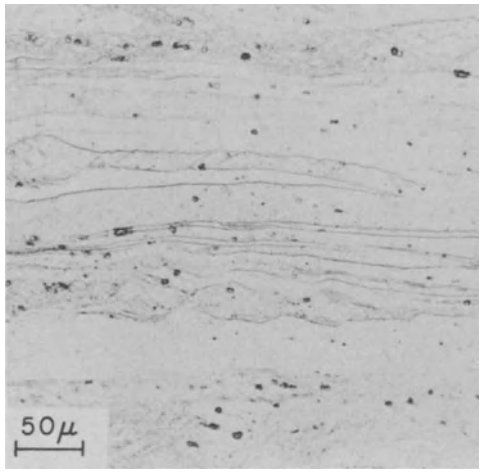

(e)

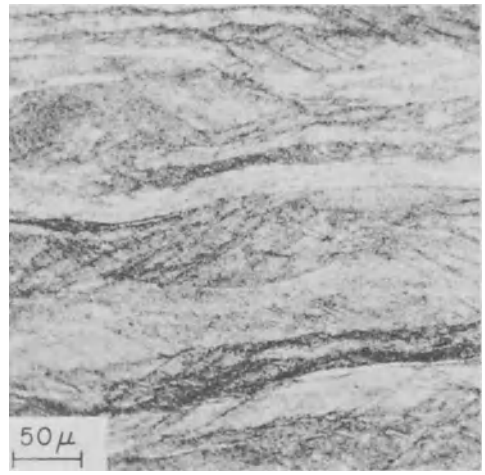

(f)

Fig. 2. (cont.) (e) Microstructure of material solution treated, cold worked 80 percent, no aging.
(f) Microstructure of material solution treated, cold worked 80 percent, aged for 2 hours at 538°C.

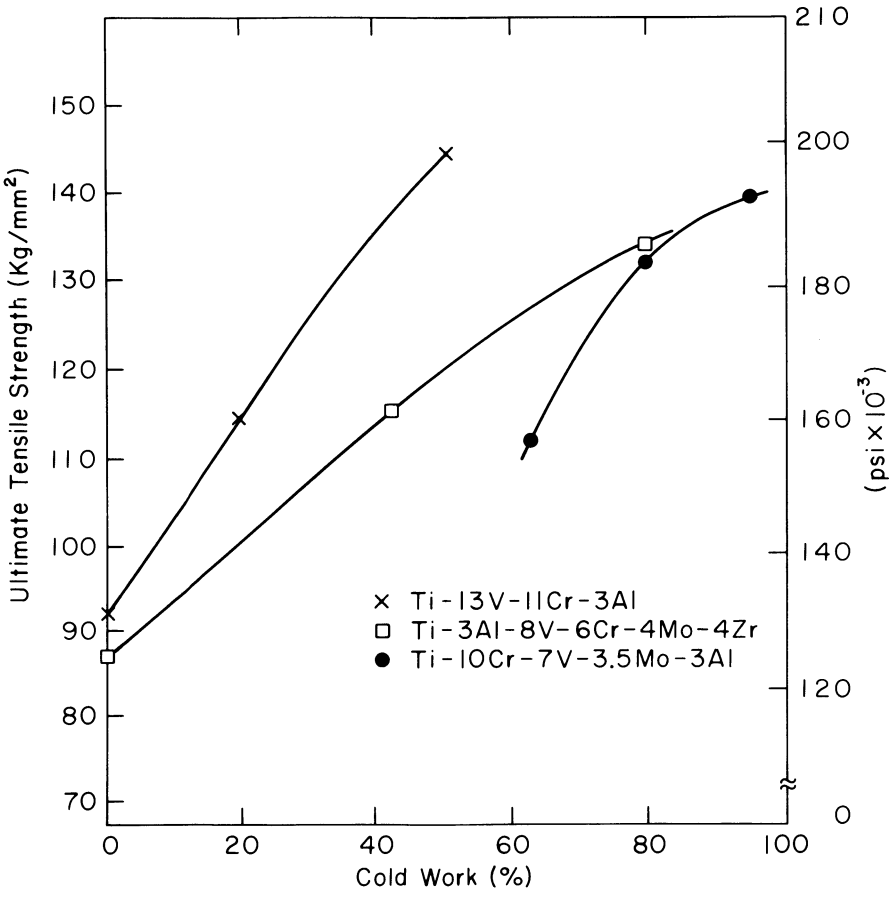

Fig. 3. Ultimate tensile strength of three commercial titanium alloys as a function of percent cold work.

Kg/mm^2 resulted from the duplex heat treat cycles (aging at 480°C for 8 hrs. followed by aging at 538°C for 1/2 hr.)

Material with zero percent cold work must be aged longer than material with 40 and 80 percent cold work to achieve maximum yield strength. In figure 4 it is shown that 40 and 80 percent cold-worked materials obtain their maximum yield strength after 2 hours aging. Material with zero percent cold work must be aged 8 to 48 hours to achieve high yield strengths. Figure 5 shows the relationship between ultimate strength and aging time. It can be seen that high strength levels can be obtained after aging for short time periods. This makes the alloy desirable for industrial applications. Although this alloy has better ductility than other beta alloys, cold working reduces the elongation sharply. Figure 6 shows the relationship between elongation and aging time.

Thermomechanical mechanical processing had a definite effect on Young's modulus of elasticity of the material. Figure 7 shows that this property was increased approximately 40 percent. The Young's modulus of elasticity of beta phase titanium is approximately 8,436 Kg/mm^2 and that of alpha phase titanium is approximately 11,250 Kg/mm^2. As aging progresses, the alloy becomes alpha plus beta and Young's modulus of elasticity increases.

After exposure in the salt cabinet for 2200 hours, the unstressed RMI 38-6-44 specimens did not show any appreciable reduction in ultimate tensile strengths and elongation. Furthermore the specimens that were stressed to 75 percent of their yield strength exhibited excellent resistance to stress-corrosion cracking. After 4000 hours in the salt fog, none of the specimens had broken. In comparison to 7075-T6 aluminum alloy specimens, which were tested under the same conditions and failed in several hours (7), RMI 38-6-44 shows promise in the area of stress-corrosion cracking.

The microstructure of a specimen in the solution treated condition shown in Fig. 2a is composed of equiaxed beta grains with a finely dispersed second phase. After aging for 2 hours at 538°C a fine alpha precipitate is formed in the beta matrix (Fig. 2b). It is the formation of the fine alpha precipitate that is responsible for the observed increase in strength and Young's Modulus. The microstructure of the specimen with 40 percent cold work in the un-aged condition is shown in Fig. 2c. The structure consists of elongated beta grains with a finely dispersed second phase. The solution treated grain structure is broken up by twinning due to the rolling reduction. After aging at 538°C

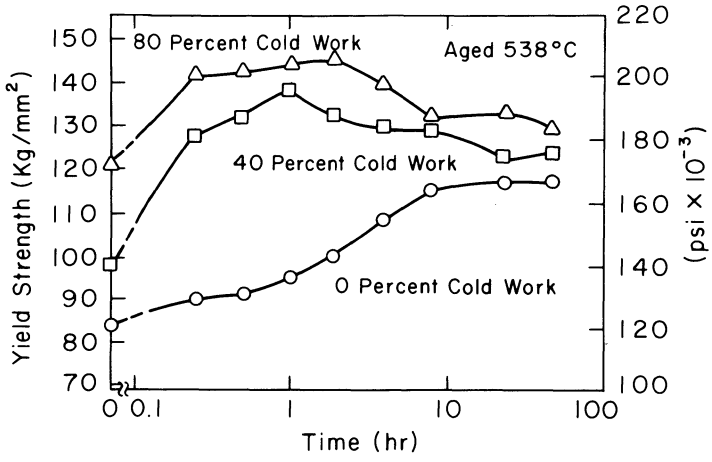

Fig. 4. Yield strength versus aging time for material solution treated and cold worked 40 and 80 percent.

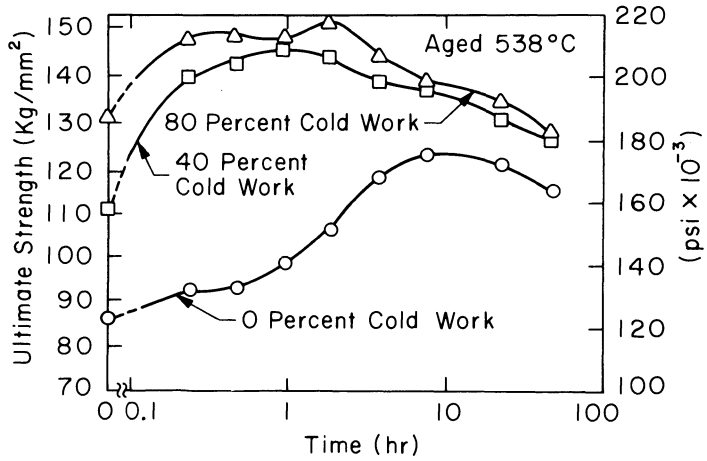

Fig. 5. Ultimate tensile strength versus aging time for material solution treated and cold worked 40 and 80 percent.

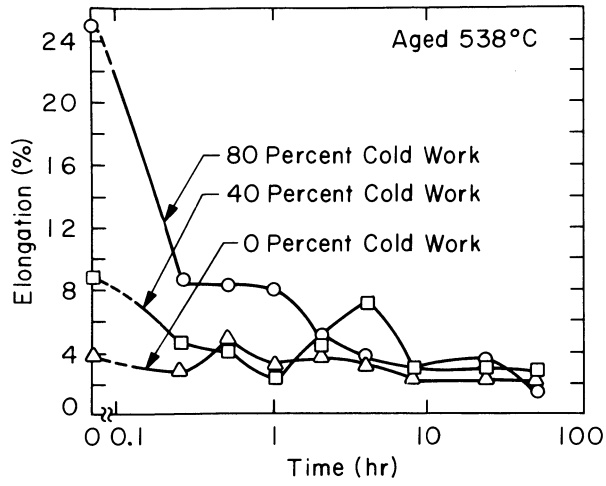

Fig. 6. Elongation versus aging time for material solution treated and cold worked 40 and 80 percent.

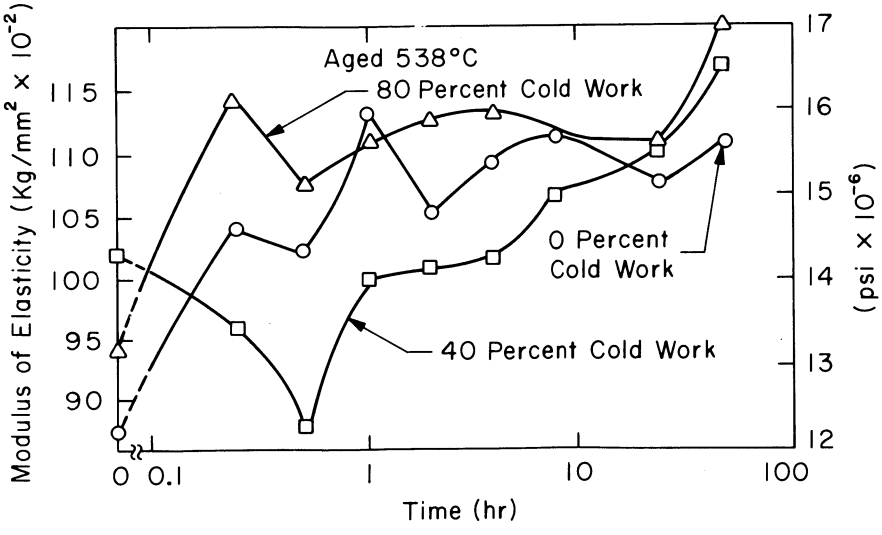

Fig. 7. Young's modulus versus aging time for material solution treated and cold worked 40 and 80 percent.

for 2 hours, the 40 percent cold-worked material had an aged structure consisting of alpha and beta grains. (Fig. 2d). A large increase in strength is observed in this material. Additional cold-work of the solution treated material continues to increase the ultimate tensile strength. After 80 percent cold work the grain structure is further broken down by twinning. (Fig. 2e). The extensive twinning may be the cause of the reduction in ductility to 3 percent. Fig. 2f shows the structure of the material which was 80 percent cold worked and aged 2 hours at 538°C. Again the elongated grain structure is broken up by a considerable amount of twinning.

5. BIBLIOGRAPHY

1. Feeney, J. A. and Blackburn, M. J., "Effect of Microstructure on the Strength, Toughness, and Stress-Corrosion Cracking Susceptibility of a Metastable Beta Titanium Alloy (Ti-11.5 Mo-6 Zr-4.5 Sn)," Metallurgical Transactions, 1970, 1, 3309-3323.

2. Jon, Min Chung, Fujimura, Hiroshi, and De Angelis, R. J., "Omega-Phase Formation in Beta III Titanium Alloy," Metallography, 1972, 5, 139-150.

3. Rack, H. J., Kalish, David, and Feke, K. D., "Stability of As-quenched Beta-III Titanium Alloy," Materials Science and Engineering, 1970, 6, 181-198.

4. Silcock, J. M., "An X-Ray Examination of the Omega Phase in Ti V, Ti Mo and Ti Cr Alloys," Acta Metallurgica, 1958, 6, 481-493.

5. Reactive Metals Incorporated, Niles, Ohio, "Preliminary Data Sheet, RMI 3Al-8V-6Cr-4Mo-4Zr Titanium Alloy for Deep Hardening Applications," Technical Bulletin, 1969.

6. Reactive Metals Incorporated, Niles, Ohio, "Facts About RMI Ti-3Al-8V-6Cr-4Mo-4Zr," 1972.

7. Stokes, Rebecca J., US Army Missile Command, Redstone Arsenal, Alabama, Unpublished Data.

TEXTURE DEVELOPMENT IN $\alpha+\beta$ TITANIUM ALLOYS*

A. Sommer,** M. Creager,**
S. Fumishiro,*** and D. Eylon****

*Research sponsored by the United States Air Force Materials Laboratory under Contract F33615-74-C-5107

**Del West Associates, Inc., 6324 Variel Avenue, Woodland Hills, CA 91364, U.S.A.

***United States Air Force Materials Laboratory, Wright-Patterson AFB, Ohio 45433, U.S.A.

****University of Cincinnati, Cincinnati, Ohio, U.S.A.

INTRODUCTION

Textures arise as a result of extensive plastic deformation, usually in one direction, and may be modified or strengthened by subsequent recrystallization annealing. In titanium alloys where the hexagonal phase predominates, the textures which develop are usually described in terms of the orientation of the basal plane (0001). The basal textures which develop in titanium alloys can be broadly classified as those in which the basal planes are parallel with the rolling plane (Figure 1(a) and those in which the basal planes are normal to the rolling plane (Figure 1(b)). The former textures are well documented to result in improved biaxial strength properties (References 1,2, and 3). The latter textures, by contrast, produce mechanical property anisotropy in the rolling plane (References 4, 5, and 6). Recognizing our intent to provide enhanced structural integrity in a single product direction, our research effort focused on providing better description of how Figure 1 (b) or basal transverse textures form and the properties such a textured material exhibits. The alloy we elected to employ in the program is 6Al-4V Ti. We shall report on results obtained with two heats of metal containing either 0.09 wt% oxygen

(ELI Grade) or 0.15 wt% oxygen (Standard Grade). In all other respects, the alloy chemistries of these two heats was identical.

Experimental Procedure

The 6Al-4V Ti alloy materials employed in this research were obtained from conventionally sized production heats, (i.e., 5000 lb. ingots). Both heats were unidirectionally forged to crossections of 6" x 4 1/4". A majority of the forging deformation was carried out below the alloys beta transi. β_T = 1760°F for ELI Grade and 1830°F for the Standard Grade of 6Al-4V Ti.

Unidirectional working below 4 1/4" in thickness was accomplished on a 7" wide, two high laboratory rolling mill. The lower oxygen content alloy was rolled either isothermally at 1710°F by reheating after each rolling pass until its final crossection of 1/4" x 6" was attained (rolling campaign #1) or was rolled continuously without reheat from 4 1/4" x 6" in crossection to 1/4" x 6" in crossection upon removal from an 1800°F furnace (rolling campaign #2). Final metal surface temperature in the second campaign was 1275°F. The higher oxygen content alloy was rolled in the style of campaign #2 employing an initial temperature of 1855°F and its surface finish temperature was 1300°F at 1/4" x 6" (in crossection). The post rolling heat treatments applied to each alloy are shown in Table I.

Table I
Heat Treatment Schedule
for Program Material

Alloy	Designation	Heat Treatment
6Al-4V Ti	Mill Annealed	1350°F/1 hour + furnace cool*
ELI Grade (0.095 wt% oxygen)	Recrystallized	1710°F/4 hours + furnace cool*
	Beta Annealed	1710°F/4 hours + 1900°F/10 minutes + 1710°F/1 hour + 1400°F/1 hour + air cool
	Duplex Annealed	1710°F/4 hours + furnace cool* to 1400°F/1 hour + air cool
6Al-4V Ti Standard Grade (0.16 wt% oxygen)	Recrystallized	1780°F/8 hours + furnace cool*

* Cool at less than 100°F per hour

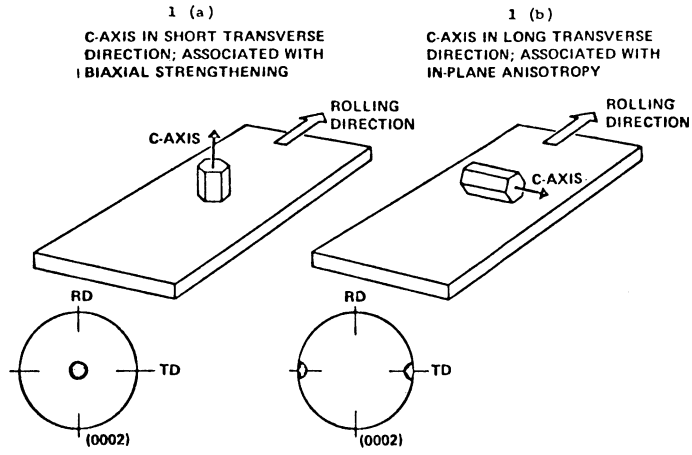

Fig. 1 - Schematic view of alpha phase textured plates and their corresponding basal plane pole figures.

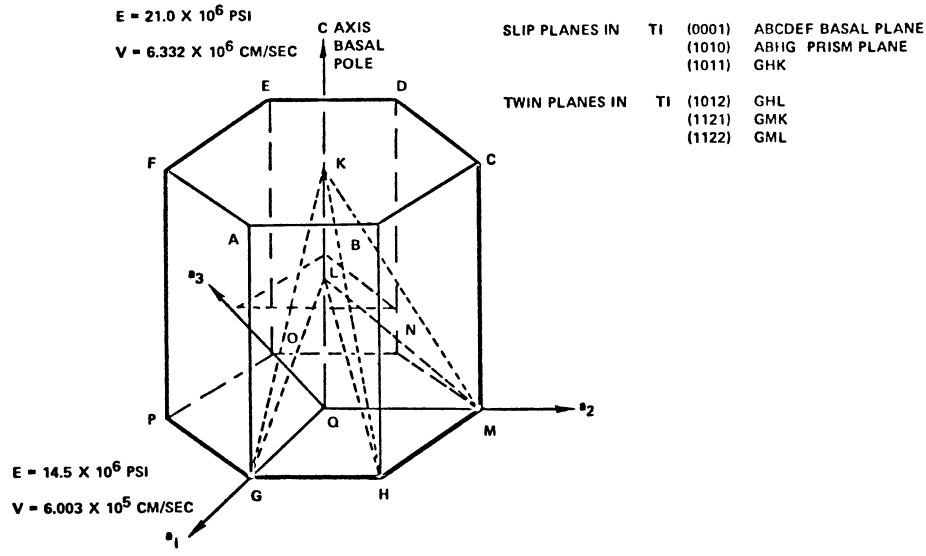

Fig. 2 - Slip and twin deformation planes in alpha titanium.

Preferred orientation or crystallographic texture was assessed employing two independent techniques. Basal pole figure quadrants were obtained using a modified Kula-Lopata X-Ray diffraction technique (Reference 7). Additionally Young's moduli were assessed for the rolling and long transverse directions of all products. The moduli measurements relate to preferred orientation in that the elastic properties of the alpha phase are anisotropic (see Figure 2).

Mechanical property measurements performed to evaluate the textured products included:

elastic modulus

monotonic stress:strain

S-N for K_t - 1

K_{ISCC} in 3.5% NaCl in H_2O

creep

In all cases properties were obtained in two orthogonal directions (rolling and long transverse) or orientations (LT or TL). All testing save the elastic moduli measurements was conducted employing MTS Corporation "closed loop" electro hydraulic equipment. Stress:strain and creep measurements were made with round bar dog-bone type samples (Diameter - 0.160"). Fatigue life data were obtained using a flatwise "dog-bone" configuration. All fracture mechanics measurements were made employing fatigue precracked compact tension samples (W = 2.5"). Young's modulus was measured dynamically employing a resonant bar technique. All elevated temperature tests were performed in air except for several creep experiments which were performed in a vacuum of 3×10^{-6} Torr. Temperature control during elevated temperature testing was always maintained within ± 3°F.

RESULTS

The relationship between rolling practice and textures is shown in Figure 3. Presented here are basal pole figure quadrants and Young's modulus determinations observed after 6Al-4V Ti ELI Grade was thermomechanically processed in two distinct manners. As one observes, isothermal working just below the alloy's beta transus produces an isotropic product whereas the same deformation reduction applied as the temperature of the product falls from 1800°F to 1275°F results in a very strong basal transverse texture (as defined in Figure 1(b)). These observations are based on two independent techniques for basal texture assessment (i.e., X-Ray pole figures and elastic moduli). When our 6Al-4V Ti Standard Grade material was processed employing a Rolling Campaign #2 practice, its X-Ray basal pole figure was essentially that shown

in Figure 3(b). Young's modulus determinations for the Standard Grade metal after recrystallization were:

Direction	Young's Modulus ($x10^6$psi)
Transverse	21.20
Rolling	16.00
Difference	5.20

The effect of post rolling thermal practice on texture is shown in Table II in terms of Young's modulus measurements.

Table II

Effect of Post Rolling Thermal Practice on 6Al-4V Ti ELI Grade Texture

Heat Treatment*	$E_{Transverse}$ ($x10^6$psi)	$E_{Rolling}$ ($x10^6$psi)	E_T-E_R ($x10^6$psi)
Rolling Campaign #1			
-Mill Anneal	18.70	16.50	+2.2
-Recrystallization Anneal	18.25	17.35	+0.9
Rolling Campaign #2			
-Mill Anneal	19.50	15.20	+4.3
-Recrystallization Anneal	20.25	15.65	+4.6
-Duplex Anneal	20.25	15.45	+4.8
-Beta Anneal	16.65	17.25	+0.55

*as defined in Table I

One notes from Table II, that a weak texture such as that produced by Rolling Campaign #1 is unstable upon recrystallization just below the metal's beta transus whereas the strong texture induced by Rolling Campaign #2 actually becomes more perfect as a result of recrystallization. Exposure to temperatures over the alloy's beta transus eliminates even the strongest texture as one would anticipate based on the degeneracy of the Burger's relation for alpha phase variants.

In Table III we report the montonic strength properties of basal transverse textured or Rolling Campaign #2 metal after recrystallization.

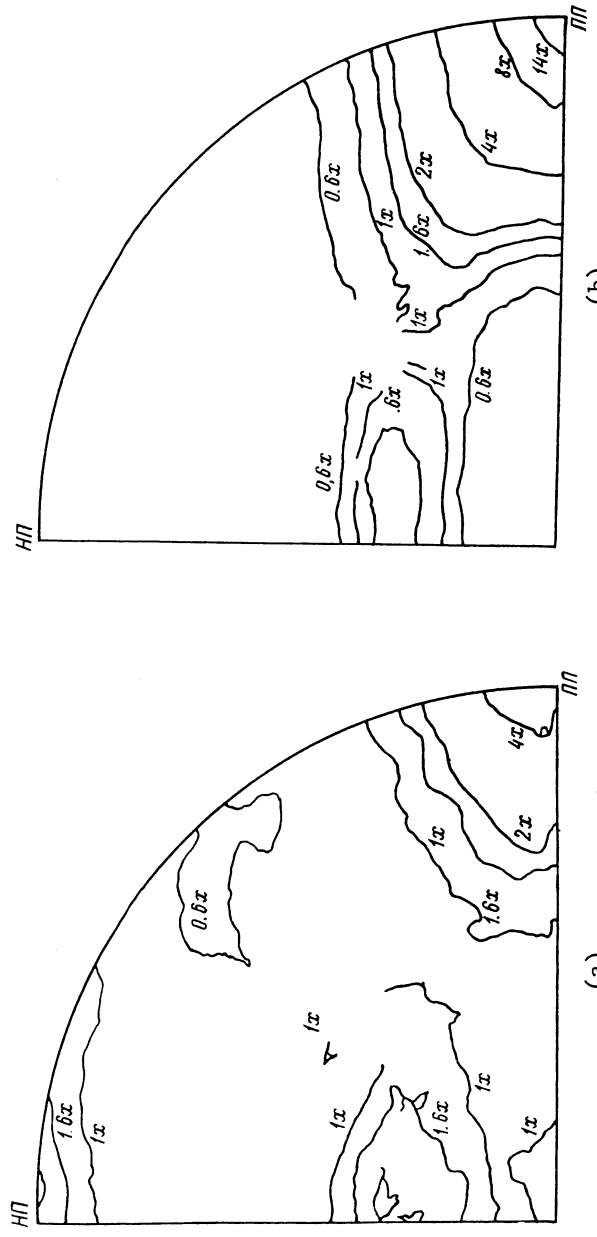

Fig. 3. Relationship between rolling practice and texture for alloy 6AL-4V-Ti with trace admixtures after recrystallization annealing: (a) Rolling Campaign #1; (b) Rolling Campaign #2.

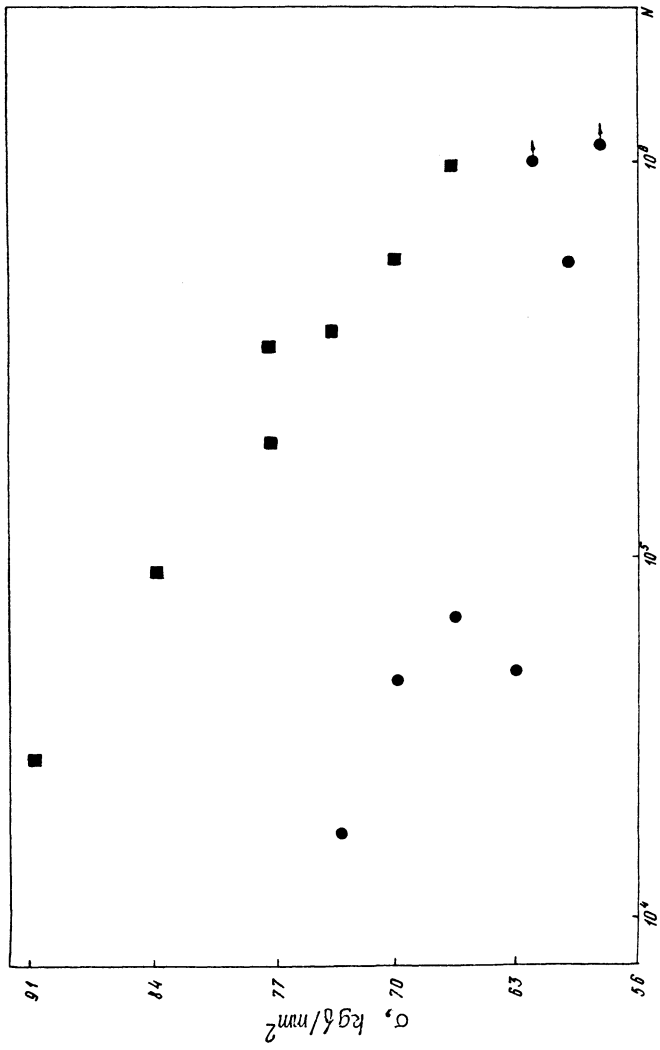

Fig. 4. Fatigue behavior of textured 6AL-4V-Ti with trace admixtures after recrystallization annealing: "c" axis perpendicular to the loads direction; "c" axis parallel to the load direction.

Table III

Monotonic Strength of Basal
Transverse Textured 6Al-4V Ti Metal

Direction	Test Temperature (°F)	Young's Modulus ($x10^6$psi)	σ_y (ksi)	σ_u (ksi)	ε (%)	R/A (%)
		ELI Grade				
Rolling	70	15.65	104	112	18	43
Transverse	70	20.25	130	138	15	38
Rolling	700	11.60	57	70	18	69
Transverse	700	17.90	91	93	16	74
		Standard Grade				
Rolling	70	16.00	128	133	13	32
Transverse	70	21.20	154	164	16	33
Rolling	700	N.D.*	66	82	19	43
Transverse	700	N.D.*	95	109	15	63

*Not determined

As one notes here, the stiffer product direction is also the stronger direction regardless of oxygen content with the anisotropy increasing at elevated temperature (compare results at 70°F with those obtained at 700°F). The increase in anisotropy with increasing temperature numerically results because on a percentage basis the stiffness and strength of the transverse direction is less temperature sensitive than its orthogonal counterpart. Strength and stiffness in both directions also increase with increasing oxygen content.

The high cycle smooth fatigue behavior of highly basal transverse textured 6Al-4V Ti ELI Grade metal is shown in Figure 4. Here we also noted the strong and stiff direction in the textured product is also far more fatigue resistant than is the weaker, less still rolling direction.

Creep in both directions has also been monitored for highly textured 6Al-4V Ti ELI Grade in both air and vacuum over the temperature range 700°F to 1000°F. At 700°F in vacuum no appreciable creep was observed after 40 hours of loading in either direction (rolling or transverse) until one applied greated than 90% of the direction's monotonic yield strength. In Tables IV and V we present minimum creep rates observed in vacuum and air respectively as a function of temperature, applied stress and orientation.

Table IV

Variation of Minimum Creep Rate of
Textured 6Al-4V Ti Alloy Tested in Vacuum

(a) Longitudinal Direction

Stress, (Ksi)	Minimum Creep Rate (in/in/hr)	Temperature (°F)	Young's Modulus (psi)
60*	4.4×10^{-6}	700	11.6×10^{6}
50*	8.3×10^{-6}	800	10.2×10^{6}
40	1.60×10^{-5}	900	10.9×10^{6}
45	3.15×10^{-5}	900	10.9×10^{6}
50	7.00×10^{-5}	900	10.9×10^{6}
30	5.15×10^{-5}	1000	9.3×10^{6}
35	1.10×10^{-4}	1000	9.3×10^{6}
40	3.10×10^{-4}	1000	9.3×10^{6}

(b) Transverse Direction

85>	(No appreciable creep observed for a total of 35 hours)	700	17.9×10^{6}
60>	(No appreciable creep observed for a total of 45 hours)	800	16.3×10^{6}
65	1.3×10^{-6}	800	16.3×10^{6}
40	4.5×10^{-6}	900	15.8×10^{6}
50	7.5×10^{-6}	900	15.8×10^{6}
60	1.70×10^{-5}	900	15.8×10^{6}
25	6.5×10^{-6}	1000	13.9×10^{6}
35	1.45×10^{-5}	1000	13.9×10^{6}
50	6.70×10^{-5}	1000	13.9×10^{6}

*No measurable creep was observed until 90% of the yield stress was applied.

Table V

Variation of Minimum Creep Rate of Textured 6Al-4V Ti Alloy in Air

(a) Longitudinal Direction

Stress (Ksi)	Minimum Creep Rate (in/in/hr)	Temperature (°F)	Young's Modulus (psi)
40*	8.5×10^{-6}	700	11.6×10^{6}
50*	4.1×10^{-5}	700	11.6×10^{6}
40	3.4×10^{-6}	700	11.6×10^{6}
50	5.0×10^{-6}	700	11.6×10^{6}
55	1.10×10^{-5}	700	11.6×10^{6}
60	1.20×10^{-5}	700	11.6×10^{6}
30	3.25×10^{-5}	900	10.9×10^{6}
35	1.55×10^{-4}	900	10.9×10^{6}
45	5.86×10^{-4}	900	10.9×10^{6}
(b) Transverse Direction			
70	2.00×10^{-5}	700	17.9×10^{6}
80	2.21×10^{-5}	700	17.9×10^{6}
35	3.86×10^{-4}	1000	13.9×10^{6}
50	5.80×10^{-4}	1000	13.9×10^{6}

* Single stress level; unless stated otherwise, stress levels were increased incrementally.

As one can note from Tables IV and V, the alloy in both directions is markedly more creep resistant in vacuum than it is in air. Additionally the stress sensitivity of the creep rate in the rolling or longitudinal direction is significantly higher than is its counterpart in the transverse direction. Rephrased, the stiffer, stronger transverse direction is also significantly more creep resistant. For example, a steady state creep rate of 5.9×10^{-4} in/in/hour is obtained in the longitudinal direction of 900°F when the applied stress is 45 Ksi. By comparison the same rate is obtained at this stress level only if one increases his temperature to 1000°F.

It is now well accepted that stress corrosion cracking in sea water (or K_{ISCC}) occurs primarily by basal cleavage. Thus one would expect a crack to grow readily in our basal transverse textured product in the TL orientation if it is exposed to salt water under sustained load. In order to ascertain the extent of any problem in this area and as well determine whether it is possible to recover sea water resistance by heat treatment without sacrificing textural intensity we determined K_{ISCC} in 3.5% NaCl in H_2O for a variety of conditions at 70°F.

Table VI

K_{ISCC} Basal Transverse Textures

Metal Chemistry	Metal Orient.	Post Roll Thermal Practice	Environment	K_{ISCC} Ksi$\sqrt{in.}$
ELI	LT	Rex'l	lab air	>72
	TL	Rex'l	lab air	>72
	LT	Rex'l	3.5%NaCl in H_2O	>70
	TL	Rex'l	3.5%NaCl in H_2O	50
	LT	Duplex Ann.	3.5%NaCl in H_2O	>72
	TL	Duplex Ann.	3.5%NaCl in H_2O	>72
Standard Grade	LT	Rex'l	3.5%NaCl in H_2O	N.D.*
	TL	Rex'l	3.5%NaCl in H_2O	<50

*N. D. Not determined

The K_{ISCC} measurements cited above were obtained by exposing fatigue precracked compact tension samples to salt water for 500 hours under sustained displacement. Loads and initial crack lengths were chosen such that K, the stress intensity, never exceeded 72 Ksi$\sqrt{in.}$ That value was shown in our lab air crack growth resistance measurements to be just below the lower bound for K_{ISCC} in lab air. As one can note in Table VI, if one leaves these products in a recrystallized condition (i.e., having furnace cooled them from their

recrystallization temperature, (see Table I), there is indeed a basal cleavage problem which reduced K_{ISCC} in salt water. Duplex annealing which simply air cools from 1400°F the metal after it has been recrystallized just below its beta transus, provides a means of eliminating this problem. Returning to Table II, for a moment, one notes that duplex annealing does not alter the product's basal transverse texture.

CONCLUSIONS

Conditions for the production of either basal transverse textured 6Al-4V Ti metal or isotropic 6Al-4V Ti material have been defined. The textured metal possesses an "in plane" direction which is simultaneously stiffer, stronger, more fatigue crack initiation resistant, and creep resistant than all other "in plane" directions. Moreover, the differences in mechanical property values between the rolling and transverse directions in the product cover a majority of the range normally observed for wrought 6-l-4V Ti products.

REFERENCES

1. Fitzpatrick, J. M. and Crossley, F. A., "Development of Improved Biaxial Strength in Titanium Alloy Rocket Motor Cases Through Texture Hardening," Phase I AFRPL-TR-67-302, December, 1967.

2. Hatch, A. J., "Texture Strengthening of Titanium Alloys," Trans Met Soc AIME, Vol. 288, January, 1965, pp 44-50.

3. Babel, H. W. and Frederick S. F., "A Review of Texture Strengthening of Titanium Alloys," Douglas Paper 4664, January, 1968.

4. Roberts, W. T., "Preferred Orientation and Anisotropy in Titanium," Journal of the Less Common Metals, Vol 4, 1962, pp 345-361.

5. Zarkades, R. and Larson, F. R., "Sheet Tensile Properties of Titanium Alloys as Affected by Texture," AMMRC TR-68-03, January, 1968, DDC No. AD66765.

6. Larson, F. R., "Textures in Titanium Sheet and Its Effect on Plastic Flow Properties," Report No. AMRA-TR-65 24, October, 1965, DDC No. AD 626410.

7. Olsen, R. H., Metallography, 5, pp 369-71, 1972.

THE EFFECT OF PHASE TRANSFORMATION ON DEFORMATION TEXTURE OF α AND (α+β) TITANIUM ALLOYS

N. V. Ageev, A. A. Babareco and A. I. Khorev

A. A. Baikov Institute of Metallurgy
USSR Academy of Sciences
All-Union Institute of Aviation Materials
USSR

Structural strength of α and (α+β) titanium alloy products strongly depends on the texture of α-phase. Investigation of the mechanism of α-phase texture formation of commercial titanium alloys is, therefore, of primary importance. *Technological processing of commercial titanium alloys includes working in the range of high temperatures of prevailing pure β-phase or a large amount of it. The texture of transformed α-phase after such processing is determined by deformation and recrystallization texture of β-phase and crystallographic mechanism of phase transformation β→α. Ready articles of thermally strengthened (α+β) titanium alloys may be subjected to strengthening treatments, including phase transformations. Analyzed in the present work is the dependence of the texture type of transformed α-phase on the type of starting texture of β-phase and conditions of phase transformations β→α.

BUILDING OF THEORETICAL INVERSE POLE FIGURES FOR TRANSFORMED α-PHASE

Texture strengthening of titanium alloys is used mainly in making spherical and cylindrical vessels. These articles are obtained by methods of sheet-forming or drop forging at high temperatures. Their optimum mechanical properties are determined by the basal and prismatic orientation of the material in unfolded surface of the sphere or cylinder. Of interest is the analysis of possible relationships between texture components of β-phase and transformed α-phase in the plane of sheets, plates and forgings, for controlling

*Editor's Note: It appears that the authors are referring to thermomechanical processing.

Table I

Textures of Hot and Cold Working of β-Phase Titanium Alloys and Transformed α-Phase

Alloy No.	Alloy Composition wt.%	Treatment: Temperature, °C	Low temperature thermomechanical treatment	Warm rolling	High-temperature thermomechanical treatment				Hot drop forging (2)
			20	800-700	850	900	1000	1050	1100-900
1	Ti-5Al-3Mo-IV			x) (α+β) 111, 100. / $1\bar{1}02 \div 1\bar{1}04$, $11\bar{2}2 \div 11\bar{2}4$, $11\bar{2}0$					
2	Ti-5, 5Al-2Mo-2Cr-1Fe-0,2Si								(α+β) 100 / $11\bar{2}0$
3	Ti-5, 3Al-2Mo-1Cr-4,5V-0,6Fe		(α+α") / 0001, $11\bar{2}2$, $1\bar{1}04$		(α+β) 100, 112, 110. / $11\bar{2}0$, $1\bar{1}00$, $11\bar{2}2$		α" / $1\bar{1}01$, $1\bar{1}00$, 0001.		

4	Ti-3Al-15Mo	(α+β) 111,112,100 $11\bar{2}0,12\bar{3}0$ $11\bar{2}2,11\bar{2}4$.		
5	Ti-3Al-6Mo-6Cr	(α+β) 100, 111 $11\bar{2}0$.		
6	Ti-2,5Al-7,5Mo-10,2Cr	(α+β) or β 111,100,112 $12\bar{3}0,11\bar{2}0$ $11\bar{2}4$.	β 112,130 $12\bar{3}0,1\bar{1}00$, $11\bar{2}0$.	β 110,112,321 $11\bar{2}0,20\bar{2}1$ $1\bar{1}05,11\bar{2}2$.

x) On top are listed the phases present during hot working or after quenching and working texture of β-phase, at bottom texture of α-phase after transformation, in decreasing order of intensity.

the process of texture formation of α-phase in articles during technological processing.

The main BCC-β-phase texture components of cold and hot upsetting, rolling and forging are orientations {111}, {100}, and {112}. With an increase of working temperature, to these orientations are added recrystallization texture components {310}, {321}, {110} and others, Table I.

On the basis of Burgers orientation relationships during phase transformation of $\beta \rightarrow \alpha$; $\{0001\}_\alpha || \{110\}_\beta$ and $\langle 11\bar{2}0\rangle_\alpha || \langle 111\rangle_\beta$, inverse pole figures have been constructed of α-phase in the plane of sheet, plate or unfolded surface of forging after transformation of β-phase with the indicated orientations, Figure 1. The figures have taken into account polyvariant nature of the transformation along all the possible habit planes $\{110\}_\beta$.

COMPARISON OF CALCULATED AND EXPERIMENTAL DATA CONCERNING THE TEXTURE OF TRANSFORMED α-PHASE

A comparison of textures of α-phase titanium alloys, which have been subjected to working in β or (α+β) region, with calculated data has produced good agreement in individual cases. For example, hot rolling of No. 1 alloy in temperature range high in the α+β phase field results in the formation of texture components of α-phase, determined by transformation

$$\beta \rightarrow \alpha \quad \text{and}$$
$$\{100\} \quad \{11\bar{2}0\} + \{10\bar{1}2\}$$

$$\beta \rightarrow \alpha$$
$$\{111\} \quad \{11\bar{2}0\} + \{12\bar{3}0\} + \{11\bar{2}4\}.$$

Additional texture components of α-phase in this alloy $\{11\bar{2}2\}$ and $\{10\bar{1}4\}$, evidently, correspond with deformation texture of α-phase, which was present in the alloy during warm working at the last stages.[1] High temperature thermomechanical treatment of No. 3 alloy by upsetting at 1000° with water quenching to α"-phase and subsequent aging results in development of texture transformed α-phase, which corresponds with the calculated value

$$\beta \rightarrow \alpha$$
$$\{110\} \quad \{10\bar{1}1\} + \{10\bar{1}0\} + \{0001\}.$$

Observed in a number of cases is preferable transformation along individual habit planes with development of not all texture components of α-phase. This is shown during analysis of relationships between textures of α and β-phases of alloy No. 6 and alloys Ti-3Al-15Mo and Ti-3Al-6Cr-6Mo after low temperature thermomechan-

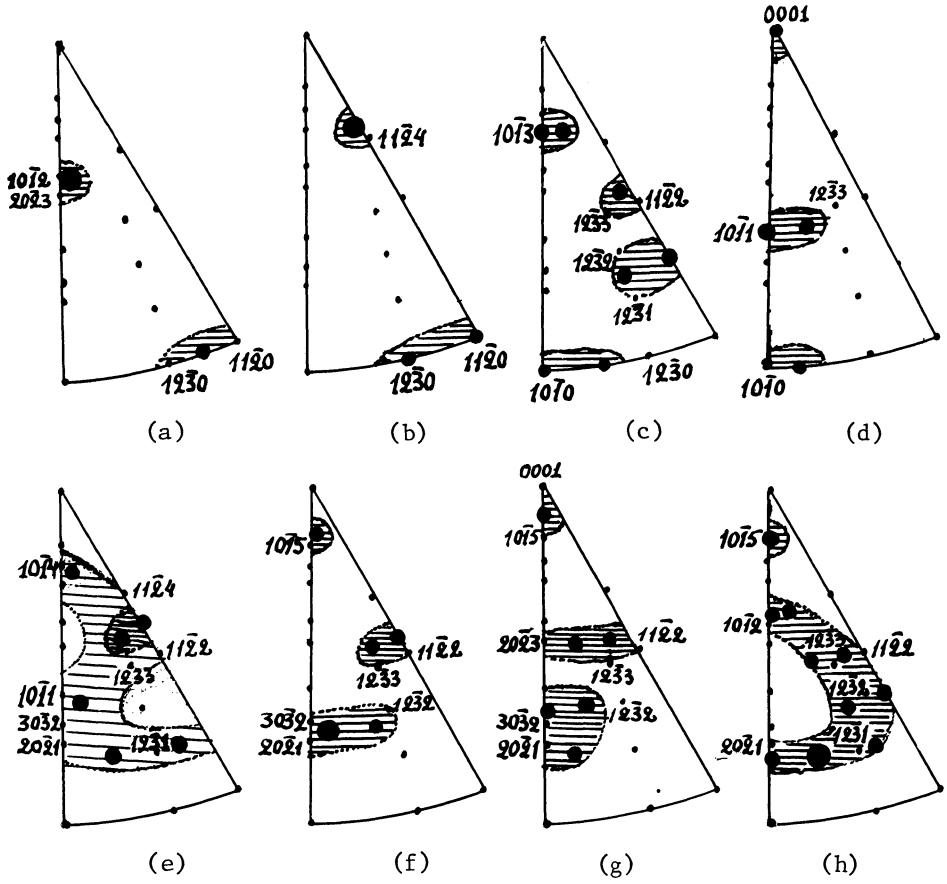

Fig. 1: Inverse pole figures of transformed α- phase from β - phase with textures: a - {100} , b - {III} , c - {112} d - {110} , e - {310} , f - {120} , g - {320} , h - {321} .

ical treatment, high temperature thermomechanical treatment and subsequent aging. Development of preferred orientations of transformed α-phase close to the prismatic, and some pyramidal orientations is observed. In the No. 2 alloy[2] the transformation of β-phase with {100} texture under load during drop forging in the β-region with chilling in the die to temperatures of (α+β) range results in the development of single component texture of $\{11\bar{2}0\}$ α-phase. Completely absent in this case was the second orientation, $\{10\bar{1}2\}$, which must appear during transformation of β-phase with such texture. Quenching and aging of the alloy after forging resulted in transformation along all the possible habit planes with development of both possible orientations.[2]

These results indicate that the texture of transformed phase depends not only on the type of starting texture of β-phase, but also on the conditions under which the phase transformation proceeds in titanium alloys.

EFFECT OF APPLIED AND RESIDUAL STRESSES ON THE TEXTURE OF TRANSFORMED α-PHASE OF TITANIUM ALLOYS

The analysis of discrepancies of α and β crystal lattices of titanium alloys during phase transformation shows that transformation is accompanied by linear anisotropic effects. From comparison values of pairs of interplanar distances $d_{(0002)\alpha}$ and $d_{(110)\beta}$, $d_{(11\bar{2}0)\alpha}$ and $d_{(200)\beta}$, $d_{(110)\beta}$ and $d_{(10\bar{1}0)\alpha}$ (respective pairs of directions are coupled with each other during phase transformation), it follows that phase transformation requires a 1-3% extension of the matrix along the normal to the habit plane $(110)_\beta || (0002)_\alpha$ and more considerable 10-12% extension along $\langle 1\bar{1}0\rangle_\beta || \langle 10\bar{1}0\rangle_\alpha$ and 9-10% compression along $\langle 200\rangle_\beta || \langle 11\bar{2}0\rangle_\alpha$ in the habit plane.

In conformity with Le Chatelier principle in the presence of external applied or internal residual stresses the transformation of β→α may proceed preferably along such habit planes, which result in maximum relaxation of internal stresses caused by phase transformation in the material. On the basis of this it is possible to explain the special features of texture formation which occur during the process of complex thermomechanical treatments of titanium alloys, and to describe the conditions of phase transformation for preferable development of some orientations of α-phase.

Of maximum interest for the problem of texture strengthening of titanium alloys are the formation condit-ons of basic and prismatic orientations. As is evident from the calculated pole figures the basal texture, or type $\{10\bar{1}5\}$ pyramidal orientations may develop in appreciable number only during transformation of β-phase with recrystallization textures {110}, {320}, {210}, {321}. Prismatic

orientations can develop from β-phase with deformation textures as well as recrystallization textures.

As an example, let us examine the effect of the state of stress on the development of either texture components of α-phase during transformation of β-phase with texture {110} or {100}. During the rolling process the transformation of β-phase with texture {110} <001> will be favorable to the development of pyramidal texture components of α-phase, whereas residual deformation stresses during transformation should facilitate the development of basic and prismatic orientations. With a {100} <110> β-phase texture the transformation during the rolling process facilitates the development of prismatic texture in the sheet plane with distribution of normals to the base plane along the transverse direction during rolling direction when rolling with sheet widening. Residual stresses after deformation of such textures of β-phase do not facilitate the development of prismatic orientations in the sheet. During analysis of texture formation in transformed α-phase it is also necessary to take into account that in thick sections of titanium alloy products the texture may differ through the thickness due to the effect of quenching stresses on the transformation crystallography.

EFFECT OF TITANIUM ALLOY COMPOSITION ON THE TEXTURE OF TRANSFORMED α-PHASE

The composition of alloys affects the type of working texture of β-phase and consequently on the texture of transformed α-phase. With an increase of the content of alloying elements which stabilize the β-phase, the tendency is observed toward development of recrystallization texture components of β-phase at lower treatment temperatures than for alloys that contain a smaller amount of these alloying elements.

In addition, the chemical composition of alloys affects the relative amounts of α and β present during different treatments of the alloys, which also affects the final texture of α-phase. For example, hardening of No. 3 alloy to α" phase during thermomechanical treatments and water quenching results, at subsequent aging, in the development of the basal component in the texture of transformed α-phase with a starting $\{110\}_\beta$ texture. Quenching during thermomechanical treatments with this β-phase texture results in the development of prismatic and pyramidal orientations during β→α transformation. These differences in texture can be explained by the influence of residual deformation stresses on the transformation crystallography of β→α" at quenching and inheritance by α-phase of the texture of α"-phase during subsequent transformation.

CONCLUSIONS

1. Phase transformations in titanium alloys during and subsequent to hot working result in the development of a texture of the transformed α-phase which is different from deformation textures in the developed while working low in the α+β phase field.

2. Conditions of phase transformation and compositon of β-phase affect the type of texture of transformed α-phase.

3. In order to obtain textures of a given type it is necessary to take into account the effect of phase transformations in the process of technological treatment of titanium alloys.

REFERENCES

1. Ageev, N. V., Babareco, A. A., Rubina, E. B., Khorev, A. I., Krasnozhon, A. I. and Betsofen, S. J., "Effect of treatment technology on the texture of VT-5-1 and VT-14 titanium alloy rolled sheets." IZVESTIA USSR Academy of Sciences, Metally, 1973, No. 5, p. 150.

2. Ageev, N. V., Morozov, B. S., Babareco, A. A., Betsofen, S. J. and Illin, A. A., "Textures of stampings and heat treatment of articles of (α+β) VT-3-1 alloy." Collection: Khimia metallicheskikh splavov. "Nauka," Moscow, 1973, p 104.

THE FORMATION OF RECRYSTALLIZATION TEXTURE IN TI-AL ALLOYS

R.A. Adamescu, D.A. Srybin, Yu.S. Bratchikov, P.V. Geld,
A.S. Shishmakov
The Urals Polytechnical Institute

U.S.S.R.

There is no information in literature on recrystallization texture of Ti-Al alloys. The significance of such information is evident as crystallographic texture to a great extent determines the anisotropy of mechanical and physical properties of sheet materials.(1-4)

The paper gives the main results of studying the recrystallization process and the formation of recrystallization textures in Ti-Al alloys.

MATERIALS AND TECHNIQUE

The alloys to be investigated were prepared from titanium sponge $_{TT}$-100 and aluminium A7 in an arc furnace. The chemical composition of 20-40 kg bars is given in TABLE I.

After forging the bars were hot-rolled to 10 mm, the temperature at the beginning of rolling being 1,100°C. Further hot rolling to 4 mm was carried out at 800° and followed by annealing at 750° for 1.5 hr.

The bars were given cold rolling in one direction only with the resulting total reduction of strips 20 to 95 pct.

Annealing the specimens being investigated was carried out with various holdings in a vacuum furnace having $\sim 10^{-4}$ torr vacuum, the temperature ranging from t_r^o - 50° to t_{cr} -50° where t_r^0 is the temperature of allotropic transformation.

TABLE I

Chemical composition of investigated alloys

Alloy No.	Inclusions and alloying elements, weight pct						
	Al	Fe	Si	V	Cr	H	O
1	0,36	0.03	0.060	<0.01	0.012	0.004	0.08
2	0.59	0.05	0.065	<0.01	0.014	0.004	0.09
3	1.04	0.04	0.055	<0.01	0.013	0.005	0.08
4	2.01	0.04	0.060	<0.01	0.012	0.004	0.07
5	3.58	0.05	0.055	<0.01	0.010	0.004	0.08

TABLE II

The temperature of the onset of recrystallization (°C) for titanium and Ti-Al alloys

Alloy No.	The amount of deformation, %						t_{cr}
	20	40	60	80	90	95	
Commercial titanium	530	510	490	480	470	460	890
1	570	530	520	480	480	470	900
2	570	540	510	480	475	470	900
3	540	530	530	500	490	480	900
4	600	570	560	530	520	510	930
5	670	630	580	560	550	550	1010

X-raying of specimens for plotting pole figures was carried out using copper radiation by means of IIPOH-0.5 device using scintillator and differential discrimination. To increase the number of grains participating in reflection, X-raying was carried out with a reciprocating movement of a specimen.

Electron microscope Y3MB-100k of 100 kV accelerating voltage was used for examining the conditions of recrystallization nucleation, and sub-grain sizes, and azimuth disorientation of sub-grains as well.

Dehardening was monitored taking into account the results of average microhardness, which was determined by means of IIMT-3 device using a 200 g load.

The onset of recrystallization was estimated according to the disintegration of Debye lines into "spots" on an X-ray film. X-raying was conducted in PKII chamber in copper radiation using defocusing.

PRERECRYSTALLIZATION ANNEALS

Some experimental data on hardness of deformed specimens before and after annealing are given in Fig.1. The curves $H(t^{o})$ show that specimens of commercial titanium and alloys containing less than 1% Al are to a great extent dehardened before the beginning of recrystallization (TABLE II).

This is likely to be due to the high value of stacking fault energy for titanium and dilute alloys [5] which facilitates polygonization processes.

Increasing Al-content reduces the amount of dehardening of cold rolled alloys which is associated with a decreasing stacking fault energy. For example, prior to recrystallization in Ti - 3.58% Al alloy the polygonization covers 50% of specimen volume deformed 90% while in specimens with = 20% the polygonization amounts only to 5-10%.

While studying the texture after prerecrystallization anneals, it was found to be intensified at the polygonization stage (Fig.2). Electron microscopic examination revealed that this intensification of the texture was due to a decrease in sub-grain disorientation with the growth of the sub-grains. One of the probable mechanisms of changing the sub-grain disorientation might be their rotation while growing by means of coalescence.[6] It should be noted that texture intensity is more essential in alloys having high value of stacking fault energy as polygonization processes in them are more vigorous.

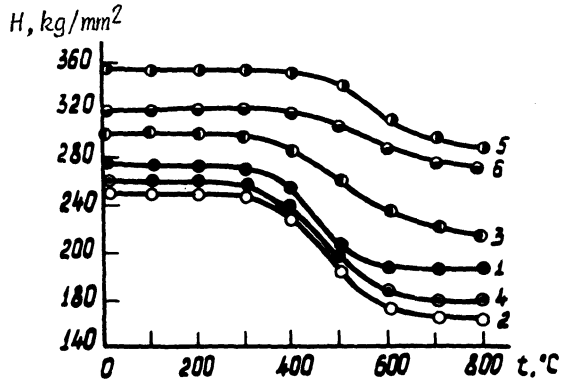

Fig. 1: The influence of annealing temperature on hardness of commercial titanium (curves 1, 2), as well as of Ti-0.36% Al alloys (3, 4) and Ti - 3.58% Al alloy (5,6).
Curves 1,3 and 5 - after deformation 90 pct.
curves 2,4 and 6 - after deformation 20 pct.

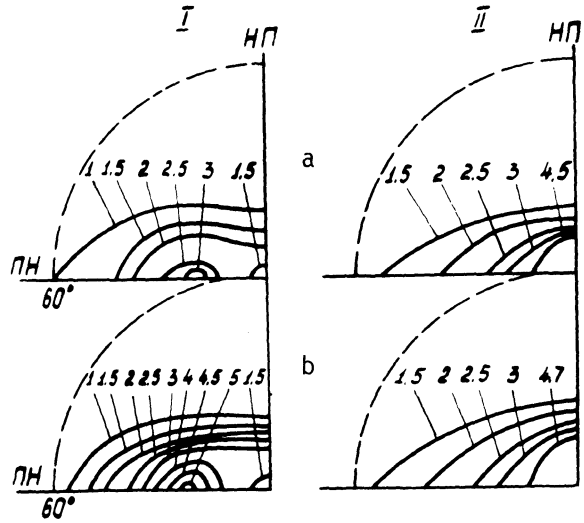

Fig. 2: Pole figures {0002} for Ti - 0.36% Al (I) and Ti - 3.58% Al (II) alloys after deformation 90 pct (a) and 1 hr annealing at $t_r°$ - 50° (b).

RECRYSTALLIZATION TEXTURE

In alloys with Al-content less than 1 pct the texture after 1 hour annealing at t_r^o +50° is similar to that observed in commercial titanium, and is characterized by (0001)±YND-CD[10$\bar{1}$0]-type orientation (Fig.3). The intensity of recrystallization texture increases with the increased amount of reduction during cold rolling.

Annealing at higher temperature results in changing the texture. For example, after annealing at t_{cr} -50° for 1 hr recrystallization texture consists of two components with all amounts of deformation studied and has the following orientations: (0001)±YND-CD[10$\bar{1}$0]-[11$\bar{2}$0] and (0001[10$\bar{1}$0] (Fig.4). If after 20 pct reduction the intensity of both components is approximately the same, an increase of deformation from 20 to 90 pct results in the growth of contribution of the first component and the weakening of the second one. The texture resulting from the deformation of 90 pct or more and 1 hr annealing at t_{cr} -50° may be characterized by an intense (0001)±20° ND-CD[11$\bar{2}$0]-component. An increase of annealing time decreases the dissipation of recrystallization texture and the scattering of basal plane inclination at = 20-70%.

The analysis of recrystallization textures of 1.04% Al alloy specimens deformed 20 and 40% and annealed at t_r^o +50° for 1 hr (Fig.3) has shown that pole figures {0002} at 40-45° inclination with respect to rolling direction were found to have zones of higher intensity, these zones being asymmetrical with respect to transverse direction. As the amount of deformation increases to 60pct, asymmetry decreases, while scattering around rolling direction increases. Recrystallization texture at $\varepsilon \geqslant 60\%$ may be characterized by (0001) 20-30° ND-CD [10$\bar{1}$0]-component.

Annealing at t_{cr} -50° results in the formation of "ideal" basal texture (0001)[10$\bar{1}$0] (Fig.4).

It should be noted that apart from the main component, there appeared (0001)± 10° ND-CD[10$\bar{1}$0]-component in specimens deformed 90-95 pct as well. An essential change in the regularities of the formation of recrystallization texture is caused by an increase in Al-content. For example, the (0001)[10$\bar{1}$0]-component was observed even in specimens of 2% Al alloys after 1 hr annealing at t_r^o +50°, the exception being specimens with $\varepsilon \geqslant 90\%$ having (0001)±20° ND-CD [10$\bar{1}$0]-component along with the above mentioned. Annealing Ti - 2% Al alloy at t_{cr} -50° for 1 hr results in (0001)[10$\bar{1}$0]-type orientation, its intensity increasing with greater amount of deformation.

The (0001)[10$\bar{1}$0]texture is also formed in 3.58% Al alloy after annealing at t_r^o +50° for 1 hr, the intensity of this component, however, being less affected by the amount of deformation during cold rolling (Fig.3).

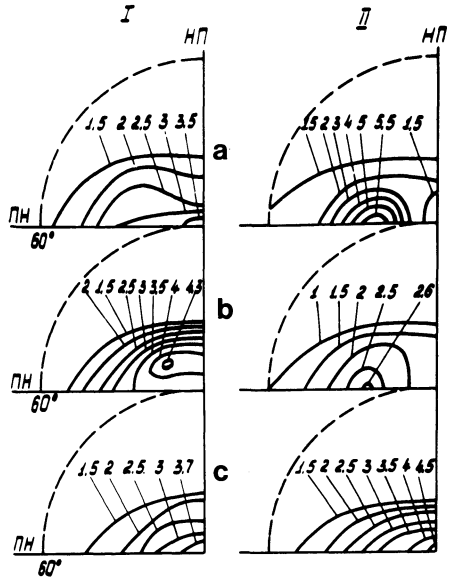

Fig. 3: Pole figures {0002} for Ti-Al alloys after 1 hr annealing at $t_r°$ + 50°.
a - Ti - 0.36% Al; b - Ti - 1.04% Al;
c - Ti - 3.58% Al; I and II - deformation
20 pct and 90 pct, respectively.

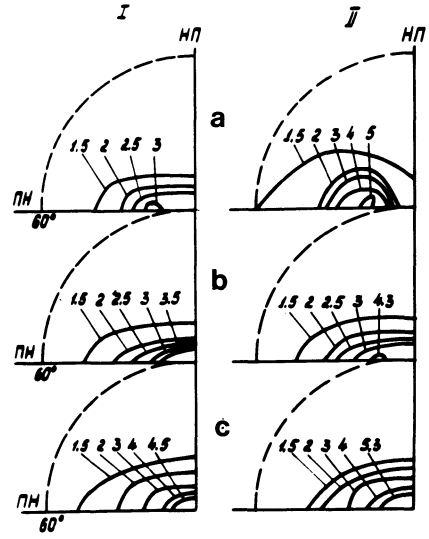

Fig. 4: Pole figures {0002} for Ti - Al alloys after 1 hr annealing at t_{cr} -50°. Notations are the same as in Fig. 3.

The type of texture does not change after annealing even at higher temperature. In particular, in 3.58% Al alloy after 1 hr annealing at t_{cr} -50° the texture in specimens with any amount of reduction is characterized by (001)[10$\bar{1}$0]-type orientation, its intensity increasing with an increase in deformation (Fig.4).

For all Ti-Al alloys an increase of annealing time from 1 to 5 hr affects but slightly the intensity of recrystallization texture. Besides, non-uniformity of recrystallization texture in strip thickness in alloys studied is low, and has been found only in specimens of reductions 20-40 pct. An increase in temperature and time of annealing is accompanied by the reduction of this non-uniformity.

Thus, in alloys with Al-content less than 1 pct during annealing at t_r^o +50° a recrystallization texture is formed which is similar to that observed in unalloyed titanium. Increasing Al-content results in emergence and further intensity of (0001)[10$\bar{1}$0]-type orientation, while in 3.58% Al alloy the texture is single-component with all amounts of deformation studied. Increasing the annealing temperature within the α-phase field has a greater affect on the resulting texture in alloys containing less than 1% Al. In alloys containing 2% Al or more, however, the texture is characterized by (0001)[10$\bar{1}$0]-component.

Electron microscopic examination of the first nuclei of recrystallization has shown that the majority of nuclei have (0001)-type orientation with the inclination of the basal planes with respect to the foil surface not exceeding 20-25°.

Taking into account the orientation relationship of these nuclei and the deformed matrix (Fig.1), as well as orientation relations between recrystallization and deformation textures, one might suppose that the recrystallization texture is formed as a result of the selective growth of new grains, the growth being governed by the orientation dependence of the migration velocity of large-angle bondaries. In the long run, the greatest part of recrystallized volume is filled with the grains of more favourable orientation relationship with the greatest number of deformation texture components.

Thus, the results obtained allow us to propose that orientation peculiarities of forming the recrystallization nuclei are not very important, and the formation mechanism of recrystallization texture may be accounted for on the basis of the theory of orientated growth.

The comparative analysis of recrystallization textures of Ti-Al alloys after annealing at t_r^o +50° and t_{cr} -50° has shown that increasing the annelaing temperature results in (0001)$\pm$YND-CD [11$\bar{2}$0]-texture instead of (0001)$\pm$YND-CD[10$\bar{1}$0] in alloys containing

less than 1% Al, and "ideal" (0001)[10$\bar{1}$0]-component in Ti-1.04%Al alloy (ε<90%). The texture type in Ti - 3.58% Al alloy remains unchanged.

The stability of the primary recrystallization texture resulting from an increase in temperature is likely to be accounted for by the fact that an increase of annealing temperature results in collective recrystallization. This process is not followed by an abnormal grain growth as anisotropy of migration of large-angle boundaries decreases greatly in this case. Similar reduction of anisotropy of grain growth velocity resulting from an increase of annealing temperature was observed in previous studies as well, namely in polycrystalline zirconium.[8,9]

The investigation has shown that secondary recrystallization doesn't take place in titanium and Ti-Al alloys after annealing at $t^o < t_{cr}$. In some cases, however, a slight abnormal grain growth is observed, producing a texture which is most characteristic of Ti - 1.04% Al alloy. The cause of changing the texture type in the above alloy is likely to be an increase in the mobility of some boundaries associated with an increase in temperature, the change of the mobility according to data [10,11] being twice as great in some cases.

REFERENCES

1. Kudryavev I.P., Tekstury v metallakh i splavakh. Metallurgiya. 1965.

2. Wasserman G., Greven I. Tekstury metallicheskikh materialov. Metallurgiya. 1969.

3. Honeycombe R. Plasticheskaya deformatziya metallov. M. Mir, 1972.

4. Michlyaev P.G., Fridman J.B. Anizoptopiya mechanitcheskikh svoistv materialov. M. Metallurgia, 1969.

5. Shishmakov A.S., Adamescu R.A., Geld P.V. Relations of the Texture and the Strain Mechanism of Alpha-Titanium Alloys to the Stacking Fault Energy. (The paper in the present issue).

6. Li J.C.M. Possibility of Subgrain Rotation During Recrystallization. J. Appl. Phys. 1962, 33, 2958-2965.

7. Shishmakov A.S., Adamescu R.A., Geld. P.V. Teksturi kholodnoi prokatki v splavakh Ti-Al. Izvestia Akademii Nauk SSSR. Metalli 1972, No.2, 123-129.

8. Keeler, J.H., Geisler A.H. Textures of Rolled and Annealed Iodide Zirconium. Trans. Met. Soc. AIME, 1955, 203, 395-399.

9. Keeler J.H. Hibbard W.R., Decker M.E. Textures of Rolled and Annealed Iodide Zirconium. J. Metals, 1953, 5, 9320936.

10. Gleiter G., Chalmers B. Bosheuglovie granitzi zeren. M. Mir, 1975.

11. Lücke K., Rixen R. Rekristallisation und Korngrösse. Z. Metallkunde, 1968, 59, 321-333.

RECRYSTALLIZATION OF Ti-Mo BASE BETA ALLOYS

S.Ohtani, M. Nishigaki, T. Nishimura and Y. Moriguchi

Kobe Steel, Ltd.
Kobe, Japan

Introduction

For Ti-15Mo-5Zr beta alloy aged at 500°C, it was observed to be remarkable difference of ductility between the specimens solution treated at 825°C and 725°C. This is considered to be due to the different precipitating conditions appearing after ageing according to the solution treatment temperature, although any difference cannot be observed in the microstructures of solution treated specimens at 825°C and 725°C. The microstructure of the solution treated Ti-15Mo-5Zr alloy at 725°C followed by ageing at 500°C, is inhomogeneous but that of the soluiton treated at 825°C and aged is perfectly recrystallized.

The effects of Al addition and different prior working conditions on the recrystallization behaviors of this Ti-15Mo-5Zr alloy were investigated.

Experimental procedures

Materials

The chemical compositions of tested materials Ti-15Mo-5Zr and Ti-15Mo-Zr-3Al alloys are shown in Table 1. The tested speciments were prepared from a one ton ingot for Ti-15Mo-5Zr alloy and a 300 kg

Table. 1 Chemical compositions and beta transus

Alloy	Form	chemical analysis (%) Mo	Zr	Al	Fe	O	N	C
15-5	bar	14.23	4.76	-	0.0046	0.183	0.0058	0.008
	plate	14.74	4.84	-	0.0046	0.179	0.0061	0.006
15-5-3	bar	14.97	5.04	2.93	0.0047	0.165	0.0129	0.006
	plate	14.81	5.06	3.00	0.0037	0.150	0.0115	0.006

	Beta transus (°C)	
15-5	bar	730
	plate	730
15-5-3	bar	795
	plate	785

Table. 2 Rolling procedure of specimens

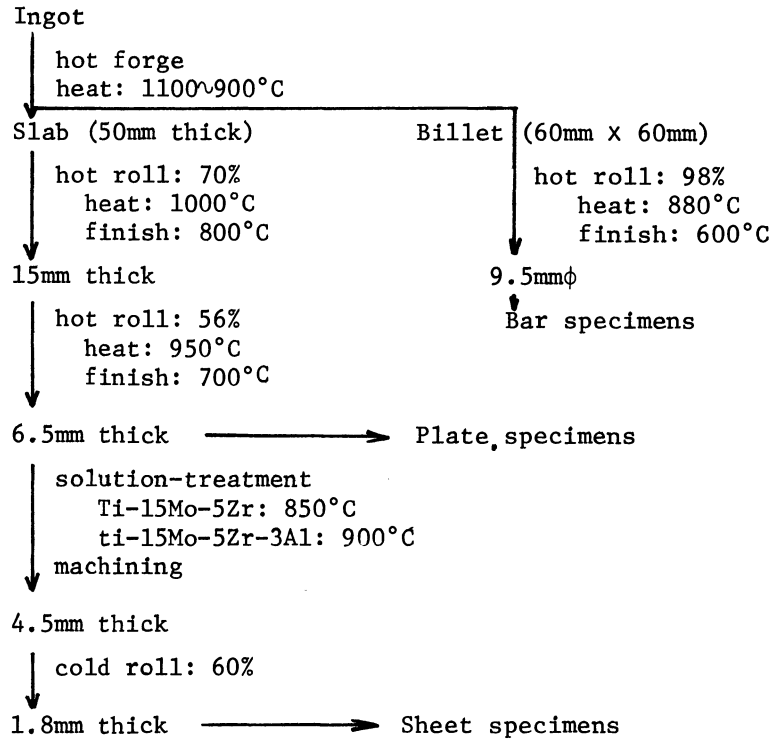

ingot for Ti-15Mo-5Zr-3Al alloy according to the rolling procedure shown in Table 2. The hot rolled plate and bar, and cold rolled sheet specimens were tested to investigate the effect of prior working conditions on these alloys' recrystallization behaviors. Figure 1 shows the microstructures of Ti-15Mo-5Zr alloy specimens as rolled. As shown in Figure 1, the most highly deformed is a bar specimen and the lowest deformed is a plate specimen.

Beta transus was determined by the microstructure change for hot rolled plate and bar specimens. It was difficult to determine the transus by a general method because it took much time to come to an equillibrium state due to these two alloys' relatively low beta transus. Finally, the following methods were found to be suitable for determining the beta transus clearly. For Ti-15Mo-5Zr alloy, the solution treated specimens were heated at 300°C for 3 hr. followed by heating again at 500°C for 6 hr. in order to perecipitate alpha grains homogeneously. The beta transus was determined by presence of alpha grains holding at a temperature for 3.5 hr. For Ti-15Mo-5Zr-3Al alloy, the solution treated specimens were aged at 600°C for 6hr to precipitate alpha grains and beta transus was determined in the same method as for Ti-15Mo-5Zr alloy specimens.

The authors define the recrystallization behaviors of these alloys as follows.

The first step recrystallization temperature; Transformation temperature from worked structure to an equiaxed beta one.

The second step recrystalliazation temperature; Temperature completely recrystallized, that is, precipitated with alpha grains homogeneously after following ageing.

The recrystallization behaviors were studied as follows. The solution treated specimens were held at the temperature of 25°C intervals between 625°C and 950°C for 10 - 300 minutes and water quenched.

The ageing condition was constant; 500°C x 100 min. A.C.

The first and second step recrystallization conditions were de-

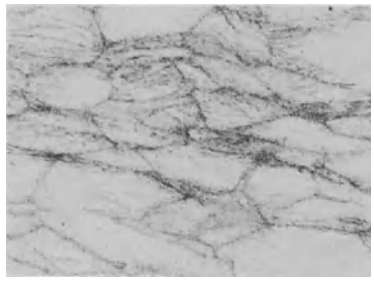

1a

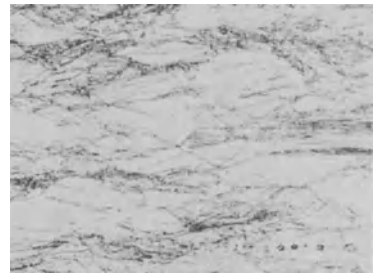

1b

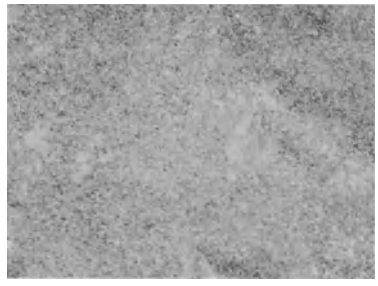

1c

Figure 1 a - c

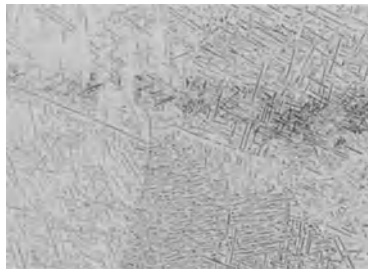

2a

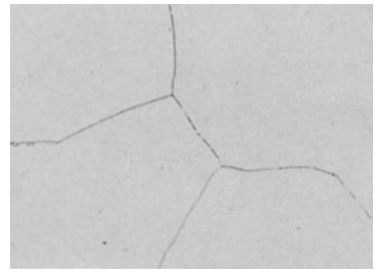

2b

Figure 2 a & b

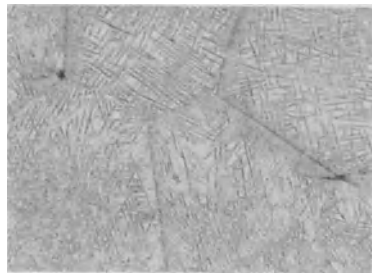

3a

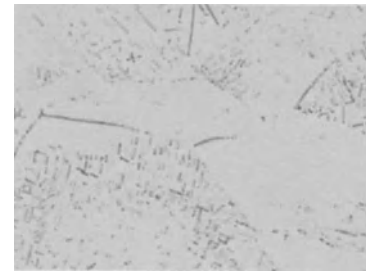

3b

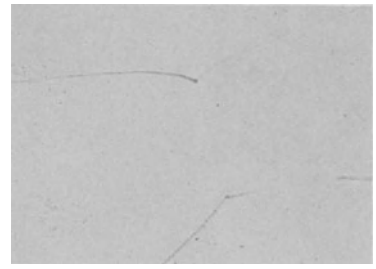

3c

Figure 3 a - c

termined by the microstructure changes.

Results

Beta transus

Ti-15Mo-5Zr alloy

The omega phase was precipitated by heating at 300°C, was transformed to alpha phase by following heating at 500°C. The beta transus of hot rolled plate, 730°C was determined by presence of alpha grains as shown in Figure 2. The same beta transus was obtained for hot rolled bar and cold rolled sheet specimens.

Ti-15Mo-5Zr-3Al alloy

The beta transus 795°C for hot rolled bar and 785°C for hot rolled plate were determined as shown in Figure 3. The temperature difference

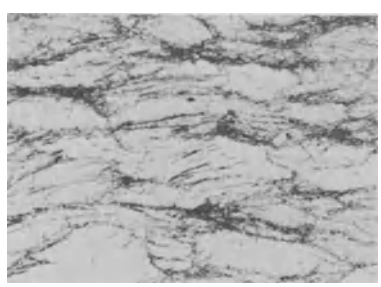

4a

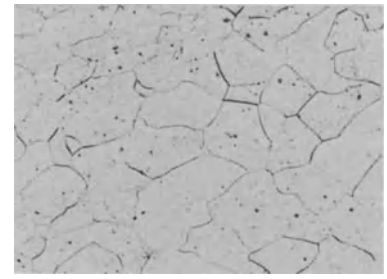

4b

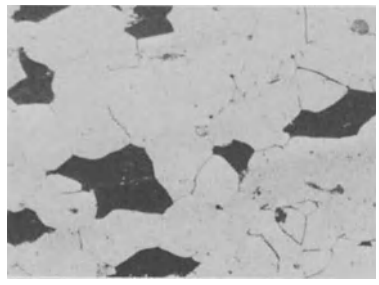

4c

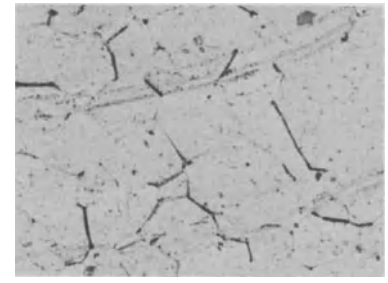

4d

Figure 4 a - d

between plate and bar specimens is considered to be an error due to experimental technique.

Recystallization

Figure 4 and 5 show the microstructures of Ti-15Mo-5Zr alloy plate specimens, and sheet and bar specimens, respectively. The first and second step recrystallization temperatures and holding periods at the temperature are shown in Figure 6. While, the first step temperatures are almost same independent of prior different working conditions, the second step temperature is affected by difference of the working conditions. That is, the lowest deformed hot rolled plate specimens show the higher recrystallization temperature than that of hot rolled bar or cold rolled sheet specimens. As the holding period at a solution treated temperature is prolonged, the first and second step temperature is approaching to the same temperature 775°C.

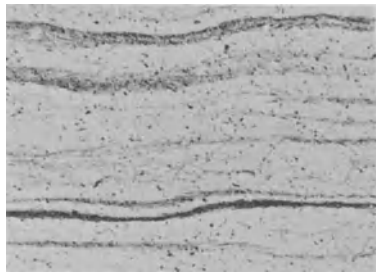

5a

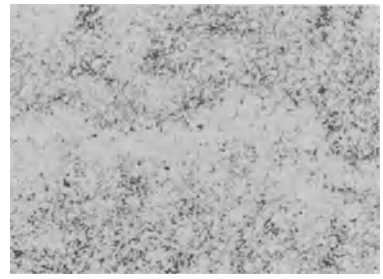

5b

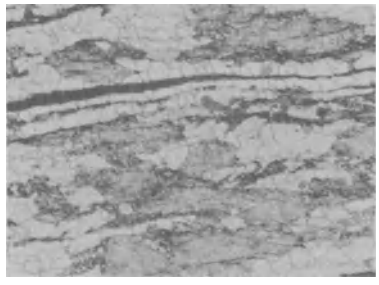

5c

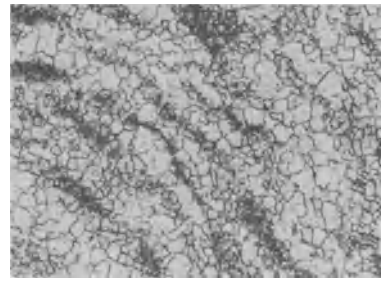

5d

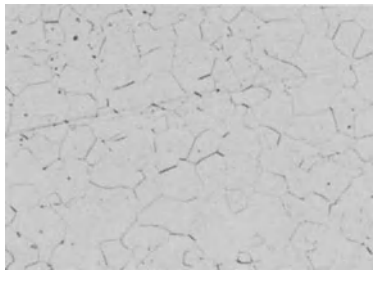

5e

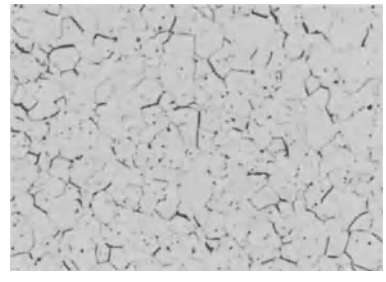

5f

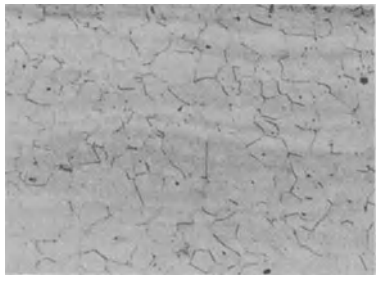

5g

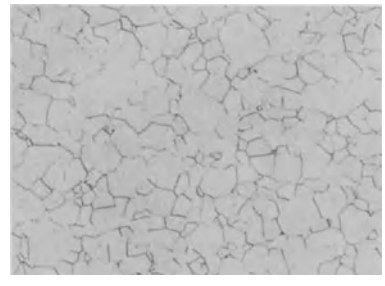

5h

Figure 5 a - h

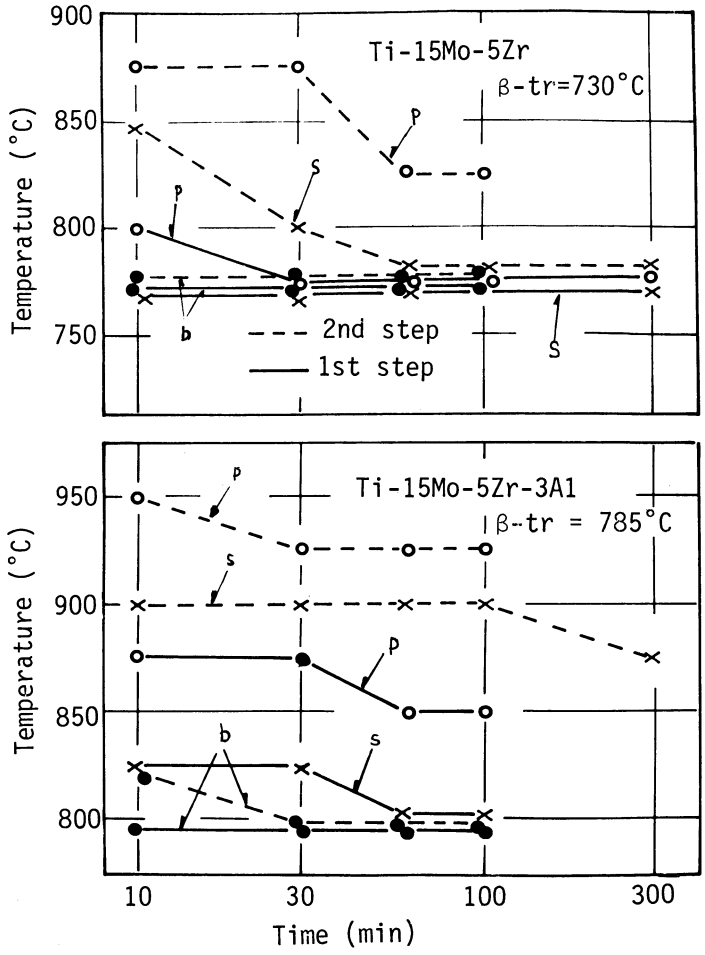

Figure 6

The recrystallization behaviors of Ti-15Mo-5Zr-3Al alloy are shown in Figure 7. While, the most highly deformed hot rolled bar specimens show the same first and second step temperature, plate and sheet specimens show the considerably higher second step temperature than the first one. But it is thought that the first and second step temperatures are apt to approach to a constant temperature of 800°C for

this Ti-15Mo-5Zr-3Al alloy with the lapse of holding time as well as Ti-15Mo-5Zr alloy.

Discussion

In the determining beta transus test, alpha precipitated at the grain boundary for Ti-15Mo-5Zr alloy and inside of the grain for Ti-15Mo-5Zr-3Al alloy after ageing at 600°C. For Ti-15Mo-5Zr alloy, direct transformation beta → alpha at 600°C is rather difficult and so alpha precipitates only at the grain boundary. On the other hand, for Ti-15Mo-5Zr-3Al alloy, beta → alpha direct transformation easily takes place on account of alpha being stabilized by Al addition and so alpha precipitates inside of the grain. For Ti-15Mo-5Zr alloy,in order to precipitate alpha inside of the grain,it is necessary to transform from beta to alpha via intermediate omega phase. Therefore, two step ageing 300°C X 3 hr → 500°C X 6 hr is effective to determine the beta transus cleary.

The two step recrystallization behaviors of Ti-15Mo-5Zr base beta alloys is considered to be due to very slow reaction rates in recrystallization process. The first step recrystallization takes place only in the highly deformed grains with much strain and it is considered not to be fully recrystallized. The recrystallization is completed with the second step.

The working conditions of these alloys are more effective on recrystallization than those of any other metals. This is considered to be due to much difference in local deformation on account of these alloys' low work hardenability. Therefore, on the recrystallization process, only highly deformed phase is mainly recrystallized at first and the low deformed phase stays as an equiaxed grains. That is, by microstructure observation, recrystallization reaction seems to be completed. This is the first step recrystallized state which the newly recrystallized grains coexist together with those containing the lattice defects had been at the working stage. The homogeneously and highly deformed hot rolled bar specimens are recrystallized at the same first and second step temperature. While, for the inhomogeneously

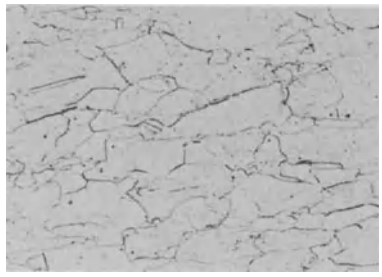

7a

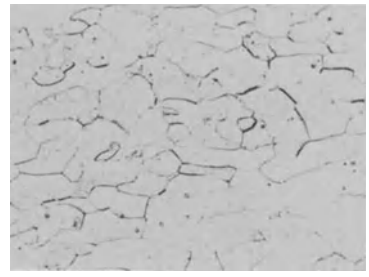

7b

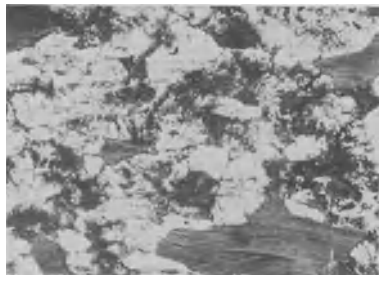

7c

7d

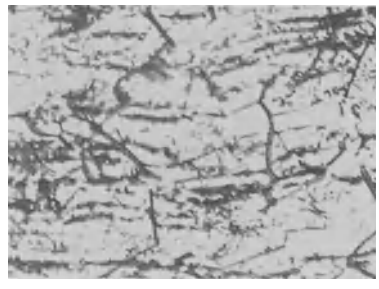

7e

Figure 7 a - e

and low deformed hot rolled plate specimens, the difference between the first and second step recrystallization temperature, is rather big and their recrystallization temperatures are higher than those of bar specimens. It is necessary for finishing recrystallization of low worked specimens to heat at a higher temperature for longer periods.

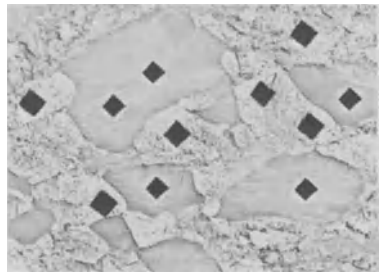

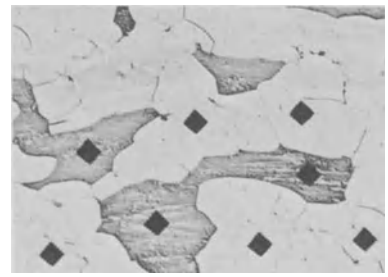

8a 8b

Figure 8 a & b

Figure 8 shows hardness of different two phases of the not fully recrystallized specimens. The dark color grains' hardness of Ti-15Mo-5Zr alloy is a little softer than that of light color grains but for Ti-15Mo-5Zr-3Al alloy, dark grains are considerably harder. The hardness difference is explained as follows. The dark grains are considered not to be fully transformed by solution treatment and are preferentially precipitated with alpha grains on account of containing much lattice defects. Alpha precipitation is not so effective to increase hardness of Ti-15Mo-5Zr alloy, but alpha precipitation containing Al element is much effective too. Hardness of these two alloys solution treated is almost the same about 290 Hv. The light color grain's hardness of Ti-15Mo-5Zr alloy is much higher than 290 Hv., but hardness change of Ti-15Mo-5Zr-3Al alloy is not observed. This hardness increase for Ti-15Mo-5Zr alloy is considered to be due to omega precipitation. For Ti-15Mo-5Zr-3Al alloy, as this omega precipitation is controlled by Al addition, hardness increase cannot be observed.

The mechanical properties of solution treated and aged Ti-15Mo-5Zr alloy bar are much affected by solution treatment temperature. This change of mechanical properties is considered to be related to above discussed recrystallization behaviors.

ANNEALING BEHAVIOR AND STRENGTHENING OF Ti-6Al-2Sn

M. Majdic, G. Welsch, and G. Zeigler

Deutsche Forschungs- und Versuchsanstalt für
Luft- und Raumfahrt
500 Köln 90, Deutschland

The microstructure of a fine globular Ti-6Al-6V-2Sn alloy was investigated after various solution treatments (700 to 1000°C) and after aging treatments in the temperature region from 350 to 600°C by X-ray diffraction and by electron microscopy. For two selected solution treatments at 700 and 850°C the mechanical properties in tension were determined as a function of aging temperature and time. Correlation of the microstructure with the mechanical properties yielded the following results: age hardening is caused by precipitation processes in the β or martensite phase and by hardening of the primary α by Ti_3Al precipitation and possibly oxygen order. After solution treatment at 850°C hardening of the (β + martensite)-areas are predominant. After solution treatment at lower temperatures (e.g. 700°C) hardening of both phases is of importance.

I. INTRODUCTION

In order to optimize the microstructure with regard to the mechanical properties it is necessary to know the transformations

that take place during deformation and annealing. The results given in the literature on the phases present after solution annealing at various temperatures are in agreement with each other for the temperature ranges below 825°C and above 900°C. However, the results obtained after solution annealing in the temperature range 825 - 900°C are interpreted in differing ways (1-5).

In general, precipitation processes are possible in both the β- and the α-phase, since upon quenching these phases are not in thermal equilibrium. For the alloy Ti-6Al-6V-2Sn precipitation processes in the β-phase have so far been registered only indirectly, by the change of various parameters. Also, precipitation within the α-phase has not been determined.

In the present work the precipitation behavior and in particular its dependence on prior solution treatment was investigated for the alloy Ti-6Al-6V-2Sn. By the combination of several methods of investigation, it was attempted to obtain information on precipitation processes in both the β- and the α-phase. The mechanical properties were determined as a function of aging temperature and aging time after prior solution treatments at 700 and 850°C. The correlation of the mechanical properties with the changes in microstructure is discussed.

II. EXPERIMENTAL

The starting material was a commercial Ti-6Al-6V-2Sn alloy with a fine globular microstructure. The chemical composition was analyzed and is given in weight percent: 5.6 ± 0.2 Al, 5.8 ± 0.1 V, 2.1 ± 0.1 Sn, 0.58 ± 0.1 Fe and 0.32 ± 0.1 O.

Discs of 3 mm thickness were used for hardness, X-ray and microscopic measurements. The tensile specimens had diameters of 5,0 and gauge lengths of 20 mm. Solution annealing was done in

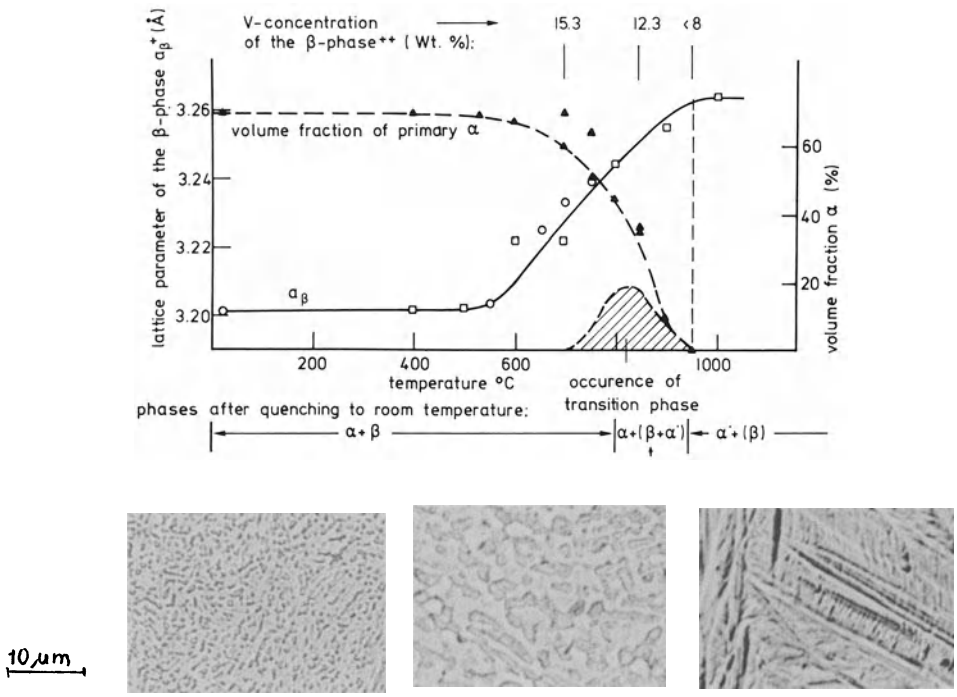

Fig. 1 Composition of phases and lattice parameters of the β-phase in various temperature regions.
+Measurements at:
□ solution temp. (corrected for expansion)
○ room temperature
++determined from changes in lattice parameter and based on the dependence found for Ti-6Al-4V (6).

vacuum of better than 10^{-3}Pa for 40 minutes each and followed by an oil or water quench.

Several methods of investigation were used to analyze the changes taking place in β and α during aging: tensile tests, hardness measurements and electron microscopy, all at room temperature; X-ray diffraction was performed on both quenched specimens and also directly at high temperatures with the help of a high temperature chamber.

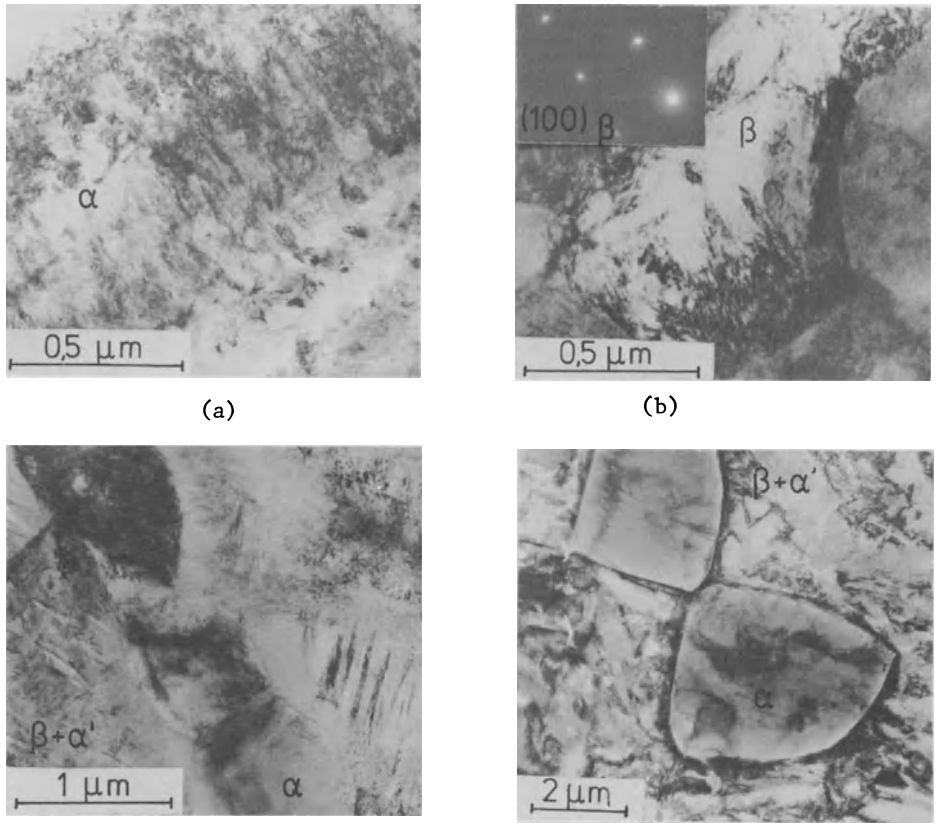

Fig. 2 Microstructure after solution treatment at various temperatures:

a) 700°C/quench: α-grain with displacement contrast.

b) 700°C/quench: β-grain with slight distortions.

c) 850°C/quench: α-grain with displacement contrast and areas of fine (β and martensite).

d) 900°C/quench: primary α + coarse martensite.

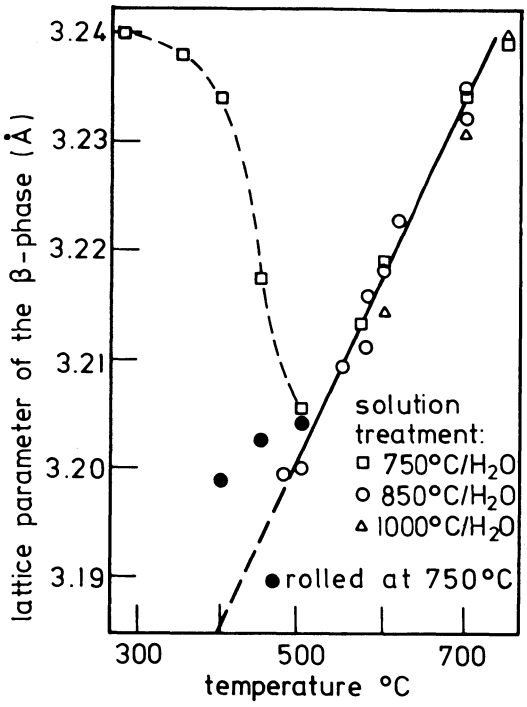

Fig. 3 Lattice parameter of the β-phase as a function of aging temperature (aging time 1 h)

III. RESULTS

3.1 Microstructure after solution annealing

X-ray results (Fig. 1):

X-ray diffraction measurements at high temperatures indicated a continuous transformation of the primary α into the β-phase starting at about 600°C. As expected from the phase diagram, the vanadium

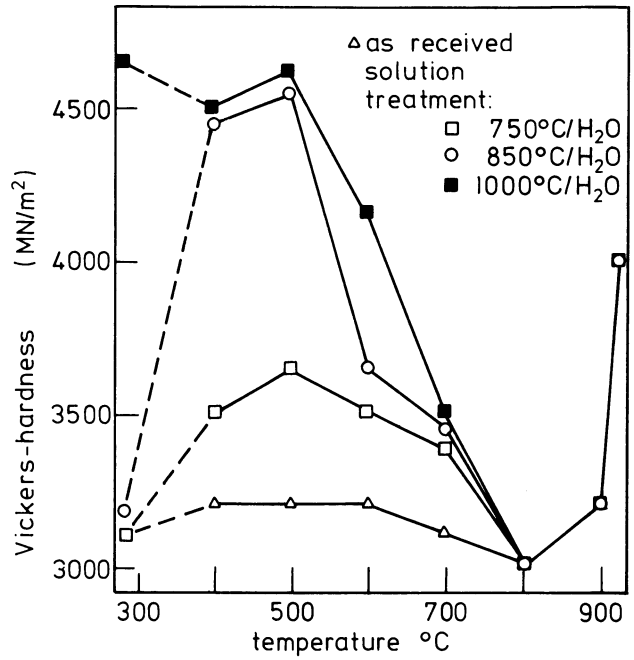

Fig. 4 Hardness as a function of aging temperature (aging time 1 h)

concentration of the β-phase decreased with increasing temperature, as is indicated by the increasing lattice parameter in Fig. 1. After quenching from above 800°C, the β-phase could no longer be identified in a definite way. Also,the line broadening of the α-reflections are a sign of martensite formation upon quenching from above 800°C. After quenching from temperatures between 700 and 950°C a transition phase was found by X-ray diffraction with an intensity maximum near 850°C. Values of 2 θ (θ= diffraction angle) for CuK_α-radiation are: 30.9, 35.9, 38.8 and 41.0 degrees. The structure of this phase is clearly distinguishable from the hexagonal structure of the martensite, which was obtained when quenching from temperatures > 925°C. The transition phase, however, does not exist at the high temperatures and is formed only when quenching.

Transmission electron microscopy (Fig. 2):

Quenching from temperatures below 800°C produced a microstructure consisting of primary α-matrix (>60 volume %) and of clearly identifiable β-grains with slight distortions (Fig. 2a,b). There was considerable displacement contrast within the α-grains, the cause of which could not be identified (Fig. 2a). After quenching from the temperature range 800 - 900°C primary α-grains with some displacement contrast were embedded in a matrix consisting of fine martensite and β (Fig. 2c). With higher solution temperatures the martensite coarsened and occupied increasingly large volume fractions (Fig. 2d). After quenching from above 925°C the microstructure was completely martensitic.

3.2 Microstructure after aging

X-ray results (Fig. 3):

Low temperature (< 500°C) aging of a 750°C solution annealed specimen produced a continuous decrease of the lattice parameter of the β-phase, which is indicative of a time dependent enrichment in vanadium. The change of the lattice parameter of the β-phase (750°C solution treated) and the reduction of the halfwidth of the α-reflections after 850°C solution treatment show that the decomposition of the metastable β- or martensitic phase takes place already at temperatures as low as 350°C. The increase of the lattice parameter of the β-phase upon aging at temperatures above 500°C shows that the β-phase depletes in vanadium. A one hour anneal is sufficient to nearly reach the equilibrium concentration.

Transmission electron microscopy (Fig. 5a-f):

The decomposition of the metastable β or of the martensite phase takes place as follows:

a) After solution treatment up to 800°C: at low aging temperatures (< 500°C) fine α-needles or platelets have precipitated (Fig. 5b,c). At aging temperatures above 500°C the α-precipitates coarsened (Fig. 5d).

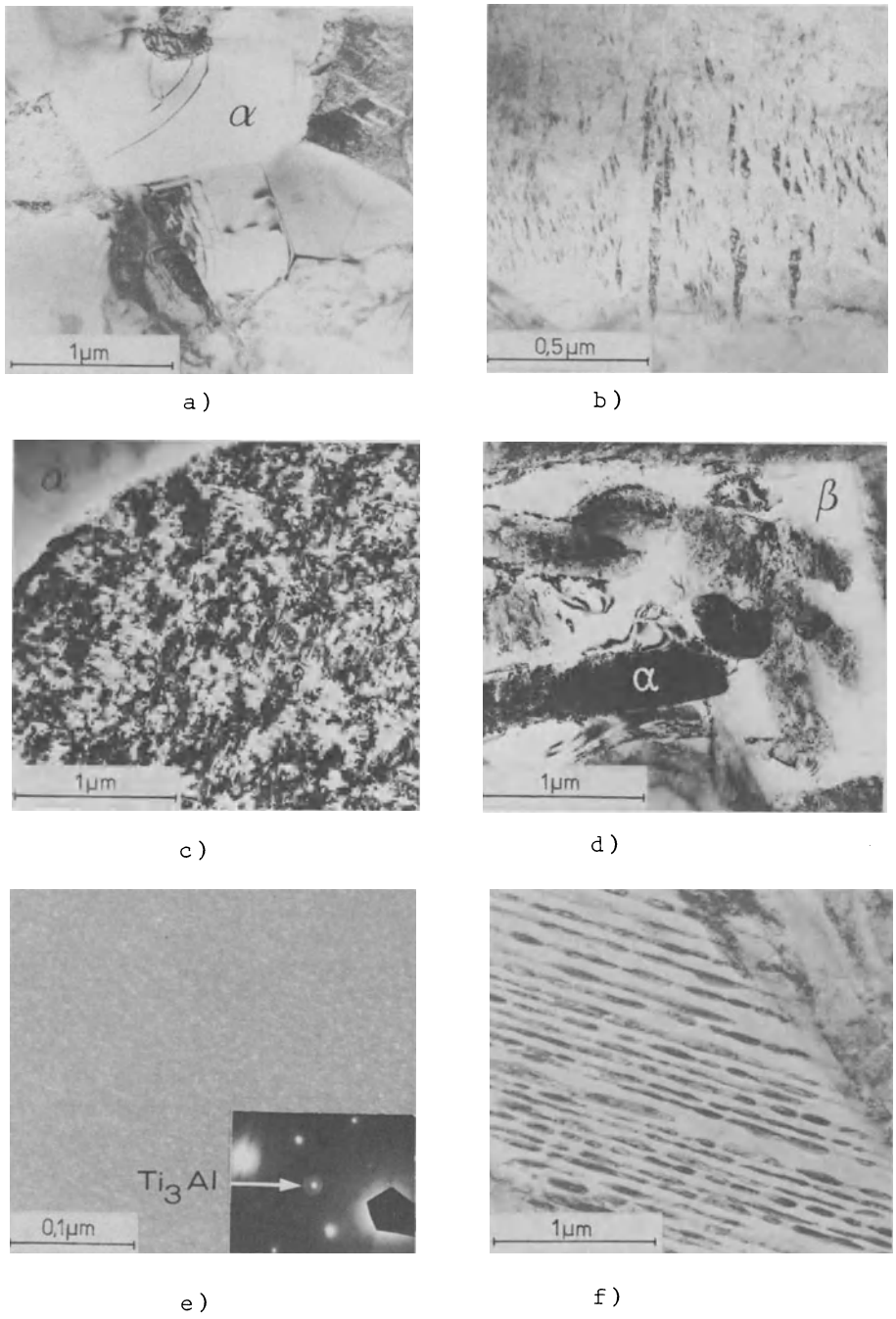

Fig. 5 Microstructure after aging

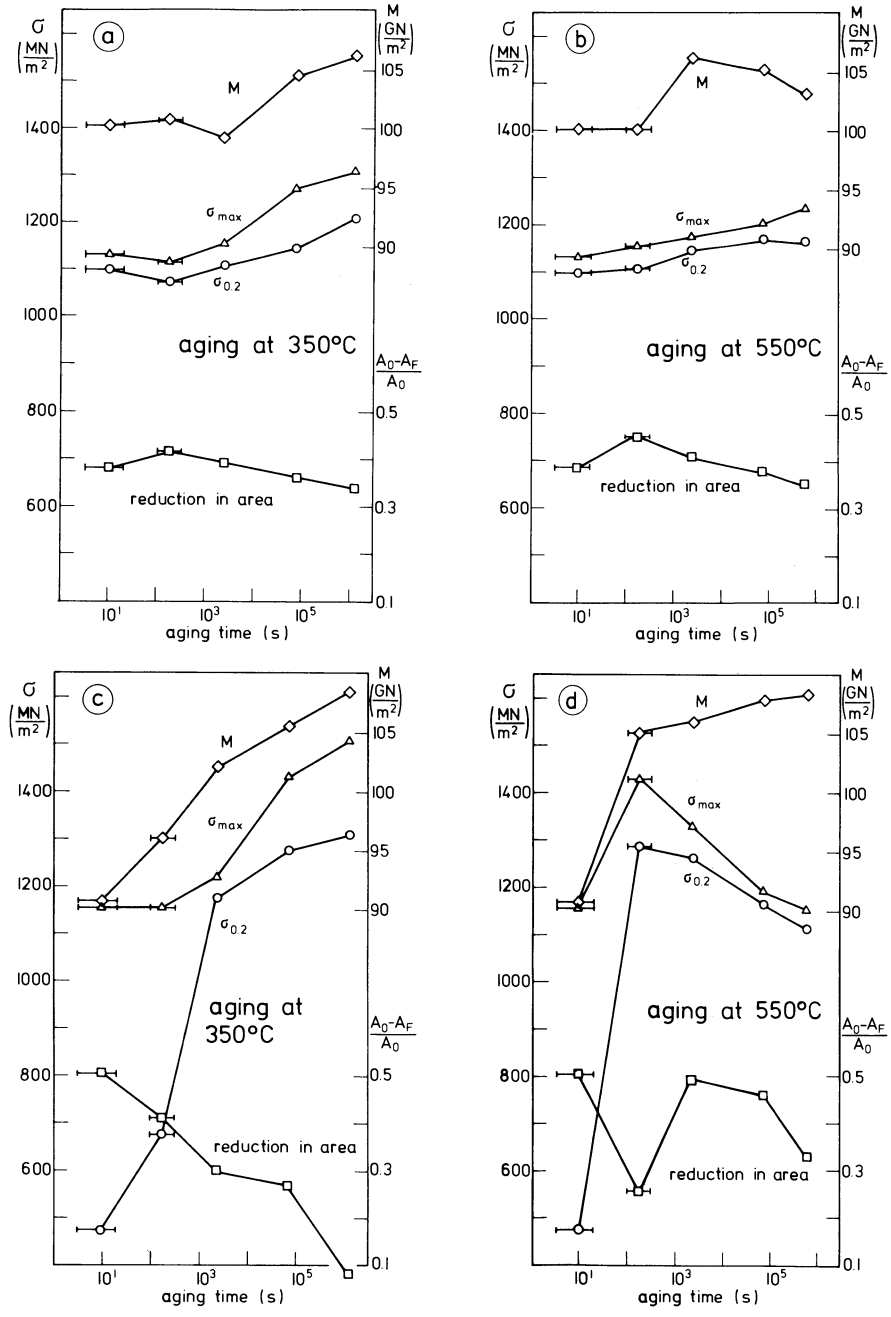

Fig. 6 Mechanical properties in tension as a function of aging temperature and time after solution treatments at 700 (a,b) and 850°C (c,d).

b) After solution treatment above 875°C the martensite decomposed at low aging temperatures (< 500°C) into fine α-lamellae , which coarsened upon aging above 500°C (Fig. 5f).

c) After solution treatment at increasing temperatures in the range from 800 to 900°C, a transition took place from needle- or plate-shaped to lamellar precipitates upon aging.

Precipitation of fine Ti_3Al precipitates (< 5 nm, Fig. 5e) in the primary α was observed upon aging in the temperature range 500 - 620°C. The displacement contrast present after quenching from above 600°C disappeared completely at aging temperatures as low as 350°C (Fig. 5a).

3.3 Mechanical Properties

Hardness (Fig. 4):

For isochronous aging treatments (1 h) a hardness maximum was found between 400 and 500°C. The maximum hardness was dependent on the prior solution treatment temperature.

Tensile tests (Fig. 6):

Young's modulus (M), tensile strength (σ_{max}), yield strength ($\sigma_{0.2}$) and the reduction of cross section are plotted in Fig. 6 for the two solution treatment temperatures 700 and 850°C as a function of aging temperature and time.The dependence on aging temperatures ranging from 350 to 600°C was investigated; representative results are given for the temperatures 350 and 550°C. The values of strength and ductility exhibit the typical shape of age hardening curves. Increasing yield strength, tensile strength and Young's modulus is accompanied by a decrease in ductility. The ductility increases again with decreasing strength after the maximum strength has been reached. It is remarkable, however, that there is again a loss in ductility after very long aging times at 550°C (Fig. 6d) and also at 600°C.

IV. DISCUSSION

4.1 Microstructure after solution treatment

After quenching from 800 to 925°C, a fine mixture of metastable β-phase and martensite phase is found, the remainder is primary α. X-ray diffraction also reveals a transition phase when quenching from the temperature region 700 to 950°C. The reflections obtained agree with the measurements of (1,4), who claim that the phase has a martensitic structure. In particular, Gueret et al. (4) interpret the result as "soft" martensite of cubic structure. Another interpretation was that Ti_3Al had formed (2,3). However, our results in electron microscopy revealed no Ti_3Al after solution treatment and quenching. The vanadium and the aluminum concentrations of the metastable phases upon quenching are probably determined by the equilibrium concentrations at the solution treatment temperature since segregation can be assumed to be negligible. The vanadium concentrations, extrapolated from the lattice paramters of the β-phase (Fig. 1), range from 15,3 to about 6 wt.% in the temperature range from 700 to 950°C. If one uses the results on the alloy Ti-6Al-4V (6) for estimating the aluminum concentration in the primary α-phase, the aluminum concentration comes out to be around 7 wt.% above 750°C.

4.2 Microstructure after aging

The following precipitation processes were found:

a) Decomposition of the metastable β-phase or of the β + fine martensite by the precipitation of the fine α-needles or plates (prior solution treatment $\leq$ 850°C), Fig. 5b,c;
b) Decomposition of the coarse martensite into α-lamellae of different orientations (prior solution treatment $\geq$ 900°C), Figs. 5f;
c) Precipitation of fine Ti_3Al ($<$ 5 nm) within the primary α, (Fig. 5e).

The fact that precipitation in the metastable β or in the martensite takes place at rather low temperatures (e.g. 350°C), whereas Ti_3Al does not precipitate until about 500°C may be explained by two factors: 1) a generally faster diffusion in the body centered cubic β-lattice and 2) the elastic distortion of the martensite can aid both nucleation and initial growth rate of the α-precipitates.

In a binary Ti-5.8 wt.% Al the precipitation of Ti_3Al was observed at 550°C (7). Vanadium and oxygen lower the solubility of aluminum in the α-phase, while tin increases it somewhat (8). The precipitation of Ti_3Al in the 7 wt.% aluminum rich α-phase of Ti-6Al-6V-2Sn is thus understandable. Based on the results on binary Ti-Al alloys (7), precipitation of Ti_3Al is possible above 450°C.

4.3 Correlation of microstructure with mechanical properties

Age hardening in the temperature range from 350 to 600°C can be caused by two reactions:

a) the decomposition of the metastable β-phase or of the martensite into α-needles, platelets or lamellae (Figs. 5b,c,f). The contribution to hardening is particularly strong in those cases, where the α-precipitates are very fine and take up a large volume fraction, as is the case after long aging times at low temperatures (e.g. 350°C, Fig. 5b). This process also contributes to the increase in Young's modulus. For the larger aging temperatures of 550 and 600°C the maximum hardening is reached after a short time, and then becomes less because of coarsening of the secondary α within the β (Fig. 5d). Such coarsening is accompanied by an increase in ductility (Fig. 6d).

b) The α-phase is hardened in the temperature range from > 450 to about 620°C by the precipitation of fine Ti_3Al (Fig. 5e). The large values of Young's modulus and also perhaps the loss of ductility after very long aging times (Fig. 6d) may be due to Ti_3Al. At low aging temperatures (e.g. 350°C) there may also be hardening due to oxygen order (oxygen concentration 0.32 ± 0.1 wt.%)(9).

The effective hardening is determined by the volume fractions of the hardenable phases and by the instability of the β or martensite phases. The stronger hardening after the solution treatment at 850°C must be due to the large volume fraction (65 vol.%) of metastable β + martensite. The respective specimens exhibit very efficient hardening at the aging temperatures of 350 and 450°C. Their increase in strength is mainly due to the precipitation of fine α-plates. The lowering of the strength after long annealing times at 550 and 600°C is most likely due to the coarsening of the secondary α within the β. The hardening of the primary α (35 vol.%) cannot compensate for this drop.

After solution treatment at 700°C the values of strength rise continuously with increasing time, even at 550 (Fig. 6b) and 600°C. This can be explained by the combined hardening of the α-matrix (60 vol.%) and of the β-remainder. Aging at 350 and 450°C hardens both phases. Upon aging at 550 and 600°C one may assume that the hardening of the (β + secondary α)-regions decreases because of coarsening. However, because of a smaller volume fraction (40 vol.%) this loss is likely to be compensated by the hardening of the primary α by Ti_3Al. A moderate rise in strength (Fig. 6b) is the consequence.

BIBLIOGRAPHY

(1) Hickey, C.F., Jr.,
Effect of Microstructure and Cooling Rate on the Mechanical Properties of Ti-6Al-6V-2Sn, Journal of Materials, 1, 1966, p. 89 - 103.

(2) Quemper, F., Beauvais, C., Hocheid, B., Roux, C.,
Etude Qualitative et Quantitative de la Phase β du Ti-A6V6E2 A Differentes Temperatures, Thèse ingénieur, CNAM, Paris, 1970, p. 143 - 160.

(3) Hocheid, B., Fontalirand, C., Beauvais, C.,
Isothermal Transformations of Ti6Al6V2Sn Alloy after Preheating in the ($\alpha+\beta$) Range, Titanium, Science and Technology, Proceedings of 2nd Intl. Conf., Cambridge, Mass. 1972, p. 1609 - 1619.

(4) Gueret, G., Houssin, B., Fries, J., Cizeron, G., Lacombe, P.,
Cinétique de Durcissement de L'Alliage de Titane $TA_6V_6E_2$.
Analyse de L'Évolution Structurale au Cours du Revenu,
Journal Less Common Metals 38, 1974, p. 31 - 51.

(5) Hickey, C.F., Jr., Fopiano, P.J.,
Heat Treatment Effects on the Mechanical Properties in Ti-6Al-6V-2Sn, Journal of Testing and Evaluation JTEVA, 1, 1973, p. 166 - 169.

(6) Castro, R., Séraphin, L.,
Contribution à l'étude métallographique et structurale de l'alliage de titane TA6V, Mém. scientifiques rév. met. 63, 1966, p. 1025 - 1056.

(7) Namboodhiri,T.K.G., McMahon, C.J., Jr., Herman, H.,
Decomposition of the α-Phase in Titanium-Rich Ti-Al Alloys.
Metall. Trans., 4, 1973, p. 1323 - 1331.

(8) Crossley, F.A.,
Effects of the Ternary Additions: O, Sn, Zr, Cb, Mo and V on the $\alpha/\alpha+ Ti_3Al$ Boundary of Ti-Al Base Alloys, Met. Soc. AIME, 245, 1969, p. 1963 - 1968.

(9) Welsch, G., Lütjering, G., Gazioglu, K., Bunk, W.,
Deformation Characteristics of Age Hardened TiAl6V4, Metall. Trans. 1976 to be published.

INFLUENCE OF GRAIN SIZE ON THE DUCTILITY OF AGE-HARDENED TITANIUM ALLOYS

A. Gysler[+], G. Terlinde[++], and G. Lütjering[++]

[+]Institute for Materials Research, German Aerospace Research Establishment (DFVLR), Cologne, West-Germany

[++]Institute for Materials Science, Ruhr-University Bochum, Bochum, West-Germany

Introduction

In precipitation hardened alloys in which the moving dislocations are able to shear the particles pronounced slip bands are formed at the beginning of plastic deformation. With increasing volume fraction of precipitated particles such alloys often show a drastic reduction in macroscopic ductility. The reason for this brittle behavior is the high stress concentration at the head of dislocation pile-ups causing the fracture of grain boundaries by intersecting slip bands [1-3]. The main purpose of the present work was to investigate how a reduction in grain size and therefore a decreasing number of piled-up dislocations within the slip bands may influence the ductility of those alloys. The investigation was mainly performed on two binary Ti-alloys, namely on β-Ti-Mo and α-Ti-Al, because the details of deformation behavior and crack nucleation mechanisms are already known for these alloys [1,2].

Experimental Procedure

The β-Ti-Mo alloy investigated had a molybdenum concentration of 20 wt.-% (11 at.-%) and an oxygen content of about 0.3 %. For a variation in grain size this alloy was cold deformed and recrystallized

in the β-phase field at 950 °C and 800 °C for various times. By this treatment the average grain diameter was varied between 30 μm and 225 μm. All specimens were finally water-quenched from 800 °C to room temperature to get equal quenching conditions for the specimens prior to aging. To precipitate ω-particles all specimens were aged at 350 °C for various times. Tensile tests with a strain rate of $5 \cdot 10^{-4} s^{-1}$ were performed at room temperature on round specimens with diameters of 4 mm and gauge lengths of 20 mm.

The aluminum concentration of the α-Ti-Al alloy was 8.5 wt.-% (14.2 at.-%). The oxygen content was 0.08 %. For a variation in grain size this alloy was hot rolled in the α-phase field at 980 °C and subsequently recrystallized for various times at various temperatures between 820 °C and 950 °C. Uniform grain sizes could be achieved by these treatments with a variation in average grain diameters between 20 μm and 150 μm. All specimens were finally water-quenched from 820 °C (single α-phase field) and aged at 600 °C for 6 hours to precipitate Ti_3Al-particles. Tensile tests with a strain rate of $3.3 \cdot 10^{-4} s^{-1}$ were performed at room temperature on flat specimens with the dimensions 5 mm x 1 mm and gauge lengths of 35 mm.

The deformation structures were investigated by transmission electron microscopy using the standard thinning procedure described elsewhere [1]. The fracture surfaces were investigated by scanning electron microscopy.

Experimental Results

Ti-20 % Mo

Mechanical Properties. The variation of tensile properties of the Ti- 20 % Mo alloy is illustrated in Fig. 1 showing the true fracture strain $\varepsilon_F = \ln A_o/A_F$ for specimens with two different grain sizes of 30 μm and 225 μm as a function of aging time at 350 °C. In the as-quenched condition the ductility was quite high (ε_F = 1.3 and 0.7). With increasing aging time the ductility decresed for both grain sizes. After aging times of about 5 hours the ductility was

zero for specimens with a grain size of 225 μm and after 30 hours for specimens with a grain size of 30 μm. The dashed line in Fig.1 shows the dependence of yield stress $\sigma_{0.1}$ which is the stress after 0.1 % plastic strain as a function of aging time at 350 °C. With increasing aging time the yield stress increased. No measurable difference in yield stress could be detected for specimens with different grain sizes as long as the specimens exhibited at least 0.1 % plastic strain at fracture. For specimens showing no macroscopic ductility the fracture stresses deviated from the dashed line in Fig. 1 to lower values.

The dependence of true fracture strain ε_F on grain size L was measured on specimens having all the same aging treatment of 10 hours at 350 °C. The results are shown in Fig. 2 with the grain size plotted as L^{-1}. Specimens with grain sizes above about 100 μm fractured without macroscopic ductility. With decreasing grain size the true fracture strain increased up to about $\varepsilon_F = 0.35$ for a grain size of 30 μm. It should be noticed that this high ductility was obtained without lowering the high yield stress $\sigma_{0.1}$ of the alloy ($\sigma_{0.1}$ = 1200 MN • m^{-2}). As may be seen from Fig. 1 the true fracture strain ε_F depends linearly on L^{-1}.

Fig. 3 shows the dependence of true fracture stress σ_F on grain size L for these specimens aged at 350 °C for 10 hours. The grain size is plotted in Fig. 3 as $L^{-1/2}$. It can be seen from Fig. 3 that the true fracture stress σ_F depends linearly on $L^{-1/2}$.

The strain hardening exponent m of the true stress - true strain curves ($\sigma = \sigma_o + k \cdot \varepsilon^m$) of these specimens was measured to be about 0.5.

Deformation Structures. In a recent study [1] on the deformation behavior of age-hardened Ti-Mo alloys it was shown for the Ti-20% Mo alloy that upon deformation the dislocations were arranged in inhomogeneous distributed slip bands piling-up against grain boundaries. Close to macroscopic failure these well defined slip bands were able to fracture grain boundaries. These results were obtained on specimens with a large grain size of about 250 μm. For comparison tensile

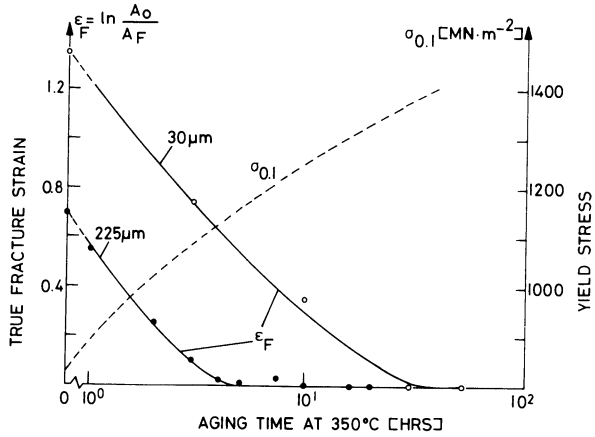

Fig. 1 - Ti-20%Mo; true fracture strain and yield stress as a function of aging time for two different grain sizes.

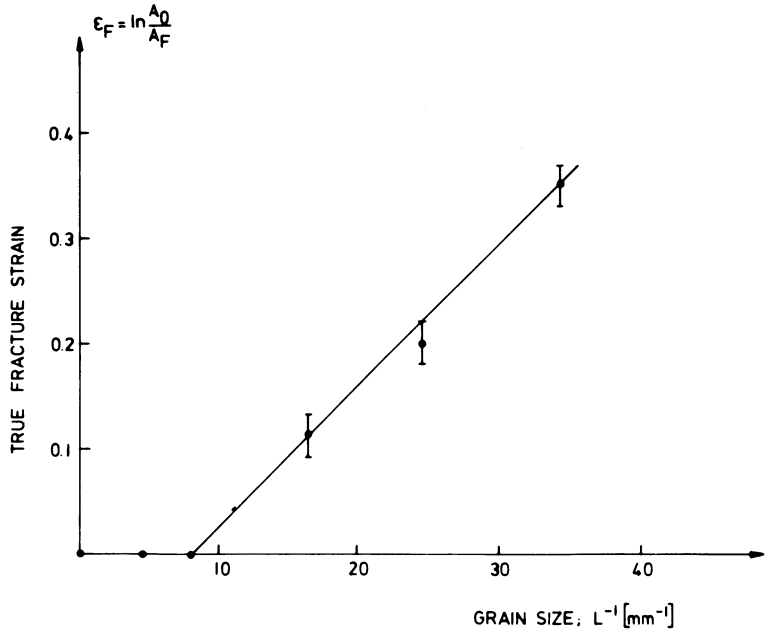

Fig. 2 - Ti-20%Mo; 10h 350°C; true fracture strain as a function of reciprocal grain size.

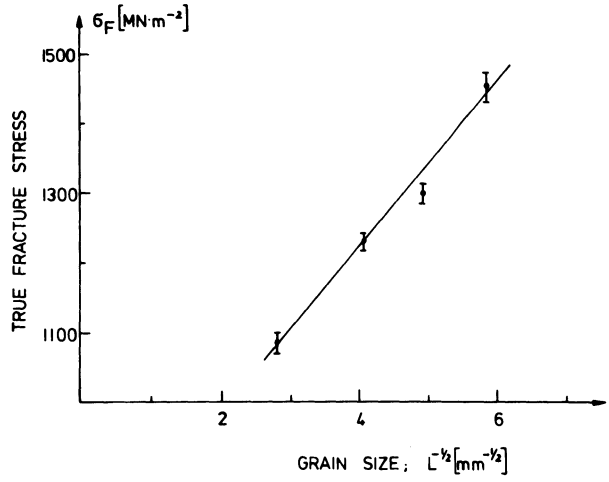

Fig. 3 - Ti-20%Mo; 10h 350°C; true fracture stress as a function of grain $L^{-1/2}$.

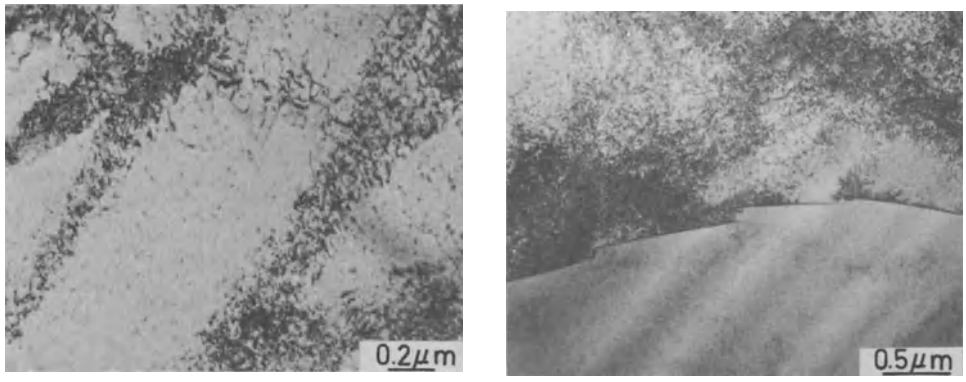

(a) (b)

Fig. 4 - Ti-20%Mo; L = 30μm; 10h 350°C; TEM; deformation structure and crack nucleation mechanism
a) 2% deformed
b) Deformed close to fracture (ε_F = 0.35).

specimens with a small grain size of 30 µm were deformed in the present study to a plastic strain of 2 % and the dislocation structure was investigated by transmission electron microscopy. Fig. 4a shows an example for a specimen aged at 350 °C for 10 hours. From the micrograph it can be seen that also for this small grain size the dislocations were arranged in well defined slip bands. Further plastic deformation close to fracture of such specimens revealed that these slip bands were finally able to fracture grain boundaries as may be seen from Fig. 4b. This crack nucleation process occured only after true plastic strains of about 0.35 as compared to nearly zero plastic deformation for specimens with a large grain size.

Fracture Surfaces. The variation of fracture surface with aging time at 350 °C is already known for the Ti-20 % Mo alloy for specimens with a large grain size of 250 µm [1]. The fracture mechanism changed from a dimple type of matrix failure over a fracture along grain boundaries to a fracture along slip bands again through the matrix. For specimens with a small grain size of 30 µm a similar variation of fracture topography was observed with increasing aging time at 350 °C. The only difference was that the transition from one fracture mechanism to the next one was delayed slightly to longer aging times for specimens with the small grain size of 30 µm. Comparing the fracture surfaces of specimens with different grain sizes all aged at 350 °C for 10 hours (Fig. 5) it can be seen that the fracture mode did not change. For all grain sizes a fracture along grain boundaries was observed, but the macroscopic failure took place after quite different amounts of plastic deformation. On a microscopic scale the intergranular fracture exhibited the features of a ductile type of failure because the flat grain surfaces were covered completely with small dimples [1]. Furthermore straight lines were visible on the flat surfaces resulting from the steps in the grain boundaries due to intersecting slip bands (Fig. 4b). On a microscopic scale no difference could be detected on the fracture surface between specimens having a large or a small grain size.

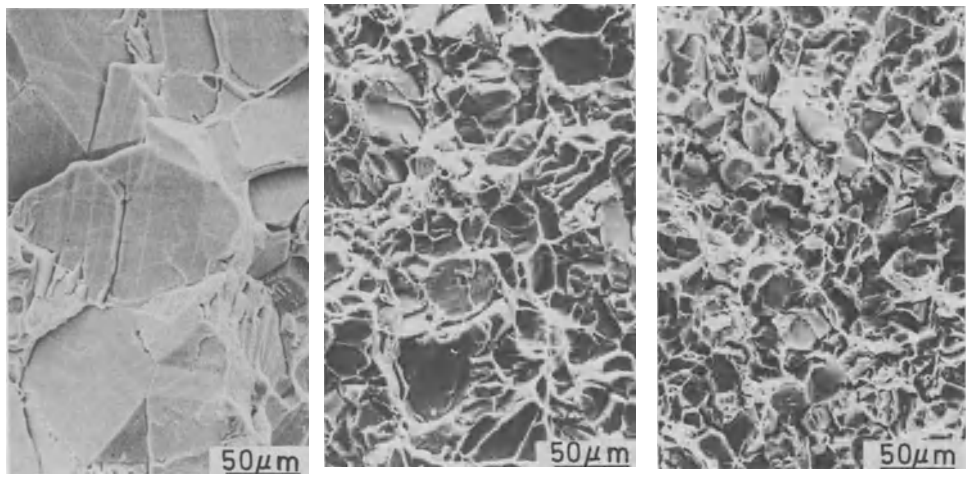

(a) (b) (c)

Fig. 5 - Ti-20%Mo; 10h 350°C; SEM; fracture topography as a function of grain size
a) L = 125μm; ε_F = 0
b) L = 60μm; ε_F = 0.12
c) L = 30μm; $\varepsilon_F = \ln \frac{A_o}{A_F}$ = 0.35

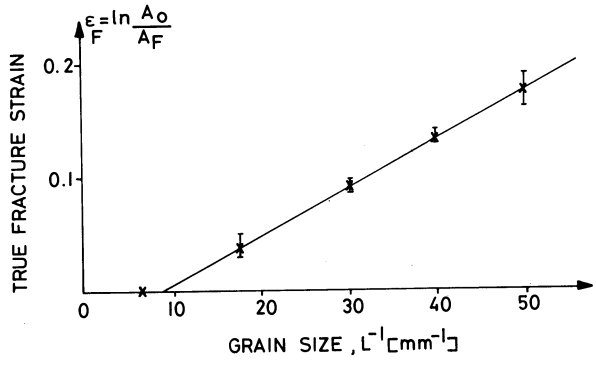

Fig. 6 - Ti-8.5%Al; 6h 600°C; true fracture strain as a function of reciprocal grain size.

Ti- 8.5 % Al

Mechanical Properties. Specimens with different grain sizes but having all the same aging treatment of 6 hours at 600 °C were deformed in tension. Fig. 6 shows the dependence of true fracture strain ε_F on the grain size plotted as L^{-1}. Specimens with the large grain size of 150 µm fractured with no measurable macroscopic ductility whereas specimens with a small grain size of 20 µm showed a high ductility, the true fracture strain ε_F being about 0.18. As may be seen from Fig. 6 a linear relationship exists between ε_F and L^{-1}. Similar to Fig. 3 the true fracture stress was approximately proportional to $L^{-1/2}$. For this alloy the yield stress $\sigma_{0.2}$ increased from 780 $MN \cdot m^{-2}$ for a large grain size to a value of 910 $MN \cdot m^{-2}$ for a small grain size of 20 µm.

Deformation Structures. The dislocation structure of deformed specimens was investigated by transmission electron microscopy. For all specimens inhomogeneous distributed slip bands piling-up against grain boundaries were observed. These slip bands were able to fracture grain boundaries in specimens deformed close to macroscopic failure. An example of this kind of crack nucleation mechanism is shown in Fig. 7. No difference in deformation structure and crack nucleation mechanism was found between specimens with different grain sizes.

Fracture Surfaces. The variation of fracture topography with grain size is demonstrated in Fig. 8. Specimens with a large grain size of 150 µm showed portions of fracture along grain boundaries as well as fracture along slip bands (Fig. 8a). For specimens with a small grain size of 20 µm the fracture path was nearly completely along grain boundaries as may be seen from Fig. 8b. At higher magnification straight lines were visible on the fracture surface resulting from the steps due to intersecting slip bands (Fig. 7).

Ti- 6 % Al- 4 % V

In a recent investigation [4] it was found that the commercial Ti- 6 % Al- 4 % V alloy could be age-hardened at temperatures of

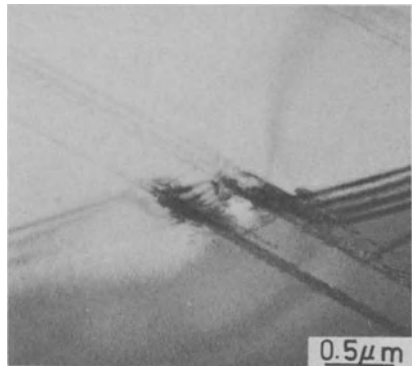

Fig. 7 - Ti-8.5%Al; 6h 600°C; TEM; grain boundary fracture by intersecting slip bands.

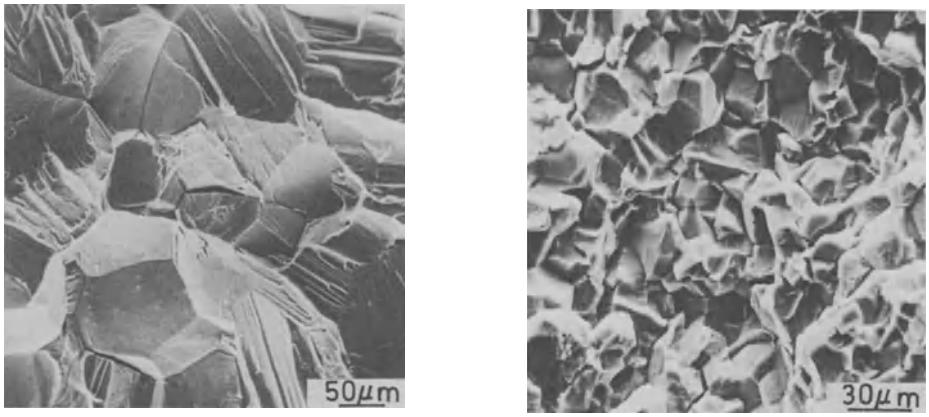

(a) (b)

Fig. 8 - Ti-8.5%Al; 6h 600°C; SEM fracture topography as a function of grain size
a) L = 150μm; ε_F = 0
b) L = 20μm ε_F = 0.18

about 500 °C. This age-hardening was due to the precipitation of Ti_3Al-particles within the α-phase. An interesting feature of the investigation was that although pronounced age-hardening occured the ductility of the alloy remained constant. Fig. 9 shows the dependence of tensile yield stress $\sigma_{0.2}$ and true fracture strain ε_F as a function of aging time at 500 °C. The alloy was quenched from 800 °C before aging at 500 °C and exhibited a globular (α+β) grain structure. It can be seen from Fig. 9 that the yield stress $\sigma_{0.2}$ increased from 800 MN • m^{-2} in the as-quenched condition to about 1000 MN • m^{-2} after aging at 500 °C. On the other side the true fracture strain ε_F remained constand at the high value of about 0.5. The globular (α+β) grain structure is shown in the electron micrograph of Fig.10a. The grain growth of the α-phase was restricted by the smaller β-grains which appear lighter in the micrograph. The size of the α-grains was quite small and ranged from 2 to 10 μm [4]. The dislocation structure within the α-grains of aged and slightly deformed specimens is shown in Fig. 10b. The dislocations were arranged in slip bands piling-up against the grain boundaries, but it was observed that they were not able to fracture the grain boundaries. The fracture surface showed a dimple type of matrix failure and was not affected by the age-hardening due to Ti_3Al-particles within the α-grains[4].

Discussion

A pronounced dependence of ductility on grain size was found for both alloy systems investigated (Figs. 2 and 6). Both alloys, Ti-20 % Mo and Ti- 8.5 % Al, exhibited particles which could be sheared by the moving dislocations leading to inhomogeneous distributed slip bands piling-up against grain boundaries and finally fracturing them (Figs. 4b and 7). This crack nucleation mechanism leads to a fracture along grain boundaries for the age-hardened conditions investigated in this study (Figs. 5 and 8). Assuming that crack nucleation by this mechanism occurs for all grain sizes at a critical local stress value σ_c^+ the experimental observed relationships can then

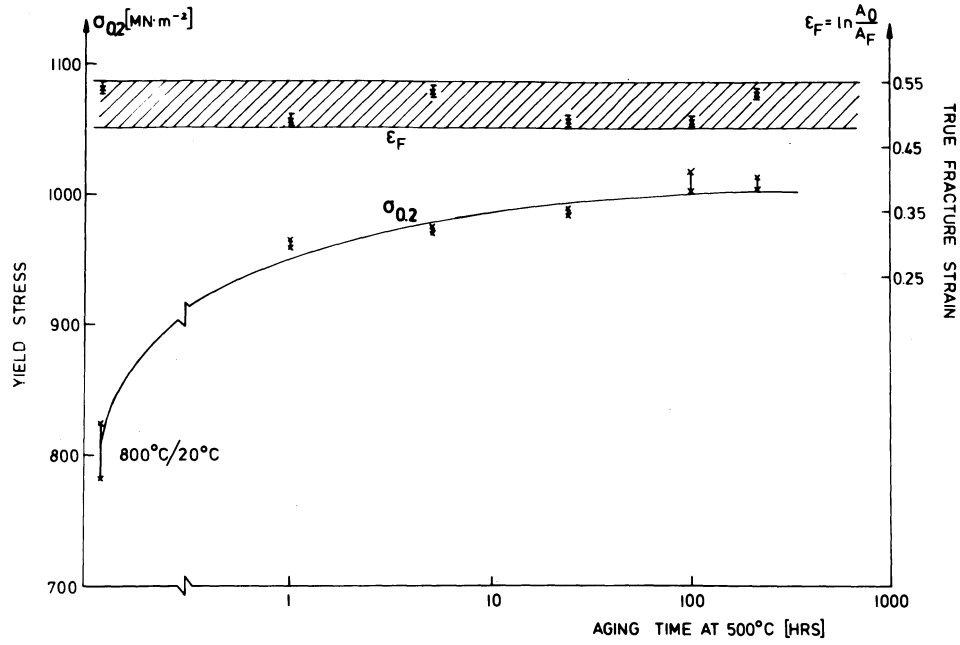

Fig. 9 - Ti-6%Al-4%V; yield stress and true fracture strain as a function of aging time at 500°C.

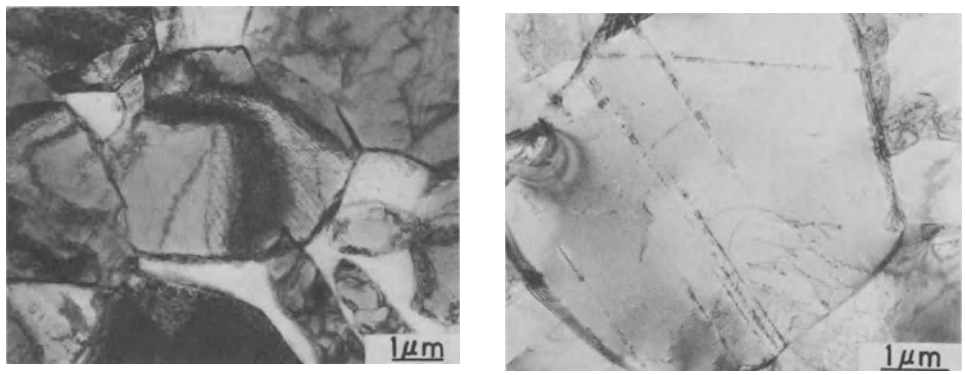

Fig. 10 - Microstructure and deformation mechanism of Ti-6%Al-4%V; TEM(4)
a) Globular (α+β) grain structure
b) Slip bands in α-grains of aged specimens after 0.2% plastic deformarion.

be explained on the following basis. The local stress σ^+ at the head of a pile-up of n dislocations against a grain boundary under an external applied stress σ_a is given by [5]:

$$\sigma^+ = n \cdot \sigma_a \qquad (1)$$

Taking the theoretical treatment by Eshelby, Frank, and Nabarro [5] the number n of dislocations in a pile-up can be expressed by the following equation:

$$n = A \cdot L \cdot \sigma_a \qquad (2)$$

where L is the pile-up length (grain size) and A is a factor depending on the type of dislocations involved. Combining both equations for the event of crack nucleation and fracture ($\sigma^+ = \sigma_c^+$ and $\sigma_a = \sigma_F$) the following dependence of true fracture stress σ_F on grain size L results:

$$\sigma_F \sim L^{-1/2} \qquad (3)$$

With the experimental observed value for the strain hardening exponent m of the true stress - true strain curves (m = o.5) the dependence of true fracture strain ε_F on grain size L yields to:

$$\varepsilon_F \sim L^{-1} \qquad (4)$$

These relationships of equations (3) and (4) were found for the two alloy systems investigated (Figs. 2, 3 and 6). Since it can be assumed that all precipitated particles are destroyed within a slip band in the moment crack nucleation occurs the friction stress which is then equal to the stress of moving a dislocation in the solid solution is very low and thus neglected in equations (1) and (2) in a first approximation.

Besides on grain size the number n of dislocations within a slip band depends strongly on the increase of yield stress due to the

precipitated particles which are then destroyed by the moving dislocations. The resulting decrease of true fracture strain with increasing aging time (increasing yield stress) was found for the Ti-20% Mo alloy (Fig. 1).

The observed high ductility of the commercial Ti- 6 % Al- 4 % V alloy in the age-hardened condition (Fig. 9) can be explained by the small α grain size of 2 to 10 µm (Fig. 10a). The local stress concentration σ^+ resulting from the slip bands (Fig. 10b) apparently did not reach the critical value σ_c^+ to fracture the grain boundaries. The fracture will then occur by a different mechanism presumably by decohesion of the α/β interfaces. This is supported by the experimental result that the true fracture strain ε_F was not depending on the age-hardening due to Ti_3Al-particles within the α-phase (Fig. 9).

The intrigant experimental result that a dependence of yield stress on grain size was found for the Ti- 8.5 % Al alloy but not for the Ti- 20 % Mo alloy is subject to further investigations.

This work was supported by the Deutsche Forschungsgemeinschaft.

BIBLIOGRAPHY

(1) Gysler A., Lütjering G., Gerold V.; "Deformation Behavior of Age-Hardened Ti-Mo Alloys"; Acta Met. 22 (1974) 901-909

(2) Lütjering G., Weissmann S.; "Mechanical Properties of Age-Hardened Titanium-Aluminum Alloys"; Acta Met. 18 (1970) 785-795

(3) Lütjering G.; "Slip Distribution and Mechanical Properties of Metallic Materials"; DLR-FB 74-70 (1974) 1-141; ESRO TT (1976)

(4) Welsch G., Lütjering G., Gazioglu K., Bunk W.; "Deformation Characteristics of Age-Hardened Ti-6Al-4V"; submitted to Met. Trans.

(5) Hirth J. P., Lothe J.; "Theory of Dislocations", Mc Graw-Hill Book Company (1968) 694-718

PROCESSING AND DEFORMATION STUDIES ON ULTRAFINE GRAINED TITANIUM

V. Ramachandran
Materials Science Division
National Aeronautical Laboratory
Bangalore 560017, India

E. P. Abrahamson, II
Materials Processing Laboratory
Department of Mechanical Engineering
Massachusetts Institute of Technology
Cambridge, Massachusetts 02139 U.S.A.

ABSTRACT

Ultrafine grain sizes in the micron range have been developed in titanium by controlled minor alloy additions and deformation processing. The deformation behavior of this material has been studied in the temperature range 77° to 973°K. The strengthening effect of grain refinement is preserved over a wide temperature range. The work hardening rate in the dynamic strain aging region is found to depend on grain size, decreasing with decrease in grain size. The tensile elongation is a minimum in the dynamic strain aging region. Just beyond this region, there is a sharp increase in the necking strain, resulting in large tensile extensions. This sharp rise in necking strain is also a function of grain size, being higher for coarser grain sizes.

INTRODUCTION

Stable ultrafine grain sizes in the micron range can be developed in alpha titanium by controlled alloy additions followed by thermomechanical processing. Considerable enhancement of mechanical strength at ambient and cryogenic temperatures has been achieved by grain refinement. The tensile deformation of alpha titanium at elevated temperatures is quite complex as strain aging occurs concurrent with deformation. This paper describes a method of producing ultrafine grain sizes in alpha titanium and a study of the effect of grain size on the mechanical behavior, especially the dynamic aspects of strain aging.

Knowledge gained from extensive investigations on the recrystallization behavior of titanium and other engineering metals as affected by small concentrations of transition metal solutes has been employed to design a series of ultrafine grained alloys (1,2). Addition of transition metal solutes such as chromium, molybdenum, tantalum, zirconium and hafnium raises the recrystallization temperature of titanium markedly (3). This effect is generally pronounced at low concentrations of the solute, in the range 0.05 to 0.2 atomic per cent. In certain systems it has been found that the rate of increase of the recrystallization temperature is linear up to a certain critical concentration beyond which the rate of change decreases, becoming negligible in some cases or even negative. Moreover, in dilute alloys, the effects of more than one solute are generally found to be additive.

Also, at these critical concentrations of the solutes, the grain growth is strongly inhibited. The important aspect in the development of ultrafine grain alloys is to restrict grain growth during processing. In alloys with such critical concentrations of solutes, the temperature and the sequence of deformation can be so chosen as to cause repetitive recrystallization during hot working, without any significant grain growth, resulting in stable ultrafine grain sizes usually in the micron range. Further refinement to submicron sizes is possible by conventional cold working and carefully chosen annealing schedules. These grain sizes are quite stable for extended periods of time at homologous temperatures up to 0.5.

The high temperature deformation of titanium is characterized by phenomena associated with dynamic strain aging (4,5). Appearance of plateaus or peaks in the flow stress-temperature diagrams, serrated stress-strain curves, low strain rate sensitivity of flow stress, minimum tensile elongation, stress transients on change of strain rate and work hardening rate maxima are some of the manifestations of dynamic strain aging (6-8). At moderate strain rates, these phenomena occur in titanium predominantly in a temperature range centered around 670°K and to a less pronounced extent near room temperature.

In the dynamic strain aging region, the work hardening rate goes through maxima which are shifted to higher temperatures with increase in strain rate. It is interesting to note that while the tensile elongation is a minimum in the dynamic strain aging region, just above this temperature range, the total tensile elongation, of which the necking strain is the major component, rises rapidly to high values, well above 100%. This sudden rise in elongation is related to the strain rate dependent work hardening rate maxima.

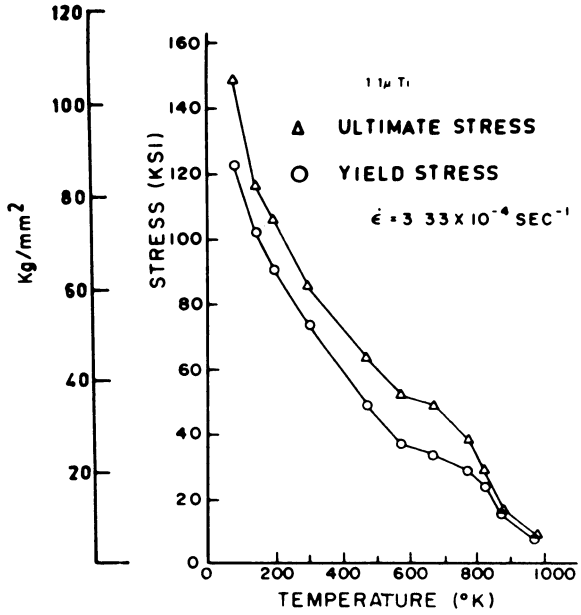

Fig. 1 - Temperature dependence of the yield and ultimate stress of 1μm titanium.

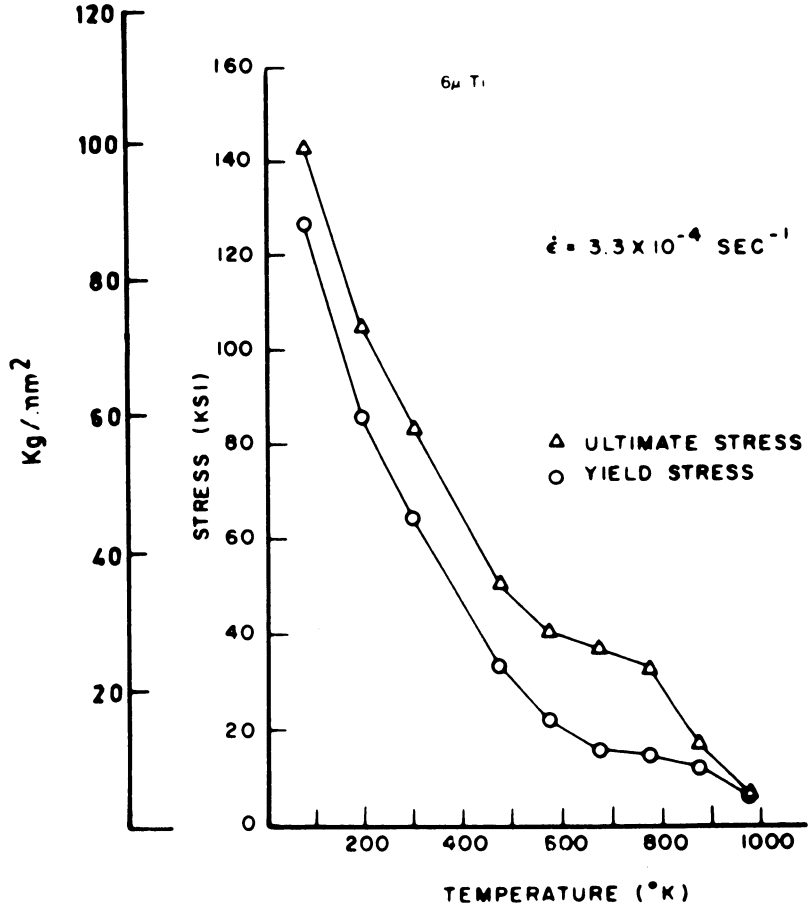

Fig. 2 - Temperature dependence of the yield and ultimate stress of 6μm titanium.

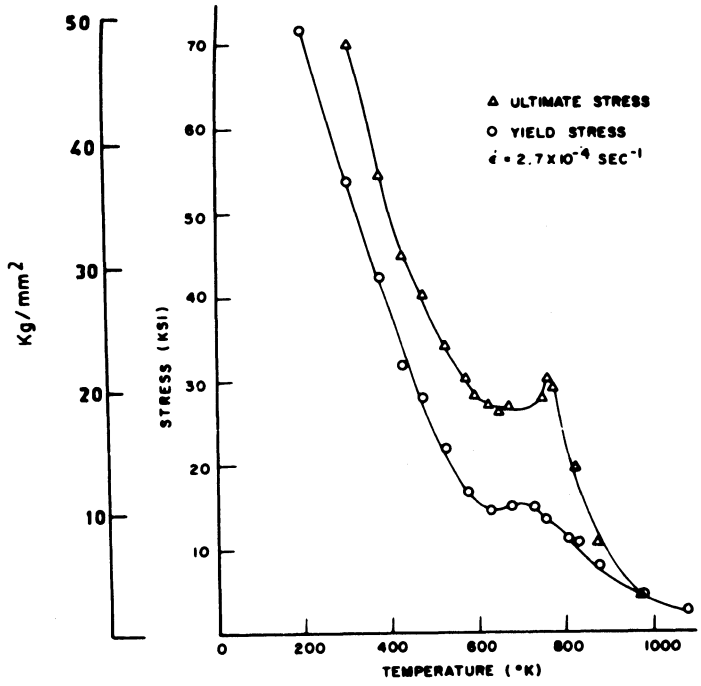

Fig. 3 - Temperature dependence of the yield and ultimate stress of commercial titanium of 16μm grain size (from Santhanam[12]).

It has been well documented that in metals exhibiting dynamic strain aging, dislocation multiplication per unit strain is greater in the dynamic strain aging region than outside this range (9-11). Moreover, the dislocation density developed in fine grained metal is greater than in coarser grains. As work hardening is related to dislocation multiplication, the influence of ultra-fine grain size on dynamic strain aging in titanium, especially the work hardening rate was investigated. In this paper, the behavior of a dilute alpha titanium alloy of two grain sizes, namely, 6μm and 1μm is presented.

EXPERIMENTAL

The titanium alloy used in the present investigation has the composition 0.15% Cr, 0.06% Mo, 0.026% Ta and 2.5% Hf, all in weight per cent. The alloy was arc melted in an argon atmosphere, homogenized by multiple melting and cast in the form of 1/2 Kg blocks, approximately 50 mm cube. The blocks were forged at 760°C and drawn to 18-20 mm round bars. The bars were cold swaged to 10 mm diameter rods. Tensile specimens were machined from these rods, with a gage length of 25 mm (1 inch) and gage diameter of 6.4 mm (0.252 inch). Annealing for 1 hour at 870°C resulted in a grain size of 6μm. The lowest temperature for recrystallization in 1 hour was 600°C and this anneal produced a grain size of 1μm. The grain sizes reported are mean linear intercepts measured from optical and transmission electron micrographs. Tensile tests were conducted at various temperatures from 77° to 973°K, with gettered argon atmosphere for the high temperature tests.

RESULTS AND DISCUSSION

Tensile Behavior. At room temperature and below, ultrafine grained titanium deforms with an upper yield point, yield drop and Luders strain, followed by work hardening. The Luders strain increases with decrease in grain size and temperature; however, the extent of Luders strain is small. The Luders strain in 1μm grain size titanium at room temperature is 1.6% and at 77°K it is still only 1.8%.

The variation of the ultimate and yield stress of the 1μm and 6μm material with temperature is shown in Fig. 1 and 2. Similar data from the work of Santhanam(12) for commercial titanium of 16 μm grain size are shown in Fig. 3 for a comparable strain rate. The room temperature yield strength of 1μm grain size titanium is 51 Kg/mm^2 which is about 50% higher than that of commercial titanium of grain size 16 μm. Even at 670°K, 1μm titanium has a yield strength of 24 Kg/mm^2 which is twice that of commercial titanium at that temperature. At various temperatures, the difference between the yield stress and the ultimate stress is smaller

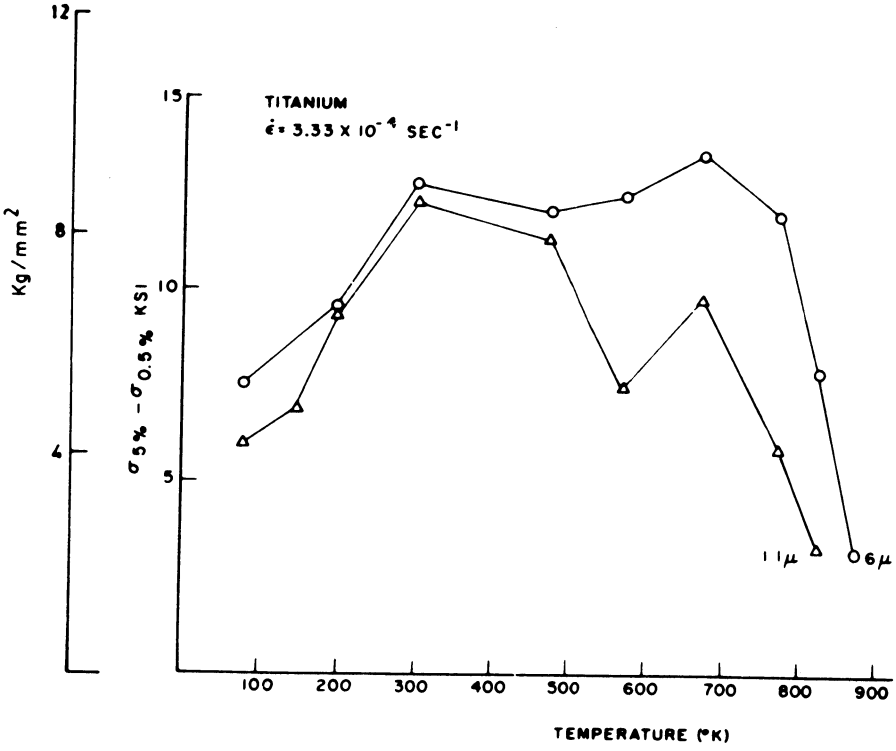

Fig. 4 - Variation of the work hardening rate of 1μm and 6μm titanium with temperature.

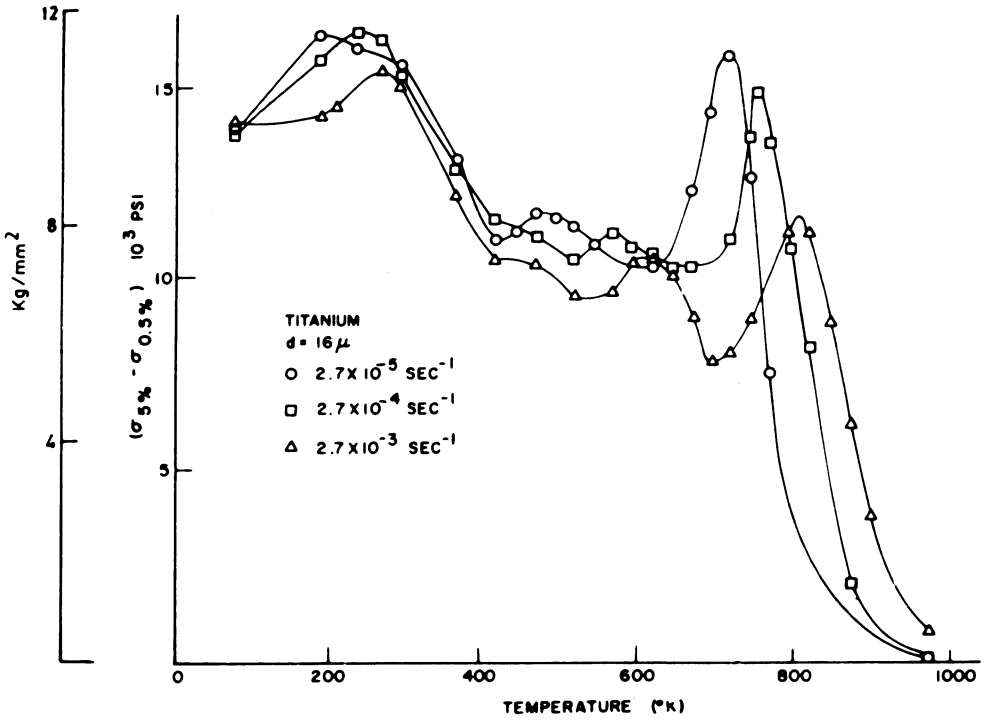

Fig. 5 - Variation of the work hardening rate of 16μm commercial titanium with temperature (from Santhanam and Reed-Hill[13]).

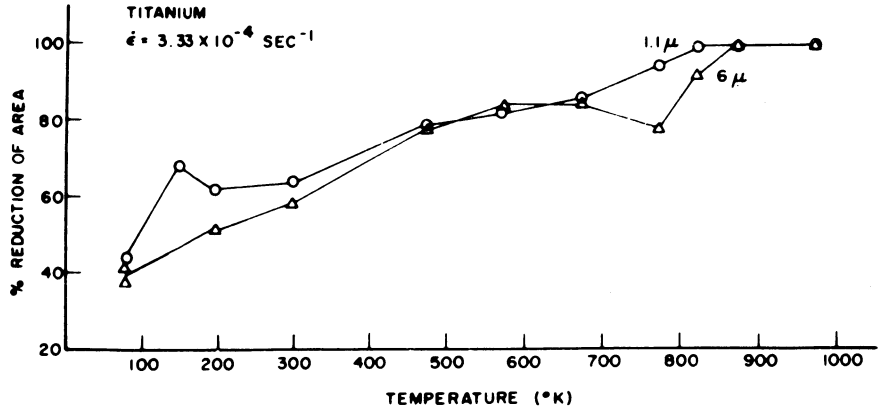

Fig. 6 - Percentage reduction in area of 1μm and 6μm titanium versus temperature.

in the finer grain size. This implies that the work hardening is also smaller in the finer grain size.

Work Hardening. The variation of the work hardening rate with temperature is shown in Fig. 4 and 1μm and 6μm grain sizes. The parameter employed to represent the work hardening rate is the flow stress difference between two strain intervals, namely 0.5% and 5%. This flow stress difference represents an average work hardening rate. In the fine grained titanium at low temperatures, the 0.5% strain level falls within the Luders strain. In such cases, the flow stress was estimated by extrapolation of the stress-strain curve back to the 0.5% offset line. In order to find whether the extrapolation could lead to serious errors, the flow stress difference for other strain intervals, such as 2.5% to 5%, which were well within the uniform strain range for all temperatures was plotted. The shape of the curves was quite similar to those shown in Fig. 4, indicating that the variation of the average work hardening rate represented in this manner is not affected by the choice of the strain interval. Similar data for commercial titanium of 16 μm grain size taken from the work of Santhanam and Reed-Hill (13) are shown in Fig. 5. Around room temperature and 670°K, prominent peaks are seen in the average work hardening rate. The peaks are found to shift to higher temperatures with increase in strain rate. The decrease in the work hardening rate below room temperature may be related to twinning which was found to occur in specimens of all grain sizes. The height of the work hardening rate peak in the upper dynamic strain aging region is found to depend on grain size. The coarsest grain size appears to have the highest work hardening rate at all temperatures.

Reduction in Area. The reduction in area of titanium is plotted against temperature in Fig. 6 for the two grain sizes. A steady increase in reduction in area can be seen with increase in temperature. Though dynamic strain aging is known to promote early necking in tensile tests leading to minimum elongation, the large reduction in area in the upper dynamic strain aging region implies that the failure of the material is by the ductile mode.

Elongation. Fig. 7 and 8 indicate the variation of the tensile elongation with temperature for the 1μm and 6μm grain size respectively. The extent of uniform strain and necking strain is also indicated in the same figures. The tensile elongation in titanium has a pronounced minimum in the dynamic strain aging region, similar to zirconium (6,13). Just above this region, there is a rapid increase in the tensile elongation, contributed mostly by the necking strain. This rapid increase in the necking strain has been rationalized in terms of the strain rate dependent

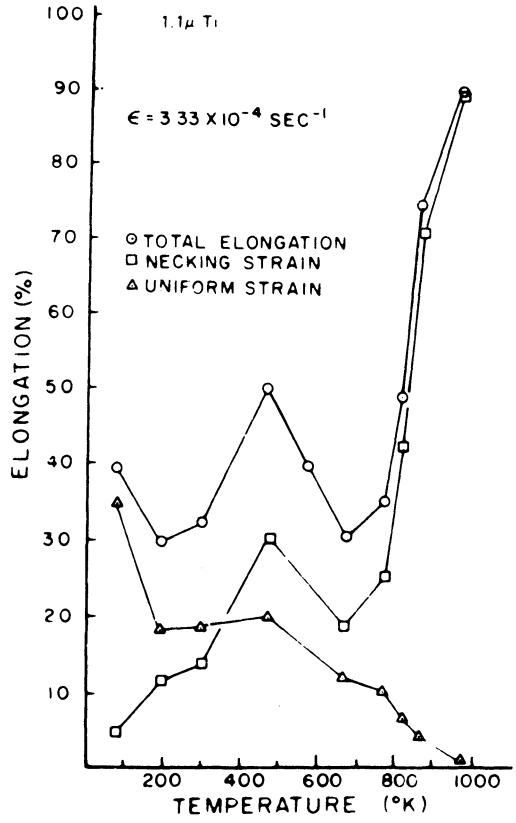

Fig. 7 - Variation of the tensile elongation of 1μm titanium with temperature.

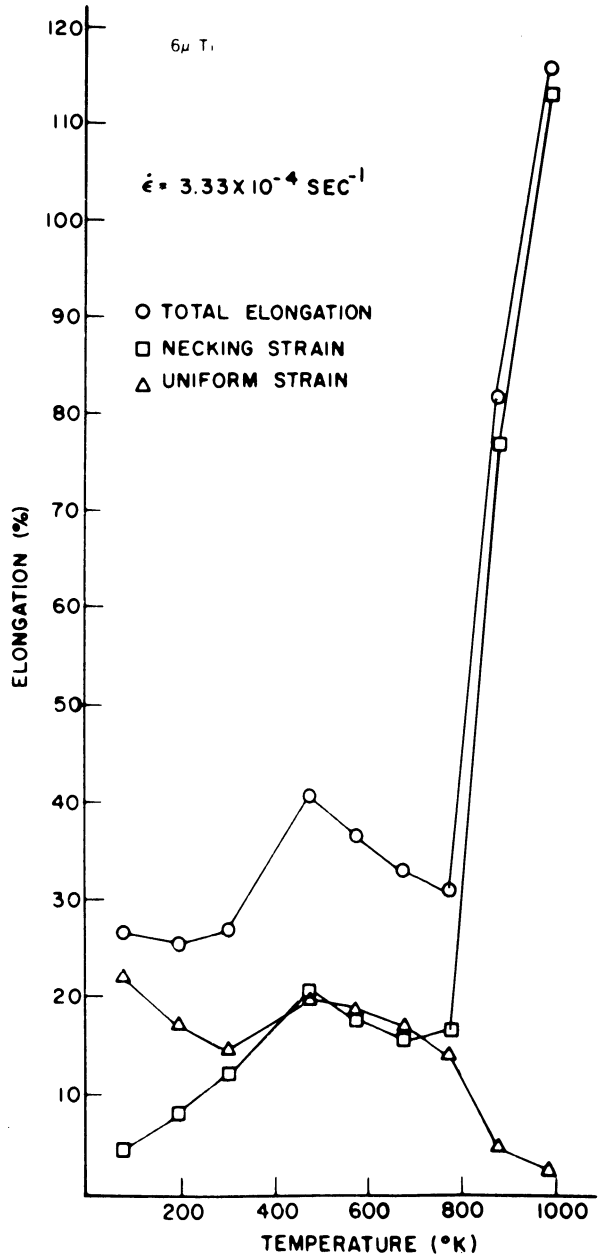

Fig. 8 - Variation of the tensile elongation of 6μm titanium with temperature.

work hardening rate maximum (13) and can be understood by reference to Fig. 5. When a neck starts in a tensile specimen, the effective gage length becomes smaller and hence there is an enhanced strain rate localized in the necked region. Consider deformation at a strain rate of the order of 10^{-4} sec^{-1} just above 800°K. In such a test, when a neck starts for the first time, the increase in the effective strain rate in the necked region corresponds to a higher work hardening rate in that region. This implies that the necked region should resist further deformation. As the deformation continues, necking should start elsewhere in the gage section and the phenomenon should repeat. This results in a diffused neck with a large necking strain as against a sharp neck in the dynamic strain aging region.

The extent of necking strain thus depends on the resistance to continued deformation of the necked region and hence on the effective work hardening rate. In the present study, the work hardening rate is found to be a function of grain size. As seen in Fig. 4 and 5, the finest grain size of 1μm has the smallest work hardening rate peak, compared to coarser grain sizes. This difference should also reflect on the necking strain and total elongation obtained for the various grain sizes. While for the 1μm grain size the total elongation is 90%, the 6μm material has an elongation of 116%. In commercial titanium of 16 μm grain size, which has the largest work hardening rate peak, elongations of the order of 125% have been recorded.

ACKNOWLEDGMENT

This work was carried out while one of the authors (V.R.) held a National Research Council Resident Research Associateship at the U. S. Army Materials and Mechanics Research Center, Watertown, Massachusetts. Support of these organizations is gratefully acknowledged. The authors are thankful to Mr. J. D. Colgate for his assistance in experimental work.

REFERENCES

1. Abrahamson, II, E. P., "Ultrafine Grain Metals", Burke, J. J. and Weiss, V., ed., Syracuse University Press, Syracuse, 1970, 71.

2. Abrahamson, II, E. P. and Ramachandran, V., Fourth Bolton Landing Conference, Bolton Landing, 1974.

3. Abrahamson, II, E. P., Trans. TMS-AIME, 224, 1962, 265.

4. Monteiro, S. N., Santhanam, A. T. and Reed-Hill, R. E., "The Science, Technology and Application of Titanium", Jaffee, R. and Promisel, N., ed., Pergamon Press, Oxford and New York, 1970, 503.

5. Garde, A. M., Santhanam, A. T. and Reed-Hill, R. E., Acta Met., 20, 1972, 215.

6. Ramchandran, V. and Reed-Hill, R. E., Metall. Trans., 1, 1970, 2105.

7. Santhanam, A. T., Ramachandran, V. and Reed-Hill, R. E., Metall. Trans., 1, 1970, 2593.

8. Santhanam, A. T. and Reed-Hill, R. E., Scripta Met., 4, 1970, 529.

9. Edington, J. W. and Smallman, R. E., Acta Met., 1, 1964, 1313.

10. Dingley, D. J. and McLean, D., Acta Met., 15, 1967, 885.

11. Keh, A. S., Nakada, Y. and Leslie, W. C., "Dislocation Dynamics", Rosenfield, A. F. et al., ed., McGraw Hill, New York, 1968, 381.

12. Santhanam, A. T., Ph.D. Dissertation, University of Florida, Gainesville, 1971.

13. Santhanam, A. T. and Reed-Hill, R. E., Metall. Trans., 2, 1971, 2619.

EFFECTS OF TEXTURE ON DEEP DRAWABILITY OF COMMERCIALLY PURE TITANIUM SHEET

A. Hasegawa, T. Nishimure and M. Fukuda

Kobe Steet, Ltd. Kobe, Japan

Introduction

The anisotropic properties of hexagonal close-packed titanium sheets have been utilized effectively for the application such as a pressure vessel under the biaxial stress condition. In general, the deformation mode of the deep drawing for sheet metals is regarded as that under the biaxial stress condition and therefore, such a normal anisotropy is considered to influence largely the deep drawability of titanium sheets. As the anisotropy in titanium sheets is based mainly on the texture, its deep drawability is considered to be improved by the texture control.

In this work, effects of the texture on the r-value(plastic strain ratio) and the deep drawing behavior were studied and further, a method for calculating the r-value directly from the pole figure was discussed.

Material and Test Procedure

1. Material

The used material is a commercially pure JIS Class 2 titanium slab with a thickness of 100mm. The chemical analysis of this material is given in Table 1.

The five kinds of 1mm thickness specimens with different textures were prepared by the rolling processes as shown in Fig. 1. Their

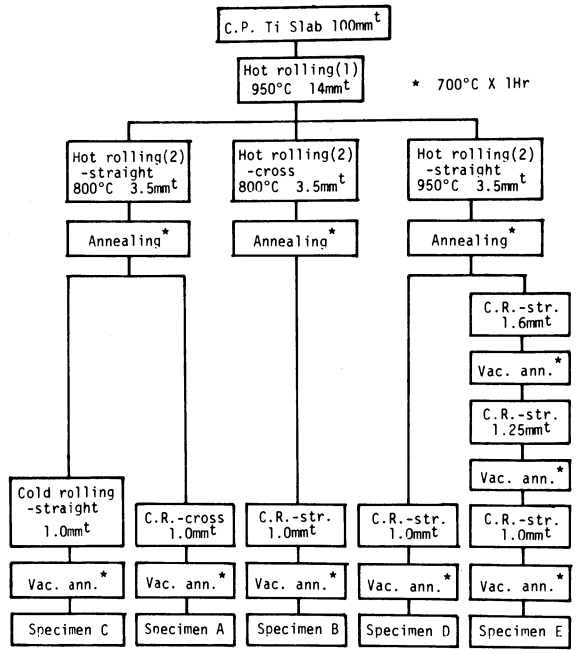

Fig. 1 - Rolling procedure for preparation of test specimens.

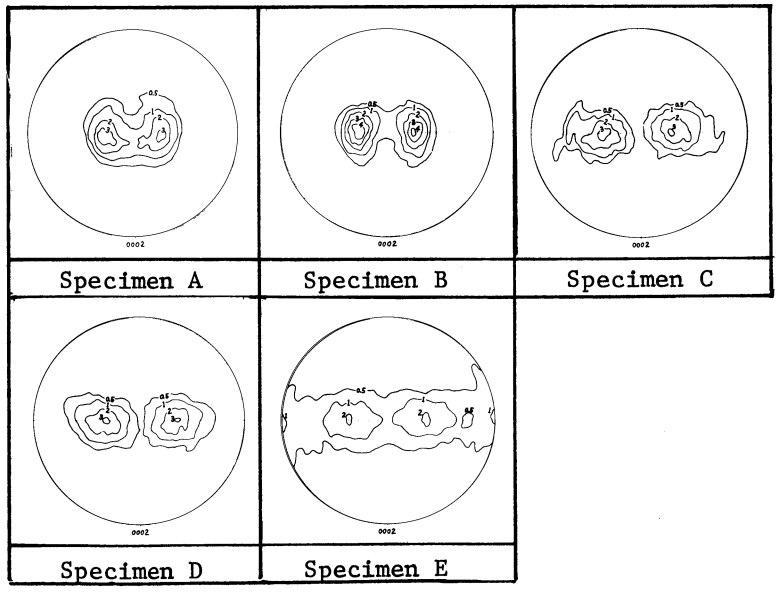

Fig. 2 - Basal pole figures of five test specimens.

microstructures were equiaxed alpha structures with an average grain diameter of 35 to 55μm.

Table 1 Chemical Analysis (weight%)

O	H	N	Fe
0.088	0.00648	0.0078	0.0056

2. Measurement of r-value and Estimation of Deep Drawability

The r-values were determined by the measurement of the tensile and the width strains after 10% plastic tensile elongations on the assumption of the volume constancy.

The deep drawability of specimens was estimated by the single blank loading test, as known as T.Z.P. method. This method is based on the conception that the deep drawing limit is determined by the relative magnitude of the maximum drawing force to the breaking strength of the cup wall. According to this method, the limit drawing ratio(L.D.R.) is described as following equation.

$$L.D.R. = Pf\ (\alpha - 1)\ /\ Pd + 1$$

Pf : breaking strength of cup wall

Pd : maximum drawing force

α : drawing ratio

3. Texture Determination

Specimens for X-ray tests were taken from the cold rolled and annealed sheets. All the specimens were polished to observe the texture at the mid-plane. The reflection pole figures were determined with CuKα radiation using the Schulz technique and the transmission with MoKα using the Decker technique.

Result

1. Pole Figures

The (0002) pole figures for five specimens are shown in Fig.2 and the histograms of the basal plane intensities are also shown in Fig.3.

It is apparent in Fig.2 that there is so much difference between the textures of these specimens as to the following points.

1. the position of the basal pole at the maximum intensity
2. the intensity distribution near the sheet normal direction (ND)
3. the degree of the pole spreading toward the transverse direction(TD)

For the specimen A, the basal pole at the maximum intensity appears at about 30 degrees from the ND toward the TD, but its pole is broadening toward the ND and the intensities around the ND are rather strong comparing with other specimens. The specimen B showed the texture nearly similar to the specimen A, but the intensities around the ND are rather weaker than those of the specimen A. For the specimen C and D, the basal poles concentrated at 35-40 degrees from the ND and they seem to spread toward the TD. However, the components near the ND appeared to be almost zero. The specimen E showed a great difference from other four specimens. It is very characteristic that the basal pole distributes in all the α ranges from the ND to the TD. Although the peaks of the basal pole appear at two angle positions of 40 and 90 degrees from the ND, their intensities are relatively weak.

2. The r-values and Mechanical Properties

The r-values and the mechanical properties of these specimens are shown in Table 2 and Fig.3.

The average r-values($\bar{r} = (r_0 + 2r_{45} + r_{90}) / 4$) of all specimens varied from 6.56 to 1.50. They decreased in the order of the specimen A,B,C,D and E. It is interesting that the r-value changes for three tensile directions take place together with a large directionality as shown in Fig.4. These behaviors of the r-value that seem to be based on the texture are different from those on the grain size. Because, in the latter case, the r-value change occurs significantly in the TD especially with small variations in the RD. As the basal pole at the maximum peak inclines more largely from the ND and its pole distribution is broadening toward the TD, the r-value tends to

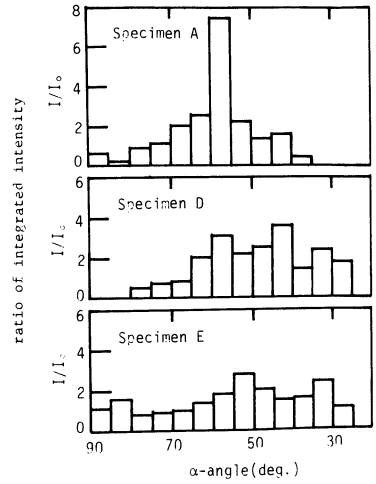

Fig. 3 - Histograms of reflection intensity from basal plane.

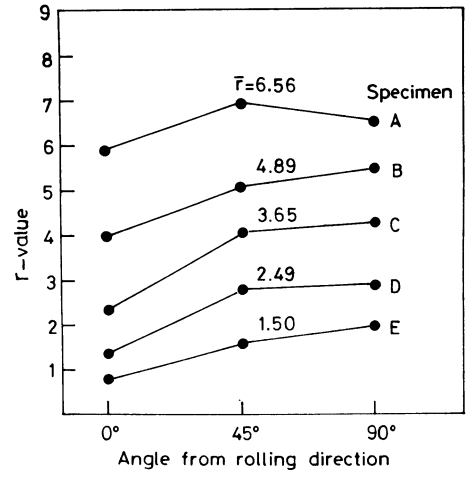

Fig. 4 - The r-values of five test specimens.

decrease. However, even if the intensities of the basal pole near the ND grow weaker, the r-value does not always decrease.

For the yield and tensile strength, they seem to have a tendency to decrease in the order of the specimen E,D,C,B and A contrary to the order of the r-value. As for the directionality of the yield strength, it tends to decrease with an increase of the r-value. These behaviors are considered to be explained from the texture similarly to the r-value.

3. Deep Drawability

The results of the conical cup test(C.C.V.) and the deep drawing test(L.D.R.) are shown in Fig.5. It indicates the influence of the r-value on the deep drawability.

For the C.C.V. test, the specimen E having 1.50 of the r-value indicated the most poor drawability(C.C.V. = 47.2). With increasing of the r-value, the C.C.V.decreases gradually and for the specimens A and B ($\bar{r} \geqq 4.89$), the drawabilities are so good as to be performed without any breaking.

For the L.D.R. test, the specimen E with the most poor drawability showed 2.42 of the L.D.R. With an increase of the r-value, the L.D.R. increased gradually(for the specimen D and C, 2.60 and 2.62, respectively) and the specimen A showed the highest value(2.82) of all the specimens.

Thus, it is obvious that the deep drawability for pure titanium sheets is improved with an increase of the r-value. It is also confirmed that the deep drawability of pure titanium sheets can be estimated properly from the r-value.

However, while the r-value is a property of the strain mode under the uniaxial tension, the deep drawability exhibits that which mean the forming limit under the biaxial stress. And so, there are some questions about what relations between the r-value and the deformation force in the forming process. With respect to this point, it is necessary to examine an effect of the r-value on the maximum drawing force and the breaking strength of the cup wall.

Further, in order to control the drawability, we should understand the effect of the texture on the r-value in detail.

Discussion

1. Maximum Drawing Force and Breaking Strength of Cup Wall

The L.D.R. method is based on the concept that the drawing limit is determined by the relative magnitude of the maximum drawing force to the breaking strength of the cup wall. In Fig.6, the behavior of these two values are shown in relation to the r-value. They are nor-

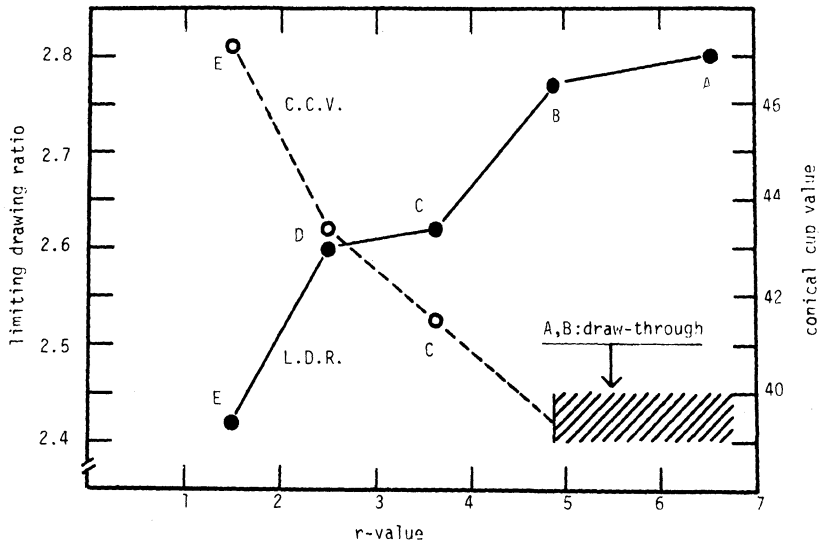

Fig. 5 - Effects of r-value on limit drawing ratio and conical cup value.

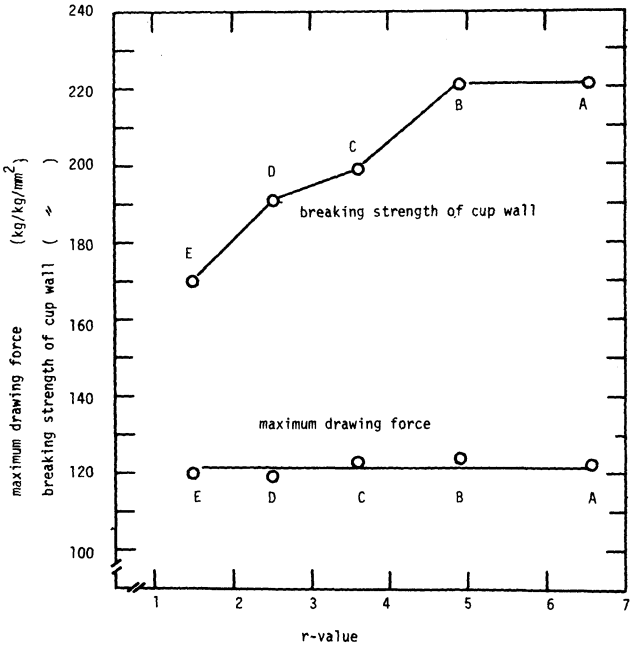

Fig. 6 - Effects of r-value on maximum drawing force and breaking strength of cup wall.

Table 2 The r-values and Mechanical Properties

Specimen No	Direction (deg.)	Y.stress (kg/mm^2)	U.T.S. (kg/mm^2)	Total elong. (%)	r-value	Average r-value
A	0	26.3	36.7	38.5	5.89	6.56
	45	26.8	35.3	38.4	6.92	
	90	27.6	35.1	40.5	6.54	
B	0	25.8	37.0	39.6	3.95	4.89
	45	27.4	35.4	38.1	5.08	
	90	29.0	35.4	35.1	5.44	
C	0	26.1	37.9	37.0	2.32	3.65
	45	28.6	36.6	35.0	4.03	
	90	31.2	37.6	31.1	4.23	
D	0	26.8	40.1	36.1	1.37	2.49
	45	29.5	37.6	34.1	2.84	
	90	33.4	40.0	33.2	2.92	
E	0	28.2	41.0	31.1	0.81	1.50
	45	30.4	39.2	32.7	1.61	
	90	33.7	41.0	33.8	1.98	

malized to the average tensile strength $\overline{\sigma}_b$ ($\overline{\sigma}_b = (\sigma_{b0} + 2\sigma_{b45} + \sigma_{b90}) / 4$).

It is shown in Fig.6 that the breaking strength increases remarkably with an increase of the r-value, though the maximum drawing force is nearly constnt independently of the r-value. It means apparently that the increase of the drawing limit is mainly caused by the breaking strength, but not by the maximum drawing force. These behaviors are well understood when considering them in relation to a yield locus under the plane stress condition. According to the yield locus, increasing the r-value increases yield strength in the plane strain remarkably and decrease the resistance to flow in the drawing deformation. As for the deformation mode in the deep drawing process, the deformation in the cup wall can be categorized as the plane strain, for any changes in the circumferencial strain are restricted. And also, the deformation in the flange part of the cup profile is classified as the drawing deformation, namely that in the 4th quadrant of the yield locus. It is generally considered that an improvement

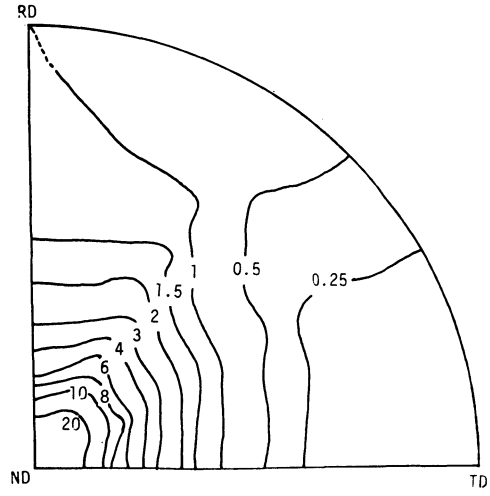

Fig. 7 - Equi-r-value net for RD tension calculated from eq (3).

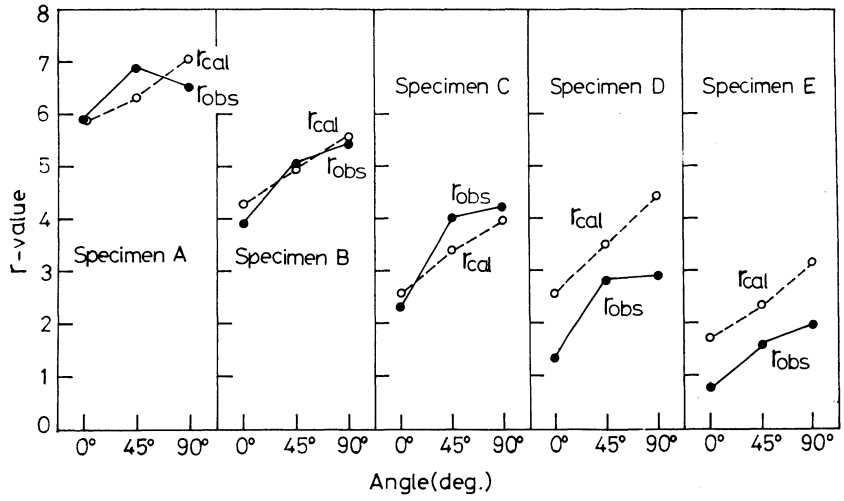

Fig. 8 - Results of r-value calculated from eq (4).

in the deep drawability with the increasing r-value is caused by the decrease of the resistance to flow in the drawing deformation, i.e., flange-softening. However, the results showed that the increase of the limit drawing ratio for titanium sheets is due to the strengthening of the cup wall under the plane strain, but not to the flange-

softening. Such a strengthening under the plane strain with the r-value is considered to be caused by the relatively higher r-value of the titanium sheets comparing with the other metals. The texture-hardening for titanium alloys in pressure vessels can be also explained by such a strengthening in the biaxial tension.

Therefore, it is considered that the drawing behaviors for commercially pure titanium sheets are identical with an extension of the yield locus in the 1st quadrant with an increase of the r-value.

2. Effect of Texture on r-value

In order to understand an effect of the texture on the r-value well, we made a try to calculate the r-value directly from the pole figure with reference to the method of Kato et al.(1).

The main points of the calculating method are as follows.

It is assumed that when the external force is applied to a grain, the active slip systems are limited to that with the Schmid factor (M) more than a critical value (Mc) and that the amounts of the strain by the slip deformation on that slip systems are proportional to the magnitude of the Schmid factor. Then, the strain, $d\varepsilon_l$, $d\varepsilon_w$ and $d\varepsilon_t$, in the tensile, width and thickness direction respectively is represented as the following equations.

$$\begin{aligned} d\varepsilon_l &= K \cdot M_{nl} \quad (M_{nl} - M_c) \\ d\varepsilon_w &= K \cdot M_{nw} \quad (M_{nl} - M_c) \\ d\varepsilon_t &= K \cdot M_{nt} \quad (M_{nl} - M_c) \end{aligned} \qquad \text{eq (2)}$$

where, Mnl, Mnw and Mnt is the Schmid factor on the nth slip system for the tensile, width and thickness direction respectively. K is the constant value. If the macro strain is equal to the summation of these strain for all the possible slip systems, the r-value of some grain with some crystallographic orientation (r') is given as the equation (3).

$$r' = \frac{\sum^{n} d\varepsilon_w}{\sum^{n} d\varepsilon_t} = \frac{\sum^{n} M_{nw} (M_{nl} - M_c)}{\sum^{n} M_{nt} (M_{nl} - M_c)} \qquad \text{eq (3)}$$

Therefore, the r-value of the practical specimen is obtained by integrating r' for all the orientation. Namely,

$$r = \frac{\sum_{\alpha\beta}^{n} [\Sigma M_{nw} (M_{ne} - M_c)] \cdot PD(\alpha,\beta)}{\sum_{\alpha\beta}^{n} [\Sigma M_{nt} (M_{ne} - M_c)] \cdot PD(\alpha,\beta)} \qquad \text{eq (4)}$$

where, $PD(\alpha,\beta)$ is the pole density at α and β angle in the (0002) pole figure.

Further, when applying this method to the titanium, three prismatic slip systems for $(\bar{1}010)\langle\bar{1}2\bar{1}0\rangle$, $(0\bar{1}10)\langle\bar{2}110\rangle$ and $(\bar{1}100)\langle\bar{1}\bar{1}20\rangle$ are selected.

From the eq(3), it is possible to construct the equi-r-value net as shown in Fig.7, which indicates that at zero of Mc for the RD tension. For the TD tension, it is opposite to Fig.7 and for the middle direction between the RD and the TD, it is rather different from that of RD tension (which is not shown). In Fig.7, the zone with the higher r-value spreads toward the RD from the ND, comparing with the TD. This means that the titanium sheet having maximum intensity on the TD in the (0002) pole figure shows the directionality with higher r-value in the TD than RD. And it is apparent from the net that in the polycrystalline titanium sheet, as the angle position at the maximum intensity goes near the ND and the distribution around its position spreads toward the ND, overall r-values increase. Therefore, as the integrated reflection intensities from the crystallographic plane such as $(10\bar{1}4)$, $(10\bar{1}3)$, $(10\bar{1}2)$, $(11\bar{2}4)$ and (0001), which lie in the zone with the r-value more than 1, grow stronger relatively, the r-value increases. On the contrary, the other components in the zone of $r<1$ will have large effects to decrease it.

In practical polycrystalline sheets, the r-value reflects the type and level of the texture. The calculated results from eq(4) for five specimens are shown in Fig.8. The calculated value, r-cal, with zero of Mc exhibits relatively a good agreement with the observed value, r-obs, especially in the cases of the specimen A, B and C, as for the directionality and level of its value. Although, for the specimen D and E, the directionality is obviously corresponding to the observed data, the difference of the level between both data seem to be rather

large. Particularly, for the specimen E, the components of the low α angle near the TD appears to be underestimated. The disagreement between both data is considered to be caused by following problems.

1. Limitation of the deformation mode
   Only prismatic slip systems are selected and twin modes are neglected.
2. Restricted conditions for the grain deformation
   Such a condition as strain continuity is neglected.
3. Accuracy for determining the pole figure
4. Development of the deformation texture is neglected.

Conclusion

In this work, we discussed about the effect of the texture on the r-value and the deep drawability for the commercially pure titanium sheets and further, about the method for the direct calculation of the r-value from the pole figure. These results are as follows.

1. The deep drawability for commercially pure titanium sheets is improved with an increase of the r-value. The improvement of its drawability is due to the strengthening of the cup wall, but not to the flange-softening.
2. The correlation between the directionality and level of the r-value and the texture can be qualitatively explained by the method based on the Schmid factor for the prismatic slip systems and the pole figure.
3. As the orientation components such as $(10\bar{1}4)$, $(10\bar{1}3)$, $(10\bar{1}2)$, $(11\bar{2}4)$ and (0001), which lie in the zone with the r-value more than 1, grow stronger relatively, they have an effect to increase the r-value and therefore, bring to improve the deep drawability of titanium sheets.

Bibliography

1. H.Kato, H.Takechi and S.Nagashima
   The Plastic Anisotropy of Polycrystalline Ferritic and Austenitic Steel Sheets Having Textures, "J. Japan Society for Technology of Plasticity," vol.7, no.60 (1966) 13-19

INFLUENCE OF PROCESSING AND HEAT TREATMENT ON THE ANISOTROPIC PROPERTIES OF SHEET AND STRIP OF COMMERCIALLY PURE TITANIUM

W. Knorr and J. Budde

Federal Republic of Germany

1. INTRODUCTION

In recent years titanium has been gaining increasing importance in the fabrication of welded tubes for heat exchangers used in power stations, desalination plants and in ships as well as for plate heat exchangers employed in a variety of applications. The choice of material for all these applications is determined by the liquid to be cooled and by the coolant.

2. Grades

The material primarily employed for the above mentioned applications are low-strength titanium grades such as the DIN materials 3.7025 and 3.7035 corresponding to ASTM B 338, grades 1 and 2, which to some extent are also supplied with small additions of palladium. For other applications c.p. titanium grades of higher strength are being manufactured to a lesser extent in the same way.

The demands imposed on the mechanical and technological properties of titanium sheet govern the choice of titanium sponge and restrict the amount of mill scrap in the charge. When exacting demands are placed on cold workability, titanium sponge containing little oxygen and iron is used to give a remelt hardness of 105 ± 5 (BHN 30). For reasons of economy, limited amounts of mill scrap, however, must also be used with these grades. Titanium sponge from the USSR is particularly suitable for making these mild titanium qualities. In the manufacture of titanium grades of higher strength, the remelt hardness may vary more widely to meet the requirements of the standard specifications.

3. Technological Properties

The characteristics of cp titanium determined by tensile testing for the purpose of inspection and evaluation are not sufficient to indicate whether the material is suitable for higher degrees of cold deformation. For applications with less exacting demands on cold workability such properties as proof stress, proof stress ratio, and bendability together with elongation and reduction of area provide adequate information. Today, however, increasing use is being made of the strain hardening exponent n ($\sigma=K.\varepsilon^n$), the uniform elongation δ_g ($\gamma_g = \ln(1+\delta_g)$ which is proportional to it, and the plastic anistropy r (the ratio between the logarithmic change in width to the logarithmic change in thickness $r = \gamma w/\gamma t$) together with the values of the mean (vertical) anisotropy r_m ($r_m = (r_o+2r_{45^o}+r_{90^o})/4$) and of the planar anisotropy Δr ($\Delta r = (r_{0^o}+r_{90^o})/2 - r_{45^o}$) calculated from the directional dependence of the plastic anisotropy.[1]

Additional simulating tests such as the Erichsen cupping test provide further information about the cold workability of thin sheet. Nevertheless, owing to the complex interaction of material, forming tool, and lubricant under operating conditions, there is still a great deal of uncertainty involved in accurately predicting the results of complex forming operations commonly combined of deep-drawing (r-value), stretch-drawing (δ_g,/E), and bending (P.S.)[2][3].

It is therefore advisable to determine these characteristics also for the c.p. titanium grades commonly manufactured today.[4] Hot rolled strip of 3 mm gauge is primarily used for making cold-rolled thin sheet. Sheet cut from strip and not subjected to any subsequent cold-rolling is used for large lots of equal-size products.

Thicknesses range from 3 to 10 mm. The demands imposed on properties generally correspond to those placed on conventionally produced sheet. The comparative properties of sheet cut from hot-rolled strip and produced conventionally are shown in Table 1.

In sheet cut from hot-rolled low-tensile strip containing 0.05 % oxygen b.w., the directional dependents of proof stress and proof stress ratio is more pronounced than in the case of conventionally produced sheet of equal tensile strength, while the directional dependence of the tensile strength is only small. The proof stress ratio is at its minimum in the direction of rolling and increases with the angle to the direction of rolling. With increasing annealing temperature, proof stress and proof stress ratio decrease in the longitudinal direction while there is only a slight decrease in the transverse direction.

Table 1: Technological Properties of Hot Rolled Coil and Sheet of c.p. Titanium

Product Thickness Heat,Treatm.	Angle to Roll.Dir.	Proof Stress Ratio (-)	Tensile Strength (MPa)	Elong. $(5\sqrt{A})$ (%)	Uniform Elong. (%)	Red. of Area (%)	Strain Harden. Exp. (-)	Plastic Anisotr. Param. (-)	Mean Anisotr. (-)	Plane Anisotr. (-)	Mean Grain Diam. (µm)
Sheet 3 mm Ingot Hardness 105 BHN 0=0,07 Fe=0,04% H.T. 700°C	0° 45° 90°	0,70 0,71 0,75	315 312 320	51 48 47	24 13 16	80 80 80	0,14 0,11 0,10	2,7 3,4 4,6	3,5	0,3	80
Sheet 3 mm 165 BHN 0=0,12 Fe=0,04% H.T. 700°C	0° 45° 90°	0,72 0,78 0,83	453 425 440	40 43 40	14 11 10	50 60 60	0,13 0,12 0,10	2,9 3,9 4,8	3,9	-0,1	60
Sheet 2 mm 188 BHN 0=0,04 Fe=0,04 % H.T. 700°C	0° 45° 90°	0,80 0,80 0,83	515 518 530	42 40 41	14 12 13	50 50 50	0,13 0,11 0,11	3,5 4,4 4,4	4,2	-0,5	60
Coil 3,2 mm 106 BHN 0=0,04 Fe=0,04 % H.T. 700°C	0° 45° 90°	0,58 0,65 0,75	360 325 330	55 66 55	38 45 10	67 77 80	0,31 0,33 0,11	1,4 2,3 4,0	2,5	0,4	104
Coil 3,2 mm 106 BHN 0=0,04,Fe=0,04 % H.T. 850°C	0° 45° 90°	0,47 0,58 0,72	365 340 335	56 62 52	38 43 9	70 67 70	0,32 0,35 0,14	1,6 2,0 6,6	3,1	2,1	118
Coil 3,0 mm 110 BHN 0=0,06 Fe=0,04 % H.T. 700°C	0° 45° 90°	0,52 0,74 0,77	315 295 315	67 59 71	35 12 14	75 77 80	0,23 0,13 0,10	1,2 2,3 2,4	2,1	-0,5	50
Coil 3,0 mm 110 BHN 0=0,06 Fe=0,04 % H.T. 850°C	0° 45° 90°	0,41 0,65 0,76	330 295 295	65 85 71	45 45 15	65 75 75	0,31 0,37 0,12	1,2 2,0 4,6	2,5	0,9	120

Longitudinal and transverse specimens show characteristic differences in the uniform elongation. In the direction of rolling there is considerable uniform elongation while in the transverse direction there is only a small amount of it together with a large amount of total elongation. At an angle of 45° to the rolling direction, the uniform elongation shows a pronounced dependence on grain size. It is small with a fine grain size which can be obtained by reducing the rolling speed in the finishing train and thus keeping the final-rolling temperature at a low value. If the grain size is in excess of 100 micron the uniform elongation increases and is above that in the direction of rolling.

The strain-hardening exponent behaves similarly. In sheet cut from strip it is higher in the longitudinal direction than that on conventionally produced sheet and shows a considerable drop in the transverse direction. At an angle of 45° relative to the direction of rolling the strain-hardening exponent shows the same dependence on grain size as in the uniform elongation.

The plastic anisotropy parameter r of conventionally produced sheet shows a small amount of directional dependence, increasing from longitudinal direction to transverse direction. As the oxygen content increases the directional dependence decreases. Sheet cut from strip having a low oxygen content shows a more pronounced anisotropic dependence at higher finish-rolling temperatures. At the same time a high plastic anisotropy is found in transverse direction. At lower finish-rolling temperatures, however, the directional dependence is less pronounced.

The influence of cold-reduction and heat treatment on the properties of sheet cut from low-tensile strip is shown in Table 2. While the tensile strength shows only a slight dependence and the proof stress and the proof stress ratio decrease with increasing annealing temperature and grain size independent on the percentage of cold reduction, the uniform elongation and the strain-hardening exponent are less dependent on direction with mean percentages of cold reduction than with high amounts of cold reduction. The plastic anisotropy parameter r also shows a smaller amount of anisotropy.

Sheet cut from cold-rolled strip is primarily made in thicknesses up to 1 mm. The demand for optimum operating properties must always be seen in close relation to the level production costs can justifiably reach. The aim therefore is to roll such strip as far as possible without any intermediate anneals. Table 3 shows the properties of two titanium grades differing in oxygen content and tensile strength obtained with different anneals after heavy cold reductions. In both grades the tensile strength is only slightly dependent on the recrystallization temperature and rolling

Table 2: Influence of Cold Deformation and Heat Treatment on the Properties of c.p. Titanium Sheet
(Ingot Hardness: 106 BHN, O= 0,04 %, Fe = 0,04 %)

Condition	Sheet Thickn. (mm)	Degree of Cold Deform. γ (-)	Degree of Cold Deform. ε (%)	Angle to Roll. Dir.	Proof Stress Ratio (-)	Tensile Strength (MPa)	Elong. $(5\sqrt{A})$ (%)	Uniform Elong. (%)	Red. of Area (%)	Strain Hard. Exp. (-)	Plastic Anis. Param. (-)	Mean Anis. (-)	Plane Anis. (-)	Mean Grain Dia. (µm)
Hot Rolled	3,2	0	0	0°	0,58	360	55	38	67	0,31	1,4			
				45°	0,65	325	66	45	77	0,33	2,3			
			700°C	90°	0,75	330	55	10	80	0.11	4,0	2,5	0,4	104
Cold Rolled	2,4	0,29	25	0°	0,52	345	65	40	75	0,20	1,4			
				45°	0,65	330	73	45	75	0,22	1,4			
		H.T.	700°C	90°	0,75	335	61	22	73	0,12	3,2	1,9	0,9	80
id.	1,6	0,69	50	0°	0,56	345	64	42	75	0,18	1,3			
				45°	0,66	320	72	36	78	0,15	2,1			
		H.T.	700°C	90°	0,73	333	63	19	78	0,12	3,1	2,1	0,1	69
				0°	0,53	355	63	42	65	0,23	1,2			
				45°	0,62	330	72	46	67	0,17	2,9			
		H.T.	800°C	90°	0,72	330	68	29	70	0,13	3,2	2,6	-0,7	85
id.	0,8	1,39	75	0°	0,54	355	55	33	63	0,18	1,5			
				45°	0,66	330	74	22	68	0,14	2,3			
		H.T.	700°C	90°	0,75	350	61	11	75	0,11	3,6	2,4	0,3	46
				0°	0,52	365	64	46	48	0,26	1,3			
				45°	0,60	350	74	57	58	0,20	1,5			
		H.T.	800°C	90°	0,73	350	57	12	63	0,10	3,7	2,0	1,0	70

direction. Proof stress and proof stress ratio are at their minimum in the rolling direction and decrease as the annealing temperature increases; perpendicular and at an angle 45° to the rolling direction the decrease is smaller. The improved workability of low-tensile titanium is shown by its high elongation and reduction of area; in transverse direction the total elongation is smaller but the reduction of area considerable. Uniform elongation and the strain-hardening exponent show the greatest directional dependence. While in transverse direction of rolling these properties are largely independent of grain size but increase slightly after annealing above the transformation temperature, there is a considerable increase in the uniform elongation at an angle of 45° to the rolling direction for grain sizes above 80 micron. This increase is not observed in material having relatively high percentages of oxygen, which also shows smaller values of uniform elongation and of the strain-hardening exponent in the rolling direction.

The Erichsen depth of cup decreases slightly with increasing grain size. It is at its maximum at a low oxygen content. The stress-strain diagrams obtained by tensile tests show the characteristic differences for different values of uniform elongation. Different percentages of final cold-reduction (50 to 80 %) do not appreciably affect the directional dependence of cold working (c.f. Table 2). Low-tensile titanium shows a lower range of plastic anisotropy than the grades of higher tensile strength. The r-value increases moderately from longitudinal to transverse direction.

The texture obtained in commercially produced strip after heavy percentages of cold reduction and annealing shows maxima at the pole figure (0001) at at angle of 30° (0.05 % O) and of 25 to 30° (0.12 % O) to the normal in transverse direction. There was no noticeable change in texture over the strip width. The texture corresponds to the well known recrystallization texture for titanium subjected to considerable amounts of cold reduction[5][6][7]. At higher annealing temperatures titanium of lower tensile strength and with grain sizes in excess of 100 micron showed maxima for the same pole figure at angles of 30° to the normal and 30° to the rolling direction. Titanium of higher strength, however, showed no major change in texture. This is held to be the reason for the varying directional dependence of the properties while slip in the $(10\bar{1}0)$-plane rendered more difficult with higher percentages of oxygen contributes to the decrease in workability.

In commercial production the material is subjected to a slight amount of plastic deformation after the final anneal by temper rolling or leveling. This is done to improve flatness and facilitate trimming, slitting, shearing or coating. It is a known fact that such slight reductions may have an adverse effect on workability. With c.p. titanium of low tensile strength the proof stress

Table 3: Technological Properties of 0,6 mm Cold Rolled Strip of c.p. Titanium

Grade	Anneal. Temp. (°C)	Angle to Roll. Dir.	Proof-Stress Ratio (-)	Tensile Strength (MPa)	Elong. ($5\sqrt{A}$) (%)	Uniform Elong. (%)	Red. of Area (%)	Strain Hard. Exp. (-)	Plastic Anisotr. Param. (-)	Erichsen Cupping Test (mm)	Mean Grain Dia. (µm)
Ingot Hardness 103 BHN 0= 0,04 Fe= 0,04% Degree of Cold Def.ε =82 % (γ total = γ_1 = ℓn t_1/t_0 = 1,7) t_0 = 0,6 mm	700	0°	0,51	330	62	36	50	0,30	1,5	12,6	44
		45°	0,74	305	68	14	60	0,11	3,0		
		90°	0,77	350	50	10	72	0,11	3,2		
	800	0°	0,44	340	67	42	55	0,35	1,4	11,6	125
		45°	0,65	305	68	52	60	0,40	2,9		
		90°	0,76	345	56	11	70	0,13	3,0		
	900	0°	0,48	345	65	38	67	0,36	1,2	11,3	100
		45°	0,65	330	60	41	67	0,34	2,7		
		90°	0,75	335	55	14	72	0,13	2,9		
Ingot Hardness 161 BHN 0=0,14 Fe=0,05 % ε = 83 % (γ total = 1,8) t_0= 0,5 mm	700	0°	0,70	470	32	18	45	0,15	3,6	8,0	37
		45°	0,76	470	33	13	45	0,13	4,0		
		90°	0,81	480	33	12	50	0,11	4,5		
	800	0°	0,67	460	34	13	55	0,13	3,0	7,3	37
		45°	0,77	450	32	12	48	0,11	3,8		
		90°	0,82	470	35	10	60	0,10	4,4		
	900	0°	0,63	450	39	18	45	0,16	2,7	6,0	71
		45°	0,69	445	35	14	48	0,12	3,9		
		90°	0,70	455	38	11	53	0,10	5,0		

ratio in the rolling direction and the uniform elongation were found to be slightly reduced but an appreciable effect on the cupping test and r-value was not observed. The aim is to reduce temper rolling to the minimum for sheet requiring a high degree of cold formability. In special cases temper rolling is fully dispensed with.

4. SUMMARY

Compared with conventionally produced sheet, sheet cut from strip shows a pronounced directional dependence of its properties, particularly its proof stress, uniform elongation, and strain-hardening coefficient. With c.p. titanium the directional dependence is most pronounced when the oxygen content is low. The proof stress decreases with increasing grain size more strongly than the tensile strength. Uniform elongation and strain-hardening coefficient are at their maximum in the direction of rolling when the oxygen content is low and the grain size small; at an angle of 45° relative to the rolling direction both properties increase considerably with grain sizes in excess of 80 micron; in transverse direction they are small and independent of grain size.

The increase at an angle of 45° to the rolling direction was not observed with higher oxygen contents.

The plastic anisotropy parameter r shows an increase from longitudinal to transverse direction. Considerable variations and differences under equal conditions of processing indicate that small changes in the preferred orientations affect the r-value very considerably. In view of the importance of this property for deep-drawing further studies still have to be carried out.

The uniformity of the properties of low-tensile strip produced economically is verified by statistical analysis. The use of uniform charge materials and constant processing conditions ensure small variations.

REFERENCES

1. Müller, R., Techn. Mitt, Krupp - Werksberichte 32 (1974) 67-74.

2. Lange, E., Bänder, Bleche, Rohre 12 (1975) 511-514.

3. Beck, G., Roth, W., Techn. Mitt. Krupp - Werksberichte 33 (1975) 41-44.

4. Wilhelm, H., Bänder, Bleche, Rohre 10 (1975) 421-426
11 (1975) 473-476.

5. Mülders, H., Schmitz, K., Tecn. Mitt. Krupp - Werksberichte 33 (1975) 83-87.

6. Williams, D. N., Eppelsheimer, P. S., Trans. AIME 197 (1953) 1378-1382.

7. Thornburg, D. R., Piehler, H. D., Titanium Science and Technology, Vol. 2, New York-London, 1973, 1187-1197.

MECHANICAL PROPERTIES OF TITANIUM ALLOY PLATES

K. Rüdinger and A. Ismer

Contimet, Titanium Division of
Thyssen Edelstahlwerke AG,
Krefeld, Fed. Rep. Germany

The production of titanium alloy plates has grown considerably in the last years. Main applications are highly loaded integral parts of airframes and parts in aero-engine constructions (1,2). Further on heavy plates up to 100 mm thickness are fabricated for deep submergence vehicles (3,4), where also a high strength-density ratio is required besides weldability, corrosion and stress corrosion resistance as well as high fracture toughness.

The alloys of major importance for plate production, on which is reported here, are Ti6Al4V, Ti6Al6V2Sn and Ti4Al4Mo2Sn. Among them, Ti6Al4V has the widest application because of its excellent combination of properties, ample experience in fabrication and service and its applicability for EB-welded structures (5). Ti6Al6V2Sn with a higher strength level than Ti6Al4V is preferred for compression loaded, unwelded parts. Both alloys are normally used in the annealed condition. Ti4Al4Mo2Sn showing superior tensile strength and ductility over the other two alloys, is only used in the aged condition. Since no water quenching is provided for that alloy after solution treating the main disadvantages of the solution treated and aged (STA) condition with other $\alpha+\beta$ -titanium alloys, namely distortion and induction of inner stresses, are avoided.

Table 1 Chemical Composition of Ti6Al4V, Ti6Al6V2Sn and Ti4Al4Mo2Sn Plate. Specified and Typical Values.

Elements		Al	V	Mo	Sn	Cu	Fe	Si	0	C	N	H
Alloy	Value	in Weight Percent										
Ti6Al4V	Spec. min	5,5	3,5	-	-	-	-	-	-	-	-	-
"	" max	6,75	4,5	-	-	-	0,3	-	0,20	0,08	0,05	0,015
"	Typical	6,3	4,0	-	-	-	0,17	-	0,16	0,02	0,01	0,006
Ti6Al6V2Sn	Spec. min	5,0	5,0	-	1,5	0,35	0,35	-	-	-	-	-
"	" max	6,0	6,0	-	2,5	1,00	1,00	-	0,20	0,05	0,04	0,0125
"	Typical	5,4	5,4	-	2,0	0,65	0,65	-	0,18	0,02	0,01	0,008
Ti4Al4Mo2Sn	Spec. min	3,0	-	3,0	1,5	-	-	0,30	-	-	-	-
"	" max	5,0	-	5,0	2,5	-	0,2	0,70	0,25	0,08	0,05	0,0125
"	Typical	4,0	-	3,9	2,1	-	0,05	0,36	0,18	0,01	0,01	0,006

Plate Production

All reported data come from plates which have been produced from double melted ingots of the customary vacuum arc furnace process (6). Table 1 lists the typical values of chemical composition of the ingots used for plate production. Since thermo-mechanical processing affects macro- and microstructure and mechanical as well as other properties, standard procedures for the production of plates were developed (6,7,8). The general production scheme includes three basic steps:

- Breaking down the coarse solidification grains of the vacuum-arc melted ingots at temperatures starting high in the β-field. Intermediate heat treatments for recrystallizing may be included.

- Sufficient working at temperatures below the β-transus- in exceptional cases also slightly above the beta-transus - to provide the desired microstructure.

- Final heat treatment to further influence the microstructure in the desired way.

Close control of the processing variables, as amount of reduction, deformation rate, starting and finishing temperatures of deformation, number of reheats, heating and cooling conditions are of utmost importance for the reproducibility of properties. It was found that the amount of final work at temperatures below the β-transus has a greater effect on the tensile properties than the amount of primary deformation (9). For all the three titanium alloys Table 2 presents the β-transus determined metallographically.

Table 2 Beta Transus Temperatures of Ti6Al4V, Ti6Al6V2Sn and Ti4Al4Mo2Sn.

Alloy	$\alpha + \beta/\beta$ Phase Transformation (^{o}C)
Ti6Al4V	995 ± 15
Ti6Al6V2Sn	935 ± 15
Ti4Al4Mo2Sn	985 ± 15

Basically two types of microstructures can be produced. Generally specified for plates of the three alloys is the microstructure resulting from final working and heat treatment in the $\alpha+\beta$ field with equiazed or short lamellar primary α-grain. In Ti6Al6V2Sn and Ti4Al4Mo2Sn a finer, more uniform macrostructure was achieved than in Ti6Al4V.

By solution treating of Ti6Al4V high in the $\alpha+\beta$ field, the amount of primary α-grains can be reduced to a desired level; the amount of transformed $\alpha+\beta$ matrix is increased. The advantage of this treatment may be higher fracture toughness and improved ultrasonic inspectability, as also reported by other authors.[9,10] Also notch time stress rupture values were found to be higher due to greater uniformity of the structure.

Structures from beta-working or heat treating are generally not accepted by specifications, although in general higher fracture toughness and creep resistance was found at moderate loss of tensile properties as previously described.[11]

Tensile Properties

A statistical evaluation was made from the data of up to 57 plates tested during final control. Fig. 1 illustrates the results. The top of the columns represents the average ($\bar{x}$) and the second line underneath shows the statistical significant line of average minus two times standard deviation ($\bar{x} - 2\sigma$).

The average values of ultimate tensile strength (Rm) and 0.2% yield strength (Rp02) do not differ much for various directions in the same thickness range. Generally, they show somewhat higher values in the transverse (LT) than in the longitudinal (L) direction. Tensile properties of the short transverse direction (ST) were determined only on over 50 mm thick plates. The Rm-and Rp02-values are about comparable to the L-values, as shown in Fig. 1 for Ti6Al4V and Ti6Al6V2Sn. Both, elongation (A) and reduction of area (Z) show similar values for L- and LT-directions. Only in the ST-direction lower values are observed. There is also a tendency that with an increasing thickness the tensile properties decrease.

For Ti4Al4Mo2Sn only LT-values for the STA-condition are available. Compared to Ti6Al6V2Sn, annealed, in the same test direction they are about 80 N/mm^2 higher for Rm, and 20 N/mm^2 higher for Rp02. Both alloys, Ti4Al4Mo2Sn in the STA-condition and Ti6Al6V2Sn in the annealed condition, have a considerably higher strength than Ti6Al4V, annealed.

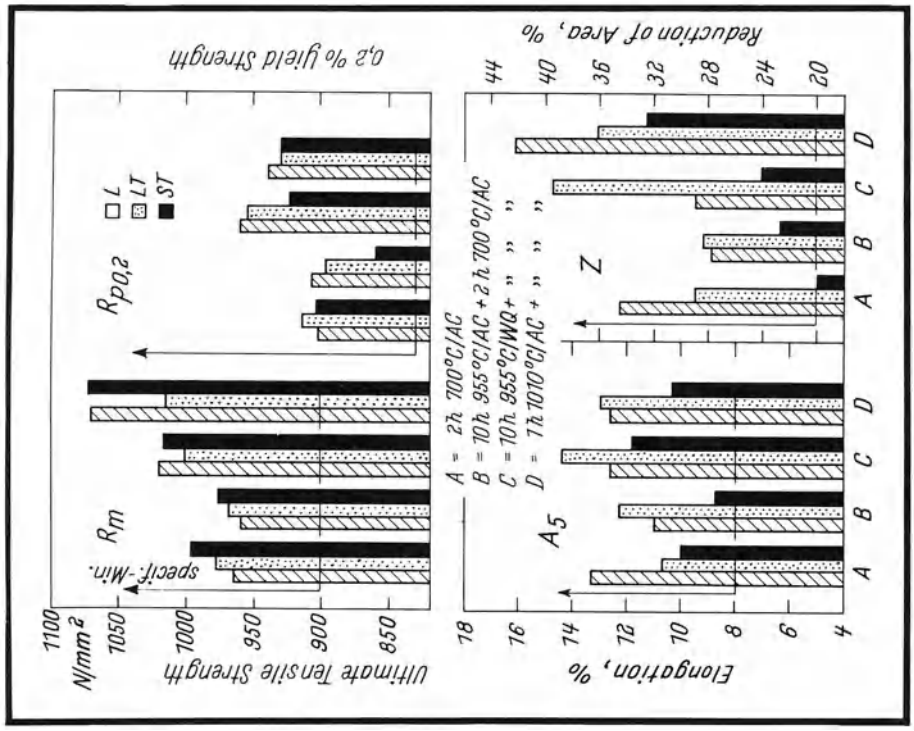
Ultimate Tensile Strength
0,2 % yield Strength
Elongation, %
Reduction of Area, %
A = 2h 700°C/AC
B = 10h 955°C/AC + 2 h 700°C/AC
C = 10h 955°C/WQ+ " " "
D = 1h 1010°C/AC + " " "
L
LT
ST
specif.-Min.

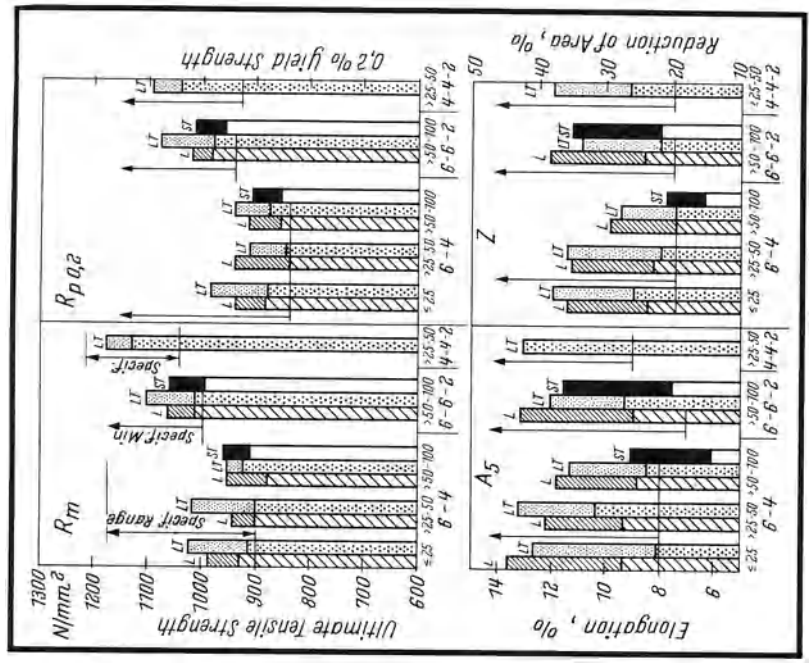
Ultimate Tensile Strength
0,2 % yield Strength
Elongation, %
Reduction of Area, %
specif. Min.
specif. Range
specif.

Figure 1

The average tensile properties were well above the minimum values of common specifications (Fig. 1), however, ($\bar{x}$ - 2 σ)-values sink in some cases below them, although all individual values meet the specification.

The effect of intermediate solution treatment on the tensile properties of Ti6Al4V plates of 85 mm thickness can be seen from Fig. 1. In this case the heat treatment was performed on cut test pieces of the plates and the mentioned results are average values from two test specimens. It was confirmed that water quenching and also β-annealing require special measures and extreme care for controlling the operation conditons.

Concerning the tensile properties of Ti6Al4V comparable values were obtained for the annealed (A) as well as for solution treated, air cooled plus annealed conditions(B). In the solution treated, water quenched plus annealed condition (C) and in the β-plus (α + β)-annealed condition (D) we achieved also similar tensile properties with the exception of the tensile strength, which reached higher values in condition D as in C and therefore also a lower Rp/Rm-ratio. The conditions C and D result in higher Rm and Rp values compared with condition A and B, including higher ductility values, in particular of reduction of area for condition D.

Fracture Toughness

Fracture toughness testing was done on ASTM-E-399-72 (Compact tension), L-(tension), LT-(notch) direction specimens taken from 85 mm-thick plates in the annealed condition. The average value of K_{IC} is 2034 $N/mm^{1,5}$ with a standard deviation of 183 $N/mm^{1,5}$. The relevant mean values of $Rp0_2$ are 934 N/mm^2 in the L- and 974 N/mm^2 in the LT-direction. Within this determined range of K_{IC}-values no tendency of rising fracture toughness with decreasing yield strength was found.

The properties of four plates showed conformance with the literature(12,13,14) in that the very fine, equiaxed microstructure shows with 1722 $N/mm^{1,5}$ the lowest K_{IC} value, while the more lamellar structures result in higher fracture toughness.

CONCLUSIONS

The plates of Ti6Al4V, Ti6Al6V2Sn and Ti4Al4Mo2Sn produced by conventional α + β-conversion and heat treating generally meet the specified tensile properties when subtracting two times the standard deviation from the mean value.

- No remarkable differences of strength were observed for the three test directions, but ductility is lower in the ST-direction. Tensile properties decrease with increasing plate thickness.

- Ti4Al4Mo2Sn in STA-condition has an excellent combination of tensile strength and ductility superior to Ti6Al4V and Ti6Al6V2Sn in the annealed condition.

- The tensile properties are not affected notably, if the content of primary alpha-phase is reduced by solution treatment below the β-transus followed by air cooling (condition B).

- Without special control measures heat treating of Ti6Al4V closely above the β-transus plus annealing and solution treating, water quenching plus annealing gave less consistant results than annealing as well as solution treating followed by air cooling plus annealing.

- The determined fracture toughness values on Ti6Al4V plates met the tentative specifications.

REFERENCES

(1) N.N. B-1's Test Components in Production, AW & ST. Vol. 99 (2, 7, 1973), p. 38/41.

(2) Hotz, R., TU 144 Aimed at 30000 Hour of Service. AW & ST. Vol. 99 (2, 7, 1973), p. 24/28.

(3) Goode, R. J., Huber, R. W., Fracture Toughness Characteristics of Some Titanium Alloys for Deep Diving Vehicles, J. of Metals 17 (1965), p. 841/46.

(4) Minkler, W. W., Feige, N., Titanium for Deep Submergence Vehicles, Undersea Technology, Vol. 6 (1965), p. 26/29.

(5) Stocker, G., Erfahrungen beim Elektronenstrahlschweißen dickwandiger Bauteile aus der Titanlegierung Ti6Al4V, geglüht. Schweißen und Schneiden 26 (1975), S. 91/93.

(6) Zwicker, U., Titan und Titanlegierungen, Springer-Verlag, Berlin, Heidelberg, New York 1974. S. 114/95.

(7) Rüdinger, K., Erzeugung und Qualitätssicherung von Titanwerkstoffen, DEW-Internationales Symposium, Krefeld, 21./22. Mai 1969.

(8) Rüdinger, K., Ismer, A., Eifluß von Mikro- und Makrogefügeausbildung auf das Schwingfestigkeitsverhalten von TiAl6V4 und TiAl6V6Sn2. Proceedings of 3. Haus-colloquium Institut II fur Werkstoffeigenschaften der Universität Erlangen-Nurnberg, 11/12, Oct. 1972, Teil 3, Seite IX/1-16.

Rüdinger, K., Ismer, A., Einfluß von Mikro-und Makrogefügeausbildung auf das Schwingfestigkeitsverhalten der Titanlegierung TiAl6V4. 6. Internationaly Leichtmetalltagung Leoben/Wien 1975. Aluminum Verlag GmbH, Düsseldorf, 1975, S. 269/70.

(9) Gerhard, A., Knorr, W., Influence of Hot Working on the Properties of the Ti6Al4V Alloy with Special Regard to Heavy Sections. Titanium Science and Technology, Plenum Press, New York-London, 1973, p. 463/75.

(10) Billmann, F. R., Rudolph, Effects of Ti6Al4V Alloy Metallurgical Structures on Ultrasonic Response Characteristics. Titanium Science and Technology, Plenum Press, New York-London, 1973, p. 693/705.

(11) Wood, R. A., Favor, R. J., Titanium Alloys Handbook, MCIC Columbus Battelle Laboratories, Columbus, Ohio, USA, 1972.

(12) Broichhausen, J., van Kann, H., Influence of Forging Conditions on Fatigue Behavior of Ti-6Al-4V, Titanium Science and Technology, Plenum Press, New York-London, 1975, p. 1785/99.

(13) Diebold, A., Hammer, M., Eigenschaften von Schmiedestücken aus der Legierung Ti6Al4V nach dem Beta-Schmiedeverfahren. 6. Internationale Leichtmetalltagung Leoben/Wien 1975. Aluminum Verlag GmbH, Düsseldorf, 1975, p. 266/68.

(14) Margolin, B., Greenfield, M. A., Greenhut, I., Yield Strength, Microstructure and Fracture Toughness. Titanium Science and Technology, Plenum Press, New York-London, 1973, p. 1709/18.

EFFECT OF HEAT TREATMENT ON THE MECHANICAL PROPERTIES IN AN ALPHA-BETA TITANIUM

T. Nishimura, Y. Tsumori, and K. Shimizu

Kobe Steel, Ltd.
Kobe, Japan

Introduction

The microstructure of the annealed alpha-beta titanium alloy Ti-6Al-4V consists of the alpha phase of 82 per cent and the beta phase of 18 per cent, and shows the various types such as the primary alpha structure, transformed beta structure and so on, depending upon the conditions of heat treatment and deformation. It is thought, therefore, that the mechanical properties of this alloy are largely dependent upon the microstructure, particularly the shape of the alpha phase. Since the shape and the amounts of various alpha grains vary by the heat treatment, the effect of the heat treatment before the final annealing was investigated using two kinds of materials with the primary alpha structure.

Experimental procedure

Hot rolled bars (22 mm diameter) and forgings (500 mm diameter x 80 mm thickness) were used. Hot rolled bars were produced by forging from 480 mm diameter ingot to 90 mm x 90 mm billets after heating at 1100°C and rolling to 22 mm diameter bars after heating at 900°C without an intermediate heating. The Forging material was produced by closed-die forging at 930°C with one intermediate heating. Specimens were cut from the forging, as shown in Fig. 1.

The chemical compositions of the materials are shown in Table 1. Hot rolled bars and forgings showed the all primary alpha structure. Twenty-two mm diameter specimens cut from hot rolled bars and forgings were heated in the high alpha-beta field from 850°C to 975°C and at 1000°C just above the beta transus for 1 hour, water quenched

Table 1 Chemical compositions of Ti-6Al-4V (wt.%)

Material	Al	V	Fe	O	N	H
Hot rolled bar	6.54	4.05	0.261	0.146	0.0066	0.0028
Forging	6.28	4.13	0.273	0.134	0.0040	0.0010

at a cooling rate of 2050°C, and subsequently annealed at 700°C for 2 hours. Since the microstructure changes depending upon the cooling rate after the solution treatment, the specimens were also cooled at various cooling rates such as oil quenching (1040°C/min), air cooling (145°C/min), and furnace cooling (1.5°C/min) after the solution treatment at 900°C and 950°C. Tensile test, notched stress-rupture test and light microscopy were carried out for solution-treated and annealed specimens. Test specimens are shown in Fig. 2. The strain rate of tensile tests was 0.5 per cent per minute through the yield strength and then increased so as to produce failure in approximately one additional minute.

The notched stress-rupture strength (NRS) was determined in the following manner. Notched specimens shown in Fig. 2 were loaded at an initial stress level of 119.5 kg/mm^2 for 5 hours. If they were not fractured, the initial stress was increased in increments of 5 kg/mm^2 at intervals of one hour. If the fracture occured at a stress of s_1 for h_1 hour, the notched stress-rupture strength was determined as follows:

$$\text{NRS (kg/mm}^2) = s_1 - 5 + 5 \times h_1/1$$

Results and discussion

1. Effect of solution temperature

The effect of the solution treatment temperature on the mecha-

nical properties of the hot rolled bar and the forging is shown in Fig. 3. The microstructures of solution treated and annealed specimens are shown in Fig. 4. The hot rolled bar showed a good combination of strength and ductility in the annealed condition which was related to a fine primary alpha structure. The solution treatment at 850°C before annealing lowered the strength and raised the ductility a little higher. This is largely due to the enlargement of the primary alpha grain, as shown in Fig. 4. The average grain diameter of hot rolled bar was 2 microns in the annealed condition and became 5 microns after the solution treatment at 850°C and subsequent annealing. Although the decrease of the amount of the primary alpha structure and the increase of the transformed beta structure are also related to the change in the mechanical properties, it is not in the case because the change of the ratio of both structure is small.

In the solution treated and annealed conditions, the notched stress-rupture strength, the tensile strength and the yield strength increased with increasing solution temperatures, which was attributed to the decrease of the primary alpha structure and the increase of the transformed beta structure. Tensile ductility did not change by the solution treatment in the range 850°C to 950°C, but decreased at 975°C and fell at 1000°C.

For the forging material with large primary alpha grains, both strength and ductility were lower than those of hot rolled bars and improved by the solution treatment. The notched stress-rupture strength of the annealed specimen increased with increasing solution temperatures in the high alpha-beta field. The tensile and yield strength also increased with increasing solution temperatures, while tensile ductility showed a slight increase by the solution treatment in the alpha-beta field but a drop by that in the beta field.

As shown in Fig. 4, it was observed that the fine primary alpha grain of 2 micron diameter in the hot rolled bar became larger with increasing solution temperatures, while the large primary alpha grain in the forging became finer from 14 to 8 microns. The en-

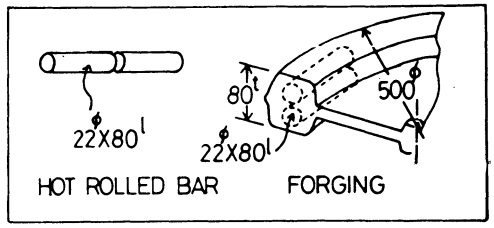

Fig. 1 - Specimens for heat treatment.

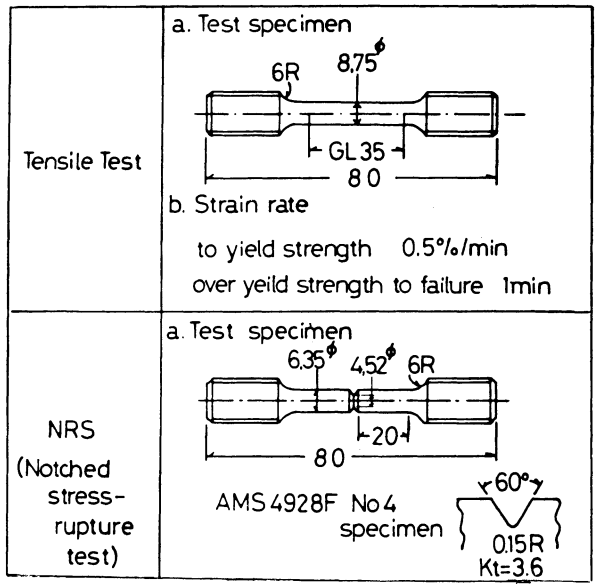

Fig. 2 - Test specimens.

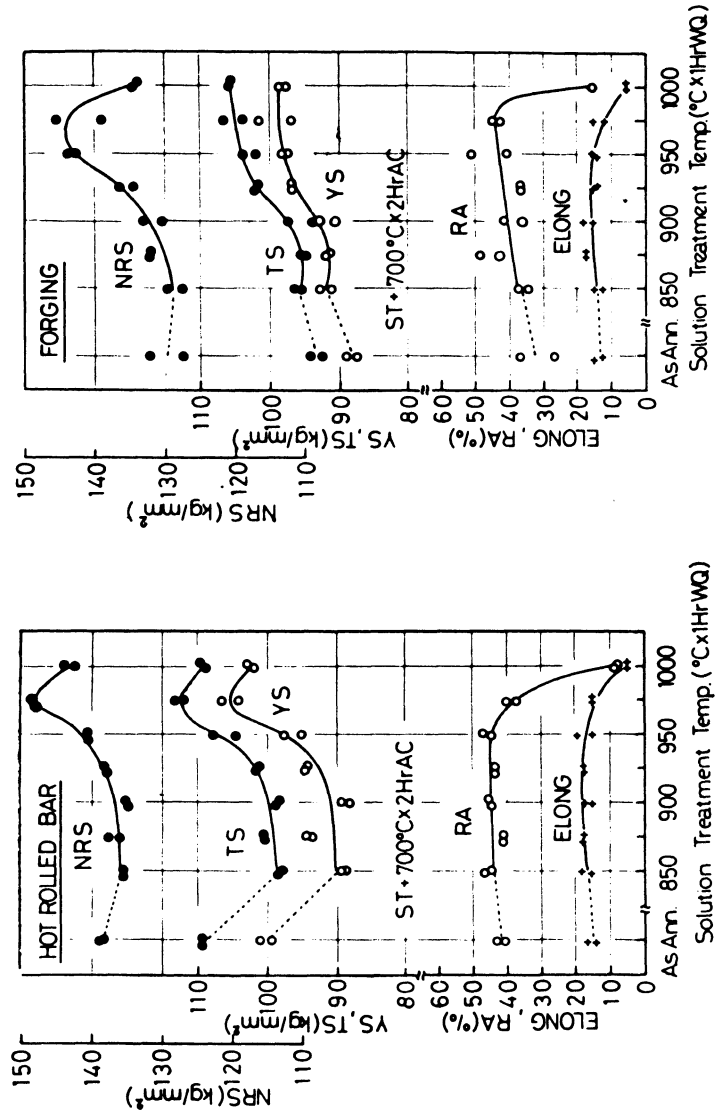

Fig. 3 - The effect of the solution treatment temperature on the mechanical properties of the solution treated and annealed hot rolled bar and forging of Ti-6Al-4V.

largement of the fine primary alpha structure may be considered to occur with alpha-beta transformation which occurs to the equilibrium fraction of the phases at the solution temperature. The difference of the effect of solution temperatures on the mechanical properties between the hot rolled bar and forging may be considered to become from the difference of the change of the primary alpha grains after the solution treatment.

The volume fraction of the primary alpha decreased with increasing solution temperatures, as shown in Fig. 5. In the solution temperatures above 900°C, the amount of the primary alpha decreased remarkably to zero at 1000°C. The decrease of the primary alpha structure is consistent with the increase of the transformed beta structure after solution treatment and annealing. The relationship between the mechanical properties and the amount of the alpha phase is shown in Fig. 6. It was found that the notched stress-rupture strength, the tensile strength and the yield strength decreased with increasing the amount of the primary alpha while tensile ductility showed a slight change.

2. Effect of the cooling rate after solution treatment

The mechanical properties of the specimen cooled at various cooling rates after the solution treatment are shown in Fig. 7. The microstructures of these specimens are shown in Fig. 8. The notched stress-rupture strength, the tensile strength and the yield strength decreased with decreasing cooling rates, and tensile ductility did not change at any cooling rate. For the hot rolled bar with good mechanical properties in the annealed condition, the improvement of mechanical properties was not observed by the solution treatment with cooling at any cooling rate due to the enlargement of the primary alpha grains.

For the forging materials with the large primary alpha grains, the solution treatment improved the mechanical properties, particularly the notched stress-rupture strength at all cooling rates. The higher strength at the higher cooling rate was related to the finer

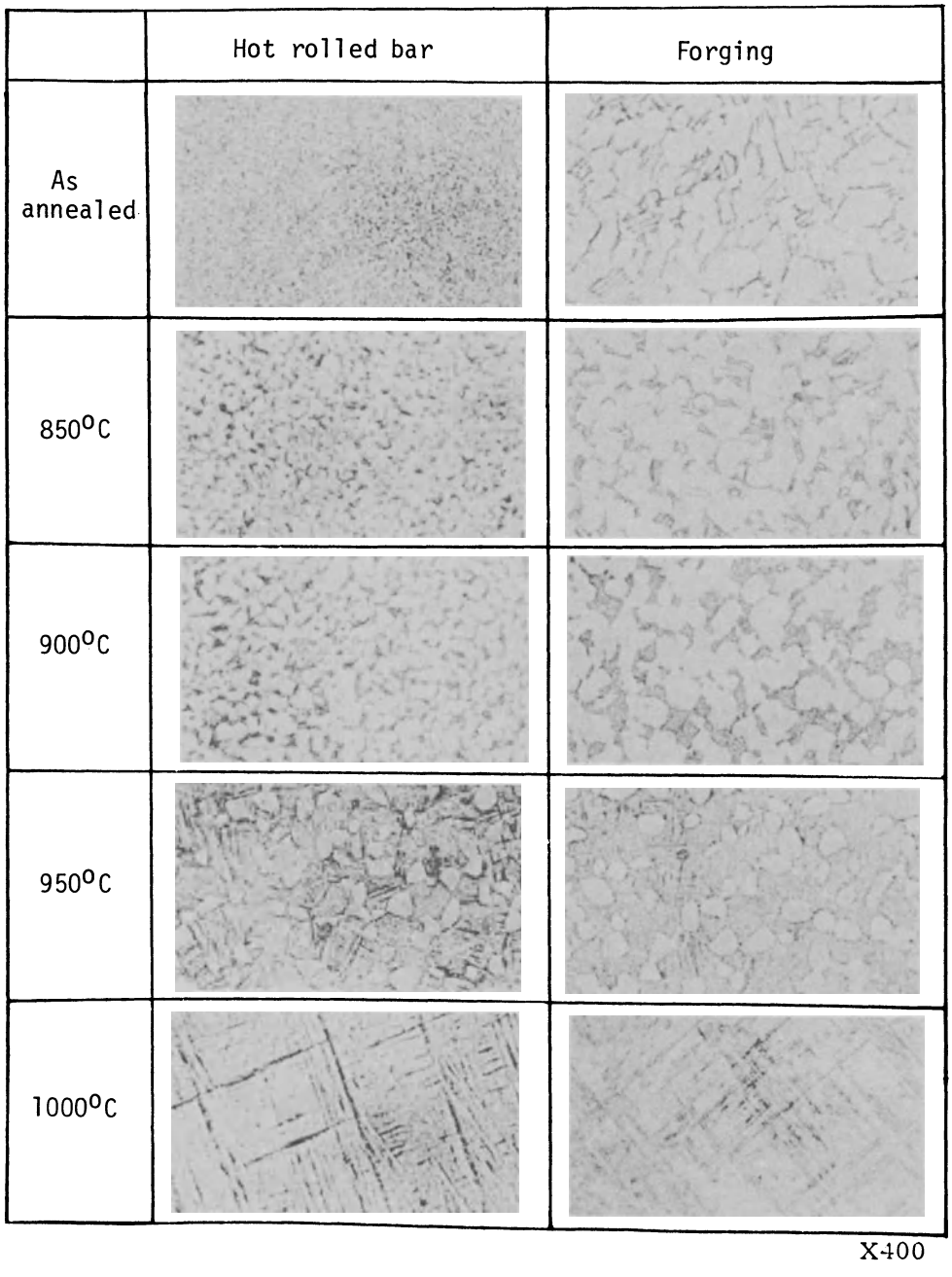

Fig. 4 - Microstructures of hot rolled bar and forging of Ti-6Al-4V, solution treated, water quenched and annealed.

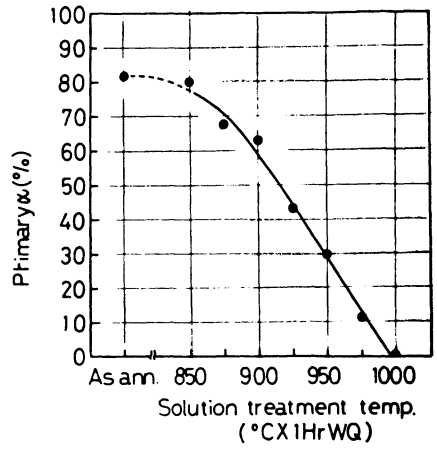

Fig. 5 - The relationship between the solution temperatures and the amount of the primary alpha in Ti-6Al-4V.

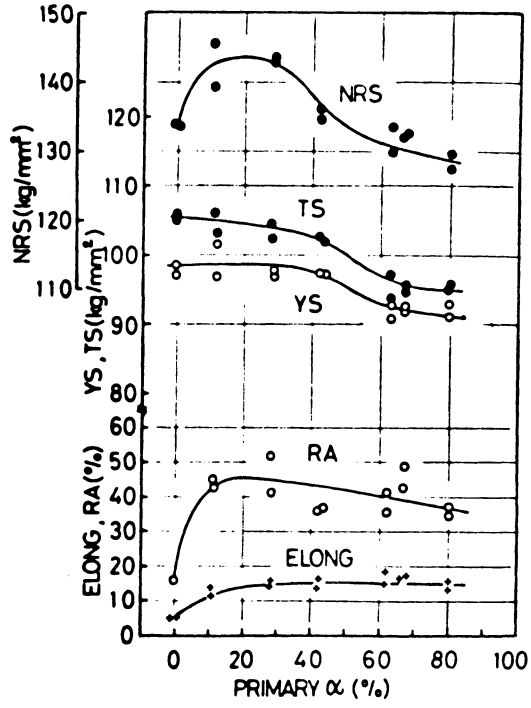

Fig. 6 - The relationship between the mechanical properties and the amount of the primary alpha in Ti-6Al-4V.

grain size of the primary alpha and the acicular alpha in the transformed beta structure between the primary alpha grains, and also related to the much amount of the transformed beta structure. The beta phase at the solution temperature in the high alpha-beta field transforms martensically during cooling and finally changes to the transformed beta structure after annealing which consists of acicular alpha phase and intergranular beta phase. At low cooling rates such as furnace cooling of 2.5°C/min , the beta phase at the solution temperature does not transform martensically, and remains between the enlarged primary alpha grains, as shown in Fig. 8. The relationship between the cooling rate after the solution treatment and the amount of the primary alpha structure is shown in Fig. 9. It was found that the cooling rate higher than air cooling is needed so as to prevent the enlargement of the primary alpha grain and to form the transformed beta structure with fine acicular alpha grains between the primary alpha grains.

Conclusion

(1) The hot rolled bar with a fine primary alpha structure showed the good combination of strength and ductility in the annealed condition, but the lower strength and a little higher ductility at the lower solution temperatures of 850°C to 900°C due to the enlargement of the primary alpha grains, and the increase in the notched stress-rupture strength and tensile strength at the higher solution temperatures.

(2) For the forging with a coarse alpha grain structure, the remarkable improvement in the notched stress-rupture strength and tensile properties of both strength and ductility was observed in the solution treated and annealed conditions, especially in the solution treatment at the higher temperatures below the beta transus.

(3) It was found from the microstructual observation that the improvement of the mechanical properties was related to the decrease of the primary alpha structure and the increase of the transformed beta structure.

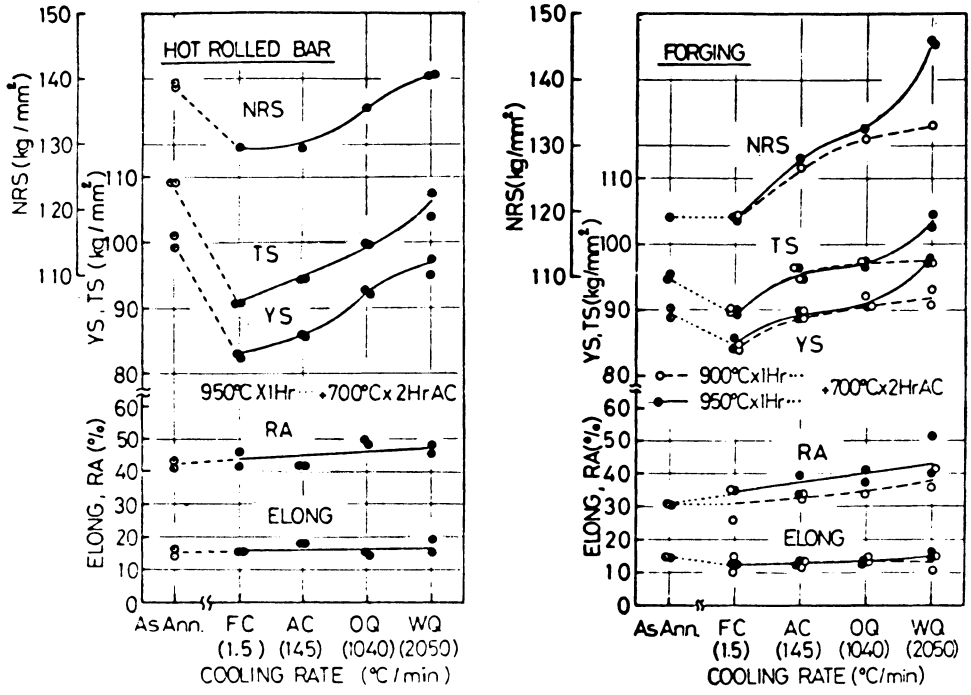

Fig. 7 - The effect of the cooling rates after the solution treatment on the mechanical properties of the hot rolled bar and forging of Ti-6Al-4V, solution treated and annealed.

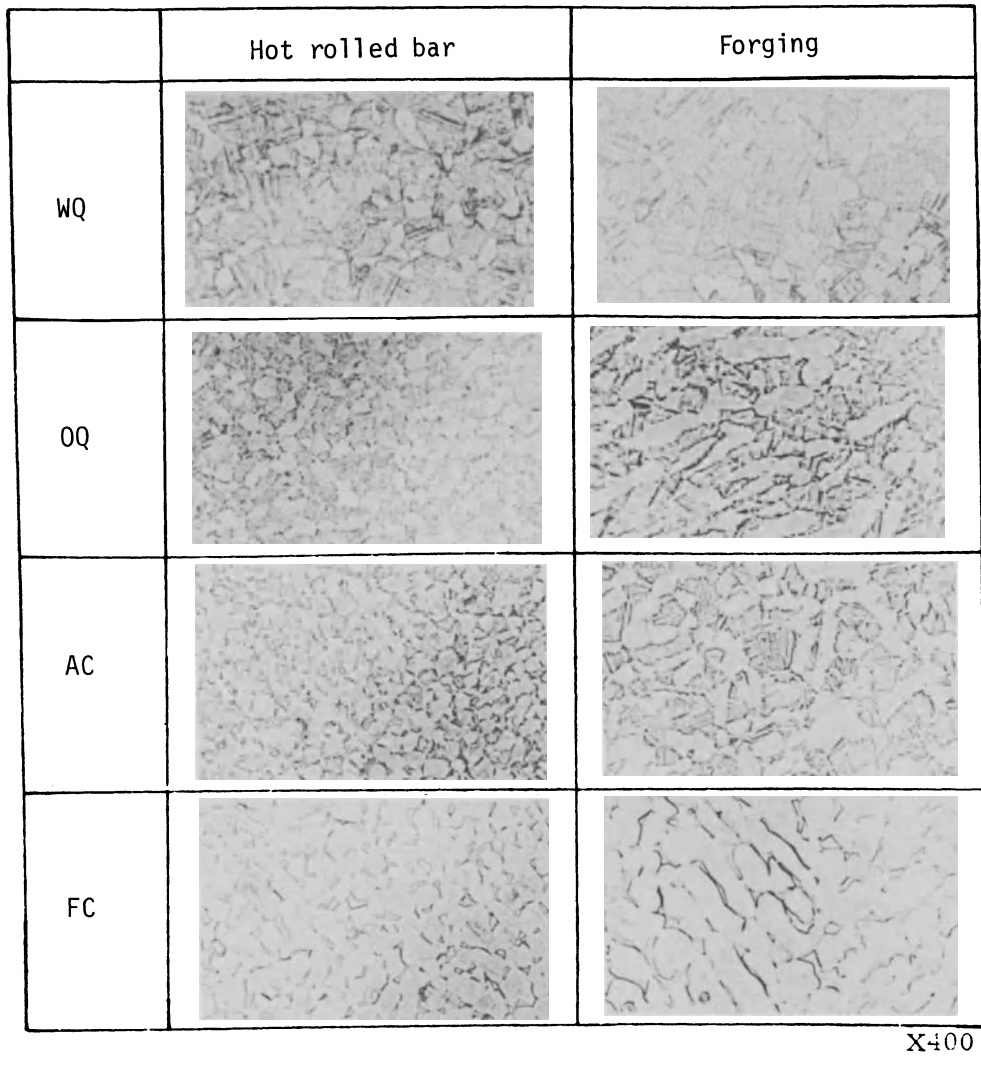

Fig. 8 - Microstructures of hot rolled bar and forging of Ti-6Al-4V, cooled at various cooling rates after the solution treatment at 950°C for 1 hour and annealed.

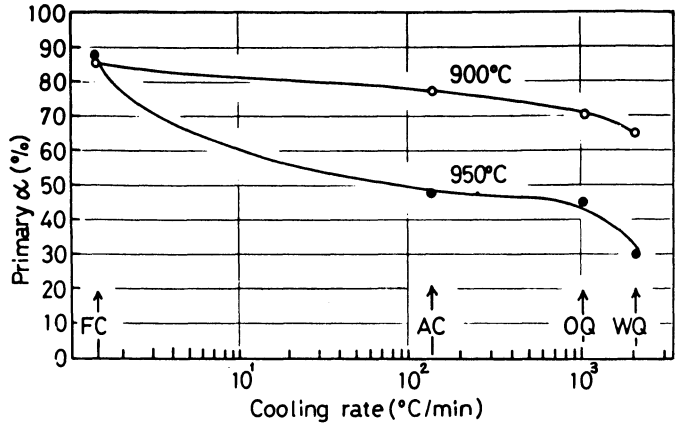

Fig. 9 - The relationship between the amount of the alpha phase and the cooling rate after the solution treatment in Ti-6Al-4V.

(4) The solution treated and annealed materials showed the lower strength at the furnace cooling, but the remarkable increase in the notched stress-rupture strength at the higher cooling rates of air cooling for both the solution temperatures of 900°C and 950°C. It was found that at the higher cooling rates after the solution treatment, the finer acicular grains formed in the transformed beta structure and the primary alpha structure decreased, and that the fine transformed beta structure with the primary alpha grains showed the better mechanical properties.

THE EFFECT OF HEAT TREATMENT ON THE FATIGUE STRENGTH OF Ti-6Al-4V

A.W. Bowen and C.A. Stubbington

Materials Department, Royal Aircraft Establishment
Farnborough, Hants, GU14 6TD, UK

Summary

An investigation has been carried out to determine the type of heat treatment likely to be most successful in increasing the fatigue strength of Ti-6Al-4V. One heat treatment only was successful, namely a solutionising and ageing treatment, which gave a microstructure of small primary α grains in a matrix of stable transformed β. It is concluded that only limited improvements in the fatigue strength of Ti-6Al-4V can be achieved by heat treatment alone, and that such treatments should be carefully controlled because of the possibility of introducing deleterious effects such as a large prior β grain size. The maximum increase in low cycle fatigue strength was obtained when the microstructure contained a high proportion of transformed β, but, unfortunately, such a microstructure did not similarly improve the high cycle fatigue properties.

Table 1

Tensile Properties of Heat Treated Ti-6Al-4V

Heat Treatment	0.2% Proof Stress (MN/m^2)	Tensile Strength (MN/m^2)	E (GN/m^2)	Elong %	Red in Area %	Fatigue Strength at 10^7 cycles (MN/m^2)	FS/TS[/]
As received (annealed)	834	906	113.7	17.5	33	496	0.55
850°C ($\frac{1}{2}$h) WQ + 500°C (8h) AC	938	1025	106	16.0	28	480	0.47
900°C ($\frac{1}{2}$h) WQ + 500°C (8h) AC	980	1070	105	15.5	24	480	0.46
950°C ($\frac{1}{2}$h) WQ + 500°C (8h) AC	1088	1158	108	12.5	34	580	0.50
900°C (1h) AC + 700°C (2h) AC	832	886	119	13.5	-	435	0.49
1050°C (1h) AC + 625°C ($4\frac{1}{2}$h) AC	913	982	120	12.0	-	510	0.52
1050°C (1h) FC to 700°C AC + 625°C ($4\frac{1}{2}$h) AC	876	917	114.5	15.0	-	448	0.49
1030°C (1h) FC to 800°C AC*	838	947	115.3	12.5	-	440	0.46
700°C TMT*	1036	1147	110.3	12.5	-	670	0.58

*from ref 3

[/] $\frac{\text{Fatigue Strength}}{\text{Tensile Strength}}$

Introduction

In previous papers the fatigue properties of commercially and laboratory processed Ti-6Al-4V bars were reported (1-3). From this work it was apparent that Stage I (shear mode) crack initiation processes were dominant in determining the smooth test piece fatigue strength of this alloy, and various methods were suggested to improve the initiation strength by thermo-mechanical treatment (TMT) (2,3). It is also possible to change the fatigue strength of Ti-6Al-4V by heat treatment, and in this paper some of these changes are reported.

Heat Treatments

The 238 mm x 57 mm forged bar used in the previous work was again studied (composition in wt %: 6.12Al; 3.97V; 0.07Fe; 0.03C; 0.001H_2; 0.072 O_2 and 0.013N_2).

10 mm square blanks were cut from the bar in the longitudinal direction and heat treated in a flowing argon atmosphere at various temperatures in the $\alpha+\beta$ and β fields. Ageing and annealing treatments were carried out in salt baths or in air. No problems were encountered with O_2 or N_2 contamination.

Heat treatments were selected (i) to study the effect of solution temperature in solutionising and ageing (STA) treatments, and (ii) to simulate fusion zone microstructures in electron beam welds. These latter treatments included a stress relieving treatment of 4.5h at 625°C which was applied to electron beam welds (4). These, and the other heat treatments, are listed in Table 1.

The hardness changes associated with the above heat treatments are shown in Fig 1; these and the microstructural changes are detailed below:

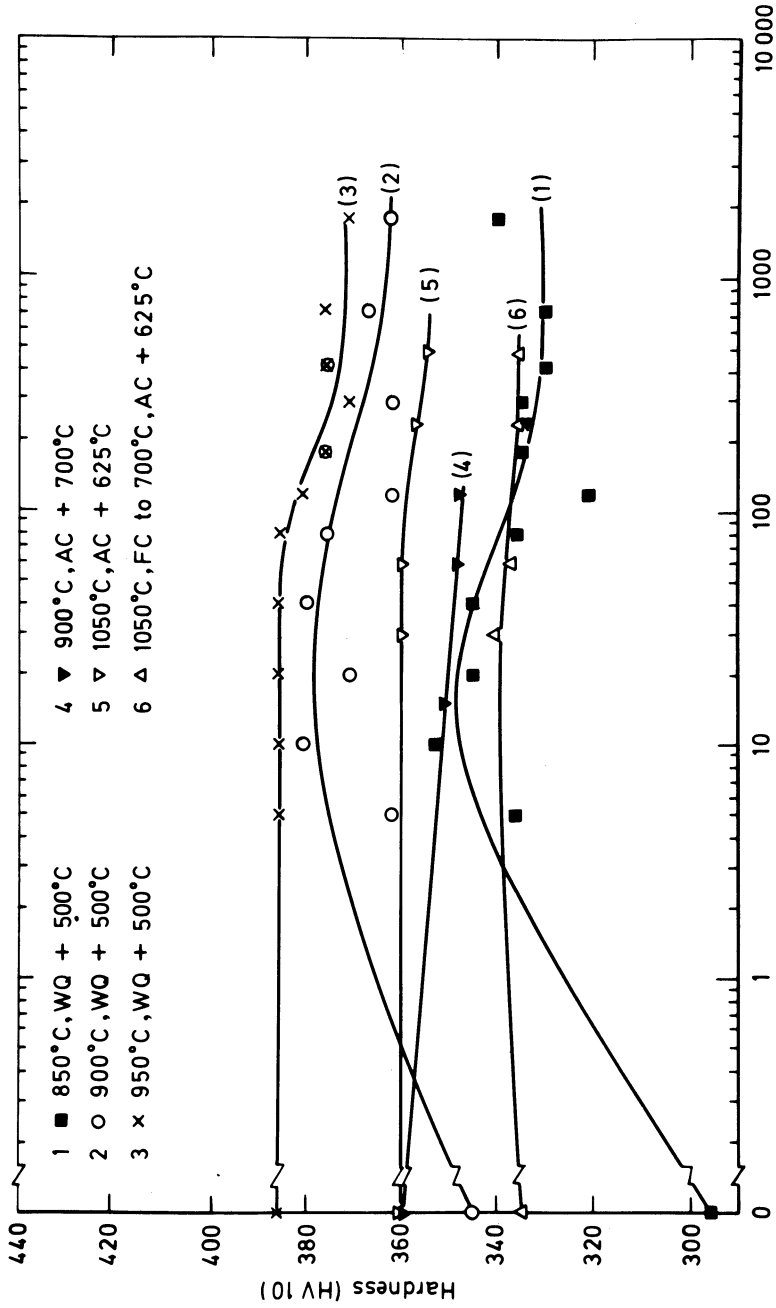

Fig. 1 - Aging curves for heat treated Ti-6Al-4V.

a. In heat treatments 1 and 2 there was an increase in hardness due to precipitation in the α' and α'' martensites*, the degree of precipitation and the hardness increment decreasing with increasing solution temperature (Figs 2(a) and (c)).

b. Heat treatments 3 and 5, however, resulted in little change in hardness, due to the much smaller degree of precipitation (Figs 2(d) and (g)).

c. Heat treatment 4 resulted in a loss in hardness, due to over-ageing and growth of both martensites (Figs 2(e) and (f)).

d. Heat treatment 6, as would be expected, produced little ageing response. The feature of interest in this microstructure is the α/β interface (Fig 2(h)), which has been shown recently to be composed of a non-equilibrium α phase (9). An example is shown in Fig 2(i) using an α phase reflection in dark field microscopy.

While a detailed investigation of phase transformations in Ti-6Al-4V was beyond the scope of this study, it is pertinent to observe that:

i α' and α'' appear to form in Ti-6Al-4V, and their ageing responses are different.

ii Ageing of α'' (which bears many similarities to that found in metastable β-titanium alloys) seems to occur by a cellular reaction (Fig 2(b)), described by Williams and Hickman in some laboratory prepared alloys (8). This is the first observation of its apparent occurrence in Ti-6Al-4V.

iii Fopiano et al (10) have also observed similarly shaped hardness curves for Ti-6Al-4V for different solution temperatures. This lends further support to (i) and (ii) above.

---

* Two martensites of different composition are believed to form (5) - a hexagonal martensite of low V content (α'), and an orthorhombic martensite of higher V content (α'') (6) (α'' is probably analogous to the initially proposed fct phase (5)). On ageing it is generally agreed that α' precipitates the β phase (6,7) but the decomposition product of α'' is less certain, although it is believed to precipitate the α phase (7,8).

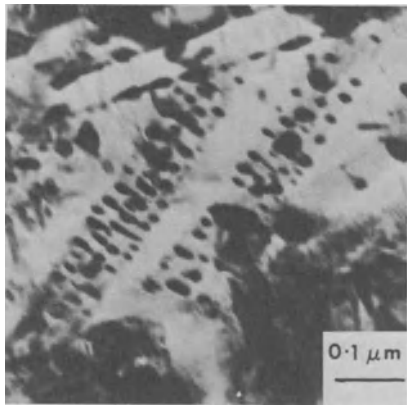

(a)

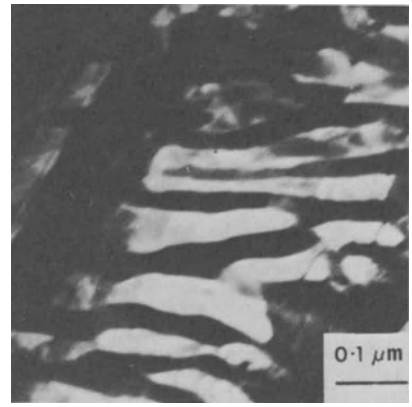

(b)

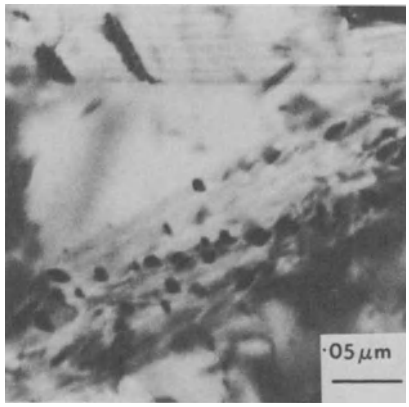

(c)

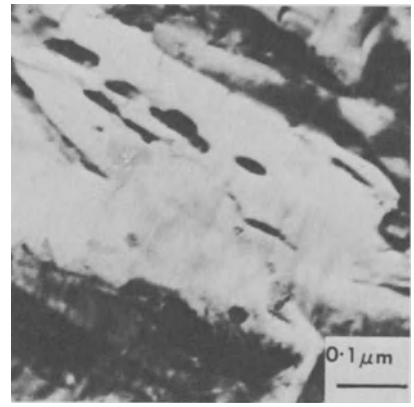

(d)

Fig. 2 - Microstructures of heat treated Ti-6Al-4V (a) and (b) 850°C/500°C (c) 900°/500°C (d) 950°/500°C (e) 900° AC (f) 900° AC/700°C (g) 1050° AC/625°C (h) 1050° FC/625°C (i) dark field from α phase reflection 1050°C FC/625°C.

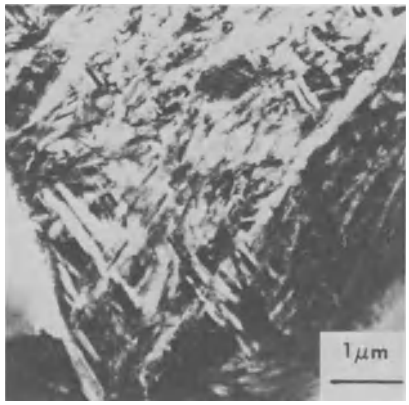

(e)

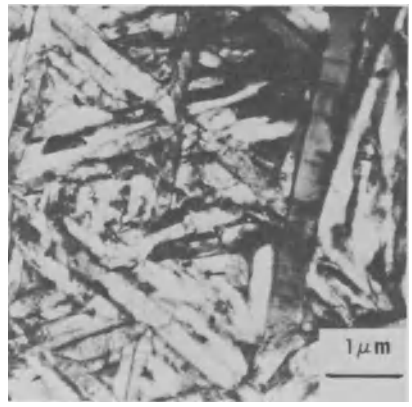

(f)

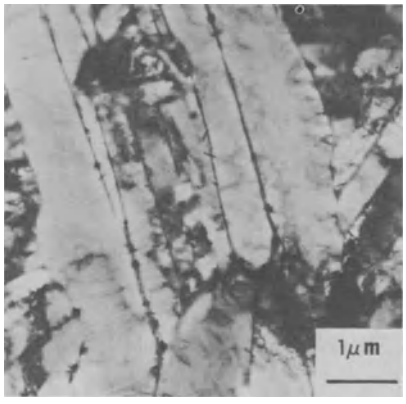

(g)

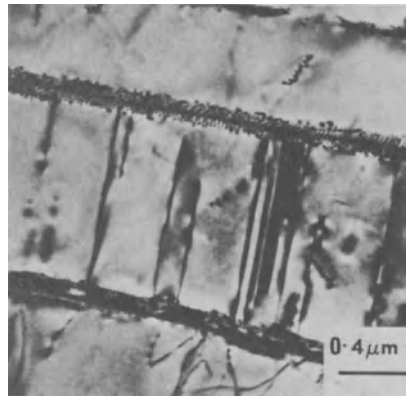

(h)

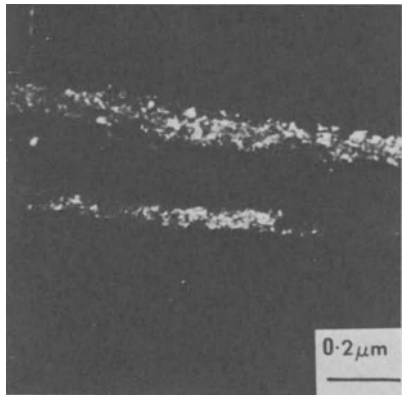

(i)

An important point to consider in any heat treatment of Ti-6Al-4V, or any other α based titanium alloy, is the possibility of texture changes. Heat treatment of the present bar below the β transus altered little the preferred orientation, but even short exposure times in the β field resulted in almost completely random textures. Thus, although the texture also changed during the present heat treatments, it is felt that the microstructural effects predominated due to the inherently inhomogeneous nature of fatigue crack initiation in Ti-6Al-4V (unpublished work).

Tensile Tests

Tensile properties were determined on machined test pieces (dimensions: 0.41 cm diameter; 3.3 cm parallel gauge length), at a crosshead speed of 3×10^{-3} sec^{-1}, and are listed in Table 1.

Fatigue Tests

S-N curves were determined on longitudinally polished rotating cantilever test pieces (0.41 cm min. diameter) at a zero mean stress and a frequency of 100 Hz, and are shown in Figs 3 (a) and (b). A noticeable feature of these results was the reduced scatter compared with the earlier as received data (11). The fatigue strengths at 10^7 cycles ranged from 435 to 580 MN/m^2. (Table 1). Metallographic studies were carried out on electro-polished rotating cantilever and torsion (3) test pieces.

Some examples of fatigue crack initiation sites are shown in Fig 4. It is suggested that the fatigue strengths of material given heat treatments 1, 2 and 4 are inferior because initiation could occur, not only in the virtually unchanged α grains (Fig 4 (a)), but also in the long α/β interfaces which are introduced (Fig 4(b) and (c)). Heat treatment 3 was superior because the primary α grain size was reduced significantly (as was the α volume fraction), and hence initiation here was virtually eliminated. Cracks formed in the transformed β (Fig 4(d)) which, although the 'weak link' in fatigue, is relatively hard (Fig 1). Heat treatment 5 was inferior

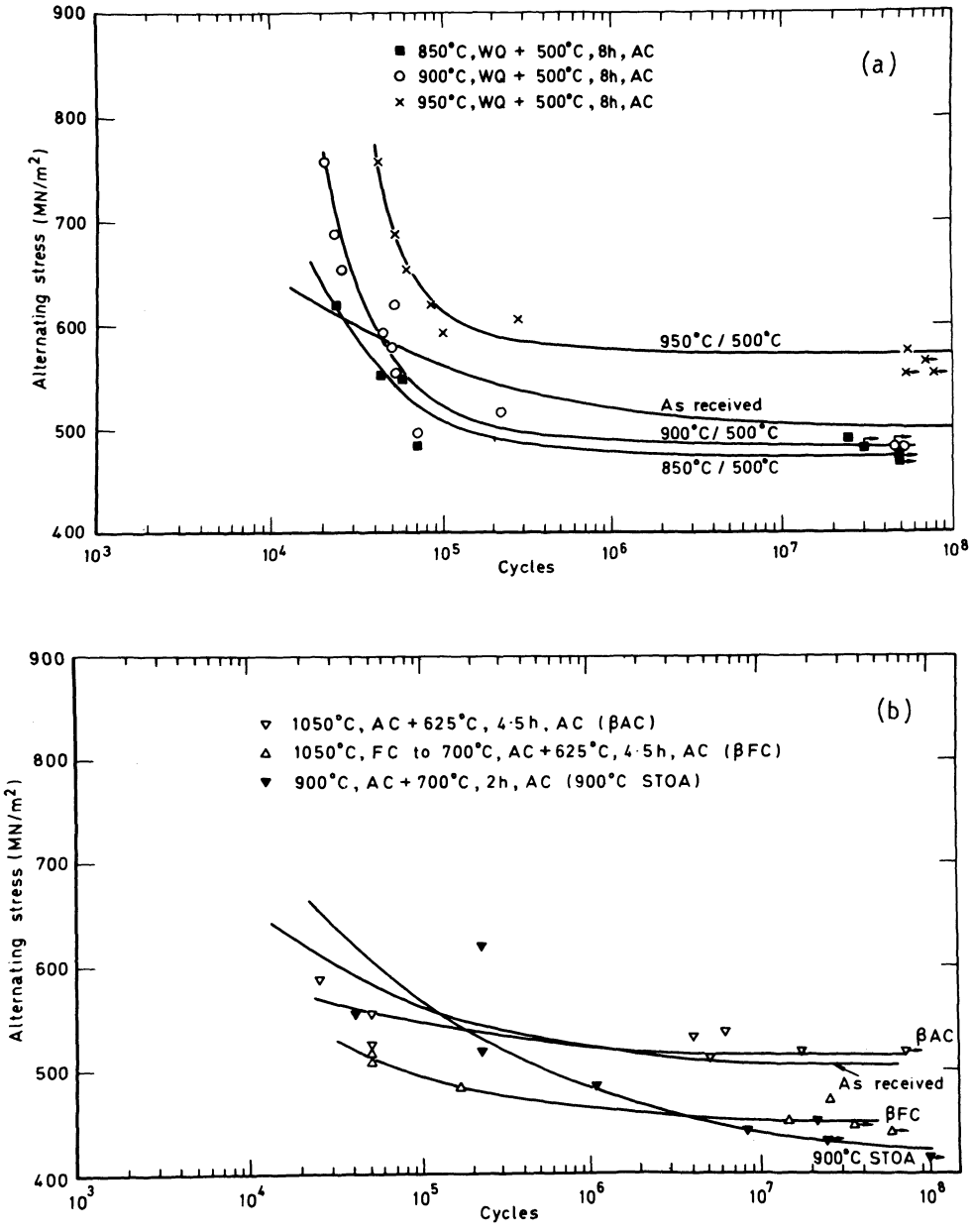

Fig. 3 - (a) and (b) S-N curves for heat treated Ti-6Al-4V.

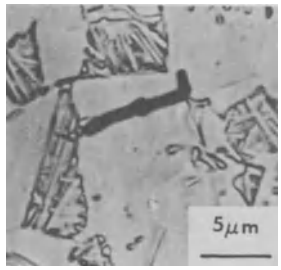

(a)

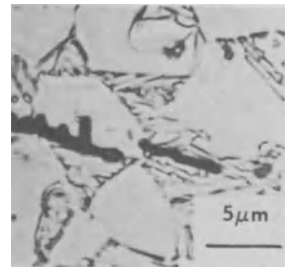

(b)

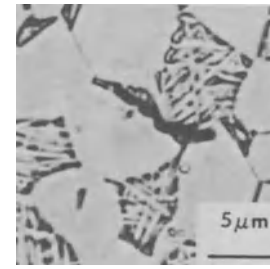

(c)

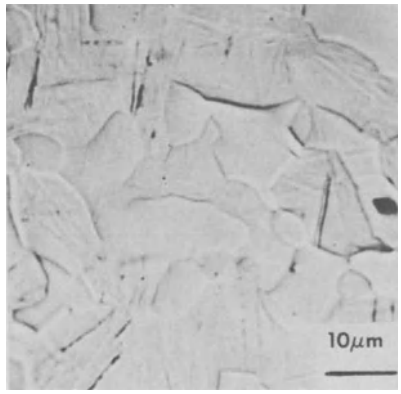

(d)

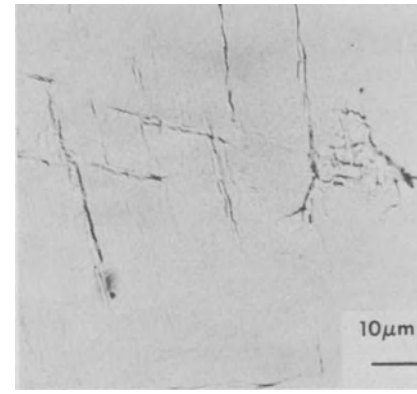

(e)

(f)

Fig. 4 - Fatigue crack initiation sites in heat treated Ti-6Al-4V (a)-(c) 900°/700°C (850°/500°C and 900°/500°C similar to (a)-(c) (d) 950°/500°C (e) 1050° AC/625°C (f) 1050° FC/625°C.

only in the low cycle fatigue (LCF) region. Thus, in spite of the moderately high hardness (Fig 1), the introduction of the large prior β grain size, and an excess of long interfaces for crack initiation (Fig 4(e)), result in a poor LCF strength. Heat treatment 6 was inferior at all stress levels due to the large prior β grain size, and long α/β interfaces which again provided an excess of crack initiation sites (A, Fig 4(f)). Transcrystalline cracking was also observed (B, Fig 4(f)).

Discussion

The present observations of fatigue crack initiation sites are in good agreement with earlier work, viz predominantly interface initiation in high cycle fatigue (HCF), and interface and transcrystalline initiation in low cycle fatigue (2,3).

The present work has shown that, to improve the fatigue strength of Ti-6Al-4V in the LCF and HCF regions, merely by heat treatment, requires:

1 A solution temperature high in the $\alpha+\beta$ field (in the present case 950°C $= \beta_T - 60°C$, where β_T is the β transus temperature), where excessive grain growth does not occur.

2 A refined primary α grain size; for example, when it is no longer the matrix.

3 A hard transformed β showing little ageing response. This phase would seem to consist only of α' martensite.

The presence of both α' and α'' martensites exerts a considerable effect on fatigue behaviour (Fig 3), and within the scope of this investigation, it is clear that:

A. Both phases are detrimental to HCF for volume fractions $\leq 100\%$, because long interfaces are introduced. This observation implies strongly that improvements in the HCF strength of heat treated Ti-6Al-4V, and other α based titanium alloys, are therefore limited.

B. 100% α' is also detrimental to the LCF behaviour because of the large prior β grain size and an excess of interface crack initiation sites.

C. Volume fractions <100% of α', and possibly α'' (and hence no excessive grain growth), seem to be beneficial to the LCF properties due, it would appear, to the inherently high strength and stability of α' and the moderate hardening response of α''.

If the improvements in fatigue strength due to heat treatment, as in the present work, are compared with those due to TMT at 850°–910°C (2), there is no difference in the HCF strength since interface initiation predominates to about the same extent in the two similar microstructures. The improved LCF strength of the TMT material is probably due to the already mentioned section size effect (1). As discussed earlier (3), the only means of further improving the HCF strength is to remove the long linear α/β interfaces which are present in the β transformation product, by lowering the working temperature to 700°C. Even in this case the primary α grain size is not refined much further, and hence the LCF strength remains the same.

Finally, it must be remembered that, in the light of the strong section size effect in Ti-6Al-4V (1), similar heat treatments of small diameter heavily worked bars would be expected to yield higher fatigue and tensile strengths than those obtained in this work. Nevertheless, the overall microstructural effects are expected to remain valid.

Conclusions

1 The only heat treatment of Ti-6Al-4V which is likely to improve the fatigue strength is a STA treatment, with the solution temperature high in the $\alpha+\beta$ field, so that the primary α grain size is reduced, excessive grain growth does not occur, and a hard stable martensite is present after subsequent heat treatment.

2 Fatigue cracks initiated in the α grains and along α/β interfaces in all microstructures. The degree of interface cracking could be modified by heat treatment, but, due to the dominant role of interface initiation, HCF improvements are limited in microstructures containing transformed β.

3 Microstructures containing 100% α' martensite are detrimental, and those containing <100% α' and α'' martensites are beneficial, to LCF strength.

4 Large prior β grain sizes, irrespective of the subsequent cooling rate, are detrimental to fatigue strength at all stress levels.

Acknowledgements

The authors would like to thank N J F Gunn for carrying out the tensile tests. Copyright © Controller HMSO London 1976.

Bibliography

1 Stubbington C A, Bowen A W Titanium Science and Technology (ed R I Jaffee & H M Burte) Plenum NY (1973) 2 1283. RAE TR 72091 (1972).

2 Bowen A W, Stubbington C A Ref 1 3 2097. RAE TR 73019 (1973).

3 Stubbington C A, Bowen A W RAE TR 73036 (1973). J Mater Sci (1974) 9 941.

4 Stubbington C A, Ballett J T Ref 1 1 601 RAE TR 72021 (1972)

5 Williams J C, Blackburn M J Trans ASM (1967) 60 373.

6 Blackburn M J, Feeney J A, Beck T R Advances in Corr Sci & Tech (ed M G Fontana & R W Staehle) Plenum NY (1973) 3 67.

7 Williams J C Ref 1 3 1433.

8 Williams J C, Hickman B S Met Trans (1970) 1 2648.

9 Williams J C, Rhodes C G Met Trans (1975) 6A 1670.

10 Fopiano P J, Bever M B, Averbach B L Trans ASM (1969) 62 324.

11 Bowen A W Ref 1 2 1271.

EFFECT OF HEAT TREATMENT ON THE MICROSTRUCTURE AND PROPERTIES OF IMI 685

P. A. Blenkinsop, D. F. Neal, and R. E. Goosey

Imperial Metal Industries (Kynoch) Ltd.
Birmingham, England

Introduction

IMI Ti 685 (Ti-6%Al-5%Zr-0.5%Mo-0.25%Si) is a weldable near-alpha alloy which was developed for high temperature creep resistance. Maximum creep resistance is obtained by beta heat treatment, allowing the alloy to be operated at temperatures up to 520°C. The $\alpha+\beta/\beta$ transus temperature of the alloy is 1020°C and the commercial heat treatment consists of a solution treatment at 1050°C followed by an oil quench and a stress relieving/ageing treatment in the range 500-550°C. IMI 685 is believed to be unique in this respect in being the only transformed beta alloy in commercial use.

Significant changes can occur in the degree of alpha phase acicularity and in crystal structure, morphology and amounts of precipitation, with variations in solution treatment and ageing parameters. These variations have been related to mechanical property changes, particularly to tensile ductility, creep resistance and stability.

Optical and electron microscopy have been used to follow microstructural changes in the alloy after heat treatment and after deformation in tensile, creep and fatigue environments.

Alloy Philosophy

In titanium and many other alloy systems, property variations can be related ultimately to the effect of the alloying constituents on transition temperatures, precipitate formation, etc and to the chosen heat treatment schedule (IMI 685 was designed to be β heat treated for maximum creep resistance, fracture toughness and weldability).

Aluminium and zirconium were added to improve tensile and creep strength of the alpha phase: their levels being chosen such that together with oxygen, the total aluminium equivalent is below that required to cause ordering instability on creep exposure ie:

$$Al\% + \frac{Zr\%}{6} + (10 \times O_2\%) < 8 \qquad (wt\ \%)$$

Molybdenum is the most potent beta stabilising element (isomorphous) in terms of its effect on tensile and creep strengthening in this type of alloy and was added to just above the alpha solubility limit. This keeps beta content and precipitation to a minimum giving good creep resistance, stability and weldability. Silicon also has the above advantages, particularly with regard to creep resistance, but has limited solubility before precipitation and consequent ductility losses occur.

In practice, therefore, heat treated IMI 685 consists of an acicular alpha titanium matrix with small amounts of beta phase precipitation.

Solution Treatment Variables

Time and Temperature

Excessive time, or more particularly temperature, above the beta transus causes grain growth which can be directly related to reduction in tensile ductility and slight strengthening. Whilst higher temperatures cause rapid average grain growth, prolonged time at slightly lower temperatures appears to cause preferential grain growth such that random grains may grow to an excessive size. Coarse grain structures are undesirable because of their adverse effects on tensile ductility, low cycle fatigue and, if slow cooled structures are present, possibly on crack propagation characteristics. Typical beta grain sizes of IMI 685 are of the order of 0.5-2 mm.

Cooling Rate

IMI 685, and indeed many similar titanium alloys are sensitive to cooling rate. Table 1 illustrates the effect of different cooling rates on room and elevated temperature tensile properties and shows the improvements obtained by oil quenching. This is particularly true of elevated temperature properties, which are illustrated in Figure 1; a plot of creep strain against cooling rate. It shows that cooling rates of the order of 1-10°C/second are required for optimum creep resistance.

From a structural standpoint, fast quenching produces a martensitic structure in IMI 685 (Figure 2); with slower cooling rates producing a progressively coarser basketweave morphology. Very slow cooling rates give an aligned nucleation and growth product (Figure 3).

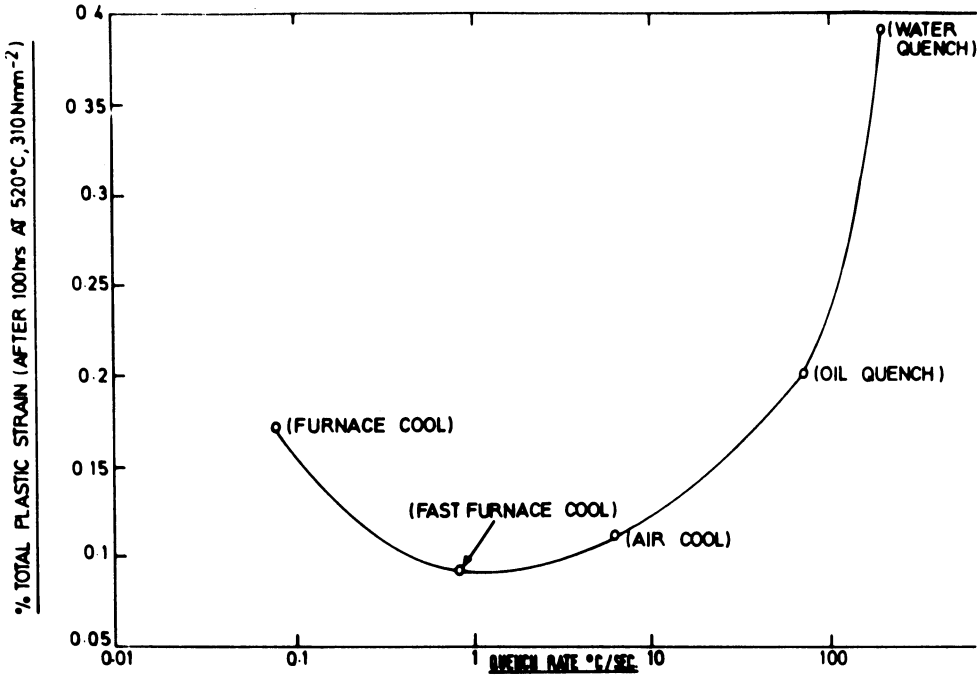

Fig. 1 - Effect of quench rate on creep resistance of IMI 685.

Fig. 2 - Typical structure of IMI 685 after oil quench.

Fast quench rates retain the precipitate forming elements Mo and Si in alpha solution and optimise alpha phase composition with respect to ductility and creep resistance. However, in larger sections. internal stress can reach high values after quenching and a compromise must be reached between mechanical properties and internal stress by careful choice of ageing/stress relieving treatments.

TABLE 1 - Effect of Quench Rate from Solution Treatment on Room and 520°C Tensile Properties of Forged Cheese

Cooling Rate from Solution Treatment	Test Temp.	0.1%PS $N.mm^{-2}$	0.2%PS $N.mm^{-2}$	UTS $N.mm^{-2}$	EL4$\sqrt{A}$ %	EL5D %	RinA %
Air cool	RT	826	846	960	11.8	9.5	18
Oil quench	RT	846	868	980	11.8	10	21
Still air cool	RT	842	849	950	10	8	16
	520°C	411	445	548	11	9.5	25
Forced air cool	RT	845	870	981	14	12	20
	520°C	448	477	609	15	12	26
Oil quench	RT	851	877	1001	13	12	18
	520°C	482	513	670	18	14.5	41

Heat Treatment 1050°C + 24 hrs/500°C

Effect of Ageing/Stress Relieving Treatments

IMI 685 exhibits fairly complex microstructural changes with time and temperature of heat treatment after beta quenching. The observable changes occur in the structure and morphology of the α needle boundary precipitation, which is always present in the alloy. Figure 4, a thin foil electron micrograph, illustrates a typical solution treated and 550°C aged structure with thin semi-continuous sheets of β phase at α needle boundaries.

Electron diffraction has shown that this precipitate may have either a body centred cubic symmetry of lattic parameter 'a' = 3.30 A, the nominal β titanium structure, or a face centred cubic structure of lattice parameter 'a' = 4.40 Å. A <110> zone axis electron diffraction pattern of the fcc structure is shown in Figure 5 and whilst this structure has been seen by the authors in other titanium alloys, it is not listed as a normal compound in these systems. Both fcc and bcc phase may occur together and the fcc

Table 2 - Effect of Ageing Temperature and Time on Creep and Tensile Properties of Billet and Disc Material

*Post creep tensile (surface retained)

Treatment	Total Plastic Strain 520°C 310 N.mm^{-2} 100 hrs %	0.2% PS N.mm^{-2}	UTS N.mm^{-2}	EL 5D %	RinA %
1050°C OQ + 24 Hours/500°C	- 0.063	888 922	1016 1013	12 11.5	23 19*
1050°C OQ + 24 hours/575°C	- 0.119	900 936	1013 1018	7 5	16 7*
1050°C OQ + 24 hours/600°C	- 0.124	883 939	999 1008	8 3	13 8*
1050°C OQ + 16 hours/575°C	-	894	1015	8.5	20
1050°C OQ + 24 hours/575°C	-	917	1016	8.5	19
1050°C OQ + 32 hours/575°C	-	942	1030	7.5	18.5
1050°C OQ + 24 hours/550°C	- 0.071	903 950	1021 1049	10 7	18 12*
1050°C OQ + 48 hours/550°C	- 0.100	912 949	1026 1048	9.5 7	15.5 13*
1050°C OQ + 24 hours/580°C	- -	912 -	1023 -	9.5 -	16.5 -
1050°C OQ + 48 hours/580°C	- -	913 -	1024 -	10 -	15 -
1050°C OQ + 24 hours/550°C	-	964	1061	9	19
1050°C OQ + 8 hours/600°C	-	965	1066	8	16
1050°C OQ + 16 hours/600°C	-	953	1049	6	15
1050°C OQ + 32 hours/600°C	-	976	1055	7	15

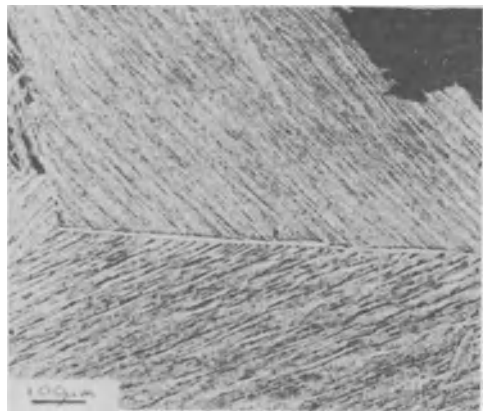

Fig. 3 - Typical structure of IMI 685 after slow cool in air.

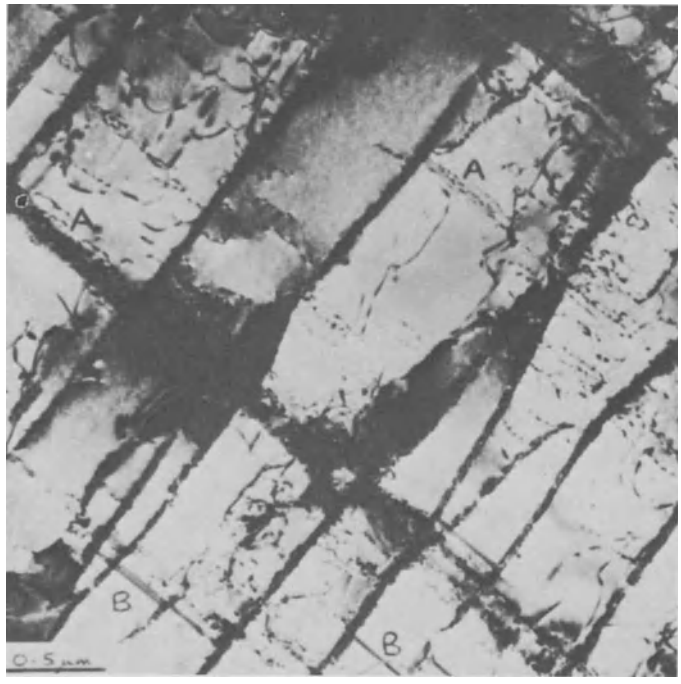

Fig. 4 - Typical structure of IMI 685 after oil quenching + 24 hr/550°C (after 5% deformation). Thin foil.

Table 3 - Effect of Intermediate Heat Treatment on Creep and Tensile Properties of Forged Billet (12 mm Section)

*post creep tensile (surface retained)

Treatment	Test Temp °C	Total Plastic Strain 520°C 310 N.mm^{-2} 100 hrs %	0.2%PS N.mm^{-2}	UTS N.mm^{-2}	EL5D %	R in A %
Control						
1050°C)	20		870	1001	9	22
Oil quench +)	20	0.056	-	-	-	-
24hrs/500°C)	520		513	638	13	45
1050°C OQ +)	20		876	986	10.5	14
950°C/1hr AC)	20	0.107	880	975	8	13.5*
+ 24hrs/500°C)	520		465	630	12	32
1050°C OQ +)	20		834	954	9	15
1000°C/1hr AC)	20	0.211	876	959	8	13.5*
+ 24hrs/500°C)	520		456	596	13.5	31
1050°C OQ +)	20	0.056	866	981	10.5	22
24hrs/500°C)	20		-	-	-	-
1050°C OQ +)	20		865	970	9	11
975°C/1hr +)	20	0.112	873	973	6.5	13*
24hrs/500°C)	520		462	603	11	23

phase tends to become more prevalent with increase in Si. There is no apparent morphological difference between these two phases and their compositions are thought to be similar.

Electron microprobe and x-ray fluorescence analysis on extracted fcc precipitate (by replica techniques), suggests that the phase consists of titanium, molybdenum and silicon and that it is related more to beta titanium than to a 'silicide' phase.

Figure 4 also illustrates a few of the deformation features of IMI 685, since the sample has received approximately 5% tensile deformation. The planar nature of the dislocation arrays is clearly seen (A) as are basal plane stacking faults (B). A feature of deformation not seen at this high magnification is that of twinning which accounts for a significant proportion of the total deformation in tensile or high stress, low cycle fatigue processes.

Planar dislocation arrays including dislocation pile-ups are seen in low cycle fatigue situations, whereas during creep deformation at temperatures around 520°C, dislocation structures are more tangled and stacking fault frequency increases.

Ageing at Higher Temperatures

Over the range 500°C to around 600°C, precipitation amounts increase without any marked change in morphology. This results in depletion of Mo and Si from the α matrix with consequent increases in yield strength and reductions in ductility and creep resistance (Table 2).

Above 600°C, morphological changes occur such that the precipitation becomes more globular (Figure 6). At around 850°C, original alpha needle boundaries, whilst still discernable, consist of dislocation networks with both inter and intra granular precipitation of globular particles. The precipitate is now a true silicide $(TiZr)_5Si_3$, and this heat treatment produces a minimum in the tensile ductility curve. These changes are basically unaffected by further lower temperature ageing treatment and properties such as those illustrated in Figure 8 are obtained.

At higher temperatures up to around 930°C, globular silicide precipitation still occurs, but at temperatures above about 930°C up to the beta transus, the precipitation reverts to a bcc sheet structure and morphology, since treatment is being carried out in the alpha plus beta phase region. Table 3 and Figure 7.

Stress Relief

The benefit of ageing above 550°C is in the relief of stress, but this also results in a loss of ductility and creep resistance.

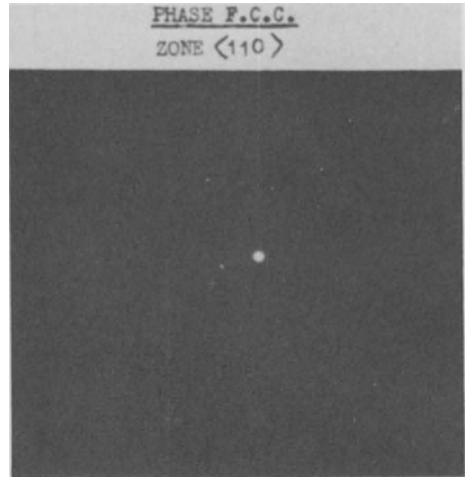

Fig. 5 - Electron diffraction pattern of FCC phase.

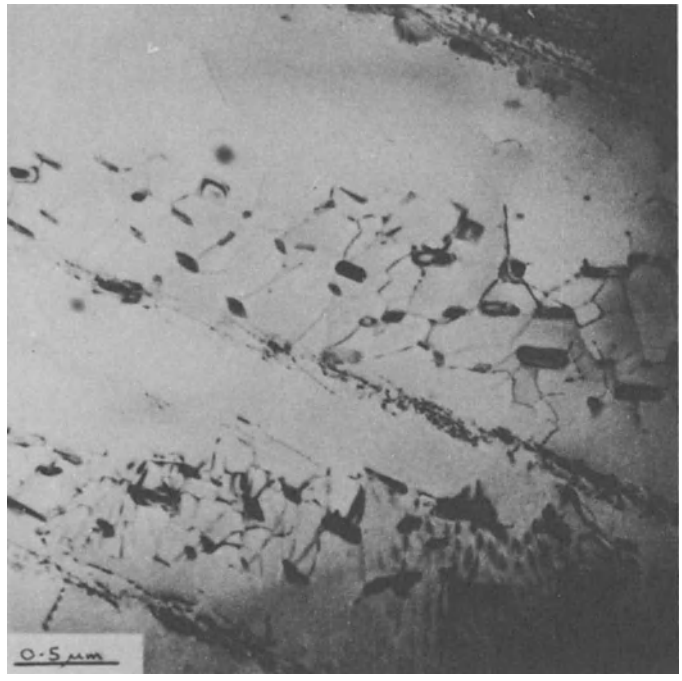

Fig. 6 - Structure after aging at 850°C. Thin foil.

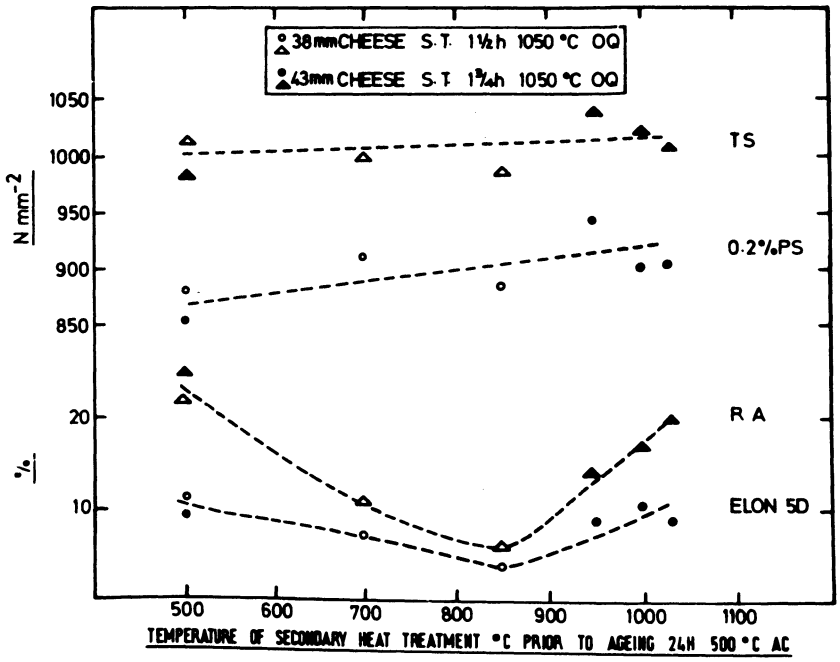

Fig. 7 - Structure after aging at 950°C. Thin foil.

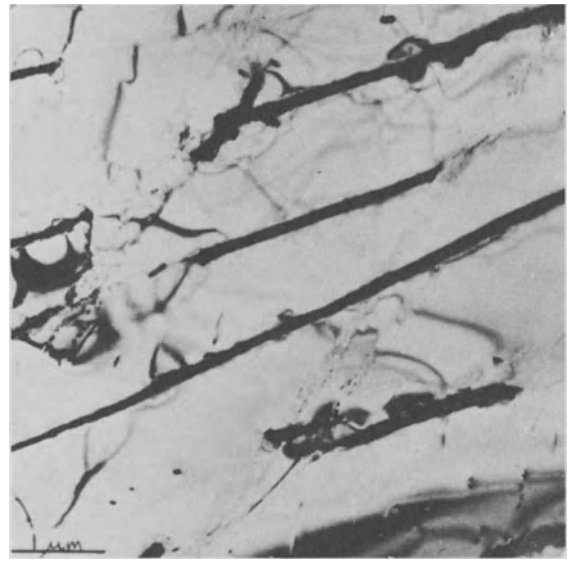

Fig. 8 - Effect of triple heat treatments on the tensile properties of IMI 685.

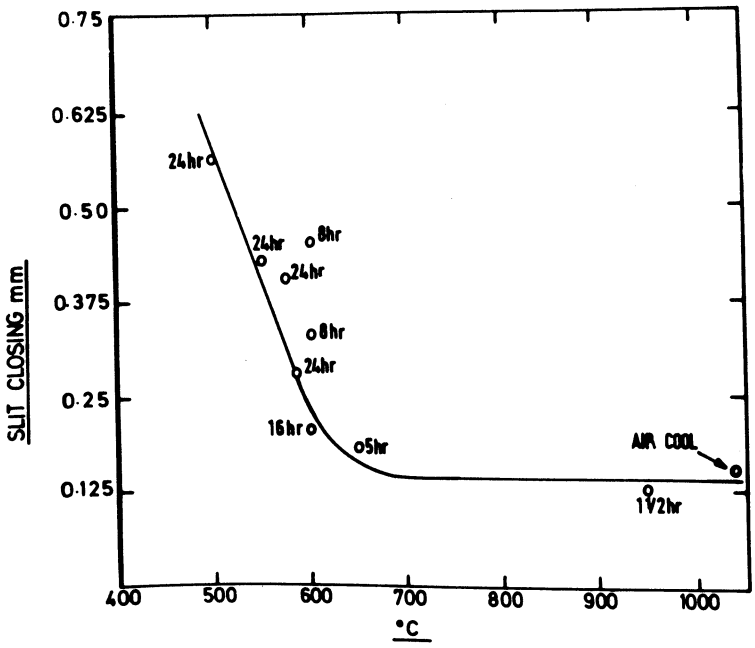

Fig. 9 - Stress relief of IMI 685. Closure of a standard slit after various stress relieving treatments.

To reduce the internal stress to that of air cooled material in large sections, treatments of around 5 hours at 650°C, or shorter times at higher temperatures are required (Figure 9). It is therefore not possible (in large sections) to relieve internal stress completely, without reductions in other properties, and this has a significant bearing on the effective stress which can be applied to such items as compressor discs. This is of much greater significance at lower temperatures because of the variation in deformation characteristics with temperature in this type of alloy. At the typical operating temperature, slip is of a more tangled nature compared with the planar slip which predominates at room temperature.

Conclusion

Alloys of the beta heat treated near alpha type containing Mo and Si are sensitive to both solution treatment and ageing parameters. IMI 685 is a typical example of this group and its mechanical properties have been related to microstructural changes which occur on heat treatment.

Increased beta quench rates which produce a change from an aligned nucleation and growth acicular α to a martensitic product,

improve tensile strength and ductility. Creep resistance, however, reaches a maximum at intermediate quench rates (1-10°C/second).

Ageing at 500-600°C increases proof stress but slightly reduces ductility and creep resistance because of precipitation of bcc beta phase or of an fcc phase which has not been previously reported. The fcc phase morphology is identical to the beta titanium and it is also believed to have a similar composition.

Ageing at higher temperatures up to ≈930°C causes precipitation of a globular silicide and a ductility minimum is reached at ≈850°C.

Above ≈930°C, the precipitation gradually reverts to a true beta titanium structure with increases in tensile ductility. However, creep resistance remains low.

Experience indicates that the very good weldability, fracture toughness and crack propagation properties of IMI 685 are little affected by these changes except in the case of high α/β heat treatments.

A COMPARATIVE STUDY OF CREEP RESISTANCE AND THERMAL STABILITY OF ALLOYS "685" AND "6242" IN AIR AND IN VACUUM

C. Quesne, C. Duong, F. Charpentier,
J. F. Friès and P. Lacombe

Laboratoire de Métallurgie Physique, Bât. 413
Université de Paris-Sud

91405 Orsay Cedex, France

INTRODUCTION

It is now well known that small silicon additions improve considerably creep resistance of titanium alloys. However, the influence of silicon on the thermal stability of these alloys is not clear. Some authors think that silicon could be the key factor responsible for instability of the alloys which contain this element (1) (2) (3). More recent studies (4) (5) have indicated that there is no appreciable hot embrittlement if the overall amount of the alloying additions is kept below certain limits.

In order to specify the role of silicium in the high temperature mechanical behavior, especially on the thermal stability of titanium alloys used in jet engines, a study of two commercial alloys of "pseudo-α" type was undertaken:

- one containing silicon : the alloy "Ti685",
- the other without any silicon additions : the alloy "Ti 6242", because it was not possible for this study to obtain a basic alloy in which small additions of silicon could be incorporated.

The mechanical properties of these alloys, creep resistance at intermediate temperatures (up to 550°C) and tensile strength at room temperature as well elevated temperature were determined and related to the microstructure resulting from different homogenizing heat treatments carried out either in β or in (α + β) range. Thermal stability (structural and superficial stabilities) of these different microstructural states were particularly studied.

1. Experimental Procedure

1.1 Materials studied. The two alloys studied* had the following composition (table 1).

Table 1 - Composition of the Alloys in Weight per cent

Alloy	Al	Zr	Sn	Mo	Si	C	N_2	O_2	H_2
685	5.87	5.18	-	0.51	0.215	0.019	0.007	0.11	0.0043
6242	6.20	3.80	1.95	2	-	0.021	0.008	0.06	0.0016

The Ti 685 was furnished in two forms:

- bars (ϕ 16 mm) heavily rolled in the (α+β) range with an initial equiaxed structure.
- plates (800x120x20 mm) forged in the β range. The structure of these plates will be called "basket weave" structure (6) and appears as criss-cross of slightly distorted coarse plate-like α grains separated by a fine edge of β phase.

The Ti 6242 was provided only in the palte form (800x120x34 mm) forged in the (α+β) range. Its structure was also equiaxed.

1.2 Heat treatments and microstructures. All heat treatments have been carried out on cylindrical samples (16 mm diameter, 60 mm length) taken directly from the forged materials. So, treatment procedure were perfectly reproducible and the cooling rate after the treatment was accurately measured (7).

* - The alloys were manufactured by UGINE ACIER Society (France).

Table 2 - Materials Studied

Forged Material	Microstructure after forming	Heat Treatment of machined bars (Ø 16 mm - length 60 mm)	Microstructure after heat treatment	N° of studied material
685 rolled bars Ø 16 mm	equiaxed	* 1050°C - 1 h-OQ + 550°C - 24 h - AC	martensitic	1
		* 1050°C - 1 h-AC + 550°C - 24 h - AC	martensitic + little Widmanstätten	2
		* 1050°C - 1 h-SC + 500°C - 24 h - AC	Widmanstätten	3
		** 900°C - 1 h-AC + 580°C - 8 h - AC	equiaxed	4
685 forged plate 120x34x800	"basket weave"	* 1050°C - 1 h-OQ + 550°C - 24 h - AC	martensitic	5
		* 1050°C - 1 h-SC + 500°C - 24 h - AC	Widmanstätten	6
		** 900°C - 1 h-AC + 580°C - 8 h - AC	"basket weave"	7
6242 forged plate 120x34x800	equiaxed	* 1050°C - 1 h-AC + 550°C - 24 h - AC	martensitic	8
		* 1050°C - 1 h-SC + 550°C - 24 h - AC	Widmanstätten	9
		** 900°C - 1 h-AC + 580°C - 8 h - AC	equiaxed	10

heat treatment normally used for "685" - 1050°C - 1 h - OQ + 500°C - 24 h - AC (8)

heat treatment normally used for "6242" - 900°C - 1 h - AC + 580°C - 8 h - AC (2)

OQ = oil quenching (33°C.s^{-1})

AC = air cooling (5°C.s^{-1})

SC - slow cooling (150°C.h^{-1})

* "beta" heat treatment

** "alpha + beta" annealing

Table 2 groups some of the treatments practiced on the alloys and indicate the microstructure obtained.

It should be noted that same heat treatment (1050°C - 1 hour) in β range, gives different ancient β grain size, depending on the original material. Mean size of the β grains is about 0.3 mm for "685" rolled bars, 1.5 to 2 mm for "685" forged plates and 0.6 mm for "6242" alloys.

For equiaxed structures, primary α grains size is about the same order of magnitude (10μm) for the two alloys (treatments n° 4 and 10), the proportion of transformed β phase being most appreciable in "6242" alloy richer in β stabilizing elements.

1.3 Creep and tensile tests. Experimental procedure used in these tests were described in details elsewhere (7) (9). However, we call again that the creep tests were carried out either in air or in vacuum (10^{-6} Torr) with continuous recording of creep curves.

The same type of specimens (4 mm diameter) were used for creep tests and tensile tests. So, it was possible to study the thermal stability by carrying out tensile tests directly on the specimens tested for creep.

2. Creep and Tensile Properties of the Alloys

2.1 Tensile properties. Tensile tests have been carried out at different temperatures between 25°C and 550°C. Tensile properties of the alloys (at 25°C and 520°C) in their diverse microstructural states are given in Table 3.

Whatever the structure or the alloy, the ductility decreases between 150°C and 300°C, then, above 350°C a PORTEVIN-LE CHÂTELIER phenomenon appears on tensile curves. These phenomena related to dynamic strain-aging, will be due to the interstitial elements specially oxygen (7).

2.2 Creep properties. Creep tests were carried out either under vacuum or in air, at different temperatures between 450°C and 540°C, and with different applied stresses. Creep properties at 520°C of the materials studied are also reported in Table 3. We remark that at this temperature, creep deformations are always higher about 480°C-500°C, then the creep curves in air show anomalous creep rates. These anomalies which we have been able to correlate directly to the oxidation phenomena (7) (9) are schematically represented in figure 1.

Table 3 - Tensile and Creep Properties of the Alloys

Alloy	N° as in Table 2	Tensile properties at 25°C			Tensile properties at 520°C			Creep properties 520°C - 31 hbar-100 h	
		0.2% proof stress (hbar)	tensile strength (hbar)	elongation (%)	0.2% proof stress (hbar)	tensile strength (hbar)	elongation (%)	elongation (%)	
								vacuum	air
	1	110	113	8	64	73	9	0.13	0.18
685	2	112	114	5	67	74	5	0.08	0.06
rolled	3	117	118	3	67	71	3	0.05	0.05
bars	4	92	99	15	48	63	17	0.45	0.77
685	5	94	101	8	53	66	9	0.24	0.30
forged	6	82	88	4	43	50	8	0.80	1
plate	7	89	94	10	48	60	11	0.32	0.40
	8	92	100	8	60	67	11	0.21	0.26
6242	9	86	95	6	47	57	9	0.18	0.24
	10	95	102	13	55	69	14	0.40	0.45

2.3 Discussion. Concerning high temperature strength, conclusions which are deduced from Table 3, are in good agreement with numerous other works.

- The homogeneization treatments in β range lead to a better creep resistance than the treatments in (α+β) domain. In the case of β treatments, it appears from our results on "685" that two simultaneous phenomena act on creep resistance:

* influence of preliminary thermomechanical treatments.

* influence of the β grains size after heat treatments.

Our observations agree with those of :

- firstly, Morton and Blenkinsop (10) who have shown that after treatments in the β range, alloy with fine β grains size had better creep resistance than the same material with coarse grains.

- secondly Parris and Russel (11) have already pointed out the existence of difference in the results of elongation (ratio 1 to 5) in the case of "Ti 11" alloy depending on whether the specimens were taken from bars forged in (α+β) range or from plates forged in the β range, this, for identical heat treatment (1050°C + A.C.) and creep conditions.

- Best compromise between creep resistance and ductility is obtained by acicular structures formed by rapid cooling from the β range.

- For similar microstructures, alloy Ti 685 possesses better creep resistance than Ti 6242. That confirms the beneficial effect of silicon on high temperature strength. Besides, the present tendency is to incorporate small additions of silicium in the basic "6242" alloy.

3. Thermal Stability of Alloys

3.1 Definition. Use of titanium alloy at high temperatures involves besides high creep resistance, a good thermal stability, that is an absence of embrittlement after long time holding at elevated temperatures (several hundreds or thousands hours) with or without applied stress. Thermal stability represents the capacity of the alloy to retain adequate toughness and ductility properties even after prolonged service at elevated temperatures. There are two factors of embrittlement or hot unstability (2):

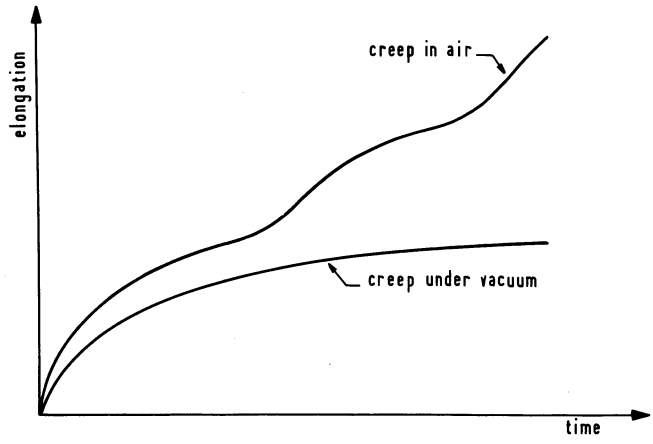

Fig. 1: Schematic creep curves of alloys tested in air and under vacuum (at same temperature and same stress).

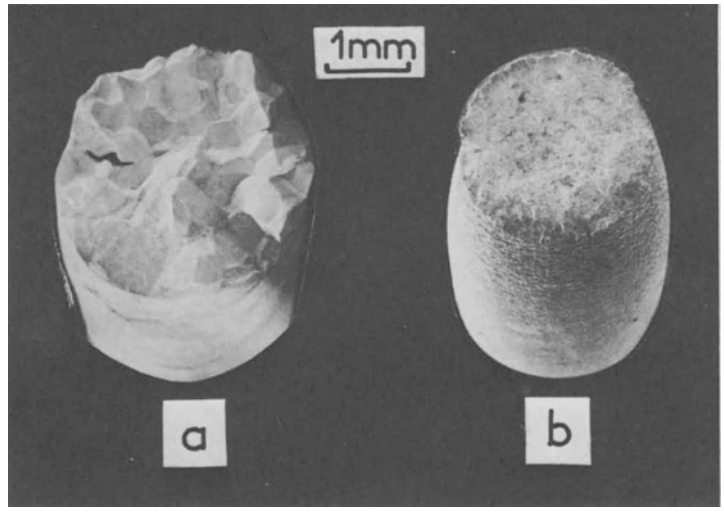

Fig. 2: Creep specimens failed in creep tests in air, at 520°C, with an applied stress of 31 hbar.
2.a: martensitic structure.
2.b: equiaxed structure.

- the first, due to structural evolution of alloys (internal unstability),

- the second, due to oxidation phenomena which are produced at the surface of the specimens (superficial unstability).

3.2 Results. In order to separate the two forms of unstability, we have carried out for each alloy (in its normally used structural state) simultaneous prolonged holdings in air and under vacuum, at temperatures between 460°C and 540°C, specially at 520°C with or without applied stress. In each case, we have studied structural evolution and compared the tensile properties at room temperature before and after holding at elevated temperature without any intermediate surface preparation, and examined tensile specimens by scanning electron microprobe.

We have observed some modifications in the microstructure (7) and a perceptible decrease in ductility only for holding time longer than 500 hours at temperatures above 500°C.

Tensile properties of two alloys after 1000 hours holding at 520°C, in different conditions are compared to their initial properties in Tables 4 and 5.

3.3 Discussion. Whatever the conditions (in air or under vacuum) for a same applied stress, the difference between properties after holding in air or holding under vacuum, will be due to oxidation phenomena.

Concerning Ti 685 (table 4) stress effect or oxidation effect alone applied, do not affect very much the ductility of the alloy. On the other hand, if these two effects are associated, we can observe a catastrophic embrittlement of the material.

In the case of Ti 6242 (Table 5) decrease of ductility after creep in air is also more important than after creep under vacuum but considering the appreciable amount of deformation in creep (about 5%), the embrittlement due to superficial contamination by atmosphere is less pronounced than for Ti 685.

It will be possible to attribute the difference between the thermal stability of each alloy, to the presence of silicon in Ti 685. In fact, the two alloys are not used in the same structural state : the structure of 685 is acicular with coarse β grains (β forged plate) while the structure of 6242 is equiaxed. It seems that the equiaxed structure will be tougher to the propagation of cracks formed in superficial oxide layer (7) (9) than the acicular structure. In order to verify this hypothesis, we have carried out "rupture-creep" tests in air and under vacuum, both for Ti 6242 with equiaxed structure and for Ti 6242 heat treated in β range

Table 6 - "Rupture-creep" Tests on 6242 (520°C-31 hbar)

Structure	Conditions	Tr (h)	$\dot{\varepsilon}$ (h^{-1})	tertiary creep
equiaxed	air	1160	1.2×10^{-4}	with
	vacuum	1430	9×10^{-5}	with
martensitic	air	750	1×10^{-5}	without
	vacuum	no failure in 1500	8×10^{-6}	?

Tr = time to rupture $\dot{\varepsilon}$ = mean creep rate between 200 and 600 h.

Table 4 - "685" thermal stability.
Evolution of room-temperature tensile properties
after 1000 hours holding time at 520°C under different conditions

holding conditions		0.2% proof stress (hbar)	tensile strength (hbar)	elongation (%)	reduction in area (%)
before exposure		94	101.5	8	28
unstressed	in vacuum	95.5	101.5	6.6	19
	in air	96	101.5	5.9	14.5
stressed 31 hbar	in vacuum	101	104	5.7	18
	in air	102.7	102.9	0.3	8

Table 5 - "6242" thermal stability.
Evolution of room-temperature tensile properties
after 1000 hours holding time at 520°C under different conditions

holding conditions		0.2% proof stress (hbar)	tensile strength (hbar)	elongation (%)	reduction in area (%)
before exposure		95	102	13	28
unstressed	in vacuum	105	109.5	10	24
	in air	107	112	8	26
stressed	in vacuum	94	94.5	10	31
	in air	102	108.8	7	16

with martensitic structure comparable to the normally used structure of Ti 685. The results of these tests are indicated Table 6.

Scanning electron micrographs of fracture surface of samples failed during creep tests in air are shown in figure 2.

In the case of an equiaxed structure (figure 2.b) the rupture is ductile, on the other hand, in the case of an acicular structure (figure 2.a), a brittle rupture appeared by sudden intergranular decohesion along the ancient β grains boundaries. The α phase which marks the ancient β grains boundaries, is a preferred path for the penetration of oxygen and/or nitrogen in the alloys because of the α stabilizing nature of these elements.

CONCLUSIONS

For similar microstructures the alloy Ti 685 possesses a better creep resistance than the alloy 6242, which confirms the beneficial role of silicon on the high temperature strength. Though a structural evolution of the alloys might be observed, phenomena of superficial oxidation are mainly responsible for the embrittlement observed after long time holding at elevated temperatures, specially if the holding is carried out with applied stress.

These phenomena of "stress corrosion" in air are very important in the case of acicular structures obtained by homogeneizing in the

β range, though these structures are more creep resistant than equiaxed structures.

These conclusions on superficial embrittlement of the alloys are in good agreement with several other authors (1) (12) (13) (14).

ACKNOWLEDGMENTS

This work was sponsored by the "Direction des Recherches et Moyens d'Essais "(D.R.M.E. Contrats n° 73/063 and 74/016) of Ministère des Armées. The authors wish to thank the D.R.M.E. for permission to publish the results of this work and to express their appreciation to Mr. G. BESSONNAT for his high interest and encouragement.

REFERENCES

1. Erdeman, V. J. and Ross, F. W., The Science Technology and Applications of Titanium. Jaffee and Promisel, London 1970, p. 829.

2. Tricot, R. and Séraphin, L., Chambre Syndicale des Producteurs d'Aciers Fins et Spéciaux, Paris, N° Spécial Aviation, Le Bourget, 5 juin 1969, p. 128.

3. Imbert, Y., Thesis - Université Paris-Sud, Orsay France, Avril 1973, S.N.E.C.M.A., Corbeil.

4. Rosenberg, H. W., The Science Technology and Applications of Titanium. Jaffee and Promisel, London 1970, p. 851.

5. Bomberger and al.
Technical Report AFML-TR 70-125, Air Force Laboratory, Air Force Systems Command, Wright Patterson Air Force Base, Ohio, July 1970.

6. Syre, R. and Saulnier, A., Revue de Métallurgie, 55, 1958, p. 442.

7. Quesne, C., Duong, C., Charpentier, F., Friès, J. F. and Lacombe, P., Communication présentée aux Journées d'Automne de la Société Francaise de Métallurgie, Octobre 1974, Paris. To be published in Mémoires Scientifiques de la Revue de Métallurgie.

8. Projet de Norme, Association internationale des Constructeurs de Matériel Aérospatial, Paris 1970.

9. Quesne, C., Friès, J. F., Cizeron, G. and Lacombe, P., 3èmes Journées d'Etudes du Titane et de ses Alliages - Tome II. E.N.S.M., Nates (France), 17-18 mai 1973.

10. Morton, P. H. and Blenkinsop, P. A., Report of Imperial Metal Industries, Kynoch, Witton, Birmingham, B. 67 B.A., 19th march 1974.

11. Parris, W. M. and Russel, H. A., Titanium Science and Technology, Boston 1973, p. 2219.

12. Antony, K. C., Journal of Materials, Vol. 1,n°2, June 1966, p. 456.

13. Shamblen, C. E. and Redden, T. K., The Science Technology and Applications of Titanium, Jaffee and Promisel, London, 1970, p. 199.

14. Zwicker, U. and Kalsch, E., The Science Technology and Applications of Titanium, Jaffee and Promisel, London, 1970, p. 299.

EFFECTS OF TiA16V4 METALLURGICAL STRUCTURES ON FATIGUE PROPERTIES

U. Zwicker, M. Blass, and U. Hofmann

Lehrstuhl Werkstoffwissenschaft (Metalle)
Universität Erlangen-Nürnberg, F.R. Ger.

Influence of hot rolling temperature on fatigue strength

There are many investigations on the influence of microstructure on the fatigue strength of TiA16V4 which have shown that large grain size material with Widmannstätten structure has a much lower fatigue strength than fine grain size material with an equiaxed structure. By aging processes the fatigue strength can be increased but the ratio between tensile strength and fatigue strength is in most cases decreased (1) - (7).

Table I: Composition of materials

Alloy	Al%	V%	Fe%	N%	C%	H%
TiA16V4 (o.12%O)	6.3	4.1	o.13	o.o11	o.o23	o.oo4
TiA16V4 (o.o9%O)	6.o	4.o	o.12	o.o2	o.o2	o.oo2
TiA17V2 (~o.o9%O)	7.o	2.o	~o.o1	~o.o2	~o.o2	~o.o1
TiV7A14.5 (~o.o9%O)	4.5	7.o	~o.o1	~o.o2	~o.o2	~o.o1

To investigate the influence of hot rolling temperature samples of 15 mm Ø TiA16V4 (o.12%O) rod, the composition of which is given in Table I, were hot rolled(65%) at 76o° in three deformation steps and at three other temperatures in two deformation steps. Between each deformation step and after the final rolling step the samples were annealed for 5 min. at the hot rolling temperature

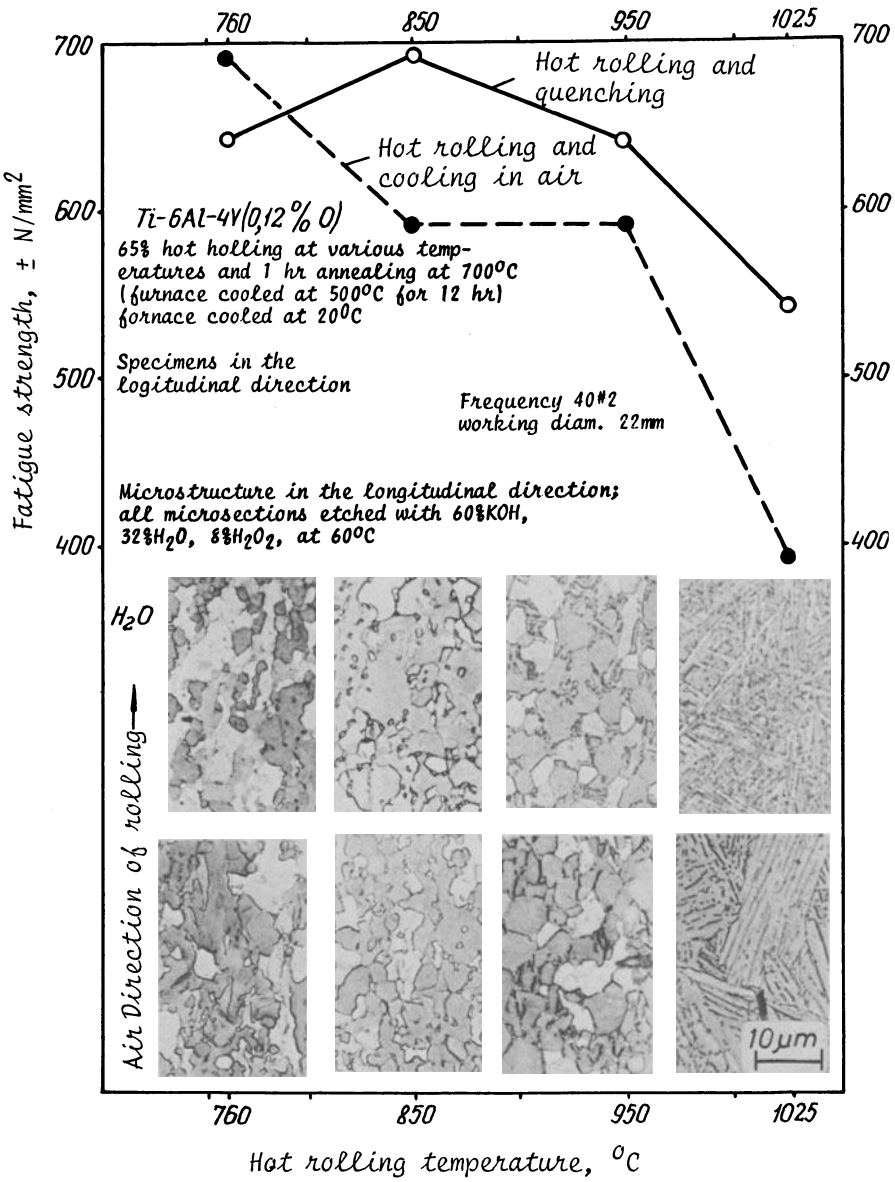

Fig. 1 - Influence of hot rolling temperature and cooling rate from hot rolling temperature of stabilized Ti-Al-6-4V on fatigue strength (10^7 cycles).

and afterwards either quenched in water or cooled in air and stabilized by annealing. From Fig.1 one can see that samples hot rolled in the β-area at temperatures higher than 950°C show a sharp decrease of the fatigue strength together with a Widmannstätten type structure. Samples which were waterquenched before they were heat treated show - besides the samples of 760°C rolling temperature - a lower fatigue strength than samples cooled in air. Optimum rolling temperature seems to be 950°C because the pressure necessary for deformation is small and because the micrographs do not yet show a Widmannstätten structure. The anisotropy of the mechanical properties in different directions of the sample geometry after rolling at 950°C is also much smaller than at lower rolling temperatures because the amount of the β-solid solution phase at the oxygen content of o.12%0 is more than 5o % (18). Fig.2 shows hardness measurements which were done on these samples on surfaces parallel (II) and perpendicular (⊥) to the rolling direction. At 950°C and 1025°C hot rolling temperature no difference in hardness after annealing occurs, whilst at lower rolling temperatures hardness on surfaces parallel to the rolling direction shows higher values than on the surfaces perpendicular to the rolling direction.

Fatigue strength and heat generation after different modes of heat treatment (hot rolling temperature 950°)

To investigate the influence of other heat treatments after hot rolling at 950°C three different modes of heat treatment were applied. The samples were air cooled after hot rolling without furher annealing at rolling temperature. The micrographs of the samples given in Fig.3a-d show that only in the 880°C/H_2O quenched and 6 h 515°C annealed samples (Fig. 3 d) the β-solid solution area was etched dark which means that the β-phase has precipitated small particles of α-solid solution (9-13). Only with these samples at a alternating stress of more than 700 N/mm^2 no measurable increase of the sample temperature by internal friction was observed. The other samples showed an increase of sample temperature up to about 1000°C at alternating stresses of ±700 and ±750 N/mm^2.

Influence of fatigue measurement variables on sample temperature after water quenching from 880°C

To investigate the effect of sample diameter between 2.2 and 5.o mm of samples with different grain size the initial 15 mm Ø rod which had a small grain size (Fig.4a) was annealed 5 min. at 1025°C air cooled and after a second heat treatment of 1/2 h at 880°C quenched in water.

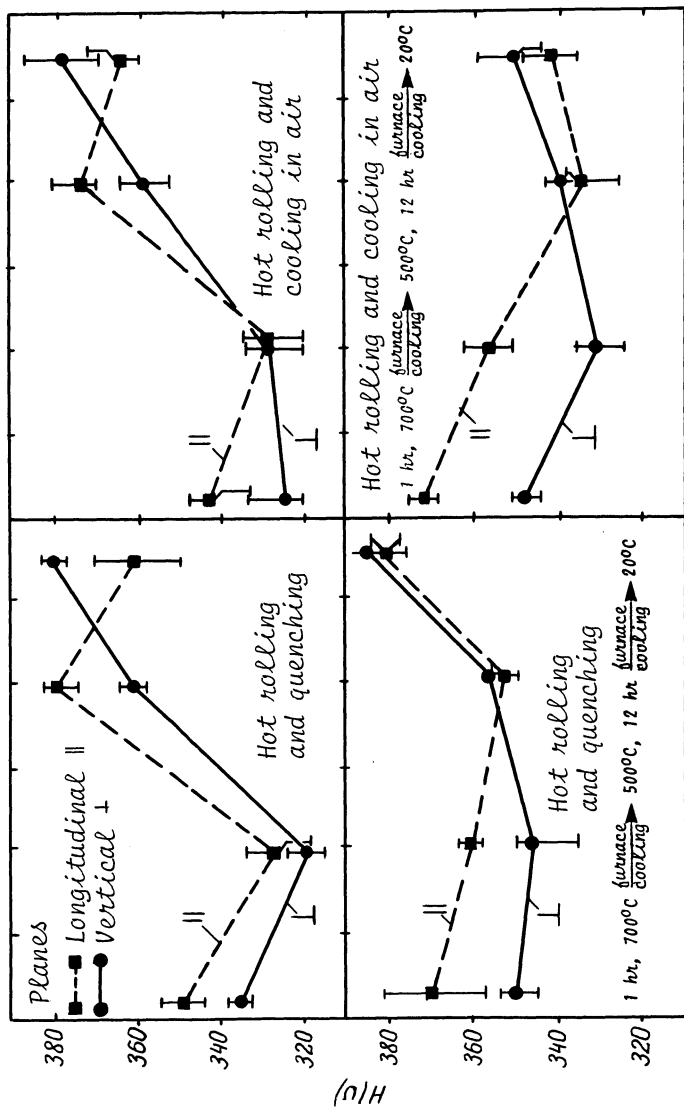

Fig. 2 - Influence of direction of the surface on VHN at different hot rolling temperatures and heat treatment.

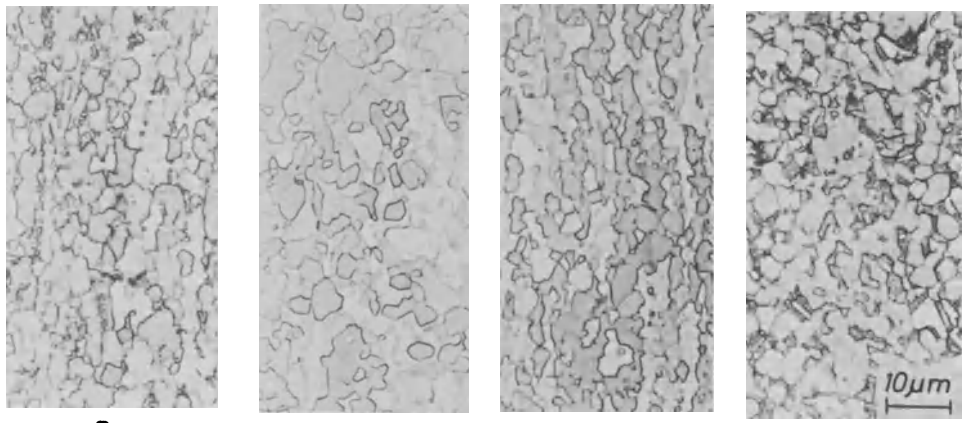

Fig. 3a-d Micrographs of samples hot rolled at 950°C (etching Fig. 1).

a) as rolled, air cooled VHN ⊥ 323±6
VHN \\ 334 (+10,-5)

b) 2h 750°C furnace cool→550°C/air VHN ⊥ 339 (+5,-10)
VHN ∥ 334 (+10,-5)

c) 30 min 880°C/H_2O VHN ⊥ 322 (=8,-6)
VHN \\ 337 (+7,-8)

d) 30 min 880°C + 6h 515°C/air VHN ⊥ 376±0
VHN ∥ 376±0

The micrograph of such a sample (Fig. 4 b) shows Widmannstätten structure. There is only a small difference of the fatigue strength values by the variation of diameter and frequency (34-12o Hz) as can be seen from Table II.

Table II: Fatigue strength of samples with different grain-size and microstructure ($1o^7$ cycles).

Sample Ø mm	frequency Hz	grain size	fatigue strength N/mm^2
2.2	4o	small equiaxed	± 6oo
3.57	12o	"	± 625
2.2	4o	grain size large, Widmannstätten	± 4oo
3.57	4o	"	± 4oo
3.57	12o	"	± 35o
5.o	34	"	± 4oo

The samples with a large grain size have in all cases a much smaller fatigue strength than the samples with a fine grain size. No measurable increase in the sample temperature during the fatigue tests in these samples was observed whilst the large grain samples increased their temperature even at the fatigue strength of ± 4ooN/mm^2. Fig.5 shows this increase of temperature at different alternating stress. Between 4oo and 52o N/mm^2 a plateau of constant temperature after 5ooo - 1o ooo cycles is observed the temperature of which is increased with increasing alternating stress. At a alternating stress of ± 525 N/mm^2 the temperature is increased at less than 1ooo cycles, breaking occurs after a maximum temperature of about 15o°C. At a alternating stress of ± 6oo N/mm^2 the sample temperature increased to more than 1ooo°C and the sample breakes because the fatigue strength at this temperature is very low.

The influence of increasing alternating stress at constant frequency on the sample temperature of from 88o°C water quenched large grain samples with 1o mm Ø in the testing area is shown in Fig.6 for TiA16V4 (o.12%O). There is a great increase of sample temperature with increasing frequency. If the frequency is increased at constant alternating stress the sample temperature at the same frequency and stress is lower than the values obtained by increasing the alternating stress at constant frequency. Fig.7 shows the increase of temperature of 1o mm Ø samples with increasing frequency at different alternating stress. Decreasing the testing diameter from 1o to 5 mm reduces the sample temperature because the volumen-

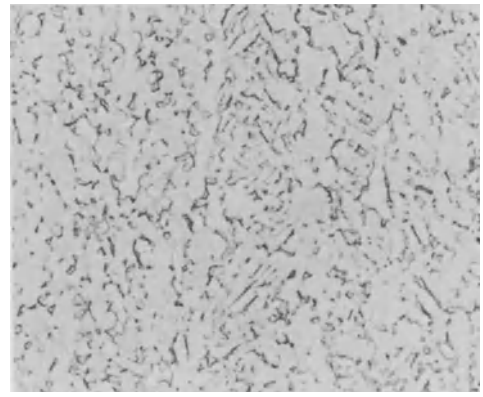

a

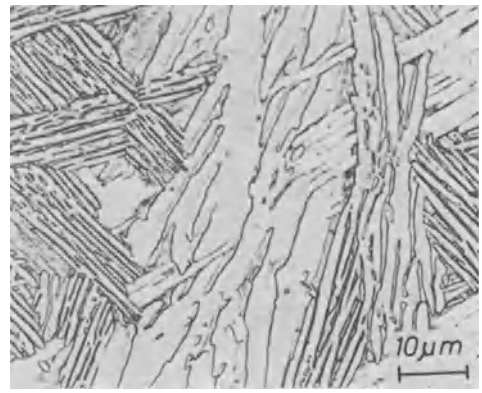

b

Fig. 4a-b Micrographs (etching Fig. 1)

a) 15 mm Ø rod as delivered, fine grain size equiaxed microstructure VHN ⊥ 337 (+8,-1)
VHN\\ 339 (+2,-9)

b) 5 min 1025°C/H_2O + 30 min 880°C/H_2O large grain Widmanstätten microstructure VHN ⊥ 331 (+5,-9)
VHN\\336 (+9,-0)

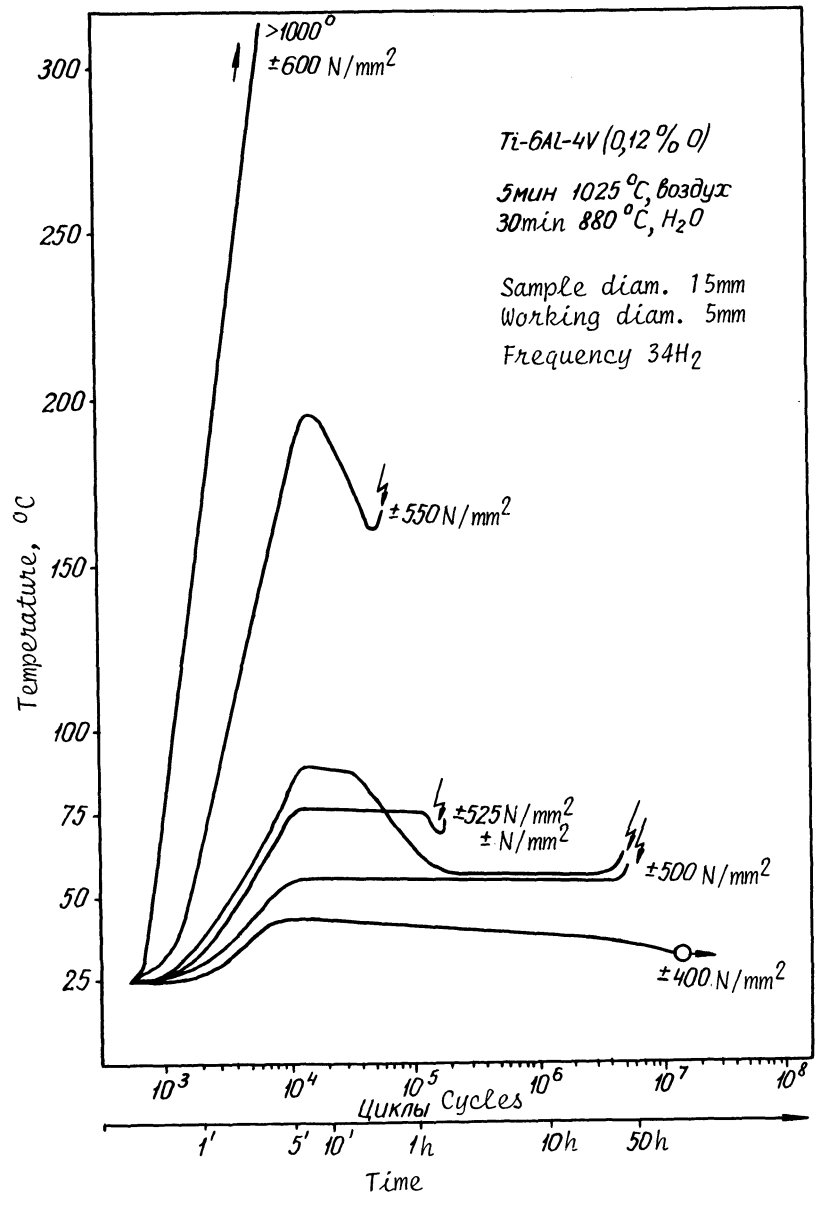

Fig. 5 - Increase of sample temperature during cycling time.

surface ratio was changed. Fig.8 shows this effect and also the influence of the oxygen content. Decreasing the oxygen content from o.12 to o.o9 % reduces the increase of the sample temperature with increasing frequency remarkably. This increase of temperature depends also to a large degree on the initial frequency. If, as Fig.9 shows the testing of the sample is started at a higher frequency the sample temperature is much higher than with samples which were stressed at lower frequency beforehand (2o ooo cycles at each frequency).
There are also differences in sample temperature by increasing the frequency at the beginning of the test compared with increasing the alternating stress. For example increasing the frequency from 1o to 7o Hz at $\pm$ 4oo N/mm^2 and lowering the frequency after that to 4o Hz and increasing the alternating stress to $\pm$ 6oo N/mm^2 increases the sample temperature to 4o°C, whilst increasing the alternating stress at 4o Hz from $\pm$ 25o N/mm^2 $\rightarrow\pm$ 3oo N/mm^2 $\rightarrow$ $\pm$ 4oo N/mm^2 $\rightarrow\pm$ 5oo N/mm^2 $\rightarrow\pm$ 6oo N/mm^2, the same final frequency and final alternating stress, increases the sample temperature to 5o°C. Fig.1o shows the area of sample temperature which was observed after different modes of increasing frequency or alternating stress. This area is increased with increasing final alternating stress.

Influence of annealing time at 88o°C on sample temperature and number of fatigue cycles

An initial fine grain size of the microstructure given in Fig.4a can be increased to about 15 µm after 9o h annealing at 88o°C (14 - 15). To investigate the influence of the annealing time at this temperature samples were annealed between o.25 and 9o h. The results are given in Fig.11. There is an increase of sample temperature which comes to an equilibrium temperature after about 1o ooo cycles at the alternating stress of $\pm$ 5oo N/mm^2 between o.25 and 4 h annealing time. Increasing the annealing time to 5o or 9o h decreases the sample temperature. A maximum sample temperature may occur after 5 h annealing time. The number of cycles for breaking the samples at the alternating stress of $\pm$ 5oo N/mm^2 was decreased from $>1o^7$ cycles (o.25 h) to $1o^5$ cycles (9o h).

Influence of α- and β-phase on sample temperature

To investigate the influence of the α-and β-solid solution on the increase of temperature three alloys were prepared by melting 2oo g ingots of TiA16V4, TiA17V2 and TiV7A14.5. The composition of the second and the third alloy corresponds to the α- and β-phase composition at 88o°C respectively.

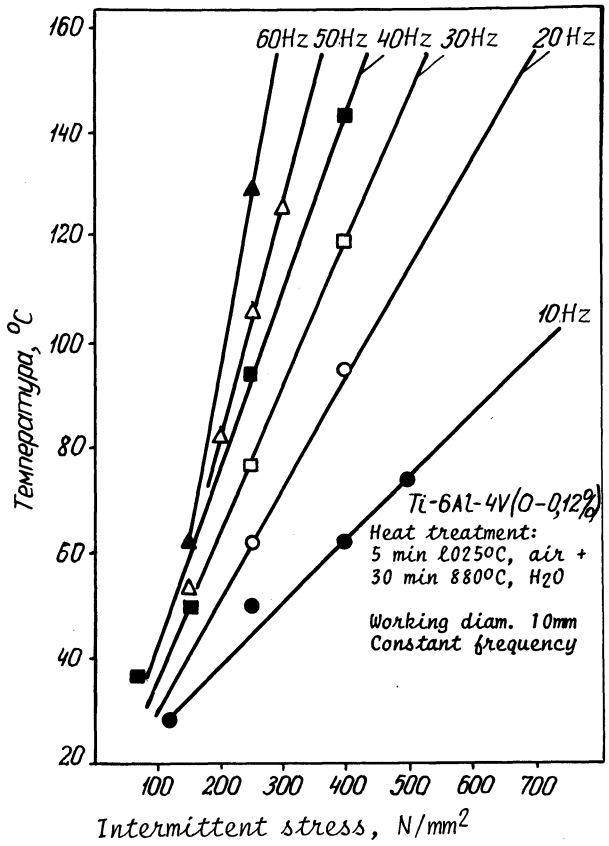

Fig. 6 - Sample temperature at 10 mm testing diameter. Stress dependence.

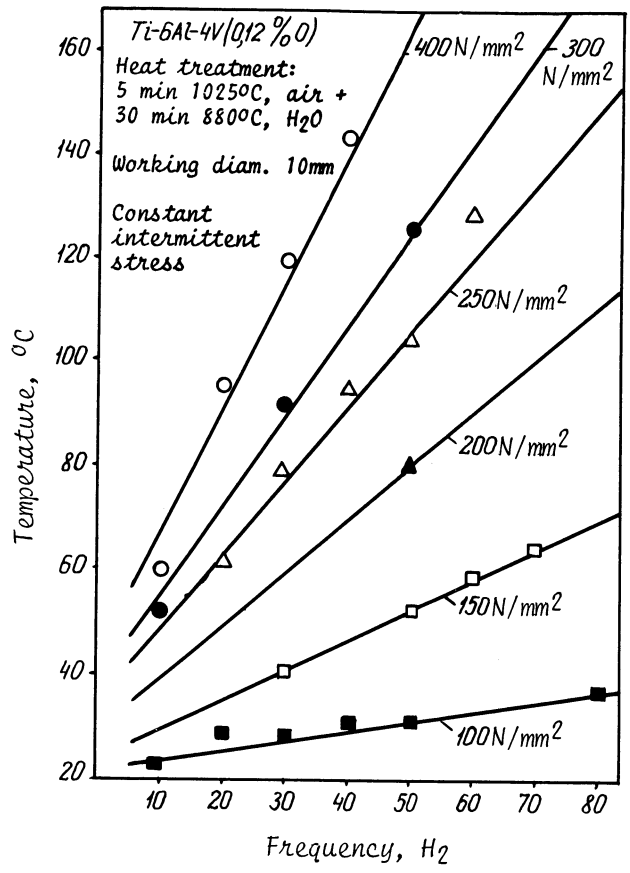

Fig. 7 - Sample temperature at 10 mm testing diameter. Frequency dependence.

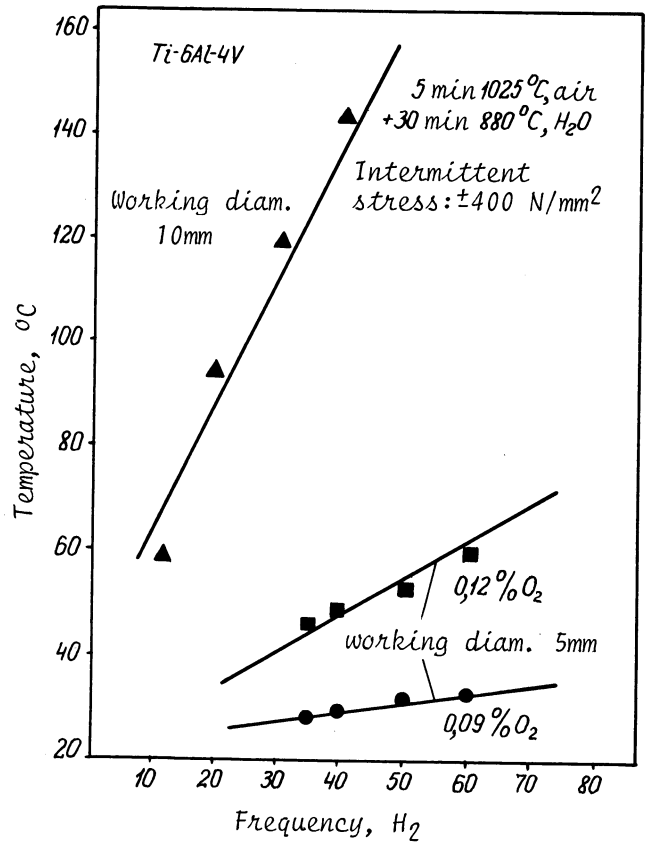

Fig. 8 - Sample temperature at different diameters and oxygen content.

This was prooved by electron microprobe analysis. The samples were hot rolled and annealed after cold deformation at 880°C. TiAl6V4 was annealed for 90 h and the other alloys for 65 h at this temperature and water quenched. The sample diameter for fatigue test was 2.2 mm, the frequency 40 Hz. The microstructure is given in the micrographs of Fig. 12 a - c, the mechanical properties in Table III.

Table III: Mechanical properties of (α+β)-, α- and β-alloys

alloy	annealing time(h) at 880°C/H_2O	UTS (N/mm^2)	$YS_{0.2}$ (N/mm^2)	Elong.%
TiAl6V4	90	960	834	12.5
TiAl7V2	65	824	785	10.9
TiV7Al4.5	65	890	789	5.3

alloy	RA (%)	E (kN/mm^2)	fatigue strength at 10^7 cycles test. Ø2.2 (N/mm^2)	VHN
TiAl6V4	51.0	103	550^x	315 ± 6^{xx}
TiAl7V2	36	113	300	$342 \pm {}^{24}_{20}$
TiV7Al4.5	15.9	98.1	250	329 ± 19

x = sample with testing Ø 5 mm ± 400 N/mm^2
xx= microhardness HV 0,01: β-phase $375 \pm {}^{29}_{17}$, α-phase $301 \pm {}^{29}_{22}$

Maximum strength and fatigue strength was observed with TiAl6V4. The influence of increasing frequency on sample temperature is shown in Fig.13. At an alternating stress of ± 500 N/mm^2 maximum sample temperature occurs at TiAl6V4 and minimum sample temperature at TiAl7V2. The surfaces of the cracks were investigated by scanning electron microscopy. Fig.14 a - c show typical areas which are characterized at TiAl6V4 (Fig.14 a) by many fatigue lines within the α-solid solution and microcracks which seem to occur at the α-β boundaries. This appearance was also observed at other investigations (16 - 18). It is suggested that the fatigue lines are only formed on the α-phase. At fatigue crack propagation studies on TiAl6V4 at growth rates of 10^{-7} to 10^{-4} mm/cycle such fatigue lines were not observed (19). The surface of the crack of the TiAl7V2-alloy (Fig. 14 b) shows a pronounced steplike breaking of the homogeneous α-phase. The main plane of these steps is tilted 60° to the sample axis which is parallel to the rolling direction. One can assume that the cracks were formed along gliding bands corresponding to $\{10\bar{1}1\}$ planes. The TiV7Al4.5 alloy (Fig. 14 c) shows another structure of the surface of the crack (Fig. 12 c). It seems that the martensitic

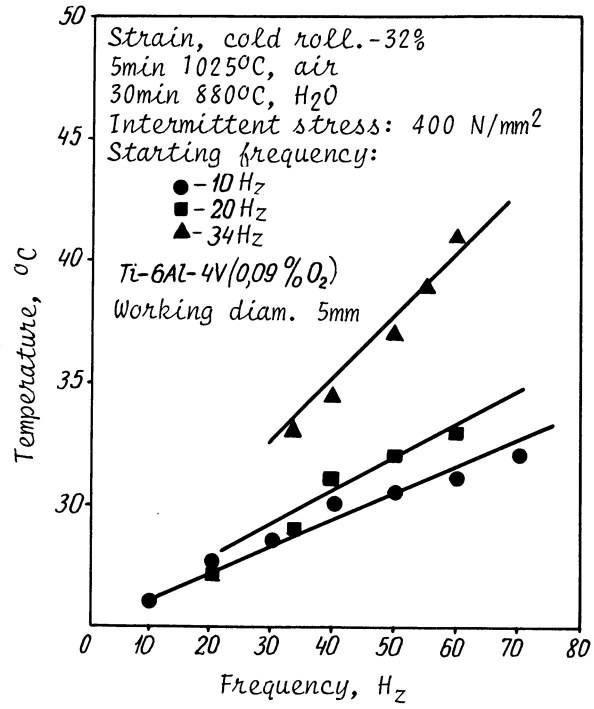

Fig. 9 - Sample temperature at different starting frequency

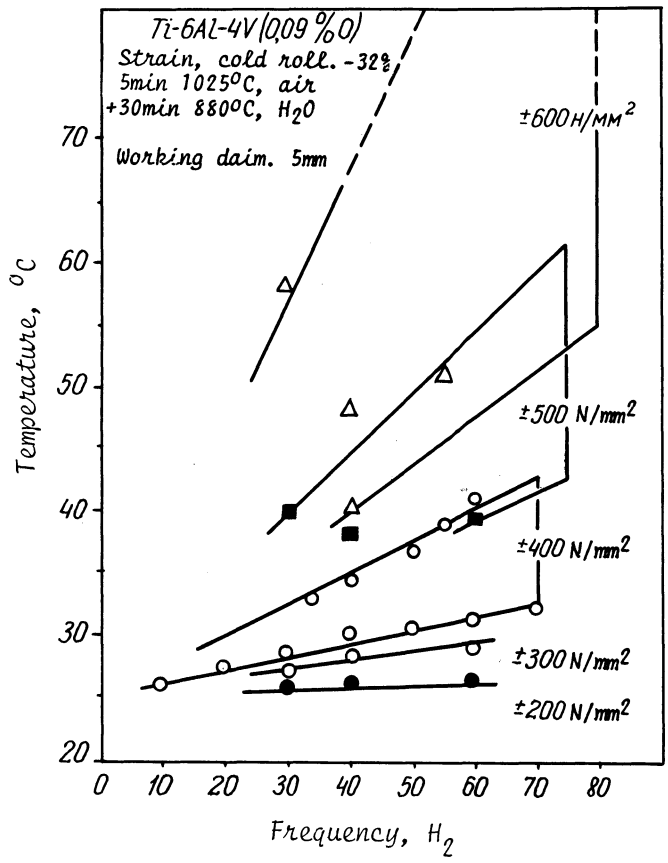

Fig. 10 - Range of sample temperature at different alternating stress.

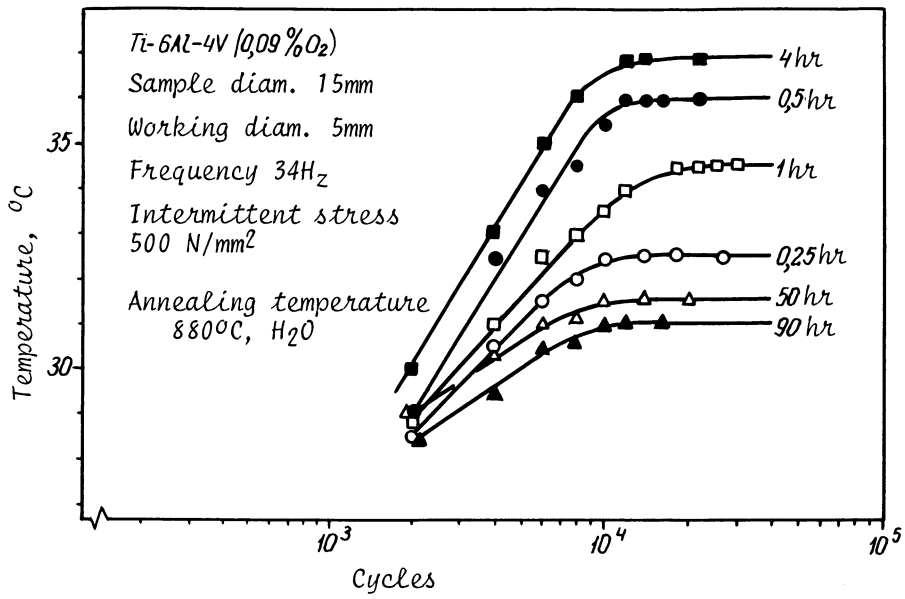

Fig. 11 - Sample temperature at different annealing time.

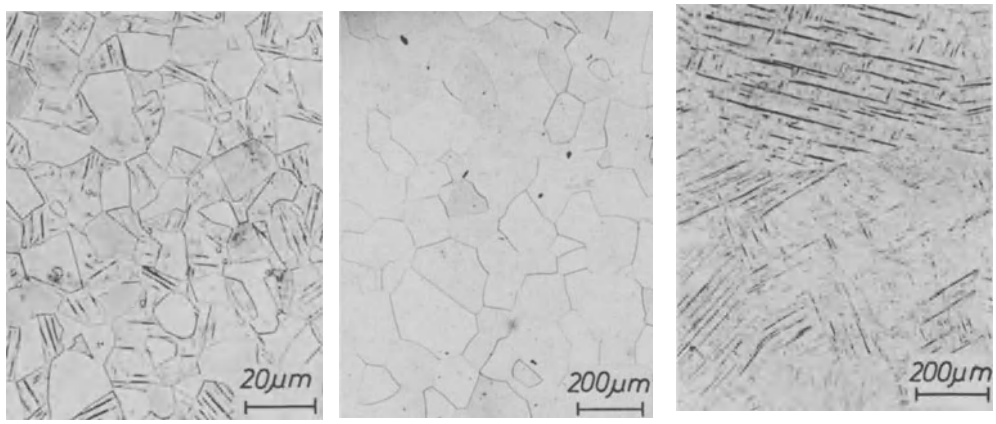

Fig. 12a-c Micrographs (etching Fig. 1)
a) Ti-Al-6-4V (0.09%0) 90h 880°C/H_2O
b) Ti-Al-7-2V 65h 880°C/H_2O
c) Ti-V7-Al-14.5 65h 880°C/H_2O

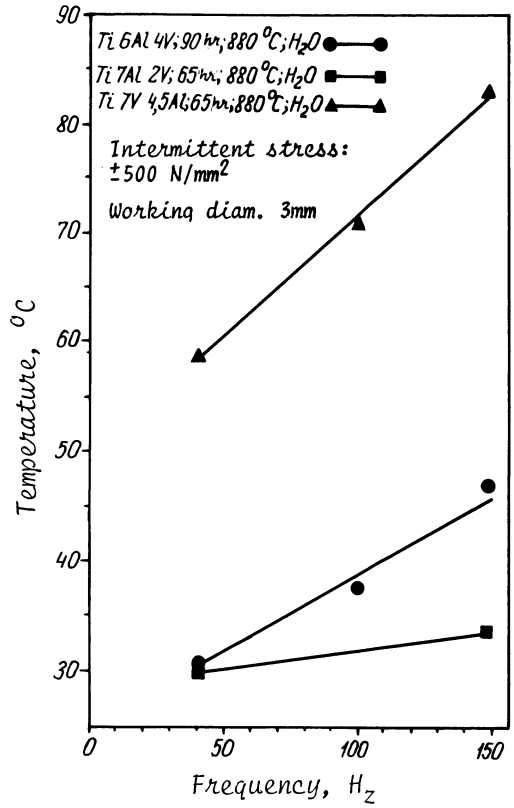

Fig. 13: Influence of frequency on sample temperature of different Ti-alloy.

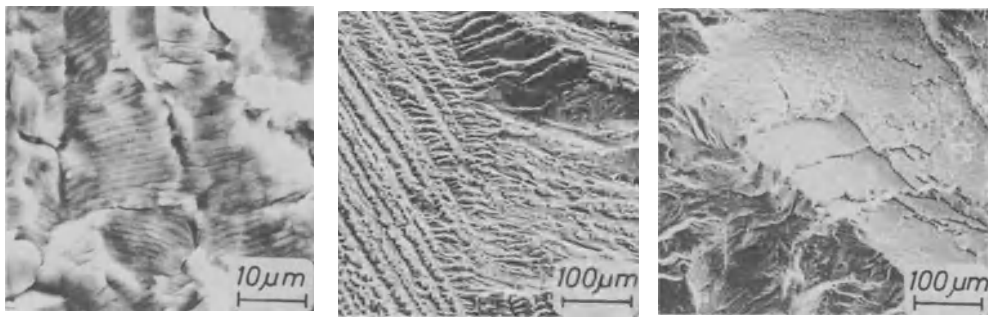

a b c

Fig. 14a-c: Scanning electron micrographs of crack surfaces
a) TiAl6V4 (0.09%0) 90h 880°C/H_2O
b) TiAl7V2 65h 880°C/H_2O
c) TiV7Al4.5 65h 880°C/H_2O

plates of the microstructure have initiated the crack growth. In the TiAl6V4 alloy the initiation of the cracks starts on the α-β-phase boundary. After the 880°C/H_2O heat treatment the β-phase has a higher microhardness than the α-phase and is therefore more sensitive to cracking.

Acknowledgement

The authors would like to thank Deutsche Forschungsgemeinschaft for financial support for some part of the experimental work and for the provision of fatigue testing facilities.

BIBLIOGRAPHY

1) Weinberg, J.G.; Hanna, I.E.: An evaluation of the fatigue properties of Ti and Ti-alloys, TML Rep.77 (1957)
2) Jungkönig, W.; Zwicker, U.: Properties of light metal alloys at increased temperature, Z.Metall 34 (1958)337-345
3) Bollenrath,F.; Domick, G.; Feldmann, H.: Properties of some (α+β)-Ti-alloys under static and dynamic stress at increased temperatures, Z.Metall 2o (1966)1256-1262
4) Bartlo, L.J.: Effect of microstructure on the fatigue properties of TiAl6V4-bar, ASTM STP 459 (1969)144-154
5) Lucas,J.J.; Konieczny, P.P.: Relationship between grain size and crack initiation fatigue strength in TiAl6V4, Met.Trans.2 (1971) 911-912
6) Bowen, A.W.; Stubbington, C.A.: The effect of α-and β-working on the fatigue and tensile properties of Ti6 Al-4V-bars, Titanium,Science and Technology,Proc.AIME 2.Int.Conf.Ti, 2.-5.5.1972,MIT,Cambridge,Mass.,USA, R.I.Jaffee, H.M.Burte, 1283-1296
7) Auvinet, R.: Mechanical properties of TiAl6V4 and TiAl6V6Sn2, Symposium materials for aviation,Le Bourget, Paris, 3.6.1971
8) Castro, R.; Séraphin, L.: Metallography and structure of TiAl6V4, Rev.Mét.58 (1966) 1o25-1o55
9) Brotzen, F.R.; Harmon jr.E.L.; Troiano, A.R.: Decomposition of β-Ti, Trans AIME 3o3 (1955) 413-419
1o) Zwicker, U.: The systems Ti-Al-Cr and Ti-Al-V and the Ti-alloys TiCr5Al3 and TiAl6V4, Z.Metallkunde 47 (1956) 535-548
11)Fopiano, P.J.; Bever, M.B.; Averbach, B.L.: Phase transformations and strengthening mechanisms in the alloy TiAl6V4, Trans ASM 62 (1969) 324-332
12)Kellerer, H.: Survey on heat treatment of TiAl6V4, Härterei-technische Mitteilungen 25 (197o) 242-253
13)Ageyev, N.N.; Petrova, L.V.; Grankova, L.P.: Decomposition ofβ-solution in β-Ti-alloys on ageing;Titanium, Science and Technology, Proc.AIME, 2.Int. Conf.Ti, 2.-5.5.1972, Cambridge,Mass.,USA, R.I.Jaffee, H.M.Burte, 1495-15o5

14) Breme, J.: Influence of microstructure on mechanical properties and creep resistance of TiA16V4, Z.Metall 27 (1973) 127-133
15) Tanone, K.; Okazaki, K.: Grain growth in commercial ($\alpha+\beta$) Ti-alloys, J.Jap.Inst.Metals 37 (1973)535-539
16) Wells, C.H.; Sullivan, C.P.: Low cycle fatigue crack in TiA16V4, Trans ASM 62 (1969) 263-27o
17) Benson, P.K.; Großkreutz, J.C.; Shaw, G.G.: Mechanisms of fatigue in mill-annealed Ti6A14V at room temperature and 6oo°F, Met.Trans.3 (1972) 1239-1248
18) Dawson, D.B.; Pellony, R.M.: Corrosion fatigue crack growth of Ti-alloys in aequous environments, Met. Trans.5 (1974) 723-731
19) Irving, P.E.; Beevers, C.J.: The effect of air and vacuum environments on fatigue crack growth rates on Ti6A14V, Met.Trans.5 (1974) 391-398

THE EFFECT OF VARIATIONS IN HEAT TREATMENT ON THE MECHANICAL PROPERTIES OF AN α+β TITANIUM ALLOY IMI 550 (Ti-4Al-2Sn-4Mo-0.5Si)

R F Vaughan, P A Blenkinsop and D F Neal

Imperial Metal Industries (Kynoch) Limited
Birmingham B6 7BA

Introduction

A number of studies[1,2,3,4] have been reported on the effect of heat treatment on the fracture toughness of titanium alloys. However, most of the experiments have been designed to establish the basic relationship between microstructure and fracture toughness, with little attempt being made to relate these changes to commercially acceptable heat treatments.

IMI 550 is an α+β type alloy with a nominal composition Ti-4Al-2Sn-4Mo-0.5Si. It was developed as a medium strength alloy for applications at both room and elevated temperatures (up to about 400°C). The alloy is now used extensively in aerospace projects in both air-frame and aero-engine components. The standard heat treatment for the alloy consists of a solution treatment at 900°C followed by air cooling to room temperature and ageing for 24 hours at 500°C. This heat treatment was devised before the relevance of fracture toughness and low-cycle fatigue properties were appreciated, at a time when creep and tensile properties were of prime importance. Although the alloy has been shown to have very good all-round properties after the standard heat treatment, it is felt that in some applications a greater potential may be realised by some modifications of the heat treatment. Therefore in the work described below, an attempt has been made to extend the theoretical approach of a basic heat treatment/fracture toughness study to include the effect of section size and the inter-relationship of heat treatment with other properties such as high and low cycle fatigue. In order to tailor the data to potential commercial applications, only simple treatments were studied, being based on variations in solution treatment temperature.

Results

Effect of Heat Treatment Temperature on the Microstructure

The nominal $\alpha+\beta/\beta$ transformation temperature for IMI 550 is 975± 10°C. Preliminary studies established the temperature/phase proportion relationship for the alloy, Figure 1. Subsequent solution treatments were chosen in terms of percentage β phase.

At the standard solution heat treatment temperature (900°C - 55% β) the microstructure of IMI 550 consists of primary α + primary β with a very small amount of Ti_5Si_3 existing as randomly distributed globular particles of approximately 1 μm diameter. Raising the temperature above 900°C has the effect of reducing the proportion of α phase and Ti_5Si_3, until at the transus temperature the structure consists entirely of β. Upon air cooling to room temperature, the primary β phase precipitates secondary acicular α, the size of which increases with solution treatment temperature. The mixture of β and secondary α is usually termed the β transformation product or transformed β. At sufficiently low solution treatment temperatures (eg 875°C) it is possible to retain the primary β phase down to room temperature and suppress acicular α formation entirely. Increasing the cooling rate from a solution treatment temperature above 900°C has the effect of refining the secondary acicular α.

Effect of Heat Treatment on Fracture Toughness and Tensile Properties

All the preliminary experiments on the effect of heat treatment variables on the mechanical properties were carried out on 25 mm diameter bar. The effects on fracture toughness and tensile properties of solution treatment temperature, cooling rate (air cool or water quench) and ageing/annealing temperature were studied, the data being presented in Table 1. All the fracture toughness testing was carried out using SEN type specimens (76 x 19 x 6 mm); the crack propagating along the transverse plane of the bar. The fracture toughness values are not valid as K_{1c} results in some cases due to the limited test specimen dimensions, but the trends shown are considered to be meaningful. (Comparisons between large compact tension CKS specimens and SEN specimens have shown close agreement, although the absolute values have varied slightly).

The highest tensile strength was found in specimens which were water quenched + aged, but generally these exhibited low fracture toughness. On the other hand, the highest fracture toughness was associated with the air-cooling treatment; ageing or annealing generally lowering the value obtained. Unfortunately air cooling produced low strength except at heat treatment temperatures which produced a large proportion of primary α. Increasing the solution treatment temperature increased fracture toughness and decreased tensile strength, except for the 100% β treatments where grain size

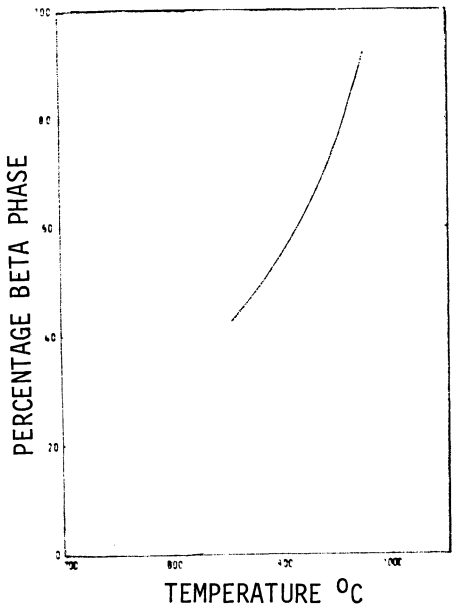

Fig. 1 - Temperature phase proportion relationship for Ti-4Al-2Sn-4Mo-0.5Si (IMI 550).

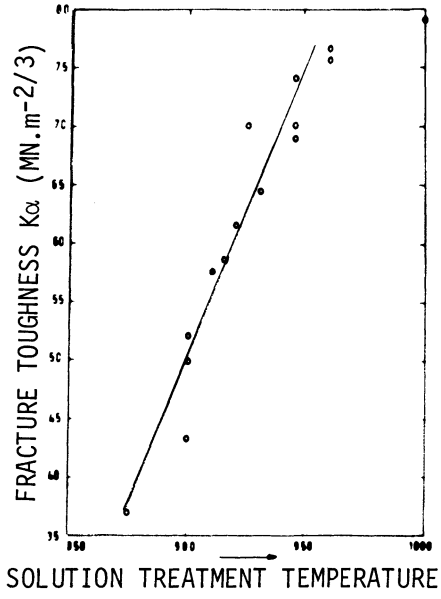

Fig. 2 - Fracture toughness - heat treatment relationship for Ti-4Al-2Sn-4Mo-0.5Si (IMI 550).

had some effect on strength. Overall, the best compromise of tensile strength, ductility and fracture toughness was found in material air cooled from either the 90% β or 75% β temperature, and aged.

TABLE 1 - Tensile and Fracture Toughness Data 25 mm Ø Bar

Heat Treatment	0.2% Proof Stress $N.mm^{-2}$	Tensile Strength $N.mm^{-2}$	Elong % on $4\sqrt{So}$	RinA %	Fracture Toughness KQ $MNm^{-3/2}$
1000°C 100% β (WQ	1127	1295	4	5½	52
1000°C 100% β (WQ + Age	1186	1315	3	4½	44
1000°C 100% β (WQ + Anneal	1119	1228	7	9	53
1000°C 100% β (AC	969	1135	16	25½	83
1000°C 100% β (AC + Age	938	1152	14	17	79
1000°C 100% β (AC + Anneal	981	1101	12	14½	69
960°C 90% β (WQ + Age	1244	1450	14	39	36
960°C 90% β (AC	947	1105	20½	51	80
960°C 90% β (AC + Age	971	1156	20½	39	77
960°C 90% β (AC + Anneal	973	1081	17½	40	55
945°C 75% β (WQ	1125	1363	15½	54½	48
945°C 75% β (WQ + Age	1252	1467	12	43	27
945°C 75% β (WQ + Anneal	1085	1204	14	36½	36
945°C 75% β (AC	965	1117	21	54	80
945°C 75% β (AC + Age	996	1152	18½	50	70
945°C 75% β (AC + Anneal	974	1101	21	40	45
875°C 50% β (WQ + Age	1089	1382	11	26	<30
875°C 50% β (AC	991	1111	19	39	57
875°C 50% β (AC + Age	1061	1231	16	35	37
875°C 50% β (AC + Anneal	970	1055	17½	32	43
Standard heat treatment 900°C AC (55% β) + Age	1045	1205	16	42	50

Age = 24h at 500°C AC Anneal = 2h at 700°C AC

The study on the 25 mm diameter bar was extended to include solution treatment temperatures in the range 910-930°C followed by air cooling and ageing. This was done to establish whether fracture toughness increased linearly with temperature. Table 2 details the additional data, while Figure 2 illustrates the overall effect of change in solution treatment temperature on the fracture toughness levels in air cooled and aged 25 mm diameter bar.

TABLE 2 - The Fracture Toughness and Tensile Properties of IMI 550 Heat Treated at 910, 915, 920, 925 and 930°C All Aged 24 Hours 500°C

Heat Treatment Details	Tensile Properties				Fracture Toughness
	0.2% Proof Stress $N.mm^{-2}$	UTS $N.mm^{-2}$	Elongation % on $4\sqrt{So}$	R of A %	KQ $MN.m^{-3/2}$
910°C AC + 24 hours at 500°C	972	1176	16	46	57.7
915°C AC + 24 hours at 500°C	966	1167	$16\frac{1}{2}$	48	58.5
920°C AC + 24 hours at 500°C	982	1141	22	52	61.3
925°C AC + 24 hours at 500°C	984	1155	19	48	70.2
930°C AC + 24 hours at 500°C	962	1137	22	51	64.4

Microstructural and Compositional Studies

Both optical and electron microscopical studies were made of the fracture toughness specimens heat treated as detailed in Table 1.

Examination of the crack path in fracture toughness specimens revealed a preference to propagate either through the beta transformation product or along the interfaces between primary α and transformed β grains.

Figures 3-5 show the optical microstructures of material air-cooled and aged after heat treatments to give 100%, 75% and 55% β phase respectively. Similar trends were seen with the water quenched and aged samples, except that the features of the tfansformed beta were irresolvable. No differences were seen optically between air-cooled specimens before or after ageing or annealing.

In the case of water quenched material, ageing did not change the optical microstructure, but annealing changed the etching characteristics of the transformed β and very fine secondary α needles became apparent. Only by use of the transmission electron microscope was it possible to monitor adequately the changes occurring

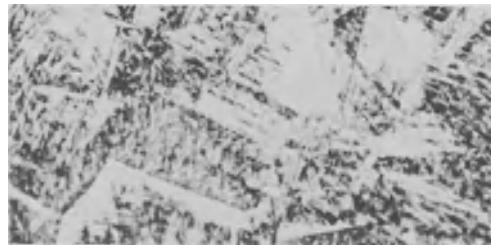

Fig. 3 - 100% β heat treatment. x400

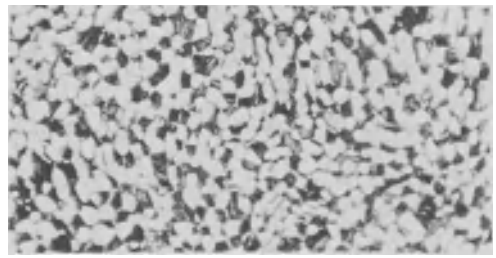

Fig. 4 - 75% β heat treatment. x400

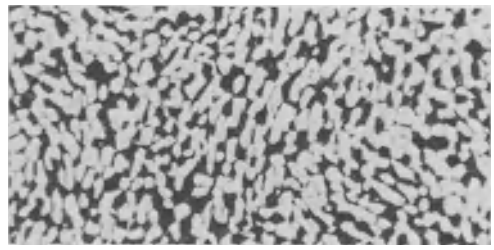

Fig. 5 - 55% β heat treatment. x400

in the primary β grains. These differences are illustrated in Figures 6 and 7. In both photomicrographs the secondary acicular α can be seen together with the associated β.

Some of the thin foils were also examined in a combined transmission electron microscope and electron probe micro-analyser (EMMA-4). This instrument has significant advantages over the conventional micro-analyser and these are referred to in the literature(5). For the purposes of the present investigation the instrument was used to analyse both the primary α and the transformed β regions. An attempt was made to determine the composition of the β and secondary α phases, but unfortunately the fineness of the transformation product precluded any direct analysis of the individual phases, and no consistent data emerged. However, the instrument did provide useful information, by an energy dispersive technique, on the composition of the primary α and transformed β regions. This data is given in Table 3.

TABLE 3 - Micro Analysis of Thin Foils on EMMA-4

Heat Treatment	Fracture Toughness $MN.m^{-3/2}$	Phase	Composition wt% Al	Sn	Mo	Si
50% β AC + Age	37	Primary α	4.12	1.95	1.40	0.39
		Transformed β	2.89	1.67	14.9	0.80
75% β AC + Age	70	Primary α	4.22	2.81	0.62	0.53
		Transformed β	3.81	2.53	6.02	0.68
90% β AC + Age	77	Primary α	4.60	2.13	0.86	0.52
		Transformed β	3.39	1.97	4.29	0.41
75% β WQ	48	Primary α	4.62	2.05	0.62	0.73
		Transformed β	3.67	2.41	5.34	1.03

Effect of Heat Treatment Variables on K_{1c} and Tensile Properties in Large Section

It was clear from the results detailed above that a solution treatment very high in the α+β phase field, followed by an air cool and age, gave the best compromise of toughness, strength and ductility. However, in choosing a heat treatment for future commercial exploitation it was felt necessary to work with a maximum heat treatment temperature of 945°C (75% β) thereby avoiding any possibility of exceeding the beta transus.

The material used was 135 mm diameter bar. Two samples of the bar were heat treated at 900°C (55% β) and 945°C (75% β) respectively

Fig. 6 - Electron micrograph of material solution treated at 960°C (90% β). x16,000

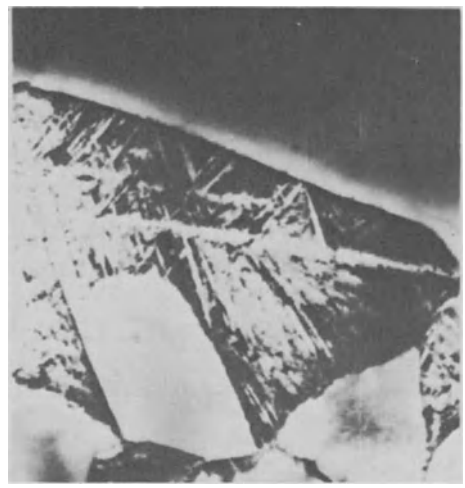

Fig. 7 - Electron micrograph of material solution treated at 900°C (55% β). x16,000

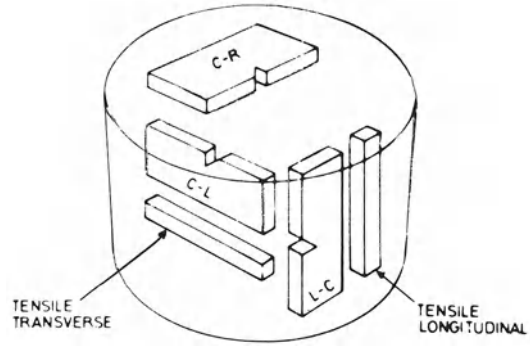

Fig. 8 - Tensile test piece directions and fracture plane identification in cylindrical sections.

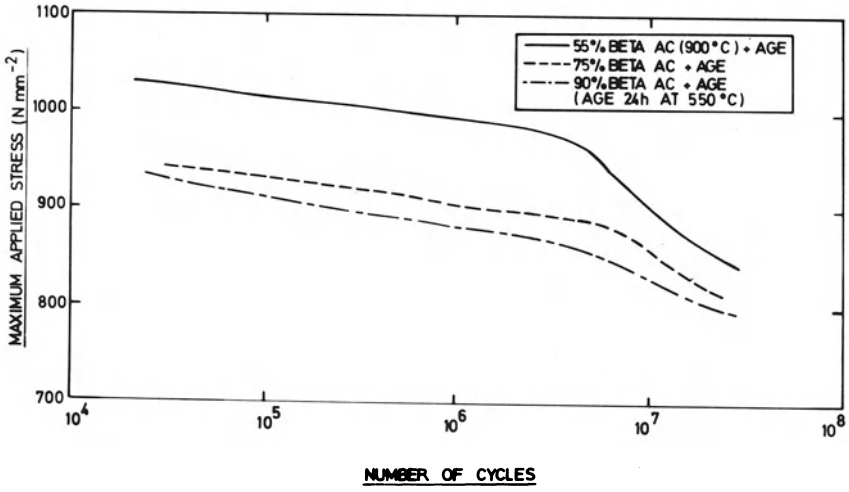

Fig. 9 - High cycle fatigue data (25 mm ∅ material).

air-cooled and aged (24 hours at 500°C). The opportunity was taken of determining the property levels in more than one direction. The specimen orientation and crack direction nomenclature are shown in Figure 8 and the test results are presented in Table 4.

TABLE 4 - Tensile and Fracture Toughness Properties (CKS) for IMI Ti 550 (135 mm Ø)

Heat Treatment Details	Fracture Toughness Notch Identification	K_{1c} $MNm^{-3/2}$	0.2% Proof Stress $N.mm^{-2}$	UTS $N.mm^{-2}$	% Elong on $4\sqrt{So}$	RinA %
3 hours at 900°C AC (55% β) + 24 hrs at 500°C	C-R	58.1	1033	1121	18½	37½
	L-C	69.6	959	1097	20½	39
	C-L	61.6	1033	1121	18½	37½
3 hours at 945°C AC (75% β) + 24 hrs at 500°C	C-R	60.4	997	1097	22	41
	L-C	78.1	918	1073	22	39
	C-L	72.9	997	1097	22	41

Effect of Heat Treatment Variables on the Fatigue Properties

(1) High Cycle Fatigue

All the high cycle fatigue testing was carried out on specimens produced from 25 mm diameter bar. An Amsler vibrophore was used under zero minimum. tensile stress conditions at a frequency of 150 Hz. The data for a range of solution heat treatment conditions is given in Figure 9.

(2) Low Cycle Fatigue

The material used was 25 mm diameter bar. Testing was carried out on a mechanical fatigue machine under constant load conditions (zero minimum) and at a frequency of 10 cycles per minute. The fatigue curves corresponding to several solution treatment temperatures are shown in Figure 10.

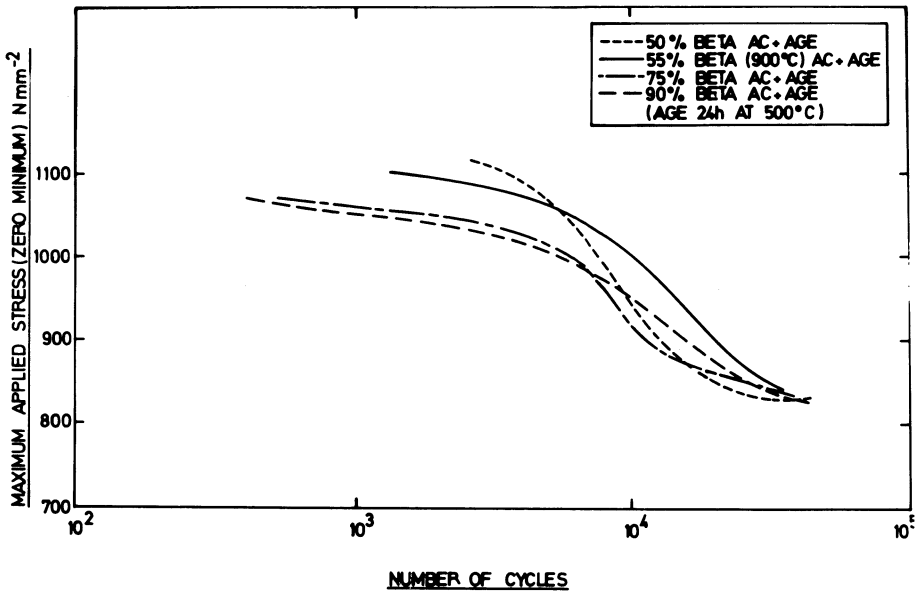

Fig. 10 - Low cycle fatigue data (25 mm Ø material).

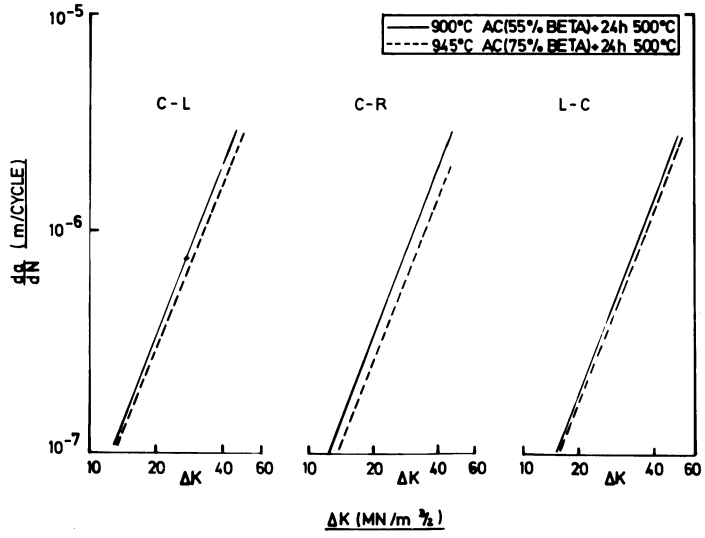

Fig. 11 - Crack propagation data (60 mm Ø material).

(3) Fatigue Crack Propagation Rate

Because the fatigue crack propagation specimens are too large (32.5 x 30 x 13 mm) to be produced from 25 mm bar, 60 mm diameter bar was used for this exercise. This provided the opportunity of producing data for crack propagation in three directions. Figure 11 shows the crack propagation data in terms of a da/dN v ΔK plot for material solution treated at 900°C (55% β), and for material solution treated at 945°C (75% β). All samples were air cooled and aged after solution treatment.

Discussion

The overall improvement in fracture toughness level with increase in solution treatment temperature is not surprising, and is in line with the observations of other workers(3,4). However, what is remarkable is the sharp increase in fracture toughness that was produced in the alloy by only small increases in solution heat treatment temperature in the $\alpha+\beta$ phase field. Figure 2 reveals an almost 100% increase in fracture toughness level in air cooled and aged bar when the solution treatment temperature is increased from 875°C to 960°C (ie the β phase proportion increased from 50% to 90%). The significance of this improvement is further emphasised by the fact that it was achieved with only 10% and 6% losses in the proof and tensile strengths respectively.

The data in Table 1 reveals not only the strong dependence of the fracture toughness level on the $\alpha+\beta$ solution treatment temperature, but also on cooling rate and ageing or annealing temperature. This data, together with the microstructural evidence does indicate a possible mechanism to explain the fracture toughness behaviour of the alloy. In this and other work(1), the observations that the crack path is predominantly either along the boundaries of, or through the transformed beta regions, emphasises the importance of these regions in controlling the level of fracture toughness. It has been observed in the present exercise that of material solution treated at an identical temperature, air-cooled or air-cooled + aged samples gave significantly better levels of fracture toughness than either water quenched or water quenched + aged. These observations indicate that the size of primary α grains and transformed β regions, distance between phases and volume of primary α/trans formed β phase boundary are not the predominant metallurgical factors affecting the fracture toughness level. Also, since ageing and annealing affect fracture toughness almost as much as solution treatment temperature, primary α/β phase proportions are not the predominant cause of good or bad fracture toughness. However, the microstructural and analytical changes noted in the study do indicate that fracture toughness is controlled by either the morphology of the secondary alpha or by the composition (and possibly amount of)β phase in the β transformation product. Of the analytical data in Table 3. the most significant is felt to be that of the molybdenum in the transformed β region; in particular the observation that the

level varies from 14.9% in the 50% β condition (KQ 37 MN.m$^{-3/2}$) to 4.29% (KQ 77 MN.m$^{-3/2}$) at 90% β. The other elements partition fairly evenly between the primary α and transformedβ; the exception being silicon. However, because of the low x-ray count rates achieved in the analysis, and because silicon tends to form Ti_5Si_3 particles, it is felt that the levels of silicon quoted are likely to be subject to a large error.

The difference in fracture toughness levels between the 50% β air-cooled and the 75% β air-cooled samples could be due to the molybdenum content of the β phase. Thus omega phase could form from the highly stabilised β in the 50% β sample. or martensite could form during straining in the metastable β in the 75% β sample. The theory of energy absorption by strain induced martensite in the plastic zone ahead of the crack has been postulated by other workers (6) and is further supported when the property levels of aged material and annealed material are compared. Whereas the microstructure in the transformed β region of air cooled samples is basically unaffected by either the 500°C or 700°C treatments, the composition and amount of β in the transformed β will be different. Unfortunately the fineness of the transformation product is such that it has not been possible to monitor compositional variations.

Similar difficulties of analysis of the products in the transformed β region have precluded any positive data on water quenched material. The analytical evidence in Table 3 shows that the composition of the β transformation product (containing beta and secondary alpha) in 75% β air cooled + aged material is similar to that in 75% β water quenched material. It can be argued that the morphological differences in the transformed β of these samples are giving rise to different levels of fracture toughness. However, cooling rate will have a marked effect on the β and secondary α compositions; considerably more diffusion is likely to have taken place in the air-cooled material, particularly of the β stabilising elements. Furthermore, comparing water quenched and water quenched + aged material, Table 1, a significant loss of fracture toughness occurs on ageing. This change would support the contention that it is the composition and possibly amount of the β phase which are the controlling factors rather than the secondary α morphology which remains unchanged on ageing.

Further studies are required therefore to quantify the effects of composition and amount of β phase, and to separate these from the changes induced by phase morphology.

On a more general level the study has shown the potential of the alloy, and that this potential can be realised in larger sections as well as in small diameter bar.

From an applications point of view the most attractive heat treatment for improvements in fracture toughness appears to be one

of solution treatment at about 75% β air-cool and age. This temperature is sufficiently far below the β transus of the alloy to allow heat treatment without the danger of overheating. On the basis of the properties determined in the present exercise the improvement in fracture toughness is achieved at the expense of some loss in tensile and fatigue strengths. However, a comparison of the data obtained in conventional heat treated material (900°C AC + 24h 500°C) with material given in the 75% β treatment (945°C AC + 24h 500°C) shows that a 40% increase in fracture toughness is achieved at the expense of a 5% loss of tensile strength, a 3% loss of low cycle fatigue strength (2×10^4 cycles), a loss of 6% in high cycle fatigue strength (2×10^7 cycles) with a marginal improvement in fatigue crack propagation resistance.

Conclusions

1. High fracture toughness can be achieved in IMI 550 without a significant loss in other properties, by use of a solution treatment high in the α+β phase field followed by an air-cool and age.

2. The fracture toughness level in the alloy is related to the phase composition and possibly proportion and morphology of the β transformation product.

Acknowledgements

The authors are grateful to Dr G Lorimer of the University of Manchester for generation of the data on EMMA-4.

References

(1) Rogers D H, Titanium Science and Technology, Plenum 1973, 1719

(2) Greenfield M H and Margolin H, Met Trans 2, 1971 841

(3) Hall J A et al, Mat Sci Eng 9, 1972, 197

(4) Hall I W and Hammond C, Titanium Science and Technology, Plenum 1973, 1365

(5) Lorimer G W, Razik N A and Cliff G, Journal of Microscopy 99 (2) 1973, 153

(6) Hall I W and Hammond C, Proc of Inst of Metallurgists Conf on Fracture Toughness, Newcastle-upon-Tyne, 1973

HEAT TREATMENT OF CAST Ti-6Al-4V ALLOY

Y. Kbaraki and T. Sasaki

Mechanical Engineering Research Laboratory, Hitachi Ltd.

Ibaraki-Pref. JAPAN

1. INTRODUCTION

Most industrial machinery, particularly blowers and pumps, possess high speed rotating parts, and recently these parts have been urged to be made in smaller size with the intent to improve their spinning speed and reliability. It is very effective to utilize titanium alloys which have high strength-to-density ratios for such parts operating at a high centrifugal force. These parts are usually in very complicated shapes which make machining almost impossible so that precision casting is required.

Factors, such as strength, cost and availability, have urged us to try casting of such parts using Ti-6Al-4V alloy. But the microstructure of this alloy as cast is acicular alpha, plate-like alpha and/or Widmanstatten structure, and it is believed that this structure cannot be changed to other structures[1] by the conventional heat treatment such as solution treatment and aging. Forging or rolling cannot be employed for these complicated shaped parts after casting, therefore, it is desirable to obtain a pre-heat treated structure that can be conventionally heat treated to yield alloys with high strength or toughness. This means that the two phase structure, alpha and beta, like that of the forged alloy is required.

In this report, we investigated the processes of heat treatment in which acicular alpha, plate-like alpha or Widmanstatten $\alpha+\beta$ is decomposed, giving desirable microstructures for the conventional heat treatment. Consequently we have obtained a desirable microstructure of cast Ti-6Al-4V alloy by application of cyclic heating. The mechanical properties of such specimens are also reported.

TABLE I

Chemical Compositions of the Materials (wt.%)

	Al	V	Fe	O	C	N	H
Cast	5.90	4.02	0.197	0.168	0.023	0.009	0.0030
Mother Ingot	6.15	4.05	0.154	0.148	0.018	0.009	0.0030
Forged	6.40	4.10	0.160	0.180	0.018	0.020	0.0065
AMS stand	5.50 6.75	3.5 4.5	<0.30	<0.20	<0.10	<0.05	<0.0125

TABLE II

Conditions of Cyclic Heating

Highest temperature (°C)	850, 900, 950,
Heating rate (°C/min.)	6.7, 13, 33, 67, 100, 200,
Number of the cycle	1, 3, 5, 20, 50,

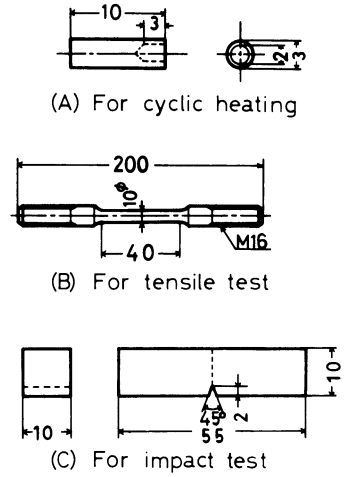

Fig. 1 - The shapes of the specimens.

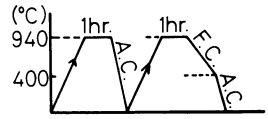

Fig. 2 - The condition of cyclic heating using an electric furnace.

2. Experimental Methods

2.1 The specimen preparation. A vacuum consumable-electrode furnace was used for melting and casting. This process, known as 'skull melting', used a consumable titanium electrode in a water cooled copper crucible. Centrifugal vacuum casting (8-109 at 10^{-1} - 10^{-2} torr) was made using graphite molds at a melt temperature about 1700°C. The size of castings was 13 x 115mm for impact test and 18 x 200mm for the tensile and cyclic heating tests. The chemical compositions of the castings and the forgings which were used for comparison are listed in Table I.

The castings were annealed in vacuum ($2x10^{-5}$ torr) at 650°C for 4hr with furnace cooling for stress relief before machining. The shapes of the cyclic heating, tensile and impact specimens are shown in Figure 1, respectively.

2.2 The conditions of cyclic heating and heat treatment. Various heating cycles utilizing high frequency (1.7MHz) induction heating were examined for decomposing the cast structure, which are listed in Table II. Figure 2 indicates the cyclic heat treatment condition of the tensile test specimen using an electric furnace. The conventional heat treatment was given after the cyclic heating, as shown in Figure 3.

3. Results and Discussion

3.1 The Effects of Cyclic Heating. Ti-6Al-4V alloy is essentially two phase alloy having alpha and beta phases. But the microstructure of the castings is not so. Figure 4 shows the microstructures of a cast specimen after stress relief anneal (A) (hereafter it is called as cast), a solution treated and aged as cast specimen (C) (hereafter it is called S.T.A.), forged (B) and S.T.A. forged specimen (D). The microstructure (A) shows acicular or fine plate-like alpha. Generally, it is difficult to obtain a structural change of the microstructure shown (A) by a conventional heat treatment like S.T.A.. This example is shown in (C). The forging (B) shows equiaxed alpha grains (light) and intergranular beta (dark). This microstructure can be changed to a desirable structure for the conventional heat treatment like S.T.A.. Therefore, we have tried a cyclic heating to change the as cast structure to the equiaxed alpha and intergranular beta microstructure by high frequency induction heating.

3.1.1 The Effect of the Highest Heating Temperature. The highest heating temperature gives a large improvement on the microstructure of castings by allowing diffusion of Al and V. Figure 5 shows the influence of the highest temperature of the heating. The

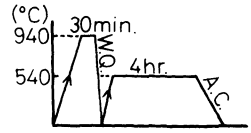

Fig. 3 - The heating cycle of solution treatment and aging.

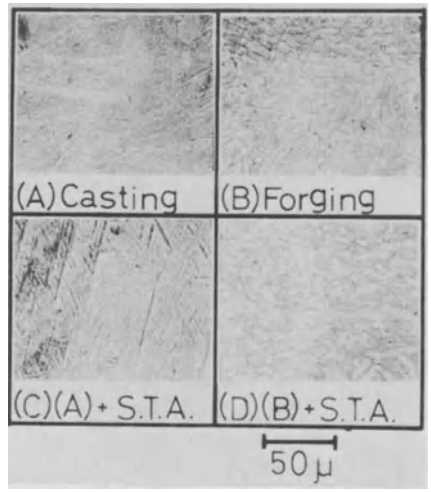

Fig. 4 - The micro structures of the specimen.

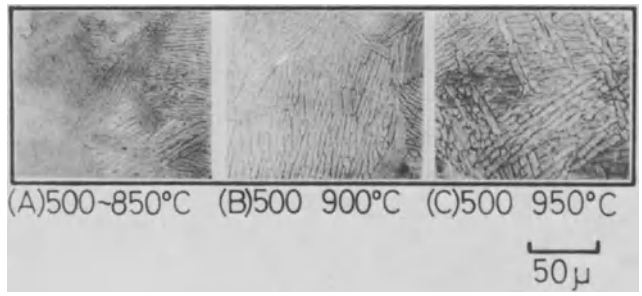

Fig. 5 - The effect of the highest heating temperature.

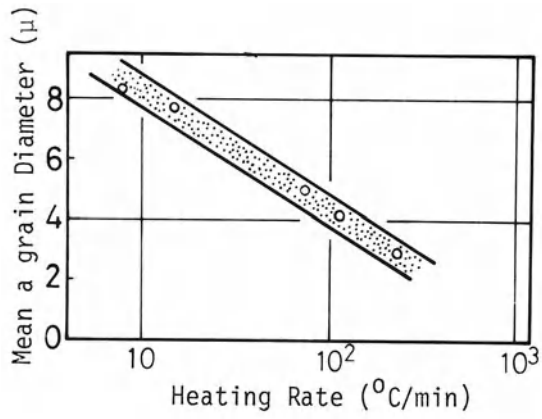

Fig. 6 - The relation between heating rate and alpha grain diameter.

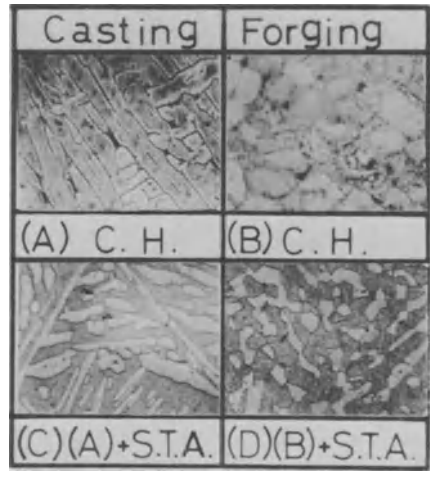

Fig. 7 - The micro structure of the specimen. C.H.: cyclic heating
C.H.: Cyclic heating ⌊_____⌋50μ

microstructure (A) shows a partial decomposition of acicular alpha with some plate-like alpha, compared with Figure 4 (A). Figure 5 (B) shows appearance of plate-like alpha throughout the structure and (C) shows decomposition to nearly equiaxed alpha with some plate-like alpha. Therefore, it may be concluded that the heating to 950°C is required to obtain a desirable microstructure at a heating rate of 67°C/min. with heating cycles of 10. The heating rate discussed in this report concerns the rate of heating from 500°C to the highest heating temperature.

3.1.2 The Effect of Heating Rate. The decomposition of acicular alpha and the other structure to equiaxed alpha with partly plate-like alpha was attained at heating rates between 67 and 200°C/min.. In this case, the mean alpha grain diameter becomes greater when the heating rate is lower. Figure 6 shows the relationship between the heating rate and the mean alpha grain diameter.

3.1.3 The Effect of the Number of the Heating Cycle. The number of heating cycles required for the decomposition of the as cast microstructure is influenced by the heating rate and the highest heating temperature, i.e., 10 cycles to 950°C, 20 cycles to 900°C at a heating rate of 200°C/min.. When the heating rate is lower (below 33°C/min.), only a few cycles are required. Practically, it is beneficial to lower the heating rate to 10-30°C/min, at which furnace heating can be used for a larger specimen. Then the heating condition, shown in Figure 2, was examined. Since a similar microstructure was obtained, compared with the induction heating, this condition was used for the tensile test specimen and other specimens reported later.

3.2 The Microstructural Change and the Diffusion of Alloying Elements

3.2.1 Microstructural Changes. The effect of cyclic heating on the microstructure was examined. Some examples are shown on a casting and a forging in Figure 7 (A), (C) and (B), (D), respectively. (A) shows transformed beta containing plate-like alpha, and (B) shows alpha grain growth caused by the cyclic heating. It may be concluded that the cyclic heating decomposes acicular or fine plate-like alpha. From these results, it was shown that the microstructure of the casting became nearly the same microstructure as the forging, except the heat treated structure contained slightly coarser and differently shapped alpha grains. Therefore, it is possible to obtain a desirable (α+β) ratio for castings similar to forgings by conventional heat treatment.

3.2.2 The Diffusion of Alloying Elements. The diffusion of alloying elements occurred during cyclic heating, the concentration of Al and V was examined by means of X-ray Micro Analyzer. Figure 8

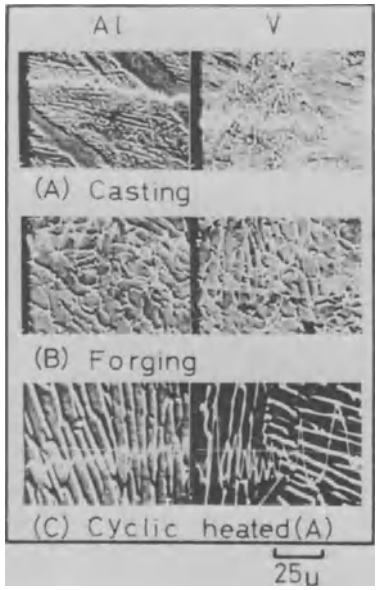

Fig. 8 - The distrubution of Al and V.

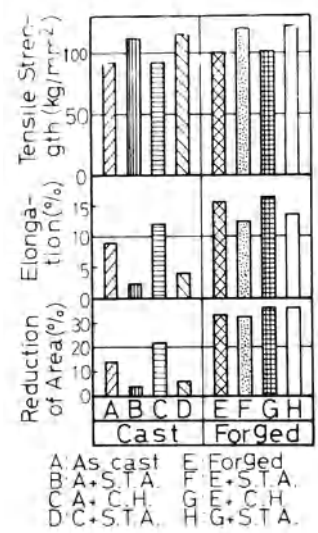

Fig. 9 - Tensile properties of the specimen.

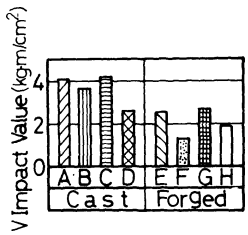

Fig. 10 - Impact values of the specimen.

(A) shows the result for the as cast specimen, showing uniform distribution of Al and V throughout the specimen. Figure 8 (B) shows the result for the forged specimen indicating a mixture of equiaxed alpha grains and intergranular beta which contains lower Al and higher V than alpha grains. Figure 8 (C) shows the effect of cyclic heating on the cast specimen corresponding to the microstructure shown in Figure 7 (A). It shows nearly the same distribution of Al and V as the forged specimen. Differences in atomic movement between the casting and forging was not observed by other heat treatment like S.T.A.. From this result, the microstructural similarity between the casting after the cyclic heating and the forging can be confirmed.

3.3 Mechanical Properties

3.3.1 Tensile Properties. The tensile properties of the castings were measured under the various heat treated conditions to compare with the forging and examine the effects of cyclic heating as shown in Figure 9. (B), S.T.A., shows a higher tensile strength with lower elongation and reduction of area than (A), the as cast specimen, in spite of a very slight structural change. Forgings (E and F) show a slightly greater tensile strength and larger elongation and reduction of area, compared with the castings (A and B). The cyclically heated specimens (C and D) show a slight increase of tensile strength, elongation and reduction of area in spite of alpha grain growth, compared with (A) and (E). It should be noted that a large increase in elongation and reduction of area was observed for (C), compared with (A), while (C) does not have perfect equiaxed alpha grains.

It has been generally accepted that the value of reduction of area is about twice the value of elongation in the equiaxed alpha-beta structure, and in the acicular alpha structure the elongation becomes nearly the same value as the reduction of area.

It has been believed that for acicular alpha, the local deformation ability decreased, which has been related to the fracture along alpha-beta interfaces.[2]

In this report, the value of elongation and reduction of area were found to be nearly the same if the microstructure was acicular or plate-like alpha, and the value of reduction of area was found to be twice as large as that of elongation for the forging and the casting subjected to the cyclic heating. The values of reduction of area of the castings subjected to the cyclic heating such as (C) and (D) were not found to be exactly twice as large as the values of elongation. It may be considered that the increase in reduction of area is related to a change in the ratio of the acicular or plate-like alpha to equiaxed alpha.

Therefore, the improvement of the casting microstructure by the cyclic heating is effective in getting larger elongations and reductions of area, while the shape of alpha grains remains to be investigated.

The values of these tensile properties measured for the castings are lower than those of the forgings. It is thought that the volume of acicular alpha, the distribution of the precipitates, the number of voids and other factors are different from those of the forgings, which affect the values of elongation and reduction of area. Further, the size of pre-beta grains may affect these differences, and macro fracture surface observation indicates coarser pre-beta grains in the casting than those of the forging.

3.3.2 Impact Value. Alpha grain growth occurred and the tensile properties were changed by the various heat treatments, as mentioned above. It is very important to measure the impact values of the specimens which were exposed to high temperature, causing alpha grain growth. Figure 10 shows the V-notched impact values of the specimens subjected to the various heat treatments. It must be noticed that the impact values of the castings are higher than those of the forgings in every heat treated condition. To examine this point, the fractographic observations were made. From this observation it appeared that the fracture of alpha grains gave a little difference between the casting and the forging showing ductile fracture. But there were differences noted in the beta phase, that is,a very fine dimple pattern in the casting and coarse one in the forging. This difference would affect the impact value.

An influence of the cyclic heating was not shown on the impact value of both the castings and the forgings, but the impact values decreased when the S.T.A. was carried out after the cyclic heating. This decrease was larger in the case of the castings than the forgings. It is thought that these results are also related to the shape and size of alpha grains.

3.4 Discussion

In this report the improvement of microstructure and strength on cast Ti-6Al-4V alloy by the cyclic heating was shown. The as cast microstructure was transformed to nearly equiaxed alpha by cyclic heating, and correspondingly the values of elongation and reduction of area increased. However, their values were still smaller than those of the forgings. This may be related to the shape of alpha grains, retained acicular alpha, distribution of the precipitates, the number of voids, and other factors. The difference of properties and structures between the castings and the forgings might be explained clearly if these factors are measured quantita-

tively or even qualitatively. In this report we could obtain the improvement of the cast microstructure without causing a decrease in mechanical properties, which can then be heat treated by a conventional method. From these results, Ti-6Al-4V alloy can be used to cast complicated shaped parts of high speed rotating machines with high reliability.

We hope that examination of other mechanical properties such as fatigue strength will widen the application of this material.

4. CONCLUSION

An improvement of the microstructure for cast Ti-6Al-4V alloy by the cyclic heating was done, and their mechanical properties were reported. We have obtained the following conclusions:

(1) When cyclic heating was applied to castings, the cast microstructure was improved and became nearly equiaxed, similar to the forging.

(2) It is possible to heat treat this microstructure by the conventional methods, and the two phase structure ($\alpha+\beta$) was obtained.

(3) We showed evidence of the diffusion of Al and V, stabilizing alpha and beta phase.

(4) The alpha grains of the forging became coarser by the cyclic heating. But the tensile properties and impact values did not decrease.

(5) The tensile properties and impact values of the casting did not decrease by the cyclic heating, while the elongation and reduction of area increased slightly.

(6) The impact value of the castings was always higher than that of the forgings for the same heat treated conditions. This is related to the fine dimple pattern observed in the beta phase of the casting.

5. REFERENCES

1. Metals Handbook; vol. 7, 8th. Ed.

2. Jaffee, R. I., "Progress in Metal Physics", vol. 7, 1958.

ON TITANIUM ALLOY RESIDUAL STRESS FOLLOWING THERMODIFFUSION SATURATION

V.V. Nikolenko, T.S. Morosova, T.A. Tumanova

Moscow Aviation Institute

U.S.S.R.

The diffusion alloying of the surface can be used for increasing the wear resistance of the friction pairs which must be manufactured from titanium alloys to provide for light weight and high corrosion resistance. In particular, the wear resistance of titanium and its alloys can be considerably enhanced by surface saturation with chromium and silicon.

The optimum composition of the alloying mixture and the procedure of diffusion saturation are selected at present not only aiming at producing in the surface layer of the part structures and phases which determine the required properties (high hardness, heat resistance, wear resistance, etc.) but also taking into account the resulting residual stresses.

The diffusion saturation gives rise to phase transformations and changes in the chemical composition of the surface which are accompanied by bulk changes which generate in the surface layer of the part the residual stresses whose magnitude, sign and character of distribution can vary over a wide range. We suggest that the working properties of the parts whose surface has been treated (surface hardening, diffusion alloying, etc.) depend to the great extent on the fact whether the distribution of the residual stresses is favourable or unfavourable for given operational conditions.

We have studied the structure and phase composition of the alloys VT1 and VT5 and determined the distribution of the residual macrostresses in the case of saturation diffusion with various mixtures of chromium and silicon. The diffusion mixture consisted of powdered chromium and silicon (in various porportions). The process was carried out in vacuum furnaces under 10^{-3} - 10^{-4} mm Hg

TABLE I

Nos.	Comp of diffusion mixture	Phase comp. of surface layer	Lattice spacing (Å)	Res stress (kg/mm^2) Compr.	Tens.	Depth of trans. layer (mm)
1.	No saturation	αTi	a=2.953 c=4.687	30	-	1
2.	100%Cr	βTi	3.195			
		αCr	a=2.722 c=4.427	-	-	-
		$TiCr_2$	6.929			
3.	30%Cr + 20%Si	βTi	3.195			
		Cr_3Si	4.558	73	-	1.7
		αCr	a=2.722 c=4.427			
		$TiCr_2$	6.929			
4.	50%Cr + 50%Si	Ti	a=2.953 c=4.687			
		TiN	4.244	35-55	-	1.
		Ti_5Si_3	a=7.465 c=5.162			
5.	20%Cr + 80%Si	-	-	5-15	-	2.
6.	100%Si	αTi	a=2.953 c=4.687			
		Ti_5Si_3	a=7.465 c=5.162	-	90	0.08

at 850 and 900°C. Cylindrical samples 0.8 mm in diameter and 10 mm long were taken to analyze the phase composition of the surface layers after diffusion of chromium and silicon into VT1 and VT5 alloys. To observe the diffusion profiles, oblique 44' sections were made. The hypotenuse length of the section was 45 mm. The total depth of the oblique sections was ϕ.5 mm. Each section was cut into six segments for X-ray diffraction studies. X-ray diffraction patterns were recorded for the six segments the first of which correspondent to the depth of about ϕ.ϕ8 mm, the second to ϕ,18 mm, the third to ϕ.28 mm, the fourth to ϕ.34 mm, the fifth to ϕ.42 mm and the sixth to ϕ.50 mm.

The X-ray diffraction studies were made using an URS-55 apparatus with an RKD chamber, copper radiator and nickel filter. For each sample two recordings were made, one with rotation and one without rotation. The recording with rotation was made to evaluate the character of the lines, whether they were solid, broken or dotted, to provide for correct identification of the phases. When the oblique sections were analyzed the section was mounted so that the angle between the primary X-ray beam and the surface of the specimen was 30°. Since the alloy was large-grained the recordings were made with the sample deciating from the middle position by ± 6°. For the small Bragg angles, determinations of the interplanary spacings were accurate to 1 - 2 at the second decimal place, for the large angles the accuracy was several units at the third decimal place. To determine the starting phase composition of the alloy prior to diffusion saturation X-ray diffraction patterns were recorded for the side surface of the sample after it had been cut.

A special mechanooptical apparatus and the layer-by-layer etching technique were used to study the residual stresses in the 70 x 10 x 1.5 mm specimens of VT1 and VT5 following thermodiffusion saturation of the surface with chromium and silicon. The etching electrolyte was selected not to produce hydrogen absorption during etching which would distort the real picture of the distribution of stresses. The electrolyte contained 88% of ethylene glycol, 6% of hydrofluoric acid and 6% of water, the current density was 0.4 A/dm^2, the voltage was 80 V and the cathode was made of stainless steel.

The experimental results are presented in the form of tables and diagrams.

The X-ray diffraction patterns show that the surface layers of the VT1 and VT5 specimens contain, apart from αTi, titanium - chromium, titanium - silicon, chromium - silicon and chromium phases. Moreover, the X-ray diffraction patterns show 8 lines belonging to unknown, probably three-component, phases.

TABLE I presents the phase composition of the surface layer

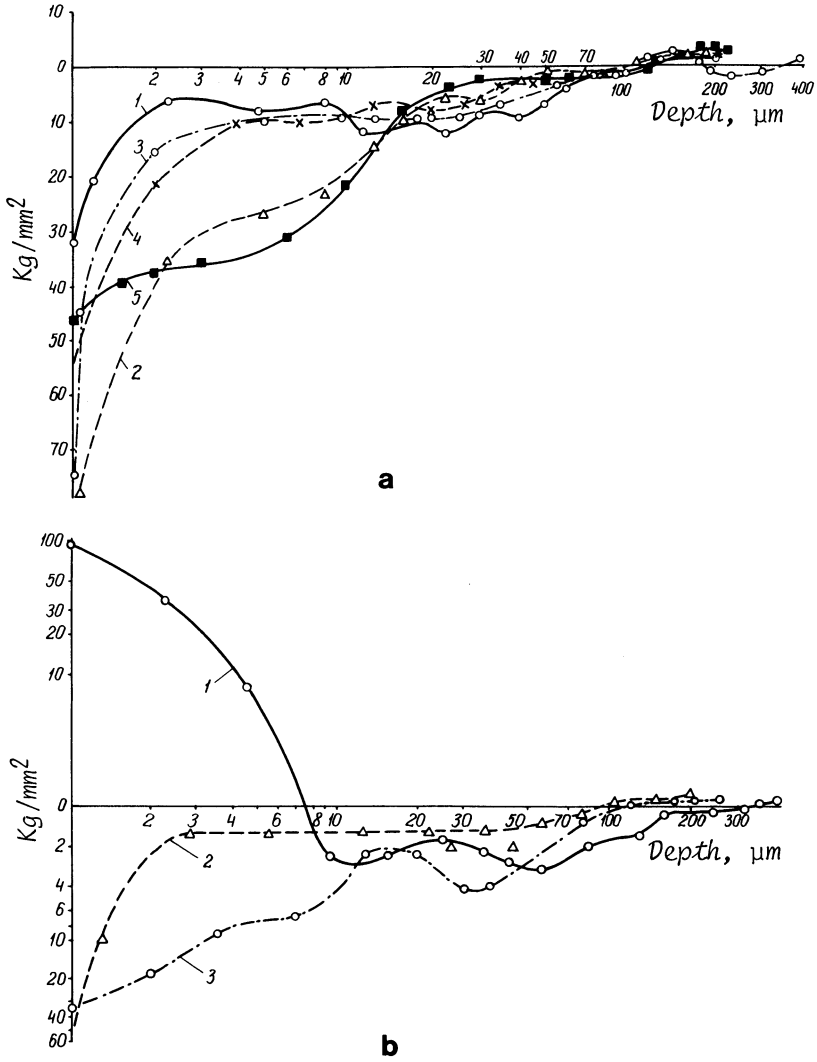

Fig. 1: The profile of the residual stresses with the depth in the diffusion layer.
a - in the alloy VT1.
1 - the initial state, without diffusion saturation.
2 - saturation with Cr-Si, 850° C, 6 hours.
3 - saturation with Cr-Si, 850° C, 12 hours.
4 - saturation with Cr-Si, 850° C, 16 hours (50%-50%).
5 - saturation with Cr-Si, 850° C, 24 hours.
b - in the alloy VT1.
1 - saturation with Si, 900° C, 16 hours.
2 - saturation with Cr-Si (50%-50%), 900° C, 16 hours.
3 - saturation with Cr-Si (50%-50%), 900° C, 20 hours.

of the VT1 specimens following saturation with mixture of various compositions as well as the highest values of the residual stresses in the diffusion layers.

The results presented in TABLE I show that after soft polishing the specimens of VT1 exhibit in the surface layer residual compression stresses of the order of 30 kg/mm^2 which are balanced by the tensile stresses at the depth about 1 mm.

Surface saturation with chromium and silicon produces changes in the distribution of stresses at the surface owing to the differences in the specific volumes of the primary metal and the phases which are formed in the process.

As may be seen from Fig.1 (a and b) the stress distributions are different for any mode of diffusion saturation down to the depth of 20 mcm and below that the distributions are practically the same as that for the initial state of VT1 without diffusion saturation. The VT1 specimens are distinguished by unfavourable distribution of the residual stresses in the case of silicon diffusion (Fig.1b) when very high (up to 90 kg/mm^2) tensile stresses are developed which can give rise to cracking of the surface layer under operational conditions (agressive medium, working stresses, etc.).

The samples of VT5 after silicon diffusion exhibit residual compression stresses, since the relationship between the specific volumes of the phases produced here is different from that of the VT1 specimens (see Fig.2, a and b). The depth of the transition region between the compression stresses and the balancing tensile stresses varies from .70 to 1.00 mm. Diffusion saturation with chromium and silicon in ammonium chloride medium increased the residual stresses at the surface from 7 to 18 kg/mm^2 (Fig.2b) owing to formation of the nitride phases of high specific volume.

The result of the electron-microscopic studies of the surface of the VT1 specimens saturated with 50% chromium and 50% silicon are shown in Fig.3 (a and b) where a is the surface and b is the base metal. A comparison of the microstructures of VT1 and VT5 specimens following similar mode of saturation shows that the distribution of the large-scale phases (Fig. 3, c and d) in VT5 is more uniform indicating the lower residual stresses; this conclusion is in a good agreement with the residual stress profiles for both alloys.

The reported studies made it possible to select the optimum mode of diffusion saturation with chromium and silicon for the parts manufactured from VT5 (precision gears). Saturation from the vapour phase for 16 hours at the temperature of 850°C with the powdered mixture of chromium and silicon (1:1 by weight) produces the diffusion layer .80 mm thick in which there are formed the

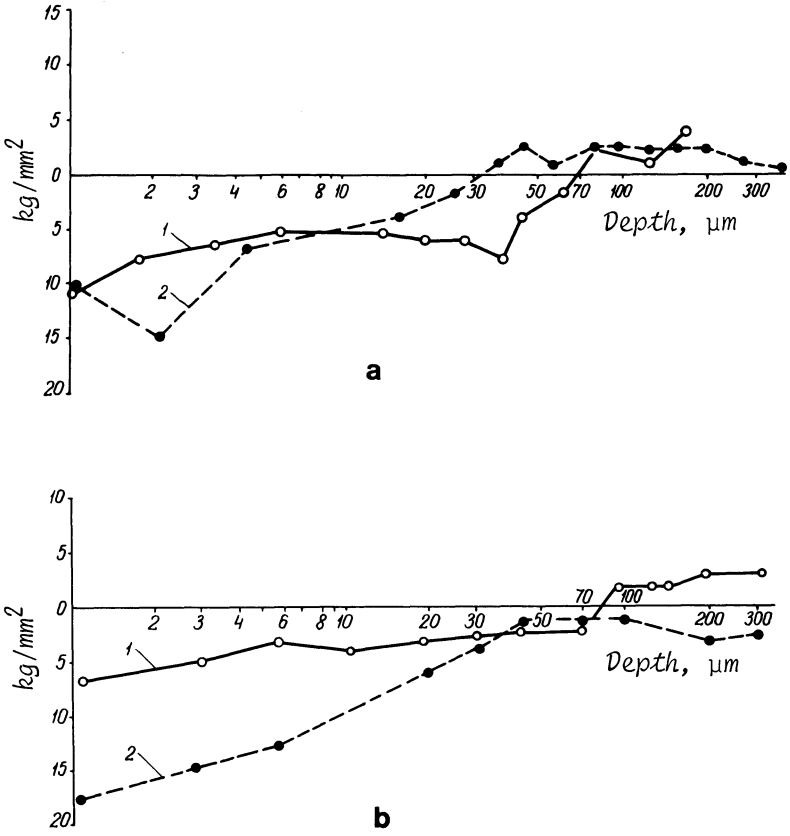

Fig. 2: The profile of the residual stresses with the depth in the diffusion layer, a - in the alloy VT5.
1 - saturation with Cr, 850°C, 16 hours.
2 - saturation with Si, 850°C, 16 hours.
b - in the alloy VT5; in the NH_4Cl medium (2).
1 - saturation with Cr-Si (50%-50%), 850°C, 16 hours.
2 - saturation with Cr-Si (50%-50%). 850°C, 16 hours.

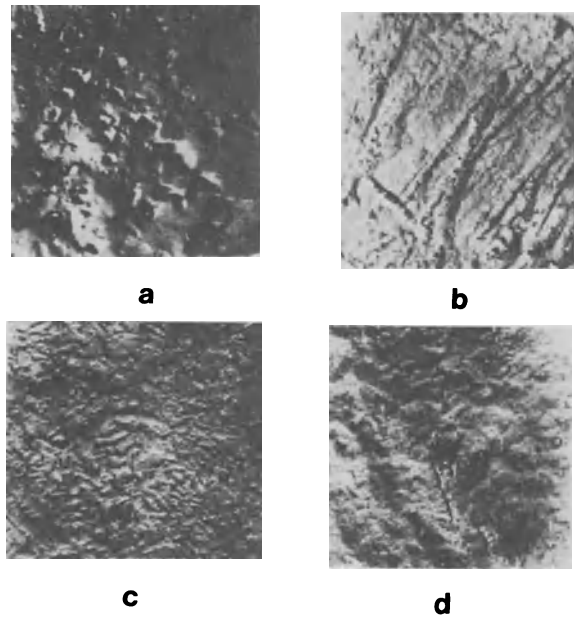

Fig. 3: Electronmicroscopic studies of the structure of the alloys VT1 and VT5 following diffusion saturation with chromium and silicon (50%-50%); x 6300.
a - the surface of the alloy VT1.
b - the bulk of the alloy VT1.
c - the surface of the alloy VT5.
d - the bulk of the alloy VT5.

phases $TiSi_3$, $TiSi_2$, $CrSi_2$ and Cr_3Si and the solid solution based on Ti with the microhardness of 1300 kg/mm^2. The residual stresses at the surface amount to 75 kg/mm^2. As a result, the wear resistance is increased 3 - 5 times.

Industrial experience with the technique show that the gears manufactured from the VT5 alloy saturated with chromium and silicon exhibit practically no wear after operation for 1000 hours at the temperatures from -60 to +80°C.

Discussion

Section X. Influence of Technological Factors on Structure and Properties of Titanium Alloys

Following P. H. Morton's Critical Review and N. F. Anoshkin's report, they and the authors of the papers were asked a number of questions followed by discussion, with the most essential subjects being presented below.

Question to P. H. Morton:

Is it possible to produce good properties, particularly fatigue life, in alloys with coarse macrostructure and fine microstructure?

Answer:

One should distinguish between two types of fatigue: the low cycle fatigue (high loads, short life) and the high cycle fatigue (lower loads and longer life).

The low cycle fatigue is the best indicator of product quality uniformity. We can have two specimens with identical conventional properties, but they can have quite a different low cycle fatigue life.

As far as the high cycle fatigue is concerned, a fine microstructure is adequately good and, in this case, it is not very important how coarse the β-grain is, i.e., what we know as macrostructure. For low cycle fatigue, both macrostructure and microstructure are important, they should be sufficiently fine.

This difference in material behavior under various loading conditions is explained by the composition difference in alloy micro-volumes, in phase composition which is indicated by the microprobe rather than the structural difference revealed by a microscrope. Macro and microstructure both influence the phase composition, α-phase composition being especially important in this respect.

Question to B. A. Kolachov:

Does hydrogen content influence titanium alloy workability?

Answer:

The favorable hydrogen effect on workability can be used for titanium alloys which are difficult to deform under normal conditions or alloys which are virtually unworkable when hydrogen is not present in them. In this case, one can introduce hydrogen, rework the material, manufacture the product required at high deformation temperatures, and then eliminate hydrogen by vacuum annealing in order to prevent low temperature hydrogen embrittlement.

I would like to stress that this hydrogen plastification effect was initially discovered by U. Zwicker. We continued his effort and found the optimal conditions at which this effect can be used for various titanium alloys, particularly, alloys that contain so much aluminum as to be fully unworkable by conventional method.

V. A. Livanov (supplementing B. A. Kolachov):

U. Zwicker added hydrogen during melting and it was observed that ingot forgability was improved. We had a reverse picture: we started with studies of harmful effects of hydrogen which tends to embrittle alloys at room temperature. And, when high temperature testing was initiated, a ductility level was obtained bordering on superplasticity.

For example, a specimen 10 mm in diameter and 15 mm high was upset forged at 900°C with the resultant forging being lens-shaped with sharp edges similar to those of a razor and without a single crack.

It should be stressed that the degassed structure was very good, i.e., the imposition of two operations - hydrogen addition and forging does not introduce any defects.

N. Z. Pertsovsky

The Critical Review, prepared by J. D. Alexander, and presented by P. H. Morton, paid a great deal of attention to the α-phase effect on mechanical properties of titanium alloys. I would like to share some thoughts in relation to this subject as they are implied in our (with M. Ya. Brun and other co-workers) report.

The main idea of our paper was to show that mechanical properties are determined only by a complex of structural parameters, rather than by a single structural parameter, as for example, grain size. These parameters were found to be: initial β-grain size, α-colony or α-plate packet size and α-plate thickness, the greatest effect being produced by the latter parameter. However, even such

combined evaluation is not always a complete one since it does not consider the effect of structural parameters such as the secondary α-phase precipitate size, the thickness of the interfacial state, the internal structure of α-plates, which as been mentioned in a number of papers during session X. Therefore, it is necessary to obtain further experimental data, desirably of statistical character, which allow a firm prediction to be made of titanium alloy mechanical properties and structures.

In addition to tensile properties, our work studied the effect of structural parameters on the design strength level, primarily impact bending strength as measured in fatigue-precracked specimens and fracture toughness K_{IC}. When reduction in area is decreased and, depending on colony size and plate thickness, it exhibits an extremum-type relationship, K_{IC} increases uniformly with coarser structures. This seems to indicate that it is possible to obtain an adequately high dependability level in semi-fabricated and finished products with coarse-grain lamellar structure.

U. Zwicker

I would like to ask Dr. Stubbington about the fatigue strength in Ti-6Al-4V alloy. He has shown some limits for various structures.

If we investigate a complex Ti-6Al-4V alloy, the change in structure is observed not only because of element concentration variations but also due to additional annealing. We can have a two-phase composition and element concentration can be different in each phase due to diffusion processes and probably No. 3 annealing, 950°C 0.5 hr., which was mentioned by C. A. Stubbington, may result in some optimization of fatigue strength. I would like to ask him whether he used a microprobe in his experiments in order to find the cause of the maximum fatigue resistance after No. 3 annealing?

C. A. Stubbington

We made no such analysis. Probably we should be more cautious in interpreting the results. We should have tested notched specimens and made evaluations of fracture toughness. Many differences disappear under these conditions.

Another important consideration is grain orientation. I feel that our future investigations will include a fuller material characterization. In the past, our work and other reported studies had detailed evaluations only of the structure. In the future, it is necessary to determine pole figures for every material and microstructure tested since we have shown that there are serious differences in the rate of crack growth in Ti-6Al-4V alloy at a constant maximum load depending on fracture plane crystallography.

I. A. Povarov

High-strength titanium alloy development in the Soviet Union follows two trends: creation of $\alpha+\beta$ alloys with extreme strengthening by alloying of α and β solid solutions and creation of alloys strengthened by precipitation hardening during heat treatment. For group 1 alloys it is, perhaps, possible to achieve a tensile strength of 120-125 kg/mm^2, for group 2 alloys the strength can be as high as 150-180 kg/mm^2. In all the cases, however, material should have uniform fine grain structure in order to insure high strength at satisfactory plasticity and toughness characteristics. The manufacture of high quality original structure in a number of titanium semi-products, particularly large press forgings, offers a very serious problem being the main limitation to increasing the component strength by heat treatment. Various attempts to eliminate this problem by the thermomechanical treatment methods, unfortunately, did not give any quality improvements. A number of presentations at this conference pointed to the significant capabilities of isothermal press forging as performed in a superplasticity state for producing precision forgings at lower unit pressures with the objective of increasing material yield.

This promising process has been viewed by us from a somewhat different angle. First, as a manufacturing method for improving original structure and in combination with subsequent active strengthening thermal treatment as a method for upgrading strength and performance of high-strength titanium alloy load-carrying members in critical structures. A number of studies stated that no significant beneficial effects on properties were observed in medium alloy content compositions, such as the Ti-6Al-6V-2Sn alloy forged under isothermal conditions. In relation to this method, two-phase titanium alloys with variable α/β phase ratio and variable polymorphous transformation temperature, in particular, BT-6 alloy (Ti-6Al-4V) containing about 7% β-phase, BT-14 alloy (Ti-5Al-3Mo-6V) with 12% β-phase, and the critical composition alloy BT-22 (system Ti-Al-V-Cr) containing approximately 35% β-phase have been studied.

It was established by investigations that, after isothermal deformation at temperatures 50-100° below the β-transus temperature and a deformation rate of 0.14 mm/s, an especially fine grain structure is formed. Alloy BT-14 had an average grain size of about 4.8 microns, alloy BT-22, 2-3 microns. This structure is equiaxed and uniform throughout the forging. Material with such structure possesses a high strength of an order of 120-150 kg/mm^2 at elongation of 14-8%, reduction 40-25%, respectively. In addition, it has been established that the most promising high-strength alloy for manufacturing parts by isothermal forging are alloys of BT-22 type with high concentration of β-stabilizing elements and high β-phase volume fractions.

These alloys are suitable for forging operations at relatively low temperatures, of an order of 790-830°C. They exhibit good die filling and are capable of producing,even during β-deformation, a finely distributed structure which effectively responds to heat treatment.

According to preliminary evaluations, use of isothermal forging, in combination with heat treatment, will permit weight reductions in structures of 15-20% to be made, to improve structure reliability and life.

E. S. Makhnev

A number of papers presented at this session demonstrated the pronounced effect of α/β phase ratio on titanium alloy properties. We have arrived at the same conclusion. Our data indicate that if the amount of α-phase is not above 10%, then the deformation slightly below the polymorphous transformation temperature will not prevent coarsening of structure. To insure process stability, α-phase should not be above 15%.

If we are to mention such a process factor as holding time, particularly during deformation in β and α+β regions with the deformation being transferred from β to α+β, the incubation period should by all means be taken into account, this period assuring such a high transformation rate that α-phase also exceeded 15%. Neglecting this process parameter will result in property unstability and structure coarsening. But, unfortunately, we do not have practical data on the time of incubation period in the upper temperature range.

Other factors which should be mentioned are cooling rate and heating temperature.

The isothermal press forging of most alloys occurs at temperatures producing α' abd α" structures on cooling. Our work shows that lamination unavoidably occurs in titanium alloys on heating and solid solution homogeneity cannot be reached. This solid solution non-uniformity leads to two types of martensite when α' and α" mixture is rapidly cooled. And, if the cooling rate is adequately high, α" martensite can be formed, having quantities of α', and the further property precipitations cannot be avoided. Thus, it seems that the manufacturing process conditions, primarily in relation to press forgings, must by all means include cooling conditions inhibiting formation of martensite.

Critical Review

TITANIUM ALLOYS FOR DIFFERENT BRANCHES OF ENGINEERING

S. G. Glasunov

Academy of Science

U.S.S.R.

In spite of its young age, as compared with other structural materials, titanium has already been tested in many areas of application. The time will probably come soon when it will be easier to enumerate the areas where titanium is not applied than those where it is applied.

The structure of titanium applications changes rather slowly, and the aerospace industry still remains the main consumer of this metal. It can nevertheless be stated that the share of this main consumer of titanium gradually decreases. New consumers enter the stage and their role constantly increases.

At the 2nd International Conference a very interesting introductory paper, "Titanium-Metal with a Past and a Future", was presented, in which it was stated that the structure of consumption in 1972 was the mirror reflection of that in 1968. The authors of the paper, Messrs. A. E. Gorum and R. Colton, stated with regret that the development of titanium industry in the USA and other countries follows a sinusoidal curve, the reason for which is, so to speak, the capricious nature of the main consumer of titanium, the aerospace industry. The authors also claim that such development of titanium industry is characteristic not only of the USA but also of all the other industrially developed countries without exception. While appraising the authority of American scientists and the achievements of American titanium industry, I shall permit myself to note that in this country the sinusoidal curve does not characterize the development of titanium. We prefer simpler regularities, e.g., an ascending straight line. To prove this one can indicate that, according to official data published in connec-

tion with the 25th Congress of CPSU, the production of titanium in the Soviet Union will increase by 40% in the coming five years.

In foreseeable future the aerospace industry will unquestionably remain the chief consumer of titanium. This area of application, however, should be differentiated and divided at least into two parts, viz., the military and the civil. The instabilities of consumption are chiefly observed in the first part. In other words, it is Mars, the god of war, who jars the titanium industry most of all. Mercury, the god of commerce and industry, personifying the civil aviation, is a more reliable consumer of titanium, and we must give due credit to the achievements of American designers who succeeded in using a great amount of titanium in huge transport and passenger planes of the third generation, whose first representative was the Boeing-747.

It is to be hoped that, due to the relaxation of the international tension, the influence of Mercury will grow to the benefit of titanium industry all over the world.

It can be argued that the main reason for the recent difficulties was the termination of the financing of the supersonic titanium passenger aircraft "SST", and not of a military project. But, had the "SST" project been completed, it would have been a reliable and permanent consumer of titanium. Incidentally, alumino-titanium "SST" aircraft, viz., "Concord" and "TU-144" have already appeared. In due time a titanium "SST" will also be built. The aerospace industry is a source of experience in titanium application for the other branches of industry, and it has already provided all the necessary titanium alloys needed to operate in various conditions.

The other branches of engineering where titanium application shows good promise are described below.

Mechanical engineering: chemical, power-generating, transport, for commodity and food industries, household appliances. Chemical engineering plants, e.g., manufacture a broad range of standard equipment, including valves, taps, pumps, tanks, filters, heat exchangers, centrifuges. Some large plants manufacture non-standard equipment for their own needs, e.g., gas flues, ventilators, driers, etc.

In power engineering titanium is used for the components of gas turbines and electric generators. This area of application has already been dealt with in the papers of Soviet specialists at the Ist and the 2nd Conferences on Titanium. As one of the recent developments we should mention the use of 1350mm long titanium blades for the steam turbine of record 1200Mw capacity.[1]

As a result of investigations conducted at research and development centers of the aviation, automotive and tractor industries, as well as at the Institute of Titanium, it has been shown expedient to use titanium in automobile transport, e.g., for automobile diesel engines.(2) For the supporting structures of automobiles it is recommended to use medium-strength sheet alloys, e.g., OT4, VT5-1; for the running gear- the VT6, VT14 and VT3-1 alloys forgings; for engine components - heat-resistant alloys VT3-1, VT8, VT9, etc.

The Institute of Titanium and the Krivorozhsky mining equipment plant have studied the application of titanium in the mining industry. The hand-operated drill, manufactured using titanium, weighs 26 instead of 32kg, which improves the labor conditions and raises the productivity. A great advantage of titanium drills is their high corrosion resistance and the absence of cold brittleness, which is important in the conditions of Siberia and the Far East.

Metallurgy: By its scope and volume of titanium application, metallurgy occupies the first place among other industrial branches after the aerospace industry. Titanium equipment has found the most extensive application in the nickel-cobalt and titanium-magnesium industries, as well as in the production of copper, zinc, tin and other metals. Substituting titanium for other metals, e.g., stainless steel, gives a substantial economic benefit due to the increased service life of the equipment. The effect is even more significant when titanium is chosen from the very beginning as the basic material for the manufacturing of the equipment and it becomes possible to utilize to the maximum the properties of this metal. This results in a considerable intensification of the existing technological processes and the development of new, more advanced ones. For example, by using titanium equipment, we succeeded in developing a new process of nickel production in our country, which makes it possible to reduce the production costs by approximately 25%.(3)

In ferrous metallurgy the application of titanium instead of stainless steel is also very effective. Titanium is stable in most of the corrosive media encountered in metallurgical, coking, ferroalloy and steel-rolling plants. At the "Zaporozhstal" plant, for example, a rubber-lined carbon steel pipeline is used to discharge the spent pickling solutions. Its service life is about 3 months. The studies carried out at the Institute of Titanium have shown that a titanium pipeline in these conditions will serve for scores of years, since the rate of corrosion in titanium, in this case, does not exceed 0.01-0.05mm/yr.

Chemical and petrochemical industry. As far as I know, ti-

tanium was for the first time used in chemical industry in 1954 when "Titanium Metals Corporation of America" applied commercial titanium to line a mixer operating in the chlorine dioxide medium. At present, practically all the industrially developed countries use titanium in these branches of industry. In Japan, for example, a great portion of rolled titanium stock serves the needs of chemical industry; in other countries quite a substantial amount of titanium is also used for these purposes.

Titanium and its alloys have good prospects of being applied in pulp and paper industry, in galvanoplastics and electroplating, food industry and medicine. More detailed data on the effectiveness of titanium application in different branches of industry are contained in the handbook, "Application of Titanium in National Economy", Kiev, 1975, which can be purchased at this conference.

At this conference, as at the two previous ones, an enormous amount of information has been presented on titanium alloys and titanium semi-finished products for the aerospace industry. In this presentation, therefore, these questions are not dealt with. In the other branches of industry, in most cases, the high resistance of titanium to corrosion is utilized. Mechanical loads being relatively small, the main structural material used is the unalloyed sheet titanium. In some cases the resistance to corrosion of commercial titanium proves insufficiently high, and titanium alloys with palladium, molybdenum and tantalum are then used. In the cases when titanium is to be used in mechanically-loaded components the titanium alloys applied are the same as for the aerospace engineering.

The character of papers presented at the previous conferences and the present one also demonstrates the increased application of titanium and its alloys in the non-military branches of industry. At the first conference there were two such papers, at the second - six, whereas in this, the third conference, eight such papers have been presented.

In conclusion, I should like to mention once again the paper of E. A. Gorum and R. Colton. It is said there that sheet must be the main type of standard titanium semiproducts for the non-military branches of industry. In my opinion, castings should be added here, especially for such products as centrifugal pumps. The American firm "Oremet", for example, has made substantial progress in manufacturing large castings of this kind for the chemical industry. Titanium mold castings are used to advantage for the manufacturing of corrosion-resistant fittings, as this results in a substantial reduction of labor consumption and makes it possible to utilize scrap extensively. Information is beginning to appear on the development of secondary titanium alloys in a number of countries,

including the Soviet Union.

At present there is every reason to believe that permanent consumers have been found for titanium in non-military branches of industry. This should strengthen the economic base of titanium metallurgy and facilitate the further expansion of the production of this metal, the metal of the XX century.

REFERENCES

1. Application of Titanium in National Economy. Ed. A. T. Tumanov. "Tekhnika" Publ., Kiev, 1975.

2. Titanium in Industry. Ed. S. G. Glazunov. Moscow, "Oborongiz" Publ., 1961.

3. Galitsky, B. A., Abelev, M. M. et al, Titanium and its alloys in Chemical Engineering. Moscow, "Mashinostroyeniye" Publ., 1963.

Critical Review

TITANIUM FOR ENGINEERING PURPOSES

C. Edeleanu

Imperial Chemical Industries Limited, Billingham
Cleveland TS23 ILD, England

Introduction

Titanium technology has made steady progress since the last International Conference and it is very difficult to select the technological areas in which the advances have been of greatest engineering significance, but the overall effect is easy to see.

Up to a few years ago, titanium could hardly be considered to be a normal engineering material, but this is no longer so, and we can now treat it in a routine manner like any other metal or alloy. In the 1972 symposium E R Rowley referred to titanium as having passed from childhood to adolescence and we can now say that it has come of age and is a fully fledged adult. We must stop thinking of titanium as a new metal; we no longer should regard it as exotic and we should remember that large and complex equipment can be built successfully out of it. Naturally it is still necessary to employ specialist fabricators as a general rule, but at least the selection of titanium for a piece of equipment does not normally pose a major procurement problem.

This is an important milestone in the history of any material because once it has been passed, potential users of the material are far more ready to consider it and there is a prospect of a rapid expansion in its use. A E Gorum and R Colton in their keynote address in the 1972 symposium stressed the need for titanium to come down to earth and now we have passed this milestone people other than

those in the aerospace industry can now consider it without further hesitation. This paper therefore deals with some of the factors which have contributed to the change and the resulting implications.

Codification

The engineers cannot use a material in a routine way until such time as there is a system of specifications and codes which describe the material and the various fabrication techniques in an adequate manner. Even then it takes a few years for the content of these papers to be fully understood and assimilated and the significance of the various available options is tested by experience. Such codes have now existed in many countries for a sufficient time to have been tested in practice and although there is a great deal more to codify, we have a good basis to work on. The present codes are perhaps too conservative and, for instance, the allowable working stresses for titanium at elevated temperatures are unnecessarily low but this creates no problem other than adding to the cost of the equipment. This is a nuisance but not a major problem.

There may be a number of scientists who may find it difficult to understand the role codes play in the process of turning the information they acquire into usable information by engineers, but it is no exaggeration to say that the clearest and the most brilliant scientific paper is virtually unusable in regular engineering design by engineers until its content is incorporated into codes. This process of incorporation does involve simplifying and even over-simplifying of data until it may appear to the originator as being unrelated to fact. Perfection, in this case, is very often the enemy of the good and if anyone wants to have his knowledge used in a routine manner he must have it incorporated into codes and accept some distortion in the process.

Confidence

Codes are necessary because they provide a basic communication system between the drawing board, those who manufacture materials, those on the shop floor in the fabrication shop, inspectors, planners and all sorts of people who all play a part in building hardware, and until a code has been used a number of times there is scope for misunderstanding and low confidence. In the early days of a material lack of confidence means that the material is not selected for use unless it offers very major advantages and even then only if there is no pressing time constraint, because one must allow time to deal with failures in the communication system. Fortunately, we are over this difficulty in the case of titanium, and particularly so in the case of the un-alloyed metal itself. Confidence in the adequacy of the code system is not however enough to allow the selection of a material for a given duty on a purely cost and merit basis because there must also be confidence that performance in service is as predicted. We

have, for instance, all known that titanium suffered no corrosion in sea water and it is an obvious material to consider for such a duty, but there is a big step between the knowledge that there will be no corrosion and the proof that exchangers made out of titanium actually perform satisfactorily, and then there is an additional step in re-designing exchangers and for that matter cooling water systems as a whole to take full advantage of the properties of titanium. This process takes time, but when it is finished there is a prospect of a snowball effect and then if there are major advantages one can expect a rapid change over from one material to another. We certainly are very much at that point in the case of sea water cooling with titanium exchangers and especially so in the offshore oil rig technology. The reason why such exchangers are popular in oil rigs are explained in another paper, but it is worth mentioning one finding with plate exchangers which illustrates how practical experience can lead to a re-assessment and, in this case as it happens, to an unexpected advantage. It is very difficult to predict fouling rates and it was not at all clear at first whether titanium exchangers would not foul more rapidly than copper based alloy exchangers in sea water and therefore what allowances should be made for cleaning and extra surface. Service experience has shown rather unexpectedly that fouling, given correct usage, could be appreciably less with titanium and this is a very important consideration.

The engineer has also to consider maintenance at the time of selection and even though he may try to opt for a design and material which will call for no maintenance, he can never be sure that he has achieved this ideal objective and he must have confidence that the equipment, especially if it is expensive, can be repaired or modified if it is necessary. With a new material and mode of construction this is difficult and when the vessels shown in Figure I were first installed at Billingham on a Urea Plant no one could be quite sure that we would be able to carry out repairs. These reasonably large vessels were multi layer steel vessels with a relatively thin titanium lining and there were a number of problems. First we were afraid that we would not detect failures in the lining should they occur, sufficiently early to prevent urea entering the shell layers and causing irrepairable damage to these important vessels. A monitoring system had to be developed, and proved in practice. This did provide some assurance but it was not until a number of liner failures had occurred in various parts of the world on similar vessels and we all started to understand the nature of the failure and proved the repair technique that the last trace of uncertainty about such vessels could be removed. This is again an example in which any doubt about the use of titanium has now vanished and we can all consider its selection without any reservation for service in large high pressure vessels.

Fig. 1 - Two 18 metre tall Urea reaction Vessels which have been in service at 225 bar since 1966 in a nominal 1000 tons/day Urea plant.

Change In Philosophy In The Use Of Titanium

Titanium was, and still is, a relatively expensive mater al, but this is not very important in those cases in which the advantages associated with its successful use makes it the obvious economic choice. The accent, however, is on the word 'successful', and in the early days when confidence was relatively low, when costs were very high, not only because of the bare cost of the material but also because so much effort had to be spent since codes did not exist, we all wanted to use as little titanium as we could. Experience has shown that we were wrong, because by using the minimum amount of titanium possible we added to the design and fabrication problems and by using very thin tubes or plates we exposed equipment to mechanical damage. Over the years there has therefore been a gradual increase in the amount of titanium used for any given application. We now use thicker tubes and solid titanium is used where liners or clad titanium was once considered. Designs are simplified to reduce fabrication costs. This trend again is important to the titanium industry. It could perhaps be slightly stimulated by increasing the allowable design rating for titanium in the codes provided the laboratory data justifies this, because the use of cladding and linings complicate design. This may be a small point, but it may also be a very important point. Trends have a strange way of accelerating given the right circumstances, and one of the necessary elements is with us now. Titanium has become an engineering material and engineers tend to think big, really big. For instance, one man in a meeting in London in April asked why not build offshore oil rig legs out of titanium. Whilst the question seems unrealistic at first sight, it may not be one we ought to dismiss out of hand. The cost of protection of such legs is high, corrosion fatigue is a problem with steel structures, safety and reliability are big problems and the only problem with titanium is that there is not enough of it manufactured in the world to consider using it on such a scale. It may also be that titanium is also slightly too expensive for such an application, and then the question is would it be quite as expensive as it is if we were to think really big? Perhaps the papers in the second session of this conference will be showing us the way ahead.

This may be interesting for the long term future, but returning to today it is worth saying something about costs even though this is a highly complicated matter and especially so in a multi national meeting of this type. Whilst titanium may be expensive, many of the other corrosion resistant materials are not cheap either, and titanium equipment is by no means always the most expensive of the available alternatives. It is worth making this point because a surprising number of people have not looked at data and just assume that titanium is expensive. Making straight comparisons between alternatives on the basis of material costs is seldom valid because

almost invariably a change in material has many secondary effects, and at times these are far more important than the differences in material costs. These secondary effects are specific to each situation and can hardly be discussed in this paper, but two general points are possibly worth making. If there is a change from one material to another and the equipment does not change physically in any way, it is almost certain that full advantage has not been taken from the change, and secondly if calculations are solely based on initial capital costs of a given item in order to decide whether to change from one material to another it would be surprising if the conclusions were valid. The really important changes normally introduce a new degree of freedom and allow us to do something which was either difficult or impossible before hand.

Successes And Failures

There have been comparatively few spectacular failures with titanium equipment and confidence in the material is high because of this. This is not entirely surprising, but if the assumption that this material is now becoming an ordinary engineering material is correct, there is a high probability that we will start having such failures. Whilst the material was considered to be an expensive and exotic material, each new application was carefully considered, only specialist and experienced people used it and inspected it carefully whilst in service. This is however inconsistent with the material being used in a routine way and mistakes will now be made with it just as they are made with all other materials.

Hydrogen has been a bit of a problem and since there is nothing in the titanium codes equivalent to the Nelson Curves for steels problems in this area are very likely to be found so long as the subject is not codified. The other area of possible concern is in the use of alloys, because those of us who are not in the aircraft industry know little about such alloys and it is not at all clear to what extent these alloys can be used for corrosive duties and what fabrication precautions are necessary. We do know that traces of iron in commercially pure titanium can have surprising effects both from a corrosion and hydrogen point of view under certain corrosive conditions, so there is an uneasy feeling that surprises with alloys are likely.

This places us in a slight dilemma because on the one hand we may be able to retain the good safety record associated with titanium by maintaining the fiction that it is a material to be used only by specialists, but do we want to do this and will it really help? Retaining control on who uses titanium, and for what, might restrict failures associated with titanium, but will it really make the world a safer place since failures will continue to occur on equipment manufactured from a less suitable material.

Turning now to successes the list is too long to deal with and there is no point in producing just a table. The more important subjects are treated in the various papers in this conference and the only thing worth saying is that by looking at these papers it is possible to sustain the claim that titanium has come down to earth and that it is an established engineering material and this general advance is made up from advances in many areas and each one has been important. However the progress made will have to be codified if it is to be useful to the engineers.

TRENDS IN THE DEVELOPMENT OF HIGH-STRENGTH TITANIUM ALLOYS

V. N. Moiseev, Yu. I. Zakharov, and E. V. Znamenskaya

USSR Academy of Sciences

U.S.S.R.

GENERAL PRINCIPLES OF STRENGTHENING TITANIUM ALLOYS

It is generally assumed at present that imparting high strength to metal materials involves an increase in the resistance to plastic deformation, which is attained by hindering dislocations in various ways. For this purpose such traditional methods of affecting the structure of metals as alloying, plastic deformation and strengthening heat treatment are used. In terms of dislocation theory, the relationship between the yield point of solid solutions and various physico-chemical factors is generally described in the following equation: (1,2)

$$\sigma_s = (\sigma_{n\text{-}H} + \Delta\sigma_{n\text{-}H}) + \Sigma(\sigma i + \Delta\sigma i) + \alpha_1 (G+\Delta G) B_i \sqrt{\rho} + K_y^1 d^{-1},$$

where $\sigma_{P\text{-}N}$ is the Peierls-Nabarro stress, $\Sigma\sigma_i$ is strengthening by interstitial impurities, G is the shear modulus, b_1-is the Burgers vector, ρ- is the dislocation forest density, d-is the grain diameter, α_1 and K_y^1 are constants for the given alloy, and $\Delta\sigma_{P\text{-}N}$, $\Delta\sigma_1$, Δ^G are values representative of the effect of alloying with the second component on $\sigma_{P\text{-}N}$, σ_i and G parameters.

The increase in the Peierls-Nabarro stress during alloying correlates with the degree of crystal lattice distortion, determined by the lattice parameter variation with the electron density variation during alloying, also with increasing shear modulus due to alloying.

The dislocation forest density and grain size are determined, mainly, by the thermomechanical parameters of alloy processing, as

well as by the deformation and heat treatment parameters.

In the case of two-phase alloys, the interphase boundary may be the most effective barrier for slip dislocations. This is due to the fact that transition through the interphase boundary brings about not only a change in orientation, but also in lattice type.

As a rule, the yield point of two-phase alloys in the equilibrium state varies linearly in proportion to the amount of the second phase. This relationship can be expressed as the following equation:

$$\sigma_S \text{ alloy} = \sigma_{S\alpha}V\alpha + \sigma_{S\beta}V\beta = \sigma_{S\alpha} + V\beta(\sigma_{S\beta}-\sigma_{S\alpha}),$$

where $\sigma_{S\alpha}$ and $\sigma_{S\beta}$ are the yield point of the alpha and beta phases, V_α and $V\beta$ are the volume fractions of alpha and beta phases.

Maximum strengthening effect due to the second phase presence is reached when this phase is distributed in the form of dispersed particles within the main phase. Structures of this type are usually obtained by appropriate heat treatment of the alloys. The increment of the yield point, due to the presence of dispersed particles of the second phase, is a function of the particle size, distance between particles, and their volume fraction, shear modulus, and the degree of misfit of the atomic radii of the particle and the matrix.[3,4,5,6]

The effects of all the above physico-chemical factors of strengthening are also used to obtain high strength titanium alloys.

Since the development of high-strength materials necessitates, along with high resistance to plastic deformation, a certain level of toughness and plasticity, it is expedient to resort to several types of strengthening at the same time, each individual factor providing for an optimum degree of strengthening.

Such an approach implies a considerable degree of solid solution strengthening through alloying, sufficient efficiency of strengthening heat treatment with precipitation of second phase dispersed particles, making use of strengthening by large second phase particles owing to an extended network of interphases, as well as toughness increase due to the high plasticity of the large second phase particles. In addition, forming in combination with heat treatment should provide for the alloy structure with optimum density and dislocation distribution, as well as fine grains.

Investigation into variations in the mechanical properties of alpha + beta titanium alloys depending on alloying has revealed some general regularities which to a great correlate with the above

propositions and can be summarized as follows.

In the annealed condition, the strengthening effect of the elements stabilizing the alpha and beta phases is the result of their strengthening the above phases and the ratio of alpha and beta phases in the structure.

The strength of alpha + beta titanium alloys is not merely the arithmetic means of the strength of the alpha and beta phases, but also a function of the distribution of the alpha and beta phases. As the amount of beta phase in the alpha matrix increases, the alloy strength increases, too, reaching a maximum in the alloys with the most uniform structure and almost equal amounts of alpha and beta phases. A further increase in the amount of beta-alloying element results in the decrease of alpha phase amount in beta matrix, with the strength of alloys decreasing from maximum to that of the alloys with beta structure.

The regularities of strength variation depending on alloying are somewhat different in case of alpha + beta titanium alloys in the thermally strengthened condition (after hardening and aging). As the content of beta-stabilizing element is increased to the critical concentration, the alloy strength is also increased, which may be attained by hardening and aging.

Alloys near the critical concentration may be thermally treated to a maximum strength.

Increasing the amount of beta-stabilizing element in the alloys of supercritical composition promotes beta phase stabilization, and the effect of strengthening through aging becomes less pronounced.

This nature of the alloys strength variation, as a result of hardening and aging, is due to the increase of structural dispersion, (just as in case of the alloys in the annealed condition) and, mainly, to the increase of beta phase amount which undergoes some changes during aging in the alloys of critical composition.

The ultimate strength of alloys and, to some extent, the effect of their strengthening after hardening and aging will depend on the strength of interacting alpha and beta phases, similar to that of the annealed alloys.[6,7]

The position of commercial titanium alloys on the diagram and their tendency to strengthening as a result of heat treatment are shown in Figure 1.

Here one can clearly see the above described regularity of the mechanical properties variation as a function of composition. Most

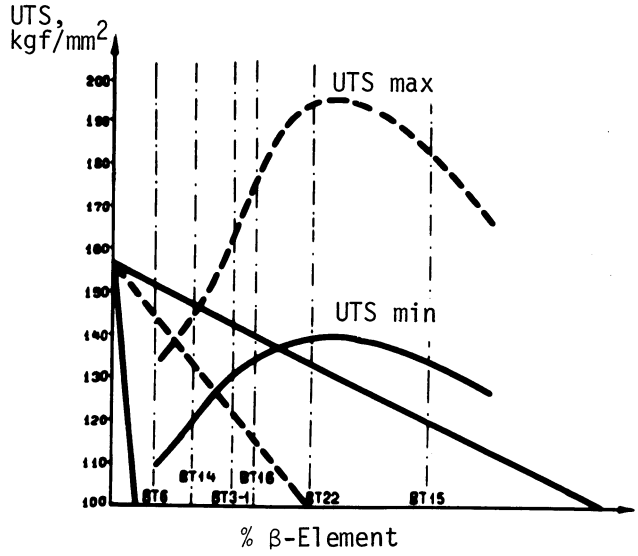

Fig. 1: Ultimate strength of industrial titanium alloys in the thermally strengthened condition versus beta-stabilizing elements content.

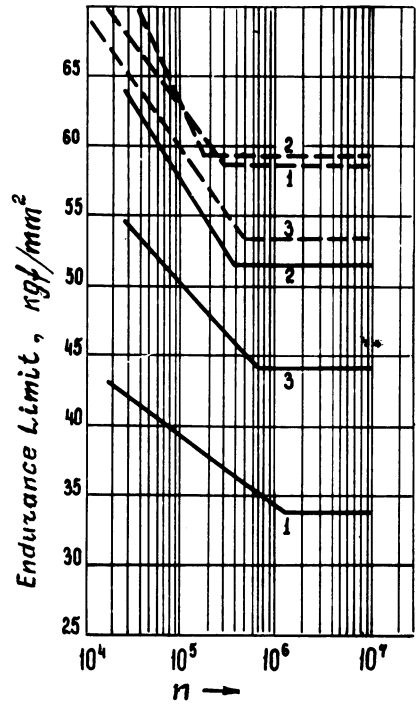

Fig. 2: Fatigue curves of VT3-1(1), VT22(2), VT15(3) alloy smooth specimens at cantilever bending (bars ϕ 20 mm (---) and ϕ 100 mm (-----).

Fig. 3: Intragranular structure of 100 mm diameter bars made of VT3-1 (a), VT22 (b) and VT15 (c) titanium alloys.

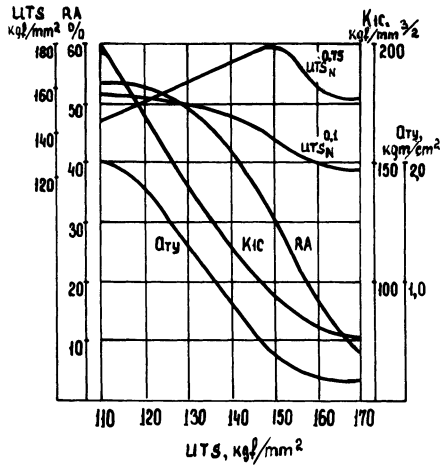

Fig. 4: Mechanical properties of VT22 alloy versus ultimate strength.

pronounced strengthening is observed in titanium alloys of near-critical composition.

Commercial Alloys

VT22 alloy belongs to the group of critical composition alloys and contains 5% Mo, 5% V, 1% Fe, 1% Cr, and 5% Al.

Various semi-products made of this alloy feature a wide range or properties depending on heat treatment conditions: σ_B = 105kgf/mm^2 to σ_B = 160kgf/mm^2.

A specific feature of this alloy in contrast to martensitic alloys is the fine-lamellar intragranular structure of the overheated metal, which provides for longer service life in case of large semi-products.

Figure 2 shows the fatigue cruves derived as a result of cantilever bending of smooth specimens made of VT3-1, VT22 and VT15 titanium alloys having fine-grained (rod 20mm in diameter; micrograin $\approx$ 300 microns) structure in the annealed condition with σ_B = 105-115kgf/mm^2.

Figure 3 shows the intragranular structure of rods 100mm in diameter made of three titanium alloys (martensitic - VT3-1, critical - VT22, and pseudo-beta - VT15), typical of large semi-products.

Since during fatigue testing the crack is initiated and propagates along the interphases, one can assume that the intragranular structure of near-critical composition alloys is more preferable than that of martensitic or beta alloys.

Alloys of these types display other characteristic features as well, namely, the ability to be effectively strengthened by heat treatment, high hardenability, etc.[8]

It should be noted at this point that the chemical composition of VT22 type alloys covers a particular range of concentrations which extends from the critical point to higher alloys. Therefore, it would be more reasonable to call them transition group alloys rather than critical composition alloys.

In this connection, it seems appropriate to introduce the value characterizing the amount and stability of beta phase in super-critical composition alloys, which could be termed as "conventional beta phase stability coefficient $K_{\beta\text{-stab}}$" and would be indicative of the ratio of the amount of beta-stabilizing element in the alloy and its content in the critical composition alloy.

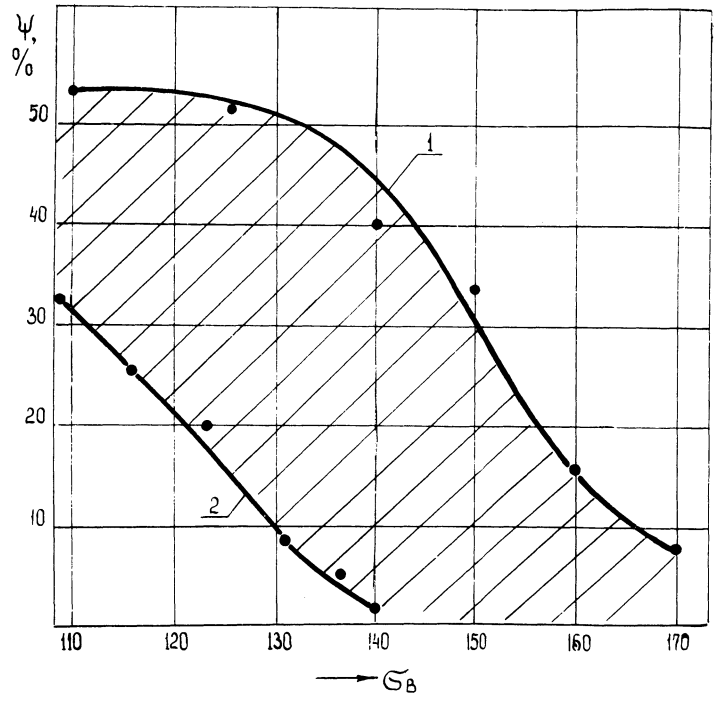

Fig. 5: Plasticity of VT22 alloy versus ultimate strength.
1 - upper technological limit (grain - 30 microns);
2 - lower technological limit (grain - 500 microns).

In case of multi-component alloys, $K_{\beta\text{-stab}}$ is calculated as the arithmetic sum of $K_{\beta\text{-stab}}$ of each beta phase stabilizing element.

A critical composition alloy features $K_{\beta\text{-stab}} = 1$, while a subcritical composition alloy features $K_{\beta\text{-stab}} \leq 1$.

In case of VT22 alloy, $K_{\beta\text{-stab}}$ ranges from 1 to 1.25 depending on the amount of alloying elements.

Thus, classified with the transition group alloys should be titanium alloys with $K_{\beta\text{-stab}} = 1 - 1.4$.

Properties and Heat Treatment

VT22 alloy, being the first commercial alloy of the transition group, has found wide use in mechanical engineering owing to a number of advantageous properties. In most cases, guaranteed u.t.s. of the alloy varies from 105 to 110kgf/mm^2. This strength permits the alloy to reliably operate under repeated static and fatigue loads at high stress concentrations (K_{IC} = 220 to 280kgf/mm$^{3/2}$).

To attain this strength level, a special heat treatment procedure has been elaborated, which is applicable to all types of semi-products with a grain size of up to 1,000 microns (regardless of their cross section and production process) according to a standard procedure: 820 - 850°C for 1 to 3 hours, furnace cooling down to 750°C, exposure for 1-2 hours, air cooling, reheating at 600 to 630°C for 2-4 hours, air cooling.

The first step of the heat treatment is carried out in alpha + beta region, at the temperature close to $\alpha+\beta \rightleftarrows \beta$ transformation temperature for structure stabilization. Then the alloy is slowly cooled down to 750°C and is exposed at this temperature until the required phase composition is attained. At this temperature, beta phase in VT22 alloy is highly stable and is fixed at low cooling rates (e.g. during air cooling in the cross section of 300mm in diameter). This is followed by high-temperature aging (overaging) at 600-630°C.

As has been mentioned above, VT22 alloy can be effectively strengthened by hardening and aging to different strength levels. The variation in the alloy mechanical properties depending on the strength level is shown on Figure 4. These results have been obtained on rolled bars 30mm in diameter with an equiaxed fine-grained structure, the grain size being no more than 30 microns.

As the alloy strength and the notch "rigidity" increase, the

ultimate strength of notched specimens substantially changes. The condition $\sigma_B^N / \sigma_B^S > 1$ is met up to σ_B = 140kgf/mm^2 for the specimens with notches of 0.75 and 0.1mm in radius and up to σ_B = 160kgf/mm^2 only for the specimens with an annular notch of 0.75mm in radius.

Tests with smooth specimens have revealed that the higher is the alloy strength, the lower is its plasticity (δ, ψ), this decrease being particularly sharp at strengths above 140kgf/mm^2.

Test results also indicate an increase in the alloy sensitivity to stress concentrators with strength increase. It should be noted, howeber, that up to 140kgf/mm^2 the alloy retains high plasticity (ψ > 40%) and has a moderate sensitivity to stress concentrators. For example, an alloy with $\sigma_B \leq$ 140kgf/mm^2 is not sensitive to a notch with a radius of 0.75 and 1mm, its sensitivity to cracking is a_{Ty}=0.8kgm/cm^2 and K_{IC} is to 130-150kgf/mm$^{3/2}$.

Processing the alloy to superhigh strength (σ_B>140kgf/mm^2) makes it possible to obtain the material with high sensitivity to stress concentrators in the form of notches and cracks.

The material with equiaxed and fine-grained structure is most promising for alloy strengthening by heat treatment. For a coarse-grained material, this possibility is limited.

Figure 5 illustrates a variation in the plasticity of an alloy with fine-grained (grain size less than 30 microns) and coarse-grained (grain size up to 500 microns) structure as a function of the alloy strength increase. The coarse-grained material plasticity curve may serve as the "lower technological limit." It is indicative of the quality of large semi-products material.

High quality material with its properties approaching the "upper technological limit" may be obtained by using progressive production processes, in particular, isothermal deformation in the alpha + beta region.

Isothermal deformation in the alpha + beta region results in uniform and equiaxed fine-grained structure with a high margin of plasticity in the annealed condition and is readily thermally strengthened.

VBT22 alloy forgings produced by isothermal deformation have the following mechanical properties in the annealed and thermally strengthened conditions: $\sigma_B \geq$110 and 140kg/mm^2, $\delta_5 \geq$ 16 and 10%, $\psi \geq$ 50 and 35%, a_n = 3 and 4kgm/cm^2, respectively.

When high-strength titanium alloys are used in modern mechanical engineering, specific features of semi-product manufacturing

phase tends to become more prevalent with increase in Si. There is no apparent morphological difference between these two phases and their compositions are thought to be similar.

Electron microprobe and x-ray fluorescence analysis on extracted fcc precipitate (by replica techniques), suggests that the phase consists of titanium, molybdenum and silicon and that it is related more to beta titanium than to a 'silicide' phase.

Figure 4 also illustrates a few of the deformation features of IMI 685, since the sample has received approximately 5% tensile deformation. The planar nature of the dislocation arrays is clearly seen (A) as are basal plane stacking faults (B). A feature of deformation not seen at this high magnification is that of twinning which accounts for a significant proportion of the total deformation in tensile or high stress, low cycle fatigue processes.

Planar dislocation arrays including dislocation pile-ups are seen in low cycle fatigue situations, whereas during creep deformation at temperatures around 520°C, dislocation structures are more tangled and stacking fault frequency increases.

Ageing at Higher Temperatures

Over the range 500°C to around 600°C, precipitation amounts increase without any marked change in morphology. This results in depletion of Mo and Si from the α matrix with consequent increases in yield strength and reductions in ductility and creep resistance (Table 2).

Above 600°C, morphological changes occur such that the precipitation becomes more globular (Figure 6). At around 850°C, original alpha needle boundaries, whilst still discernable, consist of dislocation networks with both inter and intra granular precipitation of globular particles. The precipitate is now a true silicide $(TiZr)_5Si_3$, and this heat treatment produces a minimum in the tensile ductility curve. These changes are basically unaffected by further lower temperature ageing treatment and properties such as those illustrated in Figure 8 are obtained.

At higher temperatures up to around 930°C, globular silicide precipitation still occurs, but at temperatures above about 930°C up to the beta transus, the precipitation reverts to a bcc sheet structure and morphology, since treatment is being carried out in the alpha plus beta phase region. Table 3 and Figure 7.

Stress Relief

The benefit of ageing above 550°C is in the relief of stress, but this also results in a loss of ductility and creep resistance.

PRINCIPLES OF TITANIUM ALLOYS COMPLEX ALLOYING

A. I. Khorev

All-Union Institute of Aviation Materials

U.S.S.R.

Complex alloying is one of the most promising ways to create a high strength structural state and increase the mechanical properties of titanium alloys.

Investigations have been carried out of alloy systems that contain constant amount of α-stabilizing element Al (3 and 6%) and variable amounts of the most effective isomorphic (Mo and V) and eutectoid forming (Cr, Fe) β-stabilizing elements, and also their various combinations.

Alloys have been produced with β-stabilizing elements in a quantity equivalent in β-phase stabilization effectivity to a definite amount of molybdenum (from 1 to 30%) calculated by the relation of critical concentrations (1Mo is equivalent to 1,5V; 0.6Cr; 0.55Mn; 0.4Fe), which resulted in alloys of close phase composition containing different β-stabilizing elements at separate and complex alloying.

The increase of β-stabilizing elements by a quantity equivalent to 1% molybdenum is accompanied by the increase of electron concentration by 0.01 el/at.

Alloying Effect on α and β-Phases Strength and the Alloys Mechanical Properties

The ultimate strength of α-phase was determined by the strength of α-alloy alloyed at a maximum by β-stabilizers, and ultimate strength of β-phase was determined by the ultimate strength of β-phase quenched supercritical concentration alloy.

The ultimate strength of α-phase in the alloys, alloyed by several β-stabilizing elements is higher compared to the alloys with one β-stabilizing element, which is due to the increase of the dissolved atoms number and their interaction. Complex alloying with several β-stabilizing elements has less effect on β-phase strength, since their solubility is higher in β-phase than in α-phase.

Thus, complex alloying while increasing β and α phases strength in different extent, simultaneously decreases the difference (σ_β-σ_α) in strength of phase components, which results in a more uniform plastic strain and a fuller realization of phase components strength.

In case of great difference in the strength of phase components, especially when their dimensions are large, the transfer of stress from one phase to another becomes difficult and their unequal participation in loading and plastic deformation is manifested. This non-uniformity of α and β-phases stressed state is increased due to higher value of the elastic modulus of α-phase compared to β-phase in non-equilibrium state.

During tension of α+β alloy with a certain degree of deformation in the elastic region, there is higher increase of stresses in α-phase than in β-phase, which makes greater the non-uniformity of α and β-phases loading. Such deformations are possible which for β-phase in simple alloys will correspond to the elastic region, and for α-phase to the plastic region. Repeated deformations may result in the accumulation of plastic deformation in α-phase, which in its turn will produce sources of failure.

If a comparison is made of plastic characteristics of variously alloyed alloys at a strength level of 110kgf/mm^2, in the annealed condition, it is possible to note the increase of plasticity from the alloy with Fe (δ = 13%; ψ = 45%) to the alloys with Mn, Cr; Cr + FE; V; Mo; Mo + V; Cr + Mo; Mo + V + Cr + Fe (δ = 20%, ψ = 66%). A similar comparison of mechanical properties in the thermally strengthened condition at σ_β = 120kgf/mm^2 have revealed that plasticity increases from the alloys with Cr and Fe (δ = 5%; ψ = 10-12%) to the alloy Ti-1.8Mo-3.4V-0.8Cr-0.6Fe (σ = 13%; ψ = 59%).

More effective strengthening during heat treatment of the alloys containing greater amount of aluminum (at constant content of β-stabilizing elements) is explained by greater strength of decomposition products-dispersed particles of α-phase. The same explanation holds good for greater strengthening during heat treatment of multicomponent alloys compared to simple alloys. Hence, the strengthening effect during heat treatment at identical phase composition depends not only on the degree of dispersion and homo-

geneity of decomposition, but on the strength of α-phase dispersed particles as well.

A study of β-alloys has shown that decomposition of β-phase during aging in the multicomponent alloy Ti-3Al-6Mo-4V-8Cr-2Fe is more homogeneous than in VT15 alloy (Ti-3Al-7,5 Mo-11Cr), which is connected with the decrease of alloying elements segregation as a result of the decrease of each β-stabilizing element amount. The mechanical properties of the first alloy (σ_β = 138kgf/mm^2; δ = 8%; ψ = 30%) are considerably higher than that of the second one (σ_β = 110kgf/mm^2; δ = 6%; ψ = 25%).

One of the main positive factors of multicomponent alloying, icnreasing the alloy mechanical properties, is more homogeneous and dispersed decomposition of metastable phases.

Sensitivity to Overheating of Simple and Complex Systems Alloys

The level of mechanical properties, which are obtained during heat treatment, depends on the original structure of the alloys. Heating or deformation at a temperature of β-region results in a considerable decrease of mechanical properties, which is connected with the development of chemical and structural inhomogeneity. Sensitivity to overheating, estimated by the relation of mechanical characteristics of the alloys with overheated structure to mechanical properties of the alloys with an equiaxial structure (δ overehated/δ ψ overheated/ψ) - is to a considerable extent a manifestation of unequal participation in plastic deformation of phase components having considerable dimensions. One of the main reasons of decreasing mechanical characteristics of alloys with overheated α+β structure is the presence of stress concentration in α-phase plate tip. This stress concentration is higher in simple systems alloys which have greater difference between the strength of the surrounding β-solid solution and the strength of α-phase plate, which makes difficult the redistribution of stresses in the plate tip and reduces plastic deformation, especially the local one. When cooling the alloy from β-region temperatures at moderate rates α-phase is formed in β-phase, whose specific volume is greater than that of β-phase. Tensile stresses may occur in the region of β-phase adjacent to α-plate tip. The difference in coefficients of linear expansion of α and β phases may also result in the increase of stress concentration in the plate tip.

Consequently, the alloys mechanical properties and their sensitivity to overheating will be affected not only by the morphology of phase components, but also by their mechanical and physical properties.

Strengthening treatment of α+β alloys of simple systems, resulting in strengthening of metastable β-solid solution, provides still greater difference in the strength of α-phase plate and the surrounding volume of decomposed β-phase, which intensifies the action of the plate tip as a concentrator.

On multicomponent alloying providing similar strength of α and β-solid solutions, α plates will have a negative effect to a lesser extent. Thus, the multicomponent Ti-3Al-1.3Mo-2.7 V-0.8 Cr-0.6Fe alloy with overheated structure in the thermally strengthened condition has satisfactory mechanical properties: σ_β = 110kgf/mm^2; δ = 6.5%; ψ = 12%. Alloys with isomorphic β-stabilizing elements in the identical condition have the same strength level at a lower plasticity: δ = 1.5%; ψ = 3% in the case of alloy Ti-3Al-8Mo and δ = 3%; ψ =8% in the case of alloy Ti-3Al-15V.

Mechanical Properties of Welded Joints

A study has been carried out of the mechanical properties of welded joints of three, four and six component systems of titanium alloys, made by automatic argon-arc welding.[5-8]

After annealing it is possible to obtain a strength of 100kgf/mm^2 in a system with one β-stabilizing element, and in a system with two β-stabilizers - 110kgf/mm^2 with satisfactory plasticity. Alloying with two β-stabilizing elements (Mo + V) provides a strength increase of 12kgf/mm^2 at equal plasticity compared to alloying with vanadium alone. In the alloys, alloyed with two eutectoid forming elements there is no brittle region, whereas welded joints of the alloy with 12% iron are brittle.

In the thermally strengthened condition the level of welded joints mechanical properties increases in succession, presented in Table II, which confirms the effectivity of complex and multicomponent alloying.

It has been established by X-ray microanalysis that in combined alloying with chromium and molybdenum the weld cast metal dendrites central zones are enriched with molybdenum and depleted of chromium, and in the zones adjacent to the dendrite boundaries a reverse picture is observed.[9] This distribution provides for the stability of β-stabilizing elements total number in different zones and more homogeneous strengthening of metastable solid solution during aging.

Alloying with elements which action is contrary during dendritic liquation (with the distribution coefficient higher and

Table I

α and β-Phases Strength in the Systems Ti-3Al- β Stabilizer

Phase strength	β-stabilizing elements										
	V	Mo	Cr	Mn	Fe	Mo +V	Mo +Cr	V +Fe	Mo +Fe	Cr +Fe	Mo+V +Cr+Fe
σ_α	57	64	63	62	58	68	70	70	75	76	83
σ_β	68	80	82	86	88	75	81	82	93	92	90

Table II

Mechanical Properties of Welded Joints in the Thermally Strengthened Condition

Mechanical properties	Concentration of β-stabilizing elements								
	3.6 Cr	4 Fe	3.6Cr 2.4Fe+	4.5V 1.2Fe+	6-8 Mo	3Mo+ 1.2Fe	4Mo 6V+	3Mo 1.8Cr	1.8Mo+ 3.4V+ 0.8Cr+ 0.6Fe
σ kgf/mm^2	90	100	110	110	110	115	120	133	140
o	0	0	10	16	18	20	20	22	25

lower than unity) is an important factor which should be used in creating weldable titanium alloys.

In order to prevent embrittlement of welded joints, the total amount of isomorphic β-stabilizing elements, expressed in amounts equivalent by β-phase stabilization force, must be equal to or greater than the total number of eutectoid forming elements.

Complex Alloyed Weldable VT23 Alloy

Basing on the formulated principles of complex alloying weldable titanium alloys VT23 alloy (Ti-4-6.2Al-4-5V-1.5-2.5Mo-0.6 - 1.4Cr-0.4-0.8Fe) has been developed.

The content of aluminum in the alloy, designed for making sheets is 4.0-5.5%, and in the alloy designed for making forgings and stampings - 4.8-6.2%. The alloy has been alloyed with β-stabilizing elements with distribution coefficients higher or lower than unity (K_{Mo} = 3; $K_V \approx 1.0$; K_{Cr} = 0.25; K_{Fe} = 0.7) with a total amount of isomorphic β-stabilizing elements (equivalent to 4.2-5.8% Mo) 1.5 times higher than that of eutectoid forming elements (equivalent to 2-4.2%Mo). The strength of the phase components of VT23 alloy are similar: σ_α = 88kgf/mm^2 and σ_β = 90kgf/mm^2.

The effect of heating temperature and cooling rate on the mechanical properties of VT23 alloy have been studied. The alloy has maximum plasticity and minimum strength, (110kgf/mm^2) after annealing at 750° with subsequent air cooling and at 800° with subsequent furnace cooling (Fig. 1). The increase of the alloy strength compared to the strength calculated by the law of combined effect in mixture strength of α and β phases is explained by strengthening of interphase boundaries.

VT23 alloy contains 30% of β-phase in the condition close to the equilibrium state. When quenching from β region temperature (1000°) α'-phase is fixed in the alloy, and α''-phase is fixed when hardening from α+β region temperature (900°).

When quenching from 800° 76% of β-phase is fixed in the alloy which is decomposed during aging, providing effective strengthening of the alloy up to 185kgf/mm^2, (Fig. 1).

The alloy has high long-time strength and creep characteristics, determined on sheets for 100 hours in the annealed condition at 300°: σ 100 = 72-76kgf/mm^2; σ 0.2/100 = 60-62kgf/mm^2 and at 400° σ 100 = 70kgf/mm^2: in the thermally strengthened condition at 300° - σ 100 = 110-115kgf/mm^2; σ 0.2/100 = 78-80kgf/mm^2 and at 400° - σ 100 = 70kgf/mm^2.

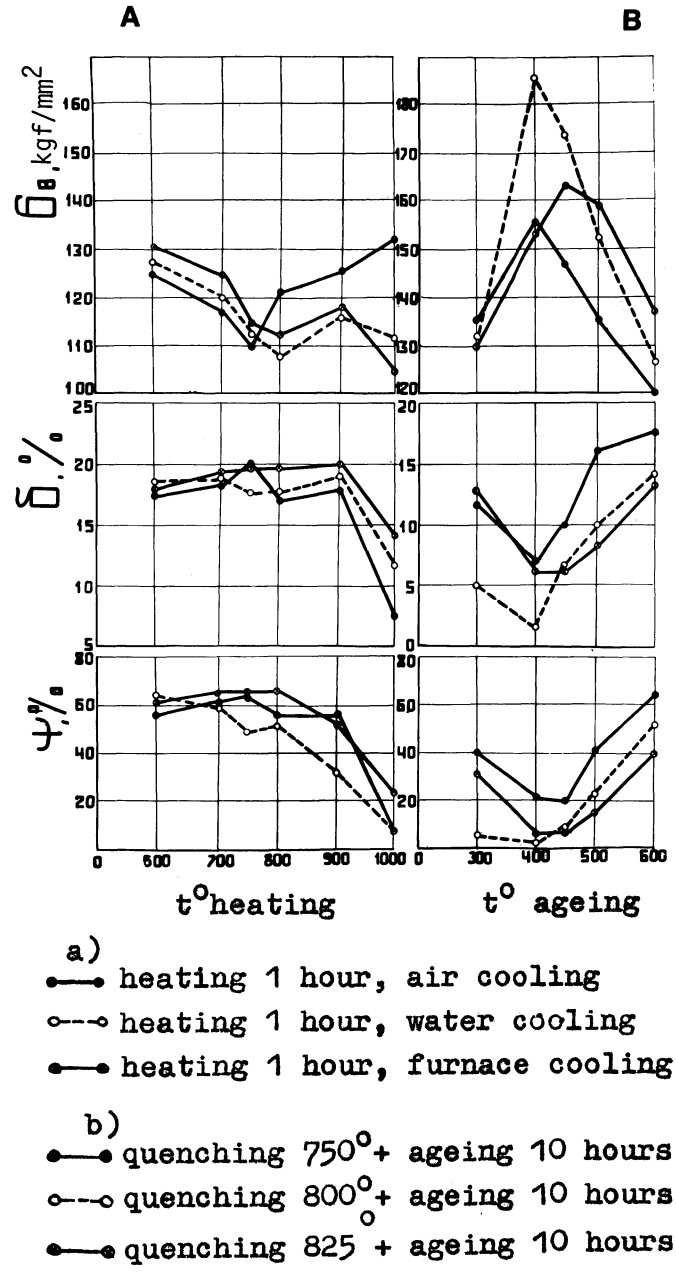

Fig. 1: Mechanical properties of VT23 alloy (rod dia. 12 mm).

Conclusions

1. The main aspects of titanium alloys complex alloying are formulated and the principal factors providing the strength increase of the basic material and their welded joints are determined.

2. The strength of titanium alloys is determined by the strength of α and β-phases, the ratio of these phases, the degree of dispersion, and the structure non-equilibrium.

3. During complex alloying of the alloys a higher strengthening of α and β solid solutions is obtained and their strength difference is reduced, due to which a more homogeneous plastic deformation on loading is provided and a fuller realization of α and β-phase strength. In this case the effect of internal stress concentrators is minimum.

4. Alloying is recommended with β-stabilizing elements which action is contrary in respect to dendritic liquation in order to provide the constancy of amount of β-stabilizing elements in different zones, more homogeneous solid solution strengthening, greater uniformity of distribution, and the improvement of phase component morphology.

5. During complex alloying it is useful to observe the ratio of isomorphous eutectoid forming elements, expressed in the equivalent values from 2:1 to 1:1.

6. Proposed is the interpretation of sensitivity to overheating taking into account not only the morphology of phase components, but their mechanical and physical properties as well.

References

1. Khorev, A. I., Glazunov, S. G. and Mukhina, L. G., Mechanical Properties of Ti-Al-Cr and Ti-Al-Cr-Mo Alloys System. "Metallovedenie i Termichesckaya Obrabotcka Metallov," 1971, No. 3, 28-34.

2. Khorev, A. I., Mechanical Properties of Titanium with Isomorphous Beta-stabilizing Elements. "Metallovedenie i Termichesckaya Obrabotcka Metallov," 1972, No. 5, 13-18.

3. Khorev, A. I. and Mukhina, L. G., Heat Treatment and Mechanical Properties of Ti-Al-Fe and Ti-Al-Cr-Fe Alloys Systems. "Metallovednie i Termichesckaya Obrabotcka Metallov," 1973, No. 9, 57-60.

4. Khorev, A. I., Complex Alloying of Titanium Alloys. "Metallovedenie i Termichesckaya Obrabotcka Metallov," 1975, No. 8, 58-63.

5. Khorev, A. I., Effect of Eutectoid Forming Beta-Stabilizing Elements on Mechanical Properties of Titanium Alloys Welded Joints. "Svarochnoe proisvodstvo," 1971, No. 2, 3-5.

6. Khorev, A. I., Effect of Alloying Elements on Mechanical Properties of Welded Joints of Ti-Al-Cr and Ti-Al-Cr-Mo Alloys Systems. "Svarochnoe proisvodstvo," 1970, No. 8, 29-32.

7. Khorev, A. I. and Gruzdeva, L. A., Strength Properties of Welded Joints of Titanium Alloys Containing Isomorphous Beta-Stabilizing Elements. "Svarochnoe proisvodstvo," 1971, No. 8, 37-40.

8. Khorev, A. I., Basic Principles of Developing High Strength Weldable Titanium Alloys. "Svarochnoe proisvodstvo," 1965, No. 10, 4-7.

9. Khorev, A. I., Gruzdeva, L. A. and Titarenko, I. I., Effect of Alloying and Heat Treatment on Mechanical Properties of Titanium Alloys Welded Joints. "Svarochnoe proisvodstvo," 1969, No. 6, 27-29.

A TITANIUM ALLOY WITH IMPROVED MECHANICAL RESISTANCE

Ti-6Al-6V-2Sn-6Zr

B. de Gélas - R. Molinier - L. Séraphin -
M. Armand - R. Tricot

Ugine Aciers - Centre de Recherches
Métallurgiques d'Ugine (France)

The alloy Ti-6Al-6V-2Sn-6Zr (Cu, Fe) is the result of an investigation dealing with thirty experimental alloys. The air of the program was an alloy with tensile strength $R \geqslant 1300$ N/mm^2, yield strength $R_{02} \geqslant 1150$ N/mm^2 with sufficient ductility i.e. elongation $A\% \geqslant 6$ reduction of area $\Sigma\% \geqslant 15$ and not susceptible to notch effect R_e (notched, $K_t = 3,9)/R \geqslant 1$.

1. Preliminary Studies : Definition of Chemical Composition

The experimental alloys studied at laboratory scale were all modications obtained from Ti - 6Al - 6V - 2Sn (Cu, Fe) with following strengthening agents:

- interstitial elements (carbon 0,05 - 0,1 %, oxygen 0,15 - 0.20 %).
- precipitation of $Ti_x M_y$ via "active" beta-eutectoid elements : cobalt 1-3 %, nickel 3 %, silicon 0,5 %, beryllium 0,5 %
- "slow" beta eutectoid elements (manganese 0,5 - 3 %), or zirconium 3 - 6 %, or replacement of vanadium by molybdenum for solid solution strengthening
- combination of two different actions : for example addition of 3 % Zr + 0,1 % C, 3 % Zr + 1 % Mo, 3 % Zr + 1 % Mo + 1 % Cr ... etc ...
- tin for strengthening the alpha phase ; raising iron (1 %) or copper (2 %) concentration.

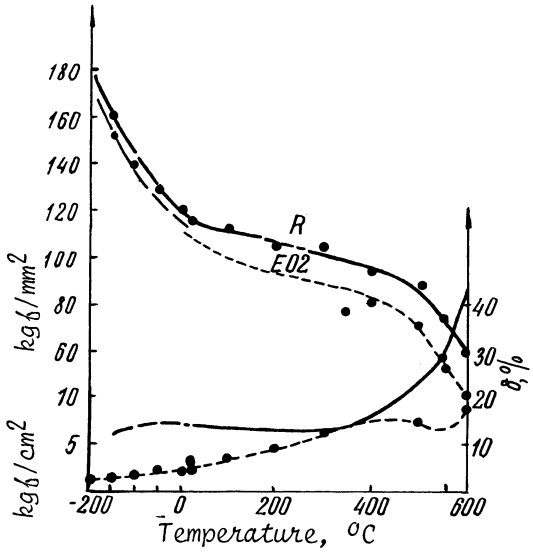

Fig. 1: Alloy selection (base + 6Zr) on tensile elongation data - 730°C - 2h anneal after forging to 15mm square.

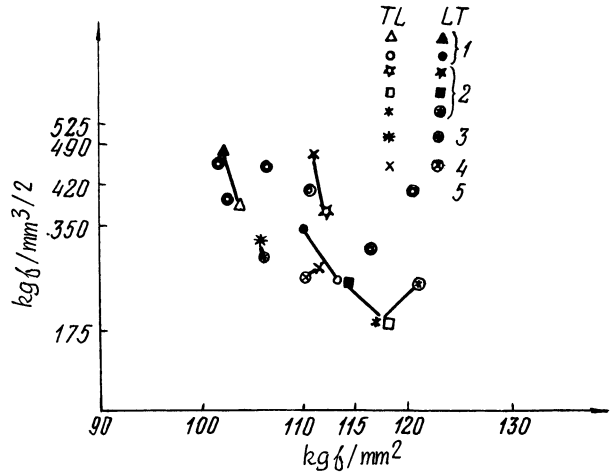

Fig. 2: Situation of Ti-662Zr alloy as compared to other alpha-beta titanium alloys.

Table 1

Preliminary alloy selection basis

Ti - 6 Al - 6V - 2 Sn - x Zr (Cu, Fe)

	R (N/mm^2)	E_{02} (N/mm^2)	A %	ε %	R_e/R
Annealed					
(x - 4,5)	1027	1155	15,5	40	1,41
(x - 6,5)	1330	1280	7,8	13	1,35
Solution treated and aged					
(x - 4,5)	1244	1210	15	38	1,34
(x - 6,5)	1380	1350	8,2	20	-
Hot rolled, annealed, welded, stress relieved					
(x - 5)	1190	1080	11	-	-

Table 2

Chemical analysis data

Products from	Al	V	Sn	Zr	Cu	Fe	Si
620 kg ingot	5,95	5,55	2,20	5,95	0,580	1,00	0,065
1260 kg ingot	6,05	5,06	2,35	5,18	0,400	0,360	<0,040
(extreme values)	6,31	5,12	2,70	5,18	0,450	0,420	

O_2	N_2	C	H_2
0.095/0,099	0,012/0,013	0,012/0,016	0,011/0,044

This part of the study is entirely described in ref. (1). Fig. 1 shows an example of results obtained on annealed products Table I given optimum mechanical properties of products fabricated from 50 kg ingots.

2. General Metallurgy of Selected Alloy

Chemical composition Ti - 6Al - 6V - 2Sn - 6Zr (Cu, Fe) defines an alpha + beta type alloy. Fig. 2 shows a representation using chemical equivalents on the following basis:

1 Al = 3 Sn = 6 Zr for Al equivalent of ref.(2)

10 Mo = 15V = 6Cr = 3,5 Fe = 13 Cu for Mo equivalent of ref(3)

Relatively high aluminum and molybdenum concentrations result from the search for best mechanical resistance and quenchability of the alloy (4).

Transformation TTT and CCT curves have been defined after solution treatment in the beta field (5) (6). Transus alpha + beta $\rightleftarrows$ beta is 920 ± 10°C. Annealing at 730°C after alpha + beta or beta forging can be most commonly used. Solution treating and aging gives better mechanical resistance : the alpha-alpha prime phase mixture obtained after quenching turns to alpha + beta hardened equilibrium structure on aging. Occasionally occurrence of an $AlZr_3$-type compound has been shown by electron microscopy after water quench. Ti_3Al has been demonstrated after 450°C 100 h - aging (7) according to prediction which can be made from fig. 2 -

Tensile strength after solution treating and aging increases with increasing solution temperature above 800°C due to increasing martensite decomposition during cooling.(4). Under 800°C tensile strength is not dependent upon solution temperature due to conservation of metastable beta phase after quenching. Two thermal treatments have then been defined :

- water or air quench from 860°C ; aging 450-625°C 8 h (450°C for best tensile strength, 625°C for best metallurgical stability). This treatment applies to sections less or equivalent to 80mm diameter.

- "slack quench" from 860° (100°C/h cooling to 700°C, then air cool) ; aging 450°C 8 h. Applies homogeneously to sections up to 150mm diameter. The beta phase after slack quench is enriched in beta stabilizing elements ; hardening results from fine alpha precipitation upon aging - (4) -

Table 3

Tensile and toughness data - 1260 kg ingot

Product	R N/mm²	E_{02}	A % (5d)	ε %	$\frac{Re}{R}$
220mm dia bar ; annealed (1)	930-1030	870-920	7-14	9-18	1,5
120mm dia bar beta forged annealed (2)	1005	905	11	17	1,5
825°C 1h AC + 450°C 6h AC (3)	1070	930	11	20	1,5
825°C 1h WQ + 450°C 6h AC	1180	980	6	9	1,25
875°C 1h WQ +450°C 6h AC (fully homogeneous long end transverse results)	1190	1015	5	8	1,25
120mm dia bar alpha + beta forged					
- annealed	1110	1020	14	38	1,5
- 825°C 1h AC + 450°C 6h AC	1118	1080	13	43	1,5
70 x 30mm alpha + beta forged bar					
- annealed (4)	1075	1030	13,5	33	-
- 825 C°1h AC + 450°C 6h AC (5)	1080	1110	12	28	-
30mm dia bar ST and aged	1285	1175	14	44	1,4

K_{cv} = 1,6 daJ/cm2 (1)

Room temp. stress rupture test (n/mm2) ≥1300 (1) ; 1350 (2) 1350 (3)

K_{1c} (MPa $\sqrt{m}$) 70:(LT) , 55 (TL) (4) ; 68 (LT), 53 (TL) (5) -

Table 4

Tensile and toughness data (620 kg ingot)

Product and heat treatment	R (N/mm^2)	E_{02}	A % 5d	ε %	K_{1c} MPa $\sqrt{m}$
120 x 25mm bar alpha beta forged					
- annealed	1175	1105	15	45	
- 960°C 1h AC + 730°C 1h30 AC	1160	1060	5	14	43 (LT) 45 (TL)
70 x 30mm bar					
beta forged, annealed	1205	1110	10	22	38,6 (LT) 39,5 (TL)
alpha + beta forged, annealed	1210	1120	14	40	49,2 (LT) 37,1 (TL)
860°C 1h AC + 625°C 8h AC	1245	1160	10	27	38,7 (LT) 26,8 (TL)
860°C 1h SQ + 450°C 8h AC	1320	1190	10	19	35,7 (LT) 27,1 (TL)
small bars, annealed	1320	1230	15	27	-

AC = air cool; SQ - water quench ; SQ - slack quench ; L - long ; T - transverse - K_{1c} data average of three determinations on ASTM-designed specimens.

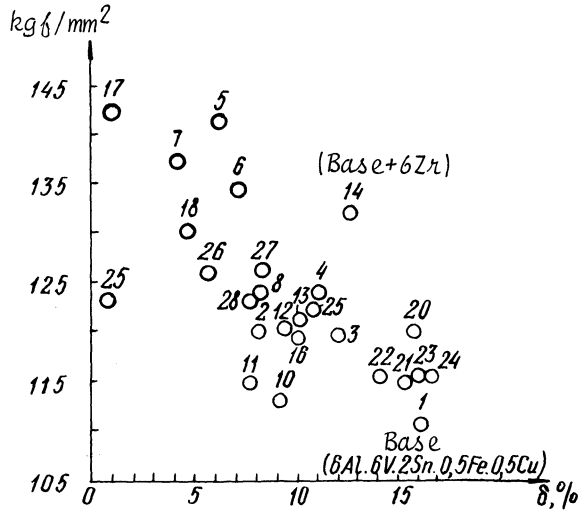

Fig. 3: Variation of tensile and Charpy V-impact values with temperature (1260 kg ingot).

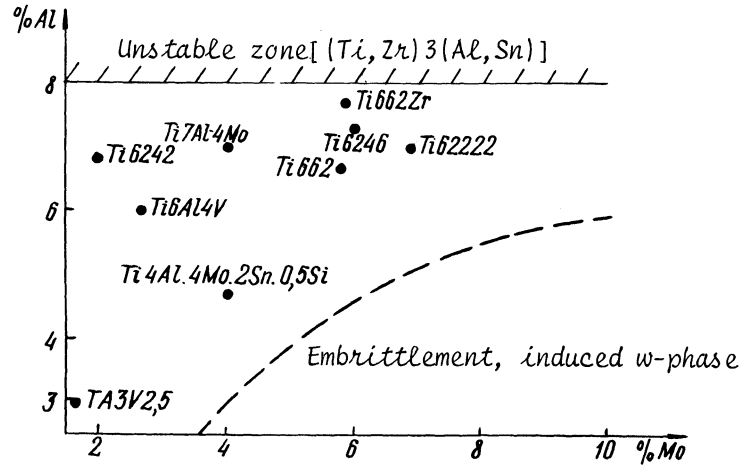

Fig. 4: Fracture toughness results.

Table 5

Tensile, fatigue and creep data (1260 kg heat)
(self and ref. (10) results)

	small bars		"pancakes"	compressors discs
	alpha + beta forged			
	annealed	825°C 1h AC + 450°C 6h AC	850°C 1h oil quench + 625/675°C 8h AC	
R (N/mm^2)	1040	1240	1210	1205
E_{02} (N/mm^2)	1070	1115	1140	1120
A %	14	12,5	10	18
ε %	43	48	24	30
Fatigue limit (L_f) 10^8 cycles, R = 1, N/mm^2)	710 ± 50	615 ± 90	590	-
$\frac{L_f}{R}$	0,62	0,50	0,49	-
Creep (100h ; 350°C)				
σR (N/mm^2)	-	-	960	-
$\sigma 02$	-	-	580	-
Low cycle fatigue (K_t = 2,5, R=0,05; 10^4 cycles)				
20°C	-	-	590	610
350°C	-	-	480	510

3. Mechanical Properties Obtained on Industrial Products

After optimization of chemical analysis and thermal treatment on 50 and 320 kg ingots, full scale evaluation was conducted on 620 and 1260 kg ingots.

Analysis of ingots are reported on Table 2. Chemical homogeneity is good. Optimum analysis is defined as follows :

Al 5,8 V 5,8 Sn 2,0 Zr 6,2 Cu 0,6 Fe 0,6 O_2 0,15

Tensile and toughness data are reported on Tables 3 and 4 after air cool and aging homogeneous results are obtained on 120mm diameter bar. Over-aging at 625°C gives comparatively low results. Tensile strength increases significantly with decreasing section of the product. Fig. 3 gives variation of tensile characteristics with temperature : the alloy can be used from 150 to +600°C.

Fig. 4 gives fracture toughness results : increasing tensile strength results in decreasing fracture toughness according to a classical trend. Interestingly compared to classical results (e.g. ref. (8)) beta forging does not improve significantly the fracture toughness but leads only to very isotropic results.

Table 5 gives some creep and fatigue results. The alloy has good rotating-beam fatigue strength and has low notch-sensitivity. Low-cycle fatigue and creep behavior make the alloy a good candidate for service up to 350°C at least. Compared to other titanium alloys we have shown superior low-cycle fatigue life with somewhat limited fatigue crack propagation resistance which would make beta forging most desirable (9).

4. CONCLUSIONS

The alloy Ti - 6Al - 6V - 2Sn - 6Zr can be used for high tensile characteristics which were defined as the aim of the program :

annealed : $R \simeq 1100$; $E_{02} \simeq 1050$ (N/mm^2)

solution treated and aged : $R \simeq 1250\text{-}1300$; $E_{02} \simeq 1150$ (N/mm^2)

Homogeneous tensile characteristics are obtained after solution treating and aging up to 80mm (water quench) 120mm (air quench) or 150mm (slack quench). Fatigue and creep data are good over + 350°C. The fracture toughness level is between 30 and 60 MPA $\sqrt{m}$ essentially dependent on the yield level.

Those results show the "Ti-662Zr" alloy as an interesting step in defining high resistance titanium alloy and the limitations introduced in that area by the need of a tensile strength-toughness compromise.

REFERENCES

1. Tricot, R., Séraphin, L., Syre, R., Molinier, R., Logerot, J. M., Rev. Met., January 70, 43-54.

2. Jaffee, R. I., Titanium Science and Technology - 2nd Internat. Conference on Titanium, Plenum Press (1973) 1670.

3. Séraphin, L., Le traitement thermique - 42 et 43 (1969).

4. Molinier, R., Séraphin, L., Tricot, R., Castro, R., Rev. Met. n° 1 (1974) 37-49.

5. Hourcade, M., Beauvais, C., Hocheid, B., C. R. Acad, Sc. 275 (1972) série C. 1239.

6. Hourcade, M., Hocheid, B., Beauvais, C., Mem. Sc. Rev. Mat. 71 (1974) n° 2,95.

7. P. Lacombe et al. - Faculté des Sciences d'Orsay - Data not yet published.

8. de Gélas, B., Molinier, R., Séraphin, L., Tricot, R., Castro, R., Mém. Sci. Rev. Met. 71 (1974) 85.

9. de Gélas, B., Tricot, R., Matériaux et Techniques. May 1975-189.

10. SNECMA YORP n° 31528 data.

EFFECT OF IMPURITIES ON THE WORKING ABILITY OF Ti-6Al-4V TYPE ALLOY

E. A. Borisova, L. A. Pastukhova, Ye. N. Starova
and I. I. Shashenkova

All-Union Institute of Aviation Materials
U.S.S.R.

I. INTRODUCTION

The aim of the investigation was to define more exactly the existing specifications on the content of silicon, oxygen, carbon and iron impurities in BT6C alloy. During the investigation, the primary attention was given to the evaluation of the impurities effect on the basic parameters determining the operational strength and reliability of the alloy, as well as low-cycle fatigue resistance as a function of the stress concentrator.

II. MATERIAL AND TEST PROCEDURE

For the investigation use was made of 2mm thick sheets, 20mm diameter rods and 30mm thick plates, made from laboratory melts weighing 40kg. The ingots were melted in vacuum arc furnaces by double remelting. The actual content of basic alloying elements in the ingots varied as follows: aluminum - from 5.7 to 5.9%, vanadium - from 4.0 to 4.2%. The content of the impurities under investigation varied as follows: silicon - from 0.03 to 0.175%, oxygen - from 0.09 to 0.24%, carbon - from 0.02 to 0.13%, iron - 0.05 to 0.21%. The following parameters have been determined as a result of the investigation:

(1) Tensile properties.

(2) Specific fracture toughness of notched specimens (according to Menager) - a_n* and cracked specimens - $\frac{V}{A}$.**

(3) Fracture toughness (K_{IC}) at eccentric tension of compact 25mm thick specimens. The tests were carried out according to a

*a_n - fracture toughness; **$\frac{V}{A}$ - cracking sensitivity.

tentative State Standard GOST, compatible with ASTM E-399-72 standard. K_{IC} was calculated from the formula $K_Q = \frac{P_Q}{t\,B}\lambda$, where λ is a known function of $\frac{l}{B}$ (l is the crack length) relationship.

If the evaluation by validity criteria

$$\left(\frac{P_{max}}{P_Q} \leq 1.1,\ t \geq 2.5\left(\frac{P_Q}{\sigma 0.2}\right)^2,\ t \geq 11.2\%\right)$$

proved that $P_Q = R_{1C}$, K_Q was assumed equal to K_{IC}.

(4) Reisstance to low-cycle fatigue, on notched round specimens.

(5) The rate of fatigue crack propagation. The specimen used for this test was a plate with a width B = 100mm and a length L = 30mm with a central open mechanically made slit ($2l_o$ = 10mm). The propagation of the crack was observed with the X24 magnifying glass. The crack growth was evaluated beginning from the moment when the total size of fatigue cracks on either side of the slit was $l_1 + l_2$ = 3mm. Prior to testing, each specimen was annealed at 800°C for an hour.

III. RESULTS

Analysis of the test results indicates that within the range under investigation carbon, iron, and silicon practically do not affect the strength and ductility in tension (Fig. 1), testing the specimens both after annealing and after strengthing heat treatment. The effect of these impurities on the results of the impact bend test is much stronger (Fig. 1). The oxygen impurity has the most adverse effect on the alloy properties. With the increase of oxygen content up to 0.24%, the resistance of the alloy to plastic deformation also increases, and the strength of the alloy in the annealed condition reached 115 kgf/mm^2, and even 135 kgf/mm^2 after hardening and aging.

Oxygen also strongly affects the fracture characteristics both under static and impact loads (Table I and Fig. 1). It can be seen that as the oxygen content increases from 0.09 to 0.24%, K_{IC} value decreases from 270-320 to 125-159 kgf/mm$^{3/2}$, the specific work of breakdown of the notched sample (a_n) is reduced three-fold (from 6.5 to 2.3 kgm/cm^2), and that of the cracked sample $\left(\frac{V}{A}\right)$ is reduced by more than 8 times (from 5.8 to 0.7 kgm/cm^2). There was no indication of any effect produced by carbon and silicon on K_{IC}. The results of 19w-cycle fatigue tests (Table II) are also indicative of the adverse effect of oxygen. Under equal stress of 44 kgf/mm^2, notched specimens containing 0.24% and 0.1% of oxygen

Table I

Mechanical Properties and Fracture Toughness of BT6C Alloy with Different Impurity Contents (plate 30mm thick)

Impurity content, %			Fiber orientation in a specimen	σ_B	$\sigma 0.2$	δ	ψ	K_{IC}
Si	C	O_2		kgf/mm^2		%		kgf/mm$^{3/2}$
0.03	0.02	0.09	crosswise	85.3	81.9	14.8	46.1	270;320
0.19	0.02	0.09	crosswise	93.3	91.8	10.8	42.8	312;308
0.03	0.13	0.09	crosswise	97.0	96.1	10.8	35	311,299, 320
0.03	0.02	0.15	crosswise	94.7	90.0	10.0	31	300
0.03	0.02	0.15	lengthwise	94.0	91.5	11.0	28	266,285, 285
0.03	0.02	0.24	crosswise	100.8	96.3	10.6	34.4	135;159

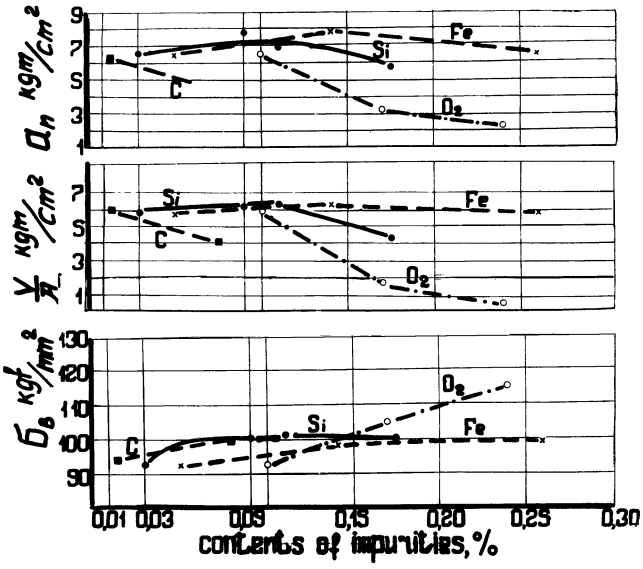

Fig. 1: Effect of silicon and iron impurities on the ultimate strength and fracture toughness (a_η, A) of BT6C alloy.

Table II

Effect of O_2 and Si on Low-Cycle Fatigue Resistance (V = 10 c/min, K = 0) of BT6C Alloy (sheet 2mm thick)

Impurity content, %		ζ_n = 0.75; K_t = 2.2		ζ_n = 0.1; K_t = 4.0	
Si	O_2	Stress, kgf/mm^2	Number of cycles	Stress, kgf/mm^2	Number of cycles
0.03	0.1	62 ($0.67\sigma_B$)	13964 16760 18792	-	-
		44 ($0.5\sigma_B$)	102 468 72 453 60 303	44 ($0.5\sigma_B$)	8675 6105
		-	-	30 ($0.35\sigma_B$)	50000 59559 47234 31673
0.175	0.1	62 ($0.63\sigma_B$)	14 651 15 091	-	-
		44 ($0.41\sigma_B$)	52 771 41 980 73 653	44 ($0.41\sigma_B$)	13837 12873
		-	-	30 ($0.30\sigma_B$)	>130000 >120000 >110000
0.03	0.24	63 ($0.58\sigma_B$	12792 10373 10135	-	-
		44 ($0.38\sigma_B$)	130000 130000 100000	44 ($0.38\sigma_B$)	8478 8196
		-	-	30 ($0.26\sigma_B$)	>130000 >120000

Table III

Effect of Long-Term Heating at 400°C on the Mechanical Properties of BT6C Alloy with Different Impurity Contents (rod 20mm in diameter)

Impurity content, %			Initial state			After 3,283 hours		
Si	O_2	C	σ_B, kgf/mm^2	a_n, kgm/cm^2	$\frac{V}{A}$, kgm/cm^2	σ_B, kgf/mm^2	a_n, kgm/cm^2	$\frac{V}{A}$, kgm/cm^2
0.03	0.1	0.025	92	0.6	5.8	99	6.0	5.5
0.09	0.1	0.025	101	7.9	6.1	106	7.0	-
0.11	0.1	0.025	101	7.0	6.2	108	5.9	5.3
0.175	0.1	0.025	98	5.7	4.3	105	5.2	3.5
0.03	0.017	0.025	106	3.2	1.83	107	3.4	1.8
0.03	0.24	0.025	115	2.3	0.68	117	3.0	0.7

Table IV

Crack Growth Rates at Different Levels

Of ΔK (sheet 2mm thick)

Impurity content, %		σ_B kgf/mm^2	δ_5,%	$\frac{d(2l)}{dN}$ mm/kc at ΔK in kgf/mm$^{3/2}$				
Si	O_2			ΔK= 175	ΔK= 160	ΔK= 110	ΔK= 125	ΔK= 150
0.03	0.24	111	12.5	0.6	1.2	2.0	2.6	4.7
0.10	0.15	101	13	0.8	1.2	1.3	1.7	3.0
0.175	0.1	98	11.7	0.5	0.8	1.1	1.5	2.5
0.03	0.1	97	10.7	0.3	0.6	0.9	1	11.6

$2l - 2l_o + l_1 + l_2$, mm - total crack length.

ΔK is the stress intensity coefficient, kgf/mm$^{3/2}$

$\frac{d(2l)}{dN}$, mm/kc is the crack growth.

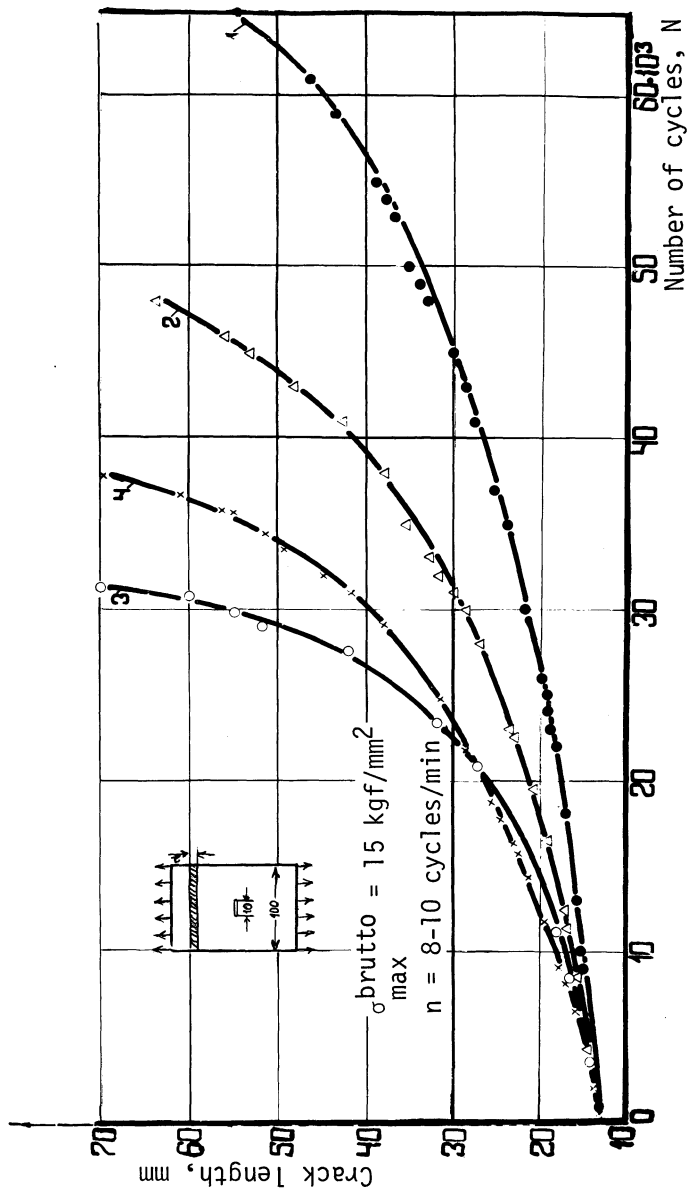

Fig. 2: Median curves of fatigue crack growth fate in BT6C alloy with different contents of silicon and oxygen impurities.

Curve 1 - 0.03 Si, 0.1 O_2
" 2 - 0.175 Si, 0.1 O_2
" 3 - 0.03 Si, 0.24 O_2
" 4 - 0.10 Si, 0.15 O_2

withstand, before failure, practically the same number of cycles, when K_t = 4.0. However, in the case of the alloy containing 0.24% oxygen, the value of these stresses is 0.38 σ_B; for the alloy containing 0.1% oxygen - 0.5 σ_B, i.e. the resistance to low-cycle fatigue is decreased by 24%. The increase of silicon content in the alloy from 0.03 to 0.175% has not resulted in the decrease of low-cycle fatigue resistance.

Taking into account the possibility of the alloy long-term service at high temperatures, its properties with different impurity content were determined after exposure to 400°C for 3.283 hours (Table III). In this case finished specimens which have not been subjected to any kind of treatment prior to testing have been heated.

It has been established that with the increase of oxygen and silicon content in the alloy, $\frac{V}{A}$ decreases, this decrease being especially high in specimens containing 0.24% oxygen. Evaluation of silicon and oxygen effect on the durability of the alloy at 400°C and a stress of 64 kgf/mm^2 has shown that silicon has a favorable effect on the durability which has increased by one order of magnitude (from 240 to 2,220 hours) with the silicon content increase from 0.03 to 0.175%. The increase of oxygen content from 0.1 to 0.24% O_2 practically did not affect the alloy durability. Experiments have also revealed a considerable effect of impurities on the rate of the fatigue crack propagation. Figure 2 shows the median curves of crack growth as a function of the number of cycles 2l = f(N) for an alloy with different impurity contents. The values of crack growth rates $\frac{d(2l)}{dN}$ for different ΔK levels obtained by graphical differentiation of curves 2l = f(N) are given in Table IV.

It can be seen from the data in Table IV that the purest, from the point of view of impurity content (Si $\leq$ 0.03%), O_2 = 0.1%), alloy of laboratory melt a crack growth rate is twice as low compared to commercial alloy (Si = 0.1% and O_2 = 0.15%). Silicon content increase and, particularly, that of oxygen results in a substantially higher crack growth rate.

CONCLUSIONS

(1) Oxygen and silicon impurities have been shown to produce a considerable effect on the mechanical properties and fracture toughness of BT6C alloy.

(2) It has been found that the content of silicon and oxygen in BT6C alloy should be limited to 0.10 and 0.15%, respectively.

Ti-6Al-4V FOR MARINE USES

G. Sorkin*, I. R. Lane, Jr.**, and J. L. Cavallaro+

*Naval Sea Systems Command, Washington, D. C.
**Metallurgical Consultant, Greenbelt, MD
+David W. Taylor Naval Ship R&D Center, Annapolis, MD

INTRODUCTION

The Ti-6Al-4V alloy is recognized as the most important alloy in the titanium industry. Because it is perhaps the most versatile grade of titanium ever developed it has grown in application until it has earned the nickname "workhorse" of titanium alloys. The Naval Sea Systems Command (NAVSEA) recognized the potential of Ti-6Al-4V and has sponsored work at the David W. Taylor Naval Ship R & D Center (DTNSRDC), the Naval Research Laboratory (NRL), and industry to investigate it for possible marine uses. A material for marine applications should possess good toughness and insensitivity to the marine environment. Properties such as seawater stress corrosion resistance and seawater fatigue resistance are of major concern. The NAVSEA investigations have been aimed at not only investigating these properties but where possible developing them to their maximum potential. Areas of interest have included plate development, weldment development, forming effects, and castings. This paper is a brief summary of some of the more significant NAVSEA investigations performed on the Ti-6Al-4V alloy in its development for marine applications.

Evaluation Factors

Important properties to be considered in evaluating a structural metal for marine applications include strength, toughness, seawater stress corrosion resistance (SCC), and fatigue characteristics. Strength properties determined in the NAVSEA investigations include 0.2% offset tensile yield strength (TYS), ultimate tensile

strength (UTS), 0.2% offset compressive yield strength (CYS), percent elongation (% El), and percent reduction in area (%RA). All strength values in this paper are expressed in units of thousand pounds per square inch (ksi). Toughness property tests include the Dynamic Tear Test (DT)[1] and the Charpy V-notch impact test (C_V). Seawater stress corrosion tests were conducted by the NRL cantilever beam stress corrosion test [2] in which the threshold K_ISCC stress intensity factor is determined as ksi $\sqrt{\text{in.}}$ In most cases a threshold stress intensity factor was also determined for specimens tested in air in the same manner as those tested in seawater. This value is designated $K_I$air. Threshold values were determined for test periods ranging from one to 100 hours. High cycle fatigue tests were conducted using rotating cantilever beam specimens and R. R. Moore fatigue specimens [3]. Fatigue strength was determined for a life of 10^8 cycles.

Ti-6Al-4V Plate

The major portion of the NAVSEA effort on the Ti-6Al-4V alloy has been spent in investigating the alloy in plate form, principally in one-inch thickness. As toughness and seawater stress corrosion resistance are of prime concern for most plate applications, investigations have been concentrated on achieving the maximum in these properties. In most of the investigations properties were determined both longitudinal and transverse to the principal rolling direction. In the interest of brevity, however, properties reported in this paper are transverse with respect to the principal rolling direction. This direction has been found to be the "weak" direction for toughness properties. Tensile and compressive strength specimens were taken parallel to the principal rolling direction. DT, C_V, and SCC specimens were made such that the notch orientation was perpendicular to the rolled surface and the fracture is driven in the principal rolling direction.

Effect of Oxygen Content. An investigation was conducted to determine the effect of oxyten content on the properties of 1-inch plate produced from 100 lb ingots. The aim for oxygen contents were 0.06, 0.08, 0.10, and 0.12 weight percent (wt %) with other elements held constant within practical limits. Plates were specified to be produced according to current mill practice. This consisted of beta forging each ingot, starting at 2200 F, to a 4-inch slab. The forged slab was alpha + beta cross-rolled to a 1-inch thickness from a starting temperature of 1850 F. Results of this investigation are summarized in Table I.

TABLE I

Effect of Oxygen Content on Ti-6A1-4V Plate Properties
(DTNSRDC Data)

Property	Oxygen Content, Wt % 0.07	0.09	0.10	0.12
TYS, ksi	118	125	131	135
UTS, ksi	129	134	139	142
% El	14	14	13	12
% RA	36	39	42	36
DT, ft lb	1392	741	672	338
C_V, ft lb	23	17	16	14
K_I Air, ksi$\sqrt{in.}$	66	51	45	41
K_I Seawater, ksi$\sqrt{in.}$	66	46	38	41

As expected, toughness decreased with oxygen content. No significent susceptibility to seawater stress corrosion was found for oxygen contents up to 0.12 wt % based on comparison with $K_I$air. Oxygen contents above 0.07 wt % appear to lower both $K_I$air and $K_I$seawater. Rotating cantilever beam high cycle fatigue tests in air were also performed on this series of alloys. Oxygen had no effect on the fatigue strength. The fatigue strength of smooth specimens is 56 ksi and for notched specimens is 26 ksi at 10^8 cycles for all oxygen levels.

Effect of Oxygen Content and Processing. An investigation was conducted to determine the effect of both oxygen content and processing on the properties of Ti-6A1-4V plate. Four 6,000 lb heats, one at each of four oxygen levels; 0.05, 0.07, 0.11, and 0.15 wt % were produced. Each ingot was upset and drawn to an 18 inch square at a forging temperature of 2100 F. The billet was cut in half. One half was alpha + beta forged and the other half was beta forged to 3-inch thickness. Each sheet bar was then rolled to 1-inch plate, one at 1400 F, one at 1700 F, one at 1900 F, and one at 2050 F. The plates were evaluated for oxygen effect and processing effect on yield strength, DT toughness, and $K_I$seawater values. $K_I$seawater tests were run in salt water in cantilever beam specimens nominally 1-inch deep, 3/4 inch wide (B=3/4 in.), and 7 inches long. The results of these tests are shown in Table II.

TABLE II

Effect of Oxygen Content and Processing on Ti-6Al-4V Plate
(NRL Data)

Oxygen Content Wt %	Roll Temp °F	Beta Forged TYS ksi	Beta Forged DT ft lb	Beta Forged K_ISW ksi$\sqrt{inc.}$	Alpha + Beta Forged TYS ksi	Alpha + Beta Forged DT ft lb	Alpha + Beta Forged K_ISW ksi$\sqrt{in.}$
0.05	1400	119	1163	73	110	2091	65
	1700	120	2446	108	122	2376	98
	1900	107	951	77	110	672	84
	2050	106	1021	95	108	1591	100
0.07	1400	131	603	70	126	1092	68
	1700	120	2305	100	123	1391	76
	1900	117	534	77	110	603	75
	2050	119	672	84	111	1022	89
0.11	1400	129	672	54	136	603	48
	1700	137	1092	74	131	741	58
	1900	121	534	71	115	534	69
	2050	118	672	76	115	741	78
0.15	1400	145	331	44	136	466	41
	1700	131	398	41	137	603	46
	1900	119	398	54	131	398	56
	2050	123	534	35	126	398	55

K_ISW = K_I Seawater

These data indicate that to maximize DT toughness and stress corrosion resistance, oxygen level should be less than 0.10 wt %. In general, no significant advantage of either beta forging or alpha + beta forging could be distinguished. The 1700 F rolling temperature produced the highest level of fracture resistance at each oxygen level. The lowest level of fracture resistance was associated with the 1900 F rolling temperature.

Materials from the processing and oxygen study were further investigated for the effect of heat treatment on the properties, i.e., strength and toughness. One study consisted of annealing at two temperatures below the beta transus, 1700 and 1750 F, followed by a water quench and aging at 1000 F with an air cool. These treatments resulted in very slight increases in DT energy and increases in yield strength of 8 to 10 ksi. Another study was made of heat treatments at and above the beta transus, 1825 and 1900 F, followed by a water quench and aging at 1000 F 4 hours

and air cooling. These treatments gave slight increases in yield strength but reduced the DT fracture toughness.

Forming Effects. Fabrication of a structure will, in many cases, necessitate hot forming of plate to achieve the desired configuration. Since the plate will undergo very little mechanical deformation, it is possible that the hot forming operation will destroy the optimum mechanical properties achieved in prime plate. Concern about the effect of hot forming operations and stress relief anneals on the properties of Ti-6A1-4V plate led to an investigation of the effect of simulated forming operation temperatures on the properties of plate. The plate used in the investigation was 1-inch thick extra low interstitial (ELI) grade Ti-6A1-4V containing 0.10 wt % oxygen. The results are shown in Table III.

TABLE III

Effect of Simulated Forming Temperatures on Ti-6A1-4V Plate

Condition	TYS	UTS	%El	%RA	C_V 32 F
As Received	126	133	14	29	17
1200 F, 2 hr	122	130	13	29	17
1750 F, 1 hr	111	129	13	31	24
1750 F, 1 hr + 1200 F, 2 hr	114	130	13	29	22
1750 F, 3 hr	110	130	12	27	22
1750 F, 3 hr + 1200 F, 2 hr	114	129	12	28	19

This investigation showed that the simulated forming temperatures reduced the yield strength, but generally were beneficial to toughness.

Ti-6A1-4V Weldments

It has been shown that Ti-6A1-4V plate can be obtained with good properties if the oxygen content is maintained below 0.10 wt % and processing is controlled. However, properties of a composite structure are controlled by the properties of the weldments that join the structure. There are fewer variables in the welding process that can be controlled that will result in changes in properties of weldments. Among these are control of weld metal composition, control of weldment heat input, and a post weld heat treatment. Another possibility for control of weldment properties is the use of the more sophisticated welding procedures such as plasma, electron beam (EB), and laser.

Oxygen Content of Weld Wire. An investigation was made to determine the effect of oxygen content of weld wire on the properties of weldments. Weldments were made out-of-chamber by the Gas Metal Arc (GMA) process using a trailing argon shield. ELI grade (0.12 wt % oxygen) 1-inch thick Ti-6Al-4V plate was used. Two different weld wires were used, one containing 0.08 and the other containing 0.10 wt % oxygen. The resulting welds had oxygen contents of 0.09 and 0.11 wt % oxygen, respectively. The test specimens were tested in the as-welded condition and with a 1200 F 2 hour simulated stress relief anneal. The results of the property evaluation are given in Table IV.

TABLE IV

Effect of Oxygen Content on Ti-6Al-4V Weldments

	Base Metal		0.09 Oxygen		0.11 Oxygen	
	As Rec'd	Annealed	Welded	Annealed	Welded	Annealed
TYS	131	133	120	128	128	133
UTS	139	139	136	141	147	148
% El	15	14	9	8	8	6
% RA	28	29	22	15	19	21
C_V 32 F	18	19	28	21	24	17

Cantilever beam stress corrosion tests were also run on the base metal and weldments shown in Table IV. No seawater SCC susceptibility was found for the as-welded materials or for the 0.09 wt% oxygen weldment after a 1200 F 2 hour anneal, i.e., there was a negligible loss in load carrying ability of the test specimen in seawater as compared to air. However, the 0.11 wt % oxygen weldment showed a seawater SCC susceptibility, losing about 10% of its load carrying capability. It should be noted that yield strength is lower in the low oxygen content weldments. Perhaps strength can be raised by higher aluminum containing wire with negligible loss in toughness or SCC resistance.

Fatigue Behavior of Weldments. High cycle fatigue tests were run on the weldments described in Table IV. Rotating cantilever beam (R= -1) high cycle fatigue strength of smooth specimens from the base metal was found to be 68 ksi in air and 54 ksi in seawater at 10^8 cycles. Fatigue strength of notched ($K_t \simeq 3$) specimens was 29 ksi in air and 28 ksi in seawater. However, there was rather severe degradation of welded specimens, a fatigue strength of only 18 ksi in both air and seawater, for both oxygen levels of filler metal.

In another investigation, a 1-inch thick Ti-6Al-4V plate containing 0.10 wt % oxygen was GMA welded with wire containing

0.08 wt % oxygen. Rotating centilever beam specimens were run in air and in seawater. The fatigue strength of the welded plate at 10^8 cycles was 17 ksi as compared to 54 ksi for the base metal. Results were identical in air and in seawater.

These instances of severe degradation of weldment fatigue strength as compared to base metal prompted further investigation. Fatigue tests were run using R. R. Moore specimens which are smaller than the previously used rotating cantilever beam specimens. The low fatigue strength of weldments was not found in tests using these specimens. Two different thermal stress relief treatments eliminated the low strength weldment failures in rotating cantilever tests. The low fatigue strength therefore appears to be related to residual stresses in weldments.

Ti-6A1-4V Castings

An investigation was made of the properties of Ti-6A1-4V castings made in rammed graphite molds and by the investment casting process [3]. Castings at three oxygen levels; 0.09, 0.11, and 0.18 st % were made in rammed graphite molds. Investment castings were made at the 0.18 wt % oxygen level. The results of these investigations are given in Table V.

TABLE V

Properties of Ti-6A1-4V Castings

	Rammed Graphite Castings Oxygen Content, Wt %			Investment Castings
	0.09	0.11	0.18	
TYS	119	129	127	121
UTS	136	146	146	133
% El	11	9	11	7
% RA	22	16	17	12
K_ISCC	69	49	43	-
K_IAir	70	65	65	-
Fatigue Strength, ksi	50	40	25	34

Oxygen level significantly influences the seawater stress corrosion susceptibility and the rotating centilever beam fatigue strength of cast Ti-6A1-4V. Cast Ti-6A1-4V at oxygen levels of 0.11 and 0.18 wt % was susceptible to seawater SCC behavior. Cast Ti-6A1-4V containing 0.09 wt % oxygen has twice the fatigue strength of the cast metal containing 0.18 wt % oxygen, 50 ksi as compared to 25 ksi. Investment cast Ti-6A1-4V at 0.18 wt % oxygen has slightly higher fatigue strength (34 ksi) than does the rammed graphite cast metal (25 ksi). Surface finish, however, influences fatigue be-

havior to a greater degree than does oxygen content. Rotating cantilever beam specimens at the 0.09 and 0.11 wt % oxygen levels were run with as-cast surfaces. The 0.11 wt % oxygen specimens with 44-70 rms surface finish had better fatigue strength (30 ksi) than did the 0.09 wt % oxygen specimens with 75-100 rms finish (25 ksi). Weldments in cast Ti-6Al-4V with 0.11 wt % oxygen were evaluated for fatigue strength with rotating cantilever beam specimens. Fatigue strength of the weldment (30 ksi) was only 10 ksi less than the unwelded base metal (40 ksi).

SUMMARY AND CONCLUSIONS

Ti-6Al-4V can be produced in one-inch plate thickness with good DT toughness and seawater stress corrosion resistance. The first requirement is low impurity content. Efforts should be made to hold oxygen content to a low level, preferably below 0.10 wt %. This alone, however, will not ensure good DT toughness. Attention must be paid to processing, especially the final rolling temperature. A temperature in the vicinity of 1700 F appears to be the optimum for finishing the Ti-6Al-4V alloy.

Thermal forming operations can change the properties of the prime plate. If the plate was produced to achieve high strength, this strength can be lowered by the forming operation. Toughness does not appear to be affected by this operation.

Oxygen content of weld wire should be at a low level, preferable 0.08 wt % maximum, to achieve low oxygen content weldments if toughness and seawater SCC resistance are of importance.

Residual stresses in thick section weldments of Ti-6Al-4V plates apparently drastically affect the high-cycle fatigue resistance. A stress relief treatment should be considered if fatigue strength is an important consideration in the application.

Oxygen content apparently affects the fatigue behavior of smooth cast Ti-6Al-4V rotating beam specimens. Surface condition is an overriding consideration, however, in achieving good fatigue properties in castings.

ACKNOWLEDGMENTS

This paper is a summary of some of the more important NAVSEA investigations concerning the Ti-6Al-4V alloy. Included are date not previously published. These data were generated by R. W. Huber, R. W. Judy, and R. J. Goode of the Naval Research Laboratory; also P. W. Holsberg, I. L. Caplan, and F. E. Brauer of the David W. Taylor Naval Ship Research and Development Center.

REFERENCES

1. Puzak, P. P. and Lange, E. A., "Standard Method for the 1-inch Dynamic Tear Test" NRL Report 6851, 13 February 1969.

2. Brown, B. F., "A New Stress Corrosion Cracking Test Procedure for High-Strength Alloys", Materials Research & Standards, Vol 6, No. 3, March 1966.

3. Morton, A. G. S. and Lane, I. R., Jr., "Titanium Castings for Marine Propellers", Titanium Science and Technology, Vol 2, 1973.

DEVELOPMENT OF A NEW MODERATE STRENGTH, HIGH FRACTURE TOUGHNESS TITANIUM ALLOY: Ti-4.5Al-5Mo-1.5Cr (CORONA 5)

F. H. Froes*, R. G. Berryman+, and J. C. Williams@

*Colt Industries, Crucible Materials Research Center, Pittsburgh, PA

+Rockwell International, Los Angeles Aircraft Division, El Segundo, CA

@Carnegie-Mellon University, Department of Metallurgy and Materials Science, Pittsburgh, PA

Introduction

The properties of Ti-6Al-4V remain attractive and provide a guideline for materials selection when considering the relative design efficiency achievable with titanium, aluminum and steel. However, the potential for further property improvements in this alloy by chemical composition modifications or by new thermomechanical processing (TMP) sequences appear to be very limited. The requirements of modern aircraft, which are designed with the aid of fracture mechanics criteria, has led to the need for an alloy whose strength is slightly greater than Ti-6Al-4V in the annealed condition and whose plane strain fracture toughness is significantly higher. To this end, an alloy development program was initiated to identify a new alloy composition together with a processing sequence which would result in an ultimate tensile strength of 135 ksi (930 MPa) or greater and a plane strain fracture toughness of 100 ksi$\sqrt{in}$. (110 MPa$\sqrt{m}$) or greater. This paper will describe the results of the first year of this on-going program.[1]

Results and Discussion

The program was conducted in two phases: Phase I which was directed towards definition of an alloy composition, with essentially constant TMP, and Phase II which was aimed at optimization of TMP to permit the goal properties of 135 ksi UTS (930 MPa) and 100 ksi$\sqrt{in}$. K_{Ic} (110MPa$\sqrt{in}$.) to be attained.

Under Phase I, nine alloy compositions varying in degree of beta stability (Table I) were evaluated.

TABLE I

PHASE I ALLOY COMPOSITIONS AND CALCULATED FRACTURE TOUGHNESS VALUES AT GOAL STRENGTH LEVEL

Alloy Number	Composition (Bal. Ti)	Estimated K_Q (ksi$\sqrt{in.}$) at Goal UTS*			
		Rex		BA	
		RW	WR	RW	WR
Goal		100	100	100	100
1	5Mo-4.5Al	67	58	107	107
2	3Mo-4.5Al-1.5Cr	82	70	111	117
3	8Mo-4.5Al	62	46	86	86
4	8Mo-4.5Al-4Zr	95	95	100	98
5	5Mo-4.5Al-1.5Cr	112	91	116	116
6	8Mo-5.5Al	55	68	98	95
9	11Mo-4.5Al-4Zr	107	107	107	-
10	8Mo-4.5Al-1.5Cr	97	81	99	103
22	4Mo-4.5Al-1.5Cr	84	70	82	87

*Goal of 135 ksi (930MPa).

Rex and BA refer to recrystallization anneal and beta anneal respectively.

RW and WR refer to loading and crack propagation directions respectively.

1 ksi$\sqrt{in.}$ = 1.099 MPa$\sqrt{m}$.

The average composition of these alloys is somewhat richer in beta stabilizer than Ti-6Al-4V and the Al content was held to a minimum of 5.5%. This Al upper level was chosen because of the tendency of higher Al contents to lower the stress corrosion resistance. Mo and Cr were the main alloying elements used to stabilize beta: the potency of Cr as a stabilizer is about twice that of Mo. The nine alloys had beta transii which ranged from ~1810F(~988C) to ~1650F (~900C). The nine compositions were triple melted as 20 pound heats and converted to 0.5 inch plate by a combined beta forging and $\alpha+\beta$ hot rolling operation. The hot rolling was con-

ducted so that each alloy received at least 50% reduction below its beta transus temperature.

After hot rolling, various recrystallization annealing (ReX) treatments were evaluated. Based on prior work with the Ti-6Al-4V alloy, the goal structure after this treatment was an equiaxed alpha-beta microstructure with both phases recrystallized; i.e., a homogeneous alpha-beta structure of low dislocation density. In addition, one piece of each alloy was beta annealed (BA). For each ReX and for the BA condition, strength and K_Q values were obtained in the longitudinal and transverse directions using standard tensile and slow bend, pre-cracked Charpy tests. These data were then used to construct strength toughness trend lines for each alloy. A somewhat unexpected result was that long time ReX annealing treatments produced inferior fracture toughness compared to that obtained from relatively short times. The reason for this became apparent during structure analysis under Phase II of the program and is discussed later. Data from these long time ReX treatments should be considered separately from that for the short time treatments and thus were not used in constructing the trend lines. Using such trend lines, the fracture toughness (K_Q) values have been estimated for each of the Phase I alloys, at the goal strength level and are listed in Table I. On the basis of the Phase I study, the composition Ti-4.5Al-5Mo-1.5Cr was selected for further study under Phase II.

For Phase II, a 500 pound ingot of Ti-4.5Al-5Mo-1.5Cr was triple melted, homogenized and forged at a temperature above the β-transus into ~4" thick slabs. These slabs were then given one of two alpha-beta hot working treatments, followed by one of six ReX treatments or one of two BA treatments (Table II). These treatments were chosen to permit evaluation of the effect of hot working temperature and final ReX and BA treatments on properties. As in Phase I, strength and K_Q values (determined from slow bend and pre-cracked Charpy samples) were determined both in the longitudinal and transverse directions for each of the eight processing/heat treatment combinations; these results are listed in Table II (overleaf). The K_Q values are not considered to accurately reflect valid K_{Ic} values at these extremely high fracture toughness levels. However, other work has shown that there is a reasonable correlation to ~120 ksi$\sqrt{in.}$ (~132 MPa$\sqrt{m}$.) level. Thus it was reasonable to assume that K_Q values >120 ksi$\sqrt{in.}$ (132 MPa$\sqrt{m}$) represented K_{Ic} values also in excess of this level. In view of the strength goal of this program (135 ksi UTS [931 MPa]) both strength and K_Q were considered in selecting conditions for further evaluation. Strength levels are lower than anticipated due to the low oxygen content - 0.069-0.084 O_2 - of this heat. On the basis of these data, three processing/heat treatment conditions were selected for compact tension K_{Ic} tests and fatigue crack propagation (FCP) studies. Of these three conditions, it was found that the best

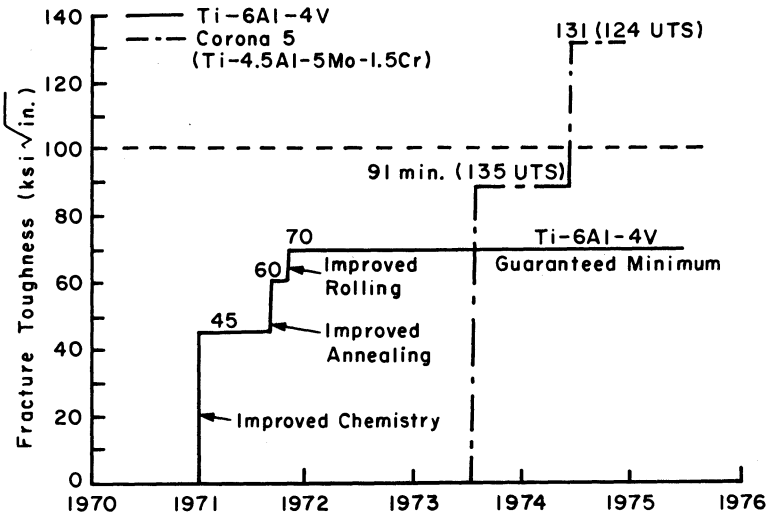

Fig. 1 - Fracture toughness improvements in titanium alloys. Fracture toughness in ksi $\sqrt{in}$ (1 ksi $\sqrt{in}$ = 1.1 MPa $\sqrt{m}$). Goal toughness of 100 ksi $\sqrt{in}$ is indicated. Tensile UTS in ksi (1 ksi = 6.89 MPa).

combinations of properties were 126 ksi (869 MPa) UTS at a K_Q^* of 131 ksi$\sqrt{in}$.(144 MPa$\sqrt{m}$). These data, coupled with the other Phase II data (Table II) show that the goal properties of 135 ksi (931 MPa) UTS at a K_{Ic} of 100 ksi$\sqrt{in}$. (110 MPa$\sqrt{m}$) are attainable with the composition Ti-4.5Al-5Mo-1.5Cr. Recent work on a third ingot of higher oxygen content, 0.14 wt. % has shown that fracture toughness values as high as 118 ksi$\sqrt{in}$.(130 MPa$\sqrt{m}$) can be obtained in this alloy at the goal strength level, thus verifying this suggestion.

Microstructural evaluation of the various Phase II conditions revealed a number of interesting features. The beta annealed condition was characterized by long alpha needles in a beta matrix (Figure 2a). Fast fracture (K_Q) occurred by a mixed transgranular/intergranular mode (Figure 2b). The fine needle-like alpha re-

TABLE II

PHASE II THERMOMECHANICAL PROCESSING AND MECHANICAL PROPERTIES, ALLOY 5 (Ti-4.5Al-5Mo-1.5Cr)

Rolling Temp. (F)	Anneal Temp. (F)	Anneal Time (Hrs)	Anneal Type	Properties Dirn.	UTS (ksi)	K_Q* (Ksi$\sqrt{in.}$)	K_{IC}* (Ksi$\sqrt{in.}$)
Start 1775 Finish 1500 (BT_r = 1650F)	1775	0.25	BA†	L (RW)	126	111	<117.3>
				T (WR)	130	156	-
	1575	4	Rex	L (RW)	116	168	<126.6>
				T (WR)	119	179	-
	1525	4	Rex	L (RW)	124	164	<131.4>
				T (WR)	125	183	-
	1525	16	Rex	L (RW)	117	155	-
				T (WR)	120	182	-
Start 1500 Finish 1300 (BT_r = 1650F)	1775	0.25	BA	L (RW)	115	162	-
				T (WR)	118	154	-
	1575	4	Rex	L (RW)	112	163	-
				T (WR)	121	143	-
	1525	4	Rex	L (RW)	114	155	-
				T (WR)	120	140	-
	1525	16	Rex	L (RW)	113	155	-
				T (WR)	120	152	-

†BA followed by 1300F-4 hour anneal, all other treatments followed by furnace cool to 1000F, then air cool.

*K_Q from slow bend pre-cracked Charpy.
K_{IC} from compact tension test.
< > failed minimum thickness requirement of ASTM E-399.
1 ksi = 6.89 MPa
1 ksi$\sqrt{in.}$ = 1.099MPa$\sqrt{m}$

---

*K_Q is specified since compact tension specimens were slightly under the minimum thickness requirements.

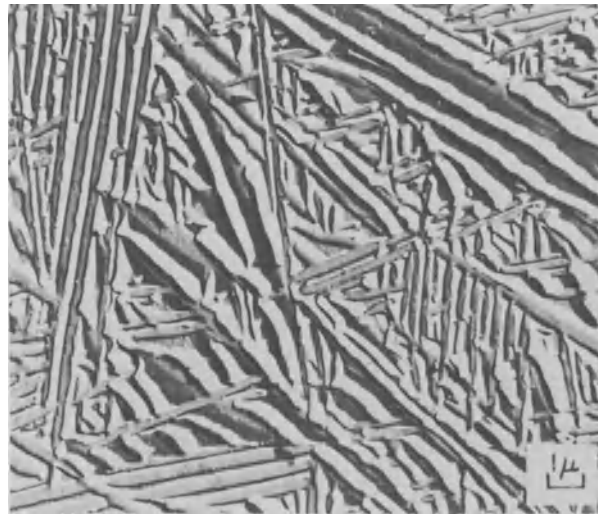

A

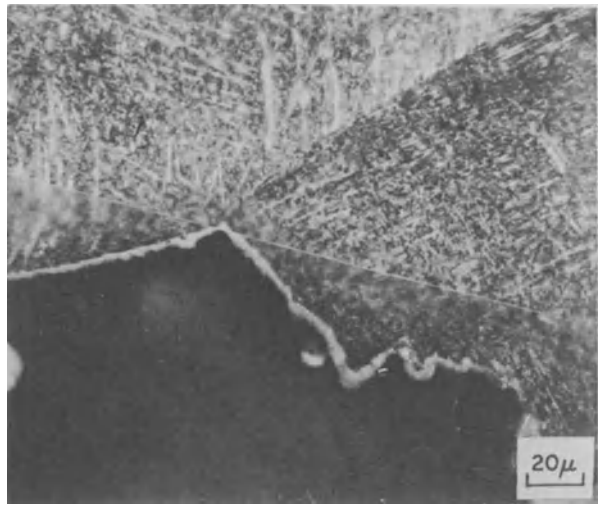

B

Fig. 2 - (a) Beta annealed 1775°F (969°C) -15 mins, air cooled plus stabilize annealed 1300°F (705°C)-4 hr air cooled. (b) As for 2(a). Fracture path, fast fracture region (K_Q sample). Note intergranular path at left, transgranular at right.

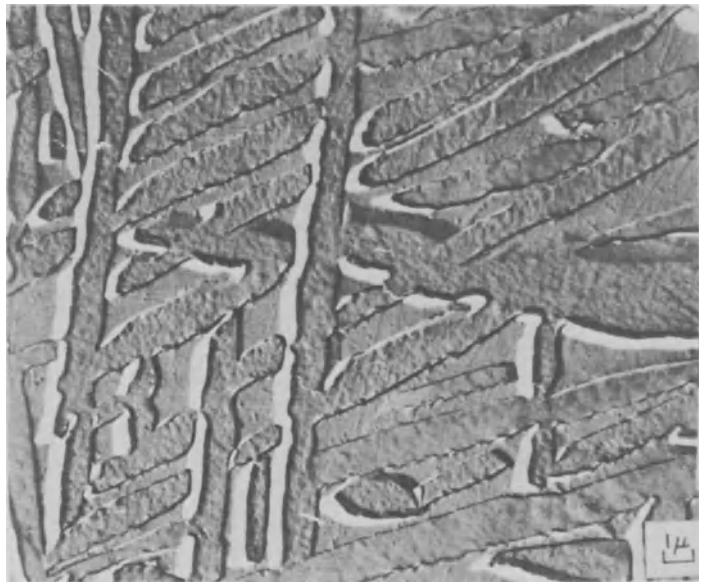

a

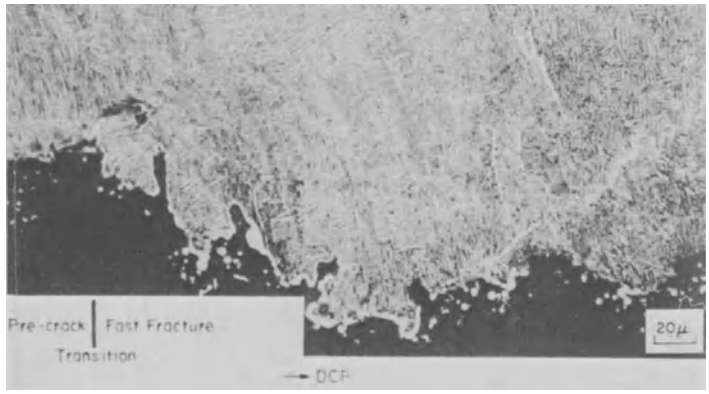

b

Fig. 3 - (a) Sub-transus annealed 1525°F (830°C)-4 hr, furnace cooled. (b) As for 3(a). Fracture path, transition zone (K_Q sample). Note transgranular fracture mode.

sults in an extremely tortuous transgranular crack path with easier intergranular crack propagation. Thus intergranular cracking is the preferred fracture mode in the beta annealed microstructure, but this is mitigated by crack branching at grain boundary triple points and by the relatively large prior beta grain size. The crack thus attempts to follow the grain boundaries. Accordingly, in order for the crack path to remain in a plane normal to the loading axis, it must periodically propagate by the relatively difficult transgranular mode until another properly oriented grain boundary segment is encountered. Sub-transus ReX annealing followed by furnace cooling resulted in alpha needles of a lower aspect ratio than after beta annealing (Figure 3a). Thus, the ReX treatment produces a structure which is different from that produced by a similar treatment in the Ti-6Al-4V alloy. In the latter case equiaxed alpha grains result, while as noted above in CORONA 5 alpha needles are produced. These needles offer substantial resistance to crack propagation by forcing a tortuous crack path (Figure 3b). There appeared to be little intergranular propagation after sub-transus annealing in direct contrast with beta annealed material. In the ReX annealed material, it appears that the nature of the grain boundary alpha makes it an efficient barrier to the crack front forcing the crack to take a transgranular route. When sub-transus annealing is carried out for a long time, the alpha regions become globular (Figure 4a) and an inferior strength-fracture toughness results. This occurs because the crack is no longer required to deviate substantially (Figure 4b) making propagation easier and hence fracture toughness lower. A detailed analysis of the sub-transus annealing results indicate that a quite well defined time-temperature annealing envelope is required to achieve the goal strength-fracture toughness values (Figure 5).

The FCP rates for CORONA 5 over the range 5×10^{-6} to 5×10^{-3} in/cycle (2×10^{-7} to 2×10^{-4} m/cycle) are compared to those reported for Ti-6Al-4V in Figure 6. Results compare very favorably although Ti-6Al-4V appears to offer somewhat greater resistance to crack propagation at low ΔK levels (the difference between stress intensity levels at maximum and minimum loads). Further work is planned to evaluate microstructural effects on FCP rates in this alloy. Thus the rates shown in Figure 6 are not necessarily optimum.

Conclusions

A titanium alloy of composition Ti-4.5Al-5Mo-1.5Cr which has been shown to exhibit extremely high fracture toughness and attractive FCP characteristics has been developed. As such this alloy is a potential replacement for Ti-6Al-4V in fracture critical applications (Figure 1).

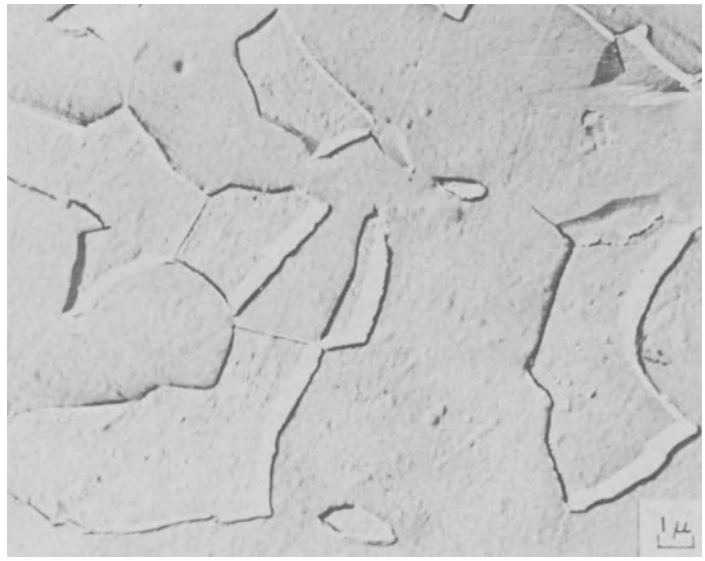

A

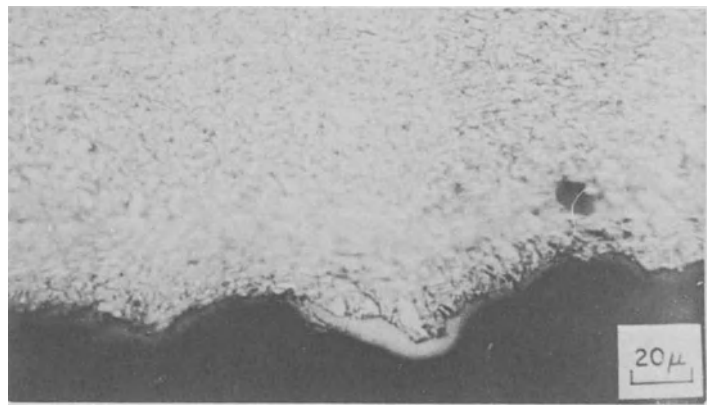

B

Fig. 4 - (a) Long time sub-transus annealed 1475°F (802°C)-48 hrs., air cooled. (b) As for 4(a). Fracture path, fast fracture region (K_Q sample).

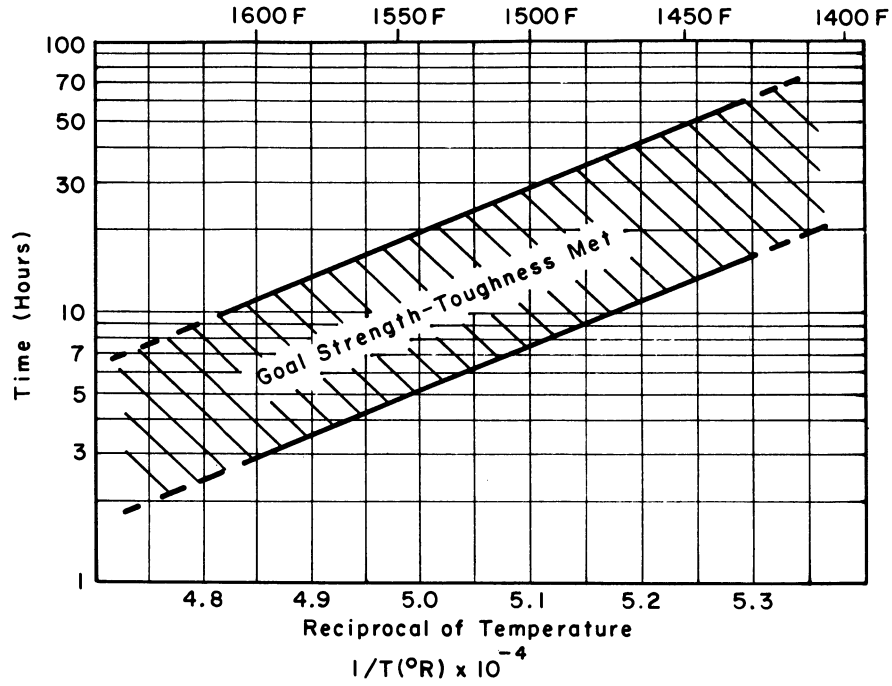

Fig. 5 - Annealing time-temperature envelope required for strength-toughness goals to be met.

Acknowledgments

The authors would like to thank Mr. W. T. Highberger of Naval Air Systems Command, Washington, D.C., for his continuing interest and guidance during this program. In addition, helpful discussions with R. F. Malone (Colt-Crucible) and Professor J. P. Hirth (Ohio State University) are acknowledged. This work was sponsored by Naval Air Systems Command under contract N00019-73-C-0335.

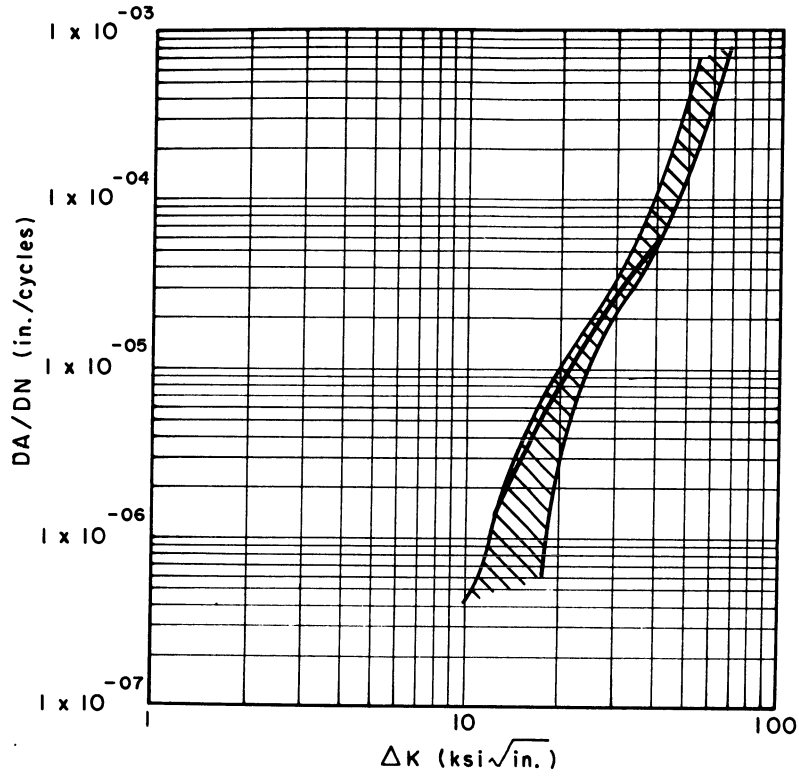

Fig. 6 - Fatigue crack propagation rates for CORONA 5 and Ti-6A1-4V (recrystallize annealed condition).

1 ksi $\sqrt{in}$ = 1.1 MPa $\sqrt{m}$.
1 inch = 0.254 meters.

References

1. Berryman, R. G., Froes, F. H., Chesnutt, J. C., Rhodes, C.G., Williams, J. C. and Malone, R. F., "High Toughness Titanium Alloy Development," Final Engineering Report, July 1974. Naval Air Systems Command Report TFD-74-657.

2. Froes, F. H., Petersen, V. C., Malone, R. F., Rhodes, C. G., Chesnutt, J. C. and Williams, J. C., "Research on Deep Hardenable Titanium Alloys for Large Airframe Structural Members," Final Technical Report, September 1975. AFML-TR-75-41.

THE METALLURGICAL SYNTHESIS OF A NEW GENERATION OF DEEP HARDENABLE TITANIUM ALLOYS. THE METASTABLE BETA TI-MO-V-CR-AL SYSTEM - DESIGN AND PROPERTIES

F.H. Froes*, R.F. Malone*, V.C. Petersen*, C.G. Rhodes+
J.C.Chesnutt+, J.C. Williams@, and J.A. Hall#

* Crucible Materials Research Center, Pittsburgh, Pa.
+ Rockwell International Science Ctr. Thousand Oaks, Ca.
@ Carnegie-Mellon University, Pittsburgh, Pa.
# Air Force Materials Laboratory, Dayton Ohio

I. Introduction

Titanium alloys are attractive for use in aircraft applications because of the weight savings arising from their high strength-density ratio. To optimize these weight savings, a number of heat treatable alpha-beta alloys have been developed to provide still higher strength-density ratios than annealed materials. However, generally low fracture toughness and deep hardening limitations have restricted the use of heat treated parts of this alloy type. In contrast, the heat treatable beta titanium alloys are inherently deep hardening because of their high alloy content which reduces the decomposition kinetics and makes the hardening reaction controllable. Furthermore, they exhibit excellent fracture toughness, far better than the alpha-beta grades. Several new heat treatable beta titanium alloys have been developed in recent years, Ti-11.5 Mo-6Zr-4.5Sn (Beta III), Ti-8Mo-8V-2Fe-3Al and Ti-3Al-8Mo-6Cr-4Mo-4Zr,[1] all of which can develop high strengths in large sections. The heat treatable beta alloys have two deficiencies which limit their potential for use in heavy sections. These are: (i) low aged tensile ductility, particularly in the transverse direction, and (ii) a low elastic modulus:density ratio. The first limitation is in large degree one of tradition since fracture mechanics tests indicate that the beta alloys are tougher than the alpha-beta alloys despite their lower tensile ductility. The second limitation is a result of the large amount of beta stabilizers in these grades which both increases the density and the volume fraction of the β -phase which has a low elastic modulus. Thus the heat treatable beta grades are not as effective in stiffness-critical parts.

The development of a new titanium alloy hardenable in section sizes greater than presently available, while maintaining good toughness and tensile ductility and relatively low density and high modulus was the goal of this program. Specific goals were to obtain the following properties in the transverse direction throughout a wrought and heat treated six-inch diameter bar:

Ultimate Tensile Strength:Density	- 1.1×10^6 inches (2.79×10^4 m) min.
Yield Strength:Density	- 1.0×10^6 inches (2.54×10^4 m) min.
Tensile Elongation	- 12% minimum.
Tensile Reduction in Area	- 18% minimum.
Fracture Toughness, K_{Ic}	- 60 ksi $\sqrt{in.}$ (65.9 MPa $\sqrt{m}$) minimum.
(K_{Ic}/YS)	- 0.095 inches (2.41×10^{-3}m) minimum.

The present paper will outline the metallurgical synthesis used in the present work, report on experimental results and indicate how the alloys developed fit into the overall titanium scenario. Complete details of the program are available elsewhere.[2]

II. Alloy Design

Alloy design pivoted in compositional range around a lean, heat treatable beta alloy. Such an alloy combines deep hardenability, high strength capability and high fracture toughness typical of a heat treatable beta alloy with the tensile ductility and elastic modulus of an alpha-beta alloy. Solution treatment below the beta transus leads to primary alpha which, in limited amounts, is beneficial to both tensile ductility and elastic modulus. The amount of primary alpha phase was restricted to $\lesssim 30$ vol. %, since higher proportions are detrimental to fracture toughness and stress corrosion resistance.[3] Primary alpha is particularly detrimental when distributed in a way which provides large alpha-beta interfaces for the initiation and growth of cracks. In all cases, the stabilizer content was sufficiently high to produce metastable beta phase whose decomposition kinetics provide deep hardenability and age strengthening.

Alloying additions which partition strongly were used to obtain the multiple goals of a matrix rich in beta stabilizers at modest total alloy content and significant amounts of high-modulus primary alpha. Virtually all the strong beta stabilizing elements and particularly molybdenum, partition strongly to the beta phase. Thus a modest addition would result in a density lower than the conventional beta alloys. Concurrently, the alpha partitioning element, Al, would strengthen the alpha phase, raise its elastic modulus and reduce overall density.

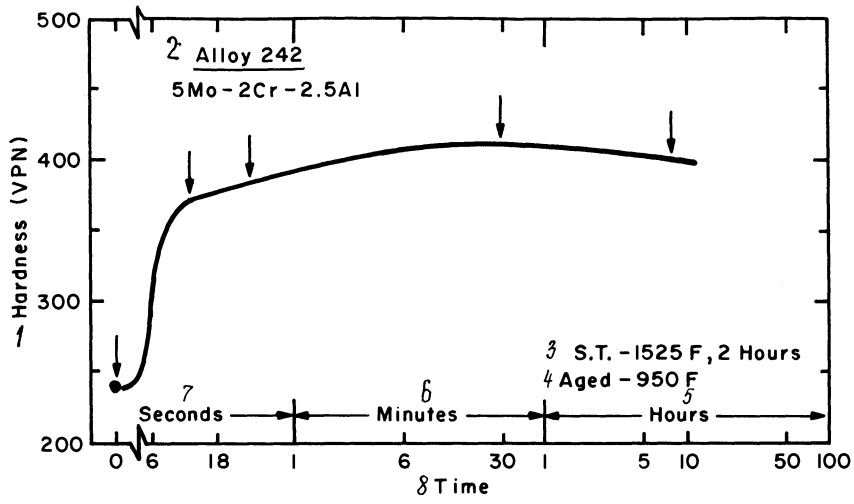

Fig. 1 - Hardening response for alloys containing primary alpha and orthorhombic martensite as solution treated. Arrows indicate aging times for samples used for microstructural analysis.

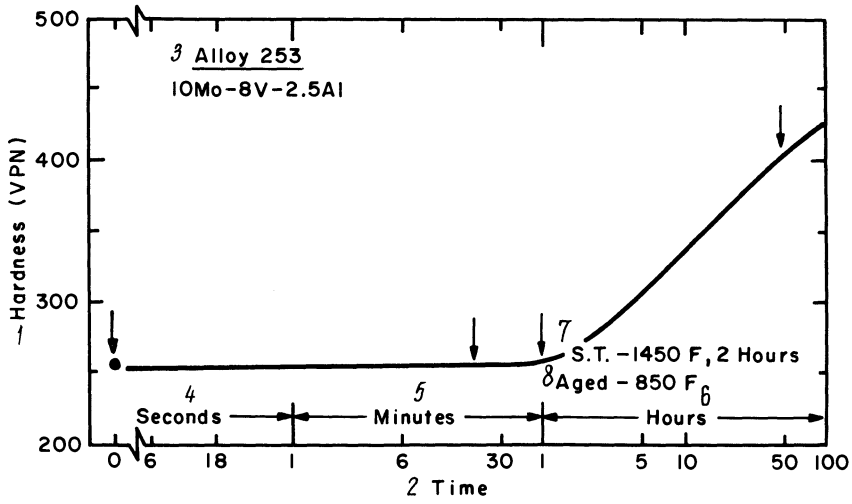

Fig. 2 - Hardening response for alloys containing primary alpha and beta as solution treated. Arrows indicate aging times for samples used for microstructural analysis.

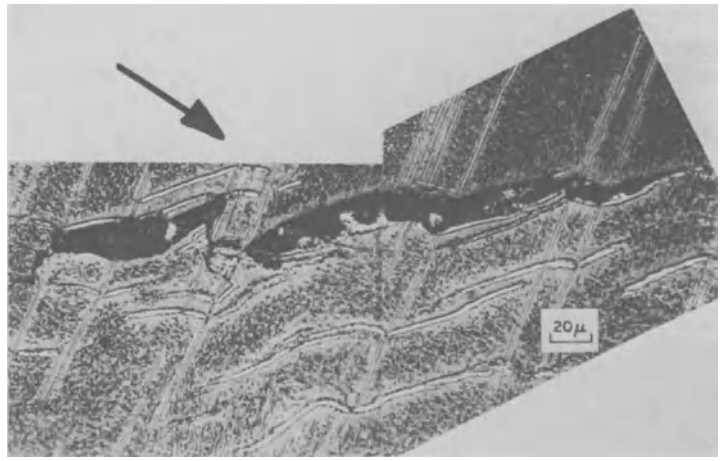

Fig. 3 - Alloy 227 (Ti-7Mo-4Cr-2.5Al). Solution annealed 1400°F (760°C) - 4 hours, aged 900°F (482°C) - 8 hours. Branch crack in fracture toughness (K_Q) sample. Arrow indicates direction of primary crack propagation. Note deviation of crack by coarse alpha phase.

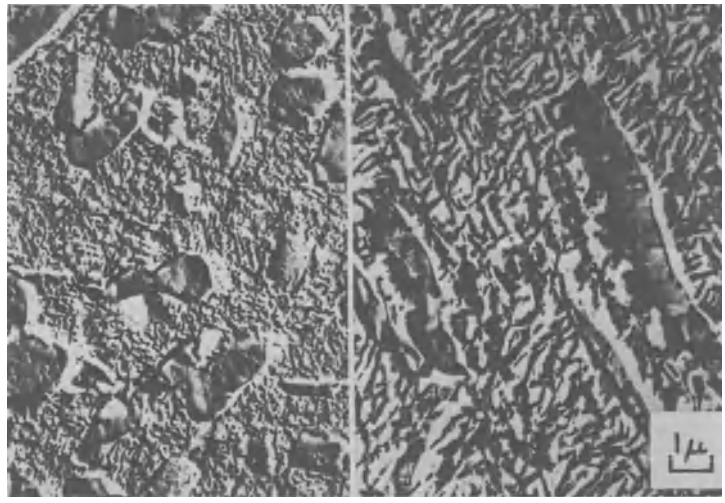

Fig. 4 - Influence of primary alpha particle shape on properties. Material containing microstructure at left exhibited low fracture toughness (K_Q) - high ductility (<20 ksi$\sqrt{in}$, [<22MPa$\sqrt{m}$] 9% elongation, 40% RA) while that containing microstructure at right exhibited high fracture toughness (K_Q) - low ductility (70 ksi$\sqrt{in}$, [77MPa$\sqrt{m}$] 2% elongation, 7% RA), yield strength 160-180 ksi (1100-1240 MPa).

Based on the criterion set out above, an alloy development and processing optimization program was initiated. As the program progress (a) thin foil electron microscopy, (b) X-ray phase identification and (c) fractographic studies using the scanning electron microscope and optical characterization of the interaction of the propagating crack with microstructural features yielded further information on alloy design. It was shown that orthorhombic martensite (α'') present as solution treated generally results in undesirably rapid hardening during aging (Figure 1). In contrast, alloys containing primary alpha and metastable beta in the as-quenched condition exhibited a desirable, relatively slow hardening response (Figure 2). Further fine structure study of this latter type of desirable alloy revealed that aging resulted in α-phase formation; the first α formed by heterogeneous nucleation at sub-boundaries and dislocations. Selected area electron diffraction showed that this α-phase exhibited the Burgers orientation relation. Continued aging resulted in general precipitation of α-phase which was uniformly nucleated within the β subgrains. This latter α-phase consisted of a high density of small particles which do not obey the Burgers orientation relation. The α-phase formed in the matrix persists as non-Burgers α even after aging time as long as 48 hours.

A study of the crack propagation path in both tensile and fracture samples revealed that it (i) occurred by microvoid coalescence, (ii) was almost exclusively transgranular and (iii) occurred in the proximity of beta-alpha interfaces. The strong influence of the alpha phase on crack path is illustrated in Figure 3 where the crack path has been constrained by the elongated coarse alpha particles. A further influence of the alpha phase on crack propagation and hence properties was primary alpha particle shape (Figure 4). The globular primary alpha promotes low fracture toughness-high ductility, while the lenticular primary alpha favors high fracture toughness:low ductility. Based on the results of the present work, a model to explain the influence of particle shape on ductility and toughness is shown schematically in Figure 5. Other workers have shown that the sites for crack nucleation during a tensile test are associated with the aged beta-primary alpha interface.[4] They suggest that crack nucleation is the result of an elastic crack, due to dislocation pile-up, being converted to a plastic crack. This mechanism then implies that larger voids (cracks) occur at larger alpha particles. Applying this to the present observations: void nucleation will tend to be easier at long lenticular particles. In addition, for a given volume fraction of primary alpha, the region plastically deformed between voids will be smaller for lenticular particles than for globular particles (see Figure 5). Thus, the ductility will tend to be higher for globular primary alpha than for lenticular primary alpha. Growth of an already existing crack also occurs along the alpha-beta interface[4,5,6] and the more intricate

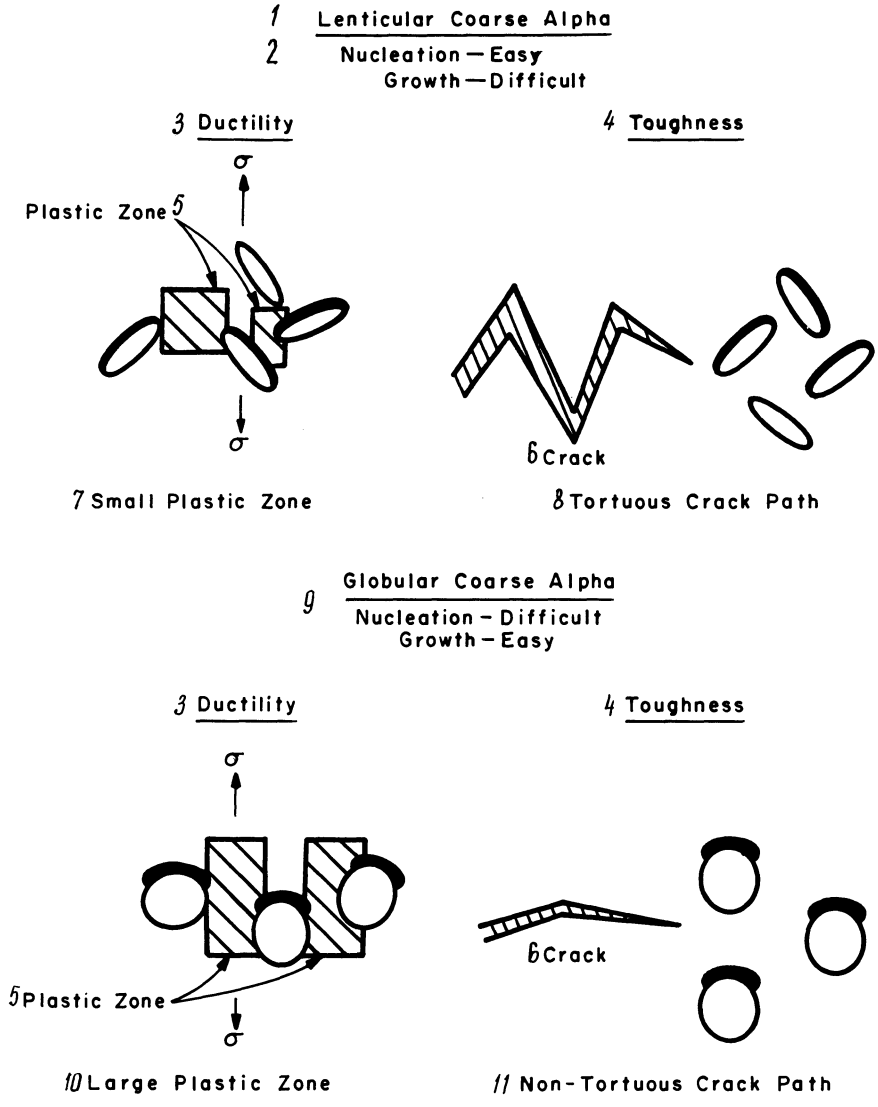

Fig. 5 - Schematic representation of effect of coarse alpha shape on ductility and toughness. For a given volume fraction of coarse alpha the total plastic zone is greater for globular alpha. However, for a propagating crack, the tortuosity factor for lenticular alpha overcomes this effect. Voids are shown as black regions.

the crack path, the greater the fracture toughness.[5] Thus with lenticular alpha particles the crack should be deviated much more than when the primary alpha is globular (Figure 5) with a result of higher fracture toughness - lower ductility combination in the former case.

A further microstructural feature which influenced mechanical properties and particularly ductility was sub-grains. The presence of sub-grains decorated with Burgers alpha particles tended to improve transverse ductility.

From the foregoing, obviously all mechanical properties cannot be optimized at the same time. For example, sub-grains are detrimental to deep hardenability but promote good ductility. However, by proper selection of composition, processing sequences and heat treatment schedules, these alloys can be manipulated to behave virtually as a composite of different constituents having individually different properties and overall a desired property combination.

III. Experimental Program and Discussion

The program was divided into three phases. In Phase I, 65 alloy compositions, ranging in compositional type from a heat treatable beta down to rich alpha-beta were melted, processed to 0.040 inch (1×10^{-3}m) sheet, and evaluated for attainable strength and deep hardening potential.

The second phase was a more extensive evaluation of the ten most promising Phase I alloys using the product of five pound (2.3 kg) laboratory melted ingots. Properties and processing variables were investigated in more detail with emphasis on strength, ductility and fracture toughness after cooling at a rate simulating[2] that of the center of a six inch (0.152 m) diameter billet.

The final phase of the contract was a detailed mechanical property evaluation of the three most promising compositions in a six inch (0.152 m) diameter billet using the product of 500-pound (230 kg) ingots. The compositions and numerical designations of these three alloys were:

Alloy 334 - Ti-10Mo-6Cr-2.5Al
Alloy 227 - Ti-7Mo-4Cr-2.5Al
Alloy 253 - Ti-10Mo-8V-2.5Al

The elevated temperature and fatigue properties of these alloys equal or exceed those of semi-commercial deep hardenable alloys.[2] However, the outstanding characteristics of the present alloys were those which were actually specified as program goals and for

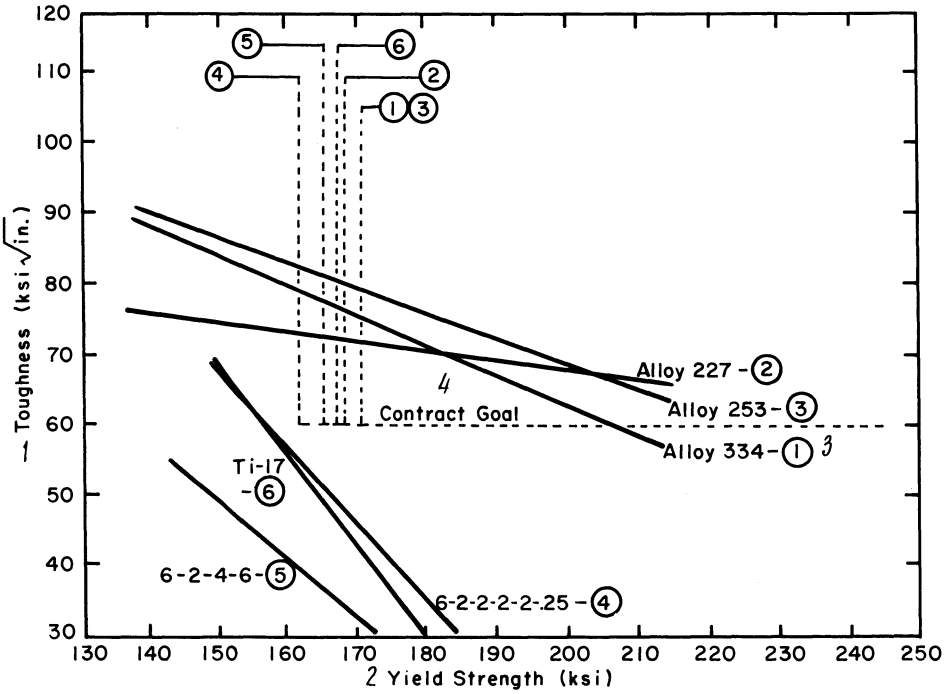

Fig. 6 - Toughness-yield strength characteristic alloy trend lines for present contract alloys and semi-commercial deep hardenable alloys. Goal properties for each alloy are density normalized (number code above).

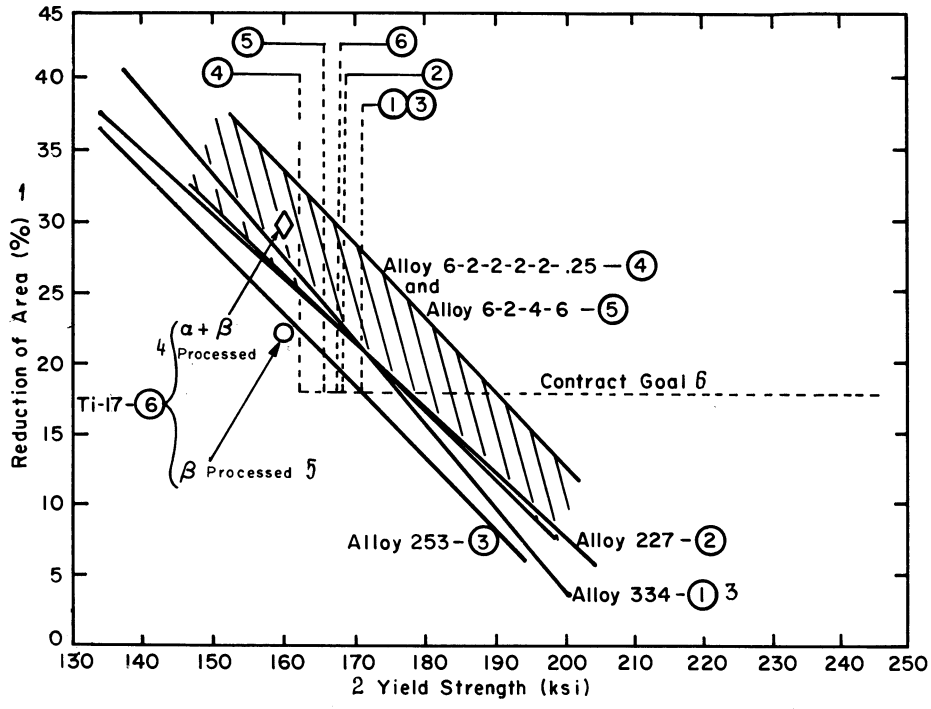

Fig. 7 - Reduction of area-yield strength characteristic alloy trend lines for present contract alloys and semi-commercial deep hardenable alloys. Goal properties for each alloy are density normalized (number code above).

which the alloys were designed - fracture toughness and ductility. The alloy characteristic trend lines for the three Phase III alloys are compared with commercial and semi-commercial deep hardenable alloys in Figures 6 and 7. The Phase II alloys substantially outperform the comparison alloys in fracture toughness behavior, in fact, they are the only alloys illustrated which exceed their density normalized toughness goal. The three alpha-beta alloys exhibit a slightly superior ductility performance. However, all three contract alloys are again at or above the required level of RA at the goal strength level.

In comparing the three Phase III alloys with the alpha-beta deep hardenable alloys, a point of concern must be the substantial edge to center differential inherent in the alpha-beta alloys. The alloys from the present contract show some property variation from edge to center of a six inch (0.152 m) section (334: ~ 2 ksi (~14 MPa); 227: ~13 ksi (~90 MPa); 253: ~3 ksi (~21 MPa). In contrast the commercial alloy Ti-6Al-2Sn-4Zr-6Mo exhibits a 14 ksi (~ 97 MPa) yield differential while the same parameter is 10-20 ksi (69-138 MPa) for Ti-17. The situation is even worse in the Ti-6Al-2Sn-2Zr-2Mo-2Cr-.25Si alloy since reported data[7] show a yield strength differential of 25-30 ksi (172-207 MPa). This strength differential between surface and center is probably less than desirable in a heavy section. However, of much more concern is the accompanying fracture toughness variation. A toughness of 60 ksi $\sqrt{in.}$ (65.9 MPa $\sqrt{m}$) in the center occurs in conjunction with < 40 ksi $\sqrt{in.}$ (< 44.0 MPa $\sqrt{m}$) at the surface. This large variability in fracture toughness implies that as an unstable flaw propagates at the stress intensity indigenous of the surface region, obviously its length increases, with a concurrent increase in the stress intensity at the crack tip. Consequently, the flaw will continue to grow into the central (higher toughness) region. Thus the effective fracture toughness is the lower (surface) value.

IV. Conclusions

1. The metallurgical synthesis of a new generation of deep hardenable titanium alloys - the metastable beta Ti-Mo-V-Cr-Al system - has been presented.

2. Culminating from a three phase program, three alloys were extensively evaluated:

   Alloy 334 - Ti-10Mo-6Cr-2.5Al
   Alloy 227 - Ti-10Mo-8V-2.5Al
   Alloy 253 - Ti-7Mo-4Cr-2.5Al

The properties exhibited by these alloys represent the "optimum" property combination for deep hardenable titanium alloys at this time.

Acknowledgments

The authors would like to acknowledge helpful discussions with E. J. Dulis, J. B. Guernsey, C. F. Yolton, Dr. M. A. Greenfield and Professor J. P. Hirth. In addition, the technical services of R. A. Hohowski, F. R. Shuss, R. A. Spurling, P. Q. Sauers and E. H. Wright are gratefully recorded.

The program was sponsored by the Air Force Materials Laboratory under contract F33615-71-C-1525.

REFERENCES

1. Guernsey, J. B., SAE Los Angeles, Ca, Oct. 5-9, 1970, publication 700856.

2. Froes, F. H., Malone, R. F., Petersen, V. C., Rhodes, C. G., Chesnutt, J. C. and Williams, J. C., Technical Report AFML-TR-75-41, September 1975.

3. Guernsey, J. B., Petersen, V. C., and Froes, F. H., Met. Trans. Vol 3, 1972, pp 339-341.

4. Greenfield, M. A. and Margolin, H., Technical Report AFML-TR-70-43, April 1970.

5. Gerberich, W. W. and Baker, G. S., ASTM STP 432, 1968, pp 80-99.

6. Hall, J. A., Pierce, C. M., Ruckle, D. L. and Sprague, R. A., Technical Report AFML-TR-71-206, November 1971.

7. Bartlo, L. J., Bomberger, H. B. and Seagle, S. R., Technical Report AFML-TR-73-122, May 1973.

STRENGTH AND TOUGHNESS OF BINARY Ti-Ni AND Ti-Mo ALLOYS

I. L. Caplan

David W. Taylor Naval Ship R & D Center

Annapolis, Maryland 21402

Titanium alloys, because of their high strength-to-weight ratios and excellent seawater properties, are leading candidates for advanced structural applications in the naval and aerospace fields. For engineering purposes, properties such as strength and toughness are traded-off to obtain desired combinations.

In most seawater applications, alpha or alpha-beta alloys are generally used. However, for naval structures where very high strength, increased reliability (in terms of stress corrosion resistance and fracture toughness), and improved formability are required, metastable beta titanium alloys must be considered.

Therefore, in this investigation two binary beta systems were chosen: titanium-nickel (beta eutectoid) and titanium-molybdenum (beta isomorphous). Alloy compositions were selected so that a range of microstructures could be obtained by appropriate heat treatments. The effect of heat treatment and percentage alloying element on mechanical properties was determined for small electron-beam melted ingots. The relationship between structure and properties will not be addressed in this paper.

Titanium-Molybdenum System

In the beta isomorphous system, the alloying element is completely miscible in the beta phase and isomorphous with it (i.e., both have bcc structures). Increasing the alloying content decreases the alpha-to-beta transformation temperature until 100% beta phase exists.

Molybdenum is an extremely potent beta stabilizer with the beta phase being stable above 28% Mo (1). Above 11-12% Mo, metastable beta is retained upon quenching (2). Omega phase precipitation occurs over certain composition ranges and is generally produced by aging or controlling the cooling rate. The solubility of molybdenum in alpha titanium is about 0.8% at 800°C (2).

Three compositions were selected for the Ti-Mo system: 0.5% Mo (alpha alloys), 6% Mo (lean alpha-beta alloys), and 12% Mo (rich alpha-beta alloys). Binaries with greater than 28% Mo (beta alloys) were not selected because of the difficulties in producing homogeneous ingots even by multiple melting procedures.

Titanium-Nickel System

The beta eutectoid system differs from the isomorphous type in that, under equilibrium conditions, the beta phase decomposes to form alpha plus an intermetallic compound. The degree of eutectoid transformation that occurs during heat treatment depends upon the eutectoid temperature and the amount of beta stabilizer(s) in relation to the composition at the eutectoid point. Eutectoid transformation is favored by high eutectoid temperatures and high alloy contents. There are many titanium eutectoid systems, and their eutectoid temperatures vary from near 540°C to above 820°C.

Nickel, one of the more active eutectoid formers, has a eutectoid temperature of 768°C at 5.5% Ni (3). The solubility of nickel in alpha titanium is less than 0.2% (3). Martensitic alpha-prime does not form from the beta phase when quenching alloys with more than 4% nickel (4). The beta phase is retained upon quenching alloys with greater than 8% nickel. With greater than 5% nickel, the non-equilibrium, submicroscopic omega phase precipitates during quenching (4).

Four compositions were chosen for this investigation: 0.1% Ni (alpha alloys), 2% Ni (hypoeutectoid alloys), 5% Ni (eutectoid alloys), and 7% Ni (hypereutectoid alloys).

Material

Titanium bar stock, 38 mm square, was used as the base material for melting. The purity of the elements used is shown in Table 1.

Table 1
Elements Used for Melting

Elements	Purity %	Form
Ti	99.86	Bar
Ni	99.50	Powder
Mo	99.93	Powder

Chemical analysis was performed after melting, processing, heat treating, and machining. One specimen for each heat treatment (two specimens per ingot) was analyzed. These data are presented in Table 2.

TABLE 2
Chemical Compositions of Processed Ingots

Ingot No.	Specimen No.	Nominal Binary Addition	Composition, wt %						
			Ni	Mo	O	N	H	C	Fe
55	5	0.1% Ni	0.13	-	0.076	0.016	0.0012	0.016	0.040
	7		0.13	-	0.072	-	-	-	-
56	3		0.16	-	0.069	-	-	-	-
	5		0.15	-	0.071	-	-	-	-
53	7	2% Ni	2.29	-	0.092	-	-	-	-
	10		2.25	-	0.095	0.014	0.0009	0.018	0.030
54	4		2.73	-	0.101	-	-	-	-
	2		2.56	-	0.096	-	-	-	-
66	8	5% Ni	6.36	-	0.100	-	-	-	-
	5		5.27	-	0.110	-	-	-	-
67	6		4.10	-	0.117	-	-	-	-
	3		5.10	-	0.110	-	-	-	-
	1		5.37	-	0.121	-	-	-	-
	7		5.28	-	0.100	0.010	0.0015	0.0015	0.014
	9		5.79	-	0.100	-	-	-	-
51	6	7% Ni	6.69	-	0.096	0.020	0.0015	0.019	0.030
	9		8.99	-	0.106	-	-	-	-
	4		6.58	-	0.098	-	-	-	-
52	7		5.10	-	0.094	-	-	-	-
	10		5.05	-	0.103	-	-	-	-
57	3	0.5% Mo	-	0.63	0.079	-	-	-	-
	7		-	0.55	0.078	0.017	0.0018	0.017	0.035
58	2		-	0.66	0.082	-	-	-	-
	7		-	0.69	0.083	-	-	-	-
59	2	6% Mo	-	4.71	0.106	0.018	0.0015	0.019	0.023
	5		-	5.44	0.105	-	-	-	-
61	6		-	6.36	0.105	-	-	-	-
	8		-	6.56	0.094	0.021	0.0022	0.015	0.030
60	2	12% Mo	-	13.80	0.140	-	-	-	-
	6		-	6.43	0.116	-	-	-	-
63	2		-	12.18	0.130	-	-	-	-
	8		-	12.74	0.130	0.010	0.0010	0.017	0.017

Experimental Procedure

Melting. Slots were machined along each titanium bar on two or four sides. The alloying addition was distributed along these slots and then, by arc melting, fused into the bar.

The arc-melted alloyed bars were fed into the plasma beam of a hollow cathode discharge melter and drip melted into a water-cooled copper crucible to form 900 gm ingots, 51 mm in diameter

and 127 mm long. Two ingots were melted for each composition and each ingot was either double, triple, or quadruple melted.

Processing and Heat Treating. Prior to forging, major surface defects were removed by machining and the top and bottom of the ingots were machined flat. Hot forging was conducted in a ram-press at either 790°C or 1040°C. The ingots were upset about 40% and then turned 90° and reduced to a forged slab of about 25 mm thick. The slabs were then heated to 730°C and cross rolled (temperature of rolls - 320°C) producing a "pancake" approximately 100 x 130 x 13 mm thick.

The plates were vacuum annealed at 700°C for one hour to remove hydrogen. Each plate also was radiographed to determine whether internal cracks and/or macrosegregation were present. Two tensile and two Charpy V-notch impact specimen blanks were cut from each plate and heat treated in an argon atmosphere prior to machining. Two heat treatments were performed per plate (see tables 3 and 4). Metallographic samples were taken from each plate to establish the as-rolled microstructure. Specimens referred to in the text are identified by two numbers, the first being the ingot number and the second the test blank number.

Results

Chemical Analysis. The chemical analysis obtained from broken halves of impact specimens (Table 2) indicated fairly uniform melting in 9 of 14 ingots. Both chemical and radiographic analysis indicated segreagation in ingots 59 (6% Mo) and 60 (12% Mo). Ingots 51 (7% Ni), 66 (5% Ni), and 67 (5% Ni) have a variation in nickel composition of 2.41, 2.10 and 1.69% respectively, but evidenced no segregation radiographically. This is due to the closeness in atomic weights of nickel and titanium. Because of the difficulty in obtaining uniform high molybdenum melts, ingot 63 was melted four times. Chemical and radiographic analysis show excellent uniformity in this ingot. The oxygen and other interstitial pick up seems to be within reasonable limits for all the ingots.

Mechanical Properties. The results of tensile and Charpy impact tests are presented in tables 3 and 4. Ultimate tensile strengths were found to vary from 407 to 1364 MN/m^2 with yield strengths ranging from 276 to 992 MN/m^2. However, there appears to be a clustering of yield data into two groups: the low strength group, 280 - 480 MN/m^2, and the high strength group, 620 - 1000 MN/m^2. The very high strength materials exhibited extremely low ductility, such as tensile specimen 60-5 which failed simultaneously in more than one location. Charpy impact values were found to

TABLE 3 - TENSILE AND IMPACT PROPERTIES OF HEAT TREATED Ti-Ni BINARIES

Specimen Number		Nominal Composition wt %	Heat Treatment			Tensile Strength MN/m^2	Yield Strength (0.2% offset) MN/m^2	Elongation (in 25 mm) %	Reduction of Area %	Charpy V-Notch Impact (0^oC) Joule
			Anneal (a)							
Tensile	Impact		Temperature ^oC	Phase Region	Aging Treatment					
55-1	2	0.1% Ni	900	Beta	—	482	365	22	42	170
3	5					448	338	21	37	208
4	6		900	Alpha + Beta	370°C	434	310	28	42	197
8	7				30 min, WQ	413	290	41	42	214
56-1	3		760	Alpha + Ti_2Ni	—	420	296	38	40	326+
2	4					420	290	36	34	326+
7	5		720	Alpha + Ti_2Ni	—	407	276	37	44	264
(b)	6					-	-	-	-	310
53-1	7	2% Ni	830	Alpha + Beta	—	634	400	17	20	45
4	8					551	372	19	20	41
3	9		830	Alpha + Beta	635°C	482	317	18	21	25
6	10				1 hr, WQ	531	345	18	14	22
54-3	4		800	Alpha + Beta	—	641	400	13	18	23
7	8					593	379	18	20	34
1	2		730	Alpha + Ti_2Ni	—	482	331	28	21	48
5	6					496	351	23	20	64
66-1	7	5% Ni	850	Beta	—	1144	992	1	3	7
4	8					1102	806	2	7	5
6	5		850	Beta	550°C	854	682	2	11	5
10	2				10 min, WQ	944	779	2	5	5
67-6	3		780	Alpha + Beta	—	786	503	9	24	5
1	7					1040	689	4	9	7
4	9		730	Alpha + Ti_2Ni	—	517	475	17	41	26
10	8					579	434	16	25	37
51-1	6	7% Ni	915	Beta	—	1164	Broke Outside Gage			5
2	7					896	620	2	2	4
3	8		845	Beta + Ti_2Ni	720°C	565	365	12	11	5
4	9				24 hr, WQ	593	379	8	8	5
52-2	7		760	Alpha + Ti_2Ni	—	600	434	7	3	26
4	8					600	434	7	3	19
5	10		730	Alpha + Ti_2Ni	—	579	427	6	5	27
1	9					565	427	7	4	19

(a) All annealing treatments involved holding one hour at temperature followed by water quench (WQ) except where noted.
(b) Insufficient material in ingot for specimen.

TABLE 4 - TENSILE AND IMPACT PROPERTIES OF HEAT TREATED Ti-Mo BINARIES

Specimen Number		Nominal Composition wt %	Heat Treatment			Tensile Strength MN/m^2	Yield Strength (0.2% offset) MN/m^2	Elongation (in 25 mm) %	Reduction of Area %	Charpy V-Notch Impact (0^oC) Joule
			Anneal (a)							
Tensile	Impact		Temperature ^oC	Phase Region	Aging Treatment					
57-1	2	0.5 Mo	915	Beta	—	482	393	23	44	214
4	3					489	400	21	43	220
5	6		900	Alpha + Beta	400^oC 1 hr, WQ	482	386	31	44	234
8	7					489	400	25	45	227
58-1	2		800	Alpha + Beta	—	462	351	23	38	287
4	3					441	351	30	36	310
5	6		720	Alpha + Beta	—	427	345	26	44	326+
8	7					441	358	26	39	326+
59-1	2	6 Mo	900	Beta	—	897	641	23	76	65
8	3					897	648	27	74	71
4	5		900	Beta	400^oC 1 hr, WQ	951	675	16	32	45
(b)	6					-	-	-	-	38
61-1	2		800	Alpha + Beta	—	779	765	15	51	93
3	6					737	696	13	50	109
4	7		720	Alpha + Beta	—	689	600	20	46	116
5	8					703	606	Broke at Punch Mark		109
60-1	3	12 Mo	815	Alpha + Beta	—	910	772	Segregation		12
(b)	4					-	-	-	-	18
5	2		815	Alpha + Beta	400^oC 1 hr, WQ	1364	Failed at 3 Locations			3 (c)
(b)	6					-	-	-	-	5 (c)
63-1	3		720	Alpha + Beta	—	854	730	25	76	31
4	2					800	641	28	75	27
6	8		720 Air Cool	Alpha + Beta	—	1020	978	10	32	14
7	9					1000	944	10	31	11

(a) All annealing treatments involved holding one hour at temperature followed by water quench except where noted.
(b) Insufficient material in ingot for specimens.
(c) Transverse charpy.

range from 3 59 326+ joules. The extremely low impact values were produced by the 5% Ni, 7% Ni, and 12% Mo binaries.

Titanium-Nickel. Generally, strength increases and toughness decreases with alloy content. The lowest strength and greatest toughness values for all ingot compositions are obtained with the alpha plus Ti_2Ni heat treatment.

The presence of omega results in very high strength but very poor toughness. This is shown by the 5 and 7% beta quenched samples which had the highest tensile strengths (>1100 MN/m^2) of all specimens. None of these materials produced impact values above 7 joules.

Titanium-Molybdenum. As in the case of the nickel alloys, the toughness decreases and strength increases with alloy content. The best impact properties and lowest tensile strengths are obtained with the alpha-beta structures. The specimens containing alpha-prime have higher strengths and lower toughness. Very poor toughness and high strength characterizes those specimens which contain the omega phase. Once again, the strength level appears to be related to the amount of omega present.

CONCLUSIONS

- As expected, strength increases and toughness decreases with alloy content.

- Most of the highly alloyed binaries (5% Ni, 7%Ni, and 12% Mo) exhibited very poor ductility and touchness particularly in the beta heat-treated condition.

- Of the alloys investigated, the 6% Mo binary seems to hold the most promise for a high strength good toughness material. However, leaner molybdenum contents (as low as 0.5-1.0%) should be considered where very high toughness is required.

REFERENCES

1. Hanse, M., Kamen, E. L., Kessler, H. D., and McPherson, D. J., Trans. AIME, 191, p. 881 (1951).

2. Dewez, P., Trans. AIME, 191, p. 765 (1951).

3. Margolin, H., Ence. E., and Nielson, J. P., Trans. AIME, 197, p. 243 (1953).

4. Barton, J. W., Purdy, G. R., Taggart, R., and Parr, J. G., Trans. AIME, 218, p. 844 (1960).

THE TECHNOLOGICAL ASPECTS OF TITANIUM APPLICATION IN THE TU-144 AIRCRAFT STRUCTURE

S. A. Vigdortchik and A. N. Tupolev

Design Bureau

U.S.S.R.

Ten years ago when our experimental design bureau initiated the design of the TU-144, the decision was made for the wide-spread use of titanium in its construction. At this time, neither we nor perhaps anyone in the world had the necessary experience or knowledge to permit reliable operation of titanium in a commercial aircraft structure with a lifetime of 30,000 flight hours. On the contrary, both practice and the literature were filled with examples of the "insidious" behavior of titanium in aircraft with even low safe-life.

This situation led not only to the creation of several specialized titanium physical metallurgy and technological laboratories in our experimental design bureau, but also to assignment of large study-contracts to our scientific research institutes.

The development and manufacturing of pilot structure assemblies, prototype aircraft and essential new equipment as well as the wide-spread testing of structural elements were all conducted simultaneously.

To permit extensive use of titanium in the TU-144 structure and to develop production techniques capable of high safe-life and reliability, it was necessary to solve several problems.

The chief problems were as follows:

1. Control of structure hydrogenation and residual stresses.

2. Control of surface embrittlement caused by oxygen, nitrogen and carbon saturation.

3. Prevent the formation of brittle phases or hardened zones during welding or heating.

4. Prevent the formation of salt stress-corrosion centers, and

5. Maximize the simplification and cost reduction for the production process after successful solution of the first four problems.

While studying the first question, the effect of hydrogen content and stress level on the slow-speed failure was investigated (using mainly the Troiano method). The tests, some of which extend for more than five years, show a definite time to failure characteristic of each hydrogen content and stress level as seen in the lower left hand curve of Figure 1. This time to failure can extend from one hour to as long as several years.

The lower right hand curves of Figure 1 illustrate the failure stress as a function of hydrogen content disregarding the time to failure. These curves show that there are threshold stresses, below which failure does not occur regardless of hydrogen content, and also that there is a threshold hydrogen content, below which failure does not occur regardless of stress level.

Similar investigations have been performed for several alloys, whose slow-rate failure characteristics are shown in the upper curves of Figure 2. These curves illustrate quite different slow-rate failure characteristics for different titanium alloys. This difference should define the designer's choice of an alloy.

The impact strength of the various alloys at room temperature as a function of hydrogen content is also shown in the lower part of Figure 2. Here also, the considerable difference between the alloys is obvious.

Investigation has shown that the slow-rate failure is defined by the peak hydrogen-content on the surface, and not by the mean hydrogen content. For both experimental as well as serial production, equipment and techniques were developed for the content of surface-as well as bulk-hydrogen content during each succeeding process step. Statistical analysis of many thousands of hydrogen content measurements has shown the majority of the production processes either induce hydrogenation or redistribute the hydrogen already present. This is caused by the inner stresses of both the first and second type leading to local concentrations of hydrogen.

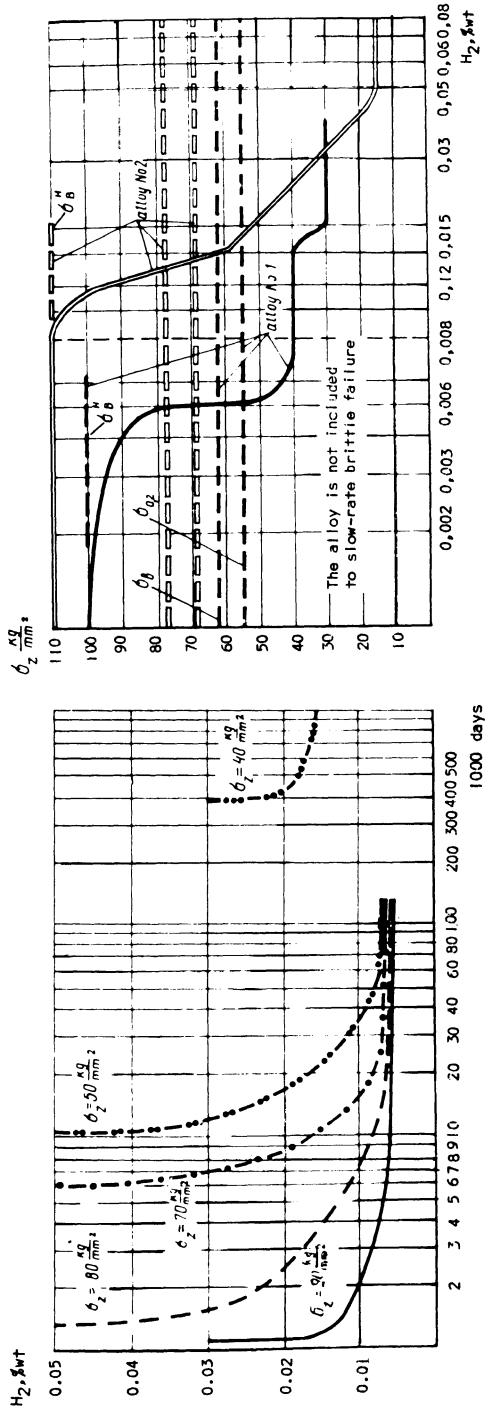
σ_z kg/mm²
110
100
90
80
70
60
50
40
30
20
10
σ_B
alloy No2
alloy No1
$\sigma_{0,2}$
σ_β
The alloy is not included to slow-rate brittle failure
0,002 0,003 0,006 0,008 0,012 0,015 0,03 0,05 0,06 0,08
H_2,%wt
$\sigma_z = 40$ kg/mm²
$\sigma_z = 50$ kg/mm²
$\sigma_z = 70$ kg/mm²
$\sigma_z = 80$ kg/mm²
$\sigma_z = 90$ kg/mm²
2 3 4 5 6 7 8 9 10 20 30 40 60 80 100 200 300 400 500
1000 days
H_2,%wt
0.05
0.04
0.03
0.02
0.01

Fig.1

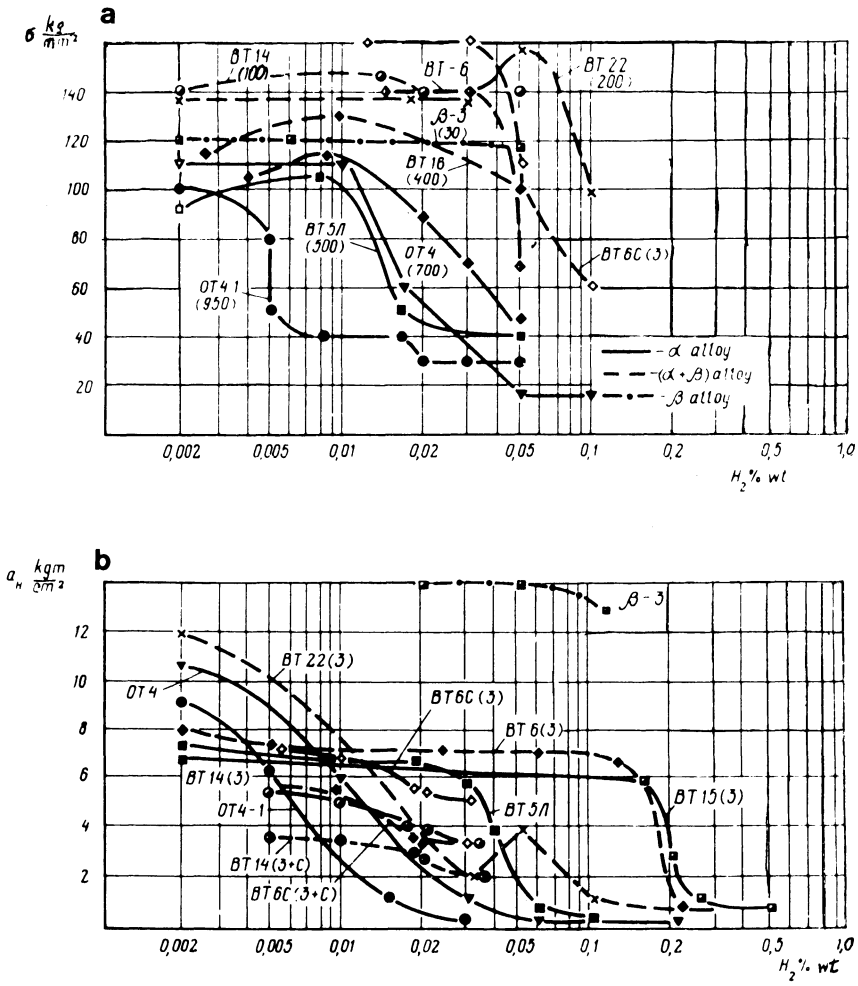
a
σ kg/mm²
ВТ14 (1000)
ВТ-6
ВТ22 (200)
β-3 (30)
ВТ16 (400)
ВТ5Л (500)
ОТ4 (700)
ОТ4-1 (950)
ВТ6С(3)
α alloy
(α+β) alloy
β alloy
H₂% wt
b
aн kgm/cm²
β-3
ВТ22(3)
ОТ4
ВТ6С(3)
ВТ6(3)
ВТ14(3)
ОТ4-1
ВТ5Л
ВТ15(3)
ВТ14(3+С)
ВТ6С(3+С)
H₂% wt

Fig. 2

Figure 3 schematically illustrates the hydrogen distribution along the cross-section of a part resulting from various processing techniques (from left to right): cutting, chemical etching, heating and welding of all types. Several processes were developed which minimize hydrogenation; e.g., a special process of chemical milling combined with refining. This technique has enabled the use of chemically milled structures (over 1500 parts) which provide savings both in weight and production costs. Typical parts produced by this method are shown in Figure 4.

Vacuum low-temperature annealing is considered the principal means for lowering hydrogen content as well as residual stresses in structural members. Several types of vacuum furnaces were developed for this purpose, among them the YBH furnace (Φ1500mmx3000mm). This furnace is capable of 10^{-5} Torr vacuum.

As seen in Figure 5, entire sections of welded assemblies can be annealed in this furnace. To avoid buckling, the temperature is smoothly changed by means of a programmed control systems and thyristor power sources. Even larger furnaces, up to 6000mm long, have been designed and operated. Now the world's largest vacuum furnace of this type, 45,000mm dia x 11,000mm long, is being constructed. In each of these furnaces, a vacuum of 10^{-5} Torr is maintained and programmed stepless temperature adjustment is provided. A sketch of this large furnace is shown in Figure 6. Following heat treatment in these furnaces, the average hydrogen concentration is about 0.003% by weight and no greater than 0.005% in areas of stress concentration. Simultaneously, the internal stresses are decreased to less than 25% of the proportional limit, which guarantees structural safety from slow-rate failure for practically any titanium alloy.

We have investigated the effects of nitrogen and oxygen saturation, on both the surface (e.g. when heating and cutting) and across the section of the part (e.g. when multilayer welding), and their relationship to the principal safe-life characteristics: fatigue, slow-rate failure and creep. As is generally known, these effects can be quite considerable, sometimes even catastrophic. In this connection, technological instructions were established to control and remove the surface saturated layer, principally by a chemical unhydrogenizing etch and finish machining. Investigations of argon arc welding show existing welding methods in an inert atmosphere (mainly, argon) cause a marked decrease in some safe-life characteristics because of contamination of the neutral atmosphere during welding.

Special inert-atmosphere welding chambers featuring continuous purification have been designed and constructed. We have developed the apparatus and methods, based principally on chromatographic

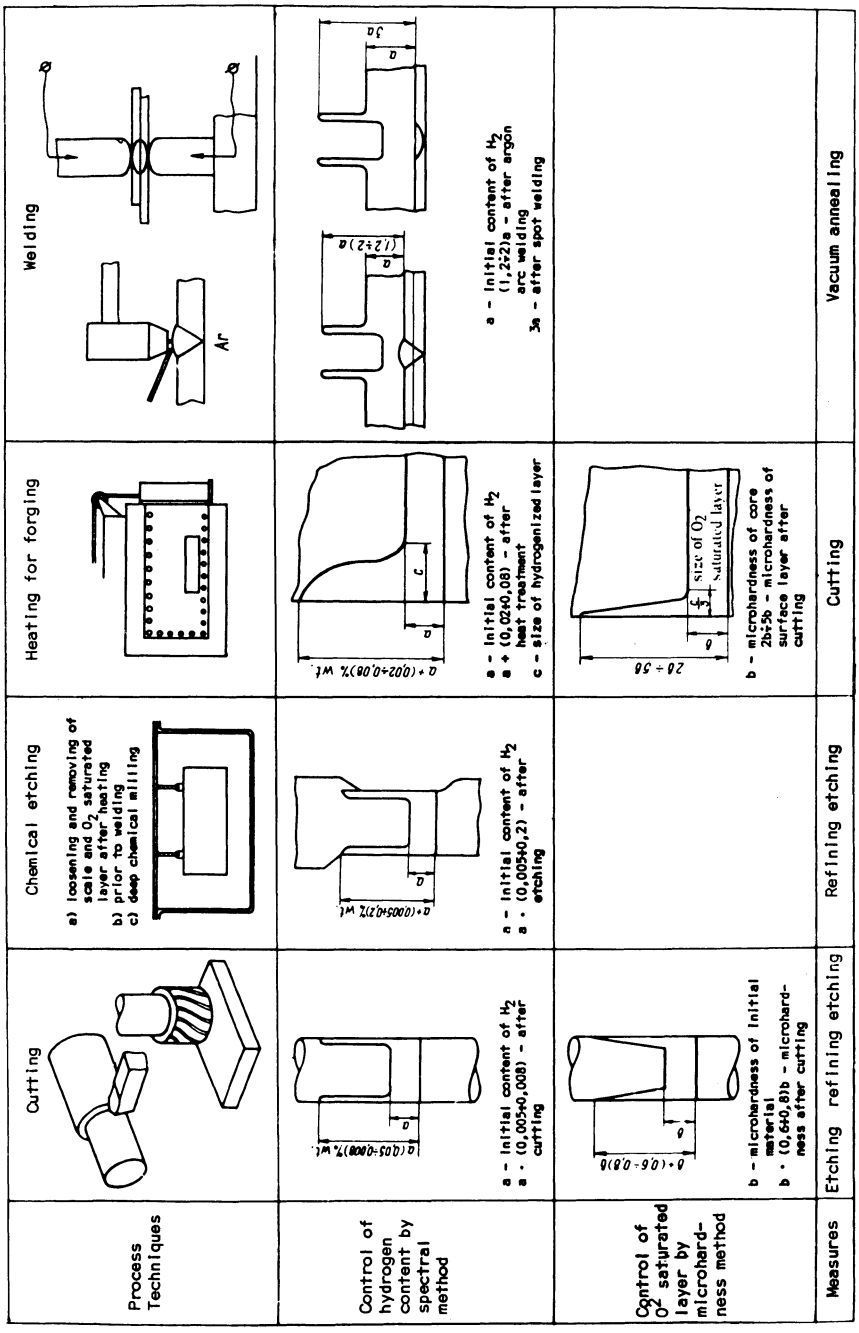
Process Techniques
Cutting
Chemical etching
a) loosening and removing of scale and O_2 saturated layer after heating
b) prior to welding
c) deep chemical milling
Heating for forging
Welding
Ar
Control of hydrogen content by spectral method
a - initial content of H_2
a · (0,005÷0,008) - after cutting
a - initial content of H_2
a · (0,005÷0,2) - after etching
a - initial content of H_2
a + (0,02÷0,08) - after heat treatment
c - size of hydrogenized layer
a - initial content of H_2
(1,2÷2)a - after argon arc welding
3a - after spot welding
Control of O_2 saturated layer by microhardness method
b - microhardness of initial material
b · (0,6÷0,8)b - microhardness after cutting
b - microhardness of core
2b÷5b - microhardness of surface layer after cutting
size of O_2 saturated layer
Measures
Etching refining etching
Refining etching
Cutting
Vacuum annealing

Fig. 3

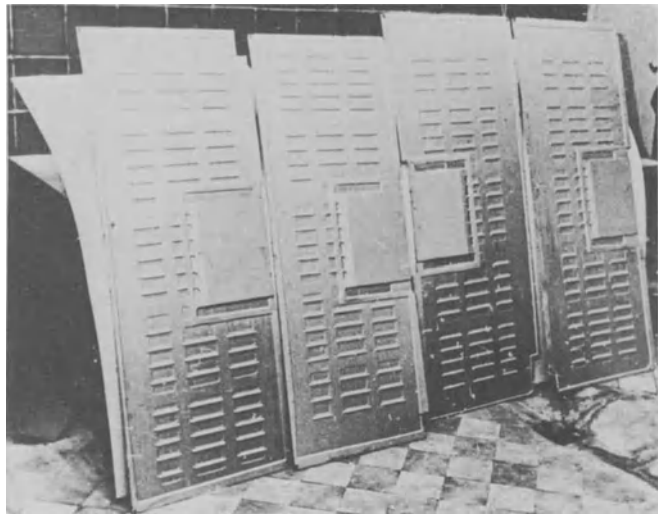

Fig. 4

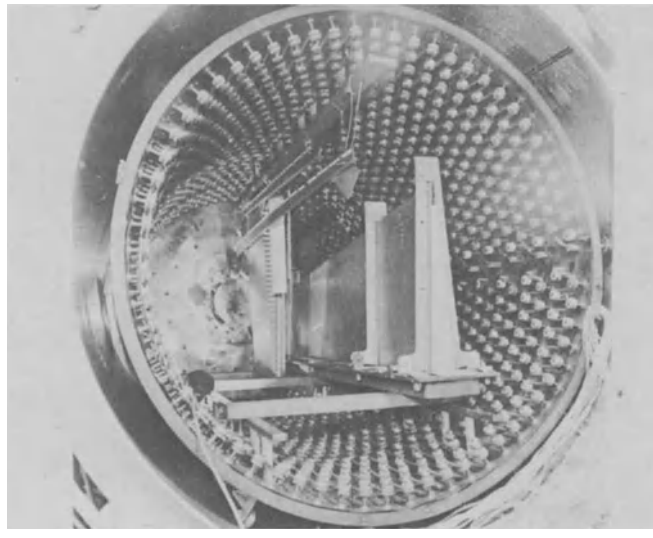

Fig. 5

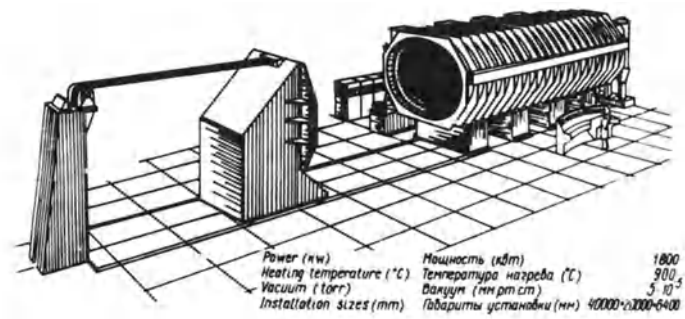
Power (kw)
Мощность (кВт)
1800
Heating temperature (°C)
Температура нагрева (°C)
900
Vacuum (torr)
Вакуум (мм рт.ст.)
5 10⁻⁵
Installation sizes (mm)
Габариты установки (мм)
40000×12000×6400

Fig. 6

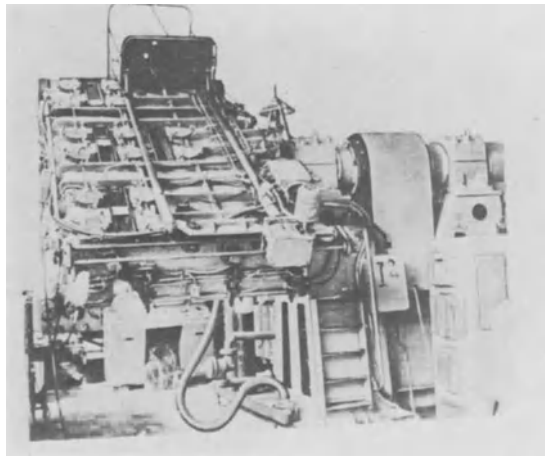

Fig. 7

analysis, for continuous precision measurement of the impurities. Figure 7 shows such a welding chamber. Large numbers of welded joints (over 1500 linear meters) are made by automatic welding with inert gas blowing from two sides. Some of these installations with keyboard clamps are shown in Figure 12. Such installations permit the production, among other things, of straight thin-walled welded T-shapes with wall thickness under 1.5mm. In this case we use pulse-arc welding with complete penetration and pilot ionic discharge.

Parts are stretched during the welding process to avoid buckling. Figure 8 illustrates the welding process for such shapes.

To straighten buckled welded assemblies of thicker elements we use roller flattening, and more extensively, thermofixation flattening in annealing furnaces. This process is widely used for straightening and forming not only welded assemblies but also sheets, extruded sections and machined parts.

In the large furnaces we perform thermal forming of complex welded structures, for example panels (see Fig.9), simultaneously with the dehydrogenation and residual stress relief.

Previously when casting parts, carbon contamination of the component surfaces was observed, even to the formation of titanium carbide. Now, because of the development of the technology and equipment for titanium casting,as discussed by comrade Anoshkin, it is sufficient to remove 0.2-0.5mm by chemical etching to produce a fine-finished surface free of oxygen, nitrogen, and carbon. Using this method, we produce over a thousand cast components, of small, medium, and large sizes, per plane (see Fig. 10 for example).

The subsequent surface hardening of cast components provides high fatigue resistance. Surface hardening is widely used for this purpose with the majority of critical titanium parts. A number of installations for vibration, pneumodynamic, shock drum, and other types of tests have been developed. The danger of salt stress corrosion, investigated by us for the principal titanium alloys employed, proved to be minimal for the operating temperatures of most titanium parts. Figure 11 shows the heating temperature and duration are expressed by the Larson-Miller parameter. In production, instructions are given to assure against the formation of corrosion centers due to the application of substances containing halogens, e.g., cooling lubricants, fluxes, etc.

Considerable research has been conducted, and even more is now being conducted, to determine the causes of formation of brittle phases and structures, and the nature of their influence on the safe life and reliability. Recently, considerable attention has been

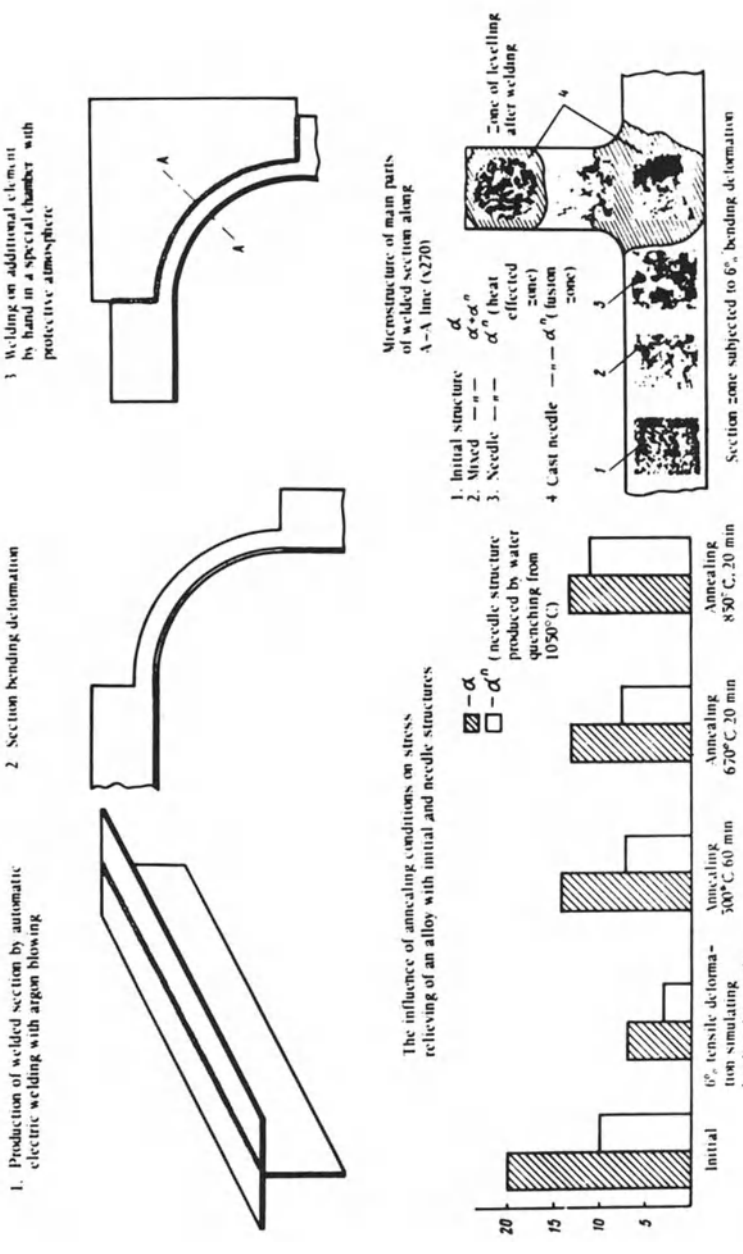
1. Production of welded section by automatic electric welding with argon blowing
2. Section bending deformation
3. Welding on additional element by hand in a special chamber with protective atmosphere
A
A
The influence of annealing conditions on stress relieving of an alloy with initial and needle structures
$-\alpha$
$-\alpha''$ (needle structure produced by water quenching from 1050°C)
Initial
6% tensile deformation simulating bending deformation
Annealing 300°C, 60 min
Annealing 670°C, 20 min
Annealing 850°C, 20 min
Elongation (%) on the basis of $11.3\sqrt{F_0}$
20
15
10
5
Microstructure of main parts of welded section along A–A line (x270)
1. Initial structure α
2. Mixed —"— $\alpha+\alpha''$
3. Needle —"— α'' (heat effected zone)
4 Cast needle —"— α'' (fusion zone)
1
2
3
4
Zone of levelling after welding
Section zone subjected to 6% bending deformation

Fig. 8 - Scheme of production of welded T-rib

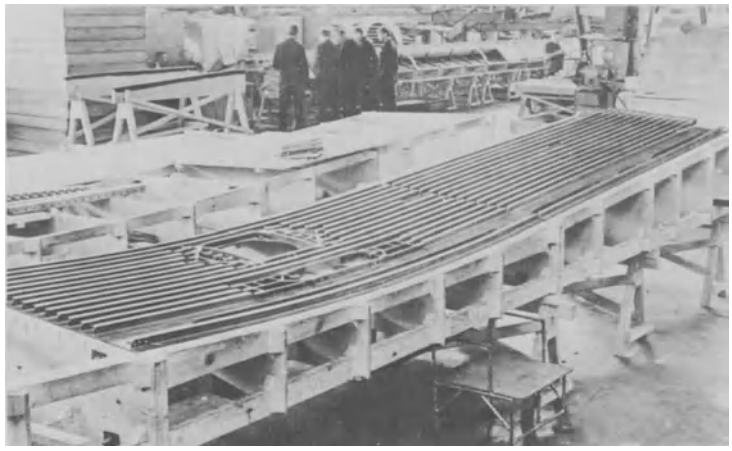

Fig. 9

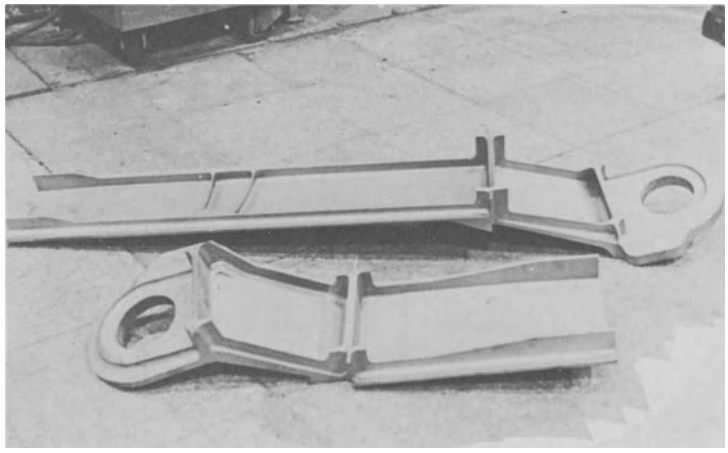

Fig. 10

given to the effect of impurities. Similar work is being conducted in the United States also, and our common conclusion seems to be the need for expanding studies in this direction. The actual measures used to prevent such structural defects, which often decrease the safe life and reliability, depend on the type of alloy, its purity, and the processing techniques. Therefore, they are not discussed in detail here. As for the alloys used in TU-144 structures, they are presented in the production instructions. The

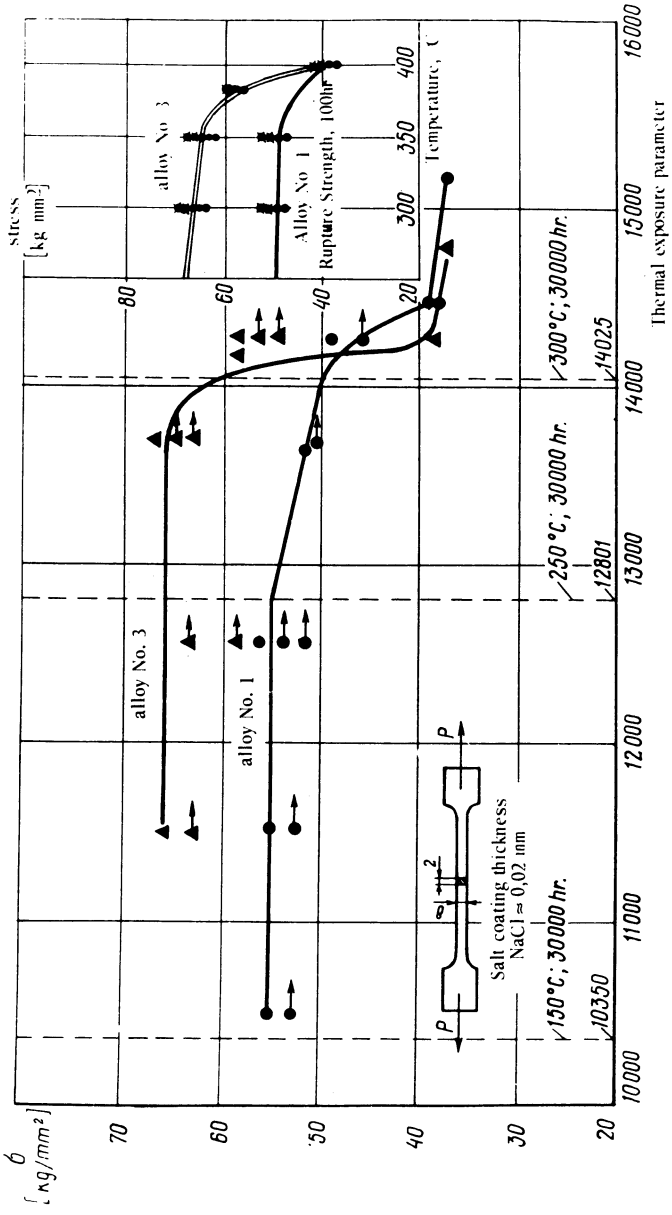
σ [kg/mm²]
70
60
50
40
30
20
10000
11000
12000
13000
14000
15000
16000
Thermal exposure parameter C – T_k(A – lgτ)
alloy No. 3
alloy No. 1
Salt coating thickness NaCl ≈ 0,02 mm
P
P
150°C; 30000 hr.
10350
250°C; 30000 hr.
12801
300°C; 30000 hr.
14025
Stress [kg/mm²]
80
60
40
20
300
350
400
Temperature, °C
alloy No. 3
Alloy No. 1
Rupture Strength, 100hr

Fig. 11

most important design and technological task is to simplify and produce less-costly production techniques for titanium structures. In this connection, a constant cost-saving effort begins with the metal itself, from the sponge and including present-day semifabricated products: precision sections, castings, and die-forgings. However, we have found that, along with the maximum application of precision and cost-saving to special semiproducts which require a minimum of machining, it is necessary to extensively use sheet-welded and section-welded structures. For this reason, we have researched the use of electron beam welding, which provides higher fatigue strength of joints, diffusion bonding, and die-stamping under superplasticity.

For sheet metal forming and section deformation we use, depending on the alloy type, not only the common cold forming methods or various forming techniques with fast heating to avoid formation of deep gas-saturated layers, but also long-term heating followed by forming or heating combined with forming, including creep conditions.

One of primary aims is an increase in productivity of titanium machining. The most serious obstacle in the application of high speed cutting is, as is well known, the short life of cutting tools combined with the non-uniformity of cutting conditions in the case of manual machine-control.

To avoid this we use quite rigid and precision machines which are program controlled.

In conclusion I would like to say that several years of extensive work by the Experimental Research Bureau, Institutes and Works were reflected in large quantities of technological instructions and new facilities. The experience developed by the Experimental Design Bureau,in the process of the production of pilot model, preserial and serial TU-144 aircraft, permitted the issuance of more precise instructions.

It is worth noting that, as a result of developing titanium structure production techniques and technology, Soviet industry not only mastered the manufacturing of numerous high-quality semiproducts of various titanium alloys, but also developed new production techniques for titanium structures of high quality, long safe-life, and high reliability.

All this permitted an increase in the total weight of titanium structures in a serial aircraft to 18% of the total structure weight.

WAYS OF INCREASING TITANIUM ALLOYS HIGH TEMPERATURE STRENGTH

S. G. Glasunov, O. P. Solonina, V. P. Kuraeva and
N. M. Uliakova
USSR Academy of Sciences

U.S.S.R.

Titanium alloys are widely used in aerospace applications because of their high specific strength compared to other structural materials; these alloys are widely used in the manufacture of engines for IL-62, Yak-40 and TU-144 airliners.

One of the decisive factors determining the high-temperature strength of titanium alloys is the polymorphic transformation temperature. Therefore, in titanium alloy development such alloying elements which raise or at least do not decrease the polymorphic transformation temperature are selected. Of all the alloying elements aluminum substantially increases the polymorphic transformation temperature of the alloy and high temperature properties. Recently, gallium, indium, antimony, and bismuth, which stabliize alpha modification of titanium, were found to be promising in this respect.

In addition to the above mentioned elements, other promising alloying additions for developing high temperature thermally stable alloys are zirconium and tin which, while producing practically no detrimental effect on the transformation temperature, improve the high temperature properties; these two are followed by molybdenum, vanadium, niobium and tantalum which are isomorphous beta-stabilizers having no eutectoid points with titanium; then copper and silicon, where etuectoid transformation is extremely fast (similar to martensitic transformation); and, finally, iron and chromium. To provide maximum high temperature strength and thermal stability of titanium alloys, the effect of impurities should also be taken into consideration.

Titanium alloys can be divided into four basic groups depending on the phases present at room temperature: alpha, alpha + beta, beta, and alpha + intermetallic phase. The ratio of the phases present in the alloy is determined by its chemical composition and heat treatment. In the Soviet Union, wide has been gained mainly by two-phase alpha + beta VT3-1, VT8, and VT9 alloys. Alloys based on alpha structure, VT20 are also widely used. The maximum operating temperature of the above mentioned alloys does not exceed 500°C. VT18 which is a pseudo-alpha alloy has an operating temperature of 550 to 600°C.

Figure 1 shows schematically a variation in the strength properties of titanium alloys as a function of test temperature. It can be inferred that for moderate temperatures the most suitable alloys are the two-phase alpha + beta alloys in the annealed or thermally strengthened condition. In the Soviet Union, alloys are mostly used in the annealed condition with the exception of thermal mechanical treatment used in blade stampings. The strength characteristics of alpha + beta alloys sharply decrease with increased in temperature, and the higher the amount of beta phase in the alloy, the lower is the temperature at which the strength decreases. At temperatures above 500°C, the most preferable alloys are the alpha alloys.

The barrier to increasing the operating temperatures of high temperature titanium alloys is their increased susceptibility to oxidation with increase in temperature and service use.

For service lives of the order of tens of thousands of hours, the effect of penetrating oxidation manifests itself, already at 400-450°C. Detrimental effects are mainly a loss in plasticity and an increase in the surface hardness. Comparative data on the thermal stability of two-phase VT3-1, VT8 and VT9 alloys as a function of heating temperature and duration are shown in Figure 2. It should be noted that after prolonged heating at operating temperatures, the strength properties at room and elevated temperatures, as well as long-term and fatigue strengths of titanium alloys slightly increase compared to aluminum alloys in which the strength properties substantially decrease after prolonged heating.

In developing titanium alloys, corrosion resistance should also be taken into account in addition to oxidation resistance.

For comparative analysis of the high-temeprature strength level of the materials one should know the long-term creep and fatigue strength values of these materials at respective temperatures.

Increasing the aircraft performance requires the improvement of commercial alloys and the development of new titanium alloys

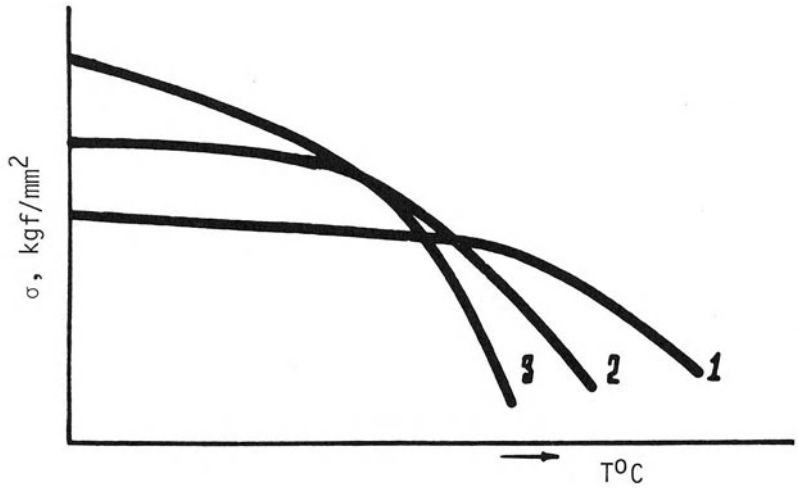

Fig. 1: Strength properties of titanium alloys versus temperature
1 - pseudo-alpha; 2 - (annealing); 3 - (thermal strengthening).

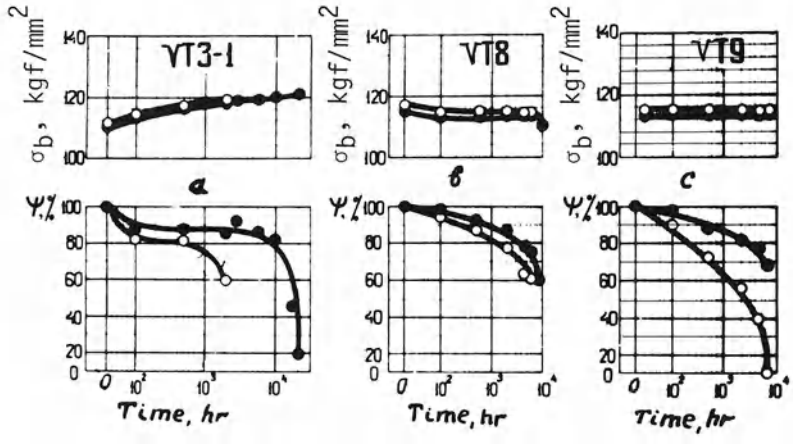

Fig. 2: The effect of exposure on thermal stability of high temperature VT3-1, VT8 and VT9 titanium alloys
(a) VT3-1: o--o 400°C (specimens) o--o 450°C (specimens)
(b) VT8: (500°C) o--o billets o--o specimens
(c) VT9: (500°C) o--o billets o--o specimens.

capable of withstanding increasingly high temperatures.

To improve the high-temperature strength of VT8 alloy at 450 to 500°C, when strengthening through heat treatment produces no effect, additional alloying with zirconium (1wt%) is used.

The addition of zirconium (1wt%) to VT8 alloy results in a substantial increase in creep strength; zirconium addition at 500°C being more effective than at 450°C. The addition of 1wt% of zirconium at 500°C results in a 70% increase of creep strength of VT8 alloy over a period of 100 hours, a 90% increase over a period of 500 hours, and a 100% increase over a period of 2,000 hours (from 13 to 26kgf/mm^2), while at 450° creep strength is increased by 7, 17 and 27%, respectively. Zirconium slightly improves the long-term and short-term strength of VT8 alloy, the short-term strength being maintained at as high as 70-60kgf/mm^2 at temperatures up to 500-600°C.

Comparison of the strength characteristics of VT8 alloy containing 1% by weight of zirconium with those of VT9 alloy containing 2.5% by weight of zirconium indicates that, in general, these characteristics are similar for both the alloys except that the creep strength of VT8 alloy (containing 1% by weight of zirconium) is slightly higher.

Studies on the effect of aluminum, zirconium, molybdenum and silicon thermal stability of VT9 alloy indicate that for reliable performance of the alloy up to 500°C, the zirconium content should not exceed 2.0wt%, while aluminum content should not exceed 7.0wt% (the concentration of molybdenum and silicon being fixed within the ranges of 2.8 to 3.8wt% and 0.2 to 0.35wt%, respectively). At a temperature of 450°C, the thermal stability of VT9 alloy is maintained over a long service life of the order of 6,000 hours, while at 500°C, over a service life of up to 500 hours. By substituting zirconium for tin in VT9 alloy, it has been possible to increase creep strength at 500°C from 28-30kgf/mm^2 to 36-40kgf/mm^2. It was shown that the service life of VT18 alloy at 600°C can be increased up to 500-1,000 hours by changing the concentration of zirconium and aluminum.

Analysis of compositions of the existing high temperature titanium alloys indicates that the presence of eutectoid-forming elements decreases their thermal stability. By comparing the chemical composition of VT3-1 and VT8 alloys, one can see that VT3-1 alloy includes two eutectoid-forming elements (chromium and iron) which are absent in VT8 alloy. Hence, the lower thermal stability of VT3-1 alloy at 450°C is due to the presence of eutectoid-forming beta-stabilizing elements.

Taking into consideration the adverse effect of etuectoid-forming beta-stabilizing elements on the thermal stability of the alloys, these elements should be excluded in developing new refractory titanium alloys designed for long service life.

However, of all the eutectoid-forming elements, tungsten plays a singular role. Owing to the low rate of diffusion of tungsten in titanium, tungsten containing alloys have substantially high thermal stability.

The results of studies on the effect of tungsten on the mechanical properties of VT3-1 alloy have shown that substitution of tungsten for chromium or additional alloying with 0.5wt% of tungsten ensures high thermal stability of the alloy, and improves high-temperature strength, particularly, the creep resistance.

As has been mentioned above, the introduction of 2.5% by weight of zirconium into VT9 alloy adversely affects its thermal stability (the plastic properties of VT9 alloy after heating at 500°C are 10 to 12 times higher than those of VT8 alloy). This is probably due to the fact that the presence of zirconium accelerates oxidation of titanium alloys.

The introduction of tungsten, tin and other metals slows down the process of redistribution of the alloying elements between alpha and beta phases, which increases the thermal stability of the alloy.

New high temperature VT25 titanium alloy developed with due regard for the above considerations, is similar to VT8 alloy in terms of thermal stability and even much superior in terms of high-temperature strength. VT25 alloy has higher thermal stability than VT9 alloy. For example, after VT9 alloy is exposed at 500°C for 6,000 hours, it loses up to 90% of its plasticity, while VT25 alloy loses by only 20-40%.

Thus, the high temperature properties of titanium alloys can be improved by alloying with appropriate elements (capable of withstanding temperatures up to 550-700°C), as well as by strengthening heat treatment (for operation at moderate temperatures).

INVESTIGATION OF SOME PROPERTIES OF VT5L ALLOY WITH RARE EARTH ADDITIONS

V. A. Kaschuk and M. B. Svetlov

Tomsk Civil-Engineering Institute

U.S.S.R.

The effects of small rare earth additions on the structure, mechanical properties at 20°, 450°, and 550°C, oxidizability, and thermal stability of VT5L alloy were investigated. The VT5L experimental alloys with additions of individual rare earth metals (REM) were smelted by consumable electrode melting in vacuum in an arc-shaped scull-melting electric furnace. High-purity elements: La, Ce, Pr, Nd, Gd, Tb, Er were introduced into the alloy separately in concentrations of 0.005, 0.01, 0.12 and 0.25wt%.

STRUCTURE OF ALLOYS

The microstructural modifications resulting from different additions were determined by the number of grains (n) per 1 cm^2 of a macrosection surface using MIM-7 metallographic microscope.

All the investigated REM effect grain refinement of VT5L alloy (Fig. 1a) with La, Ce, Pr being most effective and Nd and Tb being the least effective grain refiners.

Thus, when the REM concentrations are 0.25wt%, the reduction in grain size by La, Ce and Gd are by factors of 7, 5 and 4, respectively.

The differences in the effects of different REM on grain refinement of cast metal are mainly due to the peculiarities of the electronic structure of their atoms (the number of electrons in incomplete f- and d-shells), donor-acceptor interaction of REM atoms with those of the basic alloy - titanium - in the melt.[1] The

grain size decrease in VT5L alloy produced by the REM additions can also be caused by the interaction of the REM with impurities (O,N,C,Si) in the alloy resulting in a dispersion of refractory compounds which can act as recrystallization nuclei.

The phase diagrams of the ternary alloy system Ti-Al-REM are peritectoid type and are characterized by limited solubility in solid state in α-titanium.

The alloys containing active REM exhibit fine-grained or fine-lamellar solid solution structures in α-titanium matrix. As the concentration of an addition increases, the boundaries of grains or subgrains become wider. Pure VT5A alloy is characterzied by the oriented coarse-lamellar structure.[2]

MECHANICAL PROPERTIES AT 20°C

The tensile properties of alloys were determined in an IM-4R breakdown machine using gagarin type samples of 5mm diameter and 25mm length (type V, N7, standard 1497-73). The toughness tests were carried out in an MK-30 impact machine using menage samples 10x10mm in cross-section and 55mm long (type I, standard 9454-60).

The results showed that all the investigated REM increase the tensile and yield strengths of the alloy (Fig. 1b and 1c); the increase being maximum with the additions of La, Tb and Er and minimum with Ce and Pr. E.G., the addition of 0.25wt% La resulted in an increase in the tensile strength by 14.4% and in yield strength 17.6%. The same amount of Tb and Er increased the tensile strength of the alloy by 13.3% and 10.0%, respectively, and yield strength by 15.9 and 11.5%, respectively. All the investigated rare earth metals increase the elongation (Fig. 1d) and the relative reduction in the area of the alloy.

The additions of Tb and Er increase the plasticity of the alloy most strongly, but Pr and Nd produce the weakest effect, e.g., the addition of 0.25wt% Tb increased the elongation of the alloy by 68%, and reduction in area by 25%. The same amount of Er gave rise to 50% elongation of the alloy and 16.5% reduction in area.

The analysis of the data obtained showed that no correlation exists between the grain size and the mechanical properties of the experimental alloys.

The strength increase as a result of the REM additions is to a greater extent determined by the REM effect on the microstructure of the alloy (i.e. misorientation and decrease of subgrains).[3]

Table 1

Mechanical Properties of Alloys at 450°C and 550°C

Alloys	REM content wt.%	Test temperature, °C					
		450			550		
		Mechanical characteristics					
		$\sigma_{t,s}$ kg/mm^2	$\sigma_{y,s}$ kg/mm^2	δ %	$\sigma_{t,s}$ kg/mm^2	$\sigma_{y,s}$ kg/mm^2	δ %
pure VT5L	-	30.0	24.0	12.0	28.0	20.0	14.0
VT5L+La	0.005	32.0	26.0	13.2	29.5	21.5	14.4
	0.12	35.0	29.0	13.7	33.0	22.8	14.8
	0.25	35.6	29.5	14.0	34.0	23.5	15.0
VT5L+Ce	0.005	30.5	24.8	12.7	28.7	20.5	14.0
	0.12	33.0	27.0	13.2	31.0	21.5	14.5
	0.25	34.0	27.0	13.5	32.3	22.0	14.5
VT5L+Pr	0.005	31.0	25.3	12.5	29.2	20.8	14.0
	0.12	34.0	28.0	13.0	32.0	22.0	14.2
	0.25	34.8	28.0	13.0	33.3	22.7	14.3
VT5L+Nd	0.005	32.5	27.0	13.0	30.5	22.4	14.2
	0.12	36.5	30.0	13.3	34.5	24.6	14.6
	0.25	37.0	31.0	13.7	35.5	25.1	14.7
VT5L+Gd	0.005	33.5	28.0	14.5	31.2	23.2	15.2
	0.12	37.5	33.0	15.2	35.2	26.5	15.7
	0.25	40.0	34.0	15.5	36.7	27.0	15.9
VT5L+Tb	0.005	40.5	32.0	14.0	35.5	26.0	15.0
	0.12	46.0	38.0	14.7	40.5	30.2	15.5
	0.25	48.0	39.5	15.0	42.0	30.0	15.6
VT5L+ER	0.005	37.5	31.0	13.6	34.0	25.5	14.5
	0.12	42.0	37.0	14.0	39.5	29.5	15.0
	0.25	45.5	38.0	14.3	41.0	30.0	15.1

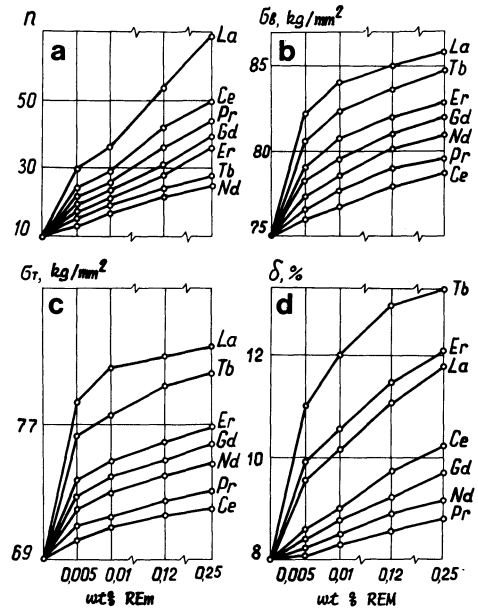

Fig. 1: The REM effect on the number of grains per I cm^2 of microsection surface (a), tensile strength (b), yield strength (c), elongation (d) of VT5L.

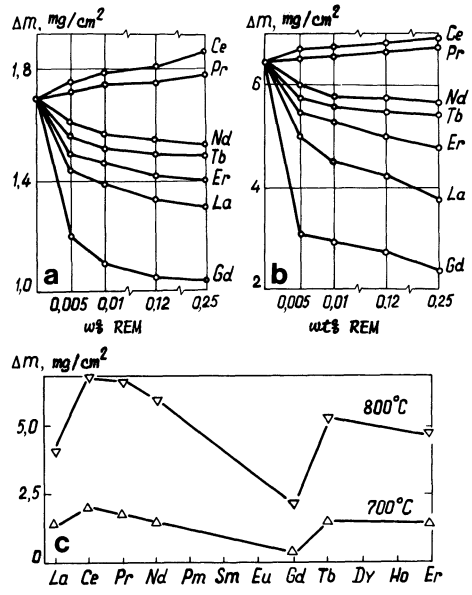

Fig. 2: The effect of the REM content on gas saturation of VT5L during 100 hours at 700°C (a) and 800°C (b); gas saturation of the alloy containing 0.25 wt.% REM depending on their disposition in the periodic system of elements (c).

The differences in the effect of the REM on the alloy strength are due, in the first place, to the characteristic electron structure of their atoms and, consequently, to differences in the capability to produce solid solution strengthening of the alloy (by altering the lattice parameters and dislocation) solute atom interaction with impurities.

The REM on interacting with O,N,C,Si available in the alloy and other impurities, oxides, nitrides, carbides, silicides, form oxides, nitrides, carbides, silicides, and other refractory compounds. These compounds being fine-dispersed are uniformly distributed throughout the grain volume and decrease the concentration of impurities by their scavenging effect. This results in an increase in the alloy plasticity. Furthermore, the REM displace "noxious" impurities from grain boundaries into grain interior. There the boundaries become free from impurities leading to an increase in strength.

All the investigated REM somewhat lower the toughness of the alloy. The toughness of REM containing alloys ranges from 4.2 kgm/cm^2 to 5.3kgm/cm^2 (the toughness of pure VT5L is 5.8kgm/cm^2).

MECHANICAL PROPERTIES AT 450°AND 550°C

The mechanical properties of the alloys under tension were determined by means of the IMASH-5S-65 with additional electronic equipment. Flat samples 1x10mm in cross-section and 20mm gauge length (standard 9651-73) were used. The samples were treated by direct passage of electric current.

All the investigated REM were found to rise the tensile and yield strengths of the alloy with Tb, Er and Gd being most effective (see Table); the addition of 0.25wt% Tb increased the tensile strength of VT5L by 60% at 450°C and by 50% at 550°C. The same amount of Er and Gd increased it by 51.1% and 33.3% at 450°C, and by 46.4% and 31.0% at 550°C, respectively.

The investigated REM increased the elongation (see Table) and relative reduction in area of the alloy at elevated temperatures.

The increase in strength of VT5L due to the REM additions at elevated temperatures and at 20°C are caused by their alloying as well as their modifying and refining effects. At elevated temperatures the increase in alloy strength is caused not only by the REM alloying of solid solution of the alloy, but by the alloying of grain boundaries as well, which is of special importance for alloy performance at elevated temperatures. Being surface-active elements, the REM are arranged along grain and crystallite boundaries in

vacancies and dislocations and "cure" these defects, thus leading to strengthening of grain boundaries.

*OXIDATION OF ALLOYS

The investigation of gas saturation of the experimental alloys was carried out in an electric muffle furnace in the atmosphere of undried laboratory air at 700° and 800°C using samples of 8mm in diameter and 10mm length.

To determine the gas absorption kinetics of the alloys a regular sample was weighed with an accuracy of 0.05mg every other hour (during 10 hours) by means of the analytical balance of the WA-33 type. The total heating interval for samples was 100 hours at the given temperatures.

The experimental points of the sample weight increments Δm during the time τ were processed by the least-squares method on the "Nairi-C" computing machine.

The (gas absorption)** of the investigated alloy was found to obey the parabolic law suggesting a diffusion controlled oxidation process.[4]

From the plots (Fig. 2) one can see that the nature of the REM effect on the alloy gas absorption remains the same during 100 hours at 700° and 800°C. The gas absorption intensity increases with increase in the temperature. All the investigated REM (with exception of Ce, Pr) increase the heat resistance of VT5L. The differences in the thermodynamical properties of different REM result in different effect of these elements on the alloy gas absorption at elevated temperatures. The additions of Gd, La, Er produce the highest increase of heat resistance in the alloy after heating for 100 hours, e.g., the addition of 0.25wt% Gd resulted in a 1.7-fold reduction of the gas saturation of 700°C, and 2.6-fold reduction at 800°C. The same amount of La and Er reduced the gas saturation 1.3-fold and 1.2-fold at 700°C, and 1.7-fold and 1.3-fold at 800°C, respectively. Additions of Ce and Pr somewhat lowered the heat resistance of VT5L.

The positive effect of the above REM additions on the heat resistance of the alloy is explained by the fact that these elements have greater affinity to oxygen and the REM oxides have higher neg-

*Editor's Note: Perhaps the use of "oxidation for "gas saturation" and the use of "oxidation resistance" for "heat resistance" is better.
**Oxidation kinetics?

ative free energy of formation than titanium oxide. Consequently, REM are the first to oxidize and to form strong compact oxide films. The protective properties of these films, according to the Pilling-Bedworth criterion, are determined by volume ratio of oxides, which are close to unity for some REM.[5] The linear coefficient of thermal expansion for the REM oxides is close to that of pure metals.

The above factors favor the formation of compact oxide films of REM with good adhesion to the principal metal, and consequently, retard diffusion of oxygen anions and titanium cations to the reaction front and, therefore, results in increased heat resistance.

Some decrease in the heat resistance of the alloy due to additions of Ce and Pr is explained by the fact that these metals can combine with oxygen not only as tri-valent but tetra-valent elements as well, and they form heterogeneous oxide films of non-uniform friable structure. This gives rise to speeding up of the diffusion processes of oxidation.

THERMAL STABILITY OF ALLOYS

Thermal stability of the experimental alloys was determined by the change of their mechanical properties and microstructure after heating for 1600 hours at 400°C.

The bars of the experimental alloys were aged at 400°C. Samples prepared from the aged bars were used to investigate the toughness and tensile properties of the alloys at 20°C. The test techniques and types of samples are described in section "Mechanical properties at 20°C."

The mechanical properties of the alloys with the REM additions (with the exception of alloys containing Ce and Pr) were not found to deteriorate after a long period of aging at 400°C. After aging the plasticity and toughness alloys containing Ce and Pr were lowered, e.g., after a long period of aging VT5L containing 0.25wt% Ce, the elongation decreased from 10.4% to 8.7%, the reduction in area - from 26.2% to 23.2%, and the toughness - from 4.6kgm/cm^2 to 3.6kgm/cm^2. Such decrease of plasticity and toughness of the alloys containing Ce and Pr can be explained by the fact that under a long exposure to high temperatures the above elements form heterogeneous friable oxide films which are unable to protect the alloys from gas saturation, particularly from hydrogen. At 400°C and higher temperatures titanium absorbs oxygen and hydrogen (up to the composition $TiH_{0.83}$) which, as a result of poor solubility in titanium at room temperature, can lead the formation of titanium hydride.[6-7]

Satisfactory thermal stability of the alloys containing the

investigated REM is explained by the fact that at elevated temperatures these metals form strong, compact, heat-stable, oxide films with good adhesion to the principal metal. These films resist gas saturation of the alloy and eliminate the brittleness phenomenon.

CONCLUSION

Small additions of the REM were found to improve the properties of VT5L at normal and elevated temperatures.

REFERENCES

1. Samsonov, G. V., Electronic structure and chemical bonding of liquid metals, from "Properties of Metallic Alloys," Metallurgy, 1967, pp. 57-64.

2. Dobatkin, V. G., Anoshkin, N. F., Andreyev, A. L. et al; Characterization of titanium alloys, Metallurgy, 1966, pp. 202-205.

3. Betekhtin, V. I., Durability and mosaic structure of metals, 1969, p. 16.

4. Bie, A. S., Liner, D. I., Slesareva, E. N. and Tsipin, M. I., Oxidation of titanium and its alloys, Metallurgy, 1970, p. 239.

5. Evans, Yu. R., Corrosion and oxidation of metals,"Mashgiz", 1962, p. 43.

6. Markovitch, K. P. and Mikheev, V. S., Heat stability of the alloy AT3 at temperatures of 250° and 400°C, "Metal Knowledge of Titnaium" in "Science", 1964, p. 243.

7. Yakimova, A. M., Examination of the mechanical properties and structure of alloys AT3, AT4, AT6 and AT8 depending on hydrogen content, "Titanium and its Alloys," USSR Academy of Sciences Publishing House, 1962, Vol. 7, pp. 166-178.

CHARACTERISTICS OF COMMERCIALLY PURE TITANIUM FOR POWER PLANT

Y. Kondo*, T. Yukitoshi*, M. Takahashi**,
H. Nagano*, H. Teranishi* and Y. Shida*

Sumitomo Metal Industries, Ltd.

* Central Research Laboratories, Amagasaki, Japan.
** Head Office, Osaka, Japan.

I. INTRODUCTION

It is reported that stainless steels and nickel alloys have suffered considerable troubles due to corrosion problems in high temperature and pressurized water environment.

The titanium is well known to have an excellent corrosion property around room temperature. However, there seems to be short of the accumulation of sufficient data for corrosion properties in the range of comparatively high temperature and pressurized water.

In this consideration, the corrosion properties of titanium were studied, at first, in the environment of high temperature and pressurized water and steam. Moreover, the method of strengthening was investigated from the viewpoint of the preferable combinations of oxygen and iron contents, reduction of cold working and the following annealing conditions.

II. Corrosion Properties

1. Material and test conditions. The chemical composition of the material used is shown in Table 1. The material was fully annealed.

Table 1
Chemical Composition of Commercially Pure Titanium (wt.%)

Alloy Mark	O	Fe	C	H	N	Ti
T0	0.094	0.028	0.007	0.0013	0.0031	Bal

After ground with 320 grade emergy paper, specimens were presented to aqueous corrosion and steam corrosion test.

Hydrogen absorption, general and crevice corrosion, and stress corrosion cracking were investigated in aqueous corrosion test. In steam corrosion test, oxidation and hydrogen uptake were studied. Test conditions are given in Table 2.

Table 2
Test Conditions

Aqueous Corrosion	Test solution	PH	4
		Temperature	300°C
		Chloride content	500ppm
		Oxygen	a) Air-saturated water was refreshed each 100hrs b) deaerated
	Duration		500hrs
Steam Corr.	Steam Condition		450°C x 1kg/cm^2-a
	Duration		max. 2400hr

2. Aqueous Corrosion. There are some data concerning corrosion behavior of commercially pure titanium in acidic solutions or seawater at high temperatures[1)~3)].

Firstly, hydrogen absorption and crevice corrosion tests were carried out by using coupled specimens, 3 thick (mm), of Ti to Ti or Ti to Fe. As shown in Tables 3 and 4, little uptake and no crevice corrosion were observed on titanium, but it is necessary to undertake longer tests for determing the high temperature behavior of titanium.

Table 3
Test Result of Hydrogen Absorption in Titanium (ppm)

Specimen*	Air-saturated		Deaerated	
	Initial	Post-test	Initial	Post-test
Ti to Ti	13	12	13	12
Ti to Fe	13	18	13	11
Ti to 4Fe	13	15	13	11

* Number means area ratio.

Table 4
Test Result of Crevice Corrosion

Specimen	Air-saturated	Deaerated	Remarks
Ti to Ti	non	non	Blue-coloured film on Ti in the crevice
Ti to Fe	non	non	Rust on Fe
Ti to 4Fe	non	non	"

Secondly, general corrosion and stress corrosion cracking tests were carried out by use of double-U bend test specimens, 75 long x 2 thick (mm), with radius of 8 (mm). Table 5 shows that titanium had only a little bit weight gain. No stress corrosion cracking occurred until 500 hours, and further tests are now under way.

Table 5
Result of General Corrosion Test

Specimen	Weight gain
T0	$3.06 \times 10^{-3} g/m^2 h$

3. Steam Corrosion. In this study, zircaloy 2 (cladding material for nuclear fuel; corrosion resistant alloy having similar properties in mechanical and structural feature) was compared to titanium. (Fig. 1)

In comparison with zircaloy 2, titanium shows superior corrosion resistance; about one magnitude less in corrosion weight gain and exhibiting no sympton of breakaway phenomena.

As for the hydrogen absorption during steam corrosion, titanium is more resistant than zircaloy 2. The latter exhibits the larger amount of hydrogen absorption in the same test condition. (Table 6) From this result, titanium is expected to absorb hydrogen up to about 200 ppm after 20∿30 year operation of this condition.

Materials with various contents of Fe, O (Table 7) were examined and the result showed little difference from TO material.

Table 6
Hydrogen Absorption of Titanium and Zircaloy-2 Due to Steam Oxidation

Alloy Mark	Corrosion weight gain (mg/dm^2)	Duration (days)	Hydrogen content (ppm)		
			Before	After	Increase
T0	24.4	101	22	48	26
T1	14.7	60	18	51	33
T6	18.1	60	19	57	38
T7	20.1	60	18	53	35
Zr2	657.0	101	12	1128	1116

III. Mechanical Properties

1. Materials. Materials examined have the systematic variations of oxygen and iron contents, and cold reduction and annealing conditions. The chemical composition of the materials is tabulated in Table 7.

In Table 8, cold worked and annealing conditions are listed.

Because the properties of titanium can be easily controlled by the oxygen and iron contents, cold worked and annealing conditions, the most preferable combination of these parameters was investigated.

Table 7
Chemical Composition (wt%)

Alloy Mark	O	Fe	C	H	N
T1	0.06	0.01	0.007	0.0042	0.0027
T2	0.06	0.31	0.009	0.0032	0.0026
T3	0.07	0.53	0.008	0.0034	0.0027
T4	0.29	0.01	0.006	0.0030	0.0027
T5	0.46	0.01	0.006	0.0031	0.0026
T6	0.24	0.26	0.008	0.0029	0.0029
T7	0.45	0.52	0.007	0.0036	0.0033

Table 8
Cold Working and Annealing Conditions

Annealing condition / Cold working	Stress Relief		Full Anneal
	450°C x 1 hr	500°C x 1 hr	700°C x 0.5 h
30%	O	O	-
50%	O	O	-
80%	O	O	O

2. Behavior of Tensile Strength.

2.1 Effect of iron and oxygen contents. The effect of iron and oxygen contents on the tensile strength is illustrated in Fig. 2. Tensile strength is affected largely by content of these elements and test temperature.

Iron can be pointed out as an effective element in improving high temperature strength, while the room temperature strength does not increase so much.

On the contrary, oxygen is not likely to be so effective in increasing high temperature strength as iron.

2.2 Effect of cold work and annealing conditions. Fig. 3 exhibits the temperature dependence of strength of the material with cold reduction and successive annealing. Tensile strength can be increased by about 10∿20kg/mm^2 in the temperature ranges examined.

Thermal stability of cold worked and stress-relieved materials was examined, considering that they are exposed to high temperature for long time. (Fig. 4)

Materials stress-relieved at higher temperature result in more stable properties of high temperature strength. And, even after the long term heating, the material with higher cold reduction shows higher strength than that with lower cold reduction.

3. Hydrogen Effect on Mechanical Properties. Since hydrogen is expected to reach an amount of about 200ppm shown in steam corrosion test, hydrogen effect was examined on mechanical properties. In consideration of the extreme and worst case, up to 1000ppm hydrogen was absorbed into specimens (Fig. 5)

It can be pointed out that the annealed materials are more susceptible to hydrogen-induced loss of ductility, but that the iron seems to reduce the susceptibility. Cold work and stress-relief has favorable effect on improving ductility loss due to hydrogen.

IV. CONCLUSION

From these results, it can be concluded as follows:

(1) Corrosion resistance of titanium can be concluded superior, though it is carried out in the comparatively short term laboratory test.

(2) The choice of preferable combination of oxygen and iron content, cold reduction and annealing temperature can lead to materials with higher and more stable strength and with comparatively lower susceptibility to hydrogen.

(3) Long term corrosion tests are now under way for the materials from various points of view.

REFERENCES

1. Grieso, J. C., Jr., Corrosion, 24, 96 (1968).

2. Bomberger, H. B. and Plock, L. F., Mater. Prot., 8, 45 (1969).

3. Feige, N. G. and Kano, R. L., Materials Protection and Performance Aug., (1970).

4. McQuillan and McQuillan, "Metallurgy of the rarer metals-4 Titanium", London Butterworths Scientific Publications (1956).

5. Conrad, H., Doner, M. and de Meester, B., Titanium Science and Technology, vol 2, p. 969, Plenum Press, New York - London (1973).

THE EFFECT OF CARBON ON THE BEHAVIOR OF THE BETA-TITANIUM ALLOYS

L. A. Petrova, E. V. Dyomina and V. S. Khlomov

A. A. Baikov Institute of Metallurgy and All-Union Institute of Scientific and Technical Information of the USSR Academy of Sciences

U.S.S.R.

The most widely known metastable beta-titanium alloys are alloys B12OVCA, BT15, TC6 and IBTI. The specific feature of the afore mentioned alloys is that the ductile high-temperature metastable beta-phase which has been obtained by quenching remains unstable and subsequent heatings will cause its decomposition with secondary phases precipitating out which will increase the strength and decrease the ductility of the alloys.

It was considered interesting to investigate how the metastable phase in higher composition alloys would behave as compared with the conventional beta-alloys upon heating. For this purpose a group of Ti-Mo-Cr-Fe-Sn-La alloys has been selected which contained more beta-isomorphous elements as compared with conventional beta-alloys. The content of beta-eutectoid forming elements (Fe and Cr) does not exceed 3% and 7%, respectively. Electron: atom ration in the structure of the alloys corresponds about of 4.4 e/a.

MATERIAL AND RESEARCH PROCEDURES

The alloys were obtained by double melting of consumable electrode in an electric arc vacuum furnace. Lanthanum was added as master alloy Ti-O, I La. After melting the ingots were turned on lathe and then were forged into 15mm diameter rod with preliminary ingot swaging of 30%.

Chemical analysis has shown the following content of interstitial impurities in beta-alloys used: *O_2 - 0.05; N_2 - 0,015-0,05; H_2 - 9m996-0.015; C - 0.02-0.05.

*Editor's Note: at%?

Mechanical properties were determined by stretching standard specimens with a gauge length of 25mm and a gauge diameter of 5mm. Impact toughness (a_n) was determined by using Menager specimens (1 - 5mm, ab - 10x10mm, notch depth - 2mm; notch radius - 1mm).

Fracture toughness (K_{IC}) was determined by using cylindrical specimens with sharp notch having a ratio d/D - 0.7 (D-specimen diameter 10mm, d - diameter of the notch, 7mm). With the established geometry of specimen and notch a value K_{IC} was calculated by the formula

$$K_{IC} = 0.414\sigma_N\sqrt{D} \quad , \qquad (1)$$

where σ_N - nominal breaking stress.

Heat treatment (quenching and subsequent aging) of specimens for metallographic and x-ray determinations was carried out in evacuated quartz capsules; as a gettering alloy iodide titanium chips were used.

In order to determine the phase composition of beta-alloys under various heat treatment conditions the radiographs* in copper K_α-radiation were taken by using both DRON-I unit complete with scintillation counter and radiography photo-type camera RKU-86. To assess eventual fluctuations of lattice parameter of beta-phase of the quenched alloy with aging time the method of back-reflection of radiographs was used which was the most convenient one for determining the relative fluctuations of the lattice parameter.

Determination of secondary phases which occurred in quenched beta-alloys as well as of distribution of alloying elements and interstitial impurities in the beta-alloys was made by microprobe x-ray spectrum analysis (Cameca MS-46 microanalyzer with 1.5μm diameter probe was employed). The fracture of specimens of the beta-alloys was studied by scanning electron microscope of kind "JSM-U3."

EXPERIMENTAL RESULTS AND DISCUSSIONS

It has been established that the beta-alloys examined retained the structure of a beta-solid solution while cooling them at various velocities from the beta-field (cooling in the furnace by switching off the furnace power, cooling in air, quenching into water by breaking the capsule). Further heating of alloys from room temperature up to 500°C for 200 hours does not cause the precipitation of a second phase from the beta-matrix and a change of hardness. This fact as well as non-varied lattice parameter of beta-phase indicate

*Editor's Note: radiographs refer to x-ray diffraction photograph.

that no phase transformations occurred in the alloys under the given heat treatment conditions and confirm the high thermal stability of beta-phase.

It should be noted that because of its nature, beta-phase in the alloys studied is metastable, i.e. results of x-ray phase analysis of sawed powder at 100% deformation, annealed at above mentioned temperatures show the presence of three phases in the alloy: beta-phase, alpha-phase and intermetallic compound $TiCr_2$. The stability of beta-phase in the alloys studied when compared with time-temperature transformation diagrams of existing industrial metastable beta-alloys indicates a considerably higher stability in the former. Figure 1 shows microstructure of one of the alloys examined after quenching and further heating for 25 hours at a temperature of 500°C in comparison with microstructure of one of the typical metastable beta-alloys - alloy IBTI (Ti-7Mo-5.5Cr-3Fe-3Al) after the same heat treatment.

Besides the microstructures, mechanical properties, impact toughness and fracture toughness of the beta-alloys after quenching and after additional heating were investigated. While examining the mechanical properties it was found that ultimate strength and relative elongation of the quenched alloys practically did not vary as a result of further heating; reduction of area became somewhat lower. Table I gives the mechanical properties of one of the highly alloyed metastable beta-alloys studied after quenching from 900°C, and also after quenching and further heating at temperatures in the range of 300-550°C for a period of 1 to 25 hours.

The impact toughness of 6-7kgm/sm^2 for quenched alloys decreased even after 1 hour treatment at the given temperatures. After 25 hours of heating the level of impact toughness did not exceed 2-3 kgm/sm^2.

According to modern point of view value of impact toughness does not give information about behavior of a metal at various stages of fracture because of its being an integral characteristic.[2] Moreover, the total fracture energy of the specimen generally consists both of the crack initiation energy and crack propagation energy under conditions where both mechanisms-ductile crack propagation (before achievement critical crack) and brittle crack propagation take place, i.e.

$$a_n = a_i + a_p$$

In connection with this, we assessed the influence of heating on the fracture toughness of the alloy by defining the parameter K_{IC}, which is characteristic of the crack propagation energy in a material. The investigation was carried out with quenched specimens (900°C, 40 min, water) and also with the specimens after quenching and heat-

Table I

Mechanical Properties of Beta-Alloy After Quemching from 900° and Heating at 300-550°C

Heat treatment	TS kg/mm^2	El. %	RA, %	a_n, kgm/sm^2	TS kg/mm^2	El. %	RA %	a_n, kgm/sm^2
Quenching from 900°C	98	19	56	6,5	-	-	-	-
Quenching +aging on		1 h.				25 h.		
550°C	97	22	42	3.0	97	19	38	2.1
500	96	18	40	3.0	96	22	42	2,7
450	96	22	55	5,1	97	19	48	3.0
400	-	-	-	5,1	96	22	44	3,0
300	96	23	58	5.0	96	26	58	-

Table II

Heat Treatment	K^Q_{IC} kgm/sm$^{3/2}$
Quenching from 900°, water	210
Quenching + heating 450° 25 h	190
Quenching + heating 500° 25 h	190

ing at the temperatures of 450 and 500°C for 25 hours.

Since the relation σ_N/σ_{a2} of the specimens studied was equal to 1, and a value of 1 corresponded to an absence of plastic flow in a notch [1], we have obtained the conventional value of K^Q_{IC}, which may be applied for the quality comparison investigations.[3] The results of determinations of the K^Q_{IC} value, given in Table II, show that the change of K^Q_{IC} value as a result of additional heating is small as compared with the value in the quenched condition, i.e. crack propagation energy varies only slightly upon further heating.

A comparison of the data of the effect of heating on K^Q_{IC} and a_n of beta-alloys allows us to make an assumption that the processes taking place during heating of the quenched specimens of beta-alloys and producing decreasing impact toughness affect mainly the crack initiation energy in the material by decreasing it.

What are, in our point of view, the reasons for the decrease in the ductility of quenched single-phase beta-alloys upon heating?

Metallographic investigation of forged and quenched specimens of beta-alloys showed the presence of precipitates in them distributed as points or chains on the surface of beta-grains (Fig. 2). A study by scanning electron microscope showed that during the time when the electron probe comes across the particle (noted by the arrow in the electron micrograph (Fig. 3),a jump in carbon concentration takes place (Fig. 4). The investigation with microprobe x-ray spectrum analyzer also showed the presence of carbon, and in some cases carbon and oxygen at the same time, in these precipitates, which in turn made it possible to assume that carbides or complex oxicarbides were formed.

It was mentioned previously that the carbon content in the alloys studied was equal to 0,02-0,05%. Presence of carbides in the beta-titanium alloys at the indicated content of carbon, and the fact that carbon is fully dissolved in the beta-phase of pure titanium, tell us that the alloying of beta-phase causes a decrease of carbon solubility in it.

The precipitation of carbide in beta-titanium alloys with carbon contents of approximately 0.02%, seems to be first noted by A. W. Bowen and C. A. Stubbington[5] who have investigated the beta-alloy Ti-14,5 Mo. Previous observations of TiC, as an impurity phase, have been made also in titanium alloys containing around 0,2%.[6]

It is known that hard and brittle inclusions in alloys,such as carbides, are most dangerous because they cause stress concentrations and promote both the process of crack initiation and crack propagation and all this decreases design strength of alloys. Thus, the

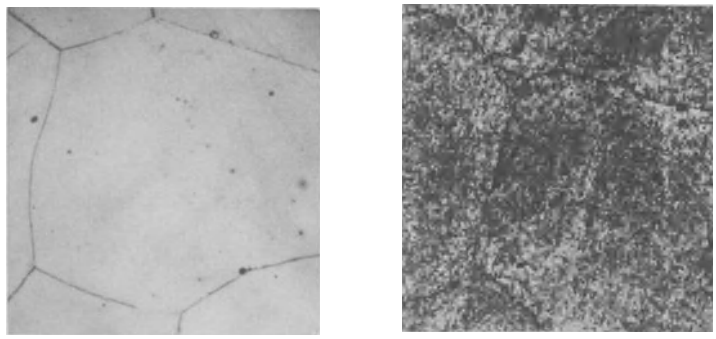

Fig. 1: Microstructure of the beta-alloys after quenching and ageing at 500°C for 25 hr: a) the examined stable beta-alloy, x 1000; b) beta-alloy IBTI (Ti-7Mo-5, 5Cr-3Fe-3Al), x 500.

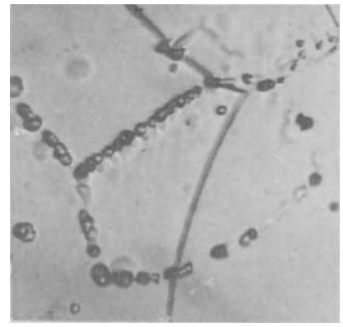

Fig. 2: The precipitates of carbides in the examined beta-alloys, x 1350.

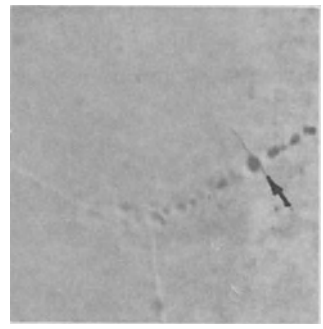

Fig. 3: Electron micrograph of the specimen surface with the carbide precipitations, x 500.

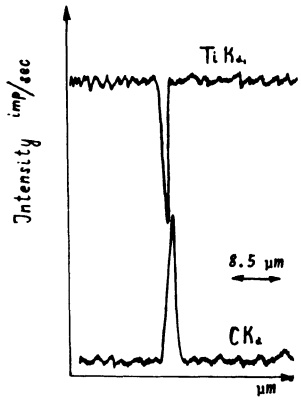

Fig. 4: Distribution of the carbon Kd intensity across the precipitated particle (Fig. 3).

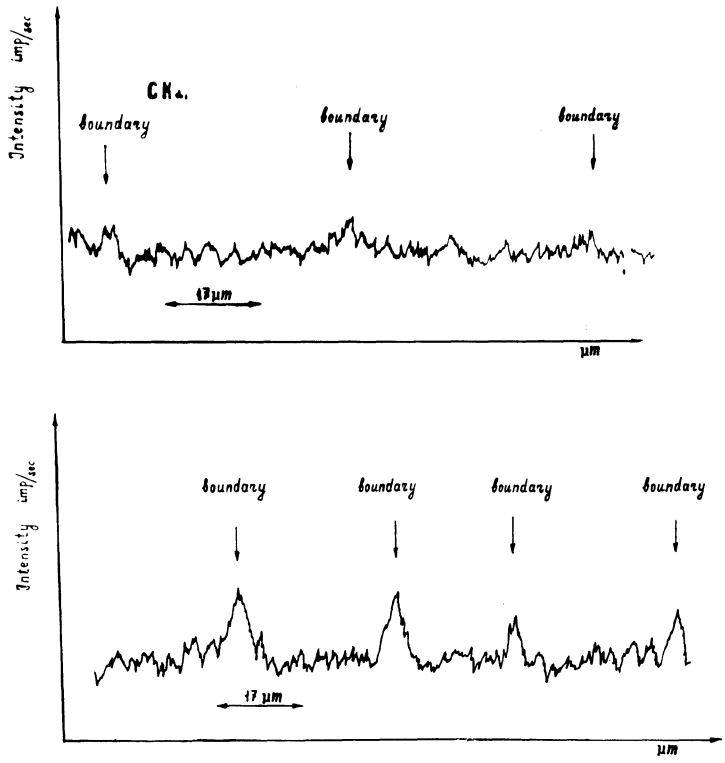

Fig. 5: Distribution of carbon (CK_α) in the interior and on the beta-grain boundaries: a) quenched alloy; b) after quenching and ageing at 500°C for 25 hr.

inclusions of carbides will cause a decrease in toughness of beta-alloys.

There is a number of investigations showing that an increase of purity of beta-alloys, carbon in the present case, effects a large increase in impact toughness of quenched alloys (up to 20kgm/sm^2). O. P. Solonina and N. M. Uljakova[4] observed a phenomenon, similar to the behavior of beta-alloys, while investigating the influence of carbon on the structure and properties of alpha-alloy, Ti-6.5Al-3Sn. Addition of carbon into this alloy in the limits of its solubility in alpha-titanium (up to 0,05%) results in maximum strengthening of alloy practically without decreasing its impact toughness. Further increases in carbon content tends to cause a drop in impact toughness, though characteristics elongation and reduction in area remain unchanged.

It is natural that carbide precipitations observed in the microstructure of quenched alloys can influence the impact toughness of beta-alloys both in the quenched condition and after additional heating of these alloys. However, they don't affect by decreasing the impact toughness upon heating of the quenched specimens.

As was previously mentioned investigations by the method of light microscopy and x-ray techniques and tests of hardness lead to the conclusions that the observed decrease of impact toughness of quenched beta-alloys as a result of further heating is not connected with phase transformations in the beta-solid solution. At the same time, metallographic investigations showed increased etchability of beta-grains boundaries even at short heatings at above mentioned temperatures. This was the reason why the method microprobe x-ray spectrum analysis was applied. Studies of the distribution of alloying elements and interstitial impurities (O,C,N) in the grain interior and across the boundaries of the quenched specimens and of those subjected to additional heating at different temperatures. The latter have an increased carbon content on the grain boundaries in comparison with the quenched state. At the samt time, the distribution of the alloying elements as well as the nitrogen and oxygen was identical for both kinds of the specimens.

Figure 5a shows the distribution of carbon in the interior and on the beta-grain boundaries in quenched alloy, Figure 5b, the same for the specimen which was additional treated at the temperature 500°C within 25 hours. Abrupt peaks of carbon concentration on the boundaries in second case show that during the process of heating at a given temperature the enrichment with carbon of the grain boundaries occurs.

In Figure 6, photographs of a section of area 50x50μm of a polished specimen, obtained by imaging in the specimen current mode and in the x-ray mode by using the characteristic radiation of carbon

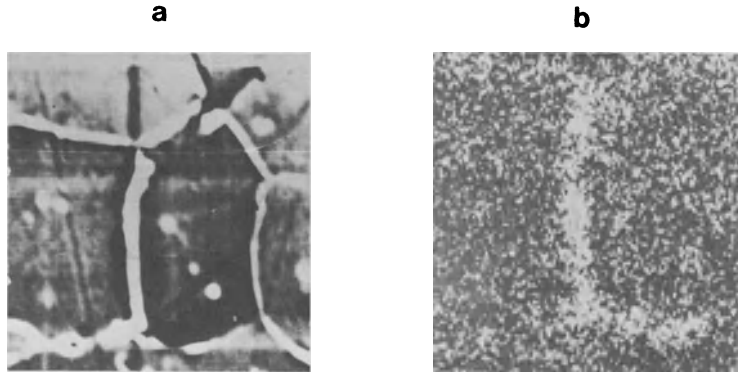

Fig. 6: Beta-alloy after quenching from 900°C and ageing at 500°C for 100 hr. Photograph of a section of area 500 x 50 µm of polished specimen.
a) in the sample current imaging mode.
b) in the x-ray imaging mode by using the characteristic radiation of carbon (CK_α).

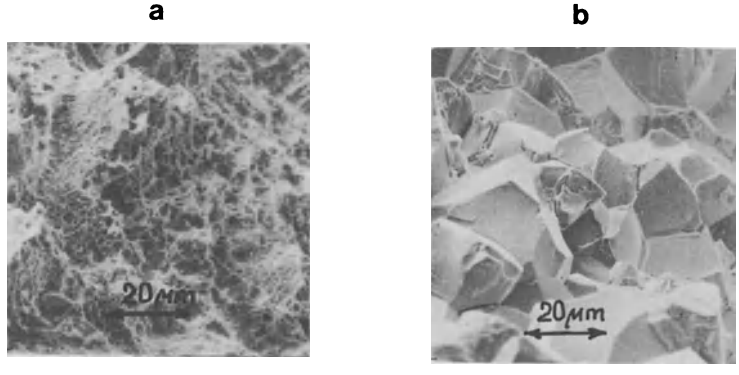

Fig. 7: Fracture surfaces of precracked notched Menage specimens:
a) quenched from 900°C;
b) quenched and aged at 500°C for 25 hr.

(CK_{α}) for the beta-alloy specimen, heated for 100 hours at 500 °C are given. In the photograph obtained by the specimen current imaging mode (Fig. 6a) configuration of the individual structural fragments and their relative positions fully match with those obtained by examination by usual metallographic microscope; light grain boundaries and dark area of beta-matrix are well seen. Elemental mapping of the specimen for carbon show that grain boundaries are enriched with carbon (Fig. 6b).

The investigation of the fracture surfaces of precracked notched Menage specimens carried out with scanning electron microscope showed dimple fracture for quenched specimens (Fig. 7a) and brittle fracture for specimens after additional heating (Fig. 7b). Thus, the redistribution of carbon and increasing its segregation on the beta-grain boundaries seem to weaken the intergrain bond and cause a decrease of impact toughness of beta-alloys upon heating, decreas being mainly in the crack initiation energy of the material.

It is evident that if we have more alloyed beta-alloys, more strictly we must estimate the carbon content value in the alloys taking into consideration the character of the interaction of carbon with titanium and alloying elements and also its distribution in alloy.

CONCLUSIONS

1. The carbides have been found in highly alloyed beta-titanium alloys at 0.02-0.05% of carbon. This means a significant decrease in the carbon solid solubility in these alloys as compared with beta-phase of pure titanium.

2. The results obtained show an increase in carbon segregation at grain boundaries of quenched beta-titanium alloys after its subsequent heating. A proposal was made that this is the reason for impact toughness decrease in quenched beta-alloys.

REFERENCES

1. Ivanova, V. S., Gurevich, S. E.,"Fatigue and brittleness of the Metal Materials." Izdatelstvo "Nauka," Moscow, 1968.

2. Georgijec, M. N.,"Toughness of the soft steel." Izdatelstvo "Metallurgija," M., 1973.

3. Gurevich, S. E. and Marijanovskaja, T. C.,"The problems of the strength," 1970, N 7, p. 22-24.

4. Solonina, O. P. et al,"MITOM," 1974, N 9.

5. Bowen, A. W. and Stubbington, C. A.,'The identification of an impurity phase in metastable β-titanium alloys." :J. Less-Common Metals," 1970, 20, N 4.

6. Ogden, H. R. and Holden, F. C.,"Metallography of titanium alloys." TML Rept. 103, Battelle Memorial Institute, Columbus, Ohio, May 1958.

AN INVESTIGATION OF SOME PALLADIUM-TITANIUM ALLOYS

L.S. Guzei*, J. Evans** and I.R. Harris**

*Department of Chemistry
Moscow University, U.S.S.R.
**Department of Physical Metallurgy
and Science of Materials
University of Birmingham, Birmingham, U.K.

Summary

The room temperature lattice spacings, micro-hardness values and magnetic susceptibilities of some Pd-Ti alloys in the composition range 0 to 30%Ti* have been determined in the present investigation. Differences in the lattice spacings of powdered and solid specimens in the early composition range have been attributed to the absorption of hydrogen by the powdered material. The lattice spacings of the solid samples indicate a progressive contraction of the palladium lattice on adding titanium, apart from the composition range from 7 to 14.5%Ti, where the spacing is invariant with composition. It is proposed that this plateau region in the spacing/composition variation is due to the compensating effects of ordering and of progressive titanium additions. Superlattice reflections indicative of a defect-type, Cu_3Au structure, have been observed at titanium contents > 16% and there is a linear variation of spacing with composition in the range 14.5 to 23%Ti. It is proposed that the behaviour of these Pd-Ti alloys is similar to that observed in the Pd-Sc system. There is tentative evidence for structural instability in the hexagonal Pd_3Ti phase at elevated temperatures. The variation of micro-hardness with

*All compositions in this paper are expressed as atomic percent.

titanium content can be correlated with the corresponding variation in the lattice spacings and both can be interpreted in terms of the appearance of short range order (S.R.O.) and eventually long range order (L.R.O.) in these alloys. The magnetic susceptibility measurements are in good agreement with a previous study and indicate an effective valency of 4.0 for the titanium atoms in solution in palladium.

Introduction

The present investigation was undertaken in order to study the alloying behaviour of titanium when in solid solution in palladium and to compare this behaviour with that of scandium[1] and zirconium[1,2], both of which form appreciable ranges of solid solution in palladium. Scandium is next to titanium in the periodic table and has one less valency electron i.e. it is trivalent, and has a nominal size factor with respect to palladium of 19%, compared with the value of 6% for titanium. Zirconium is in the same group as titanium and has an identical valency of 4.0 and a nominal size factor with respect to palladium of 16%. Appreciable solid solubility of titanium in palladium would be expected in view of the favourable nominal size factor and the ability of palladium to form appreciable ranges of solid solution with metals of widely differing atomic diameters and effective valencies. The work of Raub and Röschel[3] on the Pd-Ti phase diagram has shown that there is a significant range of solid solubility of Ti in Pd but there was uncertainty over the exact solibility limit of the disordered alloys "due to the strong similarity of properties of the disordered solid solution and the Ll_2-phase". In the present work a detailed examination has been made of the room temperature lattice spacings, microhardnesses and magnetic susceptibilities of some Pd-Ti alloys in the composition range 0 to 30%Ti. The results have been interpreted in terms of the nature of the atomic order in these alloys and the changes in the electronic state.

Materials and Experimental Methods

The alloys were prepared from high purity palladium, supplied by

Johnson Matthey and Co. Ltd., and iodide titanium, supplied by Koch Light Laboratories Ltd. The alloys were produced by arc melting in a pre-gettered argon atmosphere and the resultant buttons were homogenised for one week at 1173K. The buttons were then cut into roughly three equal sections; one section was used for lattice parameter and microhardness measurements, one was used to obtain powder for X-ray diffraction studies and one was used for magnetic susceptibility measurements.

In the first case the "as-cut" surface was abraded with emery paper to a fine finish and the specimen was then annealed at 823K for one hour to remove the surface deformation. This surface was then used for a lattice parameter measurement and then microhardness tests. The former was obtained using a specially adapted, 11.463cm. diameter Debye-Scherrer camera and CuKα radiation; this enabled the lattice spacings to be obtained with an accuracy of ±0.0005Å. The microhardnesses were obtained using a Leitz microhardness tester.

In the second case the powder was obtained by filing and was then annealed at 1173K for two hours in a vacuum of about 10^{-6} torr, achieved by a rotary pump/diffusion pump combination. The powder was quickly cooled to room temperature and was exposed to CuKα radiation in a standard, 11.483cm. Debye-Scherrer camera; an accuracy of ±0.0002Å was achieved in these measurements.

In the third case, the section was remelted in the arc furnace into a shape approximating to that of a sphere and was then rehomogenised for one week at 1173K. These samples were then used for magnetic susceptibility measurements which were performed on a Sartorious vacuum microbalance combined with a Newport electromagnet. The Faraday method was employed and, where necessary, the results were corrected for the presence of ferromagnetic impurities by the Honda-Owen method.[4] The equipment was capable of a maximum resolution of ±0.004μemu/g in magnetic susceptibility, using samples of ∿0.1g.

Experimental Results and Discussion

Lattice Spacing Studies: The room temperature (296K) lattice spacings of the f.c.c. Pd-Ti alloys obtained from both powdered and solid material, are plotted as a function of the titanium content in Figure 1. Unlike the Pd-Sc and Pd-Zr alloys,[1,2] there is a reduction in the lattice spacing on adding titanium to palladium, despite the fact that the atomic diameter of titanium (2.924Å) exceeds that of palladium (2.752Å). The major features of the lattice spacing variations are:

(i) The significant difference in the lattice spacing of the powdered and solid material in the range 0 to 8%Ti

(ii) The relatively steep fall in the lattice spacing for the solid samples in the range 0 to 4%Ti

(iii) The plateau for the solid samples in the range 7 to 14.5%Ti

(iv) The linear variation of spacing with titanium content in the range 14.5 to 23%Ti which extrapolates to the spacing of palladium (solid sample).

The significant feature of the lattice spacings of the powdered material is the expanded value observed for palladium and this expansion, together with that of the alloys in the powdered condition, can be explained in terms of hydrogen absorption. Differences have previously been observed in the lattice spacings of powdered and solid material of alloys in the pseudo-binary system, $Ce(Rh_{1-x}Pd_x)_3$;[5] this was attributed to the much greater surface to volume ratio of the powder leading to the absorption of significant amounts of hydrogen on annealing the powder in a conventional, rotary/diffusion pump vacuum system. It was proposed that the hydrogen was obtained from the "cracking" by the active alloy powder, of the hydrocarbons and/or silicone oil molecules present in the annealing environment. As a very similar vacuum annealing system was employed in the present work, it is likely that a similar process occurs in the case of Pd and the Pd-Ti alloys. The amount of hydrogen (in $^{H}/_{M}$ Values) absorbed by these materials is related to the lattice expansion on hydrogen-

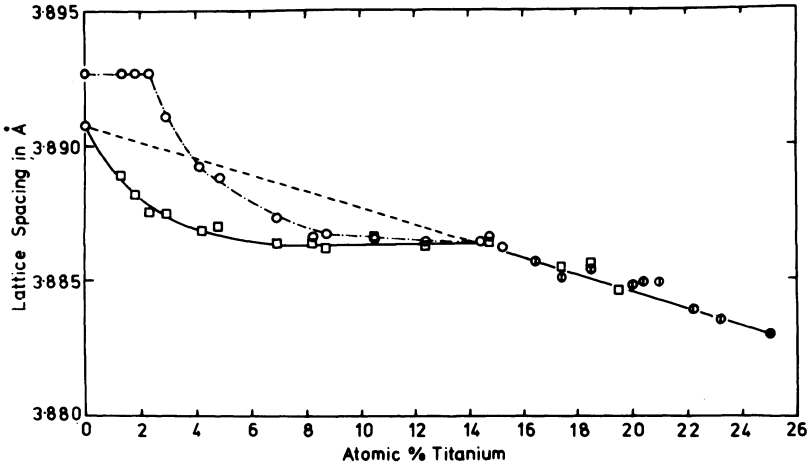

Fig. 1 - The room temperature lattice spacings of some Pd-Ti alloys. o Powdered samples o Powdered samples exhibiting superlattice reflections. □ Solid samples. ● Calculated lattice spacing of a hypothetical f.c.c. form of Pd_3Ti.

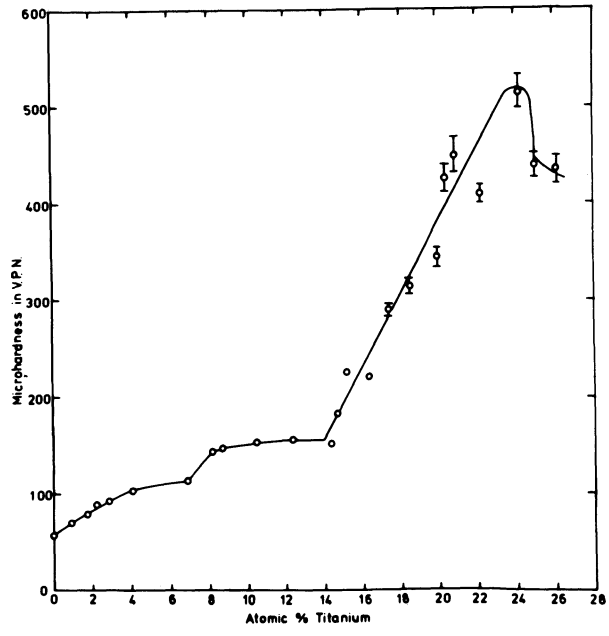

Fig. 2 - Microhardness in V.P.N. versus titanium content.

Table I

Amount of absorbed hydrogen in some Pd-Ti powder samples

Alloy Composition (%Ti)	Lattice spacing of powder (Å)	Lattice spacing of solid (Å)	Difference in spacing (Δ)	H/M value (=Δx4.074)
0	3.8927	3.8908	.0019	.008
1.3	3.8928	3.8888	.0040	.016
1.8	3.8927	3.8882	.0045	.018
2.3	3.8928	3.8875	.0053	.021
2.9	3.8912	2.8875	.0037	.015
4.1	3.8893	3.8868	.0025	.010
4.8	3.8889	3.8870	.0019	.008
6.9	3.8874	3.8863	.0011	.004
8.2	3.8867	3.8863	.0004	.002
8.7	3.8868	3.8861	.0007	.003

ation (Δ) by the expression[6,7]: $^{H}/_{M} = 4.074 \times \Delta$

In the present case, Δ is the difference between the lattice spacings of the powdered and solid material and the values of $^{H}/_{M}$ derived in this way are given in Table I. The amount of hydrogen absorbed approaches zero close to the 8%Ti composition and this could indicate, either a negligible hydrogen solubility at this and subsequent Ti compositions at the expected, very low partial pressures of hydrogen in the vacuum system, or a decrease in the ability of the powder samples to "crack" the hydrogen donating molecules. The extent of the α/β miscibility gap at room temperature in the Pd-Ti-H system has been determined by X-ray diffraction measurements[7] and according to this data the $^{H}/_{M}$ values given in Table I are well within the α-solubility range. The effect of hydrogenation on the lattice spacings of the powder samples is clearly observed in the case of the Pd-Ti alloys because of the small overall change in the lattice spacing on substituting Ti for Pd.

A pronounced feature of the lattice spacing/composition variation (Fig. 1) for the Pd-Ti alloys (solid samples) is the relatively rapid fall in the spacing between 0 and 4%Ti and the marked decrease in slope at subsequent compositions. This behaviour can be contrasted with that observed in the Pd-Sc and Pd-Zr alloys[1,2] where a linear variation of spacing with composition was observed for all the alloys within the solid solution range. Recent work on some Pd-Ce alloys[8,9] has revealed the presence of extensive short range order (S.R.O.) in the solid solution range and, in the light of this work, the lattice spacing behaviour of the Pd-R solid solution alloys (where R is a particular rare earth metal) has generally been interpreted in terms of the gradual build-up of order within the solid solution range such that there is a linear variation of lattice spacing with composition which extrapolates to the lattice spacing of the fully ordered, Cu_3Au-type, Pd_3R phase. A very good example of this behaviour is seen in the Pd-Sc system where there is an extensive range of both the "disordered" (0 to 18%Sc) and the ordered (19 - 27%Sc) alloys with a

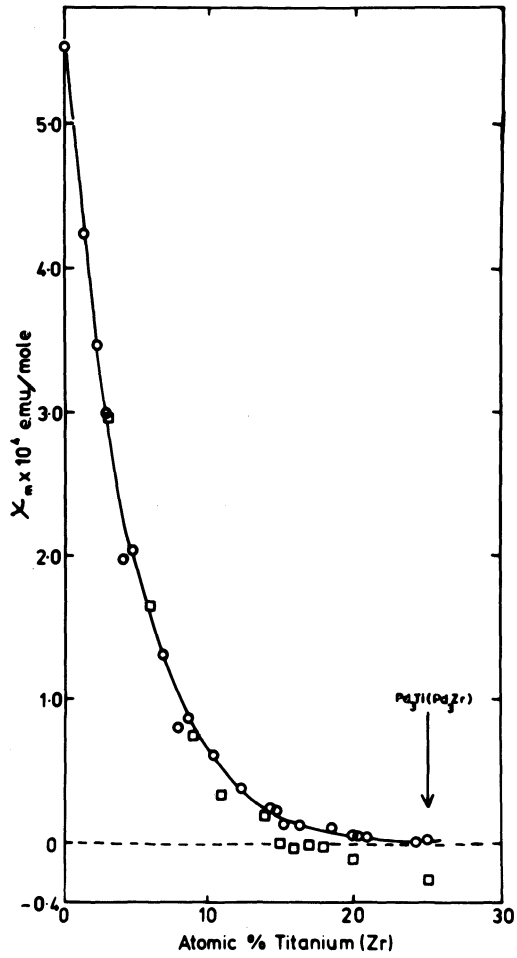

Fig. 3 - Room temperature molar magnetic susceptibilities (X_M) of some Pd-Ti alloys versus titanium content o,□ represents the values of X_M for the Pd-Zr alloys (Ref. 1).

linear variation of spacing with composition from Pd to Pd_3Sc. Normally the formation of an ordered phase would lead to a contraction of the lattice relative to the disordered state (e.g. Cu_3Au in the ordered and disordered states) but recent work[10] has shown that, in the case of Pd-R solid solution alloys, there is a net expansion as a result of S.R.O. because the dominant effect appears to be the filling of the 4d-states with a consequent decrease in the local bonding and a possible change in the screening length for the solute atoms, thus changing their effective size. The rate of filling of the 4d states with solute content will depend on the effective valency of the particular solute metal and this accounts for the dependence of the lattice spacings of Pd solid solutions on both the atomic size and effective valency of the solute metal[11].

S.R.O. is to be anticipated in those f.c.c. alloys where the solid solution range is followed by an ordered, Cu_3Au-type phase and the greater the electronegativity difference and the larger the atomic mismatch factor, the greater will be the tendency to undergo S.R.O. Both these factors are smaller in the Pd-Ti alloys when compared with Pd-Sc and Pd-Zr, and a greater range of truely disordered alloys might therefore be anticipated in the Pd-Ti system. This could explain the rapid fall in the spacing in the range 0 to 4%Ti for the solid samples, which could correspond to the truely disordered region of solid solution where the lattice spacing is not affected by the localised filling of the 4d-states due to S.R.O.

The decrease in slope and the eventual plateau in the spacing variation could be due to the growth of S.R.O. with increasing titanium content such that the effective sizes of both the palladium and titanium atoms are dependent on their particular atomic environment. This "mixed" state for the atoms could give rise to the plateau in the variation of spacing with composition. An alternative explanation for the plateau is that the alloys are in the two phase condition with both f.c.c. phases having identical lattice spacings. It will be seen however, that the microhardness and magnetic susceptibility data

support the view that the alloys are single phase in character, and it would appear that the Pd-Ti system is similar to the Pd-Sc system in that there is a transition from the "disordered" to the ordered alloys with a very narrow two-phase field between the two states.

The appearance of superlattice lines in the diffraction patterns for Ti contents > 16% indicates the presence of long-range-order (L.R.O.) in the lattice and the onset of L.R.O. probably occurs at the break in the lattice spacing composition variation at 14.5%Ti but the superlattice reflections were not visible at this composition. There is a linear variation of spacing with composition in the range 14.5 to 23%Ti and this extrapolates to the spacing of pure palladium. In this respect the behaviour is now similar to that observed in the Pd-Sc system. It is interesting to note that, by taking V_S = 4.0 for the Ti atoms, the break in the lattice spacing variation at 14.5%Ti is very close to the composition at which the 4d-band would be expected to be filled from the simple empirical correlation of the molar susceptibility (X_m) with $C_s.V_s$ (C_s is solute concentration in atomic % and V_s is the solute effective valency) observed for a number of Pd solid solutions.[5] Once the 4d-band is filled it is no longer possible for the Pd and Ti atoms to exist in a "mixed" state and the lattice spacings should then decrease regularly with increasing Ti content.

The lattice spacing of 3.8848Å for the Pd_4Ti phase is appreciably less than the value of 3.985Å reported by Raub and Röschel.[3] In agreement with previous work[12] the X-ray diffraction data obtained in the present work indicates that the structure of the Pd_3Ti phase is hexagonal, Do_{24}-type with a_H = 5.4895Å and c_H = 8.9739Å. The lattice spacing of a hypothetical f.c.c. form of Pd_3Ti with an identical atomic volume is given by the expression:

$$a_{f.c.c.} = \left[\frac{1}{8}.\sqrt{3}\ a^2{}_H c_H \right]^{1/3}$$

This expression gives a lattice spacing of 3.8830Å (full symbol in Fig. 1) and this value is identical with the extrapolated value obtained from the linear variation in the range 14.5 to 23%Ti. The

very close similarity of the atomic volumes of the hexagonal phase and the extrapolated value from the ordered f.c.c. range, indicates that the hexagonal phase is probably stabilised by electronic factors. This has been suggested previously[11] on the basis of a comparison between the DO_{24}-type phases, Pd_3Th, Pd_3Hf, Pd_3Zr and Pd_3Ti ($V_s = 4.0$) and the $L1_2$-type Pd_3R phases ($V_s = 3.0$). As in the Pd-Ti system, the lattice spacing of the hypothetical f.c.c. form of Pd_3Zr is closely similar to the extrapolated value obtained from the linear variation of spacing with composition exhibited by the solid solution alloys and the f.c.c. Pd_4Zr phase.[1]

An important aspect of the X-ray diffraction data is that very weak f.c.c. reflections are observed in the diffraction pattern of the Pd_3Ti phase and, for the 26%Ti composition, strong f.c.c. lines are observed in addition to the hexagonal reflections. The diffraction patterns of the alloys at 22 and 23%Ti did not exhibit lines due to the hexagonal phase. According to the phase diagram of Raub and Röschel[3], strong hexagonal lines should be observed in the diffraction patterns of the 22 and 23%Ti alloys and no f.c.c. lines should be present in the pattern of the 26%Ti alloy, which should consist predominantly of the Pd_3Ti phase with a small amount of second phase, Pd_2Ti. These observations imply that some modification of the phase diagram is necessary in this composition range and one possibility is that the Pd_3Ti phase transforms to the cubic structure at elevated temperatures. The variation of the c-spacings for the hexagonal phase observed in the present work, indicates a very narrow range of stability of around 1.5%.

Microhardness Measurements

The microhardnesses of the Pd-Ti alloys in the range 0 to 26%Ti are plotted against composition in Fig. 2. There is an initial rapid rise in the hardness in the range 0 to 4%Ti and this is followed by a slight plateau and then a further rise before levelling off in the range 8 to 14.5%Ti. There is an extremely steep rise in hardness with titanium content starting around the 14.5%Ti composition and reaching

a maximum value at around 23%Ti. There is a dip in the hardness at the 25%Ti (Pd_3Ti) composition.

The shape of the hardness curve in the range 0 to 8%Ti is very similar to that observed for the Pd-R solid solution alloys[9] and this behaviour was interpreted in terms of an initial, rapid increase in hardness in the more disordered alloys followed by some relief of the strain energy in the lattice by the appearance of S.R.O., which results in the hardness plateau. At later compositions the hardness again increases within the S.R. ordered alloys because of the atomic mismatch factor and possible interactions of the dislocations with the S.R.O. clusters. A similar explanation can be invoked in the case of the Pd-Ti alloys and the initial rapid rise in hardness corresponds with the rapid fall in lattice spacing observed in the solid samples (Fig. 1). There is a practically invariant hardness in the range from 8 to 14.5%Ti and this corresponds to the plateau behaviour in the lattice spacing variation. The hardness behaviour is consistent with the proposed "mixed" state of the Pd and Ti atoms in this composition range, which results in an invariant spacing and is not consistent with the plateau region in the spacings being associated with a two-phase-field. The very marked increase in slope of the hardness curve which occurs around 14.5%Ti corresponds with the onset of the defect-type, L.R.O. in the alloys and with the linear decrease in the lattice spacing. The dip in the hardness curve at the 25%Ti composition is consistent with the fully ordered nature of the Pd_3Ti phase.

Magnetic Susceptibility Measurements

The room temperature molar susceptibilities (X_M) are plotted against the titanium content in Fig. 3 together with the susceptibilities of some Pd-Zr alloys reported previously[1]. Unlike the Pd-Zr alloys, the Pd-Ti alloys do not become diamagnetic and in this respect the behaviour is more similar to the Pd-Sc alloys which do not exhibit diamagnetism in the range 0 to 25%Sc (Pd_3Sc). In contrast to the Pd-Sc alloys however, there is no discontinuity in the susceptibility/

composition curve at the composition where L.R.O. first appears (14.5%Ti). Fig. 3 shows that there is a markedly non-linear variation of X_M with composition in the range 7 to 14.5%Ti which is further evidence for these alloys being in the single phase condition. Good agreement is obtained with the results of Von Gerstenberg[13] and it is interesting to note that this worker showed that there is a paramagnetic to diamagnetic transition in Pd_3Ti close to room temperature. There is good agreement between the susceptibilities of the Pd-Ti and Pd-Zr alloys up to the 9%Ti composition and in this composition range the Pd-Ti and Pd-Zr alloys agree with the general curve of X_M vs $C_s.V_s$ for a wide range of Pd-solid solutions assuming that V_s = 4.0 for the titanium and zirconium atoms. At 15%Zr however, the Pd-Zr alloys become diamagnetic whereas the Pd-Ti alloys are paramagnetic up to, and including, the Pd_3Ti phase.

Acknowledgements

Thanks are due to the Science Research Council of the United Kingdom for support of the general research programme of which this work forms a part. Thanks are also due to the British Council for their financial support (L.S.G.).

References

1. Norman M. and Harris I.R., J. Less-Common Metals, 18, 333 (1969).
2. Catterall J.A. and Barker S.M., Plansee Proc., 577 (1964).
3. Raub E. and Röschel E., Z. Metallk., 59, 112 (1968).
4. Honda K., Ann. Phys. Leipzig, 32, 1048 (1910)
   Owen M., Ann. Phys. Leipzig, 37, 657 (1912)
5. Tay Y. and Harris I.R., to be published.
6. Baranowski B., Majchrzak S. and Flanagan T.B., J. Phys.(F), 1, 258 (1971).
7. Wise M.L.H., Farr J.P.G. and Harris I.R., J. Less-Common Metals, 41, 115 (1975).
8. Hirst J.R., Brooks J.W., Loretto M.H. and Harris I.R., to be published.

9. Hirst J.R., Wise M.L.H., Fort D., Farr J.P.G. and Harris I.R., Hydrogen in Metals Meeting, Birmingham (1976) to be published in the J. Less-Common Metals.

10. Evans J. and Harris I.R., to be published.

11. Harris I.R. and Norman M., J. Less-Common Metals, 22, 127 (1970)

12. Nishimura H. and Hiramatsu T., J. Japan Inst. Metals, 22, 88 (1958).

13. Von Gerstenberg D., Annalen der Physik. 2,236 (1958).

A TITANIUM ALLOY FOR APPLICATION IN HOT SODIUM CHLORIDE SOLUTIONS

E. I. Oginskaya and V. A. Levin

All-Union Institute of Light Alloys

U.S.S.R.

Commercially pure titanium and its structural alloys do not always satisfy the requirements of chemical machine-building. Chemical industry often needs materials of a higher corrosion resistance to be supplied. The Ti-Ni-Zr alloys are stable in hot salt solutions in which commercially pure titanium is subject to crevice corrosion.

This paper summarizes the results of a study of technological, mechanical and electrochemical properties of the Ti-Ni-Zr alloy of an optimal composition (2.5%Ni, 2.0%Zr). This alloy was shown to be a good material for producing ingots and various semifinished products.

Hot working of the alloy presents no difficulties and can take the advantage of the technology in use for low-alloy titanium systems. The resulting semifinished products have rather bad mechanical properties in their hot-worked condition (Table I). The plasticity and the impact strength may be improved considerably (Table I) by heat treatment that results in equilibrating the alloy (alpha-phase alloyed with zironcium, and a Ti_2Ni intermetallide) and in achieving the Widmanstätten structure. This contains either coagulated intermetallic phase particles (Fig. 1a) or thin alpha-phase plates with disperse precipitates of the intermetallic phase at the plate boundaries (Fig. 1b). The heat treatment makes mechanical and technological properties of the hot-worked products sufficiently good for finishing and employing them in industry.

Cold working makes the alloy very sensitive to work hardening (Fig. 2) and thus causes a need for intermediate annealing of the semifinished products. The maximum allowable cold deformation is 20%. Heavier deformations result in cracking.

Table I

Mechanical Properties of Ti-2,5Ni-2Zr Alloys Samples

Temper	Mechanical properties			
	σ_B, kg/mm^2	σ_s, kg/mm^2	δ, %	a_H, kgm/cm^2
Hot-worked	57,2	47,5	12,8	1,9
Hot-worked, annealed	48,2	36,7	18,8	4,5
Hot-worked, quenched and aged	53,6	45,2	16,4	4,0
Cold-worked, annealed	52,3	41,4	21,3	-

Table II

Corrosion Rate Obtained for Ti-2,5Ni-2,0Zr Alloy and the Commercially Pure Titanium at 70 g/l HCl at Various Temperatures (test duration is 24 hours)

Material	Corrosion rate, mm/year, at temperatures, °C			
	40	60	70	80
Ti-2,5Ni-2Zr alloy, stable structure	0,02	0,02	0,13	62,2
Ti-2,5Ni-2Zr alloy, metastable structure	0,02	1,12	36,9	57,7
Commercially pure titanium	0,93	1,93	8,7	12,4

The cold-worked Ti-2.5 NI-2.0 Zr alloy has a considerable (up to 10%) anisotropy of its mechanical properties. This is due to its strongly pronounced fibrous structure, which consists of the primary alpha-phase plates, the eutectoid reaction products, and the deformation texture formed. The parallel arrangement of the intermetallic precipitates and the anisotropy of mechanical properties are also inherited by the alloy which is thermally treated in the two-phase (α+Ti_2Ni) field (Fig. 1a). The lowest level of mechanical properties which results from annealing the material at the temperatures of the two-phase (α+Ti_2Ni) field is, however, sufficiently high (Table I). Heat treatment at temperatures higher than the eutectoid temperature eliminates the anisotropy, but the absolute plasticity characteristics are thereby impaired markedly since the structure is affected by the phase transformations involved.

Corrosion tests were made both for the Ti-2.5 Ni-2.0 Zr alloys with a stable α+Ti_2Ni structure corresponding to the optimal combination of mechanical properties and for the samples with a metastable (α'-β res.)-structure, which helped to eliminate the role of the intermetallic phase in improving corrosion resistance of the alloy.

The most probable source of titanium crevice corrosion is local acidification of the medium, caused by hydrolytic decomposition of corrosion products. Consequently, reduced tendency towards crevice corrosion may be expected for alloys that are more stable against corrosion in acid solutions than is titanium.[1,2] That is why hydrochloric acid media were used for estimating the corrosion and electrochemical behavior of the Ti-2.5 Ni-2.0 Zr alloy.

The alloy stability in hydrochloric acid was tested with the stable-structure samples subjected to the aggressive environment of variable concentration and temperatures. The criterion was the maximum temperature at which the corrosion rate was below 0,1mm/year at a given concentration of the solution. Compared with the data[3] for commercially pure titanium, the Ti-2.5Ni-2.0Zr alloy is stable at a significantly wider range of temperature and HCl concentrations than is the unalloyed titanium. Consequently, the alloy is capable of passivation under the conditions which result in noticeable corrosion rates in the case of unalloyed titanium.

The results obtained may be explained by analyzing voltage-time polarization curves obtained at 0.4 V/hr for the Ti-2.5Ni-2.0Zr alloy and for the commercially pure titanium at 70 g/l HCl (25°C). As compared with the unalloyed titanium, Figure 3a, the anode curves recorded for the alloy have no active dissolving loops while the alloy corrosion in the passivated state is somewhat faster. The cathodic curves (Fig. 4b) indicated a markedly more intense cathode process on the Ti-2.5Ni-2Zr alloy. Consequently, it is quite prob-

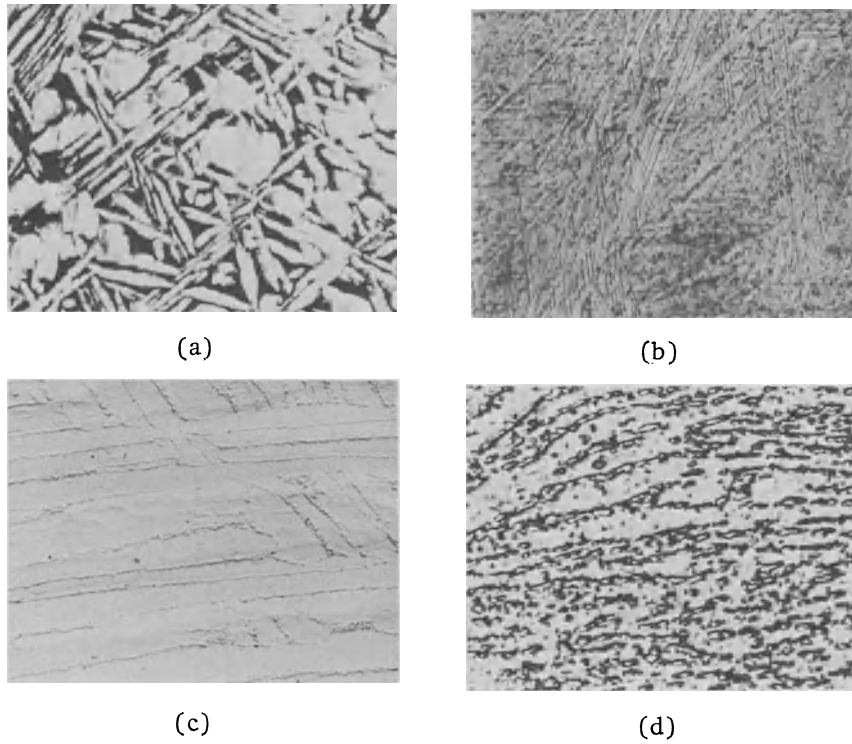

Figure 1

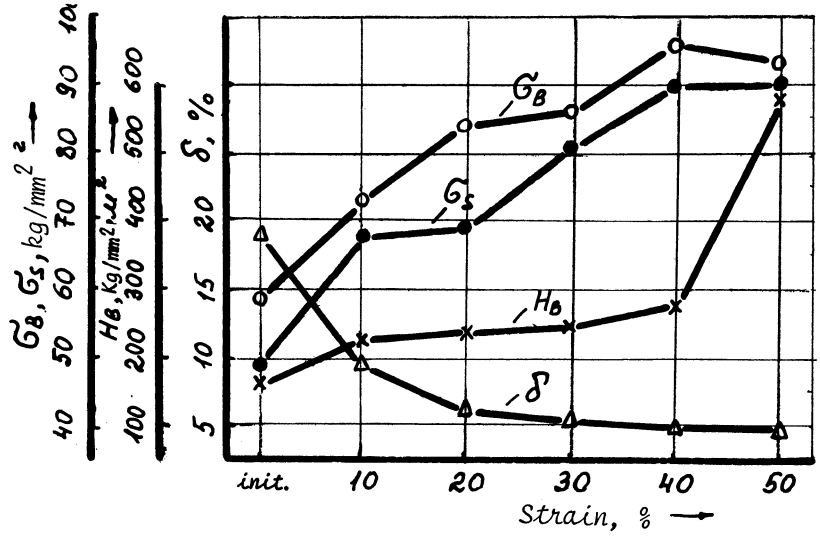

Figure 2

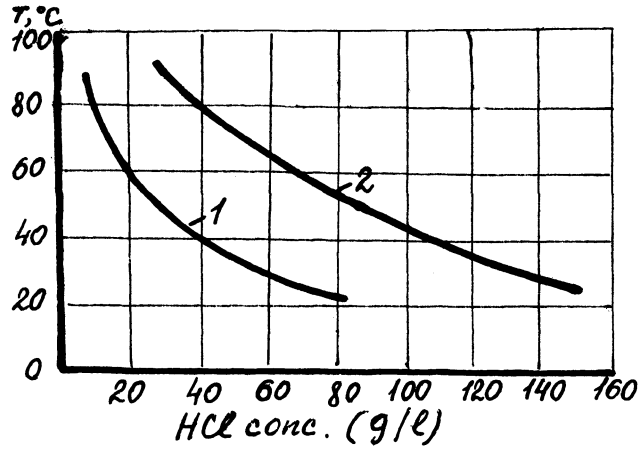

Figure 3

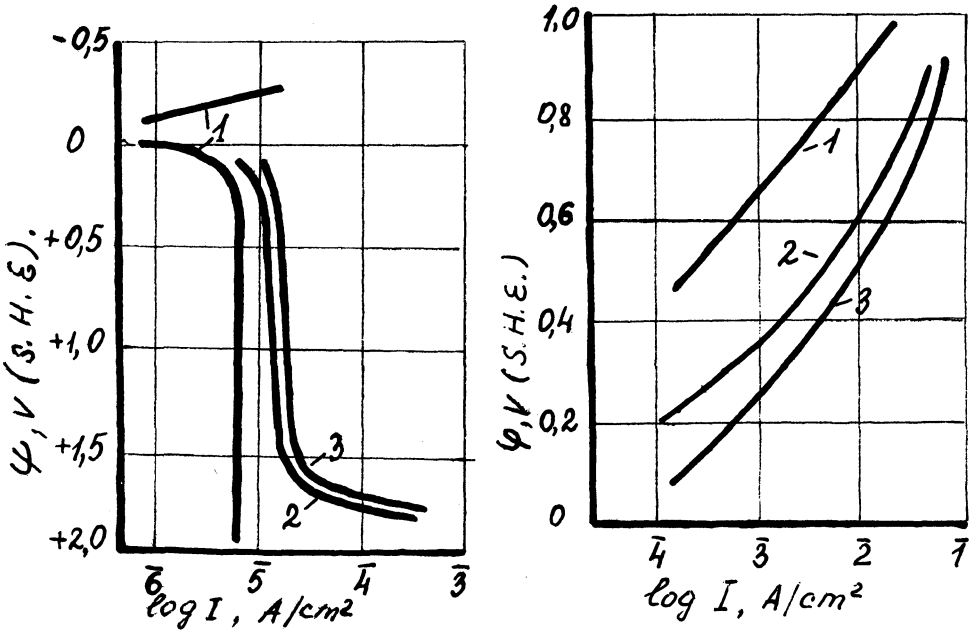

(a) (b)

Figure 4

able that the ability of the Ni and Zr alloyed titanium to acquire its passivated state is mainly due to the more effective cathode process on the alloy, whereas the unalloyed titanium is in its active or unstable passivation states.

It is noteworthy that the more intense cathode process is typical of not only the stable-structure alloy but also the metastable one that contains no intermetallic Ti_2Ni inclusions, which presumably plays the main part in the increase in corrosion resistance of Ti-Ni alloys. The data of Table II demonstrate that the Ti-2.5Ni-2Zr in both structural states is better than is the commercially pure titanium.

Corrosion rate of the alloy in the activated state is much higher than that of the unalloyed titanium, a characteristic of cathodic-alloy metals. The stable-structure (α+Ti_2Ni) alloy was shown to have higher corrosion resistance than has the metastable alloy. The intermetallic phase in the alloy structure may be thought of as an additional promoter of the cathode process. The effect may be explained by assuming that hydrogen overvoltage on intermetallide particles is lower than that on the other components of the system.

The data obtained for the alloy under study demonstrate that the alloy is more resistant to crevice corrosion than is the unalloyed metal. Indeed, the alloy tested at 270 g/l NaCl at 100-200°C for 200 hours did not display any crevice corrosion whereas the commercially pure titanium tested under similar conditions did undergo crevice corrosion above 120°C.

The present results suggest that electrochemical, mechanical, and technological properties of the Ti-2.5Ni-2Zr alloy allow one to recommend the alloy for use in making apparatus designed to work in contact with hot sodium chloride solutions.

REFERENCES

1. Ciriess, J. C.,"Corrosion," 1968, V. 24, No 4, p. 96.

2. Tomashow, N. D. and Chernova, G. P., Korroziya i Korrozionno-Stoikie Splavy (Resistant Corrosion-Alloys), The Metallurgija Publishers, Moscow, 1971.

3. Fisher, W. R., "Werkstoffe und Korrosion," 1959, Bd. 10, Nr.4, S. 243-249.

4. Sedriks, A. Y., Green, J. A. and Novak, D. L., "Corrosion," 1972, V. 28, No. 4, p. 137.

ON THE PERFORMANCE OF WHOLE-TITANIUM MADE TURBINE CONDENSER

Y. Kubo, H. Kusamichi, and H. Itoh

Kobe Steel, Ltd.

Kobe, Japan

INTRODUCTION

For the trouble-free and economical operation of the turbine condenser at the power station, such a cooling tube is needed as is perfectly free from the leakage. From the enviromental preservation point of view, it is desired of the cooling tube that the tube needs no chemical agent like ferrous sulfate, which is used to form the protective film inside the tube, and that the tube has a characteristic resistance to the high flow velocity sea-water in order to conform to the regulations of the elevated discharge water. Titanium tube can be said the best material to satisfy these requirements.

Kobe Steel, Ltd. installed No. 4 turbine condenser of Amagasaki Works in 1970 by all-titanium tubes, and the various performance tests were carried out (1). Further, No. 5 turbine of Kakogawa Works of Kobe Steel, Ltd. was installed with the whole-titanium made turbine condenser. The plant was put into operation in July 1974.

This paper will cover the outline of the design and fabrication of the titanium condenser in Kakogawa Works as well as its performance as the condenser indicated at the industrial operation.

Design

1. Specifications and Figures. Table I and Fig. 1 show the specifications and figures of this condenser respectively. Table II indicates the composition analysis of sea-water which is used as the cooling water.

TABLE I. Main Specification of Titanium Condenser of No. 5 Turbine in Kakogawa, Kobe Steel, Ltd.

Type of turbine	Mitsubishi Single Cylinder Axial Impulse-Reaction Condensing Turbine
Turbine rating	50,000 kW
Steam condition	100 kg/cm^{2}G, 540°C
Type of condenser	Mitsubishi Rectangular Radial Flow with Two Pass - Two Divided Type
Cooling surface	4,300 m^2
Vacuum of condenser	722 mmHg
Design temp. of cooling water	24°C, sea-water of Harima-nada
Quantity of cooling water	13,760 m^3/hr
Tube cleanliness factor	90 %
Cooling water velocity in tube	3 m/sec.
Overall heat transfer coef.	3,520 Kcal/m^{2}hr °C
Cooling tube	25.4 od x 0.5 t x 10,000 L (effective) mm, welded titanium tube (grade 2), 5,450 pcs.
Tube plate	(1) titanium (grade 3), 28 mmt x 2 m x 3 m, 2 pcs. (2) naval brass, 30 mmt x 2 m x 3 m, 2 pcs.

TABLE II. Composition Analysis of Cooling Sea-Water

	Temp °C	pH	DO ppm	COD ppm	Tb ppm	SS ppm	NH_4^+ ppm	NO_2^- ppm	solFe ppm	Zn ppm	Cl^- ppm
Max.	29	8.5	10.9	4.2	7.5	16.4	0.82	0.85	0.16	0.08	-
Min.	6	7.7	5.8	0.5	1.0	1.2	0.24	tr	0.01	0.01	18000
Mean	17.8	8.16	8.07	2.10	3.01	8.42	0.51	0.16	0.03	0.03	∿ 17000

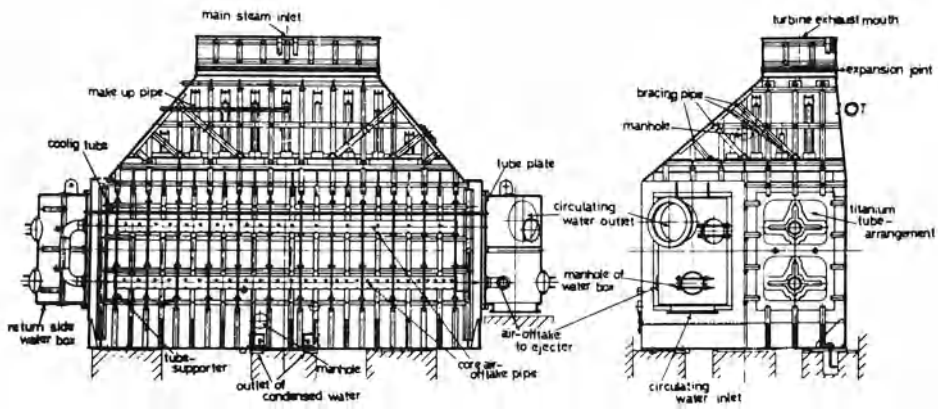

Fig. 1: Figures (front and side view) of the titanium condenser of No. 5 Turbine in Kakogawa, Kobe Steel, Ltd.

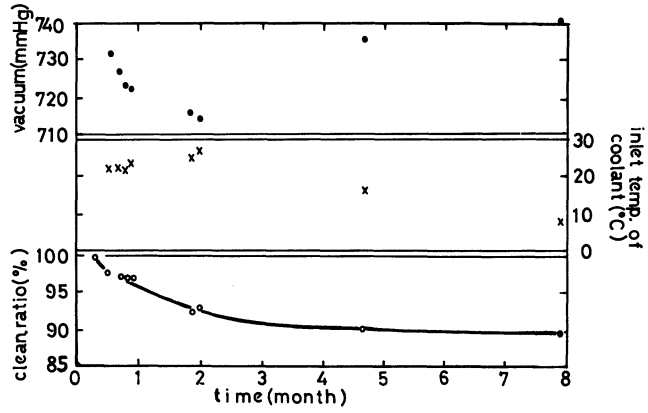

Fig. 2: Main performance curves of titanium condenser.

2. Features and Considerations.

(1) This condenser belongs to the power generation plant facility of the iron and steel work, and condensates the exhaust steam of the steam turbine and keeps the back-pressure of the turbine in vacuum. It enhances the efficiency of the turbine and at the same time recovers the condensation water, which is utilized then in the turbine cycle again.

(2) The detail engineering and fabrication works using the tin wall welded titanium tubes and titanium solid boards manufactured in Kobe Steel were carried out Mitsubishi Heavy Industries, Ltd. The calculation of the heat transfer area is performed on basis of H.E.I. Standards (2).

The cleanliness factor of the titanium tube is assumed to be 90% in the designing work of this condenser, while that of the ordinary aluminum brass tube is 80 - 85%.

(3) In the future, the use of a large amount of sea-water will become necessary in order to reduce the influence on the environment by lowering the discharge temperature of the cooling water from the condenser. To cope with such a possibility, the velocity inside the tube is designed to be increased.

In the case of the aluminum brass tube, the velocity in the tube is in the vicinity of 2.0m/sec. In this design specification, it is set at 3.0m/sec. making the use of the features of titanium tube, thus to reduce the heat transfer area and also to lower the fabrication cost. In comparison with the conventional condenser by aluminum brass tube, it is reduced by 20% in the heat transfer area.

(4) Since the tine wall welded titanium tube with 0.5mm wall thickness is used to all the cooling tubes, the sufficient study was made on the structural strength as follows:

(a) Buckling strength of tube: The distance between the tube support plates is set at 700mm. The buckling load in this case becomes to about 500 kg. However, it is not conceivable that such an excessive axial compression load is applied to one tube even when the cut-off force of the cooling water pump is considered on the water-box of the condenser.

(b) Vibration of cooling tube and tube support spacing: The spacing of the tube support plates has to be so selected that the natural frequency of the tube may not make the resonance with the revolution number of the generator and other revolution machines. Design consideration is given to the prevention of the fatigue. fretting-corrosion, etc. which are to be caused by the tube vibration. In this condenser, the tube support spacing is 700mm and the natural frequency of the titanium tube is 68c/sec. The practical experiences show no trouble with this spacing arrangement.

A kind of tube vibration strength based on many years' experience and operation records of the condenser has also confirmed the strength of about 1.4 times in comparison with the conventional tube and the safety design is achieved.

(5) The expanding is mainly adopted for the fitting of the tube plate. At the titanium plate side, a group of tubes was welded for the purpose of the test.

(6) One tube plate of the divided type condenser was made of solid titanium, while another tube plate was made of the conventional naval brass. In the former system, no cathodic protection is needed and titanium tube is free from the embrittlement problem by the hydrogen absorption, so that the performance of the literally whole-titanium made condenser can be examined.

Fabrication

1. Tube Hole Drilling at Titanium Tube Plate. The tube hole arrangement is in principle of regular triangle and the pitch is 31.75mm. The tube hole diameter is 25.4 + 0.05 - +0.1mm. The tube hole drilling conditions of 28mm thick titanium plate consist of the revolution number of 120 rpm and the feel of 0.4mm/rev.

2. Mounting of Expander Joints on the Titanium Tube - Tube Plate. The holding force and apparent wall thickness reduction rate of the expanding case are obtained by the following formula:

Holding force (kg/mm^2) = $P/\pi dL$

Wall thickness reduction rate (%) = $\frac{(d_E - 2t) - d}{2t} \times 100$

Where P : Force necessary for pushing out (kg)
L : Effective expansion length (mm). It is set at 25mm.
d : Tube inside diameter before the tube expansion (mm).
d_E: Tube hold diameter after the tube expansion (mm).
t : Tube wall thickness (mm).

3. Mounting of Titanium Tube to Tube Plate by Seal Welding. The welding was carried out by Non-Filler Pulse TIG method. The welding section was checked by the visual inspection, fluorescence detection and hydraulic test. No abnormality was found thereby.

Performance Test

1. Test Procedures. The test by the actual facility on this condenser was carried out in parallel with the test operation of the power generation turbine. The performance change by the elapse of time was investigated thereby. The vacuum degree of the condenser is changed by the load, sea-water temperature and velocity inside the tube, and it is so planned that the performance of the condenser can be easily evaluated by the measured values of various factors which constitute the theoretical formula on 1) quantity of heat rejection, 2) logarithmic mean temperature difference and 3) overall heat transfer rate, and finally by arranging them to the relations of the tube cleanliness factor.

Namely, the tube cleanliness factor Cf (%) is calculated by the following formula:

$$Cf = \frac{H}{\theta m.U.S} \times 100$$

Where H : Rejected heat (K Cal/h)
θm: Logarithmic mean temperature difference (°C)
U : Overall heat transfer rate (K Cal/m^2h°C)
S : Effective cooling surface (4,350m^2)

The main measurement factors include the following, such as 1) the turbine load, 2) the flow rate, pressure and temperature of the main steam, 3) the vacuum degree of condenser, 4) the flow amount, pressure and temperature of the cooling water and 5) the quantity of the condensate.

TABLE III. List of the Test Results of Condenser Performance

Date	July, 1974				Aug., 1974		Nov., 1974	Feb., 1975
Number of test	1	2	3	4	5	6	7	8
Turbine load, MW	25	37.5	50	50	50	50	50	50
Condenser vacuum, mmHg	731.9	726.5	721.7	720.7	715.7	714.3	733.9	742.6
Saturat, temp.equivalent to vacuum, °C	28.1	30.9	33.3	33.7	35.8	36.5	26.5	19.8
Enthalpy,turbine exhaust steam, Kcal/kg	544.0	542.8	547.6	547.8	548.7	548.9	544.0	545.2
Quantity of condensation flow, ton/hr	74.3	113.4	150.5	150.3	148.1	148.0	150.6	152.1
Quantity of radiating, X 10^6 Kcal/hr	38.3	58.1	77.5	77.3	75.9	75.8	77.9	78.3
Inlet temp.of cooling water, °C	23.4	24.1	24.0	24.5	26.5	27.1	16.7	8.1
Outlet temp. of cooling water, °C	26.7	28.8	30.4	30.9	32.9	33.6	22.8	14.6
Quantity of cooling water, m^3/hr	11980	12960	12540	12540	12265	12078	13270	12650
Cooling water velocity in tube, m/sec.	2.61	2.83	2.73	2.73	2.67	2.64	2.89	2.75
Overall heat trans. coef., $Kcal/m^2h$ °C	3250	3413	3354	3364	3372	3358	3141	2510
Log. mean temp. difference, °C	2.77	4.02	5.44	5.42	5.59	5.48	6.34	8.08
Tube cleanliness ratio, %	97.8	97.3	97.4	97.4	92.5	94.6	90.0	89.5
Head loss of cooling water, mAq	6.5	6.9	6.8	6.8	6.3	6.2	8.5	6.83

2. Test Result and Consideration.

(1) The test with the actual equipment was started from July 1974. The result of 8 month long test is summarized in Table III and Fig. 2.

(2) In the conventional condenser, where aluminum brass tube is used, the cleanliness factor is decreased below 85% after 1 - 2 month operation in a normal case, depending on the sea-water quality. Therefore, it is necessary to make the cleaning of the tube every 1 - 2 weeks particularly at the summer season. On the contrary, the performance test of this condenser showed, as indicated in Fig. 2, the cleanliness factor of well over 90% of the design value at the initial time of operation. As the time passed, it displayed a transitory reduction of the cleanliness value. However, the design point could be satisfied even after 8 months. This performance of the outstanding nature was confirmed through the test. No tube cleaning at all was conducted during this period.

(3) The quantity of the deposited scale or slime at the tube inside is substantially lower than the case of conventional aluminum brass and such a foreign deposit can be easily removed. It is considered that this favorable tendency becomes more remarkable as the velocity inside the tube increases.

(4) As to the expanding section of the tube or seal weld mounting section, no problem was found in regard to the air-tightness or durability. It was confirmed that such methods are well practically applicable.

3. Tube Withdrawal Investigation.

(1) Measurement of Overall Heat Transfer Rate; In about 6 months after the operation start, 2 titanium tubes were drawn from the actual equipment.

The measurement was made on the overall heat transfer rate. The measurement conditions were prepared experimentally. The saturated steam of 100°C was used outside the tube. The industrial water at the room temperature was given inside the tube. The flow velocity inside the tube was 3.0m/sec.

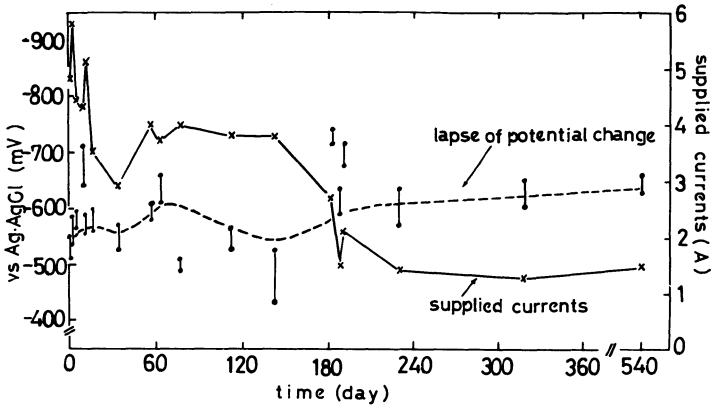

Fig. 3: Potential distribution of the naval brass tube plate face.

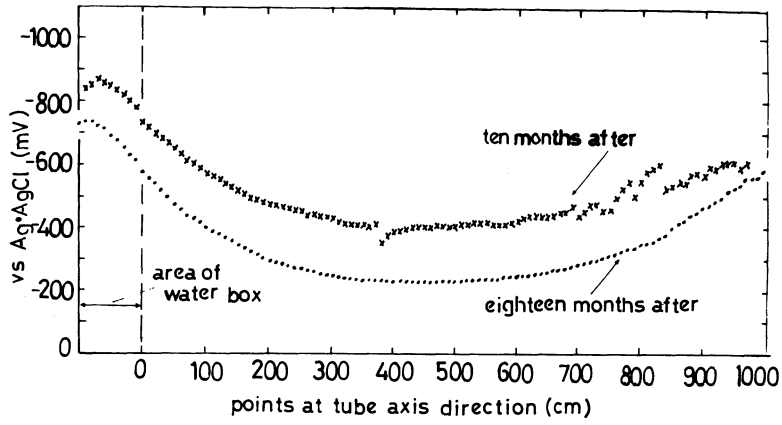

Fig. 4: Potential distribution to the axial direction inside the titanium tube.

Under the same conditions, the drawn tubes and new new tubes were tested and the fouling coefficient was obtained by the following formula (A). Based on it, the correction was made to H.E.I. Standards as to the overall heat transfer rate. The lowering rate of the overall heat transfer rate was obtained by the following Formula (B). The calculated range was 9.8 - 12.2% and the average value was approximately 11%.

$$r = \frac{1}{K} - \frac{1}{K_o} \quad \text{.....(A)}$$

$$Cf' \ (\%) = \left(1 - \frac{k}{k_o} \right) \times 100 \quad \text{.....(B)}$$

Where r : Fouling coefficient of the test speciman tube
K : Overall heat transfer rate of the test specimen tube
K_o : Overall heat transfer rate of the new tube
Cf': Reduction rate of overall heat transfer rate
k : Corrected overall heat transfer rate of the respective test specimen tubes
k_o : Overall heat transfer rate gy H.E.I. Standards

The result conformed well to the cleanliness value of about 90% of the tube, as obtained at the time of the performance test by the actual equipment in about one month ahead of the tube drawing.

(2) Deposit of the scale; The scale deposit was about 0.01 mg/cm^2 at the cooling water inlet side and 0.038 - 0.099 mg/cm^2 at the outlet side. It was extremely low at the inlet side, but the deposit at the outlet side was as much as 3 - 10 times of the inlet value. The absolute value, however, was low and about 0.1 mg/cm^2.

Protective System

In the unit at the naval brass tube plate side, the long-term measurement was made on the distribution of potential, the potential inside titanium tube, and the hydrogen absorption of titanium tube over the tube plate faces, and the proper protective potential and protective current density were checked. No cathodic protection was arranged at the titanium tube plate side.

The inner face of the water-box of mild steel was provided with neoprene rubber lining of 3mm thickness.

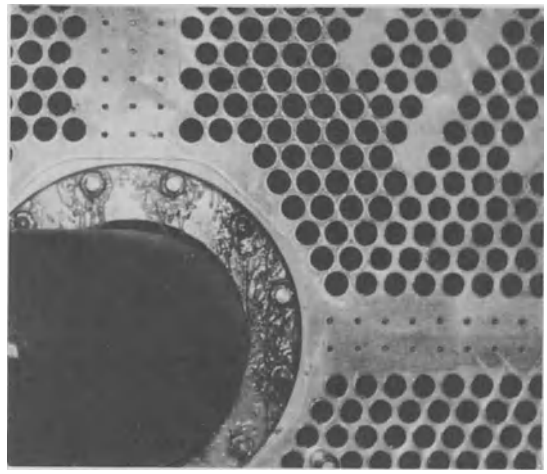

Photo 1: Appearance of titanium tube plate face directly after it was cooling down at the 5th month following the start-up of the operation.

1. Potential Distribution on Naval Brass Tube Plate Face. Zinc reference electrodes were mounted at 20 positions of the tube plate face at the sea-water inlet and outlet sides. The change by the time elapse on the distribution of potential of the respective zinc reference elec-rodes was checked.

The measured result was indicated in Fig. 3. After about 10 months, the potential was almost stabilized, as shown there. In 18 months, the potential difference at the tube plate face was within the range of several tens of mV, and it is believed that the good control condition was achieved.

2. Potential Distribution Inside Titanium Tube. The guide pipe for the measurement purpose was installed from the cock for measurement at the upper water-box at the sea-water return side, down to the tube-end of the titanium tube. By inserting the Ag. AgCl reference electrode from outside (less noble by about 10 mV vs SCE), the potential distribution to the tube axial direction was measured inside the tube.

The result was shown in Fig. 4. As shown there, the distribution of potential inside the titanium tube was hardly attenuated in comparison with the copper-base alloy tube.

3. Checking of Hydrogen Absorption of Titanium Tube. Such a method was adopted, where the measurement was made on the hydrogen

amount of the titanium plate test pieces which was adhered to the naval brass tube plate face and the test specimen tube drawn from the same tube plate side.

4. Protective Potential. The protective potential of the naval brass tube plate face was set at -550 mV + 50 mV vs SCE. The inspection after 5 months revealed a slight galvanic attack at a part of the tube plate face.

Then, the potential was raised temporarily up to -650 mV ± 100 mV vs SCE and the cathodic protection supply current to the tube plate face was increased. At the same time, the current distribution balance was rechecked.

After about 1 month, the potential was set again at -600 mV ± 50 mV vs SCE and the checking was made in about 10 months thereafter. Then, it was found out that the galvanic attack was eliminated, and the good thin electro-coating was formed on the naval brass face. The potential control was conducted thereafter by -600 mV ± 50 mV vs SCE. Photo 1 shows the clean titanium tube plate face, which was kept intact after the cooling-down in 5 months after the start-up.

SUMMARY

(1) Through the operating record and actual equipment test, the reasonable and appropriate property of the performance of the whole-titanium made condenser were confirmed, having the tube inside velocity of 3m/sec. and the tube cleanliness ratio of 90%.

(2) The maintenance can be simplified, since neither chlorine injection or ferrous sulfate injection equipment, the reverse washining device, nor the continuous cleaning system by sponge is provided. Furthermore, there is no leakage at the tube or tube-end section.

(3) It is not difficult any more than the conventional material so far as the fabrication of the titanium tube plate, processing of the tube hole drilling and the mounting of expander of the titanium are concerned. The faultless mounting can be made by Non-Filler Pulse TIG Welding.

(4) The operation is continued without the cathodic protection at the titanium tube plate side. At the naval tube plate side, the precision measurement of the potential distribution at the tube plate side and the hydrogen absorption checking at the titanium tube-end were carried out, and the optimum protective potential was selected to be -600mV ± 50 mV vs SCE.

ACKNOWLEDGMENT

The Authors were assisted by the positive cooperation of Mr. N. Ishida and Mr. T. Hiwatashi of Kakogawa Works and Mr. K. Shimogori and Mr. H. Sato of Central Research Laboratory of Kobe Steel, Ltd.

Performance test and other valuable data were offered by Mr. Y. Tadokoro and Mr. Y. Mitomi of Takasago Works of Mitsubishi Heavy Industries, Ltd., who were in charge of the design and fabrication of this turbine condenser. Mr. Y. Imoto of The Nippon Corrosion Engineering Co., Ltd., extended the collaboration in the field of the cathodic protection.

The Authors wish to express the hearty gratitude to the above personnel.

REFERENCES

1. Mimura, K., Minamoto, K., Nishihata, S., Yamasaki, M. "Karyoku Genshiryoku Hatsuden (The Thermal and Nuclear Power)" Vol. 26, No. 11 (1975), P. 71.

2. "Heat Exchange Institute Standards for Steam Surface Condensers" 6th Edition.

3. Hanson, C. F., "Titanium, Science & Technology", Vol. 1 (1973), p. 145.

MANUFACTURE AND PROPERTIES OF TITANIUM TUBES FOR POWER STATION CONDENSERS

J. Lindemann

Mannesmannröhren-Werke AG

Düsseldorf / Germany

1. MANUFACTURE

For a period of approximately 10 years, the Mannesmannröhren-Werke have been manufacturing seamless and longitudinally welded titanium tubes.

Base material for the production of seamless tubes are round bars of 167 mm diameter which are pressed to hollows on a 2.500 ton press. A typical dimension is 50 x 6 mm. These hollows are cleaned by grinding, sand-blasting or pickling and brought to final size by cold-pilgering.

The delivery program for seamless titanium tubes covers the range from 10 mm up to max. 114 mm Ø. The smallest wall thickness being manufactured is 0,7 mm; for reasons of stability larger diameters necessitate larger wall thicknesses.

For longitudinally welded tubes, longitudinally cut strip is used as base material which is continuously formed to a split tube and welded by the TIG process without filler metal. It is of importance to use an inert gas free from oxygen, hydrogen and nitrogen. Due to the high affinity of these elements to titanium, an irreparable embrittlement can occur in the weld zone. Careful guidance of protective gas has to be maintained until the weld surface is cooled down to 250°C.

In addition of the conventional methods of gauging and visual inspection for the quality assurance of welded titanium tubes, an eddy current test is carried out over the total length. In addition an underwater leakage test over the total length and an hydrostatic test with compressed air as a strength test can also be performed. Leakage testing applies also to seamless tubes. The delivery program for welded tubes comprises diameters from 10 to 57 mm with wall thickness between 0,5 and 2,0 mm.

The individual tube length we can manufacture - both seamless and welded - is essentially limited by the possibilities of transportation. Presently, fix lengths up to max. 25.000 mm can be delivered.

Material used for the manufacture of welded and seamless tubes is unalloyed titanium of the following strengths:

$$\sigma\beta 30 - 42\ kp/mm^2\ (295 - 410\ N/mm^2)$$
$$\sigma_{02}\ 18\ kp/mm^2\ (195\ N/mm^2)$$

as soft quality acc. to DIN 17860 material 3.7025 or

$$\sigma\beta 40 - 55\ kp/mm^2\ (395 - 540\ N/mm^2)$$
$$\sigma_{02}\ 25\ kp/mm^2\ (275\ N/mm^2)$$

acc. to DIN 17860 material 3.7035.

For more severe corrosion conditions especially in reducing media, tubes can also be manufactured of titanium palladium alloy.

2. PROPERTIES

2a) Corrosion. The insides and outsides of condenser tubes are subject to different conditions which they have to resist. Inside the tube the corrosion by cooling water has to be considered whereas at the outside mechanical stresses are the main factors caused by various steam conditions, such as velocity and direction of flow, beat of the blast pipe or water hammer etc.

Usual condenser materials are copper, copper-base alloys, copper nickel alloys and austenitic stainless steels. These materials have failed in various fields, especially during the last years due to the increasing water pollution. The harmful contaminations mainly consist of a high and changing content of chlorides, sulfates, free sulfides, carbonates, ammonia as well as turbidities of different concentration. Approx. 90% of the damage with condensers examined during the last 5 years resulted from the tube material corrosion by cooling water. e.g. More than 4% of the total down time in Italian power plants originated from condenser failure acc. to a report by ENEL.

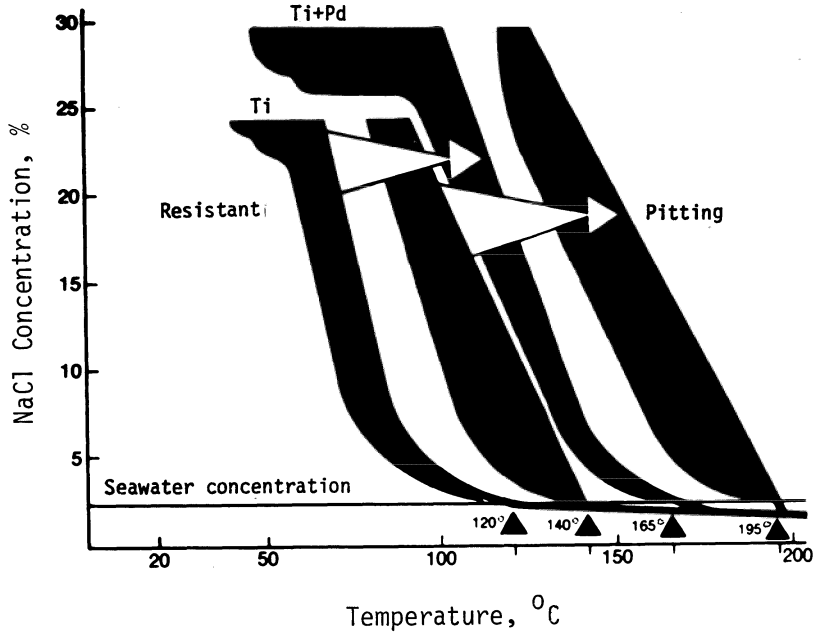

Figure 1. Resistance of titanium to pitting in neutral salt water (after N.G. Feige).

	Thermal Conductivity (Cal/cm s °C)					
	20° C	93° C	149° C	204° C	260° C	316° C
Cu Ni 90/10	0,110	0,123	0,127	0,140	0,152	0,173
Cu Ni 70/30	0,070	0,074	0,078	0,086	0,095	0,103
Monel	0,060	0,062	0,064	0,066	0,068	0,070
Titanium	0,039	0,042	–	0,043	–	0,043
CrNi Steel 18/9 W.-Nr. 1.4301	0,035	0,038	0,040	0,041	0,045	0,045

Figure 2. Temperature dependence of the thermal conductivity of various materials.

Titanium and its alloys have excellent corrosion resistance under the above mentioned water conditions. Experiments with titanium tube condensers since 1960 and practical-large-scale use since 1968 revealed that titanium is not only resistant to today's pollution of river water and also to seawater cooling but would also resist even more corrosive environments.

Within the last years titanium has been selected for nuclear and conventional, auxiliary coolers in several nuclear power stations. This type of heat exchangers are working only for limited periods and during emergency periods. That means that during the most time these heatexchangers have to keep ready under coolant conditions. Under these conditions a special type of corrosion occurs with conventional tube materials. Titanium is resistant under this corrosion phenomenas as long as the heatexchanger is out of service.

Resistance to chloride induced pitting was examined by N. G. Feige, who found that titanium is fully resistant to all loads occurring with practical condenser operation. Those results were supplemented by own examinations. It turned out that in certain areas the beginning of the corrosion is shifted to higher temperatures and chloride contents. With austenitic CrNi-steels, a content of approx. 100 ppm Cl with simultaneous stress interference can lead to stress corrosion. With Cu-base alloys, the attack as a result of destruction of the oxide surface layer is accelerated by the factor 10 - 20. (See Fig. 1)

Sulfate-concentrations up to 1000 mg/l, which were measured e.g. in the Weser river in Germany, are not harmful to metallic materials whereas structural parts of concrete may be destroyed. In non-treated water, sulfates are, however, reduced by sulfate reducing bacteria to hydrogen sulfide (H_2S) which especially attacks nickel and iron.

Titanium is absolutely resistant to the H_2S attack within the scope of the H_2S-content being present in cooling water. The Thames e.g. has a content of hydrogen sulfide up to 3 - 5% of the total content of turbidities. Also ammonia is a typical biological decomposition product which causes dangerous stress corrosion on Cu and Cu base alloys. Titanium is resistant to gaseous ammonia as well as to ammonia solved in water up to high contents and temperatures. In cooling towers with circulating cooling water it occurs that sulfuroxide from the air is forming sulfuric acid and causes tube failures.

Incrustations and other deposits in condenser tubes are of mineralia or organic nature.

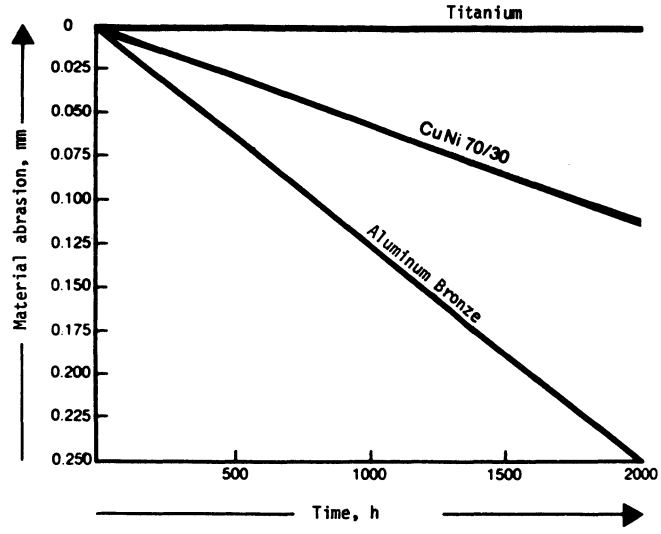

Figure 3. Material abresion by fine sand in seawater. Velocity 1.8 m/sec.

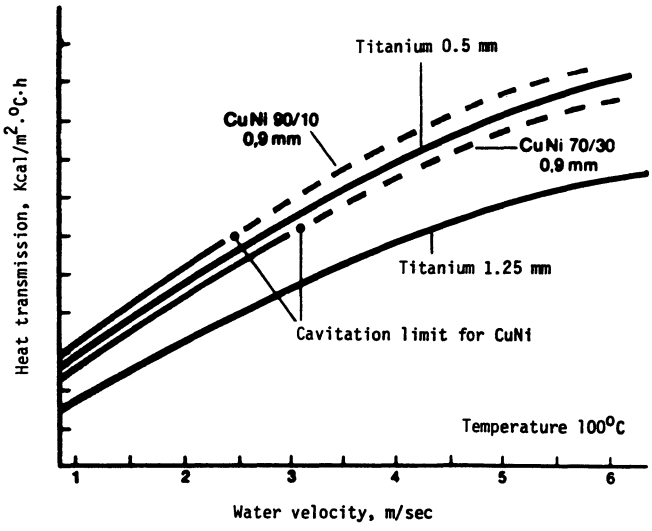

Figure 4. Heat transmission of titanium and copper-nickel alloys (after N.G. Feize and R.L. Kane).

During condenser operation, mineral deposits occur as magnesium or calcium compounds which are existing as solid layers (incrustations) or mud in the cooling system. Organic deposits are caused by the water which, depending on its origin, may contain various quantities and kinds of micro-organisms. While spring and tap water e. g. contain only slight quantities of micro-organisms, their concentration in river water, visible by more or less turbidity, is often very high. By the heating of water in condensers, life conditions improve and, thus, the growth of these organisms increases. The same applies to alga growth and with sufficient oxygen content even to the growth of fishes.

In a German power station the total amount of copper base alloys tubes had to be retubed by titanium because of the biologic oxidation of ammonia to nitrate and nitric acid. The normal pH value in this powerstation was adjusted to pH 9.2. Because of the nitric acid forming it was as low as pH 4.5. Titanium tubes work now since 2 years without any failure.

The tendency of the formation of deposits on a material is described by the cleanliness-factor. The cleanliness-factor for titanium in most of the cooling media amounts to 90 - 95% and is essentially higher than for copper-base alloys.

In the starting phase the heat transfer of a condenser equipped with titanium tubes is lower than that of a condenser with tubes on copper-base.

Conditions change when after formation of the protective oxide film and deposits the heat transfer of copper-base tubes decreases. Therefore, the heat transfer figures with both condenser materials are practically the same taking into account, that the usual wall thickness amounts to 0,9 with copper tubes and to 0,6 mm with titanium tubes. The thermal conductivity of various materials can be learned from Fig. 2.

Up to now, we do not know of any corrosion damage with condensers equipped with titanium tubes. Titanium is even resistant under corroding conditions arising by the formation of deposits inside the tubes. Titanium materials have a thin, however, tight and adhesive passive layer which effects the superior resistance to corrosion.

Often, cooling water contains sand or other solid matters. By the abrasive effect of these substances, tubes can be damaged. This problem is especially important if sea water from coastal zones with considerable tidal impulse is used for cooling. Titanium shows a very good resistance to erosion. Figure 3 indicated the material abrasion with titanium and CuNi or bronze alloys. This

type of damage was especially observed at the tube inlets, but also over the free tube length. Similar damage as that produced by erosion can also occur by cavitation in connection with whirlpools. Also in this case the special resistance of titanium can be attributed to the formation of these thin and well adhesive passive layers which are self-curing even with very low O_2 content.

Figure 4 shows that the water velocity has a substantial influence on the economy of condensers. The limiting velocity for various condenser materials is indicated in Fig. 4. When using titanium, the water velocity can be increased up to the limit of economical pump performance. For tests, velocities up to 36.6 m/sec. were effected without harming the material titanium. This property can also be attributed to the tight, solid and self-curing passive layer. Local cavitation influence does not destroy titanium tubes.

Another attack by galvanic corrosion arises from the contact of different metals in such a system. In these cases, titanium is cathodic and will not be attacked. In most cases, tube plates of copper-base alloys are used in practice. Owing to their position in the stress row, slight abrasion rates are to be expected with these materials. The materials are mainly attacked at the rolling-in point close to the titanium tubes. Nickel-containing aluminum bronze acc. to ASTM B 171 suffers the lowest attack. As the wall thicknesses of the tube plates usually dispose of a higher corrosion allowance (Thickness 12-40 mm), small corrosion rates (0,2 mm/year) are acceptable.

In case of new tube equipment unalloyed steel bottoms may be provided with titanium tubes. A protective coating is always necessary in these cases.

Titanium-explision-clad tube plates have to be used in plants where the tubes have to be welded into the tube sheets, which is often required for high integrity condensers and heat exchangers for nuclear power plants.

2b) Mechanical Loadings. The most important mechanical loadings of the tube bundle arise from oscillations and vibrations as a result of the beat of the blast pipe and the water hammer. Owing to the used smaller wall thicknesses and the relatively small E-modulus, titanium is sensitive to these loadings. Titanium tubes can replace Cu-base tubes without design changes in plants without vibration loadings. With vibration liable plants the tube distance of baffle plates be reduced to avoid undue vibration and collision of the tube. With a new tube equipment - if the distance of bottom or tube cannot be changed - it is possible to bundle titanium tubes in the endangered zone by inserted plastic tubes or clamps. Thus,

an increased bundle rigidity is achieved. In a German retubed power plant the vibration of the tubes causes problems and the problem was solved by inserted clamps.

Erosion corrosion by water drops may occur below the steam inlet. Titanium has proved extraordinarily resistant in practice and offers advantages when used in this section.

In the lower area of condenser, carbon dioxide, ammonia and oxygen are released bh condenser degassing. Also under these conditions titanium is superior compared to other materials.

Within the last years it turned out favorable - also from the economic point of view - to equip high-loaded parts, as those described, with titanium.

Costs in case of failure and standstill of the condenser are very high and therefore the world-wide trend is to construct high integrity condensers. These condensers, among other things, necessitate a tube material of high resistance to corrosion and other favorable properties regarding all occurring loads. Titanium is such a material which is now used on a large-scale basis.

TRENDS IN THE USE OF TITANIUM IN HEAT EXCHANGE

C. F. Hanson

Imperial Metal Industries (Kynoch) Limited
Birmingham, England

Introduction

Titanium's unique corrosion and erosion resistance in saline and polluted water is well known. Diminishing relative prices have resulted in dramatic growth in the use of titanium tubular and plate heat exchangers as users recognise the cost benefits of total reliability systems.

The major breakthrough has been in power generation where titanium tube has become the standard in many countries for turbine condensers and associated auxiliary exchangers cooled with coastal or estuarine water.

Titanium tubular and plate exchangers have been used for many years in chemical and on-shore refinery processes. More recently, off-shore oil development has led to use on gas and gas-oil production platforms, both for direct and indirect cooling duties; high integrity Central Coolers feeding dosed sweet water to secondary cooling circuits in cheaper materials have been specified for tanker fleets; and the practice of using thin wall titanium tube in condensers is spreading to use in multi-stage flash evaporation desalination plant, in part or throughout, as practical experience shows that in some plant locations copper base tubing has less than complete integrity. Future potential developments include those of extended surface tubing and bimetal finned tube for air or gas cooling duties in several industries.

This paper reviews present technology and future trends in what is for the titanium industry an increasingly important sector of activity.

System Concepts

Plate Heat Exchangers are particularly suitable for low pressure liquid-liquid exchange and for such are generally considered to be cheaper, more compact and lighter than equivalent tubular exchangers when either can be used for direct cooling. Important applications include cooling of demineralised water for pressure core and other duties associated with certain nuclear reactor types; brine cooling in chlorine production; and use for low pressure direct crude oil coolers, compressor interstage coolers and other ancillary duties on off-shore platforms.

Economics in indirect cooling are more tenuous where, as is often the case, higher pressure tubular titanium direct coolers can be used. Nonetheless, plate exchangers have been used as the Central Cooling system in commercial shipping, although for condensers use of thin wall titanium tubing is a more probable development; and some operators have chosen them for Central Coolers feeding carbon steel tubular exchangers for high pressure (up to 160 atmospheres) gas-oil or gas cooling on off-shore platforms.

Low Pressure Tubular Heat Exchangers - Thin wall (0.5 to 0.7mm) titanium tubes roller expanded into fixed or floating head galvanically compatible copper base, stainless steel or titanium tube plates are the basis of use in power generation, desalination and other low pressure condensing and evaporative duties.

Total integrity systems can be achieved using existing technology applied to the system as a whole; new design concepts and fabrication techniques and new corrosion resistant alloys, such as the recently introduced low nickel low molybdenum series, are likely to lead to even wider use and greater cost effectiveness in future.

High Pressure Tubular Heat Exchangers - For duties up to 300°C and pressures up to 200 atmospheres or more, thicker wall tube (1 to 5mm) is usually welded to solid or titanium clad steel tube plates, occasionally roller expanded or explosion welded to galvanically compatible non-titanium materials. Such exchangers have been used for many years in chemical plant. Design optimisation can result in clear economic advantage compared with the use of indirect systems sometimes previously preferred because of potential corrosion on conventional materials. An important example is the trend towards direct gas-oil or gas cooling using titanium tubular exchangers on off-shore platforms, where savings in weight, space and pumping power are as important

as the need to achieve very high system availability.

In high temperature process plant, scope exists for use of higher creep or rupture strength titanium grades for tubes and solid tube plates; stronger commercially pure grades such as ASTM B338-73 Grade 3 are already used in tube form in urea plant instead of the more normal Grade 2 tube product; Ti-6Al-4V alloy tube plates have also been specified in some high pressure sea water cooled plant; and ductile age hardenable alloys, such as Ti-2½Cu, may eventually be used in tube form.

Engineering and Design Considerations

The properties of titanium allow to a far greater degree than other materials the optimisation of several of the most important parameters in heat exchange systems, although some features call for more than usually careful attention to detailed design or materials choice within the whole system if the objective of total integrity throughout unit life is to be achieved.

Tube Wall Thickness - In oxidising environments, the lower limit in low pressure exchange is controlled by such engineering considerations as handling on installation, roller expansion and tube vibration. In long tube condensers, up to 23 metres, tube walls of 0.7mm are normally used in the UK (1) and in the USA (2), although on shorter lengths 0.5mm wall is common in Japan (3) and 0.6mm in Europe and in more recent American installations (2). 0.3mm wall tube has been tried in desalination plant but most commercial plant specifications call for 0.6mm minimum wall.

An important indirect advantage is substantial weight saving, a titanium tube nest is often only 30% of the weight in a copper base alloy. This should lead eventually to re-design and cost savings in turbine support structures and to fabrication of modular shells in fabrication shops as transport to site becomes feasible.

In heavy duty heat exchangers, savings are being made by careful re-analysis of mechanical design codes for titanium based on accumulating practical experience. The same applies to thermal design codes on all types of exchanger (3).

Tube Plate Materials - In sea water, practical experience indicates that of non-ferrous materials, other than titanium, the aluminium bronzes (ASTM B171 alloy D or E or equivalent) provide the best galvanic compatibility with titanium tube. Aluminium bronze is used un-coated and without cathodic protection in most recent British practice (1). Un-coated and un-protected, Naval brass has been shown to suffer preferential attack at the

tube joint, as may be anticipated from the laboratory evaluation depicted in Figure 1. This can be overcome by coating with neoprene, coal tar pitch epoxy or polysulphide rubber, in descending order of preference, and earlier United Kingdom main condenser installations have used such coatings (1). The nature of coatings is such that a regular inspection and maintenance schedule is however advocated to ensure continued integrity.

Properly controlled, sacrificial anode or impressed current cathodic protection can protect Naval Brass or Muntz Metal tube plates, but as explained later, over-cathodic protection can cause hydrogen evolution on titanium surfaces which may lead to hydriding. For this reason, other than with soft iron anodes, cathodic protection is not normally recommended.

Stainless steel tube plates, although not widely used in saline water cooled condensers, are galvanically compatible with titanium provided the grade chosen is one that does not suffer from pitting attack through breakdown passivity in the relevant cooling water composition.

Titanium tube plates have been used for smaller turbine condenser installations in the West Indies (fabricated in the United Kingdom in seamless tube, using roller expansion (1)) and in Japan (using welded tube and TIG welded joints (3)).

It has been British practice to use double tube plates on main condensers, the inner tube plate in mild steel; interspace partial vacuum guards against any finite leakage path developing in roller expanded joints into the steam space and this design is slowly being adopted elsewhere. Thus, whilst titanium plates may eventually be specified for major condenser installations, depending on developing attitudes on tube-tube plate jointing techniques and on economics, the less costly double tube plate configuration is most likely to be used.

Heavy duty chemical and off-shore oil product exchangers are usually specified with solid or clad titanium tube plates. For satisfactory welded joints on clad plate, a minimum thickness of 9 to 10mm is usually specified. Clad plate has the advantage of ease of welding to ferrous shells, otherwise in floating head designs the choice is an economic one according to the design thickness. Less than 100mm, possibly 150mm, solid titanium tube plates may be a cheaper alternative when machining and clad plate ultrasonic inspection costs are taken fully into account.

Water Box Materials - Although standard practice has been to retain ferrous water boxes in condensers and desalination plant, usually coated, the trend to more noble tube plates, including possibly titanium, and the seeking of totally maintenance free units is likely to lead to the adoption of more advanced concepts.

Already, in titanium tubed direct product coolers, water boxes clad in aluminium bronze are being specified. The technology exists already for the use of titanium loose lined or explosion clad steel units, the latter following practice in high pressure and temperature chemical process plant, and a feasible development may be fabricated thin titanium or galvanically compatible copper base materials bonded to and supported by glass reinforced plastic structures.

Tube to Tube Plate Joints - Roller expansion to non-titanium and roller expansion or welding to titanium or titanium clad steel tube plates is well established practice (1, 2, 3).

Earliest condenser installations in the United Kingdom used packed joints without any problems. Current practice on seamless tube is to roller expand using controlled torque and three roll expanders in parallel tube plate holes, ungrooved, finished by reaming to better than 32 micro-inches CLA. Tube ends are circumferentially polished to the same standard.

In aluminium bronze tube plates, joints consistently in excess of 1,000 kg mechanical push-out strength can be achieved with 25.4mm OD x 0.7mm tube even at abnormal tube to tube plate hole diametrical clearances of 0.5mm. It also appears to be difficult to over-roller expand; at higher torque settings at normal TEMA clearances, joint strengths are above 2,000 kg and thin wall tube fails before the joint.

American practice, mainly with welded tube, is to use five roller expanders and to groove tube plates, which have hitherto mainly been in Muntz Metal or Naval Brass (2).

It is clearly advisable, for each tube plate material, to run optimisation tests on roller expansion settings using standard equipment and tube of the type specified. This applies particularly with stainless steel tube plates, where pre-working of the hole surface before expansion can be beneficial; and with seam welded tube in the as-welded condition, where it is known that metallurgical and dimensional differences between the weld bead and parent strip have resulted in differential work hardening during expansion leading in extreme cases to weld cracking. For this reason various user specifications for welded tube call for annealing post welding and/or polishing of tube ends and/or a softer than ASTM B338-73 Grade 2 strip base for tube manufacture.

The TIG process for tube to tube plate welding is well established. Heli-arc welding has also been used as has explosion welding into non-compatible tube plates such as stainless steel.

Shell Side Supports - With any tube support arrangement, a primary requirement is design of spacing and tube to tube plate support hole clearance to avoid forced or induced (resonant) vibration with thinner wall titanium tube. Most titanium tubular exchangers have used conventional steel support plates, but rod and baffle designs have been developed and a future trend may be use of non-ferrous or even non-metallic support plates. Of particular interest in large re-tubing operations, where re-location of or addition to existing support plates is difficult or expensive, is the use of inert flexible plastic or rubber tubing interlaced between tubes on installation to damp vibrations.

Thermal Design - A 300 MW titanium condenser in the UK handling polluted and silted estuarine cooling water has shown a 4% improvement in thermal performance over 70:30 cupro-nickel (1). Controlled tests in another UK condenser using clean sea water show similar results - Figure 2.

Of greater importance is the fact that the threshold for impingement attack is so high on titanium, of the order of 6m per second even in high sand content water, that cooling water velocity in titanium designs can be optimised. Typically, flows between 2.6m/sec and 3.0m/sec can be used; with decreased fouling factor, savings in surface area of 10 to 20% are practicable (1, 2, 3).

Metallurgical Considerations

Material Properties - Whether in seamless or seam welded form, titanium tubing is normally the medium strength commercial purity grade corresponding to the ASTM B338-73 Grade 2 Specification. Properties of this grade relevant to heat exchanger design are given in Table 1.

TABLE 1 - Properties of IMI Titanium Condenser Tube of Relevance to Condenser Design

Mechanical Properties

U.T.S	- 345 N/mm^2(min)
0.2% Proof Stress	- 275-410 N/mm
Elongation on 50mm	- 20% (min)

Reduction in Area - 50%; Hardness HV 160-200

Fatigue Limit - Kt1 $\pm$236 N/mm^2; Kt3 $\pm$157 N/mm^2

Stress for 0.1% strain in 10^4 hrs -140 N/mm^2

Stress to Rupture in 10^5 hrs -338 N/mm^2

TABLE 1 - Properties of IMI Titanium Condenser Tube of Relevance to Condenser Design (Cont'd)

Physical Properties	
H_2-0.015%(max); N -0.03%(max); C-0.10%(max)	
O_2-0.25%(max): Fe-0.3%(max) (0.05%(max) where specified)	
Cobalt content - 5ppm; Tantalum content - 15ppm	
Density	- 4.51 Mg/m^3
Youngs Modulus	- 105 GN/mm^2
Thermal Conductivity	- 17 W/m.K
Specific Heat	- 528 J/kg.K
Linear Coefficient of Expansion ($0-100^oC$)	- 8.9×10^{-6} K^{-1}
Resonant Frequency (25.4mm o/d x 0.7mm wall)	- 78 to 80 Herz

For high temperature operation, in the range 150 to 250^oC, tensile and creep/rupture properties fall off markedly, requiring careful choice of wall thickness; the stronger ASTM Grade 3 Specification has rupture strengths some 15% higher than the Grade 2 product in this temperature range - hence its use in, for example, urea strippers.

Properties of Welds - Unfilled fusion welds in commercially pure titanium have an acicular as-cast structure usually 10 to 20 points harder (Vickers Scale) than parent material. This is typically associated with a 10 to 20 N/mm^2 higher tensile and proof strength and up to 5% reduction in ductility (3). For tube to tube plate welds and general fabrication, these characteristics are acceptable and post-weld annealing or stress relief is rarely practised.

On seam welded tube, used in the as-welded condition, the greater weld hardness, often combining with thickness variation between weld bead and strip, can result in a significant difference in the work hardening characteristics of the weld bead itself; grain size also has an effect. Hence, for satisfactory roller expansion, there is an inter-relationship between expander parameters (i.e torque, rotational speed, roller size and number and lubrication), the metallurgy, dimensions and shape of the weld bead and the general surface finish in the area to be expanded. Additional factors include the tube plate hole pitch - with welded tube adequate joint strengths may require higher torque settings, thus leading to loosening of adjacent joints; and the presence of partial weld bead disruption defects.

The requirements for a high and consistent integrity seam welded tube may thus dictate:

a) the use of post weld heat treatment (weld bead recrystallisation or stress relief) and/or cold working, with or without post heat treatment,

b) weld bead dimensional and shape tolerances,

c) polishing of OD surface at tube ends,

d) more definitive standards of non-destructive testing, and

e) restricted chemistry on iron and oxygen content

Hydriding of Titanium

Hydriding of the inlet and outlet ends of titanium condenser tube in sea water has been reported in Japan (4). This was caused by the use of impressed current cathodic protection resulting in surface atomic hydrogen evolution with subsequent limited bulk metal diffusion.

Hydriding of titanium can occur when it is used in some types of high temperature and pressure chemical process reactions and is known to be caused by use of high iron content titanium grades or through surface iron contamination. Hydriding can also result from corrosion in some reducing acid conditions. It is important to distinguish between the operating mechanisms and understand the requirements for avoidance in each case.

Hydrogen Evolution Potential - Atomic hydrogen is formed on commercially pure titanium exposed in sea water when the surface potential falls below about -700 mV with respect to a saturated calomel electrode. At the metal temperatures usually encountered in sea water cooled turbine condensers, surface adsorbed hydrogen atoms normally result only in discrete layer hydriding, which does not unduly affect the use of the material. It has previously been considered that diffusion of surface hydride layers into bulk titanium occurs only above 80°C (5), (6).

In the reported case in Japan, the welded titanium tube clearly exceeded the hydrogen evolution potential (4); hydriding to a depth of 0.1mm over 60mm from each end was observed after 1 to 2 years service, although without causing tube failure. In these condensers, titanium tube was installed amongst aluminium brass tubes in uncoated but perhaps over-cathodically protected Naval Brass tube plates, with ferrous sulphate dosing retained. In similar condensers operated without cathodic protection, hydriding was absent although brass tube plate corrosion, as predicted, was significant.

Hydrogen evolution cannot occur when titanium is coupled with any or a combination of the common copper base or ferrous materials, as illustrated in Figure 3. It may occur in systems with sacrificial zinc anodes or when any impressed current system causes titanium tube inlet ends to fall below the -700 mV evolution potential. Use of soft iron sacrificial anode cathodic protection remains feasible and has been successfully used in titanium on-shore refinery heat exchangers using copper base tube plates. Recommended practice is to avoid the need for cathodic protection by using coated Naval Brass tube plates or, preferably, uncoated aluminium bronze or titanium tube plates, with water boxes in coated steel or in a more galvanically compatible material.

Influence of Iron on Hydriding Susceptibility (7)

At iron contents greater than 0.06 to 0.07% in commercially pure titanium, presence of β phase iron-titanium compound is likely, precipitating in acicular form in weld metal. It is known that in 55-65% nitric acid, presence of acicular β phase causes preferential weld corrosion, hence for many years specifications restricting iron content to 0.05% maximum have been stipulated.

Furthermore, in certain chemical reactions, such as in the production of terephthallic acid and urea, it has been established that β| iron-titanium in weld or parent material or the presence of iron particles on the surface act as acceptors to the hydrogen atom, resulting in surface adsorbtion. At the temperatures involved, up to 250°C, diffusion to form embrittling bulk metal hydriding is inevitable (5). The remedy, substantiated over several years of operating practice, is limiting specification iron content to 0.05% maximum; use of fabricating procedures aimed at reducing or eliminating iron contamination; and a patented anodising treatment on the finished equipment which removes any remaining trace iron contamination and artificially thickens the protective oxide film (7).

Precautions of this nature are recommended when titanium is used in environments where finite corrosion occurs and metal temperatures exceed 80°C. Such procedures are not necessary in lower temperature plant handling oxidising environments where titanium is more often specified. Nevertheless, avoidance of excessive iron or other contaminant build-up in welds is essential practfce and such applies to the welding of tube.

Where hydriding is a concomitant of corrosion, the only potential remedy is to use a more corrosion resistant titanium alloy, such as those based on titanium-palladium or titanium-nickel-molybdenum, particularly applicable in weakly reducing media at higher temperatures.

Wrought Product Type, Standards and Specifications

Users face a choice between seamless and welded tube in tubular exchangers.

Seamless tube is made in finished lengths up to 25 metres by extrusion of hollow billets and cold reduction to a high standard of dimensional control and low incidence of significant defects. Full ultrasonic inspection is normal. Tube is normally supplied annealed, oxidised with ends polished suitable for roller expansion or welding.

Welded tube is made from cold rolled annealed strip, produced from hot rolled band, using continuous TIG welding. Control of strip feed quality and dimensions, roll forming and welding parameters is of critical importance to the achievement of tube shape, suitable weld bead profile, metallurgical homogeneity and avoidance of weld contamination. Of equal importance is avoidance of porosity and control of grain growth. Supply in the annealed condition is often preferred for material made from ASTM B338-73 Grade 2 strip or equivalent, to facilitate roller expansion. For supply in the cold worked condition, a Grade 1 strip base is desirable. Eddy current testing is widely preferred by suppliers for seam welded tube; for more onerous defect tolerance standards, however, both with eddy current or ultrasonic testing, it is necessary to eliminate the response interference from as-welded beads by a cold working operation to homogenise the weld structure and reduce or eliminate weld bead dimensional variances.

The considerable growth in use of titanium tube in condensers can in part be attributed to the availability of a seam welded product at prices closely related to those of the cupro-nickel family of materials. Especially is this so in the USA and Japan. Nevertheless, standardisation on titanium in UK condensers was established with a more expensive seamless product. This is a reflection both of the cost effectiveness of titanium in this application; and of different philosophies in the approach to achieving 100% reliability in heat exchange systems in high capital cost plant where integrity and safety can be crucial and non-availability a heavy financial burden.

Thus, seamless tube could continue to be preferred and justified by some users operating nuclear or other highly critical plants where absolute integrity and safety needs to be guaranteed; it is also likely to remain the choice for heavy gauge tubing for high pressure and temperature plant where it is now used almost exclusively.

For low pressure duty, in thin wall form, welded tube can however meet the onerous integrity standards demanded by many user industries, but practical experience suggests that very great care is needed in manufacture, specification and quality control to consistently sustain large scale production to standards meeting the user expectation of total leak-free service over full operating life, a standard which is more certain with the seamless product. The fact that user specifications and producer internal control standards shows such significant divergence in several important respects indicates a need within the industry to more clearly define and maintain an International standard for seam welded titanium tubing.

It is the lack of such standardisation in specifications and quality requirements that make it difficult to establish price differentials between welded and seamless titanium tubes and those in competitive material; relationships may be expected to change as the technology and scale of manufacture and use develop and as quality standards become more stabilised. Thus only with the accumulation of more practical experience and refinements in standards will there become a clearer resolution of the respective merits of seamless and seam welded tubing for the various types of application where titanium is specified.

In the meantime, the use of titanium tube is making a substantial contribution towards improving the efficiency and availability of modern high cost plant and will undoubtedly continue to do so even more effectively in future as the technology of application develops.

References

1 Hanson, C F, "Titanium Condenser Tube Application in Practice", Materials in Power Plant Conference, Institution of Metallurgists, Edinburgh, April 1975.

2 McCue, D M, "Titanium Tubes Cut Costs Even in Average Water" Electrical World, 15 February 1975, P44-46.

3 Kubo, Y; Kusamichi, H; Ito, H; Moriguchi, Y, "Thin Wall Welded Titanium Tubes for Steam Turbine Condensers", Marine Engineering Soc, Japan, December 1975.

4 Nosetani, T et al, "Experience with Welded Titanium Tubes in the Air Cooling Zone of Surface Condensers", Sumitomo Light Metals Technical Report, 1974, Vol 15, No 3, 163-173.

5 Cotton, J B and Hines, J G, "The Science, Technology and Application of Titanium", Pergamon Press, 1970, 155-170.

6 Charlot, L A et al, OSW Research & Development, Report No 624, 1970.

7 Manton, F and Turner, M E D, "Anodising of Titanium Equipment", The Science Technology and Application of Titanium", Pergamon Press, 1970, 171-178.

TITANIUM BASKET ANODES FOR METAL REFINING AND WINNING

J. R. B. Gilbert and G. M. Roberts

Imperial Metal Industries (Kynoch) Ltd.
Witton, Birmingham B6 7BA, England

Introduction

Titanium baskets have been used for many years to contain anode materials for electroplating. They have proved reliable and economical, particularly in nickel plating. This paper describes some aspects of the extension of this system into the field of metal refining, where relatively impure metal is contained in the anode basket and is refined by the dissolution and plating processes. In both these cases the principal anode reaction is the solution of metal. It has also recently been discovered that materials on which the principal anode reaction is evolution of oxygen may continue to function as anodes when contained in a titanium basket, and the application of this principle to metal-winning is described. Finally some aspects of the design of a suitable basket for operation in a commercial electrolytic tankhouse are considered.

Electro-Refining with Titanium Baskets

In conventional electro-refining, the metal to be refined is first melted and cast into the shape of an anode using an anode casting wheel. These cast anodes have integral 'ears' from which they are suspended, and which make electrical contact with the bus-bar along the side of the electrolytic cell. The advantage of using a titanium basket anode is that the scrap or impure metal can be used in particulate form. It need not be melted and cast, thereby saving, at least in the case of a new plant, the cost of a casting wheel. All the metal to be refined is immersed in the electrolyte and there are no remaining anode ears which require to be remelted. Obviously during use the level of metal within the basket drops continuously and it is necessary to provide for topping up the basket. Provided this is done, the basket system has the advantage over

cast anodes that the anode does not change shape during the electro-refining process.

A wide variety of shapes and compositions of feedstock can be accommodated and in some instances less pure material can be used, for example blister copper. Baskets may be designed to accommodate special forms of secondary metal and laboratory trials are in progress on direct electrolytic refining of chopped wire scrap.

Electro-winning with Titanium Baskets

For electrowinning the main advantage of using particulate material in titanium baskets is seen as the avoidance of solid lead anodes which can give rise to lead impurity in the cathode product or brittle intermetallic anodes such as Luilu or Chilex which can be expensive and awkward to operate.

In the development of novel anode materials to be used in particulate form, attention has been concentrated on titanium based intermetallic compositions. Using 50g alloy samples mounted in a holder, so as to expose a known surface area, three basic laboratory sorting tests have been devised. Test solutions were 40 g/l Cu (as $CuSO_4$), 150 g/l sulphuric acid at 40°C for copper winning anodes; 40 g/l cobalt as($CoSO_4$), pH6, 60°C for cobalt winning.

The first test is determination of the anodic polarisation curve for the material and over 150 specimens have been tested. The second test is a check on the behaviour predicted by this potentiodynamic scan consisting of a 24 hour polarisation at a constant anodic current density of 0.3 mA/mm^2 (300 A/m^2); variations in cell voltage and electrode potential are monitored. Thirdly, specimens are subjected to wear rate tests in which a given area (600 mm^2) is polarised anodically for 168 hours at a current density of 0.5 mA/mm^2 (500 A/m^2). Wear rate for the material in mg/Ah is calculated from weight loss of the specimen,and cell voltage recorded.

Three examples of polarisation curves produced in tests on cobalt winning anode materials are shown in Figure 1. Materials are selected for further study on the basis of the existence and location of active-passive transitions in these polarisation curves and the oxygen overpotentials displayed at useful current densities. The variation in these curves with different alloying additions has been studied.

Similar criteria are used in the evaluation of copper winning anodes. The aim of the criteria is, in both cases, to select material with the lowest oxygen overvoltage and the minimum alloy dissolution rate at likely operating current densities.

The second test, in which the samples are held at a constant current for 24 hours, has not so far changed any conclusion from

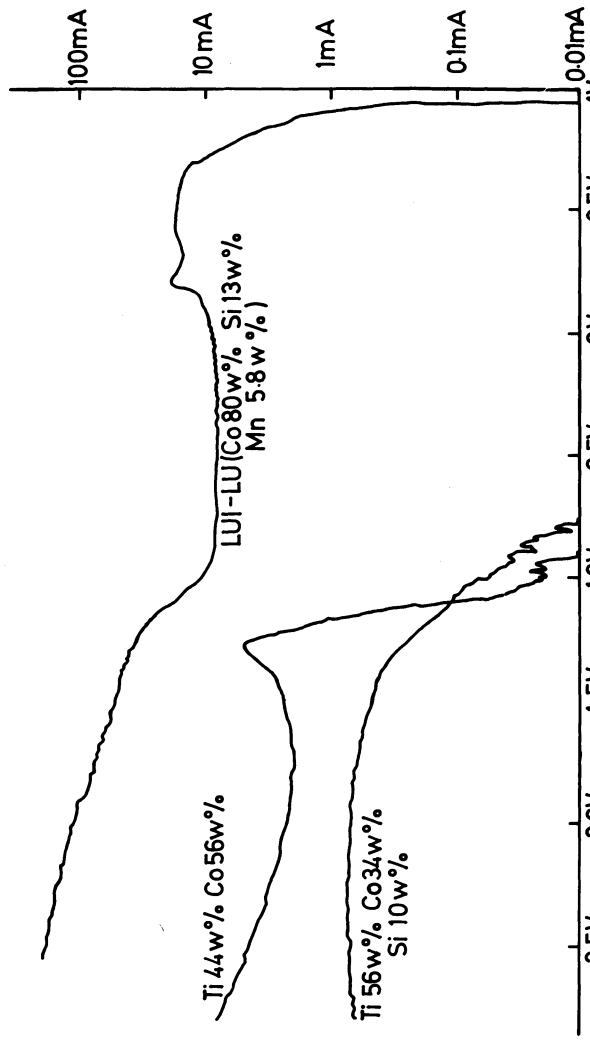

Fig. 1 - Typical Polarization curves (Cobalt winning alloys, 60°C, 40 g/l Co, pH 6.0).

the first test. It has been used on randomly selected compositions.

All alloys performing well in the first two tests are subjected to the 168 hour wear rate test; some results for these are given in Table 1.

Table 1 - Results of 168 hour Wear Test for Copper and Cobalt Alloy Samples

A : COPPER		
Alloy Composition wt%	Wear Rate mg/Ah	Cell Voltage V
Ti-40%Cu	12.4	2.23
Ti-50%Cu	16.7	2.20
Ti-49.5%Cu-1%Zr	18.05	2.22
Ti-47.5%Cu-5%Fe	15.7	2.20
Ti-2.5%Cu-1%Pt	11.3	2.09
Ti-55%Cu	17.3	2.05
Ti-54.8%Cu-25.3%Nb	8.8	1.95
Ti-57%Cu	14.6	2.13
Ti-45%Ni	12.3	1.94
Ti-38%Co	14.16	2.38
Pb-0.6%Ca	8.5	1.98
B : COBALT		
Ti-30%Co	4.5	4.50
Ti-38%Co	3.69	3.85
Ti-37.8%Co-0.5%Nb	1.3	3.84
Ti-37.6%Co-1%Zr	1.83	3.93
Zr-39.5%Co	1.87	3.82
Ti-56%Co	9.7	4.71
Ti-53.2%Co-5%Mo	9.6	4.80
Ti-70.5%Co	3.8	2.50
Luilu	8.19	3.01

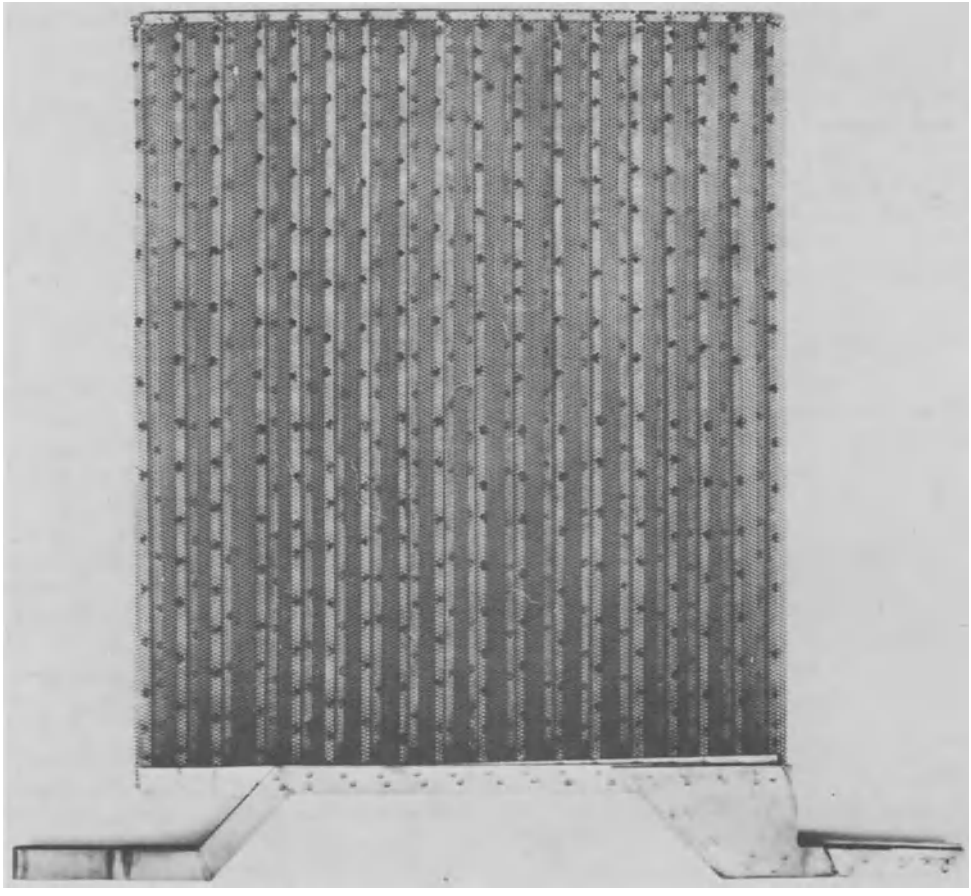

Fig. 2 - Titanium anode basket for electro-winning of Copper. 1040 mm x 880 mm x 20 mm.

For cobalt winning typical wear rates of between 1.0 and 10 mg/Ah at cell voltages of 2.5v-4.5v have been recorded. For copper values of 5-20 mg/Ah at 2.0v-2.5v are more typical. It should be noted that although total wear rate figures are quoted, the copper and cobalt contents of the consumed intermetallic are recovered in full at the cathode. Values for lead-calcium and Luilu anodes for copper and cobalt winning respectively are included for comparison.

In order to more closely simulate typical plant operating conditions and gain further information on basket design, a further laboratory test is now extensively used. In this titanium anode baskets 160 mm x 160 mm are filled with candidate anode material and operated opposite 165 mm x 165 mm cathodes.

Full size baskets, in particular for copper winning and refining, can be tested at IMI and such tests have so far duplicated laboratory results. Trials in potential customers plants are just beginning.

Titanium Basket Design

The geometry of titanium baskets for metal winning and refining, the environment which they must work, and above all the scale of the operations are very different from those met in electroplating. Inside a modern copper refining tankhouse a large proportion of the floor area is occupied by cells containing acid copper sulphate at about 60°C. Many thousands of anodes and cathodes are interleaved closely in the cells, anode to anode spacing being approximately 100 mm. To obtain access to the electrodes operators must be able to walk about on the "hanger bars" across the tops of the cathodes. Anodes and cathodes are removed and replaced at the appropriate intervals by cranes fitted with special hook frames that engage and lift up to sixty electrodes at one time.

Robust but inexpensive construction of anode baskets is vital. The baskets must occupy a volume of about 1m x 1m x 10-50 mm, hang flat and vertical, take up to 1000 amps and distribute this current evenly to the material filling them. Figure 2 is a photograph of a modern basket designed for use in a copper winning plant.

One question that arises in designing baskets for this duty is the amount of current that it is possible to pass through titanium without unacceptable temperature rise or voltage drop. The crucial area is most likely to be where the basket is joined to the member that supports it and connects it to the bus bar along the side of the electrolytic cell. Here the full current carried by the basket is funnelled into a comparatively restricted cross-sectional area of metal. The shape of the basket at this point is severely constrained by the need not only to provide easy access to the top of the basket to fill it, but also to clear the edges of the cell and settle properly on the bus bar, and to engage easily with the crane hooks when

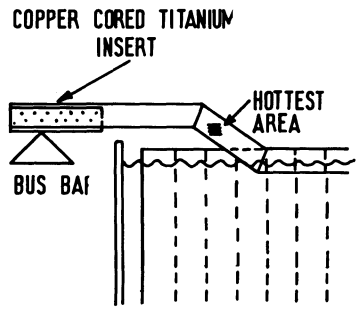

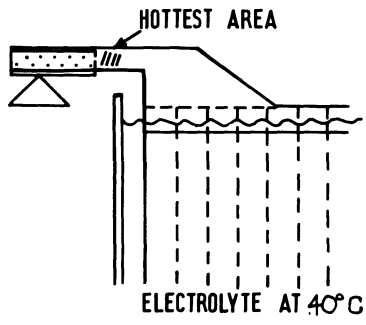

TITANIUM CROSS-SECTION IN HOTTEST AREA mm ^{2}/A	TEMPERATURE OF TITANIUM IN HOTTEST AREA AFTER 1 HOUR PASSING 400 A °C
0·6	>> 100
1·2	87
1·2	73
1·8	50

Fig. 3 - Effect of design and titanium cross section on the temperature of titanium hanger bars for anode baskets.

the anode has to be replaced or removed. It must not stick up above the general surrounding structure and thus trip the operators. A "cranked" hanger bar of the sort shown in Figure 2 may be needed to provide easy access of crane hooks to the cathodes, which have to be lifted out with the harvest of metal from the process more frequently than the anodes have to be moved. Use of copper-cored titanium solves many of the problems but there is a limit to the amount of this comparatively expensive composite that can economically be employed.

The cross section of titanium needed to carry current into a titanium starter blank or cathode is found by experience to be about 3 mm^2 per amp. The design of a basket anode is more complicated and to establish design limits it was necessary to carry out tests under realistic conditions. In order to do this tests have been carried out to measure the temperature rise on an actual basket when the appropriate current is passed through it. Clearly the basket should be immersed in electrolyte at the right temperature to the appropriate depth and have a cathode each side of it to simulate the thermal environment it will encounter in the tank house. As an example of the use of this approach, Figure 3 shows the effect of varying design on the temperature of the titanium in the hottest area of the hanger bar for a basket of the sort shown in Figure 2. Obviously design has a profound influence on the way heat is dissipated from the titanium structure, but in general a current carrying cross section of between 1.5 and 3 mm^2/A is necessary.

Summary and Conclusion

Laboratory trials on titanium basket anodes for the refining and winning of metals, in particular copper and cobalt, have given very encouraging results. Different basket designs from those used in electroplating are required. Laboratory tests have revealed compositions of titanium based materials that are sufficiently promising as particulate anode material in titanium baskets to justify plant trials in cobalt and copper winning. The search for materials with better properties continues.

RECENT ADVANCES IN TITANIUM CATHODES

B. W. H. Lowe, J. R. B. Gilbert, and G. E. Moore

Imperial Metal Industries (Kynoch) Ltd.
Birmingham B6 7BA, England

Introduction

Cathodes made of titanium are nowadays commonplace for receiving electrodeposits of copper manganese and gold as part of the processes for winning or refining these metals.

In copper refining, which has so far proved the largest market, it is mainly starter sheets rather than full weight cathodes that are grown on titanium blanks. Approximately 60,000 titanium starter sheet blanks are now in use at about 50 refineries throughout the world. The advantages of titanium blanks are well known, their corrosion resistance, their ease of stripping, the better yield and better quality of the copper starter sheets they produce and the elimination of the daily application of a parting agent. Furthermore, all aspects of their performance are being continuously improved. Recent minor advances have been made in control of surface topography and the type of surface oxide film which has previously been shown (1) has a profound effect on nucleation of electrodeposits on titanium and their adherence to it.

A major advance has now been made in techniques for joining titanium sheet to copper hanger bars. It became apparent quite early in the development of titanium blanks that it is much easier to make a satisfactory electrical joint between a copper hanger bar and a copper sheet than it is between a copper hanger bar and a titanium sheet. Advances in these joining techniques are discussed in this paper.

Mechanical Joints

Because of the ease of making good contact between copper bars and copper sheets it was common to use a method of construction in which the top of the copper starter sheet blank was sandwiched between two copper bars, the assembly being clamped together by means of bolts or rivets. However, when this system was applied to titanium sheets, very rapid deterioration of the joint occurred because electrolyte, falling from sheets just removed from the electrolytic cell, was able to enter the interface between the titanium and the copper. Thus corrosion products were very rapidly formed in this important area, leading to increased joint resistance and power dissipation with an attendant and unacceptable rise in temperature. To avoid this problem a series of slotted copper hanger bars was produced which have a closed top, and relatively thin legs through which they can be brought into contact with the titanium sheet by copper rivets or stainless steel bolts. But, although this type of joint has proved quite satisfactory provided the overall current is kept below 250 A/m^2, there are several reasons why it is desirable to have an improved form of joint.

In any type of mechanical joint, efficient current transference (which is synonymous with low joint resistance) between copper and titanium relies heavily on the contact pressure between the two metals, coupled with the maintenance of clean surfaces. This is clearly illustrated by the results of tests in which a thin sheet of titanium was clamped between two copper blocks of 320 mm^2 nominal area and the voltage drop across the joint was measured for a 40 amp current whilst the clamping load was increased. As figure 1 shows, the joint resistance is quite sensitive to contact pressure and, to a much greater extent, to cleanliness.

If one considers the thermal stresses in the copper at the contact points in a hanger bar joint, due to differences between the coefficients of thermal expansion of titanium, copper and stainless steel, it can be seen that mechanical joints must inevitably loosen after a period of time. This effect is of course less serious when making copper-to-copper joints. Once a joint starts to loosen, electrolyte can enter the gap by capillary action and a galvanic couple will arise, causing corrosion products to build up at the vital contact area. The resistance of the joint will then increase and thus the temperature will rise, further relaxation will take place and the joint will fail quite rapidly.

The joint employing stainless steel bolts is vulnerable to deterioration for a variety of reasons. If the mode of operation of such a joint is considered in detail, several points become apparent. In the first place, the bolt shanks are not in contact with the titanium sheet (and therefore carry no current) since they are fitted into clearance holes; thus, current transfer between copper and titanium can occur only via the interfacial areas that are

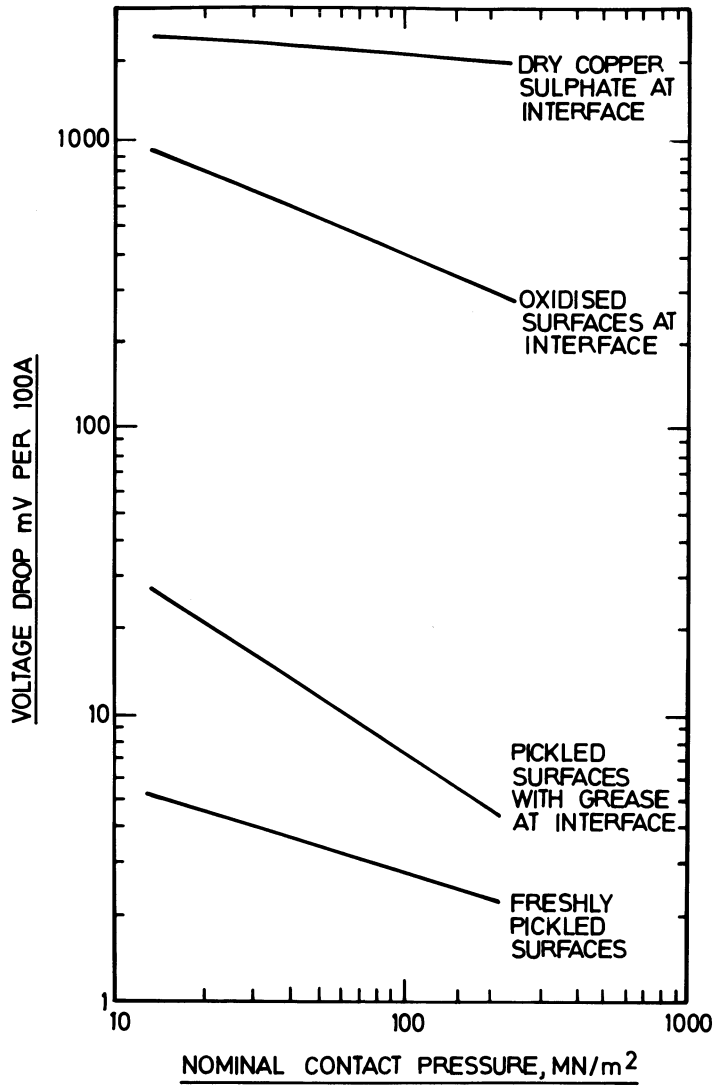

Fig. 1 - Effect of contact pressure between copper and titanium on voltage drop for various surface conditions.

brought into contact when the bolts are tightened. These areas are highly localised around the bolt holes; elsewhere in the joint there may actually be a gap between the copper and titanium surfaces, into which electrolyte is free to enter, even with a freshly made assembly. Another important point is that a significant proportion of the bolting load may be expended non-usefully in merely bending the legs of a slotted copper hanger bar before good contact with the sheet has been established. This will obviously be a function of the bar geometry and of the initial clearance between the slot and the sheet. In laboratory simulation tests on a bolted joint (using 9.5 mm diameter bolts, a size usually employed) the volt drop was measured after the bolts had been tightened to various torque values, from which the bolt loads could be deduced.

As indicated in Figure 2, volt drop is fairly sensitive to load or tightening torque. Also shown in Figure 2 is a plot obtained by loading the legs of an empty hanger bar of fairly "stiff" design and measuring the corresponding decrease in slot width at the loading position. It can be seen, for example, that for a load of 12.5 kN, which is about 50% of the safe load that a 9.5 mm bolt could carry, the slot width has decreased by only 0.3 mm. This is not a large amount in relation to the possible sheet/slot clearance that may be present initially as a result of manufacturing tolerances. With a newly made joint, it is the usual practice to tighten the bolts to a level that corresponds to the maximum safe working value, ie so that the tensile stress in the bolt is about 80% of the yield strength of the bolt material. (For a 9.5 mm bolt this would be equivalent to a tightening torque of just over 40 Nm giving a bolt tension of about 25 kN). If this level is significantly exceeded in service, for example as a result of differential thermal expansions, handling, etc then the bolt(s) will yield and the joint will relax. And since the mechanical properties of copper are not particularly high, it too will yield and cause further relaxation. Thus in a general sense a bolted joint could not be said to represent a particularly good desigh in this sort of application. And, even though some improvement can be obtained by attention to hanger bar design, and by increasing the number or size of the bolts, the principles underlying the shortcomings of such a joint remain.

In the case of a joint embodying copper rivets the same principles apply although the mode of operation is more complex. Here, in contrast to a bolt, the rivet itself plays a part in the transfer of current. Two current paths are possible: through the interface between titanium sheet and hanger bar slot, and also from the circumference of the hole in the sheet, via the rivet shank to the hanger bar. As might be expected it is the second one that plays the predominant role. There are two reasons for this. In the first place the clamping effect of a rivet is only slight in comparison to that of a bolt; whereas for a 9.5 mm bolt, as already mentioned, the clamping force may be initially up to 25 kN, with the same size of rivet the maximum force which the shank could sustain would be

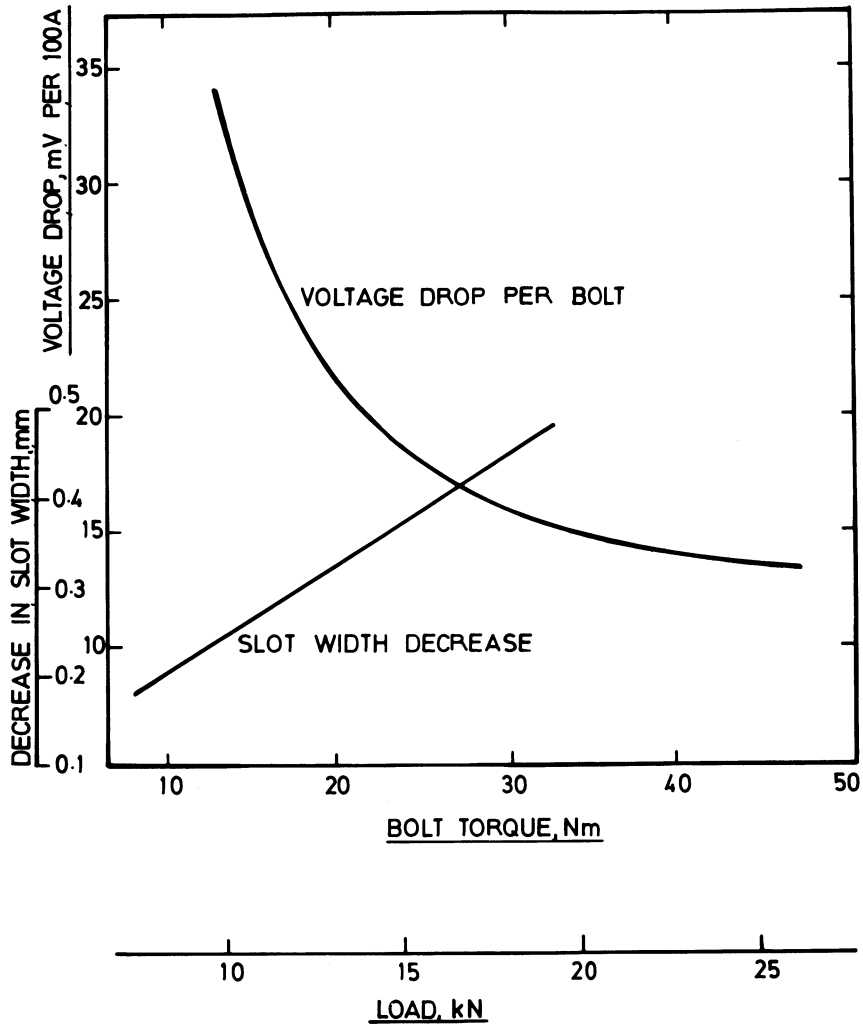

Fig. 2 - Effect of bolting-up torque on voltage drop and slot width for a joint with 9.5 mm diameter bolts.

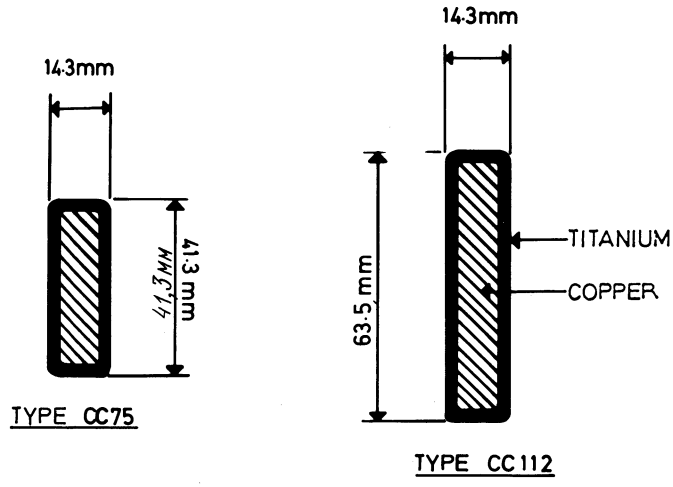

Fig. 3 - Examples of IMI copper/titanium composite bars, CC series.

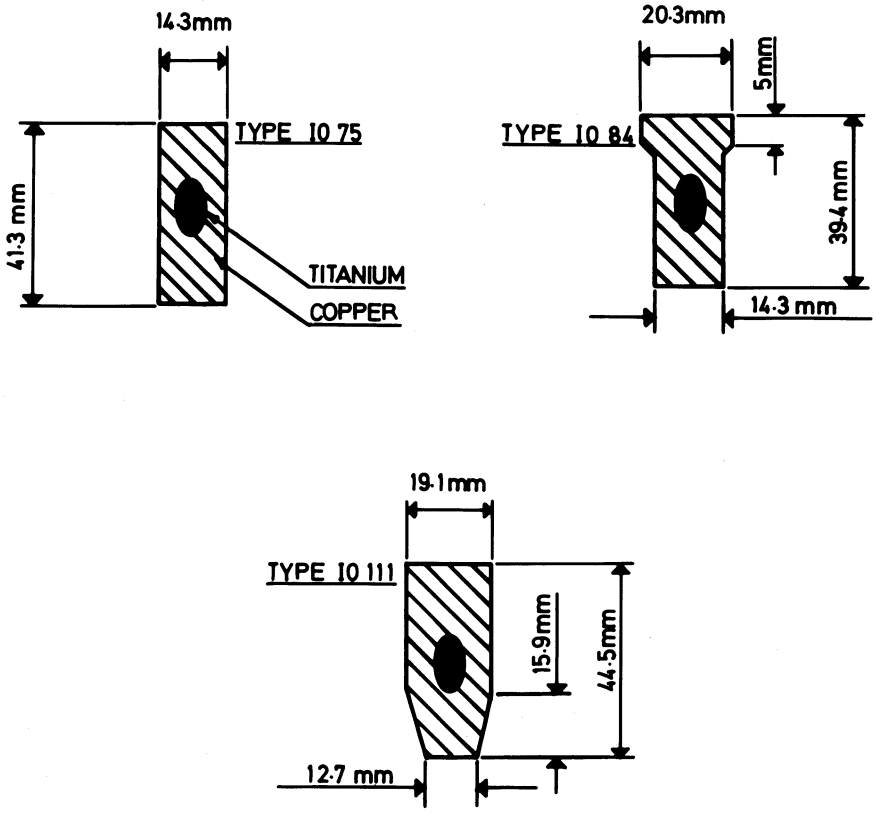

Fig. 4 - Examples of IMI copper/titanium composite bars, IO series.

only about half that value; therefore the face contact path is not very efficient. Secondly, when the rivet is "set", its shank expands and fills the hole tightly, and so good contact is established, at least initially. These points were confirmed by volt drop measurements made on three types of rivetted joint, using 6.3 mm diameter copper rivets: a standard joint, another with the rivet shank insulated, and a third in which the titanium sheet faces were insulated but the rivet shank was not. The volt drops for the standard and bare-shank joints were similar, but with the insulated shank a volt drop some eight times higher was recorded.

In service, therefore, the eventual failure of a rivetted joint is probably due to loosening of the rivet shanks in the holes through the titanium sheet, rather than to the loss of face contact that occurs with a bolted joint.

However, as with the bolts, the onset of loosening can undoubtedly be attributed to differential thermal expansions and perhaps handling damage.

With either type of joint, once loosening has occurred, some form of maintenance becomes necessary. In practice stainless steel bolts and nuts require re-tightening after between 6-12 months use, and rivets require re-fixing after 24-36 months.

At high current densities, above about 250 A/m^2, mechanical joints are not sufficiently stable, and break down after only a relatively short time. Additionally, even for lower current ratings, it is obviously desirable to eliminate the need for regular maintenance as labour costs continue to rise. Further, if the blanks in a cell have joints of differing electrical resistance, the current in that cell will be distributed unevenly between the starter sheet blanks and this will lead to copper starter sheets of differing thickness being produced.

What is required, therefore, is a permanent joint between titanium and copper, having good electrical conductivity, and mechanically strong enough to withstand the loads applied to it.

Permanent Joints

At first sight, fusion welding might seem the most suitable method to use. However, the alloys of copper and titanium that are necessarily formed during welding are extremely brittle; thus the direct welding of copper to titanium is not practicable.

Joints of limited ductility can be made if pure silver is used as an intermediate metal. But in practice a life of no more than six months was obtained under normal operating conditions for silver brazed joints, and in any case the use of pure silver is a relatively expensive solution.

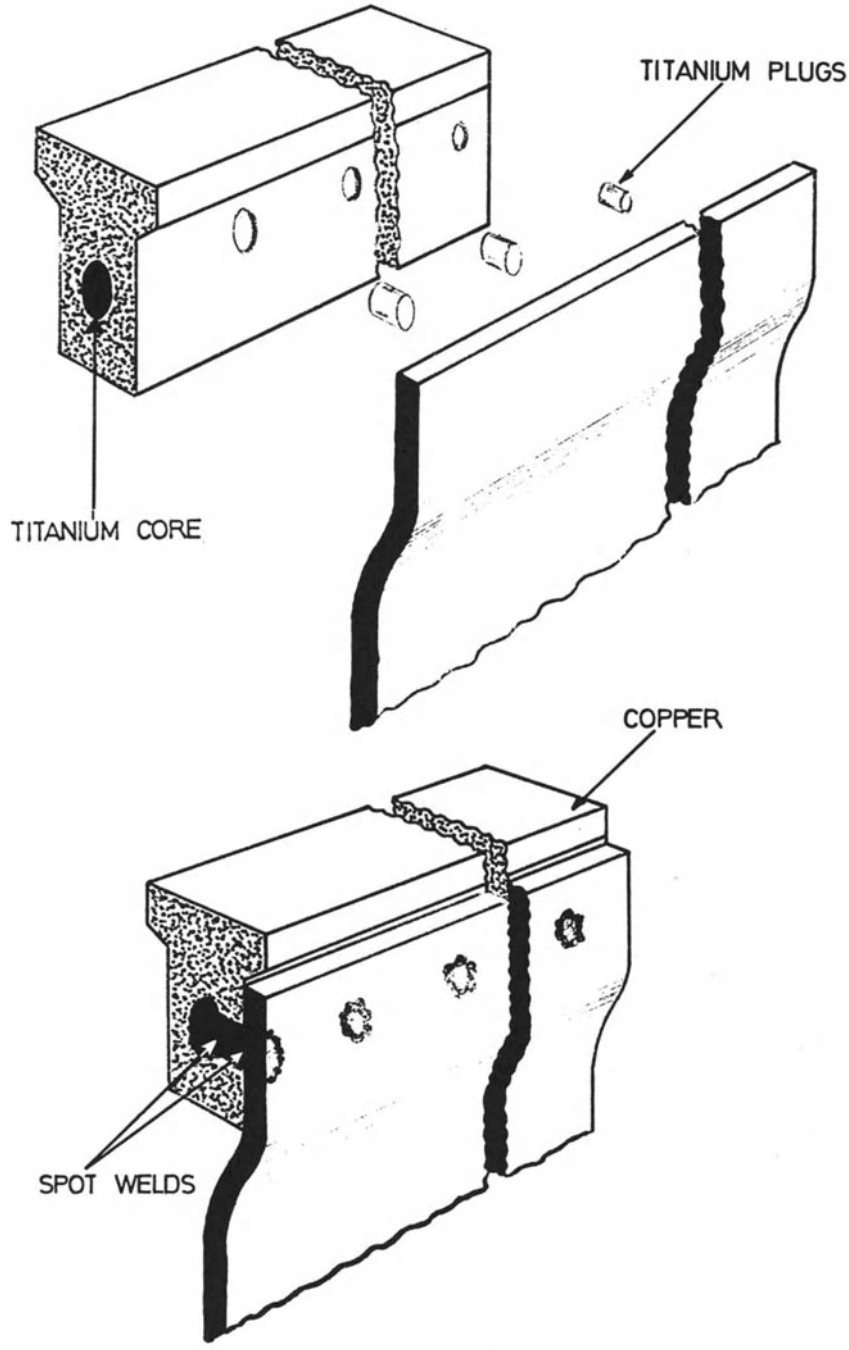

Fig. 5 - Procedure for spot welding with I0 series bars.

Soft soldering techniques have been devised, but these have failed due to the solder corroding, or melting when overheating occurred.

A solution to the problem has now been found by the use of composite copper/titanium hanger bars.

Copper Cored Titanium Bars

This type of bar consists of a solid core of copper covered by a continuous sheath of commercially pure titanium approximately 1.3 mm thick, the two components being metallurgically bonded together; examples are shown in Figure 3. Attachment to the starter sheet blank is secured by a series of up to 40 spot welds (titanium to titanium) each of which will carry at least 50A. For symmetry the top edge of the sheet is usually cut and cranked in such a way that spot welds are made to both faces of the hanger bar.

The joint when correctly made is capable of withstanding high mechanical and thermal stresses and is also able to pass very high overall currents. For example, in out-of-cell tests to compare the performance of spot welded and bolted joints, the results shown in Table 1 were obtained. In these tests a full size starter blank of each type was subjected to a range of impressed currents from 500 to 2500 A, with hanger bar temperature and joint voltage drop being measured at selected positions. Despite the fact that the bolted construction embodied a solid rectangular copper hanger bar of cross-sectional area about 40% greater than that of the spot welded titanium-clad one, its performance was clearly inferior.

Table 1

Current A	Equilibrium Temperature of Hanger Bar, °C		Voltage Drop on Joint mV	
	Spot Welded	Bolted	Spot Welded	Bolted
500	27	33	8	14
1000	50	68	16	32
1500	82	98	30	46
2000	109	159	44	87
2500	164	212	72	126

From the user's viewpoint, it might be argued that starter blank assemblies involving a "permanent" joint are at a disadvantage

compared to those with mechanical joints since the latter are readily disassembled should it become necessary to replace the starter sheet blank or hanger bar. In practice this is not the case, since spot welded joints can also be disassembled by removing the weld nuggets with a flat-ended drill, and then re-made by spot welding at new locations.

Other minor criticisms of the titanium-clad bar, which are perhaps more valid, are first that it is difficult to produce in cross-sectional shapes of greater complexity than simple rectangles; secondly it is relatively expensive; and thirdly the titanium has to be locally removed at the end to provide good copper-to-copper contact with the bus-bar.

In order to overcome these objections, further development work has recently been carried out on titanium/copper composite, and this has led to the manufacture of the I/O series of bars described in the next section.

Titanium-Cored Copper Bars

With this type of bar, the titanium element, which is necessary to permit permanent attachment to the starter sheet blank is positioned within the copper (and is again metallurgically bonded to it), instead of being on the surface. Superficially, therefore, the product is indistinguishable from solid drawn copper bar, and can within limits be manufactured in comparable shapes and sizes with corresponding dimensional accuracy and smoothness. Some examples are shown in Figure 4.

Permanent attachment to the starter sheet blank is again obtained by spot welding; the titanium core of the bar is exposed by drilling a series of flat-bottomed holes into the copper, small cylindrical slugs of titanium are inserted, and the assembly is then completed by spot welding on the sheet in one operation, as shown in Figure 5.

Field trials on blanks equipped with this type of bar have been in progress for 18 months and equivalent performance to titanium clad copper bars has been obtained.

Concluding Remarks

There seems no doubt that titanium will be used increasingly as a cathode material in electrowinning and refining. It is therefore important that totally reliable yet economical methods should be available to provide titanium/copper joints of high current-carrying capability with minimal power loss.

This paper has sought to show that mechanical methods of attachment are inherently unable to fulfil such requirements, and so these methods must be regarded as obsolescent.

The provision of a current path from the copper of the hanger bar to the titanium cathode via metallurgically bonded interfaces, which has been made possible by the development of the composite hanger bars that have been described, is therefore seen as a major advance.

Reference

(1) "Nucleation and Growth of Copper Electrodeposits on Titanium"
A G Ives, J R B Gilbert, J P A Wortley
Paper presented at 103rd Annual Meeting AIME, Dallas
25 February 1974

Discussion

Section XI. Titanium Alloys for Engineering Purposes

The critical reviewer, C. Edeleanu, was asked questions concerning economic efficiency of chemical industry applications of titanium and experiences in titanium usage for lining purposes.

C. Edeleanu answered that, according to the available data, titanium parts are only 1.1-1.5 costlier than similar stainless steel parts, but when reliability and life expectancy of titanium parts is considered, titanium can be classified as the most inexpensive material for these purposes. C. Edeleanu also noted that he was aware of many uria reactors where titanium had been used as a lining.

The critical reviewer, S. G. Glasunov, was asked about titanium applications in zinc plants. S. G. Glasunov reported that titanium application in thi field was a great success.

G. Sorkin was asked about the use of the Ti-6Al-4V alloy in ship building and its efficiency. G. Sorkin answered that expermental work is being currently carried out indicating high corrosion and pitting resistance of the parts from this alloy.

B. de Gélas was asked about maximum strength of titanium alloys which can be used in components and fabricated structures. B. de Gélas answered that the problem of optimal tensile strength should not be considered without taking into account other characteristics (yield strength, fracture toughness) and the answer is usually a compromise between different parameters for every specific case.

B. A. Kaschuk was asked to specify rare earth element concentrations used in the study and the form these elements are to be found in the alloys.

V. A. Kaschuk gave a brief account of the results presented in the report.

The speakers discussed on various aspects of the development and use of titanium alloys for different service conditions.

E. A. Borisova treated the problem of titanium alloy cleanliness from the point of view of impurity effects on performance

efficiency and reliability of finished products. He stressed the need to specify impurity concentrations, especially in high strength weldable titanium alloys.

A. I. Khorev, in his presentation, covered the problem of developing new high-strength titanium alloys. Included was the problem of complex alloying which had been thoroughly examined in his report.

V. N. Moiseev has described various aspects of development of new alloys, including their manufacture. He examined, as an example, the experience gained in creating a "self-hardening" titanium alloy for heavy-weight welded structures. By heat hardening components from this alloy in argon vacuum furnaces, it is possible to fabricate welded high-strength structures in a non-iodized fully stress-relieved condition, without any distortion.

V. N. Moiseev also described development of the BT-16 alloy which has improved processing characteristics; use of this alloy contributed to a rapid development of mass production of inexpensive fasteners.

G. Sorkin, in his presentation, pointed to the need to use the research results to which the present conference reports have been dedicated as regards specifications, standards and other technological documents promoting titanium use in various fields of technology.

Critical Review

POWDER METALLURGY OF TITANIUM

V. S. Arunachalam

Defence Metallurgical Research Laboratory
Hyderabad, India

INTRODUCTION

Powder metallurgy offers an attractive alternate strategy for producing titanium parts. The advantages include an efficient material utilization, near-net shape products with better mechanical properties. It is not without significance that the initial pioneering experiments by the U.S. Bureau of Mines were first in producing titanium powder compacts. Interstitial pick-up encountered during reduction prevented the exploitation of the powder route. Early experiments on the production of titanium powder during the metal reduction stage itself were carried out in the Soviet Union using the calcium hydride process. These efforts were only marginally successful because of impurity pick-up during reduction. More than anything else, non-availability of a good quality powder is responsible for titanium powder metallurgy remaining dormant for a number of years.

Now, this scene has changed. Methods are available today which can produce quality powder with acceptable interstitial content. These techniques are largely derived from centrifugal atomization. In addition to producing high purity titanium powder, successful consolidation techniques have now been developed for compacting to theoretical densities. Fully dense titanium powder products are mandatory for their large scale utilization as most of the components find their way to aerospace industry. Hot Isostatic Pressing to near-net shape, or Hot Isostatic Pressing, followed by isothermal forging, are two established routes available for compaction. Other routes of fabrication include hot swaging, hot extrusion and vacuum hot pressing.

In this paper we shall consider various powder production routes that have come in vogue recently as also the consolidation techniques. We shall also review some results that have been obtained on the mechanical properties of the powder products. The economics of the powder route is also discussed as this would determine whether titanium powder metallurgy would be commercially viable or not.

TITANIUM POWDER PRODUCTION

Even though there are a number of methods available to produce titanium powder, there are only two routes that hold promise for producing quality powder. These are: Hydride - dehydride route and centrifugal atomization. The first method involves producing titanium hydride, comminuting it to powder which is subsequently dehydrided in vacuum followed by further comminution. The dehydrided powder could be used for pressing and sintering. It is also possible to use the hydride powder itself for hot pressing in vacuum where dehydriding and consolidation could go together.(1) There are some disadvantages in hydride - dehydride process:

Dehydriding generally involves considerable time, running to almost thirty hours and this route does not guarantee the prevention of interstitial pick-up during powder manufacture. Powder shapes are not spherical leading to poor green strength and tap density.

Conventional inert gas atomization is not possible for titanium and its alloys because of the difficulty of containing liquid titanium. The need for newer methods for producing liquid droplets of titanium for solidification has led to the development of the Rotating Electrode Process (REP). This process in its simplest detail involves the rotation of consumable titanium electrode in a chamber filled with inert gas. Arc is struck between this electrode and a non-consumable tungsten electrode leading to the melting of the consumable titanium. The centrifugal force exerted on the rotating rod is sufficient to make the liquid metal fly in the form of fine droplets, solidifying into spherical micro-castings. This technique is the first one to have produced quality powder with acceptable interstitial content. A disadvantage is that large quantity of powder could not be produced and the process would only be of batch type. Secondly, the tungsten electrode which is stationary during atomization also contributes to some tungsten pick-up in the powder. Recently, there have been a number of modifications to the REP process. The first one is to store a number of electrodes either in the chamber itself, or alter the feeding mechanism to bring in a continuous supply of electrodes ensuring a semicontinuous production of powder. These modifications could lead to a capability of producing about 2 tons of titanium per week. Further modifica-

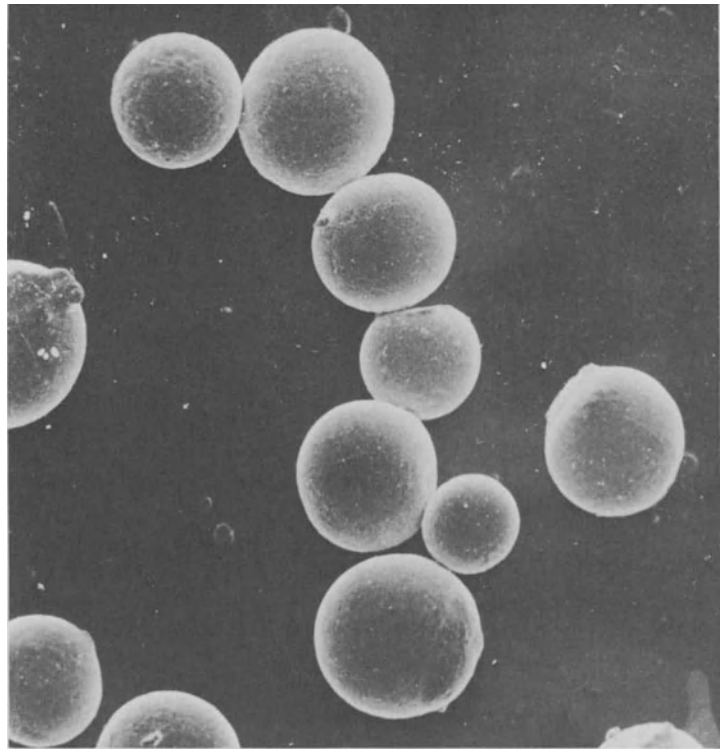

Fig. 1 - A typical spherical fraction (200 microns approx) of titanium powder obtained through spin disc atomization.

tions have included the removal of tungsten electrode and the replacement of tungsten electrode by another titanium rod. By this process, the tungsten pick-up is totally eliminated. A newer innovation of this process at Nuclear Metals consists of rotation of both the rods resulting in the melting of both the electrodes.[2] Scaling up of this process could lead to a larger production of titanium powder by the REP route itself.

The REP machine using a plasma source for melting has been designed and developed in the Soviet Union at the All-Union Institute of Light metals & Alloys.[3] This equipment, which is not dissimilar to the REP equipment in the U.S., can melt titanium powder at a rate of two kilograms per minute and tungsten pick-up during atomization is avoided by not using tungsten electrodes. The purity of the powder also appears to be reasonable with the oxygen content lower than 1000 ppm.

A variation of the REP process is the Centrifugal Shot Casting (CSC) developed at AERE Harwell, Great Britain.[4] In this process, the crucible containing liquid metal is rotated instead of the electrode. By this rotation the liquid metal crawls up to the tip of the crucible and flies away. This process may have advantages especially in melting refractories as also in not needing stringent dynamic balancing of the electrodes for melting. The disadvantage is the production of various types of powder ranging from spheres to ligaments. Spheres constitute only a fraction of the total yield.

A process that we have been working in India for a number of years involves the utilization of electron beam for melting titanium in conjunction with spin disc atomization for producing titanium powder. In the first process, titanium sponge was melted in a water cooled crucible and the crucible was tilted so that the liquid metal could fall into a fast rotating water cooled disc.[5] The yield in this process was poor, barely exceeding 60% and the impurity pick-up was significant, especially the chlorides. These impurities contaminated the chamber interior walls resulting in continuous contamination in subsequent experiments as well. A typical scanning electron micrograph of the spherical powder produced in these experiments is shown in Figure 1.

In the second process, a vertically mounted titanium rod,which could either be a compressed sponge or a cast-and-forged round, is rotated at a high speed when the surface is melted by the electron beam. This is identical to the REP except that the melting process is through the electron beam and the liquid droplets have to cool in vacuum rather than in an inert gas medium. Another small modification is the feeding of consumable rod from the bottom of the setup which facilitates an almost continuous feed. Experiments in this system have produced largely spherical particles with a narrow size

range (between 150 to about 500 microns).[6] If the consumable rod were compressed sponge, there were occasional massive particles arising from a decohesion of small particles in the sponge upon the electron beam impingement.

Using the electron beam technique for powder atomization has been pioneered by Stephan and his co-workers at Leybold-Heraeus in Germany. They have shown that for making powder production economical, it is necessary to produce large ingots which could later be atomized by the electron beam. These large bars could be cast by skull melting the scrap with consumable electrode of compressed sponge melting over the molten scrap. By tilting the skull, it is possible to cast large ingots which could later be used as the consumable rod for producing powder. In this process the diameter of the rod could be around 250 mm and the length could be as high as 5000 mm. The maximum atomization speed could be 5 Kg/minute.[7] Although it is claimed that by adjusting operating parameters hundred percent spherical particles could be produced in this process of disc atomization, it is likely that this technique could more easily lead to a mixture of spherical powders and flakes, rather than spheres only. The tap density of spherical powder works out to be about 60% of which the flakes approximate to about 28%. This process is now being scaled up to produce titanium powder of high purity at acceptable price range.

CONSOLIDATION OF TITANIUM POWDER

Earlier experiments on the consolidation of titanium powder were limited to pressing-sintering operation, and only occasionally novel techniques like spark sintering and explosive compacting were attempted to produce titanium compacts of near theoretical density. As the major usage of titanium structural parts is still in the aerospace industry, and as the components could be load bearing members, it is necessary that the consolidated and sintered titanium compact has not only high density but theoretical density.

This condition has practically eliminated all routes except hot pressing, hot isostatic pressing, hot extrusion and hot swaging. The hot pressing method has been attempted successfully for consolidating titanium powder to theoretical density both in the hydrided and in the dehydrided condition. Experiments by Mallik have shown that good theoretical density with reduced oxygen pick-up could be obtained when hydride powder is hot pressed.[1] Compared to this, hot pressed dehydrided powder comes only second best.

Hot extrusion with a blank die has been used for consolidating the titanium powder. With a proper choice of temperature and extrusion ratio, it is possible to obtain theoretical density on extruded preforms. A number of experiments conducted in the U.S. have shown

that theoretical density could be obtained when cans containing spherical titanium powder particles are extruded near beta transus.[8]

With increasing availability of Hot Isostatic Press (HIP), numerous experiments are now being carried out to consolidate titanium powder using autoclaves. For consolidation, the particles are filled into a can and the can is subsequently evacuated and sealed by welding. This is later subjected to isostatic gas pressure ranging up to 2 kilo bars at temperatures over 1000°C. The experiments using this route have shown that titanium compacts of theoretical density could be obtained when the cans are consolidated around one kilo bar pressure at temperatures around 800°C. HIP'd ingots can later be forged through isothermal forging to final shapes. The attraction of HIP lies in its potential to produce directly near-net shape components at theoretical density. In this process, there need be no further forging and the component could be ready after HIP-ing is to be followed by isothermal forging.

Recently there have been a number of experiments to test the quality of powder and also its potentiality to achieve the desired mechanical properties by consolidation. Two experiments in this connection are worthy of attention: One is the technique developed by Birla and DePierre[9] which involves hot swaging of a can containing powder particles. It is possible to obtain through this route the required densities and test the efficacy of the powder and its consolidation characteristics by preparing tensile samples from the swaged powder preforms. The other experiment was concerned with the Hot Isostatic Pressing of REP powder versus the dehydrided powder. These experiments conducted at Nuclear Metals, Inc. have shown that REP powder generally consolidated to preforms with better ductility and fracture toughness than dehydrided ones (Table I).[8] Similar experiments on Hot Isostatic Pressing of REP and centrifugally shot cast powder have been carried out.[10] These results showed that both these powders consolidate in a similar manner.

While Hot Isostatic Pressing is considered for producing preforms with theoretical density, there are also instances where Hot Isostatic Pressing appears to be the only route for producing preforms. A case in point is the recent development of titanium aluminides. As these intermetallics are brittle, casting and forging them to required shapes becomes impossible. Components from these intermetallics thus have to come from powder consolidation by Hot Isostatic Pressing. Hot Isostatic Pressing of TiAl is now being carried out from REP powder to assess its suitability for high temperature applications.[11]

TABLE I

	HIP CONDITIONS Time/Temp/Pressure			TENSILE				FRACTURE	
	hr	°F	ksi	u(Ksi)	y(Ksi[a])	% E[b]	%RA	WA (in-lb/in^2)	K_C^c Ksi.in$^{1/2}$
	1/2	1780	15						
R.E.P. Powder				138.6	132.0	18.8	40.2	447	36
"				138.3	132.7	19.6	40.6	339	34
Hydride-Dehydride				147.0	142.4	7.9	12.4	202	26
"				148.2	144.7	5.3	9.0	-	-
	2	1780	7.5						
R.E.P. Powder				138.2	132.2	18.3	38.9	369	32
"				138.0	132.1	18.4	39.2	410	32
Hydride-Dehydride				147.6	143.1	8.0	10.4	157	23
"				147.0	144.5	5.0	9.0	130	23

a. 0.2 percent offset
b. one inch gage length
c. crack propagating in a direction perpendicular to forging axis and in a plane parallel to it.

MECHANICAL PROPERTIES

As the purity of powder has reached acceptable limits and as HIP is capable of giving components of total theoretical density, it is important that the mechanical properties of powder preforms are also evaluated to confirm the acceptance of the powder metallurgy route for producing components for load bearing applications.

Recent experiments on the mechanical properties have shown that, generally, components produced through the powder route have the same yield strength and ultimate tensile strength with good ductility as their wrought counterparts. Experiments on Beta III titanium alloy have shown that the fracture toughness of the powder preforms could be higher than the forged samples.(12) An important point that has to be considered in evaluating the mechanical properties is the microstructure generated during the hot pressing of the powder preforms. It has been suggested that any difference in the mechanical properties between forged and powder stocks could be traced to the microstructures, rather than to differences in the method of manufacture.

A significant shortcoming as far as mechanical properties are concerned is the low fatigue strength of the powder products. Most of the powder components are having lower fatigue properties both in notched samples as well as in smooth specimens. This has been observed in the Beta III as well as in Ti-6Al-4V alloy.(13,14) Poor fatigue strength could perhaps be traced back to abnormal fracture initiation in powder components at inclusions and at regions of inhomogeneity. Considering that about 85% of the total life of the component is associated with generation of a critical crack and only 15% with respect to its propagation, it is necessary that crack initiation sites are identified and eliminated from the powder preforms. This, in turn, would call for producing higher purity powder of slightly larger sizes and extreme care in handling, canning, and in welding the powder cans. Oxide inclusions, or even high oxygen pickup would affect the local microstructure significantly leading to heterogeneity and subsequent crack initiation. There are a number of experiments now underway to examine the cause for a low fatigue strength. Irrespective of these experiments, it is safe to suggest that by exercising extreme care in preparing and handling powders, it is possible to reduce heterogeneity in the microstructure. Elimination of tungsten in the powder would also help in this direction. When conditions are optimized for producing powders of high purity and in handling them, it is likely that the fatigue life could exceed that of the forged products because of the chemical homogeneity of powder products.

ECONOMICS

There have been a number of articles discussing the economic advantages of the powder metallurgy route in titanium.[15] This advantage can be significant in titanium because of a very poor utilization of metal: Almost 80% of the material ends as scrap. Powder route by its inherent advantage of minimal scrap can offer significant cost advantages in titanium technology. Unfortunately, this is yet to materialize. For one thing, titanium powder is produced from melted, forged and machined rods and not directly from sponge and this results in a considerable price hike. To make titanium powder route competitive, it is necessary that the powder price comes down at least to that of ingot price. This is possible only by utilizing a sizeable percentage of scrap in producing powder and by fabricating large size ingots for atomization. This is being attempted by Stephan and his colleagues in West Germany. If powder could be produced directly from sponge, then the cost advantage could be very significant indeed. Volatile impurities are mainly responsible for making this route difficult. A greater utilization of titanium powder would also bring down the cost. The world consumption today barely amounts to 100 tons per year. Compared to the production of ingots, this is a very small fraction.

Lastly, there is a case for a second look on producing titanium powder chemically. Reduction of $TiCl_4$ or TiO_2 to high purity titanium powder, if achieved directly and economically, would bring in a much needed breakthrough to titanium powder metallurgy.

ACKNOWLEDGMENT

The author is grateful to Dr. H. Stephan, Dr. M. J. Blackburn, Dr. H. A. Lipsitt, Mr. G. I. Friedman, Dr. N. C. Birla and Professor O. V. Roman for discussing various aspects of titanium powder metallurgy with him. He expresses his sincere appreciation to his colleagues at the National Aeronautical Laboratory, especially Dr. A. C. Raghuram, Dr. R. V. Krishnan and Sri Sundaresan for stimulating discussions on titanium extending over a period of years.

REFERENCES

1. Mallik, R. K., Progress in Powder Matallurgy 1975, Ed. by G. D. Smith, Metal Powder Industries Federation, p 277 (1975).

2. Friedman, G. I. Private communication.

3. Bochvar, G. A. et al. Proceedings of the Third International Conference on Titanium, Moscow (1976).

4. Hodkin, D. J. et al, Powder Met. 16 (32), pp 277 (1973).

5. Arunachalam, V. S. et al. Proceedings of the Symposium on Powder Metallurgy - 1973, Minsk U.S.S.R. (1973).

6. Raghuram, A. C. et al. Proceedings of the 29th Annual Meeting of the Indian Institute of Metals, Jamshedpur (1975).

7. Stephan, H.,Proceedings of the AGARD Meeting on Advanced Fabrication Techniques in Powder Metallurgy and Their Economic Implications, Ottawa (1976).

8. Friedman, G. I., Air Force Materials Laboratory Erport AFML-TR-75-9 (1975).

9. Birla, N. and DePierre, V., Air Force Materials Laboratory Report AFML-TR-75-171 (1975).

10. Vaughan, R. F. et al, Proceedings of the AGARD Meeting on Advanced Fabrication Techniques in Powder Metallurgy and Their Economic Implications, Ottawa (1976).

11. Lipsitt, H. A. Private communication.

12. Birla, N. C. et al, Air Force Materials Laboratory Report AFML-TR-76-22 (1976).

13. Birla, N.C. et al, AFML-TR-76-89 (1976).

14. Keinath, W., Proceedings of the AGARD Meeting on Advanced Fabrication Techniques in Powder Metallurgy and Their Economic Implications, Ottawa (1976).

15. Sutcliffe, P. W. et al, AGARD Report No. 627 (1975).

A NOVELTY IN THE FIELD OF TITANIUM POWDER METALLURGY

V. S. Ustinov, A. N. Petrunko, Yu. G. Olesov and R. K. Ognev

Titanium Institute

U.S.S.R.

When producing articles of titanium and titanium alloys by conventional technology, 70 to 80% of the input metal is lost as scrap between the ingot and the final product. The yield of usable product does not ordinarily exceed 20 to 25%.[1-2] Powder metallugy allows a four to five-fold increase in metal utilization and a one and one-half to two-fold decrease in labor consumption when machining articles, thus resulting in a savings of six to ten thousand roubles per ton of final product.[3]

Powder metallurgy permits the production of new types of articles which cannot be made by the conventional methods, for example, porous filter elements. Titanium filters as compared to ceramic filters are characterized by considerably higher mechanical strength, resistant to hydraulic and temperature shocks, and resistant to attack of most aggressive industrial media. With the benefits of increasing equipment life, enhancing equipment capacity and reducing losses of in-process material and products, the savings due to the application of porous titanium elements amounts to from 400 to 1000 roubles per year per $1m^2$ of articles.[4]

The production of filler electrode material for titanium welding can be effected by the extrusion of titanium powders (welding electrodes) or the mixture of powders and carbides and borides of metals (build-up electrodes) with a considerable simplification of technology, improvement of quality and lowering of their cost as compared to conventional methods.

A considerable economical effect is due to the direct use of titanium powders as fillers for corrosion-resisting coatings in

electrode and hard-alloy operations, alloying additives for high-manganese and carbon steels.[6] Titanium powder, for example, improves noticeably physico-chemical and mechanical properties of epoxide resin-based corrosion-resisting coatings. The application of powder as filler allowed use of these coatings as corrosion-proof coatings for metallic and reinforced constructional structures, gas conduits, galvanic baths and various equipment subjected to the attack of acids, alkalines, gases and condensates. The economical effect due to the application of 1t of titanium powder included in the composition of a coating attains 5-6 thousand roubles per year.[7]

There are many known variants of titanium powder production flow sheets.[8] Some of them - grinding of spongy and compact titanium, spraying of liquid metal - have been tested only in laboratory and large-sized laboratory scales. Others - calcium hydride reduction of titanium oxide and electrolysis of melts with a soluble titanium anode - have been put into practice and allow obtaining titanium powders which are applied in many engineering fields.

Titanium powders have been obtained by the reduction of titanium dioxide with calcium and calcium hydride.[9] This technique can also result in obtaining titanium-based alloy powders by calcium hydride reduction of the mixture of titanium oxides and alloying elements.

Pure titanium metal is notable for a high malleability and viscosity, which makes the operation of obtaining powders by mechanical grinding rather difficult. There has been developed the technique of obtaining titanium powders based on the utilization of highly brittle hydrogenated metal and relative simple transformations in the system of titanium-titanium hydride.[10] The main advantage of the method is the facilitation of grinding operation.

There is known the technique of obtaining titanium powders by spraying of liquid metal.[11] The technique consists in melting down a fast rotating rod of titanium or its alloys (up to 15 thousand revolutions per min.) in an electric arc. Molten metal drops thrown away by centrifugal force solidify in a protective atmosphere of argon or helium before they get to the chamber walls.

The recent time has seen the practice of the technique to produce titanium powders by electrolysis of melts with a solute anode of titanium wastes.[12] The main advantage of this process is the attainment of a high purity powder, as far as the impurities of concern, especially oxygen and nitrogen, as well as the possibility to regulate powder properties within wide limits by the change of electrolysis parameters.

Titanium powder particle shape is determined by the method of

Table I

Chemical Composition of Various Types of Titanium Powders

Type of powder	Fractional composition, mm	Content of impurities, mass %%					
		Iron	Chlorine	Nitrogen	Oxygen	Silicium	Hydrogen
Hydride-calcium reduced	-0,04	0,15-0,20	0,003--0,005	0,05--0,06	0,025--0,30	0,06--0,07	0,20 -0,40
Obtained by hydrogenation-dehydrogenation of titanium sponge Ti-100	-0,63+0,18	0,07--0,10	0,05--0,08	0,03--0,05	0,06--0,10	0,01--0,02	0,06--0,15
	-0,18	0,08--0,12	0,06--0,10	0,05--0,07	0,15--0,30	0,02--0,03	0,15--0,25
Electrolytic	-0,63+0,18	0,02--0,08	0,03--0,08	0,015--0,030	0,30--0,09	0,005--0,010	0,02--0,04
	-0,18	0,02--0,18	0,05--0,15	0,02--0,03	0,05--0,30	0,01--0,02	0,03--0,06

their obtaining: for powders obtained by spraying of liquid metal it is spherical or droplike; powders obtained by reduction have a spongy, porous structure; hydrogenated powders have a fragmented shape of particles and electrolytic powders - a dendritic one (treelike). Chemical composition and titanium powder properties also edpend on the technique of their obtaining (see Table I). The fields of powder application are determined bin the same way as well.[8]

Powder obtained by the reduction of titanium dioxide with calcium hydride is highly fine - divided and heavily contaminated with impurities: therefore, it is not fit for making structural articles by the methods of powder metallurgy and applied, on the main, as gas getters in electrovacuum industry.

The quality of titanium powder obtained by the method of hydrogenation - dehydrogenation depends on the purity of basic raw material. In the case of hydrogenation of high quality titanium sponge, the obtained powders contain few impurities and are fit for making various articles by powder metallurgy methods. Because of an abrupt increase of a specific metal surface when milling titanium hydride and the inevitable formation of oxide films thereon, the content of gaseous impurities in dehydrogenated powder becomes higher as compared with basic titanium. The method of hydrogenation is expedient to be used in obtaining cheap powders of titanium scrap for consumers who do not make great demands of the content of gaseous impurities and technological properties of powders.

Powders of titanium and its alloys obtained by spraying of liquid metal are characterized by a high purity and a regular spherical shape of particles. They provide for a uniform structure and good physico-mechanical properties of articles, but can be treated only by the methods of hot pressing.

Electrolytic powders have the highest extent of purity as compared with other types of titanium powders. They have found a wide application in producing design parts of instruments, porous filter elements, gas getters (sprayed and unsprayed) having a high sorption power, and as basic raw material in producing titanium compounds (hydrides, carbides, nitrides and others).

Electrolytic titanium powders are used in producing small-sized design parts as bushes, flanges, lids, bush sleeves.[3] The content of impurities in basic powder must not exceed, weight%: iron - 0.06; oxygen - 0.08; hydrogen - 0.04. In sintered articles hydrogen content does not exceed 0.0008% and oxygen content - 0.14%.

The billets compacted at a pressure of 6-7T/cm^2 are sintered in vacuum having a residual pressure of 10^{-3} - 10^{-4} Torr at a temp-

Table II

Porosity of Sintered Articles

Parameters	-0,5+0,25			-0,25+0,044			-0,044		
Compaction pressure, kg/cm^2	1600	2700	5400	1600	2700	5400	1600	2700	5400
Density: g/cm^3	2,99	3,52	3,91	2,77	3,51	3,50	2,85	3,50	3,95
%of theoretical	67,10	79,10	87,86	62,24	78,87	87,64	64,04	78,65	88,76

Table III

Properties of Titanium Filter Elements

Parameters	Groups				
	1	2	3	4	5
Pores main diameter, mm	30-50	50-80	80-110	110-180	180-300
Porosity, %	30-35	35-40	35-40	40-45	45-50
Permeability coefficient, no less than, pm^2	0,5	15	20	30	40

erature of 1100-1150°C.

Sintered parts are machined according to 7-8 classes of purity and the first class tolerances. The recent time has shown the possibility to produce tubes of electrolytic powders by the methods of hot pressing. The properties of these tubes are approximate to those of tubes of cast metal.[13]

Filter elements of titanium powders can be made as tubes and bands (4;8). Tubular filter elements are made with a diameter from 20 to 120mm and a length up to 1000mm with wall thickness from 2 to 10mm, and porous mill product of a size of 300 x 600mm and 600 x 600, from 1 to 5mm thick. Elements are tooled by metal-cutting machines and welded by argonarc, contact and diffusion welding.

The change of pressing and sintering conditions as well as particle size distribution of basic powder enables regulating within wide limits the porosity and, thus, the throughput of filters. The data concerning the dependence of article porosity on powder particle size and compaction pressure are given in Table II. A considerable influence on article porosity is due to sintering conditions. As sintering temperature rises the physico-mechanical properties of articles become improved and the porosity becomes reduced.

The data on main properties of titanium filter elements are represented in Table III. As consumers require, the porosity of filter elements is regulated within the limits of 30-50%, main diameter of pores from 10 to 300mu and strength limit, when tested under hydraulic pressure, from 10 - to 50kg/cm^2. With the view of enhancing filtration purity, increasing throughput, and improving regeneration, double-layer filters are produced. Titanium filter elements find a wide application in various designs of cartridge and candle filters, aerators built in the units for regeneration and benefication by flotation method, Bush filter, gas and liquid sprayers and gas getters.

The analysis of the results shows that the techno-economical efficiency of powder metallurgy methods appears especially clear when applicable to titanium. This efficiency is shown by such parameters as a marked reduction of specific metal consumption, lessening of labor consumption, lowering of costs of semi-finished and finished articles. Titanium powder metallurgy permits making of new types of materials and articles possessing high physico-chemical and mechanical properties.

REFERENCES

1. Dobatkin, V. I., Anoshkin, N. F., Andreev, A. L. et al, Titanium alloys ingots, M., Metallurgia, 1966.

2. Galitsky, B. A., Abelev, M. M., Shwartz, G. L. et al, Titanium and its alloys in chemical machine-building, M., Mashinostroinie, 1968.

3. Voroviev, B. J., Olesov, U.G., Ustinov, B. S. et al, Making of serial structural parts of titanium powder by the metalloceramic method "Tsvetniye metalli," 1970, N 7, 65-66.

4. Olesov, U. G., Ognev, R. K. and Zapadnia, V. I., Large-sized titanium filters, "Tsvetniye matalli," 1968, N12, 84-85.

5. Dobatkin, V. I., Anoshkin, N. F., Andreev, A. L. et al, Titanium alloys ingots, M., Metallurgia, 1966.

6. Shitikov, V. S., Sherstiuk, A. A., Ognev, R. K. et al, Complex deoxidizers made of titanium production, "Liteynoe proizvodstvo," 1971, N6, 35-36.

7. Ognev, R. K., Zisman, E. B., Maximenko, V. M. et al, Corrosion resisting composition to protect constructional structures and technological equipment. "Industrial construction and engineering erections," 1975, N3, 19-21.

8. Ustinov, V. S., Olesov, R. G., Antipin, L. N., Drosdenko, V. A., M. Metallurgia, 1973.

9. Garmata, V. A., Gulianitsky, B. S., Kramnik, V. U. et al, Titanium metallurgy. M., Metallurgia, 1968.

10. Rubtsov, A. N., Olesov, U. G., Antonova, M. I., Hydrogenation of titanium materials. Kiev, Naukova dumka, 1970.

11. Glazunov, S. G., Solonina, O. P., Chereshneva, N. F, Dispersed granulation of metals and alloys. Selected Works. "Non-ferrous metals alloys." M. Nauka, 1972, 32-41.

12. Ustinov, V. S., Olesov, U. G., Antipin, L. N. et al, Pilot-industrial testing of titanium powders production by electrolysis of melts with a soluble anode. "Tsvetnije metalli, 1969, N12, 40-43.

13. Zhivov, L. I., Pavlov, V. A., Kolesnik, F. I. et al. Compaction of tube of metalloceramic titanium. "Tsvetniye metalli, 1971, N1, 69-70.

PRODUCTION OF DIE-FORGED DISCS FROM BT9 ALLOY POWDER

G. A. Bochvar, K. M. Borzetzovskaya, V. G. Govorov,
T. I. Bolotina and E. N. Bilibina

All-Union Institute of Light Alloys
U.S.S.R.

It is well known that one of the problems connected with the production of a homogeneous structure with good properties is to remove segregation associated with a cast structure. Increased productivity and reduced initial cost of the product calls for the use of high-capacity equipment and consequently leads to an increase in ingot size. However, an increased ingot diameter leads to increased heterogeneity of chemical composition, due to the processes of solidification and segregation and associated increased grain size and coarser second phases. Despite the fact that an increase in the ingot size results in an increase in the total reduction accompanying the fabrication of a given type of semi-finished product, the casting defects of a large-size ingot are generally liable to affect the product quality. The use of a powder approach eliminates completely the problem of segregation and coarse phases, since the as-cast powder structure may be optimum. It is formed in conditions of high solidification and cooling rates and results in homogeneous properties (Fig. 1). In addition, the fabrication of products from titanium alloys using the powder metallurgy approach makes it possible to reduce cost due to a lower labor consumption and higher output.

The present paper discusses the results of an investigation of the fabrication of a large-sized semi-finished product - a compressor die-forged disc - from high-temperature titanium alloy powder.

The processing steps used in the fabrication of products from powder includes the following: (1) production of powder; (2) encapsulating; (3) out-gassing and sealing; (4) compacting and (5) die-forging (if necessary).

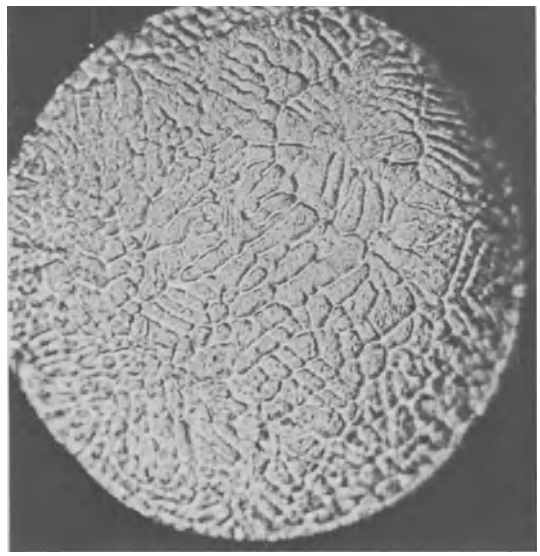

Fig. 1: Microstructure of BT9 titanium alloy powder, x 500

The powder used in the present work was obtained on the Soviet-made installation "BGY-2M" which features a unique melting design. This installation provides a large increase in the production capacity and decrease in the process cost involved in the fabrication of powder. The processing steps for the production of titanium alloy powder includes operations discussed in subsequent sections of this paper.

In the process twenty electrodes are cast in a skull furnace; this quantity being sufficient for two cycles on the powder making facility. The cast electrodes are conditioned, faced and converted to powder. The powder from ten electrodes is collected in a bin at the bottom of the installation. The installation is then opened, the powder unloaded from the bin and fed to an automatic screening set-up for sizing while the magazine is reloaded with the second set of ten electrodes.

The interstitial content in titanium alloy powders generally does not exceed that which is present in the starting electrodes. This is well illustrated in Table I.

Table II lists the results of a chemical analysis of the BT9 alloy powder, at various powder sizes. The alloying element content is practically the same in each case.

The data shown in Tables I and II suggests that the rotating electrode process (in which the titanium is melted) leads to a high-quality alloyed titanium powder exhibiting a homogeneous chemical composition.

The powder was compacted using a hydraulic press with a closed die. Prior to this the powder was placed in a capsule made of stainless steel and evacuated at a temperature of 500°C. The capsule containing the powder was heated at temperatures corresponding to the upper part of the $\alpha+\beta$ region. The pressure during compaction was 40 - 50kgm/mm^2. Using the closed die compaction method pieces from the BT9 and BT3-1 alloy powder with diameters of up to 400mm were obtained. After turning the compacted discs did not exhibit any cracks or other defects. The density of the discs throughout was close to the theoretical value with variations from 99.6 to 100%.

The macrostructure of the pieces fabricated from powder are homogeneous and fine-grained (Fig. 2), with the structure independent of the size of the product produced. The large pieces are characterized by a fine-grained structure, in direct contrast to the structure of vacuum electric-arc melting ingots of the same diameter. The structure is developed in the process of heating the powder for the subsequent hot compaction. The dendritic powder structure changes to a fine-grained mixture of α and β phases as a result of heating for the subsequent hot deformation. Comparison of the powder structure prior to compaction with that after compaction reveals that this process takes place without any noticeable deformation of the powder particles (Fig. 3).

When selecting the compaction temperature, it should be remembered that at higher temperatures diffusion welding, which is responsible for the joining together of the individual particles, will occur more rapidly. On the other hand, the compaction temperature should not exceed the temperature of the $\alpha+\beta/\beta$-transition temperature in order to prevent growth of the β-grain. The structure obtained by compaction at 900°C and 980°C is practically identical. But the pieces obtained at a higher temperature are characterized by greatly improved mechanical properties, and intergranular fracture is not observed. This is explained by the increased diffusion welding of separate particles. Table III lists the mechanical properties of pieces compacted at a temperature of 980°C.

Note the good plasticity characteristics and impact resistance which are approximately two times the required level. The values of the short-time and long-time fire resistance, in the operating temperatures range for the alloys under study, satisfy the requirements for ingot products.

There are possibly two techniques for producing powder parts. In one of them the product is fabricated directly by compaction of

Table I

Interstitial Contents of Electrode and Resulting Powder

Product	Interstitial Content, %		
	O_2	H_2	N_2
Electrode	0.10 - 0.11	0.001	0.02 - 0.03
Powder	0.09 - 0.14	0.009 - 0.01	0.02 - 0.03

Table II

Chemical Composition of BT9 Alloy Powder of Various Sizes

Powder size, mcm	Alloying element content, %			
	Aluminum	Molybdenum	Zirconium	Silicon
70	6.2	3.2	1.5	0.21
70 - 150	6.2	3.2	1.5	0.21
150 - 450	6.1	3.1	1.5	0.22
450 - 630	6.2	3.1	1.6	0.23
630 - 900	6.2	3.2	1.6	0.22

Table III

Mechanical Properties of Compacted Discs

Alloy	σ_b kg/mm^2	δ %	ψ %	a_H kg/cm^2	AT_4 kg/cm^2
BT9	103	16	35	3.8	1.46
	104	16	35	3.6	1.42
	105	12	37	3.8	1.42
BT3-1	114	20	42	4.3	1.03
	113	19	40	4.6	1.12
	115	16	47	-	-

Table IV

Mechanical Properties of Discs Made from BT9 Alloy Powder (Deformation Temperature, 1050°C)

σ_b kg/mm^2	δ %	ψ %	a_H kg/cm^2	σ^{500} kg/mm^2	r prior to fracture at σ = 60kg/mm^2 and T = 500°C, h.
115	12	33	4.9	73	>100
115	14	34	4.5	74	>100
108	16	32	4.9	-	>100
107	17	41	5.2	-	>100

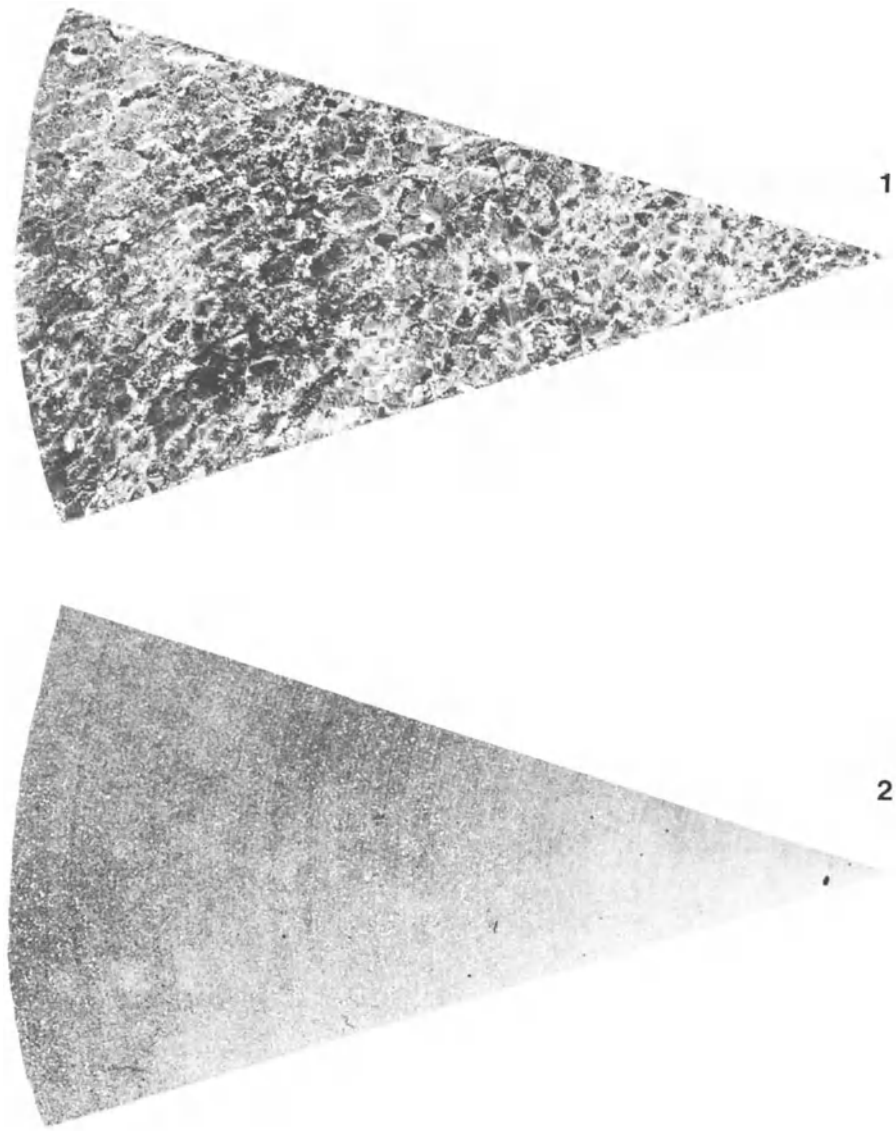

Fig. 2: Macrostructure of the BT9 alloy, 1 : 1
1. 350 mm in diameter ingot
2. Compacted piece 400 mm in diameter

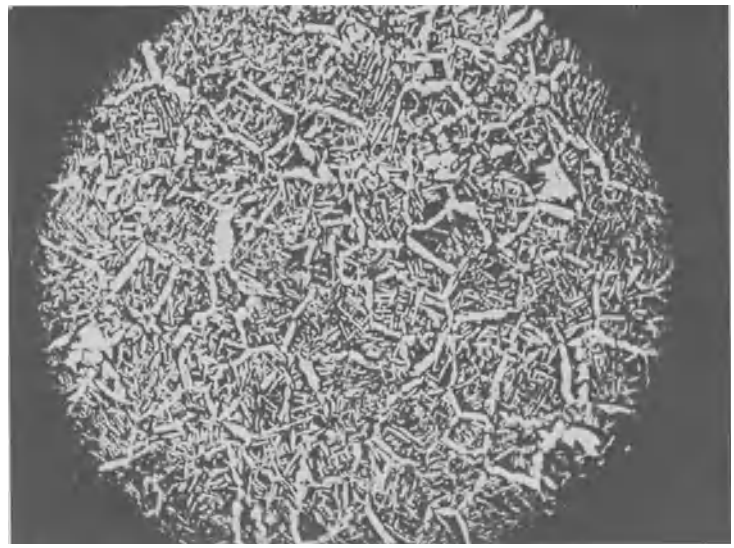

1

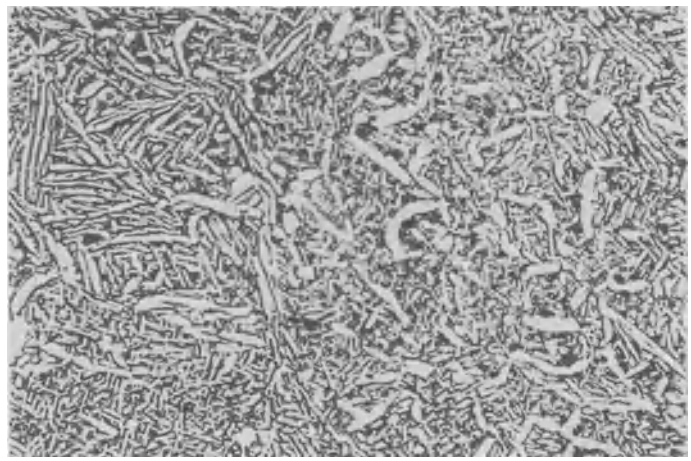

2

Fig. 3: Microstructure of the BT9 alloy, x 500
1. Powder following annealing at 900°C for 20 hours.
2. Compacted piece 400 mm in diameter.

the powder,in the other the parts are compacted and hot deformed. It is interesting to study the structure and properties of the compressor discs made from compacted pieces. The structure of the resultant discs is extremely homogeneous despite the great difference in reduction of the wheel rim, boss and body: 10, 18 and 87%, respectively. The structure of the resultant discs is fine-grained, similar to the compacted pieces. The corresponding mechanical properties exceed the required minimum level (see Table IV).

Thus a new method of producing alloyed titanium powder - by rotating electrode melting - has been developed. This powder is characterized by a uniform spherical shape, homogeneous chemical composition and low interstitial content. The use of powder as a starting material enables one to obtain titanium alloy products characterized by a fine-grained homogeneous structure and mechanical properties equal to those of ingot product. In addition, powder metallurgy method offers economical advantages and may result in cheaper titanium products.

PRODUCTION OF TITANIUM PARTS, APPARATUS AND MACHINERY BY METHODS OF POWDER METALLURGY

V. S. Rakovsky

All-Union Institute of Light Alloys

U.S.S.R.

I. INTRODUCTION

Making components of titanium powder is a powerful approach to the higher techno-economic effectiveness manifested as a drastic decrease in material consumption, lower prime cost and higher productivity as compared with their making by machining the wrought blanks.

At the present time the Soviet industry produces titanium components within a fairly wide range of products and, more particularly, new technological methods have been developed relating to the fabrication of fastening nuts from titanium powder, i.e. titanium-based dispersion-strengthened alloy.

II. MANUFACTURING PROCESS

At present there exist three major ways of making titanium powder, viz.: calcium hydride, electrolytic and hydrogenation-dehydrogenation methods. Following is the description of these methods.

Calcium-hydride method. Used as raw material in this case is titanium dioxide TiO_2 which is subjected to reduction by calcium hydrige CaH_2 at 1150 - 1200°C. The reduction process proceeds both through the effect of calcium on TiO_2 according to the reaction $TiO_2 + 2Ca \rightarrow Ti + 2CaO$ and through the effect of atomic hydrogen being formed in the decomposition of CaH_2: $TiO_2 + 4H \rightarrow 2H_2O + Ti$.

Table I

Chemical Composition of Titanium Powder

Processing method	Chemical composition (%) Ti	Total gas content	Other impurities
Calcium hydride	98.5 / 99.0	0.62 / 0.77	0.258 / 0.555
Electrolytic	99.8 / 99.9	0.025 / 0.050	0.070 / 0.111
Hydrogenation-dehydrogenation	98.9 / 99.5	0.17 / 0.21	0.058 / 0.098

Table II

Some Properties of Titanium Powders

Processing method	Particle shape	Bulk weight (g/cm^3)	Average size of particles (mm)
Calcium hydride	Fragmentary	1.15 / 1.18	12 - 15
Electrolytic	Dendritic	1.20 / 1.25	150 - 200
Hydrogenation-dehydrogenation	Spherical-fragmentary	1.50 / 1.55	48 - 50

A key role in this process is played by the former reaction. The reduction product is washed in water containing HCl and in spirit, and then it is subjected to drying and screening.

Electrolytic method is realizable in two versions: (a) as a direct method of making titanium powder and (b) as a refining method. In the former case the direct current electrolysis is performed on the electrolyte containing the melt of titanium, potassium and sodium chlorides. The content of the titanium chlorides is within 0.5 - 5.0%. In the latter case the electrolyte is added with titanium waste.

In both cases the titanium powder with a various grain size and a various content of oxygen impurities deposits on the cathode.

By varying the concentration of titanium in the electrolyte and the current it is possible to control the size of the powder obtained; here the higher dispersion of the powder is associated with the higher oxygen content. This dependence may be expressed by the following formula:

$$l_{av} = 40 + 45\left(\frac{C}{d_k}\right)^{1/3},$$

where l_{av} is the average size of the particles (mcm);

C is the concentration of titanium ions in the electrolyte (%);

d_k is the cathode current density (A/cm^3).

Hydrogenation-dehydrogenation method. Used as raw material in this case are a titanium sponge or some titanium waste. The material is subjected to hydrogen treatment at 750 - 900°C, thereby titanium hydride (TiH_2) is formed. Then the titanium hydride thus obtained is subjected to mechanical grinding which is readily effected as TiH_2 is a brittle product, and further to the process of dehydrogenation, i.e. heating under vacuum at 700 - 720°C, as a result of which the the titanium hydride breaks down to titanium and hydrogen.

Listed in Table I is the chemical composition of titanium powders and in Table II - some of their properties.

The titanium powder obtained by the first method is the most "rigid" one and it is resultant in the products with the highest strength and hardness but, at the same time, with the lowest plasticity. The powder obtained by the hydrogenation-dehydrogenation method exhibits quite the opposite properties, while the electrolytic powder takes place in between the two others.

Table III

The Properties of Sintered Titanium

Property	Value			
	CH		E	
	s	ad	s	ad
Specific gravity (g/cm^3)	4-4.2	4.30-4.35	3.8-4.0	4.2-4.3
Hardness (kg/mm^2)	235 / 240	275 / 280	135 / 140	150 / 160
elong.(%)	4-5	8-10	8-10	18-22
σy.s.(kgm/cm^2)	1.5 -2.0	5-6	3-4	9-10
(kg/mm^2)	65 / 70	85 / 90	35 / 40	45 / 50

where CH = calcium hydride method
E = electrolytic method
S = sintered products
ad = sintered products subjected to additional deformation

The products from titanium powder are made by cold pressing under pressures of 4 - 5 tn/cm^2 and the vacuum sintering of the formed products at 1250 - 1275°C for 4 - 5 hours.

Some types of the products can be subjected to additional pressure shaping (sizing reduction) through all-around reduction in order to get rid of residual porosity which normally makes up 2 to 3% in sintered titanium, and to arrive at the exact dimensions of the product.

Table III gives the properties of the sintered titanium whose deviations depend basically on the type of the starting powder and processing method.

The electrolytic powder which is rather coarse in its granulometric composition can be worked over to the thin dispersed powder by the hydrogenation-dehydrogenation method.

The general view of the products made of titanium powder is shown in Figure 1. Also, powder metallurgy can be used in making porous strips or finished elements of filters by a direct rolling of the powder, and also various compact semi-products, such as sheets, wire, bars, etc.

ROLLING OF TITANIUM POWDER AND ITS ALLOYS

V. G. Khromov

Gorky Polytechnical Institute

U.S.S.R.

INTRODUCTION

One of the methods of titanium metal production is the manufacture of powders with a wide particle size range from 20 microns to 1.5-2.0mm (hydride, calcium, hydride and electrolytic methods). A great number of studies have been carried out in this direction in the USSR, and as a result, powders of 0.02-2.0mm particle size have been obtained: calcium hydride and electrolytic processes developed by the Central Research Institute of Ferrous Metallurgy (CRIFM) named after I. P. Bardin[1,2,3] and an electrolytic method developed by the Institute of Titanium (Zaporozhye). The degree of purity in fine and coarse powders varied as a result of the high chemical reactivity of titanium. Fine powders were more contaminated especially with oxygen, while the coarse ones approached the chemical composition of iodide titanium. Titanium powder metallurgy has been further developed with the production of titanium metallic powders in the USSR.

Rolling of titanium powders began at the Gorky Polytechnical Institute names after A. A. Zhdanov (GPI) in 1955.[4] Good rollability has been achieved for fine titanium powders from which strips from 0.2 to 2.0mm thick 10-40% porous were produced by rolling with 50,70,120 and 340mm dia. rolls. Pore-free strips were produced with the same plasticity as in the cast, rolled and forged material (σ_B=65-68kg.force/mm^2: δ=23-25%) by means of several cycles of "cold rolling-annealing."

ROLLING OF PURE TITANIUM POWDERS

In the following years work on hydride calcium powder rolling was continued[5] and later a number of studies on powder rolling of different fractions in 600 and 900mm dia. rolls were carried out together with the CRIFM in connection with the development of electrolytic titanium powders and high chemical purity particles.[6,7,8]

For the first time the linear dependence between the roll diameter and strip thickness in the large diameter range was confirmed; formerly this dependence was observed for rolls as large as 350mm in dia. As a result billets 8-9mm thick, 600mm wide with 30% porosity were produced.

In rolling titanium powders the main power parameters of the process were defined:
Total rolling pressure:

$$P = 4.10^{-5} \cdot HB \cdot R \cdot B \quad \text{tons},$$

Where: HB is Brinell hardness of the rolled strip in kgf/mm^2 (this hardness may be defined through pressing hardness of the same porosity which is necessary for the strip);
R is the roll radius in mm;
B is the strip width in mm.

Taking into account the friction in the roll bearings the moment of rolling is:

$$M_{\zeta oll} = P_{p\zeta} \cdot R^2 . B(0.02 + 0.6 \cdot f \cdot \frac{\zeta}{R}) \cdot 10^{-5} \text{kgm}$$

and taking into account expenditures for friction in the bearings the power required for powder rolling is:

$$N = 17.10^{-9} \cdot P_{p\zeta} \cdot R^2 \cdot B \cdot n(0.02 + 0.6 \cdot f \cdot \frac{\zeta}{R}) \text{ kwt}$$

where Pp_ζ is the specific pressure of briquette pressing adequate to the strip t/cm^2,
R is the roll radium in mm,
ζ is the roll trunnion radius in mm,
B is the strip width in mm,
f is the friction factor in roll bearings,
n is the rolls rotation speed in rev/min.

From the above expressions the strip rolling pressure in 600mm dia. rolls with the same strip width and 30% porosity is about 500 tons. At the roll rotation speed of 5 rev/min the rolling power (without friction in trunnions) will be 8-12 kw. Obtained theoret-

ical calculations of the above values coincided with those practically measured by measurers under check screws and in measuring the torque on the spindles and further recalculation to power values with a ±10% discrepancy.

With large thickness rolled sheets particular attention was paid to edge formation and the production of strip equally dense across the width. For this purpose special devices for edge formation with a density equal to that of the rest of the strip were developed.[9,10] As a result, strip with an equally dense edge was produced and a reduction of 75% without edge trimming was possible. The yield of strip in width was about 80%.

Figure shows a strip edge view of 5mm thick after rolling of electrolytic powder without special device (a) and with that for dense edge formation (b), and also the dense edge state of such a strip after a reduction of 75% in 4 cycles (c).

For the first time it became possible to produce strips of 0.8-1.0mm thick and sized 250x600mm with the following mechanical properties by means of "cold rolling-annealing" cycles (4-7 cycles): σ_B=33-35kg.force/mm^2; $\delta_{10}\approx$45%; HV_5=115-120kg.force/mm^2. Erichsen cup depth is 8.5-10.0mm with the 20mm diameter punch. These properties were slightly below iodide titanium properties. Oxygen didn't exceed 0.1%, nitrogen 0.05%, hydrogen 0.001-0.005, silicon less than 0.02%, 0.01% carbon, iron and nickel traces were observed. Thinner strips and foil produced from these sheets found application in the electrovacuum industry. Sheet of 1.5-1.8mm thick with the same properties was produced from 9mm thick billet. Hardness and other characteristics largely depended upon the original size fraction of the rolled powder which is associated with the degree of contamination of the smaller size fractions. Thus, strip hardness from particle fractions - 1.6+1.0mm was equal to 100-110HV, and from fraction - 0.2-0.1mm was equal to 150-160HV. Attaining a pore-free state was found to depend not only upon the total deformation on further conversion after the first sintering, but also upon the original powder state, in particular, upon the size distribution. The process of pore (void) elimination in rolling and annealing of sintered billets influences the surface condition. On achieving an essentially pore-free state the strip surface becomes smooth and brilliant. From Figure 2 one can see that one large fraction - 1.6+1.0mm requires the largest number of cycles (six) and 87% reduction to achieve the same surface condition as in the undiffused powder strip after four cycles and 60% deformation. Maximum plasticity is achieved with large additional deformations after achieving a pore-free state. The total deformation required at 30% porosity of the sintered billet is 85-95%.

A number of common production operations (milling, etching,

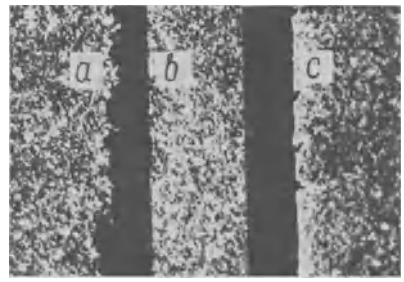

Fig. 1: Rolled strip 5 mm thick edge view in rolling without special apparatus (a) and with apparatus (b) for the dense edge formation and after compression to 75% for 4 cycles (c).

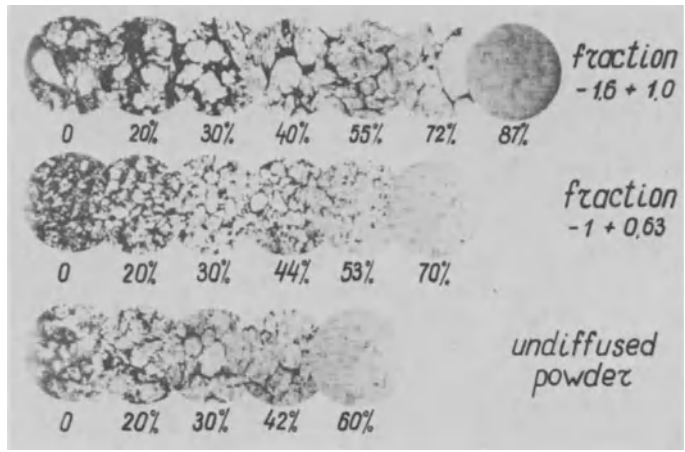

Fig. 2: Surface strip view after different compression degrees in the process of conversion.

etc.) are eliminated in producing strip and foil by means of rolling powders and original powder purity is retained.

Hot rolling of the sintered billet in a pressurized rolling mill filled with inert gas or in vacuum greatly reduces conversion time. Hot rolling of sintered billets in a pack gives good results. After hot rolling and annealing of the sheets there were no boundaries between the sheets, i.e. the metal became monolithic at less total compression. Hot rolling produces maximum mechanical property values with significantly less total compression (60-70%). Pack rolling titanium is not new,[11,12] However, when previously packed sintered billet is rolled, the active metal surface value is significantly lowered and the air evacuation operation and back filling of the pack with inert gas may be eliminated although it results in insignificant oxygen and nitrogen pickup.

Strips 0.3-6.0mm thick and with 10-40% porosity were produced by rolling powders of different size fractions. After sintering these strips found application in chemical and other branches of industry[13,14,15,rtc.] as filters for measuring and as other material.

ROLLING OF ALLOY TITANIUM

In the production of porous titanium materials a number of disadvantages have been found (lower strength, brittleness, large sintering shrinkage etc.). This necessitated carrying out work on porous titanium sheet strengthening and sintering shrinkage control. Rolling of alloy titanium powders (titanium-aluminum) and titanium-aluminum powder mixtures with those of tin, molybdenum, zirconium and other powders was carried out. Molybdenum was found to increase shrinkage in sintering, but it does not allow production of sheets of great porosity and throughput capacity. Aluminum and tin if introduced into the charge in the form of powders results in the growth of compacts during sintering. If pure titanium had a linear shrinkage of 8%, the addition of 6% aluminum reduced it to 1%, and the addition of tin resulted in a linear growth of 1%. Together with the influence of these elements on shrinkage the strength of the porous sheets greatly increased (to 30kg.force/mm2) when compared with the strength of pure titanium of 10kg.force/mm2 with the same 30% porosity.

Figure 3 shows sheet strength values with different porosities and with alloying titanium with aluminum and molybdenum. The porosity range before sintering was the same (20-40%). After sintering for 3 hours at approximately 1200°C the titanium-molybdenum porosity range displaced to the left, to the area of lower porosity to 8-25%, which is caused by a significant shrinkage. This effect is signifi-

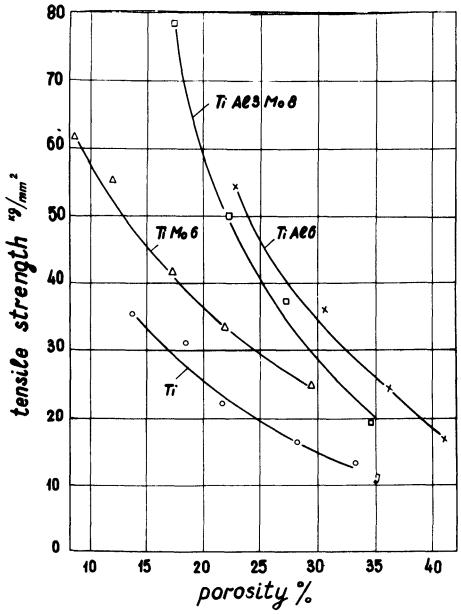

Fig. 3: Strength dependence of titanium powders, titanium +6% molybdenum and titanium +3% aluminium +8% molybdenum on porosity after sintering at 1200°C for 3 hours.

cantly lower in titanium-aluminum and titanium-aluminum-molybdenum alloys. Molybdenum showed a 1.5 times strengthening increase and aluminum more than twice. The titanium -3% aluminum -8% molybdenum composition showed sharp strengthening of the strips with low porosity as compared to titanium (almost 3 times).

With porosity of 20-35% the strength proved to be somewhat lower than that of titanium-aluminum alloy. Thus, by alloying titanium with aluminum and molybdenum powders it is possible to produce materials with a wide range of properties.

Rolling of titanium powders opens great possibilities in the production of composite type materials including dispersion strengthened products.

Rolling of composites titanium + zirconium dioxide + titanium + magnesium oxide and titanium + aluminum oxide carried out under different conditions has not resulted in complication of the process.

Sintering at 1100-1200°C with a further compressive pinch pass rolling to 30% followed by annealing allowed production of composite-

type materials of different densities. Porous titanium rolled in steel of 0.5-2.0mm thick may be rolled up in 60mm and more diameter tubes which can be welded longitudinally and on circumferentially by argon-arc, electron-beam and other welding techniques.

CONCLUSION

Rolling of pure titanium powders, titanium alloys and mixtures of titanium powders with those of other metals and non-metallic materials is a stable highly productive technique of manufacturing porous and pore-free materials. On rolling in 900mm dia. rolls at roll speeds of 3-5 rev/min (the speed of rolling is respectively 8-14 m/min) the capacity of the mill will be 10-16 tons/hour of billets of 8-9mm thick and 600mm wide. The production equipment is simple. Usual resistance furnaces with special containers may be used for sintering. Rolling mills may be applied for rolling of alternative metallic powders. Sheets and strips are characterized by the stability of mechanical properties, for such common metallurgical conversion problems of titanium and its alloys as zonal segregation, cracks, etc. are eliminated. The yield of material is increased. The cost of the metallurgical conversion is significantly lower than that of conventional manufacturing of titanium sheets and strips.

REFERENCES

1. Borok, B. A., Gavrilin, V. I., Teplenko, V. G., Gavrilova, V. K., Lobashov, B. P., Shegoleva, R. P., Golubeva, L. S., Malin, A. P., Solovyeva, Z. V.,"The production of titanium, its alloys and products by powder metallurgy techniques." The advanced scientific - engineering and service experience. The manufacture of parts by powder metallurgy technique. GOSINTI, Moscow, 1957.

2. Suchkov, A. B., Borok, B. A., Ermakova, T. N., Rodny, M. I. and Boldina, L. D., "Some problems of titanium production by electrolysis of molten media using soluble anodes." Journ. "Nonferrous Metals," N6, 1959.

3. Suchkov, A. B., Borok, B. A., Rodny, M. I., Ermakova, T. N., Morozova, L. I. and Boldina, L. D., "Some problems of titanium production by electrolysis of molten media using soluble anodes." Journ. "Nonferrous Metals," No. 8, 1959.

4. Aksenov, G. I., Khromov, V. G., Nikolayev, A. N. and Semenov, U. N., "Rolling of titanium powder into a strip by the Gorky Polytechnical Institute method." Coll. "Titanium and its alloys," iss. III, PHysical Metallurgy of Titanium, Academy of Sciences USSR.

5. Khromov, V. G., Borok, B. A., Gavrilova, V. K. and Karpman, G. M., "The production of titanium strip by powder rolling," Journ. "Nonferrous Metals," No. 11, 1960.

6. Khromov, V. G., "The production of high plasticity titanium by powder rolling technique." "Powder Metallurgy," Transactions of all Union Joint High School Conference, iss. XVI, Kujbishev, 1963.

7. Borok, B. A., Malin, A. P., Markelov, V. V., Andreyev, P. S., Kutirina, V. M., Loginov, G. V., Aksenov, G. I., Khromov, V. G., Groswald, V. G. and Tikhonov, G. F., "Experience of powder rolling on the mill of industrial type." Transactions of CRIFM, iss. 43. "Metallurgy," Moscow, 1965.

8. Malin, A. P., Khromov, V. G., Tikhonov, G. F. and Suchkov, A. B., "The production of high purity sheet and strip by means of direct electrolytic titanium powder rolling." (Ibid).

9. Khromov, V. G., "Strip edge formation in metal powder rolling," Transactions of the Leningrad Polytechnical Institute named after M. I. Kalinin, No. 222, 1963. Moscow-Leningrad "Mashgiz."

10. Spinov, V. A., Tikhonov, G. F., Khromov, V. G., Maltsev, M. V. and Bokova, L. S. Authors' License No. 186949, 1966.

11. Long, J. R.,Metal Progress, v. 55, No 2, 1949.

12. Gonser, B. W., Industrial and Engineering Chemistry. 42 (2), 1950.

13. Tikhonov, G. F., Sorokin, V. K. and Khromov, V. G., "High porosity strip rolling from titanium powder for filters." Trans. of the Leningrad Polytechnical Institute named after M. I. Kalinin, No. 222, 1963, M-L, "Mashgiz."

14. Tikhonov, G. E., Piryalov, L. A., Sorokin, V. K., Nikolayev, A. N., Khromov, V. G. and Shmelev, L. S., "The production and properties of porous rolled steel." Journ. "Powder metallurgy," No 12, 1973.

15. Vinogradov, G. A. and Musikhin, O. M., "Titanium porous sheet production." "Vestnik of the Academy of Sciences of the Ukranian SSR, No 1, 1974.

THE MECHANICAL PROPERTIES OF P/M Ti-6Al-4V ALLOY

K. Obara, Y. Nishino, H. Nishie and M. Yokomizo
Central Research Laboratory, Mitbusishi Metal Corporation
Ohmiya, Japan

Extensive efforts to fabricate titanium alloy components by powder metallurgical technique have been made in recent years.[1-10] In almost all cases, however, completely alloyed powders produced by various processes, such as the hydride-dehydride process, mechanical attrition process or rotating electrode process, were used as the starting materials.

In previous studies,[11-13] the present authors pointed out that some advantages can be gained if we adopt the master alloy powder process for making typical titanium alloys, such as Ti-6Al-4V, Ti-5Al-2.5Sn, Ti-8Al-1Mo-1V etc.. These advantages are (1) excellent compressibility of the mixed powders, (2) better sinterability of the resulting green compact, and (3) good mechanical properties of the products obtained by an appropriate choice in fabrication process variables etc.

In order to further improve mechanical properties of the product obtained by the master alloy powder process, the following points

appear to be most important in fabricating the products: (1) the sufficient diffusion of alloying elements for attainment of homogeneous microstructure of sintered products (2) elimination of residual voids in sintered products to less than 0.1% in volume through some additional metal working process (3) development of desirable microstructure through forging and subsequent heat-treatment.

These points were taken into account in the present work; the effects of major process variables, such as particle size of raw materials, sintering and forging temperatures, subsequent heat treatment conditions, on the mechanical properties were investigated.

Experimental Procedure

Powder Table 1 shows the chemical composition of soda-reduced and crushed commercial titanium powder (-60 mesh).

Table 1 Chemical analysis of soda-reduced Ti powder

	O	H	N	C	Fe	Others	Ti
wt%	0.095	0.014	0.0035	0.0093	0.009	0.251	99.62

The master alloy powder, Al-40%V, was made by arc-melting and crushing. To investigate the effect of the particle size of the master alloy powder on the microstructural homogeneity of sintered Ti-6Al-4V alloy, master alloy powder with three kinds of particle sizes, namely -100, -200 and -250 mesh, are prepared by sieving the crushed Al-40%V ingot. Titanium powder and the master alloy powder are mixed in weight ratio of 90:10 to obtain the powder with the composition of 6%Al-4%V-Bal Ti.

Compaction The mixed powders were compacted by a hydraulic press with the pressure of 5 Ton/cm^2. The size of green compacts was 10x10x55^{mm}.

Sintering To investigate the effect of the sintering temperature on the uniformity of the product, green compacts were sintered for 1hr in high vacuum (10^{-5}Torr) at temperatures 900-1500°C.

Forging Sintered preforms were heated at 700-1200°C for 1min in purified argon and forged in a closed die. As a result of preliminary tests, the reduction in height and the maximum load of the forging were determined as 10% and 13 Ton/cm^2, respectively, to densify the preform to almost full density.

Heat treatment In some cases, hot forged products were subjected to two types of heat treatments; (1) solution treatment at 925°C for 1hr in a vacuum, cooling into water and aging at 500°C for 1hr, (2) the same treatment as (1), except for cooling in furnace after solution treatment.

The former heat treatment is one of the standard STA treatments. The specimen subjected to the latter heat treatment is considered to be in full annealed state, since this corresponds to heating at $\alpha+\beta$ field, followed by slow cooling.

Results and Discussion

Homogenization of microstructure during sintering During sintering of the mixed powders, homogenization of microstructure occurs through the diffusion of aluminum and vanadium atoms to titanium matrix and titanium atoms to Al-40%V master alloy powder particles. It is generally expected that the degree of the microstructural homogenization is considered to depend on (1) geometrical factors such as the size of the master alloy powder and titanium powder particles, (2) sintering temperature and keeping time, and (3) the diffusion velocities of three kinds of atoms etc.. The diffusion velocities of three kinds of atoms, in turn, are substantially determined by the diffusion constants, the effective area for the diffusional current, and the concentration gradient of

the diffusing atoms, etc.

Fig. 1 shows the typical microstructure and distribution of titanium and vanadium elements of the specimen sintered at 1100°C for 1hr. The master alloy powder particle (Al-40%V) can be identified in the center of the photograph. Vanadium is primarily concentrated in this particle; whereas the concentration of titanium is somewhat lower there than in the matrix.

Fig. 2 shows the distribution of alloying elements in the area containing a master alloy powder particle with the specimen sintered at temperatures 950-1300°C. The diffusion of aluminum is shown to be almost completed in the specimen sintered at 1100°C. However, this is not the case for vanadium and titanium even with the specimen sintered at 1200°C; the region of higher vanadium concentration and lower titanium concentration in comparison with matrix is still observed. As shown in Fig. 2(s), sintering at 1300°C is enough for the alloying elements to diffuse into matrix and for titanium atoms to diffuse

(a) BSE

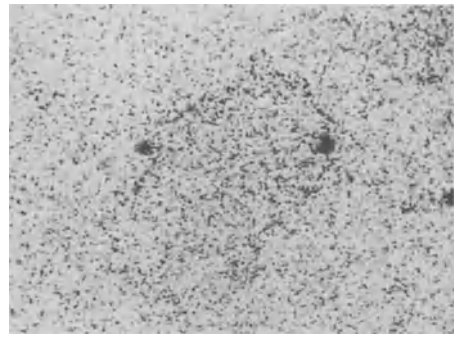

(b) Ti

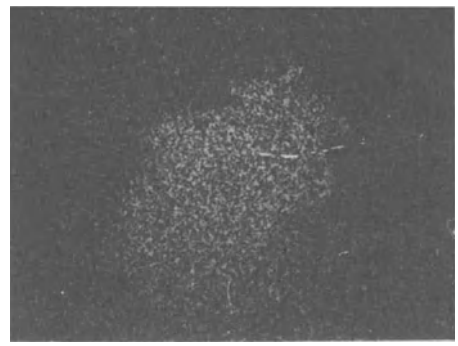

(c) V

200 μ

Fig. 1 Distribution of titanium and vanadium in and around a master alloy powder particle (sintered at 1100°C).

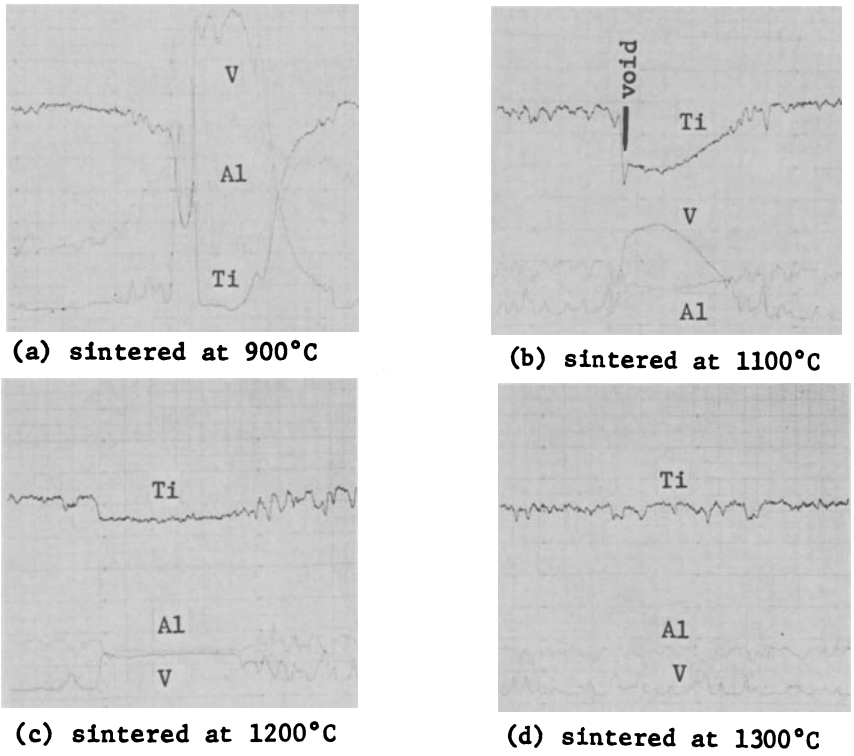

Fig. 2. Distribution of alloying elements in the specimens sintered at various temperatures (-200 mesh master alloy powder)

into the master alloy powder, resulting in the homogeneous microstructure which consists of Al rich α phase and V rich β phase. It is to be noted that in Fig. 2(b), the concentration gradients of titanium and vanadium in the left side of the master alloy powder particle is steeper than those in the right side. A possible explanation for this is that diffusion of titanium and vanadium atoms is disturbed by a void which intervenes between the master alloy powder particle and matrix, and this void reduces the boundary area through which the pertinent atoms diffuse each other.

The effects of size of the master alloy powder and sintering temperature on the microstructural homogeneity are shown typically in Fig. 3. In the case of the use of -100 mesh size-master alloy

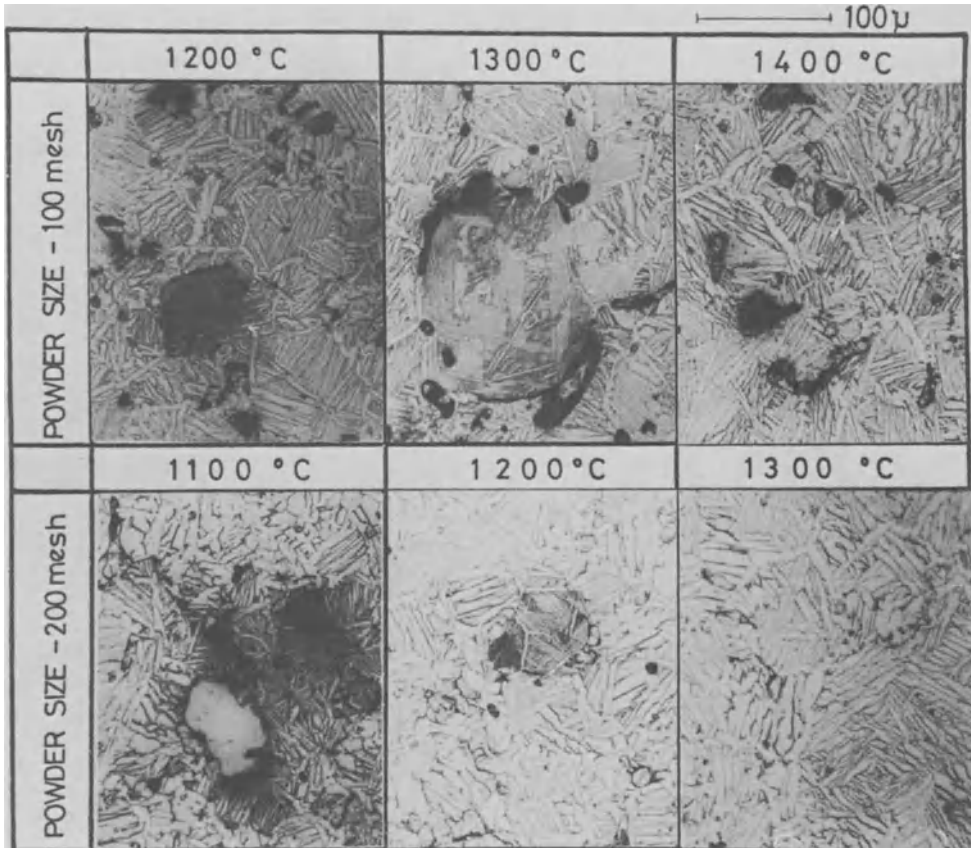

Fig. 3. The effect of the size of the master alloy powder and sintering temperature on the homogeneity of as sintered microstructure.

powder, the sintering above 1400°C is necessary for obtaining homogeneous microstructure. On the other hand, in the case of the use of finer master alloy powder (only the case of the use of -200 mesh powder is shown in Fig. 3), homogeneity of microstructure is almost complete through sintering at 1300°C. No evidence of liquid phase sintering was observed on the products sintered even at temperatures as high as 1400-1500°C. According to the phase diagram, Al_3V, which is similar in composition with Al-40%V master alloy powder, begins to melt at 1360°C.[14] This can be explained as follows. Since rapid diffusion of aluminum into matrix takes place

even at comparatively low temperatures, the composition of the master alloy powder varies to that of higher vanadium concentration in comparison with Al_3V. This results in the elevation of the melting point for the master alloy powder, and consequently, in no occurrence of liquid phase sintering even at 1400°C or 1500°C.

The effect of microstructural homogeneity on the tensile properties of as sintered specimen Fig. 4 shows the effect of sintering temperature and the size of the master alloy powder particles on the density and tensile properties of the sintered specimen. The density increases with the sintering temperature, but has no relation with the size of the master alloy powder particles. This shows the use of finer master alloy powder brings about a favourable effect only for microstructural homogenization. Meanwhile, the tensile strength and elongation increase with sintering temperature. The size of the master alloy powder particles again has no effect on the tensile strength. However, the use of the finer master alloy powder is effective for increasing tensile elongation at sintering temperatures above 1200°C, owing to better microstructural homogeneity of the sintered specimen in comparison with the case of using coaser (-100 mesh) master alloy powder.

Densification through forging As described above, the sintered specimen with excellent microstructural uniformity can be obtained by using finer master alloy powder and sintering the compacts at comparatively high temperatures. However, they still contain more than 7 volume% of micro voids; to improve the mechanical properties, micro voids must be eliminated through some additional metal working process. Fig. 5 shows the effect of forging pressure on densification of the sintered specimen; the forging was carried out at various temperatures. In the case of cold forging between closed dies, the forging pressure of more than 14 Ton/cm^2 is necessary for obtaining full density product. On the other hand, in the case of hot forging, the higher the forging temperature, the lower the forging pressure required for the full densification; i.e. 10 Ton/cm^2 at 900°C and

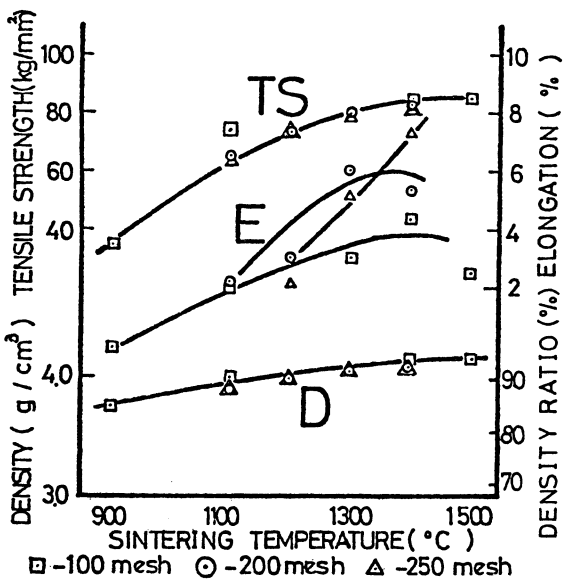

Fig. 4. The effect of the size of the master alloy powder and sintering temperature on the density and tensile properties

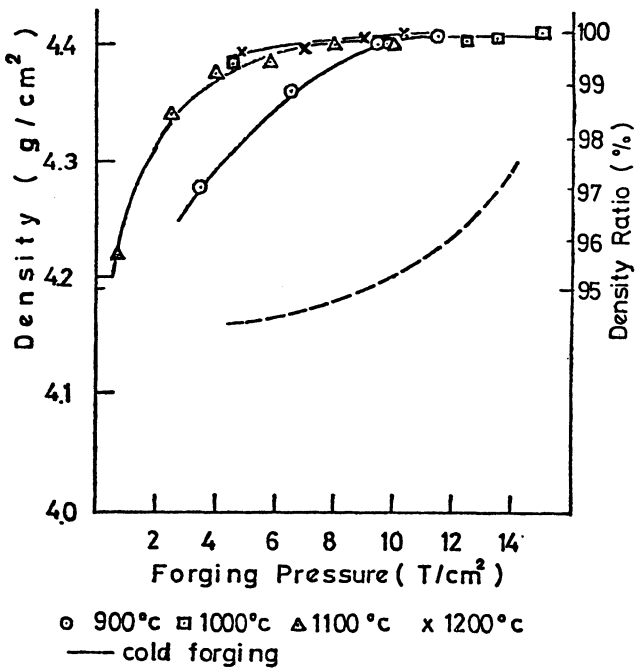

Fig. 5. Densification curves for various hot forging temperatures

7 Ton/cm^2 at 1200°C. There is no significant difference among the densification curves in case the hot forging temperatures exceed 1000°C. In comparison, densification is considerably retarded at the forging temperature of 900°C. It is to be noted that at 900°C as much as 62% of alpha phase still remains and this appears to cause rather poor densification since alpha phase is known to be more difficult to deform than beta phase.

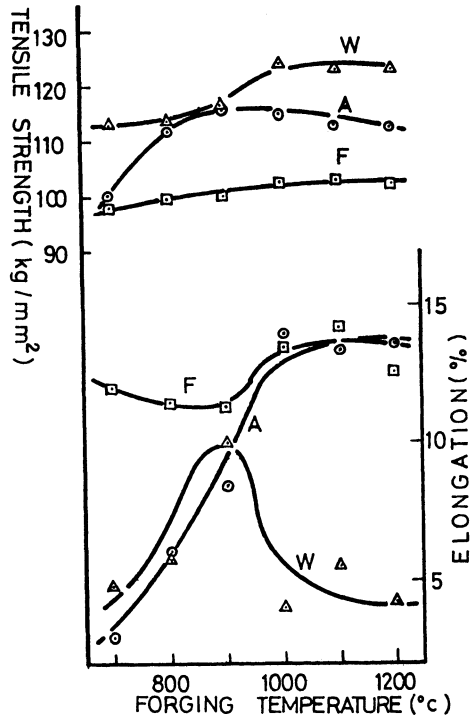

Fig. 6. Tensile properties vs. forging temperature
A: as forged
F: 925°Cx30min/FC+500°Cx4h
W: 925°Cx30min/WQ+500°Cx4h

The effect of the forging temperature and heat treatment condition on the tensile properties

Fig. 6 shows the tensile properties of the as forged and as heat-treated specimens. The relation between the forging temperature and tensile strength can be summarized as follows. (1) In the case of as forged specimens, both strength and elongation increase with forging temperature up to 900-1000°C, and above these temperatures they become almost constant or slightly decrease. (2) In the case of furnace cooled specimens, the strength slightly increases with the forging temperature; while, the elongation of the

specimens forged at temperatures below 900°C ($\alpha+\beta$ field) is lower than that of the specimens forged at temperatures above 1000°C (β field). (3) In the case of water quenched specimens, the strength gradually increases with the forging temperature up to 900°C; in β

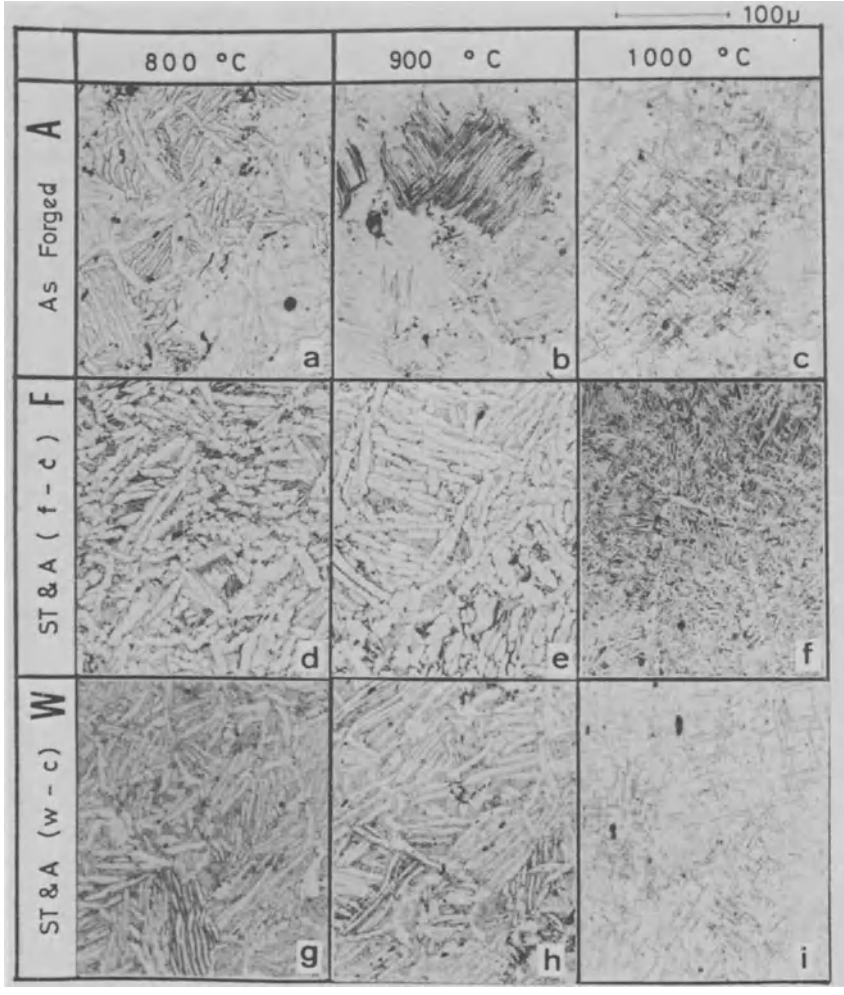

Fig. 7. Microstructures of as forged and subsequent heat-treated materials.

field forging, the strength becomes constant at a level which is higher than that for $\alpha+\beta$ field forging. The elongation, on the other hand, increases rapidly up to 900°C; in the range for β field forging, however, it suddenly decreases to a level which is less than one half of that of 900°C forging.

The major factors which are considered to affect on the tensile properties are (1) the quantity of the residual voids, (2) the bonding strength of the grain boundaries generated by the collapse of the residual voids through hot forging, and (3) the microstructural features which may differ with variation in working temperature and heat treatment. The observed tensile properties of the specimens forged at temperatures below 900°C seem to be essentially explained by the quantity of the residual voids. Since the relevant forging pressure in Fig. 6 is kept constant at a level of about 13 Ton/cm^2 which is near the maximum pressure applied in usual hot forging in a closed die, the average volume of the residual voids of the specimens in general varies with the forging temperature, i.e. 1.0% for 700°C, 0.6% for 800°C and 0.1% for 900°C forging. The increase of the volume of the microvoids in the $\alpha+\beta$ field forgings with decrease in forging temperature usually leads to weakening and embrittlement. In addition, since stronger bonding of the collapsed void area is usually supposed to have taken place with the specimens forged at higher temperatures, it is reasonable to consider that the higher the forging temperature, the better the tensile properties. The case of elongation of the furnace cooled specimens appears to be an exception. The reason is not clear at present.

Meanwhile, microstructure can affect tensile properties of the specimens. As shown in Fig. 7, the microstructures of the specimens forged at 800°C and 900°C are similar when the specimens were subjected to the same heat treatment. Main features of the microstructures in this temperature range are as follows. As forged specimens consist of plate-like alpha (slightly deformed through forging), alpha at prior beta grain boundary, alpha prime, and

intergranular beta (dark area). In the furnace cooled specimens, coarse plate-like alpha constitutes a dominant phase; a small amount of equiaxed alpha and transformed beta appear between the plate-like alpha phase. Water quenched specimens somewhat differ from the above two cases in microstructure; the microstructure is characterized by a relatively small amount of plate-like alpha and a large amount of transformed beta. A much more rapid cooling rate from solution treatment temperature in the case of water quenching, where about 50% (in volume) of beta phase exists in equilibrium condition[15] appears to be mainly responsible for the occurrence of such a microstructure. The variation in tensile properties in this temperature range is, therefore, considered to be essentially related to the effect of residual voids mentioned above and not to the effect of the microstructure.

The highest strength obtained with water quenched specimens forged at β field, can be attributed to the effect of boundary strengthening of alpha phase which appears along the prior beta grain boundary and strengthening of the dispersed fine acicular alpha as shown in Fig. 7. The rapid drop of elongation of beta forged specimens from 10% at 900°C to less than 5% at temperatures above 1000°C appears to be in harmony with the published data of wrought Ti-6Al-4V alloys; the elongation decreases from 15-16% for α+β field forging to 10% for β field forging.

As shown in Fig. 6, the furnace cooled specimens, which are substantially in the annealed state, slightly increase in elongation for the β field forging in comparison with that for α+β field forging. This should be compared again with the case of annealed wrought alloys; their elongations remain almost constant in both cases of α+β forging and β forging (12-14% elongation for α+β and 12-15% for β forging).

The as forged specimens give a medium level of strength in comparison with water quenched or furnace cooled specimens as shown

in Fig. 6. This can be explained by a small strengthening effect of alpha prime (martensite) produced by rapid cooling from the forging temperature.

Conclusions

1. Ti-6Al-4V alloy of excellent microstructural homogeniety can be made through solid state sintering of the compact which contains titanium powder and Al-40%V master alloy powder. Aluminum diffuses quickly into titanium even in a comparatively low sintering temperature of $\leq$1100°C, while complete diffusion of vanadium needs much higher sintering temperature of $\geq$1300°C or $\geq$1400°C, depending on the size of the master alloy powder particle. The use of fine master alloy powder improves tensile elongation at relatively high sintering temperatures, but has no effect on tensile strength.

2. Sintered preform of Ti-6Al-4V alloy can be densified to almost full density through hot forging in a closed die at temperatures higher than 900°C.

3. Tensile properties of as forged and heat treated products are affected by the microstructural features which are determined by the process variables such as forging temperature, heat treatment conditions, etc. In an appropriate choice of these variables, the products with tensile properties equivalent to those corresponding to the specifications of wrought materials, e.g. MIL-T-9047 (for bars and forgings), can be obtained.

Acknowledgement

The Authors wish to thank to Dr. Doi, Director of Powder Metallurgy Division, for his critical advices.

References

1. C. G. Goetzel et al, Modern Developments in Powder Metallurgy, Vol. 4, Plenum Press, 1971

2. S. Abkowitz et al, Modern Developments in Powder Metallurgy, Vol. 4, Plenum Press, 1971

3. G. I. Friedman, J. M. Kazazoff, Modern Developments in powder Metallurgy, Vol. 5, Plenum Press, 1971

4. R. E. Peebles, AFML-TR-71-148, 1971

5. E. Thellmann, Progress in Powder Metallurgy, Vol. 28, 1972

6. G. I. Friedman, International Journal of Powder Metallurgy, Vol. 6, No. 2, 1972

7. R. F. Geisendorfer et al, Titanium Science and Technology, Vol. 1, Plenum Press, 1973

8. R. H. Witt et al, Modern Developments in Powder Metallurgy, Vol. 8, Plenum Press, 1974

9. H. Seilstorfer, Preprints of 4th European Symposium for Powder Metallurgy, 1975

10. R. J. Malik, Powder Metallurgy & Powder Technology, Vol. 10, No. 2, 1974

11. K. Obara, Y. Nishino, Preprints of Funtai-Funmatsu Yakin Kyokai (Japan Society of Powder & Powdermetallurgy) Shunki Taikai, 1973

12. K. Obara, Y. Nishino, H. Nishie, Preprints of 4th European Symposium for Powder Metallurgy, 1975

13. K. Obara, Y. Nishino, H. Nishie, M. Yokomizo, Preprints of Funtai-Funmatsu Yakin Kyokai (Japan Society of Powder & Powdermetallurgy) Shunki Taikai, 1975

14. M. Hansen, Constitute of Binary Alloys, McGraw-Hill, 1958

15. P. J. Fopiano et al, Trans. ASM, Vol. 62, 1969

16. H. J. Henning, Beta Forging of Titanium Alloys, DMIC Report S-24, Battelle-Columbus, Aug. 1, 1968, AD 843480

DISPERSION HARDENING OF TITANIUM

R. V. Krishnan, R. Rangaraju and V. S. Arunachalam*

Materials Schience Division
National Aeronautical Laboratory
Bangalore - 560 017, India

ABSTRACT

The strengthening of titanium and beta III alloy by dispersions of ceria, yttria and misch metal oxides is investigated. The oxides were incorporated in the matrix by internal oxidation. The warm-rolled strips of these materials were annealed at high temperatures. The recovery of the mechanical properties and microstructure were followed by hardness and tensile testing and by optical and electron microscopy. These studies revealed that whilst the dispersoids do not prevent recrystallization, they hinder grain growth. High temperature tensile tests indicate that increase in strength brought about by dispersoids is temperature dependent and falls off above 600°C.

INTRODUCTION

The most effective way of strengthening titanium is through precipitation hardening. This is achieved either by precipitating intermetallic compounds, or, by stabilising both the alpha and beta phases in the matrix by appropriate alloying. Most of the commercial titanium alloys are thus alpha-beta type possessing high strength with good ductility. The increase in strength brought out by precipitation hardening is strongly temperature dependent; at high temperatures the precipitates coarsen, or dissolve, losing their efficacy.

* Now at Defence Metallurgical Research Laboratory,
Hyderabad 500 258, India.

Dispersion hardening with inert oxide particles appears to be a promising method of strengthening for high temperature applications. The second phase particles do not coarsen, or dissolve, and thus any decrease in strength levels at high temperatures is more or less due to a decrease in the Young's modulus. The mechanism of dispersion hardening is both direct and indirect: direct strengthening due to dislocations having to either loop around, or climb over the particles, and the indirect one due to the microstructure being altered to contain elongated grains with high aspect ratios.

It is the object of this investigation to explore the feasibility of strengthening titanium by dispersion hardening. Experiments were carried out to study the mechanical properties of titanium and titanium alloy containing rare earth oxides as dispersoids. More specifically, microstructural changes occurring on annealing the warm worked alloy were studied. This is of interest as experiments have shown (1) that the high temperature strength of some nickel base alloys like thoria-dispersed nickel (TD-Nickel), is more due to a stable microstructure containing elongated grains as in a hot worked metal.

EXPERIMENTAL

Commercial purity titanium and a beta titanium alloy of the following nominal composition Ti-11.5 pct. Mo-5.5 pct Zr-4.5 pct Sn (Beta III), were used as matrix materials for dispersion hardening. The dispersoids were yttria, ceria and misch metal oxides as these are a few oxides that have a higher free energy of oxide formation as compared to oxides of titanium. Dispersions were carried out first by melting together the matrix material with the required quantity of the appropriate rare earth metal in a non-consumable arc furnace. To ensure homogeneity, the alloy was melted a number of times. The nominal composition of the rare earths were around 1 and 2 weight percent. As there is some solubility of yttrium and cerium in titanium at elevated temperatures (2), it was presumed that internal oxidation would not present any problems. The alloy fingers were homogenised at 1000°C for about 72 hours and were then warmed-rolled at 700°C to thin strips (0.5 mm thick) after encapsulation. It was found that after rolling a special step of internal oxidation was not required as the alloys got internally oxidised during hot-rolling itself. The oxides were fine (1000 Å) and uniformly distributed. A typical microstructure of a titanium -1% ceria alloy is shown in Fig. 1. The alternative route of powder metallurgy is equally well suited for this purpose and allows the introduction of multiple oxides (3).

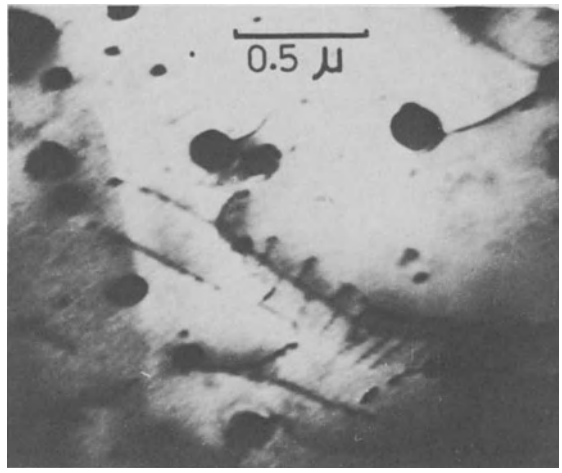

Fig. 1 - Transmission electron micrograph showing oxide particle distribution in the titanium-1%ceria system.

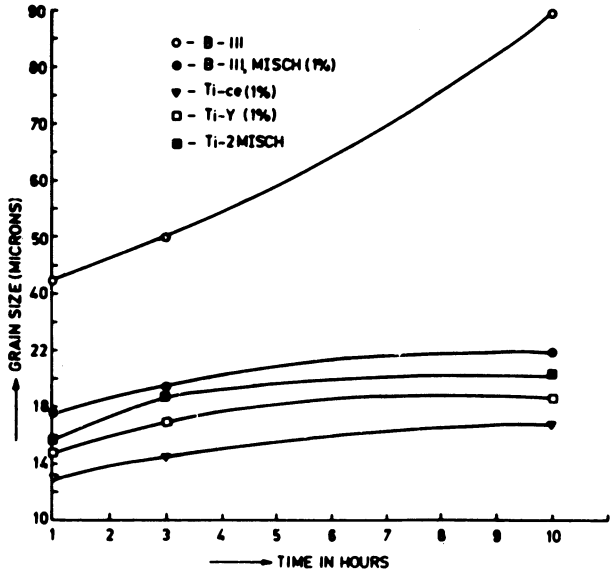

Fig. 2 - Effect of annealing time on grain size for different systems.

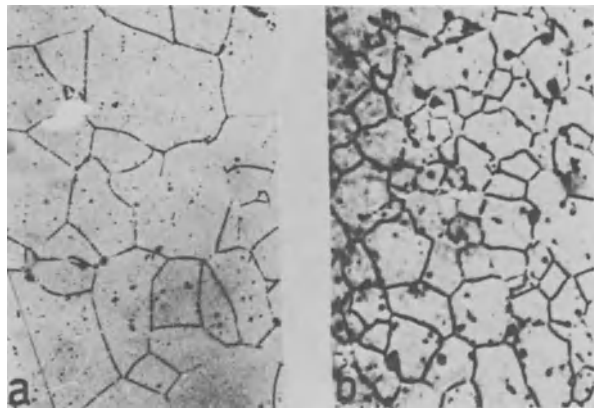

Fig. 3 - Optical micrographs showing the effect of oxide dispersions on grain size after annealing at 800°C for 10 hours.
a) Beta III without dispersoids (x 250)
b) Beta III with dispersoids (x 250)

Fig. 4 - Transmission electron micrograph showing the typical hot worked structure.

The warm-rolled strips were annealed in a vacuum better than $3x10^{-6}$torr at temperatures of 600°, 700°, 800° and 900°C for periods ranging from one hour to ten hours. The recovery of the mechanical properties and microstructure were followed by hardness and tensile testing and by optical and electron microscopy.

Tensile tests were carried out at 500°C and 600°C at a cross head speed of .05 cm/minute in an Instron machine. These tests were carried out in a high purity argon atmosphere. The tensile samples were loosely wrapped with titanium foil and a few buttons of titanium sponge were kept in the Inconel capsule for gettering. Thin foils for transmission electron microscopy were prepared by an initial chemical polishing in a bath of 1 part HF and 2 parts HNO_3 followed by electropolishing in a solution of methanol, butanol and perchloric acid (400:175:30).

RESULTS AND DISCUSSION

(i) Dispersoids and Recrystallization

Grain size measurements on annealed samples were made to evaluate the influence of dispersoids on grain growth. Fig. 2 shows the grain size as a function of time. It is seen that the grain growth is sluggish in specimens containing dispersoids. This effect is striking in Beta III alloy where the grain size doubles itself within ten hours when there are no dispersions. This is confirmed in Fig. 3 where the microstructures of Beta III are shown with and without misch metal oxides after annealing at 800°C for ten hours. Recrystallization does not appear to have been prevented, nor the grain shape appears to have been altered by the presence of dispersoids. This is in direct contrast to the results obtained in thoria dispersed nickel.

Electron microscope investigations proved this point further. Fig. 4 is the micrograph of a warm worked alloy showing a typical banded structure. Fig. 5 is the corresponding structure after an hour's annealing at 900°C. Recrystallizing grain growing at the expense of banded structures can be clearly seen supporting the inability of dispersoids to pin the migrating grain boundaries. Even though recrystallization does not appear to be prevented by dispersoids, they at least seem to retard the rate of grain growth considerably.

Reasons for this behaviour are not easily understood. Absence of a highly uniform distribution of dispersoids would be responsible for not pinning the grain boundaries. However, the more plausible one could be due to the relative ease with which recrystallization nuclei can form in anisotropic metals. Twin intersections, strains arising due to alpha-beta transformations, or even due to

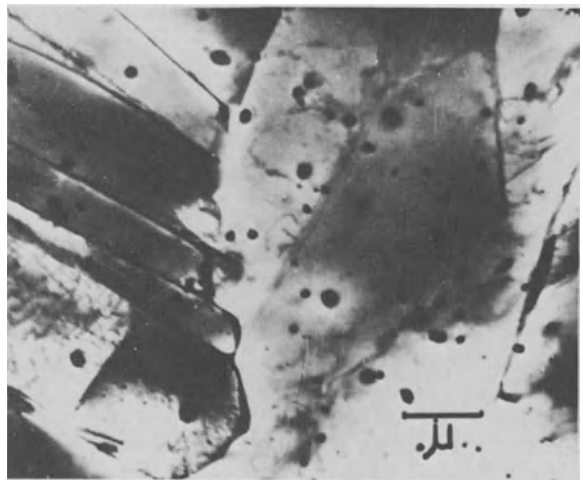

Fig. 5 - Transmission electron micrograph showing a recrystallizing grain growing into the banded hot worked structure in Ti-Y_2O_3 alloy.

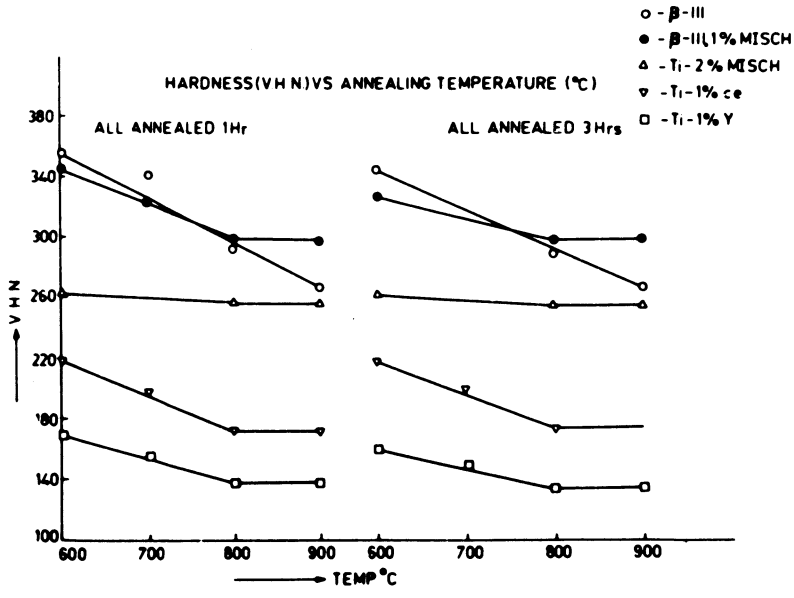

Fig. 6 - Room temperature hardness data as a function of annealing temperature.

difference in thermal expansion or contraction between adjacent grains of different orientations could generate recrystallization nuclei. A ready and large availability of such nuclei in this system as compared to nickel where polygonised boundaries would have to acquire large angle characteristics before turning out to be recrystallization nuclei may perhaps account for this discrepancy.

(ii) Strength Characteristics

Fig. 6 shows hardness of these alloys at room temperature. Hardening due to dispersions can clearly be seen in these curves. The sluggish grain growth is responsible for only small variations in the hardness number at high temperatures. Ceria seems to be a more potent hardener than yttria presumably due to the

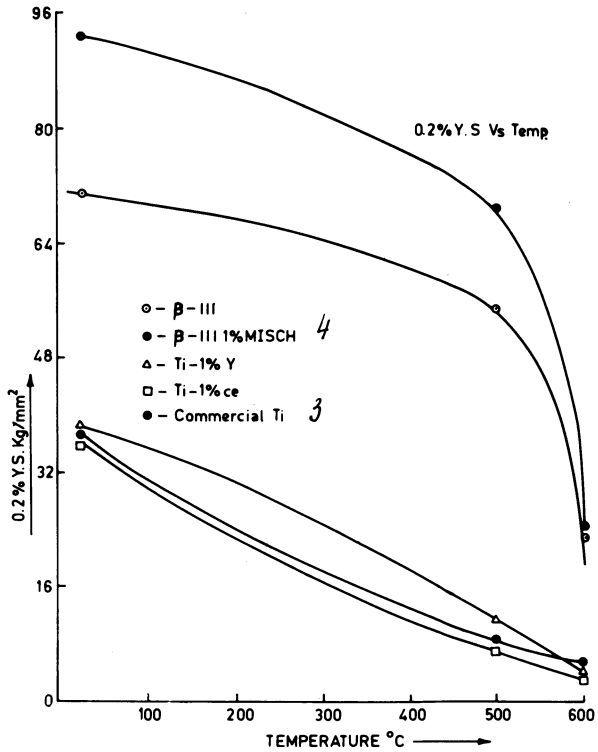

Fig. 7 - High temperature yield stress data for the different dispersion systems chosen.

increased solubility of cerium in the matrix leading to better dispersions.

High temperature tensile tests were carried out in the range of temperatures where precipitation hardening in titanium ceases to be effective and thus sets the limit for the high temperature capability of commercial titanium alloys. Results of these tests (Fig. 7) shows that the increase in strength brought out by dispersions is not temperature independent and falls off above 600°C. Increases in strength observed in Beta III alloy are not exclusively due to the presence of dispersions: alpha separation could also contribute for hardening (4).

These results suggest that titanium is not amenable to dispersion strengthening for increasing the high temperature strength and this is due to the inability of dispersoids to modify the microstructure to contain elongated grains. However, their influence is seen in the sluggish grain growth. This property may perhaps be used with advantage in titanium alloys subject to beta processing where excess grain growth is a factor to contend with.

ACKNOWLEDGEMENT

This work was carried out in the Materials Science Division of the National Aernoautical Laboratory. The authors are grateful to Dr. M. K. Asundi of the Bhabha Atomic Research Centre, Bombay for his help in getting the alloys melted.

REFERENCES

1. B. A. Wilcox and A. H. Clauer:
Acta Met., 20 (1972) 743.

2. E. K. Molchanova:
Phase Diagrams of Titanium Alloys
Israel Program for Scientific Translations,
Jerusalem, 1965.

3. I. G. Wright and B. A. Wilcox:
Tech. Report AFML-TR-72-238 Part II

4. D. E. Gordon and J. W. Hagmeyer:
Jour. of Matl. Science, 10 (1975) 1725.

PRODUCTION OF HIGH PURITY TITANIUM POWDER

BY ELECTRON BEAM TECHNOLOGY

H. Stephan and J. Fischhof

Leybold-Heraeus GMBH & Co. KG.
Wilhelm-Rohn-Str. 25
6450 Hanau - Germany

SCOPE

When we were confronted with the economical production of metal powder of highest purity we determined that our main interest should be laid on reactive metals and such ones where a low oxygen content is essential to meet the high demands of PM parts.

Before carefully studying the processes and furnaces available and under development we wrote down the scope of such a process. Bearing in mind that the highly developed aircraft industry was going to be the most critical user of the powder to be produced we have listed up the demands for quality , which means in detail:

(a) No contamination of the metal to be melted and the powder to be produced by the heat source, the atomizing system and the environment.

(b) The gas content of the powder should be, if necessary, as low as possible, which means that the melting process should be a refining process.

(c) The particle size should be between 50 and 600 microns, for special application particle sizes of 5 - 50 should also be producible.

(d) The process should allow production of either spherical particles of a 100 density, smooth surface and high tap density or flakes of 20 to 400 mesh with a high green strength and of very small grain size.

(e) The losses of volatile alloy elements should be neglectable.

(f) The process should be automatable to achieve a constant quality of the product.

Since a product of highest quality will only find a very small field of application if the prices cannot be significantly reduced, the second feature of our aims was the economical production of high quality powder. In order to bring the powder price very close to the ingot price high economy can be achieved, if:-

(a) Large and consequently cheap loads can be melted and atomized etc. by direct usage of small and medium VAR and VIM ingots;

(b) A high productivity can be achieved by having a high melting and atomizing speed, a continuous production over several days and weeks and a high material efficiency;

(c) The costs for material preparation, powder packing and transportation and quality control can be kept down.

Trying to meet all these points of our scope the result must be a sophisticated expensive furnace. In order to keep the capital costs at a reasonable level it is necessary to extend the application of the furnace to all metals and alloys, which means that all metals with a melting point above 1400° C should be powderizable in an economical way.

PROBLEMS IN THE PRODUCTION OF METAL POWDER

In order to meet all the above-mentioned aims of the specification the following main groups of powder production should be carefully considered:

Melting - Atomizing - Solidification and Cooling and at last the most important one - Collection of the Powder.

In melting we are convinced that the usage of the electron beam as source of heat, using the end of an electrode and vacuum would be the best combination to avoid contamination of the material to be melted and atomized. For atomization we have decided for a

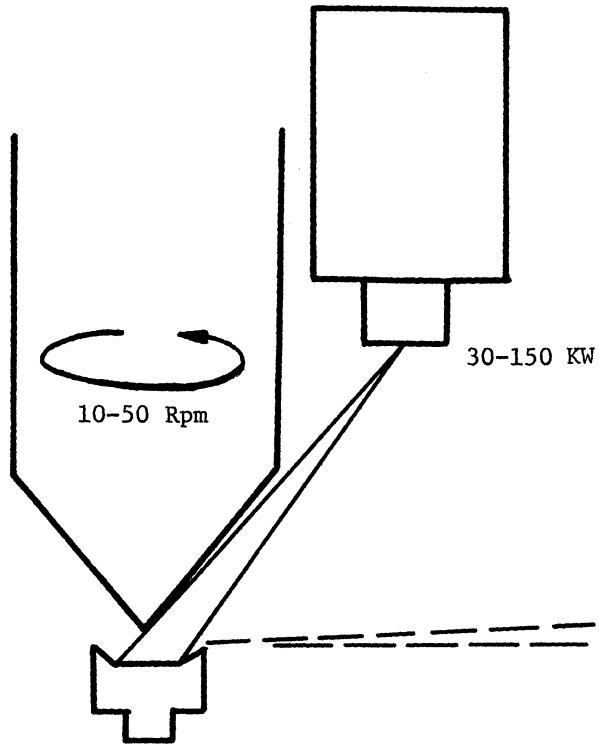

	Steps of development	
	1	2
Loaded mat.	consumable	electrodes
Max. Ti-charge	60	850 kg
Max. Ni-charge	120	1600 kg
Max. atom. speed	60	150 kg/h
Production	batchtype	continuous

Fig. 1 - EBRD - Process and its main data.

rotating disc, because only this system allows the best control of the particle size and its size distribution. Solidification and cooling down should be made slowly to avoid gas free shrinking holes even in large particles. Only energy transmission by radiation should be allowed.

Collection of particles is the most important and most difficult problem in high quality metal powder production. A collection of 100% without touching the powder by any tool must be a necessity, in order to

(a) maintain the cleanliness of the metal powder;

(b) keep the tank clean and easily inspectable so that, if changing the metal or metal alloy, crosswise contamination be avoided.

Melting, atomizing and cooling down in vacuum is especially very important in the production of Ti-powder. Evaporated metal can condensate in massive layers on the melting tank wall. Doing the same step in a reduced noble gas pressure the evaporating metal condensates in a loose sponge-like layer, which can be eroded by the powder particles and spoil the particle surface. Arousing of explosions when opening the tank must be considered and avoided by well-proven steps of tank venting.

PROCESS

Figure 1 shows that the EBRD (Electron Beam Rotating Disc) Process is a combination between a vertical drip-melting and an atomizing process with a rotating disc.

The vertical fed, slowly rotating electrode will be drip-melted as in all drip-melting furnaces. The well programmed e.b. assures a pencil-shape of the electrode tip, so that all material will run down the conical electrode tip and that the material will drop into the centre of the rotary disc.

The programmed beam provides that the outspreading metal film at the disc surface will be atomized at the edge of the disc in small particles. The size of these particles is given by the surface tension of the material to be atomized and the centrifugal force.

The particles start to solidify on their way to the chamber wall.

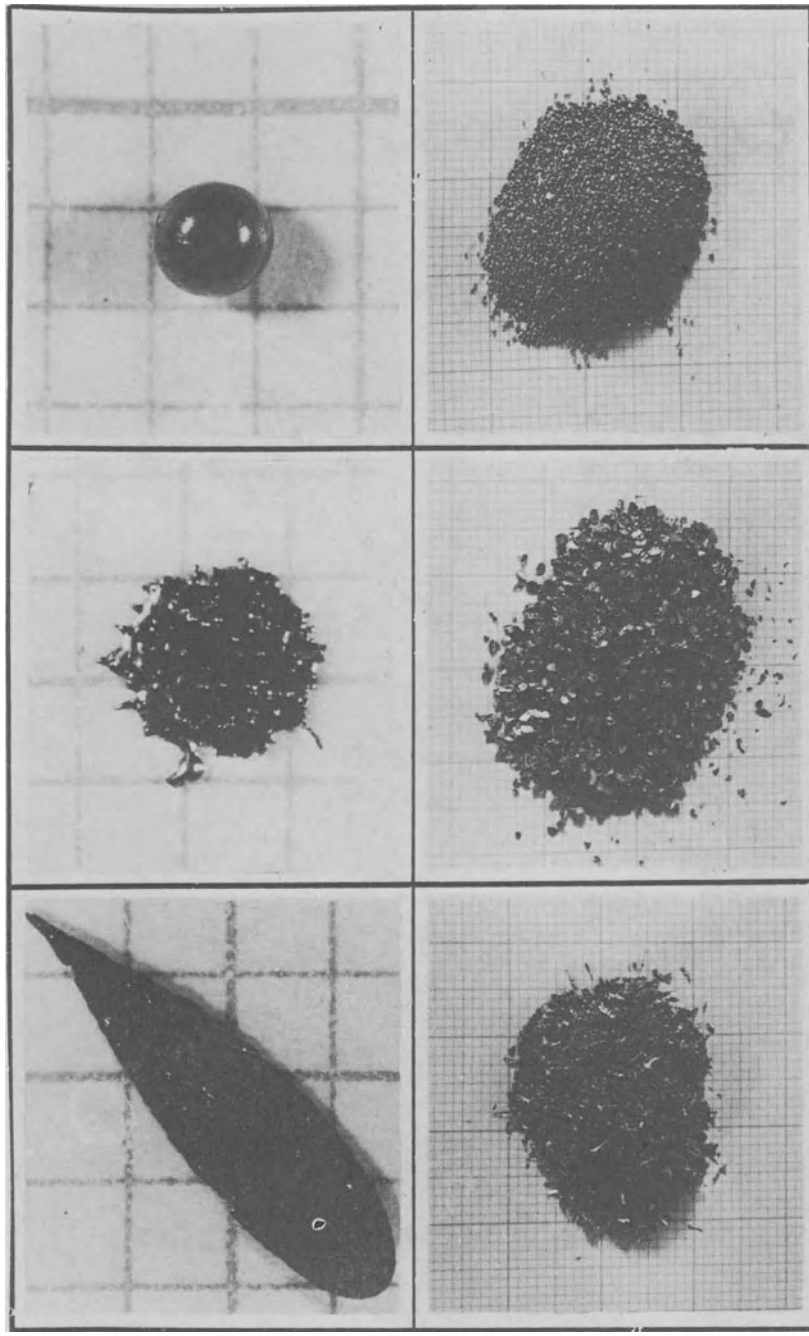

Fig. 2 - Shapes of metal powder particles
Microspear-head flakes
Micro potato pancake flakes
Spherical

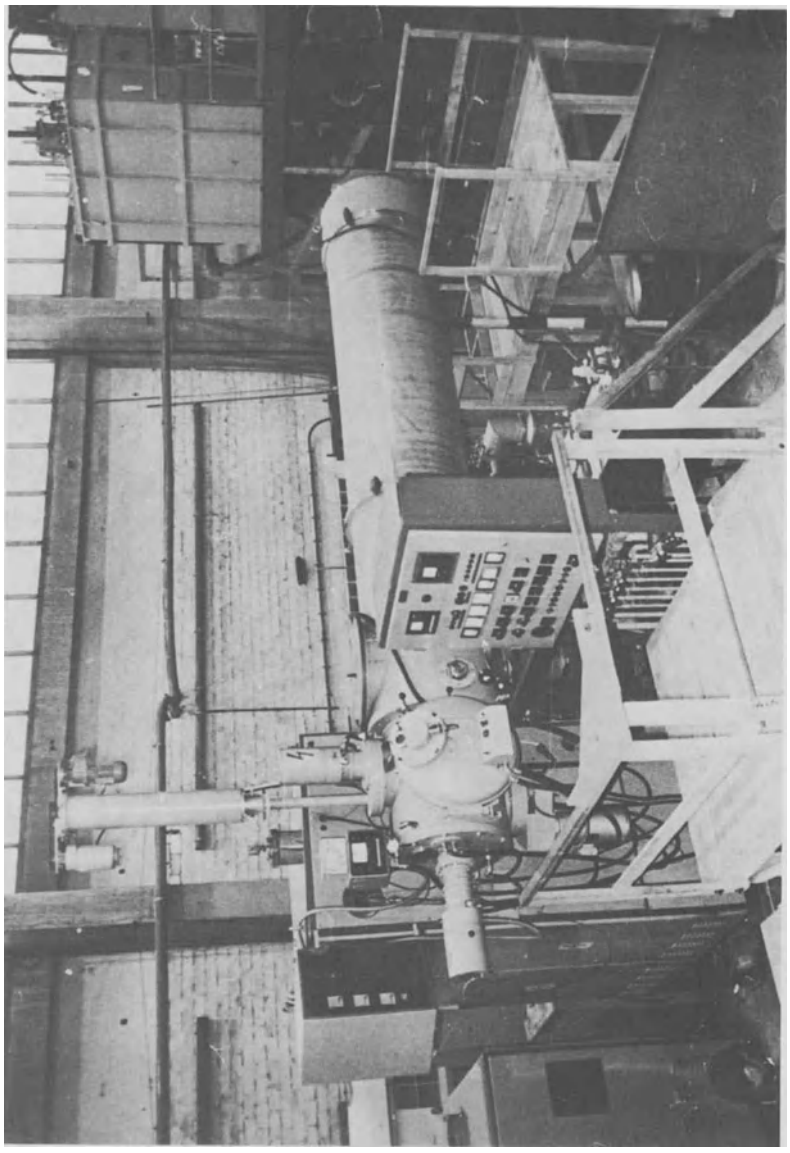

Fig. 3 - Small laboratory EBRD atomization plant.

Ti - alloys	Al	V	Fe	O_2	H_2
Starting material	6,6	4,2	0,11	0,20	0,007
Spherical powder	6,4	4,1	0,11	0,21	0,005

	Al	Zr	Mo	Si	Fe	O_2
Starting material	6,2	5,0	0,5	0,24	0,023	0,14
Spherical powder	6,0	5,1	0,5	0,24	0,021	0,13

	Al	V	Fe	O_2	H_2
Starting material	6,0	4,1	0,11	0,11	0,007
Splashed powder	5,9	4,1	0,12	0,12	0,005

Ni - super-alloys	Al	Cr	O_2	N_2	H_2
Starting material	5,0	9,0	60	8	6
Spherical powder	4,95	8,95	64	10	9

Fig. 4 - Chemical analysis data of Ti- and Ni-alloys.

Depending on the process parameter it is possible to produce

100% spherical powder or
100% flakes or a convenient
mixture of both shapes.

Also depending on the beam programme the shape of the flakes can be changed between microspear-heads and micro potato pancakes - Figure 2 -.

In the first stage of process development the electrodes to be atomized are of 100 - 150 mm diameter and 400 - 800 mm length. The atomization speed should be in the range of 1 - 2 kgs/min and the process is of the batch type.

In the second stage the electrodes could be of 200 mm, probably 250 mm diameter and 5 m length. The atomization speed will be 2 - 5 kgs/min. The process will be continuous.

In both steps the powder will be collected in vacuum tight stainless steel cans. The powder can be stored under vacuum. If the storing time will last long the cans can be e.b. welded.

As starting material several types and qualities can be used. For first-grade powder double melted VAR-Ti-alloy ingots with sand blasted surface or single melted VIM-Ni-base super alloys can be used. For second grade powder large solid scrap pieces, scrap mosaic electrodes or e.b. consolidated small scrap or virgin material can be used.

The application of cheap but high value scrap material is one of the main points to reduce the powder costs and one of the main advantages of the EBRD process.

PRELIMINARY RESULTS FROM A SMALL LABORATORY FURNACE

In a small laboratory furnace - Figure 3 - we have studied the function of atomization with e.b. We have seen that our ideas could be realized and powder could be produced. In the first step we have atomized just by bombarding the metal disc.

The chemical analyses of Ti- and Ni-alloys are given in Figure 4. For Ti atomization speed has been around 1/2 kg/min and for Ni-super alloys around 1 kg/min with an e.b. power of only 15 kW.

The spherical particles have led to a 100% density up to a particle diameter of 0.7 mm. The grain size of the Ti-spheri-

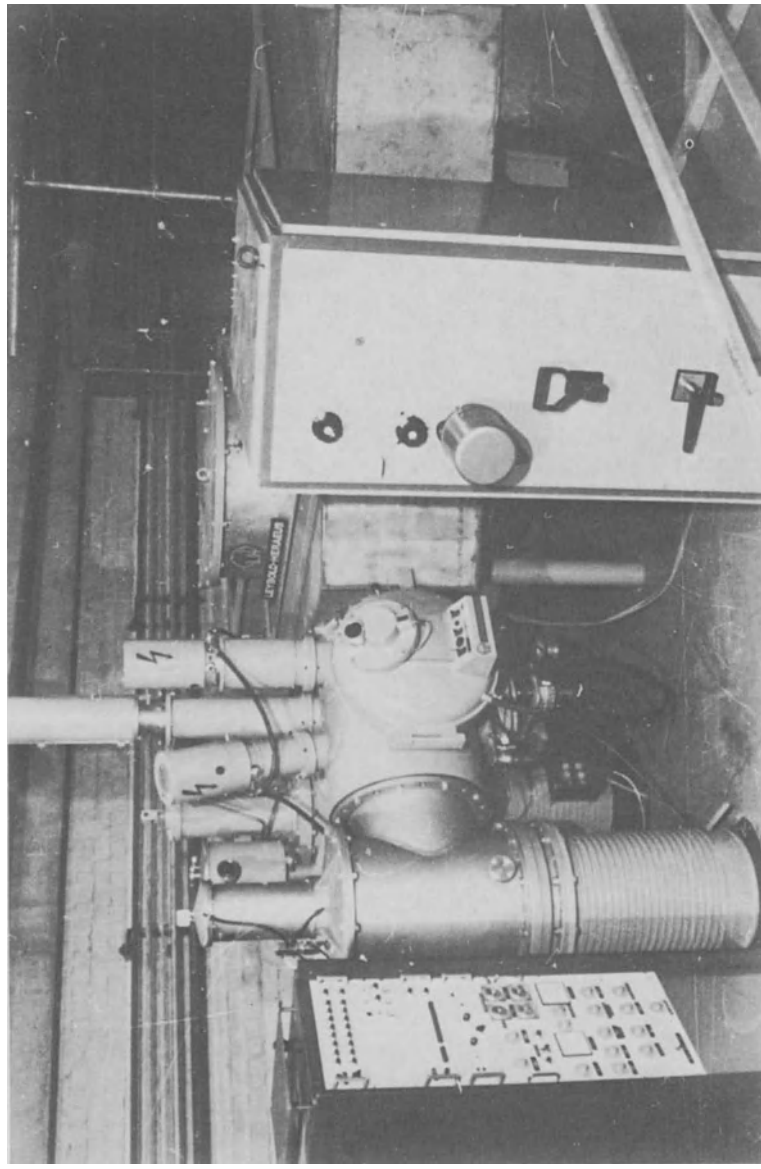

Fig. 5 - EBRD atomization plant for production of metal powder.

cals is for 0.380 mm balls about 20 microns, of Ti micro potato cake flakes of 5 - 10 microns.

The top density of spherical Ti-powder is approx. 60%, of flakes approx. 28%.

In the second step we have drip-melted on to the rotating disc and seen that this process works also to our satisfaction if the e.b. is programmed according to the sophistication of the process.

So far so good. In the course of development we have been confronted with housekeeping problems. We have learnt how many impurities are contained in a visible clean high vacuum furnace and in the environment of the furnace.

The consequence of that long development period has led to the decision to build a production furnace which is now ready for the first test runs. This furnace - Figure 5 - is able to atomize all metals with a melting point higher than 1400° C. It allows the atomization of electrodes of 150 mm diameter and 800 mm length and can be extended to atomize electrodes of 250 mm diameter and 5 m length.

FIRST RESULTS FROM THE PRODUCTION FURNACE

The results will be shown during the conference in Moscow.

CONCLUSION AND ASPECTS

It has been shown that the electron beam rotating disc process offers the possibility to produce economically very pure Ti- and Ni-base super alloys in large quantities. The existing furnace is applicable to a growing powder market. If the market demands for large quantities of second or third grade powder the process can be changed so that raw material or scrap can be atomized in a direct way and e.g. Ti-powder of high purity can be delivered at a lower price than double melted ingots and forged bars.

COMPARATIVE EVALUATION OF FORGED Ti-6Al-4V BAR MADE FROM SHOT PRODUCED BY REP AND CSC PROCESSES

R. F. Vaughan, P. A. Blenkinsop and P. H. Morton

New Metals Division, Imperial Metal Industries (Kynoch) Ltd., Witton, Birmingham B6 7BA

Introduction

Like other studies[1,2] of titanium alloy powder, the present evaluation was targetted towards potential aerospace applications of consolidated material, in particular use in rotating aero-engine components.

The initial approach to the question of titanium alloy powder has been similar to that of other organizations in the field. After first considering the alternative forms of powder, i.e. hydride - dehydride, elemental, gas atomized, and shot, the conclusion was reached that the latter route offered the best prospects of success, particularly when interstitial and surface contamination and ease of handling were considered.

The data presented in this paper detail the preliminary evaluation of Ti-6Al-4V alloy shot obtained from two sources; the Rotating Electrode Process[3] (REP) and from the Centrifugal Shot Casting Process[4] (CSC). An initial assessment of the shot was made prior to consolidation of two billet sizes by hot isostatic pressing (HIP). Comparative data was then produced on the mechanical properties (tensile, low cycle fatigue and fracture toughness) of the consolidated material both as-HIP and after rolling and forging.

Assessment of Shot

The Ti-6Al-4V alloy shot was obtained from AERE Harwell, UK (CSC) and Nuclear Metals Inc. US (REP). The details of the pro-

cesses are given elsewhere.[3,4]

The CSC shot was produced from a 50 mm Ø x 500 mm long cast and wrought bar. The shot was formed in an argon-helium atmosphere with a yield of about 60% usable material. (The yield of shot is limited by the size of the furnace chamber and not by any basic limitation of the process). The analyses of the starting electrodes and the shot are given in Table 1 and the sieve analysis is detailed in Table 2.

The corresponding analytical and size information for the REP shot are given in Tables 1 and 2, respectively. No information was available on the composition of the starting electrode for REP shot.

Consolidation of Shot

Although a number of consolidation processes were considered for the alloy shot, it was felt that hot isostatic pressing offered the best and most reliable route, particularly as comparative data was being generated.

Both types of shot had a tap density of about 65%. All encapsulation was in mild steel cans. Two sizes of cans were used, one 150 mm x 25 mm Ø and the other 216 mm x 100 mm Ø. Both electron beam and TIG welding techniques were used in the construction and sealing of the evacuated cans. No significant difference was observed in the subsequent behavior of the cans, irrespective of which welding process was used.

All cans were HIP pressed for 4 hours at a temperature of 950°C and a pressure of 1.03 kbar. The pressing reduced linear dimensions of the cans by about 10%. The mild steel cans were removed from the titanium alloy billets by machining prior to further evaluation and processing.

Thermo-Mechanical Processing

(1) Small Billets

After removal of the cans, the billets were approximately 20 mm Ø. A section was first removed for assessment of the as-HIP + heat treated properties of the material. The remaining material was then rolled at 950°C to 12 mm square; a reduction of about 56%. Both types of consolidated material deformed in an identical manner, similar in fact to the normal cast and wrought product.

Table 1 - Analysis of Shot and Electrode Material

Type	Al	V wt %	Fe	O_2 ppm
CSC Electrode	6.56	4.50	0.14	1600
CSC Shot	6.56	4.54	0.16	1650
REP Shot	5.8	4.4	0.08	1159

Table 2 - Shot Sieve Analysis

Sieve Size µm	1180	710	500	355	250	180	125	90	PAN
% Retained on Screen CSC	0.28	5.4	21.79	39.24	21.85	7.52	2.73	1.17	0.27
% Retained on Screen REP	-	-	-	7.20	26,79	39.42	18.13	5.83	2.63

All samples were heat treated at 960°C air colled + 2 h at 700°C.

(2) Large Billets

The as-machined billets were approximately 175 mm x 85 mm Ø. A slice was taken from each billet for evaluation of the as-HIP material, and the remaining material was forged.

The material was forged between flat plattens. A small amount of preliminary deformation was carried out at 1125°C to square the section, but the majority of the processing was performed at 950°C, to 50 mm square (54% deformation). Figure 1 shows the final shape of one of the forgings. Although some cracking occurred it was limited to the surface. Both forms of consolidated billet performed in a similar manner, and were not significantly different from conventional material.

The forged REP and CSC billets were heat treated at 960°C, water quenched and annealed for 2 hours at 700°C.

Metallurgical and Mechanical Property Evaluation

The microstructures of the as-HIP + heat treated material, in both the small and large billets, were very similar. The only difference between the CSC and REP material (Figures 2 and 3) was in the fact that the former contained more alpha phase. This fact was due to the difference in β-transus of the two materials, it being higher in the CSC case, due to the higher level of oxygen in the alloy.

Room temperature tensile values for the as-HIP + heat treated material (20 mm Ø) are given in Table 3. The small quantity of rolled bar produced from the 20 mm Ø billet was used entirely to generate low cycle fatigue data. All the testing was carried out at room temperature under constant load (zero minimum) conditions and a frequency of 10 cycles/minute. The results are presented in Figure 4.

A more extensive mechanical property evaluation was possible on the forged billet. The tensile property levels in the as-HIP + heat treated condition were similar to those observed in the small billet material. Both transverse and longitudinal tensile tests were carried out on the forged bar. The results are presented in Table 3, together with the fracture toughness level in the materials. Microstructurally the materials appeared similar, Figure 5 shows the structure in the CSC shot forging, while Figure 6 shows the structure of conventional cast and wrought material for comparison.

Table 3 - Tensile and Fracture Toughness Properties

Material		0.2% Proof Stress $N.mm^{-2}$	UTS $N.mm^{-2}$	Elong $4\sqrt{So}$ %	R in A %
CSC HIP + Heat Treated (20 mm)		957	1075	18	36
REP HIP + Heat Treated (20 mm)		907	1030	21	40
CSC HIP + forged + heat treated	T	922	1038	16	38
	L	942	1053	15	39
REP HIP + forged + heat treated	T	940	1048	20	40
	L	903	1026	19	40
Conventional material (75 mmØ)	T	951	1032	20	37

Fracture Toughness	K_Q $MNm^{-3/2}$
REP	68
CSC	67
Conventional material	57

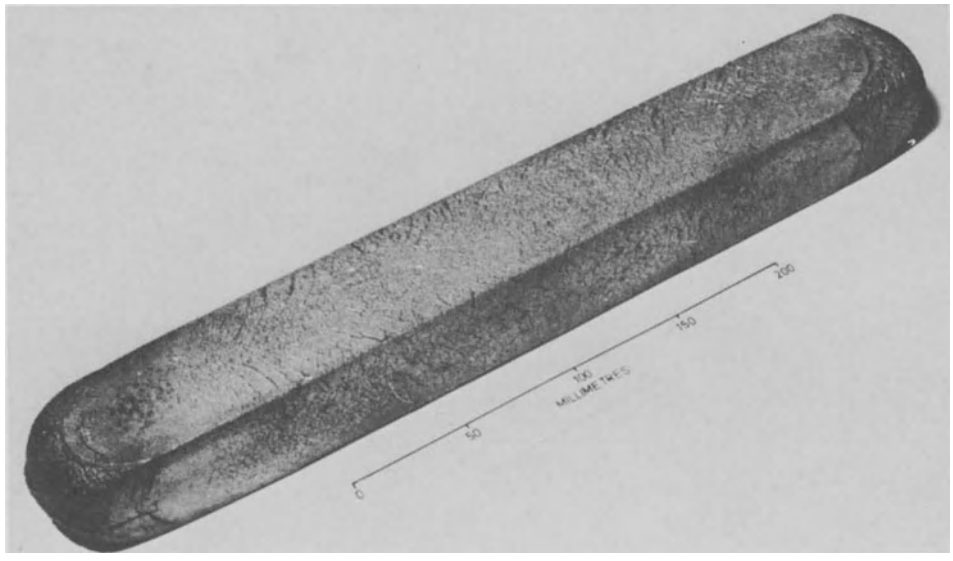

Fig. 1 - HIP + forged CSC shot billet.

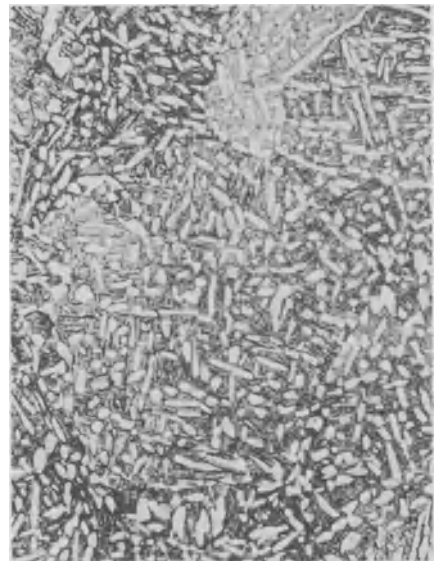

Fig. 2 - Microstructure of CSC, HIP and heat treated billet. x150

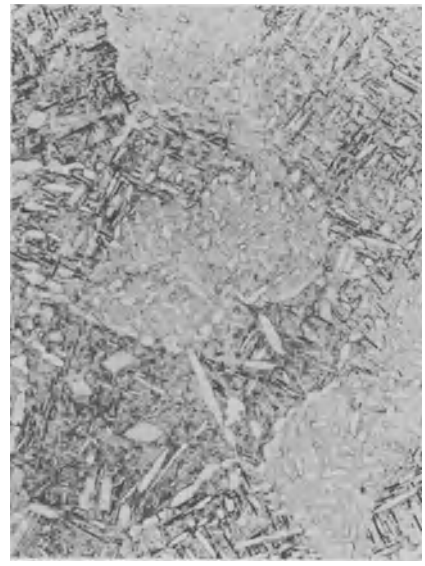

Fig. 3 - Microstructure of REP, HIP + heat treated billet. x150

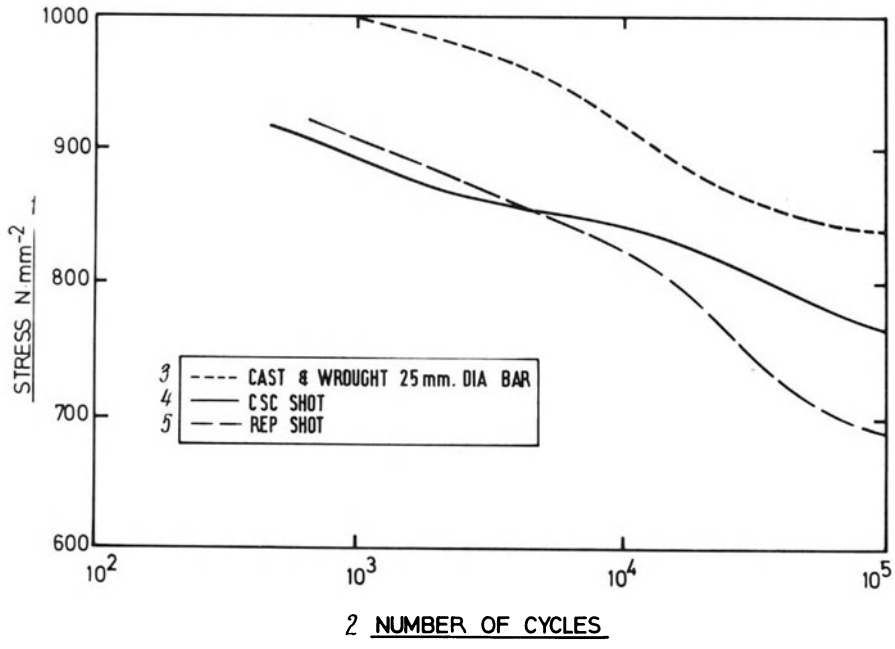

Fig. 4 - Low cycle fatigue data for alloy shot bar (12 mm square) and conventional. 25 mm Ø bar.

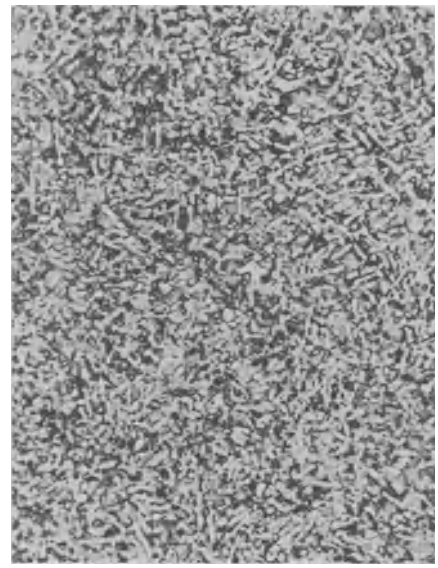

Fig. 5 - Microstructure of CSC, HIP + forged + heat treated billet. x150

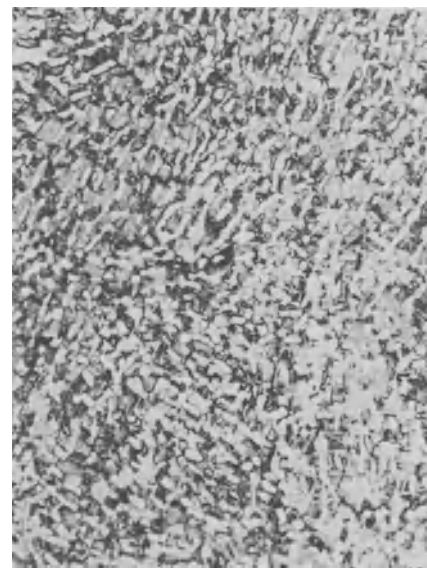

Fig. 6 - Microstructure of conventional cast and wrought billet. x-150

Low cycle fatigue data was obtained on longitudinal specimens and is presented in Figure 7.

A striking feature of all the low cycle fatigue data was the degree of scatter and the presence of internal initiation sites. Both optical and electron metallographic techniques were used to study the phenomenon of internal initiation. Metallographic sections through the REP material revealed the presence of a significant number of angular particles, Figure 8. The particles were up to 200 μm long and were identified by electron probe micro-analysis, as tungsten. Scanning electron microscopy and electron probe micro-analysis were used to study the fracture surfaces of the failed fatigue samples. In fact, all the internal origins were found to be associated with tungsten particles.

A similar examination was made of the CSC fatigue specimens. Once again the internal origins were found to be associated with foreign particles. In this particular instance the origin was an alloy steel shot particle.

Discussion

One of the observations to come out of the results is that although there was a significant difference in the size range between REP and CSC shot, the two materials handled in a similar way. No differences were observed in the way they consolidated or subsequently deformed. The chemistry of both the CSC and REP shot was controlled and the interstitial contamination appears to be a function only of the tank size and not a fundamental limitation of the method.

In general, both consolidated materials behaved in a normal manner and the tensile and fracture toughness levels were at least comparable with conventional cast and wrought material. However, a major divergence from normal was detected in the low cycle fatigue behavior of both materials, in particular the degree of scatter, the levels of results and the presence of internal initiation sites.

The internal initiation sites were readily explained by the presence of 'foreign' particles. However, the observation does underline the necessity of entirely eliminating defects, if an alloy shot route is ever to be successfully used for rotating components. Furthermore, it is significant that only the fatigue test revealed the presence of the defects, unlike the tensile and fracture toughness tests which were apparently unaffected. The sources of the defects in the present batches of material are known. Tungsten particles have been seen before in REP shot,[5] and come from the non-consumable electrode. They could clearly be eliminated by a

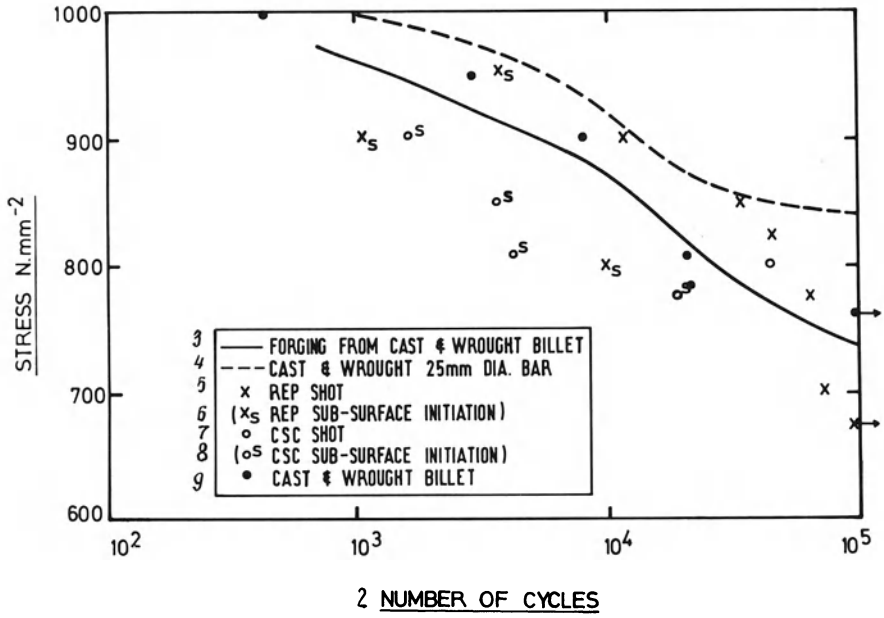

Fig. 7 - Low cycle fatigue data for alloy shot forgings (50 mm square) and conventional billet and bar.

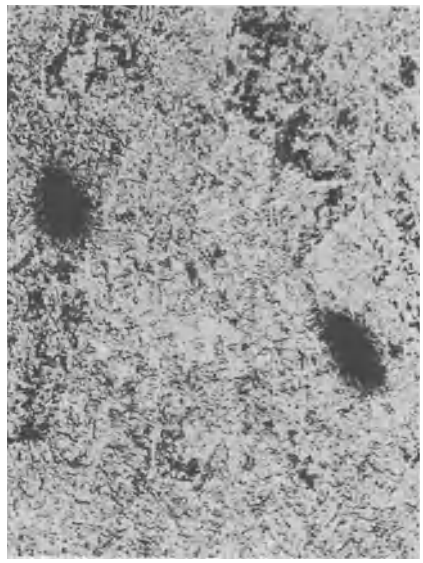

Fig. 8 - Tungsten inclusions in REP billet. x70

change in the electrode material. The contamination of the CSC shot is not a basic problem of the process, but due to cross contamination from previous runs. The situation should be overcome by the exclusive use of a furnace for titanium alloy melting and redesign of the tank for ease of cleaning.

Although the presence of internal origins reduced the fatigue life significantly, the general trend in surface initiated specimens, in both the small and large billet material, was for lower fatigue strengths and a greater degree of scatter than in conventional cast and wrought material of a similar section size (Figures 4 and 7). It is perhaps relevant to compare the results on alloy shot with the fatigue data of conventional billet, which has had about 80% work from the ingot (solid circles Figure 7). Whereas no internal origins were seen in the conventional material, the scatter in the fatigue results is similar to that of the consolidated materials, which have had about 54% work from the as-cast state. The microstructure in the conventional billet (Figure 6) is similar, though slightly coarser than the consolidated and deformed materials (Figure 5). An explanation of the fatigue behavior of conventional billet has been sought in the degree of chemical segregation, texture and grain size. Work has been shown that a minimum amount of reduction of the order of 100:1 is required to maximize the fatigue properties. The fatigue results of the consolidated and forged materials would also suggest that further work is necessary to maximize the levels. It could be argued that this deformation is necessary to minimize the content of micro-segregation within the former shot particles and possibly to strengthen the inter-particle bonding. However, although the evidence is not conclusive, because of the presence of defects leading to internal fatigue origin and premature failure, it does support observations of other workers[3] on the high cycle fatigue properties of consolidated REP shot. The results presented do call into question some of the possible advantages of the alloy shot route. In particular, the claim that because of the fine grain size, components can either be pressed to shape or nearly to shape, requiring either none or little subsequent forging; such components may have significantly inferior fatigue performance compared with conventionally cast and wrought materials.

Conclusions

1. The behavior and performance of CSC and REP consolidated shot are similar.

2. Microstructures and tensile and fracture toughness properties in HIP and HIP + deformed materials are at least as good as those in cast and heavily worked material.

3. Scatter and fatigue strengths in HIP + worked material are inferior to those in conventional material of an equivalent size.

4. The fatigue properties in HIP + worked material are highly susceptible to the presence of foreign particles, which lead to internal initiation origins.

REFERENCES

1. Friedman, G., Int. J. of Powder Met. 6 (2), 1970, 43.

2. Abkowitz, S., Titanium Science and Technology Vol 1, New York Plenum Press, 1973, 501.

3. Friedman, G., Metal Prog. 107, 1975, 81.

4. Hodkin, D. J., Sutcliffe, P. W., Marden, P. A. and Russell, R.E., Powder Met. 16, 1973, 277.

5. Geisendorfer, R. F., Saidak, R. J. and Harth, G. H., Titanium Science and Technology, Vol. 1, New York Plenum Press, 1973, 399.

ACKNOWLEDGEMENTS

The authors wish to thank the Ministry of Defence (Procurement Executive) for their financial support of the work and their permission to present this paper.

Critical Review

TITANIUM MATRIX COMPOSITES

G.J. LONDON

Head, Structural Materials Branch
Aero Materials Laboratory
Naval Air Development Center
Warminster, PA, USA

ABSTRACT

Titanium matrix composite systems are reviewed with emphasis on two systems; those containing silicon carbide coated boron filaments (B/SiC-Ti) and those containing beryllium metal either in powder or continuous filament form (Be/Ti).

Both of these composite systems have properties generally superior to aluminum matrix composites, with certain noted exceptions in the 0° direction (tensile strength and fatigue). Notable are the good transverse properties of titanium matrix composites; Be/Ti flat filament composites appear outstanding in this respect. Be/Ti composites have the disadvantages associated with machining and handling beryllium, a hazardous material. This is offset by the potential ease with which standard metallurgical processing techniques may be applied to both co-extruded powder and filamentary types of these composites.

INTRODUCTION

Titanium matrix composite systems have been studied for about

the past ten years.[1-13] Many of the systems studied were promising to a degree but have not, as yet, found specific use as structural materials. It is the purpose of this paper to review the broader aspects of the various systems and to describe in somewhat more detail two of these systems which appear to offer the promise of ultimate engineering use.

Titanium matrix composite systems may be categorized as follows:

(1) Filamentary - short fibers

(2) Filamentary - continuous fibers

(3) Particulate

These have been produced principally by vacuum hot pressing.[5] Hot isostatic pressing has been examined for mixed powders and hot extrusion has been used for more ductile composite systems such as Be/Ti.[8,9] These systems offer, as their principal advantage, the superior strength and toughness of titanium alloys. Although specific strength or specific modulus is not as high as aluminum or resin matrix composite systems the combination of strength, toughness and elevated temperature service capability has proven atractive for selected turbine engine application such as compressor blading[1] and engine control accessories.[3]

Systems studied in recent years have included filaments of Boron, Boron Carbide, Al_2O_3, SiC (whiskers), SiC (filaments), B/SiC, and Beryllium. Only a few of these systems have shown significant promise. These are the B/SiC-Titanium and Beryllium/Titanium composite systems.

Al_2O_3/Ti(6Al-4V) composites proved difficult to consolidate by normal foil-filament techniques[4] (96MPa, 815°C, 15 minutes). SiC/Ti(6Al-4V) composites exhibited properties essentially similar to the B/Sic-Ti system.[10] The B/SiC-Ti and Be/Ti systems will be reviewed in somewhat greater detail.

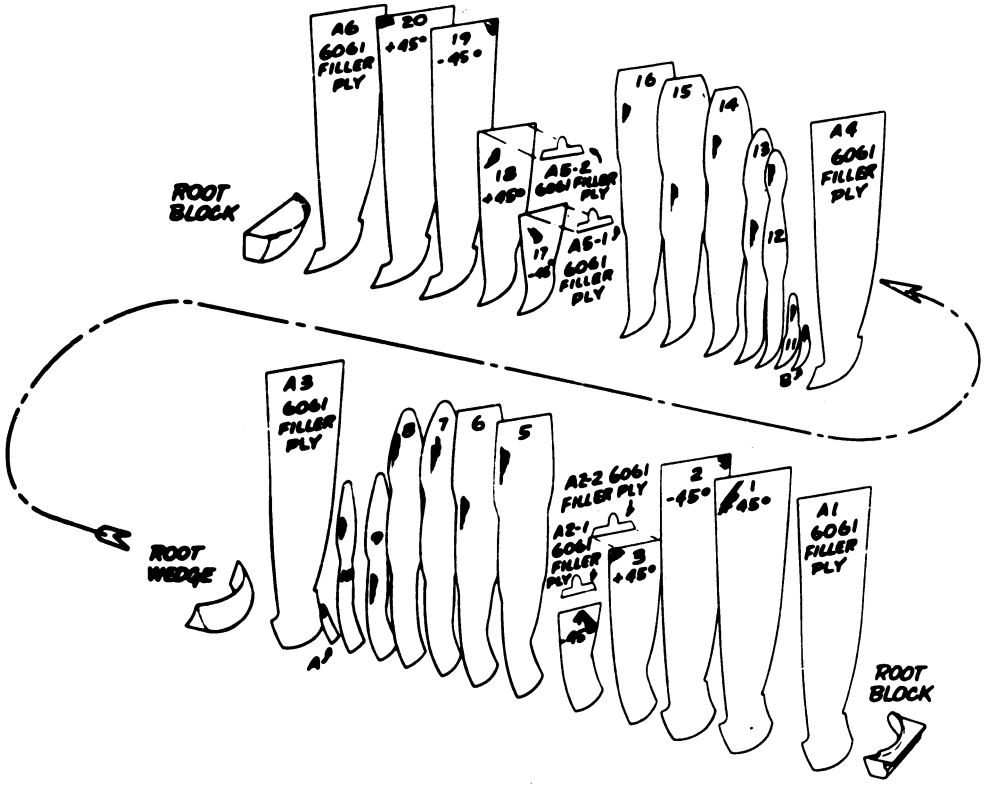

Fig. 1: B/Al composite fan blade configuration of plies root pieces.

B/SiC-Ti COMPOSITES

Early studies on Boron/Titanium composites showed that the boron fibers were not compatible with titanium or titanium alloy matrices at hot pressing temperatures normally required for full consolidation of these composites (i.e., 815-870°C). Silicon carbide coated boron filaments, although still somewhat reactive, were used in subsequent studies which will be reported here.

Fabrication

Several fabrication methods have been studied.[10] All of these use vacuum hot pressing of layered filament/matrix assemblages. The most successful methods have been the vacuum hot pressing of both foil-filament layers and pre-consolidated filamentary monotapes. The monotapes have been produced by drum winding followed by consolidation between layers of titanium alloy foil, forming a single layer composite. Turbine fan blades have been fabricated by assembling many layers of this monotape in shaped dies and isothermally vacuum diffusion bonding to complete the composite and simultaneously form the desired turbine blade shape. Figure 1 shows a schematic diagram of such an assemply for a Boron/Aluminum blade. Figure 2 shows the fabrication sequence for the foil-filament method.

BERYLLIUM/TITANIUM COMPOSITES

The Beryllium/Titanium composite system has been of interest principally for improved specific modulus with better retention of base metal ductility than other composite systems.[6,8,9,11] This is because beryllium, although not as strong as B or B/Sic filaments, exhibits useful tensile ductility especially in the form of fine wire or extruded filaments.

A second attractive feature of this composite system is that both components achieve substantial ductility in the 450-750°C temperature range. This means that composite and component fabrication may be accomplished using normal metal working techniques such as extrusion and forging. This is an important economic factor bearing

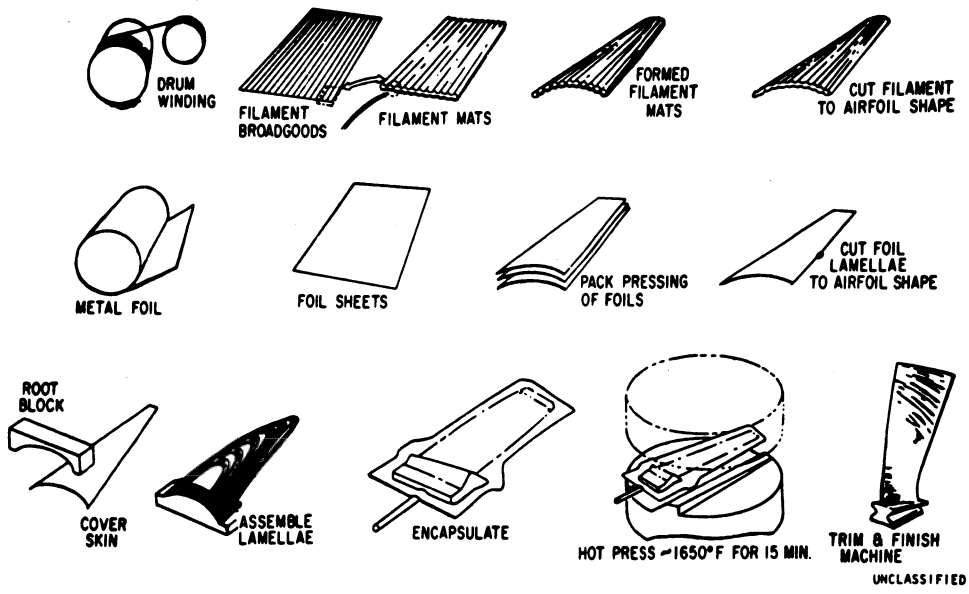

Fig. 2: Foil-filament method fabrication sequence.[5]

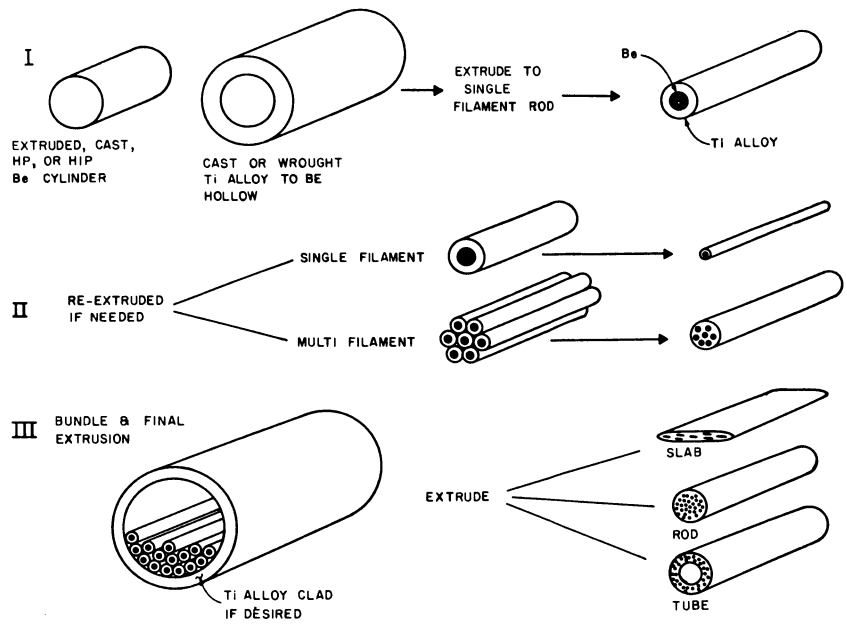

Fig. 3: Be/Ti filamentary composites - multiple extrusion process.

on the ultimate applications to be found for such generally costly products.

Beryllium appears as a unique reinforcement since it is a high specific modulus metal with a relatively low yield and ultimate strength. Thus, specific modulus is improved but yield and ultimate tensile strength are reduced.

Fabrication

Early composites in this system were fabricated by vacuum hot pressing essentially as described for the B/SiC-titanium system. Fine wire (0.13 mm diameter) was co-wound with Ti6Al-4V wire to form composite tape, interlayered with Ti alloy foil and vacuum hot pressed to produce consolidated material. Properties of this type composite were excellent but the unfavorable economics of manufacture led to evaluation of other fabrication methods.

Co-extrusion has been used to produce two distinct Be/Ti composite systems. A continuous filamentary composite with the final appearance closely resembling conventional wire composites is produced by multiple co-extrusion (Figure 3). Discontinuous filamentary composites are produced by co-extrusion of mixed beryllium and titanium or titanium alloy powders.

Secondary fabrication by isothermal forging and hot rolling has been applied successfully to both of these composite types. Figure 4 shows hot extruded eliptical pre-forms and Figure 5 shows forged turbine compressor blades produced by isothermal forging at 704°C from these preforms. Experimental engine control parts (nozzle-links) produced by hot extrusion of mixed Be/Ti (6Al-6V-2Sn) powders and normal metal machining processes are shown in Figure 6.

Note that the continuous filaments have the aspect of flat ribbons (Figure 4) in the extrusion and forging. Such a ribbon geometry, as will be seen below, has the desirable result of improving composite transverse properties when compared to conventional systems (i.e., B/SiC-Ti) or to the powder/powder discontinuous filament type Be/Ti composite.

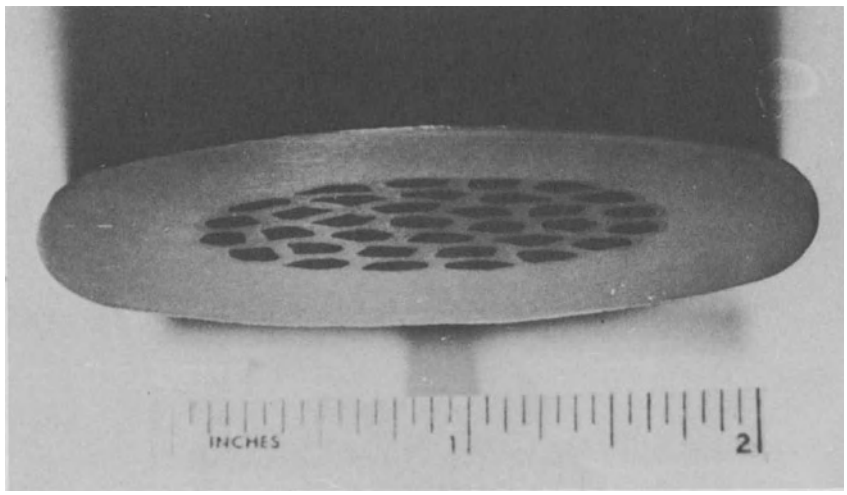

Fig. 4: Hot extruded Be/Ti (6Al-4V) forging preform.

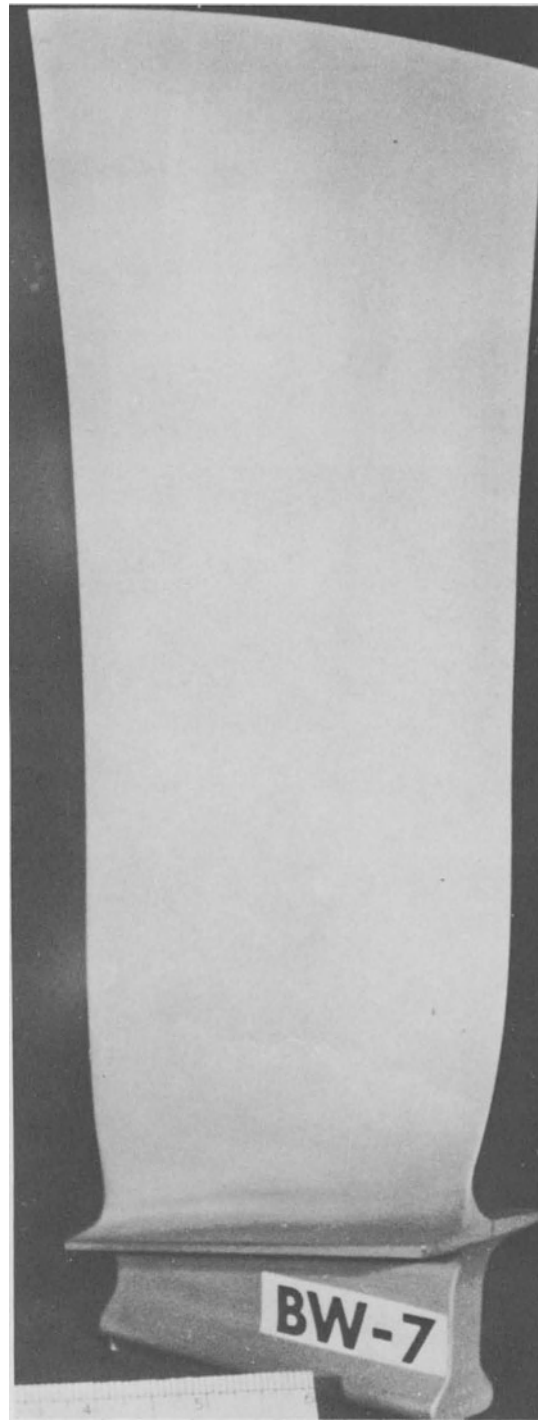

Fig. 5: Hot forged and machined turbine blades (photo - courtesy Detroit Diesel Allison Division of General Motors Co.).

Typical microstructure of these composites is shown in Figures 7 and 8. The interface region usually shows some evidence of intermetallic $TiBe_{11}$ compound formation when extrusion or forming temperatures in excess of 700°C are used. Small amounts of intermetallic do not appear to seriously degrade mechanical properties but no systematic study in this area has, as yet, been reported.

PROPERTIES

Properties achieved with these composite systems are a function of v/o filament, Ti alloy, and with the Be/Ti system, of extrusion reduction ratio and stress-strain history of the composite.

Two factors contribute to low proportional limit of composites in the Be/Ti system. First, the thermal expansion coefficient for beryllium is 2 to 3 times that of titanium. Cooling from the forming temperature, therefore, produces a residual tensile stress in the beryllium component. Second the high beryllium modulus and relatively low (compared to Boron) beryllium yield strength results in a low proportional limit followed by very rapid strain hardening in the 0 to 0.2% strain region. Figure 9 shows a schematic diagram of the modulus effect described. Two interesting effects consistent with the presence of a high residual stress in the beryllium/titanium composites are: First, compressive proprotional limit is much higher than that in tension (Table I); second; tensile proprotional limit <u>increases</u> or remains approximately constant with increased testing temperature. Small tensile pre-strain treatments, therefore, would be expected to have a significant effect on the relative tensile and compressive properties of Be/Ti composites.

<u>Tensile Properties</u>

Both B/SiC-Ti and Be/Ti composites show good strength properties parallel to the filament axis. Neither composite is as strong as comparable B/Al composites but both show superior off axis tensile properties. Figure 10 shows a comparison of tensile properties for Be/Ti, B/SiC-Ti and B/Al composites containing 50 v/o composite

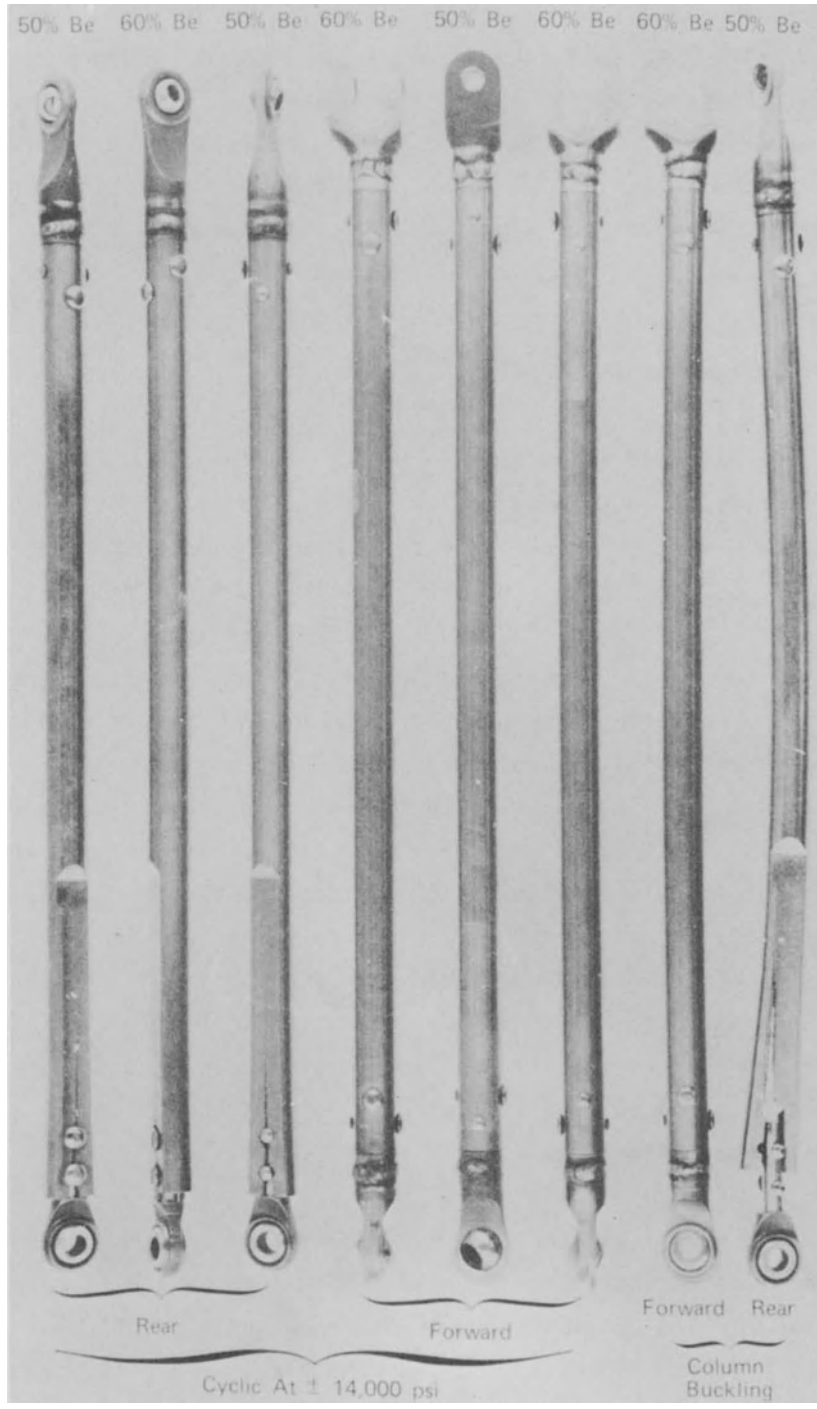

Fig. 6: Experimental Be/Ti nozzle links after 315°C testing.[3]

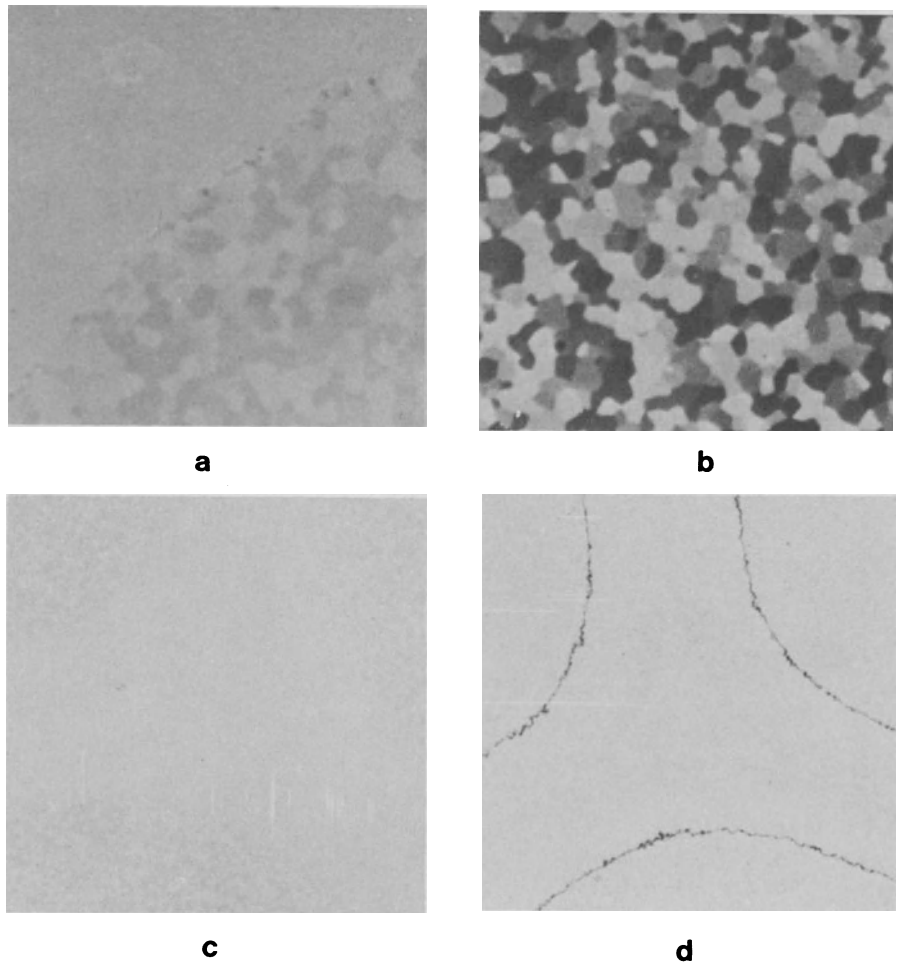

Fig. 7: Photomicrograph showing typical structure of co-extruded Be/Ti filamentary composites. Transverse sections.
a) Sensitive tint,800X.
b) Polarized light, Be filament, 800X.
c) Sensitive tint, unetched, 160X.
d) Bright field, Keller's etch, 160X.

Table 1: Tensile and Compressive Properties of Be/Ti Powder Composites Showing the Proportional Limit Effect

	v/o Be	P.L. (MPa)	T.S. (MPa)	Elong. o/o	Modulus (GPa)
Tensile					
25°C	50[3]	104	846	1.5	192
	60[3]	131	766	~1.0	180
	20-30[6]	90	1075	1.4	143
315°C	50[3]	141	685	4.1	154
	60[3]	133	590	1.6	153
	20-30[6]	227	868	~3.0	107
Compression[6]			CU (MPa)		
25°C	50	1030	1282	-	-
	60	992	1269	-	-
315°C	50	848	1175	-	-
	60	977	1113	-	-

Notes:

P.L. - Proportional Limit
T.S. - Tensile Strength
C.U. - Compressive Ultimate Strength

filament. The extruded filamentary Be/Ti composites show virtually no loss in properties in the 90° direction because of the above mentioned flat ribbon aspect of the extruded flat composite forging pre-forms. Extruded mixed powder Be/Ti composites do not show this transverse strengthening effect and exhibit a drop in properties at the 90° orientation roughly comparable to those shown for the B/SiC-Ti composites. This is apparently because with the extruded powders it is either difficult to achieve good bonding in the transverse direction or the flattened aspect ratio of the fine powder particles is not sufficient to effect the strengthening observed with

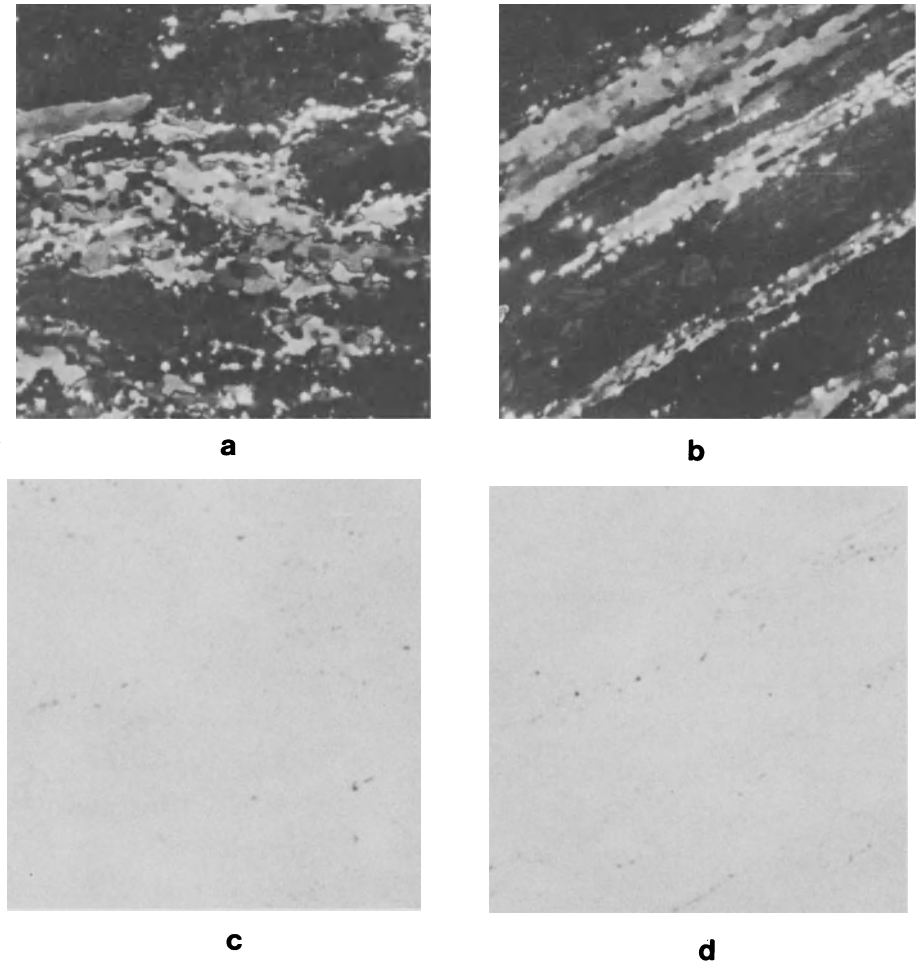

Fig. 8: Photomicrograph showing typical structure of co-extruded Be/Ti mixed powder composite. 200X.

the larger continuous filaments.

True tensile plasticity is an important attribute of the Be/Ti composites. The co-extruded filamentary composites have exhibited as high as 6% tensile plastic elongation. The 40 v/o Be powder composites have shown as high as 10% tensile elongation. B/SiC-Ti composites show essentially linear elastic stress-strain behavior with no plasticity in the 0° direction at room temperature. They do show 1.5-3% tensile elongation in off-axis tests where matrix properties become predominant.

Both Be/Ti and B/SiC-ti composite systems show a relatively small decrease in tensile properties of about 10-15% with increased temperature up to 315°C, the usually considered operating temperature range.

Hot forging at 705°C, an operation unique to Be/Ti composites, results in some tensile property reduction (See Figure 11).

Fatigue Properties

Parallel to the filament axis, titanium matrix composites exhibit about the same low cycle fatigue strength but much lower high cycle fatigue strength than comparable aluminum matrix composites. (Table II) This situation is reversed in the off axis direction with B/SiC-Ti composites greatly superior to B/Al composites. Direct comparison of B/SiC-Ti with Be/Ti composites is difficult because of the limited data available for the latter system. Present data shows that in the axial direction Be/Ti composites have significantly lower low cycle fatigue strength and somewhat lower high cycle fatigue strength than B/SiC-Ti composites. Even these lower fatigue strength values, however, appear satisfactory for most design applications.[1,2,3]

Ballistic Impact Resistance

Ballistic impact resistance is an important composite property where the design application requires damage tolerance. Such is the case for turbine engine fan or compressor blade applications. Titanium matrix composites retain much of the excellent impact re-

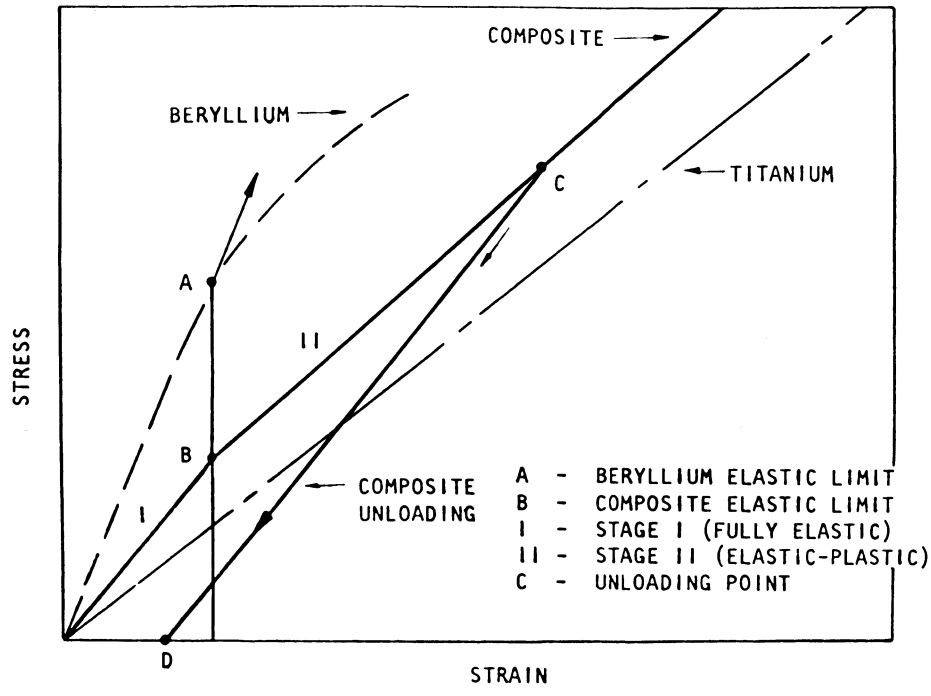

Fig. 9: Schematic diagram: - composite stress-strain behavior based on analysis of component modulii and elastic limits.

Table II: Comparative Fatigue Strength of B/SiC-Ti, Be/Ti and B/Al Composites

Material Orientation	Strength (MPa) at Indicated Cycles	
	10^4	10^7
30 v/o B/SiC-Ti(6Al-4V)[10]		
0°	1089	414
90°	379	207
30 v/o Be/Ti(6Al-4V)[6]		
0°	448	345
90°	-	-
40 v/o B/Al(6061)[10]		
0°	1048	931
90°	103	69

sistance of the matrix titanium alloys and are superior to aluminum matrix composites.

A common measure of ballistic impact resistance is to measure the residual strength after a given energy ballistic impact usually from steel balls or pellets. Other tests such as real and simulated bird impacts have qualitative utility but quantative comparisons prove difficult. Figure 12 shows the residual strength of Ti-6Al-4V, B/SiC-Ti, Be/Ti and B/Al as a function of impact energy.[6,10] The superior properties of the titanium matrix composites are clearly evident.

DISCUSSION

Titanium matrix composites, although the subject of relatively limited study, exhibit an attractive combination of properties. Projected weight savings as a high performance structural material is not as great as with either organic or aluminum matrix composite systems. When one considers serviceability, however, especially where damage tolerance or elevated temperature service is required

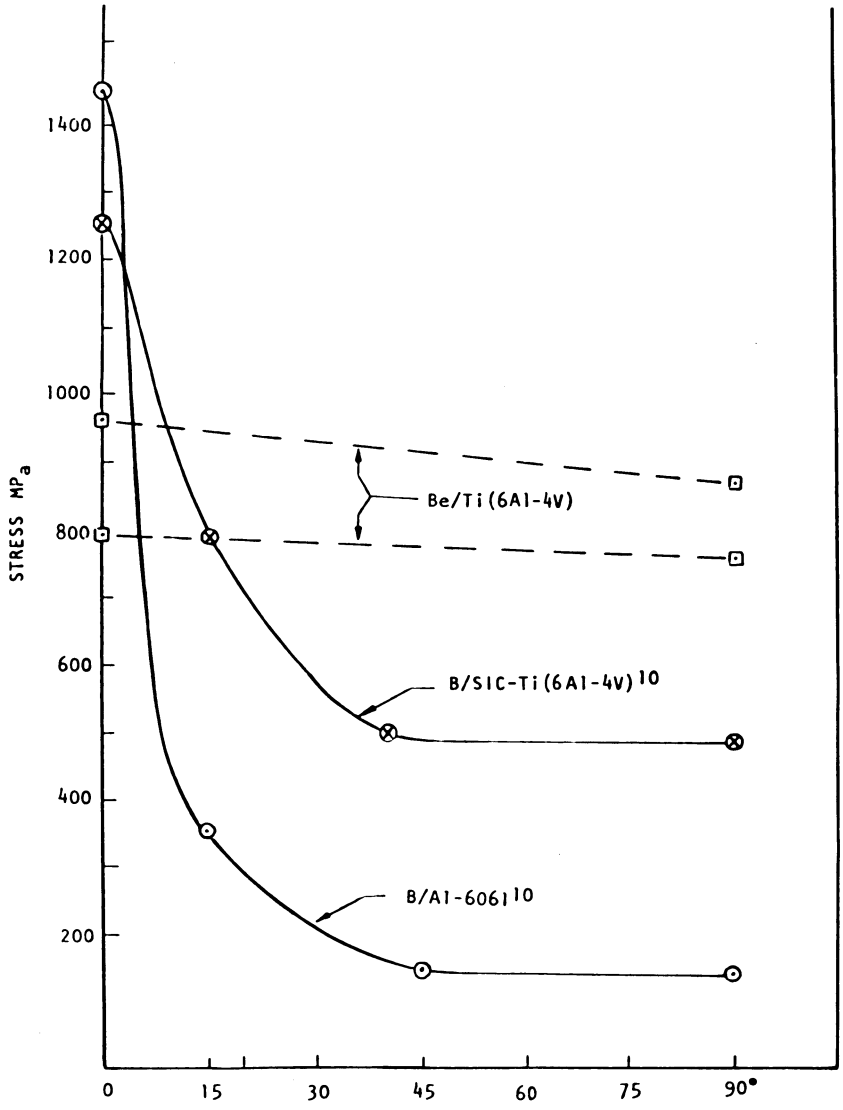

Fig. 10: Comparison of off-axis tensile strength (50% composites).

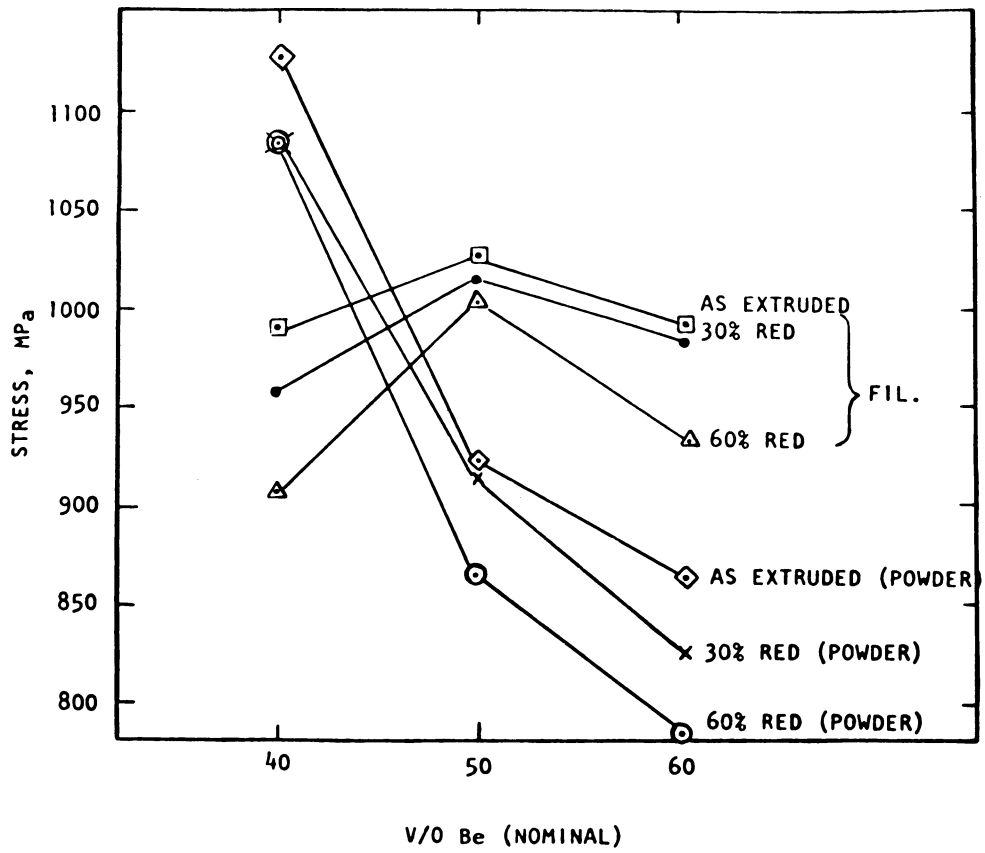

Fig. 11: Ultimate tensile strength vs V/o Be, various forging reductions (705°C), data from refs. 6,7.

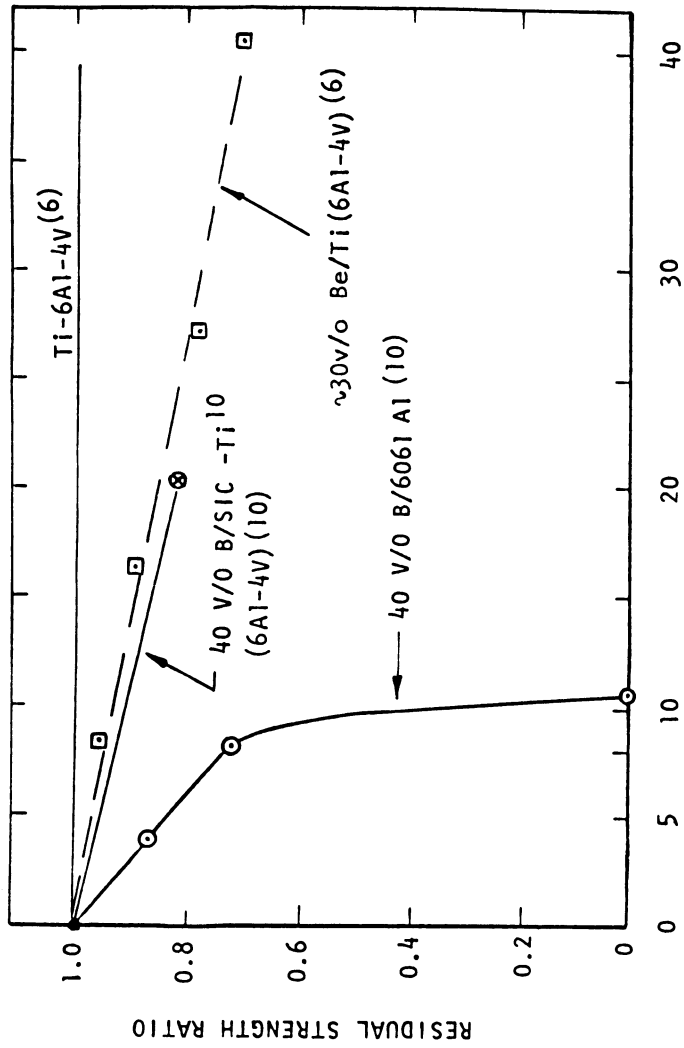

Fig. 12: Comparison of ballistic impact resistance of Be/Ti B/SIC/Ti and B/AC composites.

titanium matrix composites are clearly superior.

Strength of both B/SiC-Ti and Be/Ti appears adequate for most stiffness critical design application, i.e. where specific modulus is the principal design property. Fatigue properties both at ambient and elevated temperatures also appear adequate. Extruded flat Be/Ti filamentary composites have transverse strength properties superior to other systems because of the flat filament aspect produced by the extrusion process.

Although cost factors have not been emphasized in this discussion, they play an important role in the actual utilization of any new material system. The question always arises concerning the relative merit of a given improvement in performance (i.e. lighter weight, longer range or increased load carrying ability) compared to the cost of achieving such improvement.

B/SiC-Ti composites are relatively costly. The coated boron filaments have remained high priced. Titanium alloy foil is considerably more costly than aluminum foils. Substantial labor is needed to assemble and vacuum hot press the composite part. One analysis[5] does suggest competitive costs for this system but this must be proven in practice.

The beryllium-titanium composite systems, either mixed powders or filamentary, appear attractive from a cost point of view. Properties remain adequate after such operations as hot forging or hot rolling. The potential exists for direct extrusion of needed shapes such as "T" sections or tubing. Future studies should focus on improving the utility of this system.

The toxicity of any material containing beryllium metal is also a factor which must be considered when evaluating the Be/Ti system. Such a problem must be understood and properly handled from a personnel safety point of view and will certainly add to the cost of utilizing these composites. Many aerospace companies, however, have successfully established maching and handling techniques for the safe utilization of beryllium metal. If other fac-

tors remain favorable, therefore, the toxicity problems should be manageable.

SUMMARY

Two titanium matrix composites, B/SiC-Ti and Be/Ti have received considerable attention in recent years. Both of these composite systems have properties generally superior to aluminum matrix composites with certain noted exceptions in the 0° direction (tensile strength and fatigue). Notable are the good transverse properties of titanium matrix composites; Be/Ti flat filament composites are outstanding in this respect. Be/Ti composites have the disadvantages associated with machining and handling beryllium, a hazardous material. This is offset by the potential ease with which standard metallurgical processing techniques may be applied to both co-extruded powder and filamentary types of these composites.

REFERENCES

1. Sippel, G. R. and Herman, M., *Optimization and Design Criteria for Beryllium/Titanium Composites*, Detroit Diesel Allison Division of General Motors, Report No. EDR8159, Naval Air Systems Command Contract N00019-74-C-0103, March 1974
2. Goodwin, V. C. and Herman, M., *Structural Requirements of Compressor and Fan Blading of Beryllium Composite Materials*, National Materials Advisory Board Conference on Beryllium, Washington, D. C., March 1970
3. Cox, A. R., *Beryllium/Titanium Bimetal System*, Pratt and Whitney Aircraft Division, United Technologies Company, Report N00019-74-C-0117 (Naval Air Systems Command Contract), Sept 1975
4. Tressler, R. E. and Moore, T. L., *Mechanical Property and Interface Reaction Studies of Titanium-Alumina Composites*, Metals Engineering Quarterly, Feb 1971, pp 16-22

5. Toth, I. J., *Metal Matrix Composite Blade Fabrication Methods*, Paper of 19th SAMPE Symposium, Buena Park, California, April 1974

6. Spees, J. A. et.al., *Optimization and Design Criteria for Beryllium/Titanium Composites*, Detroit Diesel Allison Division of General Motors, Report EDR8600, Naval Air Systems Command Contract N00019-74-C-0103, Sept 1975

7. Stonehouse, J., Brush-Wellman Corporation, Cleveland, Ohio, USA, Private Communication

8. Kovacs, W. J. and London, G. L., *Synthesis and Material Characterization of Beryllium/Ti-6A1-4V Composites*, Accepted for Publication, Metallurgical Transactions 1976

9. London, G. L., Taylor, W., and Herman, M., *Co-Extruded Beryllium-Titanium Composites for Light Weight Structures*, National SAMPE Technical Conference, Space Shuttle Materials, Oct 1971

10. Toth, I. J., *Comparison of the Mechanical Behavior of Flamentary Reinforced Aluminum and Titanium Alloys*, Composite Materials: Testing and Design (Third Conference) ASTM STP 546, American Society for Testing and Materials, 1974, pp 542-560

11. Isserow, S. and Rizzitano, F. J., *Titanium-Beryllium Microcomposites: A State-of-the-Art Review*, Composites, July 1974, pp 141-150

12. Schmidt, R., *Method of Making a Beryllium-Titanium Composite*, U. S. Patent No. 3, 667, 018, June 6, 1972

13. Goodwin, V. L., *Method of Fabricating a Beryllium-Titanium Composite*, U. S. Patent No. 3, 774, 290, Nov 27, 1973

INVESTIGATION OF STRUCTURE OF TITANIUM MATRIX FIBER COMPOSITES

M. Kh. Shorshorov, V.I. Bakarinova, V.I. Antipov

A.A. Baikov Institute of Metallurgy, USSR Academy of Sciences,

U.S.S.R.

When developing metal-base composites including those with a matrix of titanium and its alloys reinforced with fibers of boron, silicon carbide, etc., it is necessary to solve the problem of compatibility between the fiber and the matrix that determines the mechanical properties at elevated temperatures. The difficulty involved in making the matrix and fiber compatible in these materials already arise at the stage of their production. This is due to the fact that while the composites are formed in a short period of time, the temperatures exceed the operating ones. Mutual diffusion between the elements of the matrix and fiber can occur under operating conditions, thereby impairing the properties of the composites.

EXPERIMENT PROCEDURES

This study is devoted to investigating the conditions required to obtain sheet fiber composites by the vacuum hot pressing method and the compatibility between the alloy of the Ti-Al-V system and the reinforcing fibers of boron and silicon carbide in the process of production and subsequent heat treatment. The matrix alloy in the initial state had an ultimate strength of 70 kg/mm^2. The outer diameter of fibers amounted to 100 μm, the diameter of the tungsten core was 12-18 μm, the thickness of the silicon carbide coating applied to boron fiber was about 4 μm.

The hot pressing method is most suitable for the production of these composits due to excellent possibilities of controlling temperature and time-dependent parameters, as well as force parameters of the process. The production temperature was varied within 880-1000°C, the hold time - within 10-30 min., the specific pressure

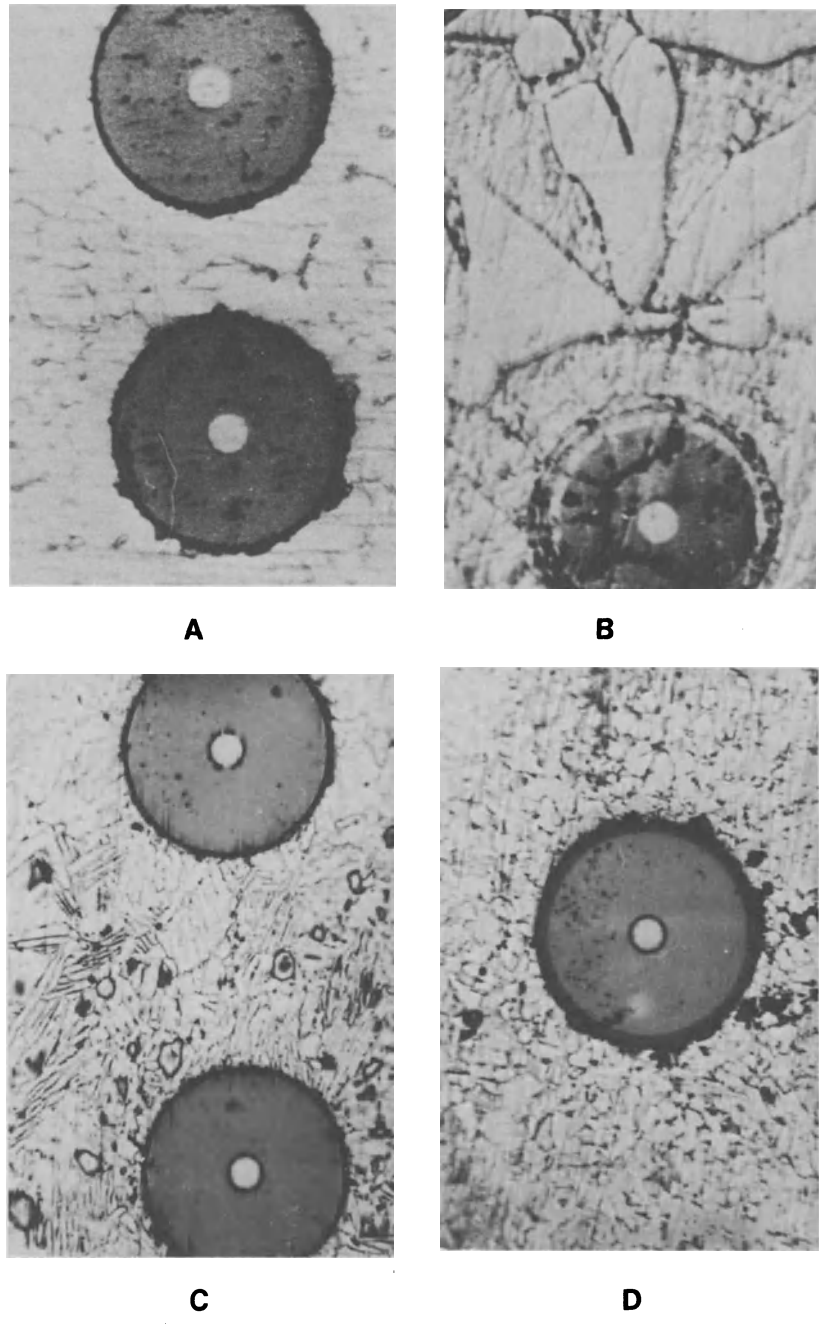

Fig. 1: Microstructure of composites after annealing Ti-Al-V-alloy/SiC for 50 hours at 840°C (a) and 1000°C (b); Ti-Al-V-alloy/B (c) and Ti-Al-V-alloy/BORSIC (d) in initial state, x 300, after etching.

was in the range of 0.4-3 kg/mm^2. The quality of finished composites was evaluated by micostructure and mechanical properties.

The comparison between the thermal stability of the composites and the fibers of boron and silicon carbide was made after vacuum annealing at 800-1000°C with hold times of up to 100 hours according to the results obtained in the cross-sectional investigation of the microstructure of specimens. The composition of the interaction area at the boundery between the fiber and matrix was assessed by means of a local X-ray spectrum analysis. The fractures in the specimens of the composites were studied with the JSM-U3 scanning electronic microscope.

EXPERIMENTAL DATA AND DISCUSSION OF RESULTS

It is known from literature that the fiber of silicon carbide is more stable in the matrix made of pure titanium than the boron fiber under the same conditions but due to the lower density the boron fiber with various coatings including that with silicon carbide is recommended for the reinforcement of titanium.(1,2)

When using a three-element alloy as a matrix, as was the case in our study, it was necessary to investigate whether the same dependence was preserved, what its kinetics were, and to make an attempt by using these characteristics to evaluate the durability of the silicon carbide coating on the boron fiber.

Fig. 1 illustrates the change in the microstructure of the Ti alloy/SiC,B compositions after different temperatures and time conditions of annealing. An increase in the annealing temperature causes an increase in the size of the matrix grain, the formation of a diffusion interactive area at the interface between the fiber and matrix; the thickness of the area grows and its inner structure changes. On the boron fibers the area is formed at a lower temperature, and the formation of pores that seem to be of a diffusion origin is observed at the boundaries between the core and fiber and the area and fiber.

The quantitative studies made on the microstructure of the composites containing fibers of boron and silicon carbide have shown that the diffusion area that results after annealing has a larger thickness with boron fiber than with silicon carbide. Fig. 2 represents the variations in the thickness of the interaction zone that is being formed depending on the annealing time at a constant temperature in boron-reinforced composites (dashed lines) and silicon carbide-reinforced composites (solid lines). A noticeable difference in the rate of thickness growth at the interface has been observed at similar temperatures. Thus, while the interaction zone thickness in the silicon carbide composite amounted to 6 μm after 50 hours of annealing

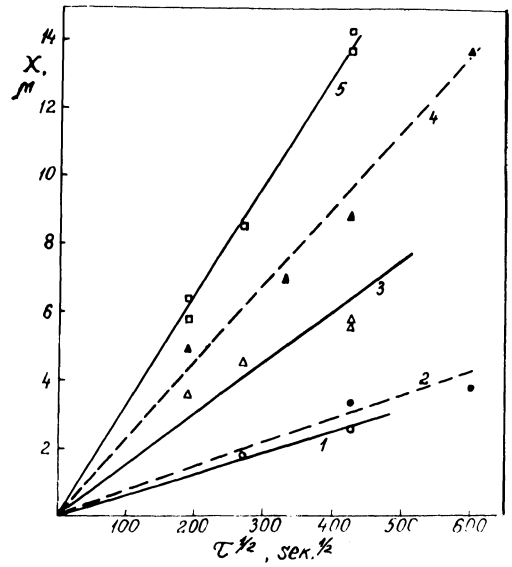

Fig. 2: Relationship between the diffusion area (x) in the composites of Ti-alloy/SiC (solid lines), and Ti-alloy/B (dashed lines) and the annealing time ($\tau^{\frac{1}{2}}$) at temperatures of: 1, 2-800°C, 3, 4-900°C, 5-10000°C.

at 900°C, in the boron fiber-reinforced composite it was 1.5 times higher. The linear character of the relationships represented in Fig. 2 makes it possible to determine approximately the expected thickness of the diffusion zone or the extent of interaction between the fiber and matrix, establishing this extent by the change in the fiber diameter at a pre-determined temperature and annealing time. As a result, assuming that there is a slight diffusion of boron through the silicon carbide coating, it is possible to show that the 4 μm-thick area should be formed at 1000°C at the boundary of Ti - alloy/SiC in about 8 hours. Therefore, it has been assumed that a 4 μm-thick coating should not be dissolved during the process of hot pressing.

For titanium alloy and silicon carbide composites it is interesting to note how the alloying elements of the matrix are distributed in the area and its adjacent layers. The curves for the distribution of relative intensity of the Ti, Al, V. Si, C, W, radiations have been obtained by the method of local X-ray spectrum analysis. These studies were made with specimens annealed for 50 hours at 1000°C, the microstructure of such a cross section is given in Fig. 1c. The distributions was recorded by shifting the electron beam from the matrix through the interaction area, fiber and up to the

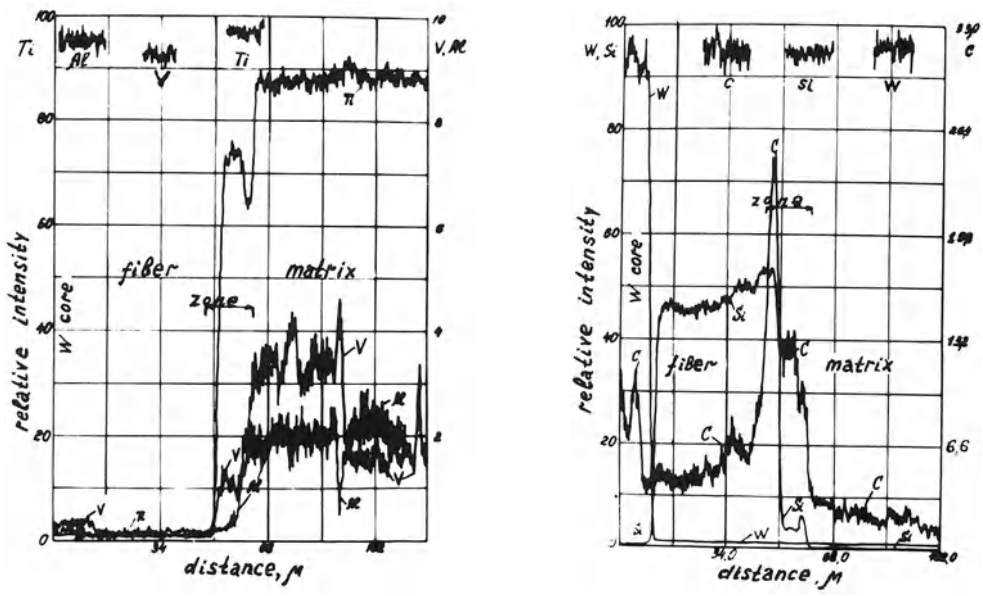

Fig. 3: Curves for distribution of relative intensity of Ti, Al, V (a) and W, Si, C-radiations in the cross section of the specimen of the Ti-Al-V-alloy/SiC composites after annealing for 50 hours at 1000°C.

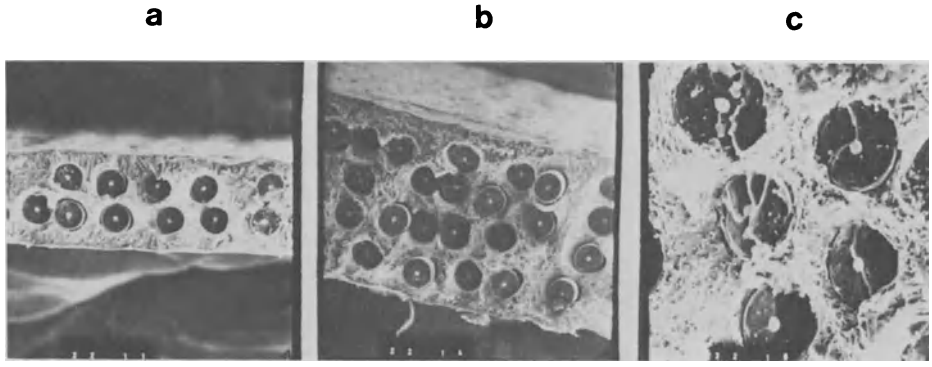

Fig. 4: Fractography of failure in the specimens of the Ti-Al-V-alloy/BORSIC obtained at 1000°C (a), 880°C (b), x 50, 900°C (c), x 250.

middle of the fiber core. After the mentioned annealing conditions the area has dimensions which are clearly distinguished on the microanalyzer. It can be noted in Fig. 3 that the matrix alloy is characterized by a constant level of titanium and aluminum intensity, while in terms of vanadium a variable level of intensity was observed in different matrix grains.

A noticeable maximum of intensity was observed on the carbon radiation curve when transferring from the diffusion area to the fiber. However, in terms of such light elements as carbon, considerable errors are possible. The silicon carbide fiber after annealing, judging by the microanalysis data, had two parts in its structure which differed by the level of intensity of silicon and carbon radiations. A considerable concentration of carbon was also observed in the tungsten core of the fiber. Titanium, silicon, carbon were the main elements that built up the diffusion area. Vanadium was also present in the area while aluminum did not take part in the formation of the area. This analysis makes it possible to draw a conclusion that silicides and titanium carbides are formed in the interaction area, this being in agreement with the data published earlier on the interaction in the non-alloyed titanium and silicon carbide composite.[3,4] The alloying elements of the matrix seem to effect the rate of formation and growth of the area, but not its composition.

The mechanical properties were determined by using composites with titanium alloy matrix reinforced with fibers of silicon carbide or BORSIC. The maximum ultimate strength of the composite amounted to 88 kg/mm^2, while the modulus of elasticity calculated by extension curves reached 20000 kg/mm^2. These mechanical properties were obtained in the alloy reinforced with BORSIC fibers whose concentration was to 20% by volume.

Specimens subjected to tensile tests were studied by the fractography method on a scanning microscope (Fig. 4). It is possible to see clearly the needle-type structure of the matrix and the brittle character of its failure in the composite formed at 1000°C, and the equiaxial grain, as well as the ductile character of failure of the composites obtained at 880 and 900°C. The silicon carbide coating on the boron fiber was preserved under all conditions for the production of composites.

Thus, the titanium alloy and BORSIC fiber composite can be produced under conditions similar to those which are used to obtain silicon carbide-reinforced composites, and they are of quality as long as the integrity of the coating is preserved. The utilization of BORSIC fibers to reinforce titanium alloys makes it possible to produce composites which are stable in terms of temperatures and time both in the fabrication process and under operating conditions.

REFERENCES

1. Dzyadykevich Ju.V., Isvestija Academie Nauk SSSR, Neorgancheskie Materialy, 1974, IO, NI, 44-46, (Russ.)

2. Burte H.M., Lynch C.T., Metal Matrix Composites, ASTM STP 438, 1968, 3-25.

3. Galasso F., Pinto J., Fiber Sci. and Technol., 1969, 2, 89-95.

4. Burykina A.L., Kosolapova T.Ja., Dzyadykevich Ju.V., Priluzkii E.V., Gorski V.V., Poroshkovaja Metallurgia, 1973, N3, 57-64, (Russ.).

MODEL COMPOSITE (LAYERED) MATERIAL ON THE BASIS OF TITANIUM

L. A. Petrova, L. P. Grankova, V. I. Belyaev and
A. P. Korshenevsky
A. A. Baikov Institute of Metallurgy

U.S.S.R.

Modern technology demands of material more and often incompatible requirements, for example, the combination of very high strength along the high fracture toughness and lightness. cently there appeared many publications on titanium alloys possessing much higher mechanical properties as compared with those known before. There are many publications about the improvement of properties of known alloys by using new kinds of heat treatment. By the latter is meant mild quenching including cooling in the furnace from the β-field to the temperature of α+β field followed by cooling in air (1);two stage aging, namely at first aging at the temperature of existing ω-phase and then at temperature field of (α+β) phases (2); different variants of thermomechanical treatment (3,4). Additional doping of known grades of alloys is widely used with the purpose of increasing strength and toughness. New composites are being developed using multicomponent alloying and such elements as Cu, Si, As.[5,6]

However, the shortcomings of all high strength titanium alloys ($\sigma_{0,2} > 100 kg/mm^2$) are the loss of their strength in parts of large sections. For example, fatigue strength of parts of large sections greatly decreases. According to[7] the fatigue strength of parts of large section is 60% of that of thin rods. In this case the decrease in strength is attributed, according to the authors, to the absence of uniformity of structural condition in large sections. In addition to this, conditions of stress of the material at the tip of the crack become more severe in large sections, namely the crack propagation in large sections occurs in the conditions of the plane strain instead of plane stress condition of the material at the crack in thin sheets. It decreases fracture toughness of the

material in large sections and results in the fact that the inherent strength of the material is not fully realized. Therefore, high strength properties of new developmental titanium alloys (150-180 kg/mm^2) cannot be realized in the products of large sections.

To circumvent this loss in usable strength of the material with the increase in the thickness of the section, it is possible to use layered titanium material. Optimal fabrication of layered semi-products must exclude the loss of strength properties due to non-uniformity of the structural conditions in the thick sections. The loss of fracture toughness (due to more severe condition in the material at the tip of the crack) must also be prevented due to the specific mechanism of destruction (delamination) of the layered material consisting of alternate strong and ductile components.

Model samples of multilayered material were fabricated by two methods, i.e. by rolling in vacuum and explosive welding.

Multilayered Material Fabricated by Method of Rolling

One of the age hardened metastable titanium alloys with $\sigma_c \sim 150 kg/mm^2$ was employed as a high strength component and the titanium foil (0.1mm thick) or technically pure titanium (plates 1-2mm Thick) or α-alloys with $\sigma_c \sim 75 kg/mm^2$ were used as a ductile component.

The choice of the two latter materials was determined because of the need for structural stability of the material at the temperature of aging necessary for obtaining a high strength condition of β-titanium alloy. Composite samples containing various volume percentages of the ductile component (10-50%) were fabricated by hot rolling in vacuum of the respective packet at 1000°C. The fabricated composite plates 6mm thick were quenched in water and subjected to aging. Bonding of sheets of α and β titanium by the method of rolling proved to be technologically difficult.

Irregular thickness of sheets of the α and β titanium alloy were observed while studying the microstructure of five layered composite material and showed that plastic deformation of sheets occurs unequally. This resulted in lack of agreement in the predicted relationship of strength and ductility and correspondingly large scatter of mechanical properties of the samples cut out of this plate.

The study of microstructure and physicochemical interaction on the interface between layers using microprobe x-ray analysis and

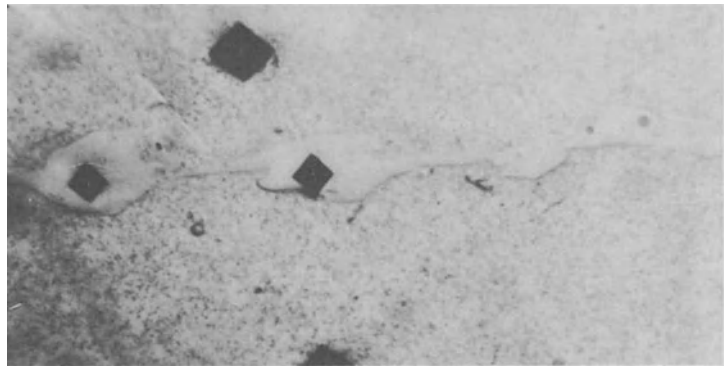

Fig. 1: Multisheet sample of OT_4 alloy: Section of bonding zone between layers ("white phase") by 340.

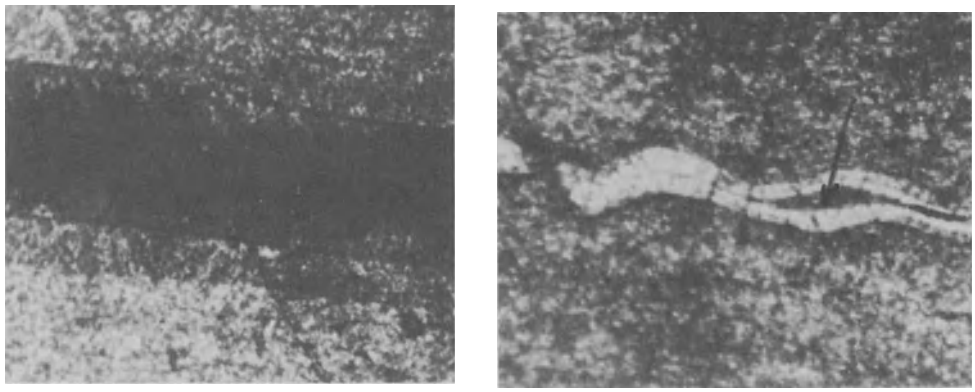

Fig. 2: a,b. Two types of interface of layers in bonding zone of ten layered sample of OT_4 alloy. x by 500.

x-ray structural analysis allowed us to note the following important factors:

1. While studying microstructure of the samples of composite material large segregations such as TiH_2 were observed on the surface of grains of α-Ti. With the help of x-ray structural analysis (in copper K_α-radiation) these segregations were identified as TiH_2.

The diffraction pattern showed reflections of TiH_2 - (111), (002) and (022) at angles (2θ) equal to 35°, 7°; 41° and 59°, respectively. Only traces of TiH_2 were detected in the parent foil. Visible increase in the amount of TiH_2 is most likely due to etching of foil sheets in diluted HF prior to rolling. This processing is not desirable without subsequent dynamic vacuum annealing.

2. A visible intermediate zone between the sheets was practically absent immediately after rolling. However, it appeared after heat treatment of the composite. (The heat treatment included quenching in water and subsequent aging, which is necessary for obtaining high strength of β-alloy). According to microprobe x-ray analysis the thin sheet of the foil of α-Ti, 0.03-0.05mm thick, was bound to be saturated through the thickness with alloying elements from β-alloy. This resulted in the foil sheet no longer behaving as the high ductility component, and this composite therefore exhibited low ductility. Thus, minimum thickness of the ductile component to preserve its role should be chosen after considering the depth of penetration of alloying elements from β-alloy.

Model Samples Fabricated by Explosive Welding

The method of explosive welding allows us to obtain multisheet products practically ready (i.e. without additional heat treatment) from the components with highly different properties. As our studies showed, the bounding quality is greatly dependent on the flatness of sheets. It was shown previously that to achieve high strength condition of metastable β-titanium alloy, it is necessary to quench and age the sheets. Quenching of sheets results in distortion which is not permissible in bonding these sheets by explosive welding. To eliminate the quenching deformation special steel plates 20mm thick were fabricated. Deformed sheets were inserted into the plates in this "enprisoned" condition and aged at desirable temperature. Aging in the plates restored flatness to the sheets. Multilayered structures 10-12mm thick and up to 40mm thick in some cases were obtained by explosive welding. Plates of alternate layers of high strength and ductility components and ten layered plates of the sheets of the same material were obtained. The latter had two purposes: 1. To facilitate understanding the

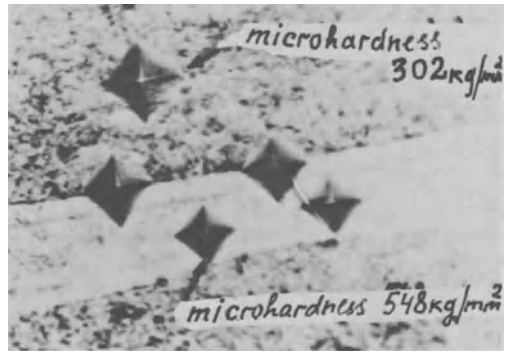

Fig. 3: Bonding zone of sheets (same as in Fig. 2a). Not etched. by 500.

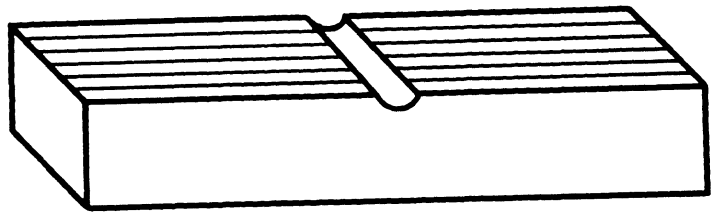

Fig. 4: Scheme of notch grove with respect to arrangement of layers on samples according to Menage of multisheet composite material titanium base.

process taking place on the interface of layers bonding by explosive welding. 2. To compare mechanical properties of multisheet sample with those of monolytic samples of the same material.

Multisheet plates of the same material were fabricated from sheet alloy OT_4 (Ti-3.3% Al-1.4% Mn-0.3%Fe) as-received; alloys BT14 (Ti-4.5%Al-3.0%Mo-1%V-0.5%Fe) and HBT1 (Ti-7Mo-5,5Cr-3Fe-3Al) in strengthened condition.

In the samples of all above mentioned alloys there were observed formations of the so called "white phase" (Fig. 1) in some parts of the bonding zone between sheets. This formation is often considered by certain authors to be a chemical compound between the components. The existence of this formation on bonding sheets of the same alloy shows that "the white phase" is a structural condition characteristic of the materials obtained by explosive welding. The "white phase" is most likely parts in which the material was melted. Much higher values of microhardness in the bonding zone as compared with the parent material may be accounted for by solubility of interstitials (namely O and H) in these zones. Oxygen and hydrogen as a rule saturate the surface layer of the sheet material. The common observation for multisheet samples consisting of the same material was the fact that their strength proved to be higher than that of the monolithic samples of the same alloy. The strength of multisheet samples of the OT_4 alloy was higher than that of the monolithic samples of 25% but for the BT14 alloy - 12% under (by other equal conditions). This means that strength properties of alloys decreasing in large sections may be maintained and even increased by fabricating plates of large sections in the form of multisheet material of the same alloy. It is necessary to note that impact toughness of the like layered material determined on the standard notched samples "Menager" (l x b x h = 55x10x10mm), exactly corresponded to the impact toughness of the monolithic samples of the same material.

Some increase in strength of multilayered samples as compared with the strength of monolithic samples of the same material is due to the contribution of high strength layer appearing on the interface between the layers. Particularly interesting results were obtained on the multilayered samples of the OT_4 alloy. Two types of boundaries in the bonding zone of the ten layer samples are given in Figure 2a and b, i.e. the boundary resembling the band of deeper etching (Fig. 2a) and the most typical form of the bonding zone - wavelike boundary with light (not yielding to etching) parts and vice versa dark parts of deeper etching shown with arrows in Figure 2b. Microhardness of parts with deeper etching in the bonding zone appeared to be equal to 521-609kg/mm^2 as compared with 204-270kg/mm^2 for the material inside the layer - Figure 3. Microhardness of the light parts in the bonding zone varied from 317-378kg/mm^2.

Microprobe x-ray analysis was carried out for the parts of higher microhardness. Distribution of the alloying elements (Al, Mo, Mn) and interstitials (O) in the bonding zone and inside the sheet were studied. No difference in the concentration of these elements both in the bonding zone and inside the sheet was observed. The phase composition of multilayer samples of OT_4 alloys determined by x-ray structural analysis (x-rayed surface included all bonding zones) revealed the presence of α (α'), α'', β and ω-phase. Two very pale but main reflections: $(11\bar{2}1)$ and $(11\bar{2}2)$were obtained for ω-phase at angles of 2θ equal to 79° and 51°, respectively. Only $\alpha(\alpha')$ and α''-phase with traces of β-phase were observed as a result of the determination of the phase composition of sheet alloys as delivered. Thus, the difference in the value of microhardness between separate parts along one and the same bonding zone and from zone to zone can be explained by the non-uniformity of the structural condition of the samples of the OT_4 alloy.

We explain observed parts with the highest hardness due to the presence in them of the ω-phase. The ω-phase probably appears as a result of the local phase transformation because of the high pressure and the local heat in some bonding zones. The increase in quantity of the β-phase in the material after explosive welding as compared with the as-received material allows us to conclude that decomposition occurs in accordance with the reaction $\alpha''\rightarrow\alpha+\beta(\omega)$ in the bonding zone by explosive welding due to high impact energy.

It is necessary to note that considerable contribution to the increase in microhardness in the bonding zone may cause dissolution of the interstitials in these zones. Particularly oxygen greatly increases hardness of α and β-titanium solid solutions on dissolving of oxygen in minute quantities which may not be observed by microprobe analysis.

The results obtained demonstrate the possibility of obtaining high strength layers (or layers with properties differing from the properties of the as-delivered material) right at the moment of joining sheets by explosive welding.

The investigation of model samples of composite material fabricated from alternate layers of high strength and ductile material (total thickness of the plate 10-12mm) revealed that their strength properties are somewhat higher than those calculated in accordance with mixture rule. The test titanium alloy in strengthened condition with σ_c = 150-180kg/mm^2, δ = 3%, a_H = 3-1.5kgm/cm^2 was used as a high strength component. The titanium alloy with $\sigma_{02} \sim$ 90kg/mm^2, δ = 19-16%, $\psi \sim$ 50% and a_{H_2} = 5-6kgm/cm^2 was employed as a ductile component. $\sigma_{02} \sim$ 145kg/mm^2, $\delta \sim$ 5% and a_H = 8-10kgm/cm^2 were obtained on the samples of the composite multilayered material. Impact toughness was carried out on the standard Menager samples.

The notch was made in such a way as to be directed toward or along the position of sheets. If the notch is made as it was shown in Figure 4, the impact toughness of the same material was low ($3kgm/cm^2$). The latter clearly reveals the importance of the sheet structure for increase in toughness. Fracture toughness of the multilayered material was determined on the samples with side cracks in the conditions of static yielding.[8] Preliminary notch positioned as in Figure 4 was made by electrospark method. The fatigue crack was produced by cyclic bending. The fracture toughness of this layered material was determined to be K_{IC} = 150-170$kg/mm^{3/2}$ as compared with $111kg/mm^{3/2}$ for the material of the high strength component.

References

1. Auvinet, J., Leleu, G., Notton, G. and Marquier, G., "Mem. Sci. Rev. met.," 1973, 70, NII, 809-821, II, III, V.

2. Alheritiere, E., Morinier, R. and Syre, R., "4 eme Sornee etude aciers el alliag. Spee. sew. aviat. Bourget, 1971," Paris, 1972, k/I-k2. Duscuss k/23-k26.

3. Boyer, R., Taggart, R. and Polonis, O. H., Metallography 7, 241-251 (1974).

4. Nyffengger, W. and Schweisstechn., Z., 1972, 62, N 3, 61-76.

5. Seagle, S. R., Hall, G. S. and Bomberg, H. B., "Metals and Quart" 1975, 15, N I, 48-54.

6. Goosey Richard Ernest. Titanium-base alloys. (Imperial Metal Inds (Kynoch) Ltd.). Great Britain Pat. N 1298923. Cl.C7A. Int. cl. C22 015/00. Filed January, 7.71. Published December 6, 72.

7. Stubbington, C. A. and Bowen, A. W., The effect of section size on the fatigue properties of Ti-6Al-4V bars. "Titanium Sci. and Technol. Vol. 2", New York - London, 1973, 1283-1296. Discuss. 1427-1428.

8. Collection. Applied questions of fracture toughness. Publisher "Mir,"Moscow, 1968.

THE INVESTIGATION OF SOLID-PHASE INTERACTION OF TITANIUM WITH REFRACTORY COMPOUNDS

V. M. Anohin, R. K. Ognev and N. I. Shirokova

Titanium Institute

U.S.S.R.

The study of the regularities of a solid-phase interaction in the system of titanium-refractory compound is of a theoretical and practical interest, since its results can be used in various fields of metallurgy and engineering, particularly in powder metallurgy when creating titanium powder-based composite materials. The character of such an interaction governs the choice of sintering and heat treatment conditions and to a considerable extent determines the mechanism of strengthening and finally the properties of sintered titanium articles.

The interaction of titanium in contact with zirconium oxides, carbides, nitrides and silicides was investigated.

The Evaluation of the Possibility for Titanium Interaction with Refractory Compounds

Thermodynamic calculations of the possibility for solid-phase reactions between titanium and zirconium-based compounds, performed with the use of published thermodynamic calculations[1,2] have shown that the expected reactions proceed within the range of positive magnitudes of Z, that is, they are unlikely (Table I).

The isobaric-isometric potentials of titanium with zirconium carbide reaction in a temperature range of 1000-1500°K have low positive magnitudes, within the error limits for thermodynamic values determination, therefore, the calculation results may not be conclusive for the possibility or impossibility for each reactions to proceed.

Table I

Magnitudes of Isobaric-Isometric Potentials of Interaction Reactions of Titanium with Compounds

System	Reaction	Z^o $\frac{cal}{mole}$ Temperature, K^o 1000	1100	1300	
Ti-ZrO_2	$ZrO_2 + 2Ti = 2T10 + Zr$	+13800	+13750	+13800	+13200
	$3ZrO_2 + 4Ti = 2Ti_2O_3 + 3Zr$	+52400	+53450	+51300	+48800
	$5ZrO_2 + 6Ti = 2Ti_3O_5 + 5Zr$	+118200	+115650	+113000	+107600
	$ZrO_2 + Ti = TiO_2 + Zr$	+33750	+33550	+33250	+32700
Ti-ZrN	$ZrN + Ti = TiN + Zr$	+6450	+7500	+6550	+6400
Ti-ZrC	$ZrC + Ti = TiC + Zr$	+2900	+2970	+3110	+3250

Table II

X-ray Analysis Results and Microhardness of Titanium-Carbide Compositions, Annealed at a Temperature of 1150^oC

Charge composition analysis	Phase microhardness kg/mm^2	Phase composition	Titanium crystal lattice parameters, Å	
			a	c
Initial Ti	165	Ti	2,945	4,690
Ti+5%TiC	260	Ti+TiC	2,949	4,688
Ti+5%ZrC	320	-Ti based -solid solutions + TiC	2,957	4,706

Besides the chemical interaction the following processes are possible between titanium and compounds.

1. Titanium is dissolved in an initial compound.
2. Metal of a compound (zirconium) is dissolved in titanium.
3. Non-metal of a refractory compound is dissolved in titanium.
4. Both components of a compound are dissolved in titaniu
5. Titanium-based compound interacts with initial compound or initial single-based compounds formed.

In the former 4 variants the character of interaction is determined by the conditions of the elements solubility and dimension factor is used as a criterion of approximate evaluation of solid solutions formation.[3,4] Titanium and zirconium form a continuous series of solid solutions. All the non-metals included in the composition of refractory differ considerably in their structure and atomic diameters dimension from titanium and have a limited (oxygen, nitrogen) or very limited (carbon, silicon) solubility in titanium.

As for the fifth variant of the interaction "compound-compound" the following may be assumed. The main conditions for the compounds to form continuous series of solid solutions are a mutual solubility of metals, included in their composition, the same time of crystal lattice and chemical coupling in compounds.

The formation of continuous solid solutions of titanium and zirconium oxides is impossible due to the difference in crystal lattices: titanium dioxide has a tetragonal and rhombic cell, and a TiO_2 structural type, zirconium dioxide is characterized by a cubic and monoclinic crystal system and a Mn_2O_3 structural type.

Titanium carbide and zirconium carbide can form continuous series of solid solutions, since these carbides are crystallized within the same crystal system (cubic), have the same dimensional group, refer to the same structural type (NaCl), and the metals which form them are compatible. The same reasoning may be used to assume the possibility for the formation of a continuous series of solid solutions during the interaction of titanium and zirconium nitrides. Among the silicides the most probable formation occurs between Ti_5Si* and Zr_5Si_3.

*Editor's note: probably Ti_5Si_3.

Experimental Investigations of the Interaction

To investigate a solid-phase interaction of refractory compounds with titanium, double-layer samples were prepared. That is, a layer of powder of the compound under investigation was pressed on a polished surface of billets compacted from electrolytic titanium powder under a pressure of $8t/cm^2$. The double-layer samples were placed in evacuated ampules and annealed at temperatures of 700, 850, 1000, 1150°C for 1, 5 and 10 hours. Sections were prepared in a plane perpendicular to the contact surface.

The metallographic investigations were carried out on a MIM-7 microscope. Microhardness measurements were made on a PMT-3 unit at a load of 20g. X-ray analysis of the diffusion zone depth by means of an electronic probe was performed on a REMP-2 unit. Measurements of zirconium K radiation intensity were carried out to determine the depth of the diffusion zone. Pulses were picked up for 10 seconds at 5μm spacings.

Titanium oxides. Titanium microstructure at the interface with titanium dioxide displays a solid solution layer with oxygen after annealing at a temperature of 700°C. As temperature and annealing time increase the depth of the strengthened layer thickens and at a temperature of 1150°C attains 200μm (Fig. 1).

The interaction of titanium with zirconium dioxide resulted in the formation of platey structure; plates being formed in the direction of zirconium diffusion (Fig. 2).

The change in zirconium K radiation intensity according to the depth of diffusion zone is in agreement with the change in microhardness (Fig. 3).

Since the coefficients of zirconium radiation absorption for zirconium and titanium are approximate, the relative intensities coincide reasonably with zirconium and titanium percentages. Therefore, using the data in Fig. 3, the concentration of zirconium in titanium in any point of a diffusion zone can be calculated according to the formula[5]

$$W_{Zr} = \frac{I_{Zr} - I_{\infty}}{I_{100Zr} - I_{100_{\infty}}} \ 100\%$$

where:

I_{Zr} = zirconium X-ray intensity in the given point of a sample;

I_{∞} = background intensity in a point;

I_{100Zr} - 100% zirconium standard (reference) X-ray intensity which equals 3000+500 $\frac{\text{pulses}}{\text{sec.}}$;

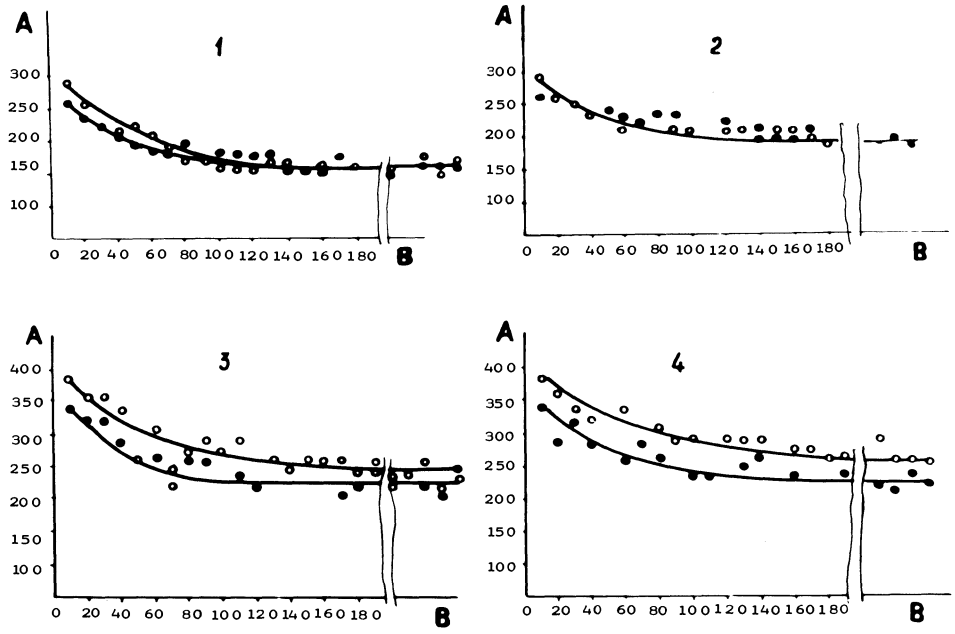

Fig. 1: The change in a microhardness according to depth for a titanium sample, annealed in contact with titanium dioxide at the temperatures of 700°C (1), 850°C (2), 1000°C (3) and1150°C (4) during 1 hour (---) and 5 hours (——).
A - microhardness, kg/mm^2
B - distance from contact surface, μm.

Fig. 2: Titanium microstructure in the zone of contact with zirconium dioxide after annealing at a temperature of 1150°C.

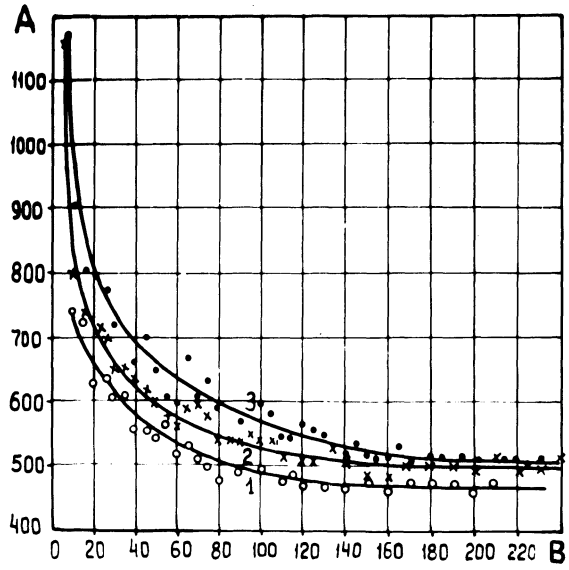

Fig. 3: The change in K zirconium radiation intensity according to the depth for a titanium sample, annealed in contact with zirconium dioxide at the temperatures of 850°C (1), 1000°C (2), and 1150°C (3) during 5 hours.
A - zirconium K radiation intensity pulses/sec.
B - distance from titanium sample surface, μm.

I_{100_∞} = reference background intensity which equals 600 $\frac{\text{pulses}}{\text{sec.}}$.

After 5 hours annealing of a double-layer sample at the temperatures of 850, 1000, 1150°C, the concentation of zirconium in titantium at a depth of 5μm equaled 1,3; 2,7; and 2,9%, respectively.

Proceeding from the fact that the relationship between zirconium and oxygen dissolved in titanium corresponds to the formula of zirconium dioxide, then the concentration of oxygen in this point at the above cited temperatures should amount to 0,44; 0,92 and 0,99%,respectively. The microhardness of titanium at a depth of 5μm when annealed in contact with zirconium dioxide at a temperature of 1150°C, equals 450kg/mm^2 (Fig. 2), which corresponds to the microhardness of titanium alloy with 1% oxygen.

Titanium nitrides. The investigation of microstructure and microhardness in the zone of titanium contact with nitrides shows that a notable diffusion of nitrogen is observed at temperatures of 1000°C and above, particularly with annealing time of 10 hours and longer. A notable difference in titanium microstructure in the zone of contact with TiN and TiO_2 is not observed, since the influence of nitrogen and oxygen on the titanium structure is similar. In the zone of contact there are several areas which are clearly distinguishable: a layer of loose unsintered nitride, a zone of titanium solid solution in titanium nitride with the microhardness of 700-750kg/mm^2, and finally a titanium-based solid solution with a microhardness of about 400kg/mm^2.

When in contact with zirconium nitride, titanium structure is characterized by a platey solid solution texture; the growth of plates being observed with temperature increase along with a notable thickening of boundaries. The diffusion curves, plotted according to the intensity of a characteristic radiation, confirm that a notable diffusion of zirconium into titanium, that is the interaction of ZrN and Ti, is observed at a temperature of 1000°C and above.

Titanium-carbides. Some interaction of titanium with TiC and ZrC has been noted at temperatures of 1000°C and above. It manifested itself in the formation of a thin, rather dense layer of carbide phase on the titanium surface. Apparently, this layer serves as a barrier, inhibiting the diffusion of carbon and zirconium into titanium, and accounts for a minor strengthening of titanium in the contact zone. However, zirconium diffusion into titanium occurs less intensively than from zirconium oxides and nitrides, the evidence of which is a titanium platey structure in the zone of contact with zirconium carbide, particularly notable after annealing at a temperature of 1150°C, and the curves of zirconium K radiation intensity.

Table III

Coefficient "n" Magnitudes for the Equation

Compound contacting with Ti	Annealing temperature °C	Coefficient "n"	Compound contacting with Ti	Annealing temperature °C	Coefficient "n"
TiO_2	1000	2,8	ZrN	1000	8,6
	1150	2,2		1150	6,7
ZrO_2	1000	1,9	TiC	1000	12,4
	1150	2,4		1150	12,8
TiN	1000	8,2	ZrC	1000	9,1
	1150	8,1		1150	8,8

To make more precise the character of titanium interaction with carbides, the compositions Ti+5%TiC and Ti+5%ZrC were investigated.

The samples of powder mixtures of initial substances were compacted at a pressure of 8t/cm^2 and sintered at a temperature of 1150°C for 3 hours. Rounded carbide particles strongly bound with the base were found in the sintered samples. In the composition of Ti+5ZrC, titanium particles acquired a platey texture, characteristic for the alloys of titanium with zirconium. X-ray pictures of samples with 5%TiC and 5%ZrC are identical and correspond to the mixture of titanium and titanium carbide (Table II).

This confirms the occurrence of titanium interaction with zirconium carbide in solid state resulting in the formation of titanium carbide.

Titanium-silicides. No changes have been found in the microstructure of titanium, annealed in contact with titanium disilicide at temperatures up to 1150°C. Probably, the titanium surface forms a very thin, dense SiO_2 film, inhibiting diffusion of the components; the methods used failed to disclose such a film.

Interaction Regularities

The curves describing diffusion zone width vs. annealing time are in the form of parabolas and, consequently, obey the general equation:*

After logarithmation we find n=ctg (-angle of straight lines inclination to axis lg). The coefficient magnitudes vary in a rather wide range - from 1,9 to 12,8 (Table III).

When interacting with oxides, the coefficient magnitudes is approximately 2, which characterizes this interaction as a diffusion process. It has been shown above that the metallographic and radiographic investigations confirm the absence of intermediate phases or chemical interaction in the system titanium-nitrides and titanium-carbides is connected with chemical reactions, occurring in them, as well as the formation of intermediate layers, which is confirmed by metallographic and radiographic investigations of the interaction zone.

CONCLUSIONS

The solid-phase interaction of titanium and refractory compounds are determined by the diffusion processes of compound components

*Editor's note: parabolic equation left out.

dissolution in titanium matrix. The kinetics of dissolution processes in a solid state are greatly influenced by such factors as chemical interaction, formation of new phases, their structure, and the difficulty of the components to enter the reaction zone.

The interaction of oxides with titanium was observed at a temperature of 700°C with component oxides dissolving in titanium. A considerable interaction of nitrides and carbides with titanium occurred at a temperature of 1000°C with compound components dissolving to form titanium carbides or nitrides or more complex compounds. Minor interaction of silicides with titanium was found at temperatures as high as 1150°C.

The kinetic curves describing the diffusion zone width vs. time are satisfactorily described by the equation*. The exponent "n" is approximately 2 when titanium interacts with oxides, which gives evidence of a diffusional dissolution of oxide components in titanium; the magnitude of "n" increases for other compounds, which form intermediate layers and interact chemically with titanium.

The results of metallographic and radiographic analyses allow a listing of titanium and zirconium refractory compounds, according to decreasing affinity to titanium: oxides - nitrides - carbides - silicides.

REFERENCES

1. Uiks, K. E. and Block, F. E., Thermodynamic properties of 65 elements, their oxides, halides, carbides and nitrides. Publishing house "Metallurgia," M., 1965.

2. Voitovich, R. F., Refractory compounds. Thermodynamic characteristics. Reference book. Publishing house "Naukova Dumka," Kiev, 1971.

3. Kornilov, I. I., Matveeva, N. M., Priahina, L. I. and Poliakova, R. S., Metallochemical properties of the periodical system elements. Publishing house "Nauka," M., 1966.

4. Um-Rozeri. The structure of metals and alloys. GONII, M, 1938.

5. Birks,L. S., X-ray microanalysis by means of electronic probe. Publishing house "Metallurgia," M., 1966.

*Editor's note: parabolic equation left out.

THE INFLUENCE OF RELEASE AGENTS ON PROPERTIES OF THE TITANIUM FOIL PRODUCED BY VACUUM EVAPORATION

O. T. Rashevitz, V. S. Fedyakina, A. I. Vovsi,
N. S. Kashpur, Yu. B. Ulanovsky and E. V. Yadin

All-Union Institute of Light Metals

U.S.S.R.

It is well known[1-3] that to impart to thin metal foil the plasticity desired requires that the precipitation of its metal vapour be effected on a heated substrate. The substrate preheat temperature is determined by the material the foil is made of, and for titanium it amounts to as high as 40% of its melting point.[2] At such temperatures processes of mutual diffusion usually set in vigorously at the interface; these processes contribute to the formation of a strong bond between the condensate and the substrate. Release agents serve to facilitate the separation of such condensates.

There are a number of papers[3-5] containing suggestions for the selection of release agent materials when producing various foils, including those of titanium. It is known, however, that the process of solidification from a vapour phase essentially depends on the material of a substrate and the structure of its surface; the role of the substrate in that case being played by the release agent. According to our knowledge, no experimental data on the influence of the release agents on the properties of foil produced are available in literature.

In the present paper, calcium and magnesium flourides were used to study the influence of release agents on the separability, structure, and mechanical properties of the titanium foil produced at various temperatures of the substrate.

Experimental Technique

Titanium foil was produced by using as a substrate specimens

of 12X18H9 grade polished steel having dimensions 80 x 0.5 x 140mm. Prior to the application of a separating layer, the steel specimen underwent degassing annealing in a vacuum of about $5x10^{-4}$ Torr at a temperature of about 950 to 1000°C for a period of 2 to 3 minutes.

The release agent was applied by the evaporation of condensed powders of magnesium and calcium flourides from a boat in a vacuum of about $5x10^{-4}$ Torr, and by depositing at a rate of about 0.2 to 1.0μm/min on a substrate preheated up to a temperature of about 300 to 400°C. The thickness of the separating layer was 0.5 to 1.0μm.

Titanium was evaporated from a copper, water-cooled crucible in a vacuum of about $5x10^{-5}$ Torr by the aid of two electron-beam guns each having a capacity of about 12kW. The condensation rate of titanium amounted to about 3 to 5μm/mm the thickness of the foils studied about 30 to 35μm/mm. In order to exclude the influence of the sedimentation parameters, titanium was applied simultaneously onto substrates with calcium flouride and with magnesium flouride, the substrates being arranged in one container. The substrates were preheated by the aid of an electron beam, the preheating temperature was measured by means of chromel-copel thermocouples.

The mechanical properties of the titanium foil (e.g., ultimate strength and elongation) were tested by subjecting foil specimens to tension on the "Instron"-type tensile test machine.

The structure of titanium condensates and of separating layers was examined with the aid of the Neophot optical microscope.

The separability of the titanium condensate was evaluated with the naked eye and was considered to be satisfactory if the foil separated from the substrate without ruptures and breaks of its continuity.

The gas evolution analysis was carried out with the MX-7301 monopole mass-spectrometer.

The through porosity of the release agents deposited on steel was determined by the superposition of filter paper according to the State Standard "GOST 16875-71".

Experimental Results and Their Discussion

Researches done have shown the following: under the aforementioned preparation conditions, using calcium and magnesium flourides as a separating layer, satisfactory separation of the

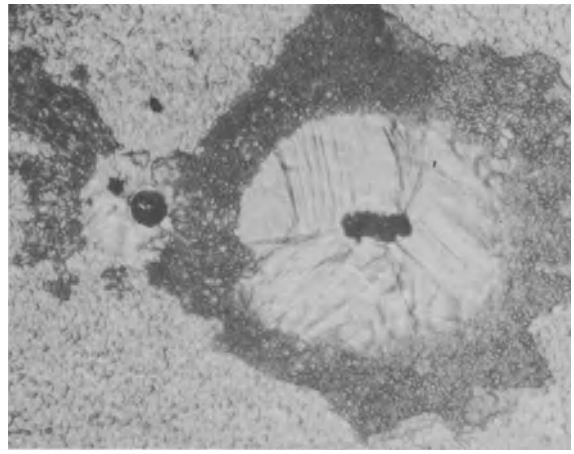

Fig. 1: Microphotograph (x 340) of the surface of a magnesium fluoride layer after preheating it in a vacuum up to a temperature of 900°C.

titanium foil from the substrate was effected up to a condensation temperature within the range of 800 to 900°C. In this case, for most specimens the release agent remained on the surface of a steel substrate. The separability was found to deteriorate as temperature was raised, and the foil produced exhibited damages and through pores that formed during its removal from the substrate.

It has been established that the maximum temperature of titanium, at which the satisfactory separation of the foil is still possible, depends upon the material the separating layer is made of and is raised by as much as 100 to 150°C when calcium flouride is used.

With a view to studying the causes of the deterioration in the separability of titanium condensates that are deposited at a temperature in excess of 800 to 900°C, research was done on the state of the surface of the release agent just at the moment of the titanium condensation. As is shown in Fig. 1, when the steel substrate coated with a layer of magnesium flouride was preheated in a vacuum up to a temperature of about 900°C, we detected bare portions of steel, resulting evidently from the partial evaporation of magnesium flouride. When titanium atoms deposit on the bare portions of the substrate, interaction occurs between titanium and steel, the interaction being accompanied, as was pointed out in paper[6], by the formation of brittle metallides that impair the separation of the foil and damage it during the course of its tearing off.

A similar phenomenon, however, at higher temperatures, say be-

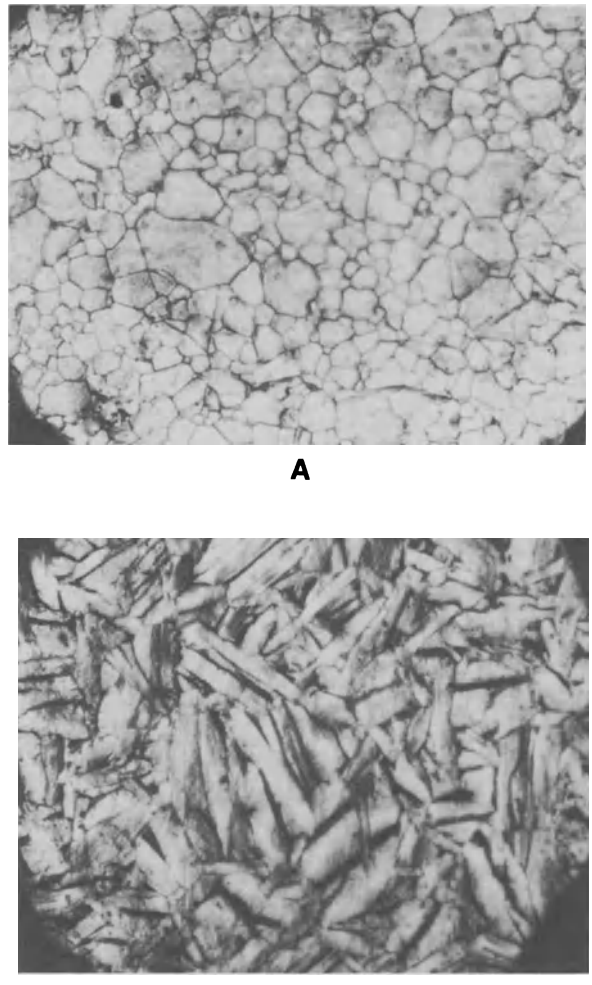

Fig. 2: Microstructure (x 340) of the titanium foil deposited at a temperature of 800°C on: a) magnesium fluoride, and b) calcium fluoride.

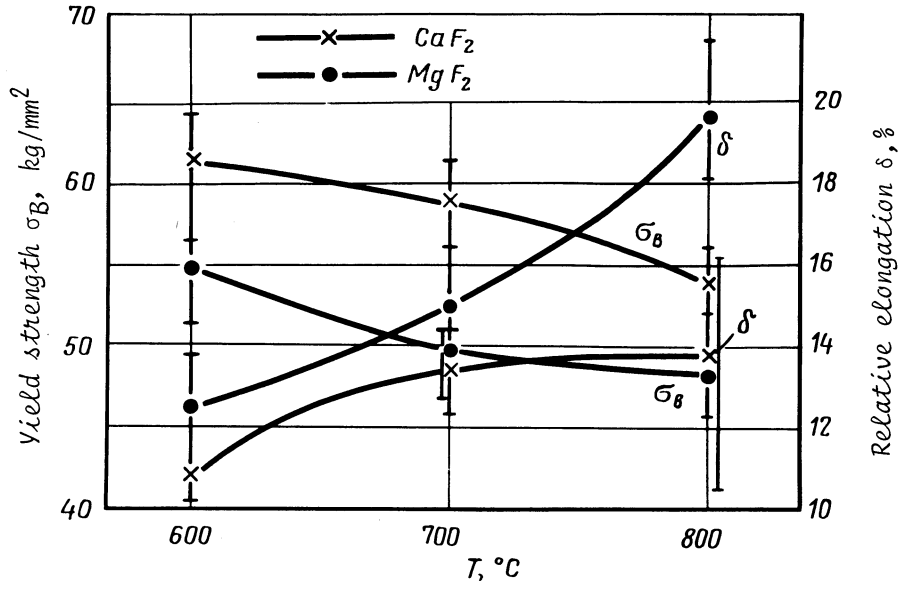

Fig. 3: Dependence of the mechanical properties of the titanium foil on the condensation temperature and the material the separating layer is made of.

tween 1000 and 1050°C, was also observed for calcium flouride. In the case of calcium flouride, an increase in the maximum temperature for titanium condensation is attributed to its lower vapour pressure as compared with that of magnesium flouride at the same temperatures.

When examining the structure of the titanium condensates deposited on the substrates coated with magnesium and calcium flourides, we have established that the influence of the material the release agent is made of, begins to become noticeable only at the condensation temperatures in excess of 700°C. The titanium condensate deposited at a temperature of about 800°C on a substrate coated with calcium flouride, possesses an acicular structure which is characteristic of the transformed β-phase, in contrast to the equixial structure of α-titanium, which was obtained under the same conditions on a substrate coated with magnesium flouride (Fig. 2).

Figure 3 shows the dependence of the mechanical properties of titanium foil on the condensation temperature and the material the release agent is made of. From this figure it is apparent that, irrespective of the material the release agent is made of, the plastic properties of the titanium foil improve as the condensation temperature is raised from about 600°C to about 800°C. Yet, within the entire temperature range under investigation, the foils produced

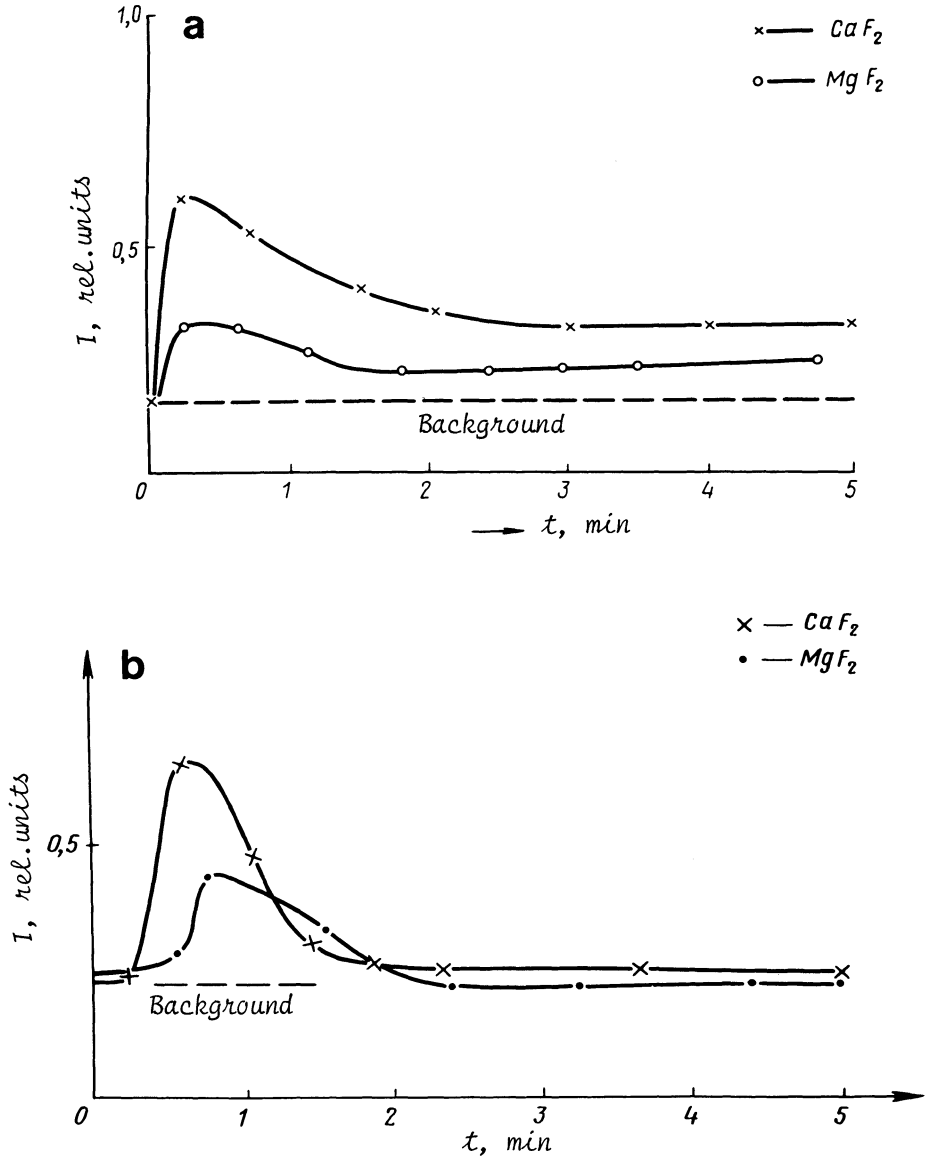

Fig. 4: Evolution of gases from a steel plate coated with calcium and magnesium fluorides at a temperature of 800°C: a) $CO+N_2$, and b) H_2.

on magnesium flouride exhibited a higher elongation than did the foils produced on calcium flouride. Here, the most striking difference was observed at the condensation temperature of about 800°C.

It is well known that gases can strongly affect both the allotropic transformation temperature[7] and the mechanical properties[8] of titanium. With a view to explaining the laws formulated above, we have analyzed the gas evolution at a temperature of 800°C from substrates coated with calcium and magnesium flourides, as well as the porosity of such coats. As is apparent from Fig. 4, the substrates coated with calcium flouride evolve a considerably greater amount of gases than did the substrates coated with magnesium flouride. Moreover, a higher porosity (about 2.0/1cm^2) is characteristic of a condensed layer of calcium flouride, as compared with that characteristic of a condensed layer of magnesium flouride (about 0.6/1cm^2).

The results thus obtained enable us to suppose that the more intense gas evolution from the steel substrate through pores of the applied calcium flouride layer determines the effect referred to above, which is characteristic of variations in the structure and in the mechanical properties of the titanium foil deposited at a temperature of 800°C.

Consequently, the researches done in the present work have shown the following: when producing metal foils by vacuum evaporation the release agent material should be selected by taking into account its influence, not only on the separability, but also on the physics-mechanical properties of the foil produced.

REFERENCES

1. Smith, H. R., Kennedy, J. K. and Boericke, J. S., The Journal of Vacuum Science and Technology, 1970, 7 No. 6, pp. 48-51.

2. Smith, H. R., US-Patent Specification No. 3,270,381.

3. Hugnes, Y. Z., Metals Engineering Quarterly, 1974, 14, No. 1, pp. 1-5.

4. Smith, H. R., British Patent Specification No. 3,729,046.

5. Kennedy, K. D., US Patent Specification No. 3,729,046.

6. Roikh, I. L. and Koltunova, L. I., Protective Vacuum Coatings on Steel (in Russian), "Mashinostrojenie" Publishing House, Moscow, 1971, p. 280, with figures.

7. Eremenko, V. N., Titanium and its alloys (in Russian), published by the Ukranian Academy of Sciences, 1955, p. 394, with figures.

8. Glazunov, S. G. and Moiseev, V. N., Structural Titanium Alloys (in Russian), "Metallurgiya" Publishing House, 1974, p. 367 with figures.

THE APPLICATION OF TiC AND TiN THICK FILMS BY PVD PROCESSES

K. Nakamura, Y. Fukube, K. Inagawa,
and Y. Nozawa
Institute for Super Materials, ULVAC
Corporation 523 Yokota Sambu-cho,
Sambu-gu, Chiba-Pref. 289-12 Japan

1. INTRODUCTION

Recently, several processes of physical vapor deposition have been developed to obtain hard refractory carbide and nitride films. Reactive sputtering[1], activated reactive evaporation with a probe electrode and grounded substrate (A R E)[2] and activated reactive evaporation with a biased substrate (Low Pressure Plasma Deposition: L PP D) were successfully used to produce TiC and TiN thick films. This paper describes the examination of these films coated on the steel plate and the WC-Co cemented carbide throw away tips by latter two processes, and also describes the distinctive feature of TiC thick films for corrosion resistance to molten Aluminum.

2. Apparatus and Experimental Procedure

Fig. 1 shows the schematic diagram of the apparatus used for coating of TiC and TiN films. After evacuation of the chamber to 5.10^{-5} Torr, Titanium was evaporated by electron beam (Beam power: max. 5 Kw) with closing the shutter. And then, after a constant evaporation rate was obtained, bias D.C. voltage was supplied on the probe or the substrate to the predecided current. Then the C_2H_2 or N_2 gas was flowed into the chamber to a predecided pressure. After the steady state was obtained, the shutter was opened then the coating was started. The thickness of the film was measured with coating time under a constant evaporation rate. The substrate temperature was kept by radiant back heating of Ta resistance heater. The substrate temperature and the partial pressure of the reactive gas were controlled in order to obtain the best coating condition. The flank face of the cemented carbide tip was coated by rotating tip around the axis perpendicular to the rake face at a constant evaporation rate. Cemented carbide used was SNG432-ST20E (JIS,P20)

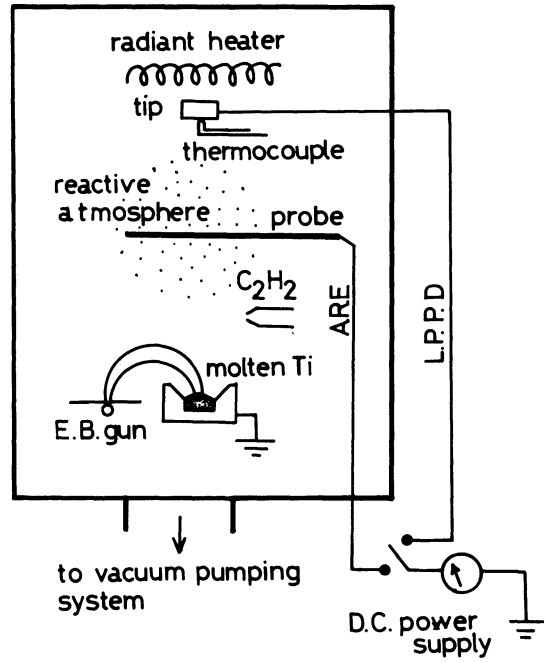

Fig. 1 - Schematic diagram of apparatus used for ARE process and LPPD process.

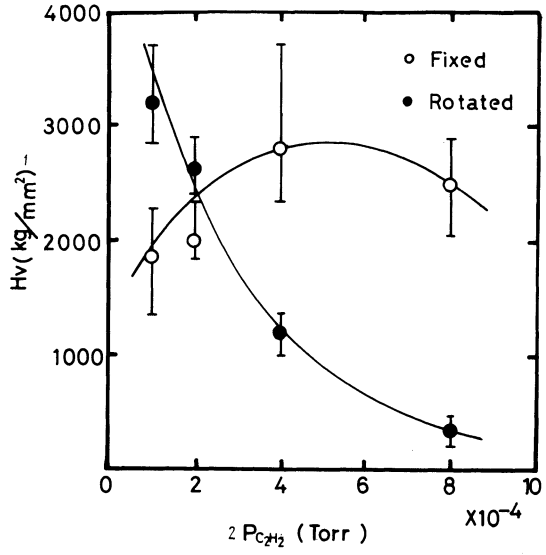

Fig. 2 - Effect of Pc_2H_2 on the hardness of TiC film.
(o: Fixed, •: Rotated)

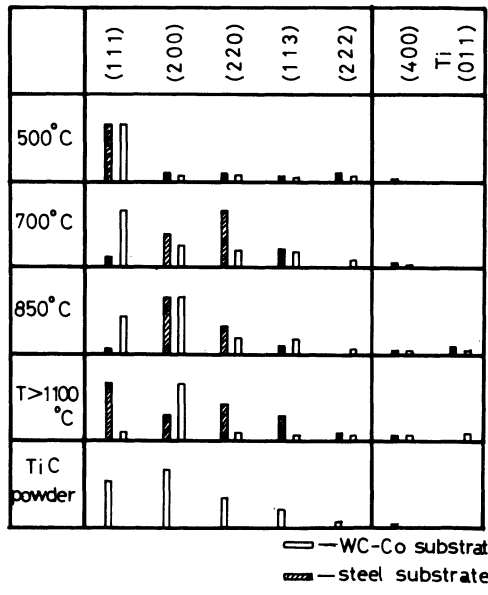

Fig. 3 - X-ray diffraction pattern of TiC film coated on WC-Co Tip and steel substrate at different temperature.
(Pc_2H_2: 8.10-4 Torr)

made by Sumitomo Electric Co. Titanium used for evaporation was degassed beforehand by high vacuum melting and its purity was 99.9%. The gas used was the welding grade one for C_2H_2 gas and high purity grade one for N_2 gas. The pressure of the chamber was measured by ionization gauge calibrated with N_2 gas. The hardness was measured by micro-Vicker's hardness tester at the load of 25g. The wear resistance test of the coated tip was done by a lathe machining of a Ni-Cr-Mo steel (JIS. SNCM 8.) rod with feed of 0.4 mm/rev, the cutting depth of 0.5 mm and the cutting speed of 225 to 175 m/min. After each 3.5 minutes cutting test, flank wear length and crater depth was measured by surface roughness tester. On this lathe machining test, we compared two kinds of TiC coated tips, the one is coated by P.V.D. process and the other was by C.V.D. process. In order to obtain the best cutting properties, the films of various thickness were tested on machining. Stoichiometry and orientation of the TiC, TiN films were measured by X ray diffracto-meter. After wear resistance test, surface of the tip was observed by Scanning Electron Microscope to see the wear resistance mechanism. Corrosion test of the TiC film was done by cyclic dipping into Aluminum melt. Aluminum melt tested was diecasting alloy (JIS.AD3.), tested temperature was 630°C and dipping cycle was 1000cycle/2hr. Tested material was TiC coated steel (SKD-6.) and uncoated SKD-6 steel. After dipping test, weight loss of the test piece was measured.

3. Results and Discussion

3.1: TiC Thick Film. Fig. 2 shows the effect of the partial pressure of C_2H_2 on the hardness of the TiC thick film coated on mild steel (substrate condition: rotated and fixed) at the temperature of 550°C by A R E process. On the fixed substrate, maximum hardness was obtained at the partial pressure of $C_2H_2 = 4 \cdot 10^{-4}$ torr. On the rotated substrate, maximum hardness was obtained at the partial pressure of $C_2H_2 = 1.6 \cdot 10^{-4}$ torr. This difference must be attributed to the low vapor density of Titanium around the substrate in a case of substrate rotation. Fig. 3 shows the diffraction pattern of the TiC film coated on WC-Co tip and mild steel at different temperature. When coated at low temperature, preferred orientation was observed and at the higher substrate temperature it becomes randomly. Fig. 4 shows the relation between crater depth/ flank wear and cutting time of TiC coated tips made by P V D process at two kinds of temperature and by C V D process and also shows the same relation of uncoated tip. Here, CVD processed tip was doubly coated with TiC (under), and TiN (upper). As shown in Fig. 4, crater depth and flank wear becomes low at higher substrate temperature respectively. Regarding to flank wear, P V D process looks more feasible method than C V D process. (Fig. 4. b.) Fig. 5 shows the relation between flank wear and TiC film thickness after 14.4 minutes cutting. Flank wear becomes minimum near the film thickness of 2 μm. Under this thickness, flank wear rises sharply

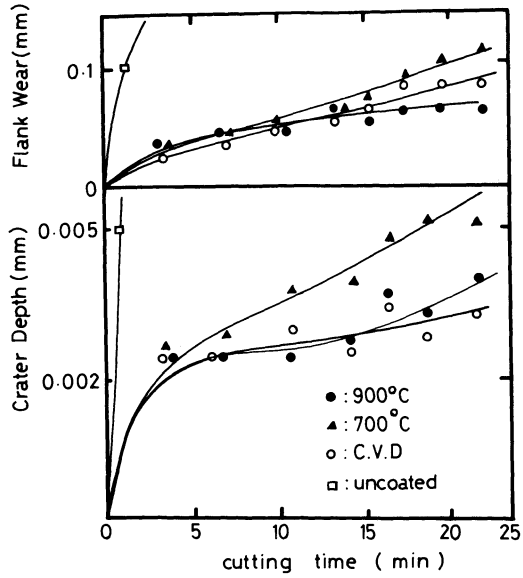

Fig. 4 - Relation between the Flank wear, the Crater depth and the cutting time of the TiC coated tips.
(▲: 700°C, ●: 900°C, o: CVD.
□ : uncoated tip).

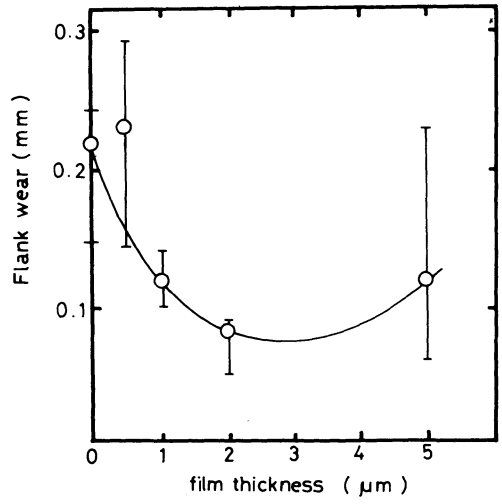

Fig. 5 - Effect of TiC film thickness on Flank wear of WC-Co tip after 14.4 minutes cutting test.

and over this thickness, it rises slowly. Fig. 6 shows the relation between the cutting time and crater depth of the tip coated by two process that is A R E and L P P D process. No difference was observed between two process. Figure 7 shows the S.E.M. micrography of the crater weared surface and flank weared surface after 14.4 min. cutting test of the uncoated tip and the TiC coated tip. We can see the remarkable difference of the crater wear pattern after machining test between the uncoated and TiC coated tip as shown in Figure 7 (a), (c). Regarding to the TiC coated tip's surface, the flow line of TiC surface parallel to the chip's flow was observed. Table. 1 shows the corrosion loss of the TiC coated SKD-6 steel cyclicaly dipped in die-casting aluminum melt in 630°C. A remarkable effect of the TiC coating was observed and the film thickness above 20 μm is sufficient for the corrosion resistance. The corrosion loss of the coated steel, of which the thickness of TiC film is 20 μm, in a molten aluminum alloy at 630°C was about 1/350 of that of the uncoated steel.

TABLE I

Corrosion Loss of TiC Coated SKD-6 Steel and Uncoated SKD-6 Steel in Molten Aluminum

Thickness of TiC film	Corrosion Loss
0 (uncoated) μ	350 - 400 (mg/cm^2)
10	2.8
20	1.2

3.2 TiN thick film. Table II shows the effect of the substrate temperature and the N_2 partial pressure on the formation of TiN film on mild steel by A R E process. Table III shows the effect of N_2 partial pressure on the formation of TiN films on steel by L P P D process and on the hardness of the films at the substrate temperature of 300"C. As shown in the Table 2, when the N_2 partial pressure was low, TiN was formed at low substrate temperature and at higher substrate temperature, higher partial pressure of N_2 was necessary to form TiN. Under a constant substrate temperature, hardness of the TiN film was decreased by increasing N_2 partial pressure. This phonomemon may be related to the structure of the films. When Ti_2N was contained in the film, hardness of the film increase remarkably as shown in the Table II and Table III.

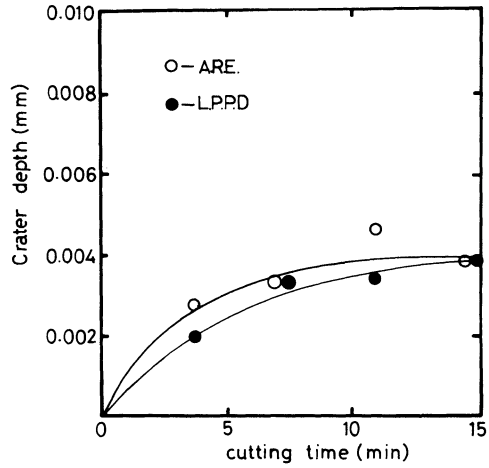

Fig. 6 - Relation between Crater depth and cutting time of WC-Co tip, TiC coated by ARE and LPPD process.

4. CONCLUSION

TiC and TiN films were coated on steel and WC-Co tips by A R E and L P P D process. Its stoichiometry and the orientation was examined and hardness of these films were measured. The wear resistance of TiC coated WC-Co throw away tip was measured by lathe machining test and feasibility of TiC coating by two processes was obtained. Corrosion test of TiC coated steel in aluminum melt was done and remarkable corrosion resistance of TiC coating was obtained. Concerning TiN films coated by A R E and L P P D process, an effect of N_2 partial pressure and substrate temperature on the hardness and the stoichiometry was obtained.

REFERENCES

1. Nakamura, K., Shinoki, F., Ito, A. Preparation of TiC Film by RF Reactive Sputtering. Journal of the Japan Institute of Metals, Vol. 38, No. 10, 1974, pp 913-919.

2. Bunshah, R. F., Raghuran, A. C., Activated Reactive Evaporation for High Rate Deposition of Compounds, Journal of Varuum Science and Technology, Vol. 9, No. 6, 1972, pp 1385-1388.

3. Raghrun, A. C., Bunshah, The Effect of Substrate Temperature on the Structure of Titanium Carbide Deposited by Activated Reactive Evaporation, Journal of Vacuum Science and Technology, Vol. 9, No. 6, 1972, pp 1389-1394.

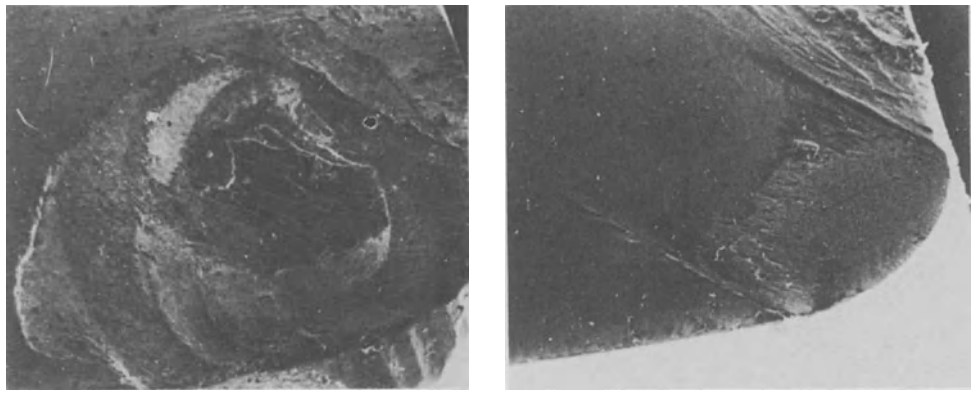

(a)
crater surface of
uncoated tip

(b)
flank surface of
uncoated tip

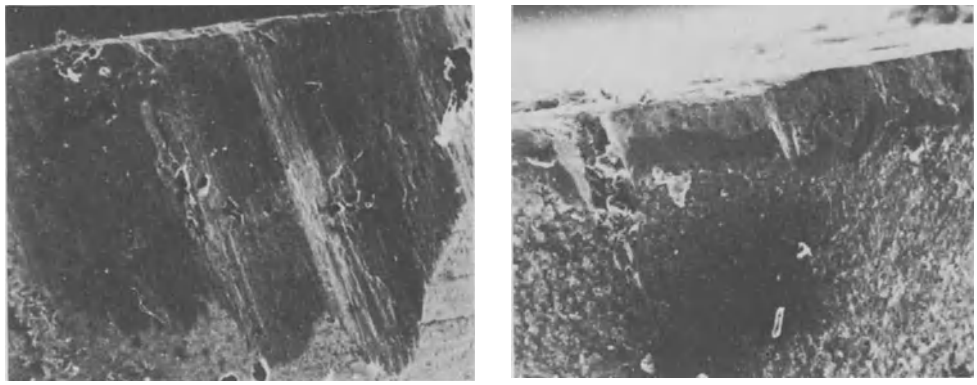

(c)
crater surface of
TiC coated tip

(d)
flank surface of
TiC coated tip

Fig. 7 - Scanning electron microscope micrography of the surface of TiC coated and uncoated WC-Co tips after lathe machining test. Cutting time: 14.4 minutes - Magnification: 33

TABLE II

Effect of N_2 Partial Pressure and Substrate Temperature on the Stoichiometry and Hardness of the TiC Film on Mild Steel. (A R E process)

sub.temp. (°C)	PN_2 x 10^{-3} (Torr)			
	0.8	1.5	1.8	2.0
500	H_V=1900 Ti_2N	1300 TiN+(Ti_2N)		
250	1700 Ti_2N+(TiN)	1900 TiN	1000 TiN	600 TiN
150	1500 TiN			

TABLE III

Effect of N_2 Partial Pressure on the Hardness and the Stoichiometry of the TiC Film Coated on SKH-9 (steel) at the Temperature of 300°C (L P P D process)

PH_2 (Torr)	thick. (μ)	Hv (kg/mm^2)	phase
$0.5x10^{-3}$	6.5	2800	Ti_2N
1.3	4	1400	"
1.7	3	1300	"
2.2	3	650	TiN+(Ti_2N)
3.0	1.5	340	TiN
1.7	6.5	1400	TiN+(Ti_2N)
2.2	3.5	750	TiN
2.2*	4	1000	"

*ARE

Discussion

Section XIII. Titanium Matrix Composites. Semi-products Produced by Vacuum Evaporation Methods

K. A. Portnoy

I would like to point to the need to use all means available for improving the strength characteristics of composites. One such approach is the utilization of coatings on reinforcing fibers not only as barrier-forming layers, but also for additional strengthening.

Silicon carbide and nitride used at the present time act as barrier layers but make no contribution to strength. Meanwhile, by using boron carbide as a barrier-forming layer, it is possible both to raise titanium composite tensile strength levels by 20% and to obtain corresponding fatigue resistance increases. We should extend the search for completely new reinforcing methods capable of substantially changing our present outlook as regards interaction and property strengthening in composite materials.

In his presentation, C. Edeleanu properly noted that utilization of titanium alloys first require confidence. This comment can be extended to include composite materials since they are development products seeking new applications. To realize a wider utilization of composite materials, it is necessary to broaden the research on the complex interaction between various properties of new materials.

M. H. Shorshorov

Allow me to make a few comments in relation to the selection of titanium as a matrix for reinforcement by borsic and silicon carbide. First of all, one should point to the desirability of alloying the matrix with stabilizers which affect the energy of titanium self-diffusion and slow down the interaction reaction. This is one point. The second is if there is a necessity to raise titanium matrix strength thereby "pulling up" composite material properties? Another question is if there is a possibility of stress relaxation in the matrix, particularly during thermocycling? Only by considering all three of these points is it possible to establish the benefits of titanium matrix alloying.

The work conducted at the Institute of Metallurgy have shown the necessity of considering the occurrence of stress relaxation, especially for abrupt changes of heat conditions.

I also call for caution in matrix alloying from the standpoint of interaction reaction.

A. I. Khorev

Allow me to recall the remark stated in A. T. Tumanov's (USSR) presentation about improving performance of multi-layer composition materials (MCM), as compared with conventional materials. The latter is attributed to the strengthening of interfaces.

On the basis of our own experience, we suggest that the following MCM design principles should be used. The composite design is determined by the following:

1. The strength level required: the greater it is, the higher is the required strength level of composite components.

2. Structural safety factor providing for continuous structure performance when one of the high-strength layers is broken.

3. The high-strength layer thickness should be less than critical crack length for the given test method.

4. The capability of crack localization at a certain stage of its development also depends on the soft component properties, its ability to produce a plastifying effect on the high-strength component.

L. P. Grankovoy

I feel I ought to comment on two subjects. First, the interest to the use of laminated titanium composite materials in heavy sections which make it possible to eliminate the major limitation of titanium alloys: the reduction in toughness.

Second, the strong promise of explosive welding. In a sample 10-12 mm thick we obtained a yield strength of 145 kgf/mm^2 at an impact strength of 8-10 kgf/cm^2.

INDEX

Acid corrosion
  effect of prior oxidation, 943, 949, 952 (graphs), 1010
  elemental effects
    Al, 955, 959, 1006
    Cr, 959, 967
    Fe, 959, 1030
    Ni, 1033
    O, 1030
    Pd, 1033
    Si, 959
  hydrogen absorption, 995, 1005
  industrial media, 935, 1007, 1039
  inhibitors, 1039
  microstructural effects
    BT-14, 996
    BT-15, 996
    Ti-Cr, 971 (Table)
    Ti-Fe, Ti-O, 1030
    VT-15, 970 (Table)
  multi-component alloy systems
    AT-3, 941, 949
    AT-6, 949
    BT-6C, 1009
    BT-14, 995, 1009
    BT-15, 995, 1009
    BT-20, 1009
    BT-22, 1009
    BT1-0, 952, 995
    BT3-1, 1009
    OT-4, 1009
    TC-5, 1009
    Ti-Al-Mn, 1006
    Ti-Al-Mo, 1006
    Ti-Al-V, 1006
    Ti-Mo-Nb-Zr alloys, 927
    VT-14, 967
    VT-15, 967
    VT1-0, 1039
    welds, 937
Acoustic Emission
  fracture of oxides, 1097
Age hardening response
  for Ti-39V-0.6Si and beta C, 556
Aging
  of β Ti alloys, 1675
  of Ti-8823, 1717
Aging behavior
  of Ti-6Al-6V-2Sn, 1913
Alloy composition
  effect on texture, 1881
α-phase precipitation, 1477
α-Ti alloys
  influence of peculiarities of boron, 189
α-Ti, diffusion of H in, 1377
Anderson structure, 65
Anodic polarization curves of Ti & Ti_4, 898 (figure)
Anosvite, 65
Applications of titanium alloys, 35
Artificial titanium minerals, 65
Bardinite, 65
Base corrosion - elemental effects
  Al, 959
  Cr, 959
  Fe, 959
  Si, 959
Bauschinger strain, 560
Beta flecking
  in large forgings, 417

Beta forgings, 231
Billet production of titanium, 10, 14
Boron
  peculiarities in α-Ti alloys, 189
  modified VT-5 alloy, 209
Boronizing, 1741
BT-5 alloy
  with 0.01 Boron additive, 191
BT6-C
  vacuum rolling, 264
Bulk deformation, 359
Cathode modified Ti-Alloys, 915
Charpy impact value
  effect of β grain size in Ti-15Mo, 577
  relationship with K_{IC} value, 584
Chemical dissolution
  mechanisms, 978, 995
  rate, 995
Chemisorption of oxygen, 1063
Chloride corrosion-elemental effects,
    Al, 959, 981
    Cr, 959
    Fe, 959
    Si, 959
Chlorination process, 33, 68, 70
  of titanium dioxide, 68
Cleavage facets in vacuum fatigue, 804 (figure)
Coefficient of diffusion, 1512
Cold rolling, 235, 283
Compositions,
  of ferromagnetite concentrates of placer deposits, 82
  of ilmenite concentrates of bedrock deposits, 80
  of ilmenite concentrates of placer deposits, 83
Compressor wheels, 337
Cooling rate effects, 1119
Corrosion, 847
  corrosion rates of various Ti alloys, 859 (figure)
  effect of Mo additions, 903
  effect of Ni addition, 921 (Fig.)
  in dilute HCl at elevated temperature, 881
Corrosion (cont'd)
  of cathode-modified Ti-alloys, 915
  of Ti & Ti-Pd alloys, 881, 917
Crack initiation
  hot salt stress corrosion, 1081
Crack propagation, 1601
  hot salt stress corrosion, 1081
  in air and sea water, 825
  relationship with mechanical properties, 791
Creep rate
  influence on texture, 1872
Critical crack length
  use in estimating K_{IC}, 769
Crystallographic structure
  stress-induced martensite, 1567
Crystals orientation relationship, 1531
Cyclic fracture toughness, 829
Cyclic stress-strain response
  cyclic instability, 553
  cyclic softening, 557, 589
  cyclic stress-strain curve for beta C, 560
Decomposition
  α', α'+β+ω, β+ω, β, 1509
  β, 1559, α", 1613
Defects, resulting from
  heterogeneous and coarse grained macrostructure striations, 1772
  local manifestations of the coarse α-phase, 1777
Deformation flow studies, 337
Deformation and fracture, 1357
Deformation hardening, 837
Delayed failure, due to hydrogen,783
Dendrites
  dendritic freezing in ingots,130
  secondary arm spacing for four Ti-Mo alloys, 134
  dendritic segregation, 148
Die-forgings, 230, 347
Diffusion bonding, 1112
Diffusion in Ti
  oxygen, 1055
  vacancies, 1060
Diffusion
  of ions through oxides, 872
  of oxygen in metal substrates, 874

Disc forging, 351
Dislocations
  effect of oxygen, 531
  interstitial alloys, 497
Drawing, 296
Ductility
  influence of grain size, 1919
Effect of oxygen
  skull produced ingots, 184
  sponge drums, 156
  sponge size, 158
Elastic modulus, 1511
Electrochemical properties
  elemental effects
    Al, 983
    Cr, 960, 974
  multicomponent alloy systems
    BT-14, 996
    BT-15, 996
    VT-1-0, 1018 (Table), 1041
    VT-14, 973
    VT-15, 973
Electrolytic production of titanium, 55-57
Electrolytic titanium powders
  characteristics, 121
Electron beam melting, 197
Electron beam welding, 1245
Electrorefining of titanium, 117
  cell arrangements, 118
Electroslag remelting process
  impurity content, 164
  mechanical properties of ingots, 164
  power required, 166
  slag temperature, 165
Electroslag welding, 1259, 1269, 1279
Electronic bonding in Ti alloys, 1391
Electronic specific heat of Ti alloys, 1407
Electronic structure, 1281
Embrittlement
  high strain rate, 781
  of hardened α+β alloys, 1641
  slow strain rate, 781
Environmental effects sustained load cracking, 1221
Eutectoid reaction, 1294
Explosive plating, 760
Extrusion
  hydrostatic, 369
  of PM billets, 355
Fatigue
  S-N curves for Ti-8823 alloy (Figure), 1722
  strength of Ti-6Al-4V, 1821
Fatigue behavior
  effect of β-grain size in Ti-15Mo, 577
  effect of heat treatment in Ti-6Al-4V, 637
  effect of mean stress in Ti-6Al-4V, 589
  S/N curves of Ti-6Al-4V, 593
  torsional fatigue of Ti-6Al-4V, 640
Fatigue crack initiation
  fatigue crack initiation sites of Ti-6Al-4V and Ti-11, 674
  mechanism for the fatigue crack initiation in Ti-6Al-4V, 645
  of aircraft structural components, 570
  subsurface initiation, 599
Fatigue crack propagation
  effect of hold-time, 671
  effect of microstructure in Ti-6Al-4V, 691
  effect of microstructure in Ti-11 and Ti-6246, 664
  effect of texture, 794, 799
  in air and sea water, 825
  measurement of crack extension by the electrical potential method, 653
  of aircraft structural components, 569
  relationship with mechanical properties, 791
Fatigue limit
  vs. critical crack length, (Figure), 772
Flow stress and strain in TiAl,739
Flow turning, 725

Forging, 1221, 1277
large forgings, 413
of PM billets, 355
shock loading effects, 765
Ti-6Al-4V, 397
Ti-6Al-4V, 413
Fractography
of vacuum fatigue, 799
Fracture
fatigue, 483
monotonic loading, 480
oxide scale, 1097
review, 467
sustained load cracking, 1221
Ti-6Al-4V, 383
Fracture mode
appearance and development of the cracks in Ti-Al, Ti-V and Ti-Cr alloys, 615
ductile fracture mechanism in titanium, 686
pore formation of α Ti alloys at the temperatures above 0.5 Tm, 707
transgranular ductile dimples, 608
void nucleating Ti_5Si_3 particles, 608
Fracture toughness
effect of alloying, 631
effect of microstructure in Ti-11 and Ti-6246, 664
effect of microstructure in Ti-6Al-4V, 649, 693
effect of pressure shaping and thermal treatment, 629
effect of specimen dimension on K_{IC} of Ti-6Al-4V, 650
index diagram, 611
Ti-6Al-4V, 383
Fracture toughness, plane strain
dependence on chemistry, 814
effect of hydrogen, 785, 811
effect of sea water, 825
estimation of, 769
influence of texture, 818
values for Ti alloys, 769, 826
Friction coefficient (rolling), 251
Galling
of IMI 318, 1750
γ-phase in Ti alloys, 1357
Goodman diagram, 589
Grain size
influence on ductility, 1919
influence on work hardening,1933
Habit plane, 1532
Hall coefficient in Ti alloys, 1391
Heat treatments
of α+β alloys, 1583, 1605
of β alloys, 1675
Helical rolling mills, 313
High temperature deformation, 1357
Hollow hinge shapes, 302
Homogeneity
of the plastic strain, 616
Hot corrosion
effect of preoxidation, 989
effect of water, 987
multicomponent alloy system, IMI 685, 987
scale morphology, 991
Hot hoisting tests, 324
Hot plasticity of Ti alloys, 324
Hugoniot graph
effect of Al & V additions (Figure), 759
Hunter process, 33
Hydride formation, 892
Hydrogen
diffusion of in Ti, 1377
effect of pressure of arc furnace, 157
effect on fracture toughness,811
embrittlement, 781
evolution in Ti-Mo alloys, 903
in solid solution, 781
influence on Ti alloys, 1833,1840
sponge pickup, 159
Hydrogen-titanium system, 1365
Hysterisis of Ti-Mo-Zr alloy, 1691
Impact ductility effect of hydrogen, 782
Inclusions
high density types, 129
in ingots, 127
Ingot casting of titanium, 10, 34, 127, 141
grain morphology, 144

Ingot casting of titanium (cont'd)
microstructure, 144
skull furnace, 179
In-Situ electron microscope
observations of crack propagation, 715
Interaction between alloying elements, 1521
Interdiffusion, 1731
Interface phase, 695, 1437
Intergrain creeping, 617
Intergranular fracture of titanium α alloys, 705
Intermetallic compounds, 1281
$(Ti_{0.4}Zr_{0.6})_5Si_3$, 1527
$ZrFe_2$, 1576
Internal friction, 1521, 1543, 1555, 1661
effect of oxygen, 531
Internal twinning, 1531
Iron alloys
40X, 837
Y8, 837
Isothermal forgings, 232, 327, 337, 347
K_{ISCC}
influence on texture, 1873
Kroll-type titanium products, 26
Large Ti-billet rolling, 273
Lattice parameter, 1614
Low cycle fatigue, 1177
Coffin-Manson plots for Ti-6Al-4V, 595
effect of hold-time in IMI 685, 671
of VT5, 211
Machining
theoretical aspects, 762
Macrosegregation
ingots, 137
alpha stabilized streak, 137
Macrostructure
of rolled billets, 278
Magneli phase, 65, 866
Magnesium chloride electrolysis process, 33
Magnesium-thermic process, 44, 45
kinetics, 47
thermodynamics, 46-53
titanium sponge production, 101
Magnetic anistropy
in Ti alloys, 1461
Magnetic susceptibility
measurements in Ti-alloys, 1407
of Ti-Al alloys, 1391
Martensite
α' substructure, 1623
formation in Ti alloys, 1477, 1703
strain induced, 1567
Mechanical properties
after aging, of β alloys, 1675
after slack quenching, 1595
cooling rate dependence, 1583
effect of ingot section, 210
effect of microstructure, 1916
effect of texture, 1863
grain size dependence, 1501
of rolled Ti-rings, 309
of VT5 alloy, 210
oxidation effect, 955
spontaneous cracking of α+β alloys, 1641
Metal flow in rolling, 290
Metallothermic production of titanium, 42, 45, 72
Method of evaluating the validity
of α+β titanium alloys, 601
of K_{IC} values, 626
relationship with strength or ductility, 601, 611, 634
SEN specimen, 602
sustained loading of Ti-6Al-4V, 656
Microsegregation, 130, 133
alloy temperatures, 132
dendritic structures, 133
segregation ratios, 134
Microstructure
after aging of α+β alloys, 1605
after slack quenching of Ti-6Al-6V-2Sn, 1595
effect on fracture toughness, 816
in large section forgings, 413
influence on forgeability, 397
of α/β alloys, 1437
of Ti-6Al-4V, 383
Microstructure and properties
in Ti-11.5Mo-6Zr-4.5Sn, 1421

Mineral formation of artificial titanates, 66, 67
Modulus
elastic, 1691
Multi-layered sandwich structure, 828
fatigue crack growth, 828
Multi-roll passes, 281
Nitrogen
in ingots, 158
skull ingots, 184
Non-destructive testing
ultrasonic testing, 1231, 1277, 1279
Non-uniform plastic deformation during flow twinning, 1726
Notch toughness, 1521
Omega phase, 1161
effect on acid corrosion, 969
formation in Ti alloys, 1477
in Ti-alloys, 1403
precipitation, in Ti-11.5Mo-6Zr-4.5Sn, 1421
Ordering in Ti-alloys, 1403, 1477
Oxidation, 864
AT3, 950
AT6, 950
effect of chloride, 987, 1015
effect of mechanical properties, 955
IMI685, 987
kinetics, 866, 1046, 1057, 1089
mechanisms, 1051, 1097
pure Ti, 1045, 1057
scale morphology, 950, 991, 1046, 1089, 1097
Ti_3Al, 1089
Ti_3Sn, 1089
Oxides of titanium
composition, 870
microstructure, 870
structure, 866
Oxygen
effect on deformation, 514
effect on dislocations, 531
effects during extrusion, 370
in large forgings, 417
Panels, 302
Passive film
composition, 850, 883
formation processes, 887
thickness determination, 854, 883
Passivity, 850, 881, 891
experimental methods for investigation, 850
influence of alternating current, 851
influence of Mo addition, 903
of cathode-modified Ti-alloys, 915
Peritectoid reaction, 1298
Perovskite (celanite), 65
Phase composition of artificial titaniferrous products, 97
Phase diagrams, 1281
Ti-Al-Zr-W system, 1319
Ti-Hf-O system, 1327
Ti-Mo system, 1335
Ti-Si-Cu, 1351
Phase transformations, 1281
after stop aging, 1651
$\alpha'' \rightarrow \beta$, 1614
$\alpha \rightarrow \omega$, 1633
during heating, 1509
effect on texture, 1875
in Ti alloys, 1477
on rapid heating, 1499
upon quenching, 1559
Physical properties, 1281
Physico-chemico analysis, 1281
Plastic deformation, 841
during rolling, 253
interstitial alloys, 431, 497
kinetics in Ti-Al and Ti-Sn, 513
review, 429
slip and twinning modes, 429
substitutional alloys, 442
Plasticity of Ti alloys, 324
Polarization
anodic, 982, 996, 1017
cathodic, 982
surface condition effect, 1016
Pourbaix diagram, 847, 848 (Figure), 893 (Figure)
Precipitation
α, of Ti-8823 alloy, 1725
α, of Ti-Mo-Zr alloy, 1693

Precipitation (cont'd)
β, of Ti-Mo, Ti-V, TiNb, 1714
ω, of Ti-Mo-Zr alloy, 1693
Pressure shaping, 229
Production of titanium in the USsr, 7, 41, 63
Pseudo-elastic range, 598
Pulse load bonding, 1112
R-curve, 650
R-value
Ti-sheet, 1947
Radial reduction, 303
Recrystallization
during forging, 405
effect on texture in Ti-Al alloys, 1883
of Ti-Mo base beta alloys, 1893
Recycling
of Ti scrap, 213
Refining titanium sponge wastes
alloyed, 122
applications, 125
unalloyed, 119
Remelting of ingots, 161
impurity contents, 164
mechanical properties of, 164
rectangular ingots, 161, 162
round ingots, 162
Residual stresses
effect on texture, 1870
Rib structures, 329
Rolled Ti-products, 229
Rolled wire, 295
Rolling, 304
Rolling force, 294
Rolling pass design, 286
Rolling of Ti-rings, 305
Sandwich rolling, 253
Section rolling, 289
Segregation in Ti-6Al-4V, 604
Segregation temperatures for several titanium alloys, 132
Seizing, 1755
Selection evaporation, 197
Semi-finished shapes, 299
Serrated flow
Ti-Hf alloys, 539
Ti-Zr alloys, 539
Shape memory
of Ti-Ni alloys, 1843
Sheet rolling parameters, 243
Shock loading effects, 757
Skull-melting, 10, 169
applications, 176
chemical homogeneity, 182
effect of revertible scrap content, 185
experimental procedure, 171
ingot macrostructure, 180
ingot manufacturing, 179
melting rate, 173
schematic of vacuum arc skull furnace, 170
Sodium-thermic reduction method, 43, 45, 53-55
Solubility of H in titanium, 1365
Sponge production in Japan, 32
Stacking fault energy texture effects, 747
Strain aging, 1933
Strain induced martensite, 717
Strain induced precipitation of titanium hydride, 717
Strain rate sensitivity
in forging, 405
in superplasticity, 446
negative value for α+β Ti-15Mo, 584
Strength to toughness rates, 773
Strengthening
by grain refinement, 1919, 1933
of Ti-Al alloys, 1919
of Ti-Mo alloys, 1919
of Ti-6Al-6V-2Sn, 1905
Strengthening mechanisms
omega phase, 476
review, 467
second phase, 474
solid solution, 468
Stress corrosion
of RMI38-6-44, 1853
Stress corrosion, chloride solution
IMI685, 1081
kinetics, 1083
polarization, 983
stress intensity factor, 1081
Ti-Al, 981

Stress corrosion cracking
in 3%NaCl, 825
Stress intensity factor
threshold for stress corrosion
K_{ISCC}, 1083
Stress relaxation in Ti-Al
alloys, 741
Structure
polygonized, β-Ti, 1799
Substructure
in superplastic forming, 837
Superplasticity, 232, 837, 841
in Ti-5Al-2.5Sn, 446
in Ti-6Al-4V, 446
review, 429
Superconductivity in Ti alloys,
1407
Surface segregation under high
vacuum, 1069
Tagiorvite, 65
Tensile behavior
correction factor (σF/σf) of
titanium, 681
effect of β grain size in
Ti-15Mo, 577
effect of strain rate on
reduction of area and pore
nucleation, 710
effect of temperature, inter-
stitial content and grain
size in titanium, 683
Hall-Petch plots for the four
purities of titanium, 683
Tensile properties
effect of Al additions, 739
effect of hydrogen, 783
effect of superplastic form-
ing, 838
of Ti-6Al-6V-2Sn, 1905
of Ti-20Mo, 1922
of Ti-8.5Al, 1926
of textured Ti-sheet, 1954
relationship to crack
propagation, 791
yield strength, 826
Texture
back-reflected pole figure
method, 731
cold rolling of α-Ti, 747
Texture (cont'd)
development in α+β Ti alloys,
1863
direct pole figure method, 729
effect of Al additions, 739,
747 (Figure)
effect of applied and residual
stresses, 1870
effect of phase transformation,
1875
effect of Sn addition, 747,
750 (Figure)
effect on alloy composition, 1881
effect on deep drawability, 1947
effect on fatigue crack propaga-
tion, 794, 799
effect on fracture toughness, 818
effect on mechanical properties,
1867
effect on r-values, 1956
hot rolling α-titanium, 740
influence on creep rate, 1872
influence on K_{ISCC}, 1873
recrystallization texture, 1883
texture formation during flow
turning, 729
Ti-6Al-4V; oxygen influence, 1863
Texturing in Ti alloys, 1461
Thermomechanical processing, 1477
Thermodynamic parameters, 1307
Thermodynamics, 1281
Thermodynamics of Ti-H system, 1365
Time temperature transformation
diagrams of Ti-Mo-Zr alloy,
1696 (Figure)
Ti-alloys, 513, 1357, 1461
Beta III, 784 (Figure), 1903
Beta III, (Ti-11.5Mo-6Zr-4.5Sn),
1421
Beta III, (11.5Mo-6Zr-4.5Sn),
1161
BTI-1M, 791
BT-5-I, 829
BT6C, 791, 837
BT-14, 829, 837
BT-15, 791, 826
BT-20, (Ti-6Al-2Zr-1Mo-1V), 1145
CT-6, 826
influence of grain size on
ductility, 1919

Ti-alloys (cont'd)
NBT-I, 826
NBT-2, 826
ordering in, 1451
recrystallization textures, 1883
Ti-Al, 739, 747, 916
Ti-Al, Zr-W, 1319
Ti-C, 497
Ti-Cr, 859, 1307
Ti-Cr-Pd, 859
Ti-Hf, 539
Ti-Hf-O, 1327
Ti-Mo, 859, 903, 1307
Ti-Mo-Pd, 859
Ti-N, 497
Ti-Nb, 1307
Ti-Ni, 866, 921 (Figure)
Ti-O, 497
Ti-Pd, 859, 881, 916
Ti-Si-Cu, 1351
Ti-Sn, 513, 747
Ti-Ta, 1307
Ti-V, 1307
Ti-W, 1307
Ti-Zr, 539
Ti-1%Ru, 923
Ti-1.5Al-4.5Mn, 783
Ti-2.5%Cu, 866, 1189
Ti-3Al-1.5Mn, 916
Ti-4Al, 469 (Figure)
Ti-4Al-3Mo-1V, 1119, 1131
Ti-5Al-2.5Sn, 446, 469 (Figure)
Ti-6Al-2V-4Zr-6Mo, 450
Ti-6Al-4V, 383, 397, 413, 446, 469 (Figure)
Ti-6Al-4V, 1119, 1189, 1221, 1231, 1245
Ti-6Al-6V-2.5Sn, 858
Ti-6V4, 375
Ti-6wt%Al-4wt%V, 1437
Ti-8Al-1Mo-1V, 450
Ti-8Mn, 450
Ti-8%Ni-.2Ru, 923
Ti-8wt%Mn, 1437
Ti-11Cr-7.5Mo-3.5Al, 916
Ti-13Cr-3Al-11V, 450
Ti-16Mo, 450
Ti-25Al, 1451
Ti-26Mo, 469 (Figure)
Ti-alloys (cont'd)
Ti-43Mo, 531
Ti-56V, 531
VT1-0 (commercially pure),1197
VT3-1, 784 (Figure)
VT3-1 (2.5Mo-2Cr), 1209
VT4-1, 784 (Figure)
VT5-1, 784 (Figure)
VT5-1 (Ti-5Al-2.5Sn), 1145
VT6, 784 (Figure)
VT6 (Ti-6Al-4V), 1119, 1131, 1145, 1177, 1209
VT14 (Ti-4.5Al-3Mo-1V), 1119, 1131, 1145, 1177
VT15, 784 (Figure)
VT16, 784 (Figure)
VT20, 784 (Figure)
VT22, 785
VT22 (Ti-5Al-5Mo-5V-1Fe-1Cr), 1119, 1145, 1177, 1269
VT22M (Ti-6Al-5Mo-5V-1Cr-1Sn-1/2Cu), 1177
6-4, 784, 799, 811, 866
Ti-Al phase diagram, 1391
Ti-2Al-2Mn, 35
mechanical properties, 36
weldability, 36
Ti_3Al formation in Ti-alloys, 1477
Ti_3Al precipitation
in Ti-6Al-6V-2Sn, 1905
Ti-5Al-2Co-2V-0.2Si, 35
mechanical properties, 36
weldability, 36
Ti-5Al-3Mn, 35
mechanical properties, 36
weldability, 36
Ti-6Al-2Co, 35
mechanical properties, 36
weldability, 36
Ti-6Al-6V-2Sn
annealing behavior, 1905
strengthening, 1905
Ti-6.5%Al-2.5%Mo-1.5%Cr-0.5%Fe-0.3%Si
macrostructural studies of ingots, 144, 148
macrograph size in ingot 430mm, 147

Ti-15Mo-5Zr, 35
mechanical properties, 36
recrystallization behavior, 1893
weldability, 36
Ti-15Mo-5Zr-3Al, 35
mechanical properties, 36
weldability, 36
Ti-52.5Ni-1.56Fe-1.79Mo, 35
mechanical properties, 36
weldability, 36
Ti-castings
effect of grain modifiers, 209
Ti-commercially pure, 1189
Ti-extrusions, 230
Ti-Mo alloys
influence of grain size on ductility, 1919
Ti-Mo-base beta alloys
effect of recrystallization, 1893
Ti-pipe production
in USSR, 321
Ti-scrap, 213
Ti-sheet
texture effect on deep drawability, 1947
Ti tube manufacture, 321, 313
Titanium developments in USA,14
Titanium hydrides, 781
Titanium ingot solidification
inclusions, 127
macrosegregation, 137
segregation, 128
solute partitioning, 130
tree rings, 136
Titanium in Europe, 19
Titanium in Japan, 31
Titanium in ship building, 37
Titanium-oxygen phase diagram, 864
Titanium slags, 42-79
initial slags, 81-92
mineral structures, 86
slag-making, 81
thermodynamics, 86-92
where produced, 81
intermediate slags, 92-96
final slags, 95-98
structure characteristics,93
Titanium sponge
alloyed, 107
gas pickup during melting, 153
Nb alloyed sponge, 114
photo, 48
production process, 57, 101, 104
welding of sponge compacts, 154
Zr alloyed sponge, 112
Titanium tetrachloride, 73
activation energy, 73
production, 102
thermodynamics, 103
Titanium in thermal power stations, 37
Titanium (unalloyed), 829, 866, 881, 916
Titanium wrought products, 8, 14
Transformations
diffusional, 1691, 1712, 1731
displacive, 1691
martensitic, 1712, 1737
Tree rings, 136
Two-phase titanium alloy ingots
dendritic segregation, 148
ingot microstructure, 144
ingot properties, 150
phase growth patterns, 142
pool depth, 141
solidification rate equation, 141
solidification skin thickness, 142
Ultra-fine grained Ti, 1933
Universal strength diagram, 769, 774 (Figure)
Use of Titanium in the USSR, 7, 63
Vacuum rolling, 263
VT5 alloy, 210
Warm drawing, 303
Web structures, 329
Weld cavitation, 1171
Weld defects, 1171, 1177, 1189, 1209, 1278
Weld fluxes, 1201, 1259
Weld heat effected zone, 1161
Weld impurities, 1278
Weld porosity, 1189, 1277, 1278
Weld process effects, 1119, 1177, 1201
Weld processes
diffusion bonding, 1209, 1277

Weld processes (cont'd)
electroslag, 1259, 1269, 1279
electron beam, 1245
Weldability, 1119
Welding
applications, 1253
arc forge effects, 1171
filler metals, 1201, 1279
general, 1107
effect of hydrogen, 1113
effect of microstructure, 1108
techniques, 1108
Welding
computer simulation, 1145
crack growth, 1221, 1245, 1269
ductility, 1197, 1209
fatigue, 1277
low-cycle fatigue, 1177
mechanical properties, 1131
of sponge compacts, 154
O_2 and N_2 contents in welds, 155
hardness in welds, 155
post-weld heat treatment, 1131, 1139, 1145, 1269, 1279
Weldments
hydrogen-induced failures, 783
Work hardening
in ultra-fine grained Ti, 1933
Zirconium alloys, α_2-phase, 1761